The Palaeoceanography and Glacial History of the Greenland Sea and Spitsbergen Ice Cap over the last 200ka

By
Jeremy Lloyd

Thesis submitted for the degree of
Doctor of Philosophy

University of Edinburgh

February 1994.

Declaration

I certify that the work presented in this thesis is my own, except where otherwise stated, and has not been previously submitted as a degree at this, or any other, Universitv.

Jeremy Lloyd

Acknowledgements

I would like to thank my supervisors Geoff Boulton and Dick Kroon for initiating the project in the first place, and N.E.R.C. for providing the funding. Thanks must go to Cees Laban and the Dutch Geological Survey who provided the cores and the x-ray photographs used in this project, and allowed several re-sampling trips.

Special thanks must go to Dick Kroon, whose boundless enthusiasm and encouragement made this project so much easier and enjoyable. Thanks to Anne Payne and Erwin Bach for help with initial sampling, and to Ian Alexander, Kate Darling and Al Matthewson for help with the second sampling trip.

Terry Donnelly and Tony Fallick of the S.U.R.R.C. at East Kilbride must be thanked for advice and endless help with samples run on the Mass Spectrometer. I would also like to thank Bill Austin for help with identification of some of the foraminifera, and Alasdair, Yani and Stewart for reference checking.

I must also thank the many people who have made my time in Edinburgh so enjoyable. To Alasdair for teaching me to ski (!?), Anne, Ian, Alan and Rachel for skiing (and patching me up afterwards), and especially to Alan for the many climbing trips to the highlands. Thanks to Kev, Jon and many other squash partners. Special thanks to Rachel for dancing and fighting the photocopier.

Finally I would like to thank my parents, who may have been wondering what I've been doing these past 3 years, well here it is!

Abstract

Piston cores from the continental slope of Spitsbergen were analysed using micropalaeontological, stable isotope and sedimentological techniques. The study attempted to determine the palaeoceanographic history of the Norwegian-Greenland Sea, and the glacial history of the Spitsbergen ice cap over the last 200ka. The chronostratigraphy of the cores was determined using stable oxygen isotope analysis of planktic foraminifera. These records were correlated to a composite benthic foraminiferal $\delta^{18}O$ stratigraphy from the Norwegian Sea (Duplessy *et al.*, 1988), as well as to other radiometrically dated records from the Norwegian-Greenland Sea to produce an age model.

X-ray photographs were used to assess the ice rafted detrital (IRD) content of the cores, dropstones were counted from these x-rays. IRD content was used as a measure of calving rate from the outlet glaciers of the Spitsbergen ice cap. From these counts and the $\delta^{18}O$ record a model of relative advance and retreat of the Spitsbergen ice cap was produced. It was found that moisture supply was the over riding factor controlling dropstone input to the Spitsbergen margin. Periods of high moisture supply lead to rapid ice advance and hence high calving rate producing peaks in IRD. Peak IRD events were found during interstadial periods, such as substage 5c, as well as during glacial periods when ice was at the shelf edge, and during deglacial periods.

Absolute abundance counts of foraminifera suggest glacial periods had a much higher productivity than interglacial periods. This strongly suggests the Spitsbergen margin was at least seasonally ice free during glacial periods. Melting events were recognised from the $\delta^{18}O$ record of planktic and benthic foraminifera. The influx of North Atlantic surface waters during deglaciation have been identified from the $\delta^{18}O$ record and the faunal assemblages. The initial influx of North Atlantic water during the last deglaciation took place at about 12.3ka, disappeared at 12ka, was present again from 10.5 to 10.3ka, and then from 10ka onwards. The strength of North Atlantic water influx increased from 10ka onwards, evidence for this comes from the increase in percentage of subpolar planktic foraminifera at this time. Evidence from benthic foraminiferal $\delta^{18}O$ measurements and benthic foraminiferal faunal assemblages suggests that renewal of deep water circulation began at 10ka. The North Atlantic influx before this time was too weak to drive deep water circulation.

Faunal analysis provides no evidence for the influx of North Atlantic waters during any part of stage 5. The $\delta^{18}O$ record identifies two periods of strong melting during substage 5a and substage 5e. The benthic foraminiferal $\delta^{13}C$ record and the benthic foraminiferal assemblage changes suggest renewed deep water circulation took place during stage 5. This implies North Atlantic surface waters did reach the Greenland Sea during stage 5. The absence of subpolar foraminifera may be due to the strong meltwater lid present, in which the foraminifera can not live. Atlantic waters would sink below this low density surface layer at too deep a depth to support foraminifera and drive a deep water circulatory system recognised in the benthic foraminiferal record.

TABLE OF CONTENTS

List of figures, tables and plates

List of figures

Chapter 6

Chapter7

List of Tables

Plates

Chapter 1. Introduction

1.1. Background

During Quaternary ice ages thick sedimentary sequences were produced on continental margins, which can be studied in great detail. Cycles of growth and decay of ice sheets during glacial periods lead to changes in the sediment flux to the oceans. The Spitsbergen continental margin preserves thick sedimentary sequences originating from glacial erosion of the Spitsbergen ice mass. Outlet glaciers from this ice mass flow across the continental shelf within major troughs. Where these reach the shelf edge large depositional fan complexes are produced. These fans not only preserve the record of the sediment influx from the glaciated Spitsbergen landmass deposited during the late Quaternary, but they also contain evidence for changes in palaeoceanography in the Fram Strait. The calcareous tests of foraminifera get buried in the sediments and are of primary importance for the reconstruction of palaeocirculation and palaeoproductivity. The fans are unique because the high sedimentation rates provide high resolution stratigraphy to meet the need for a high temporal resolution.

The ice cap of Spitsbergen at the present is significantly smaller than it has been in the past. The western half of the Spitsbergen island is a mountainous terrain, and drops steeply to sea level at its western margin. The interior mountains of western Spitsbergen and, to a greater extent, eastern Spitsbergen are still heavily glaciated. Outlet glaciers extend down to the fjord head of the major outlet fjords draining the Spitsbergen ice cap along the west coast of Spitsbergen (for example Kongsfjorden, Isfjorden, Hornsund and Bellsund). The input of glacier sediments to the continental shelf edge and slope is very low at the present day. Input of ice rafted detritus from calving icebergs is very low. During the major glacial phases the Spitsbergen ice cap grew to a much larger size coalescing with ice masses from the other Svalbard islands to produce a major Svalbard ice cap. It is now generally accepted that during the last glacial maximum (oxygen isotope stage 2 or the Late Weichselian) outlet glaciers extended across the continental shelf of the western Spitsbergen margin, filling the glacial troughs present, and reached the shelf edge (Svendsen *et al.*, 1992; Mangerud *et al.*, 1992). Ice at the shelf edge would produce large quantities of glacial sediments enlarging the above mentioned fan complexes.

The extent of Spitsbergen ice, however, during the Early and Middle Weichselian (oxygen isotope stages 5 to 3) is less clear. Mangerud and Svendsen (1992) suggest two significant ice advances during this period from evidence from land sections. The first advance is postulated to have occurred during the Early Weichselian during oxygen isotope substage 5d. The maximum extent of this advance is uncertain, but it is thought to have reached the continental shelf. A major advance is identified during the Middle Weichselian; the outlet glaciers extended out onto the continental shelf during oxygen isotope stage 4.

The material analysed in this project comes from the continental margin of Spitsbergen. A series of cores have been studied from the mid-upper continental slope at various positions on the fan complexes mentioned above. Details of these cores are given in table 1.1 below, and their geographical position is shown in fig. 1.1. The cores were taken during an expedition of the Geological Survey of the Netherlands, with the survey vessel Hr. Ms. Tydeman of the Hydrographic Survey of the Netherlands in 1988.

Core	Position	Water depth	Length	Sampling frequency
PCM5	Lat. 78° 29'N Long. 7° 43'E	2139m	6.86m	2.5cm
PCM7	Lat. 78° 37'N Long. 7° 54'E	1073m	7.32m	5cm
PCM30	Lat. 79° 34'N Long. 6° 41'E	1137m	6.36m	5cm
PCM56	Lat. 79° 54'N Long. 8° 48'E	468m	7.56m	5cm

Table 1.1. Details of cores examined

Due to their position on the continental slope these cores preserve a unique record of local terrestrial fluctuations in ice activity as well as a more regional record of oceanographic changes. In the past, many studies have been carried out on deep marine sedimentary sequences of the major oceans of the globe. Cyclical changes in parameters such as the oxygen isotope composition of foraminifera, and the composition of foraminiferal assemblages themselves, have been identified. These changes have been related to the major continental glaciations and, subsequently, a chronology of ice sheet fluctuations on land has been produced from the deep marine record (Emiliani, 1955, 1966; Imbrie et al., 1984). Due to the relatively stable and slow sedimentation rate of the deep ocean environment, the records produced are relatively long ranging and uninterrupted, but have a relatively low resolution (often 1000 years or less). Cycles of continental glaciation have been recognised from marine records over the past several million years.

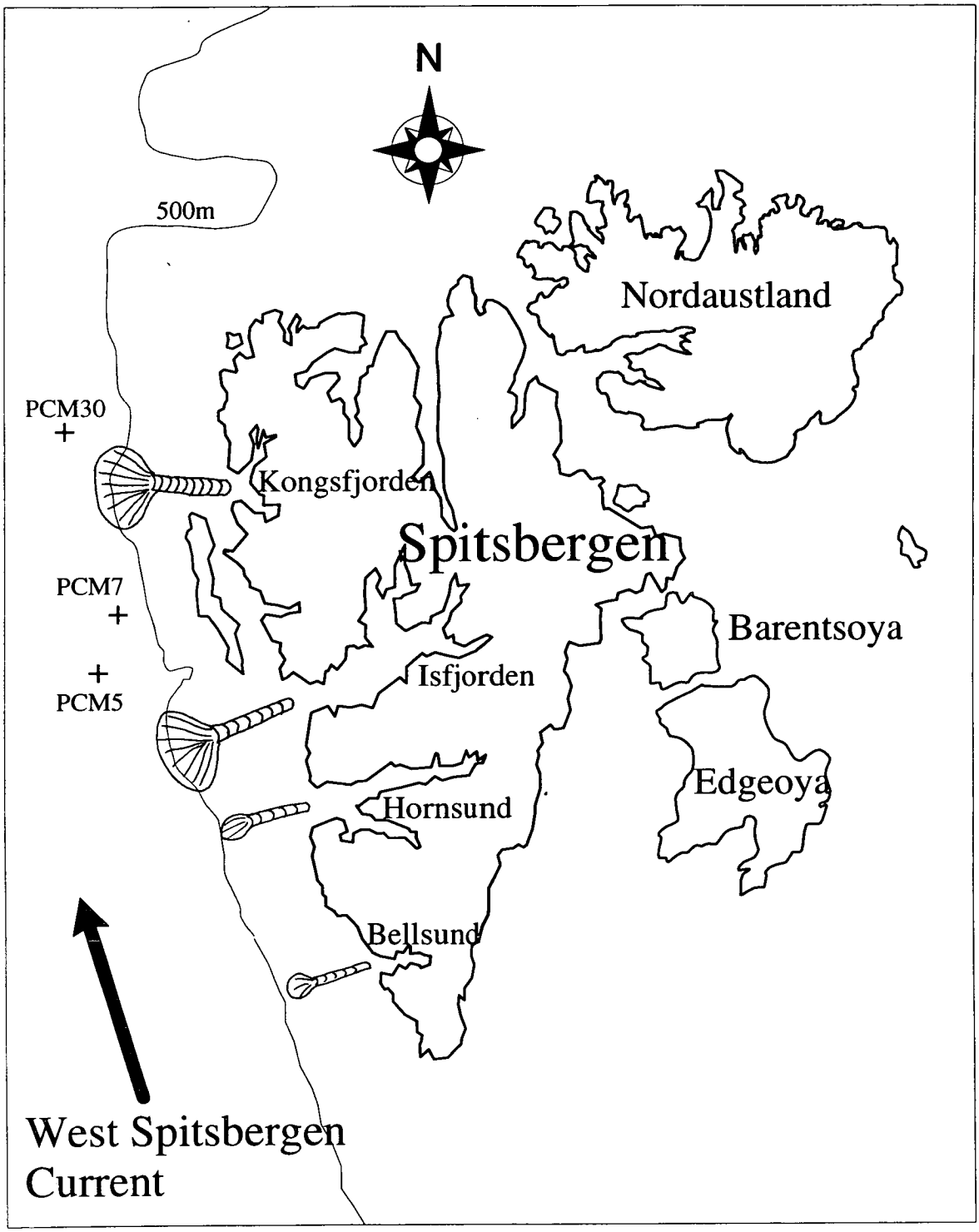

Fig. 1.1. Location map of the Svalbard Archipelago showing the location of the cores sampled in this study. The main outlet fjords of the western Spitsbergen margin are labelled, and the major trough and sediment fan complexs from this area are shown.

Trough;  Fan; 

Records from the terrestrial environment have been used to reconstruct the size and movement of continental ice sheets also. These records tend to be discontinuous, and relatively short compared to marine records. The advance of the most recent glaciation often destroys the evidence of previous advances. The results, however, give a far more detailed picture of the history of ice sheet growth and decay compared to deep marine records. The material used in this study lies half way between the two extremes of long, uninterrupted deep marine records of poor resolution on the one hand, and short, fragmented but very detailed terrestrial records on the other. Sediments at the shelf edge and upper slope should provide a link between the land and ocean records, producing relatively complete and high resolution records over moderately long timescales.

1.2. Study objectives

The objectives of this study can be split into two main groups: 1) Those which focus on the relative size and activity of the local Spitsbergen ice mass; 2) Those which focus on the palaeoceanographic changes over the last 200 ka. A time frame for this study is produced using an oxygen isotope chronology based on measurements from planktic and benthic foraminifera (outlined in chapter 2). The oxygen isotope curves, produced in this study, are compared to a composite isotope record produced by Duplessy *et al.* (1988) from the Norwegian Sea, which has been accurately dated, to produce an age model. This has been refined by further correlation with accurately dated oxygen isotope records from the Norwegian Sea, of which one (Sarnthein *et al.*, 1992) was dated by radiocarbon methods. Radiocarbon dates have not yet been produced for the cores of this study at the time of writing unfortunately. Cores from this study record sedimentation over the last 200 ka, covering the last seven oxygen isotope stages as defined by Emiliani (1955).

One objective was to try to identify and characterise periods during which ice rafted detritus (IRD) was produced by the Svalbard ice mass. From this it was hoped to recognise the factors affecting ice rafting, and to produce a model explaining the production of IRD from the Spitsbergen continental margin, which could be applicable to other high latitude glaciated continental margins. In recent years ice rafted events, termed Heinrich Events, have been recognised throughout the North Atlantic (Heinrich, 1988; Bond et al., 1992; Broecker *et al.*, 1992 Andrews and Tedesco, 1992 and Grousset *et al.*, 1993). It has been postulated that these events were produced by internal oscillations of the Laurentide ice sheet during deglaciation,

leading to rapid ice calving (Oerlemans, 1993). The possibility that Heinrich events in the North Atlantic could be recognised in the IRD events seen in the Greenland Sea is investigated. The IRD chronology relating to ice sheet movement is also compared to the glacial chronology of Spitsbergen from terrestrial data (Boulton *et al.*, 1982; Miller *et al.*, 1989; Mangerud and Svendsen, 1990; Mangerud *et al.*, 1992 and Svendsen *et al.*, 1992). In this way an attempt is made to produce a link between the marine record and the terrestrial record.

The palaeoceanographic objectives of this project involved an effort to improve our understanding of the processes of palaeoceanographic change over glacial-interglacial cycles in the Fram Strait. An attempt is made to reconstruct ocean circulation during glacial and interglacial periods, and to document associated productivity changes. Stable oxygen and carbon isotope measurements on planktic and benthic foraminifera are used for palaeoceanographic interpretations, along with foraminiferal faunal analysis. The timing and intensity of influx of North Atlantic surface waters to the Fram Strait-Spitsbergen margin is assessed from planktic foraminiferal assemblage changes, and planktic oxygen isotope methods. The initiation of deep water circulation during the transition from a glacial to an interglacial period is investigated using oxygen and carbon isotope analyses, and changes in foraminiferal planktic and benthic fauna. The changes in deep water circulation in the Greenland Sea have very important implications for global ocean circulation and heat transfer. The Greenland Sea during the present day is a major area of production of deep water, which, on flowing south, forms a major proportion of North Atlantic Deep Water (NADW). This flows into the North Atlantic and down the length of the Atlantic Ocean having an important influence on the global circulation system. The present day circulation system of the Greenland Sea is outlined in more detail below. During glacial periods the production of NADW is prevented in the Greenland Sea by the presence of sea ice and the absence of North Atlantic surface water in the area (which cools and sinks to form deep water). This reduces the intensity of global circulation reducing the redistribution of heat from low to high latitudes, encouraging glacial growth at mid-high latitudes. It is, therefore, of great interest to understand the timing and intensity of deep water circulation in such a high latitude area. The palaeocirculation is investigated in most detail over the last glacial-interglacial transition because of the greater resolution over this period. An attempt is then made to reconstruct the palaeoceanography of the previous glacial-interglacial transition from oxygen isotope stage 6 to stage 5. The oceanography of the Greenland Sea is poorly understood for this period, which is due to the lack of records studied for this time period and the low resolution of those that are available.

1.2.1.List of objectives

1. The IRD supply to the continental margin of Spitsbergen is characterised from clast counts and particle size analysis of marine cores PCM5, PCM7 and PCM30.
2. A model is produced to explain the variations in IRD supply to the Spitsbergen margin in terms of the relative size of its ice mass, moisture supply, timing and rate of ice movement.
3. A comparison is made between the estimations of the size and nature of the Spitsbergen ice mass from data from the marine cores with the terrestrial information of ice advances. We are also trying to produce a link between the marine and terrestrial records.
4. An accurate reconstruction of the meltwater history of the Fram Strait over the last deglaciation from oxygen isotope analysis of planktic foraminifera of core PCM7 is made. The influence of meltwater on benthic foraminifera is also estimated.
5. The productivity of surface waters is investigated using planktic and benthic foraminiferal abundance counts. Comparisons are made between the productivity of glacial and interglacial periods.
6. The timing and intensity of influx of North Atlantic surface waters into the Fram Strait after the last glacial period is assessed from planktic foraminiferal faunal changes, and planktic foraminiferal oxygen isotope evidence.
7. Changes in the benthic foraminiferal assemblage and stable oxygen and carbon isotope signature are used to assess the timing of renewed deep water circulation. The importance of North Atlantic water inflow on the deep water circulation system is investigated.
8. An attempt is made to reconstruct the palaeoceanography of stage 5, a period about which relatively little is known in terms of palaeoceanography and ice advance compared to stage 1.
9. The palaeoceanographic history of the Fram Strait over the last 200 ka is compared to other records from the Nowegian-Greenland Sea, the Summit ice core and the solar insolation record for 80°N to put the Fram Strait records in a global context.

1.3. Present day ocean circulation

The present oceanography of the area will now be outlined in more detail. The surface circulation system is summarised in fig. 1.2. There are three main surface water masses affecting the Greenland Sea (Swift and Aagaard, 1981). The North Atlantic Current flows up the eastern side of the basin where it forms the Norwegian

Atlantic Current and West Spitsbergen Current. This is a relatively warm high salinity current originating from the North Atlantic and supports a subpolar foraminiferal fauna. Polar surface water flows to the south from the Arctic Ocean. This forms the East Greenland Current flowing along the eastern Greenland margin, and is a cold low salinity water mass supporting a polar foraminiferal fauna. The third surface water mass in this area lies between the former two, and is termed Arctic water (Helland-Hansen and Nansen, 1909). This is a mixture of warm saline North Atlantic water and cold fresher Polar water. It forms an anticlockwise circulating gyre in the central Greenland Sea. It is bounded to the west by the Polar front and to the east by the Arctic front.

At the present time the Greenland-Norwegian Sea is one of the main areas of formation of North Atlantic Deep Water (NADW) (Mantyla and Reid, 1983; Aagaard *et al.*, 1985). The present day deep water circulation system is summarised in fig. 1.3 (adapted from Aagaard *et al.*, 1985). The warm, highly saline North Atlantic surface waters of the West Spitsbergen Current mix with the cold, low salinity Polar waters forming Arctic waters in the central Greenland Sea. This new water mass has a temperature-salinity composition between that of the two parent water masses. It is cold and moderately saline and, after further cooling, forms a dense surface water mass, which sinks to form Arctic Intermediate Water (AIW) (Swift and Aagaard, 1981). This can be split into two water masses, the upper and lower AIW. Below the AIW Greenland Sea Deep Water (GSDW) is found, very cold and dense and therefore stable (Carmack and Aagaard, 1973; Swift and Aagaard, 1981 and Quadfasel and Meincke, 1987). GSDW is formed from dense waters cooling on the continental shelves, which sink, and mix with the lower AIW. The upper AIW flows to the south into the Iceland Sea, across the Jan Mayen Fracture Zone, where a similar intermediate water mass forms. This upper AIW constitutes a major proportion of overflow of dense water into the North Atlantic through the Denmark Strait forming NADW (Swift and Aagaard, 1981). The southerly flow of AIW is produced by the northerly flow of surface waters, cooling and subsequent sinking producing a conveyor belt circulation (a term initiated by Broecker, 1982). During glacial periods the global circulation system is more sluggish. The northward flow of North Atlantic water is much reduced, not entering the Norwegian-Greenland Sea. A stable water stratification system is produced in the Greenland Sea causing stagnation. As mentioned above, this reduces the transport of heat from low latitudes to high latitudes, leading to intensification of glacial growth at mid-high latitudes. It is the renewal of this deep water circulation system that can have such a major impact on the global climate.

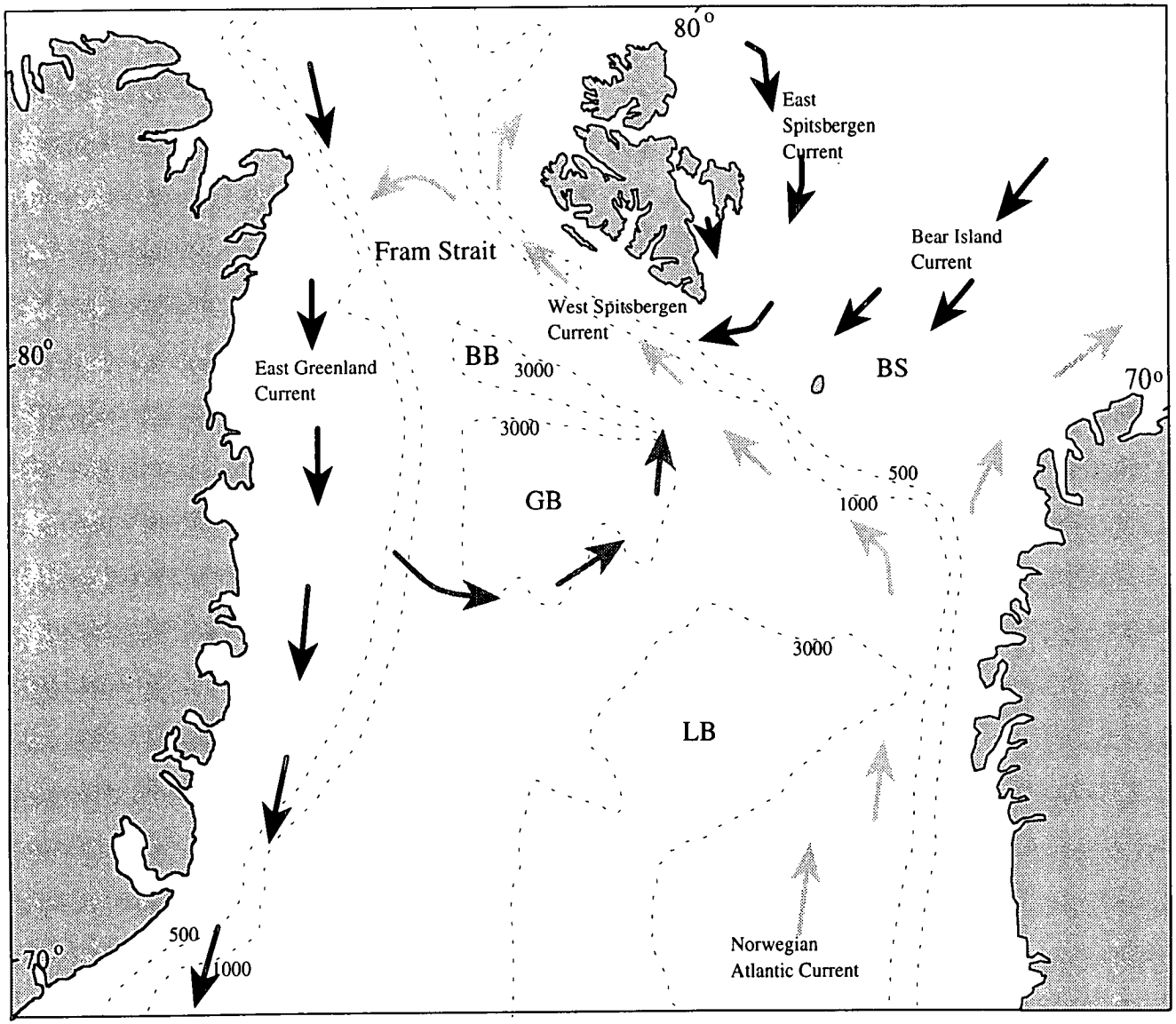

Fig. 1.2. Map of Greenland Sea showing surface current circulation of the present day.

Warm currents, light shading;
Norwegian Atlantic Current
West Spitsbergen Current

Cold currents, dark shading;
East Greenland Current
East Spitsbergen Current
Bear Island Current

BB - Boreas Basin
GB - Greenland Basin
LB - Lofoten Basin
BS - Barents Shelf

Broecker *et al.* (1988) suggested that salinity changes could induce major circulation changes, in turn causing significant ice mass fluctuations. The influx of large amounts of low salinity meltwater can produce a low density lid preventing the sinking of surface waters, and thus, preventing the formation of deep water and reducing the intensity of circulation. A more sluggish global circulation system reduces the flow of warm currents to the high latitudes. This reduces the heat flux from tropics to poles allowing the poles to get colder, promoting ice growth. Therefore, the palaeoceanographic history of the Greenland Sea has important implications for global ice fluctuations.

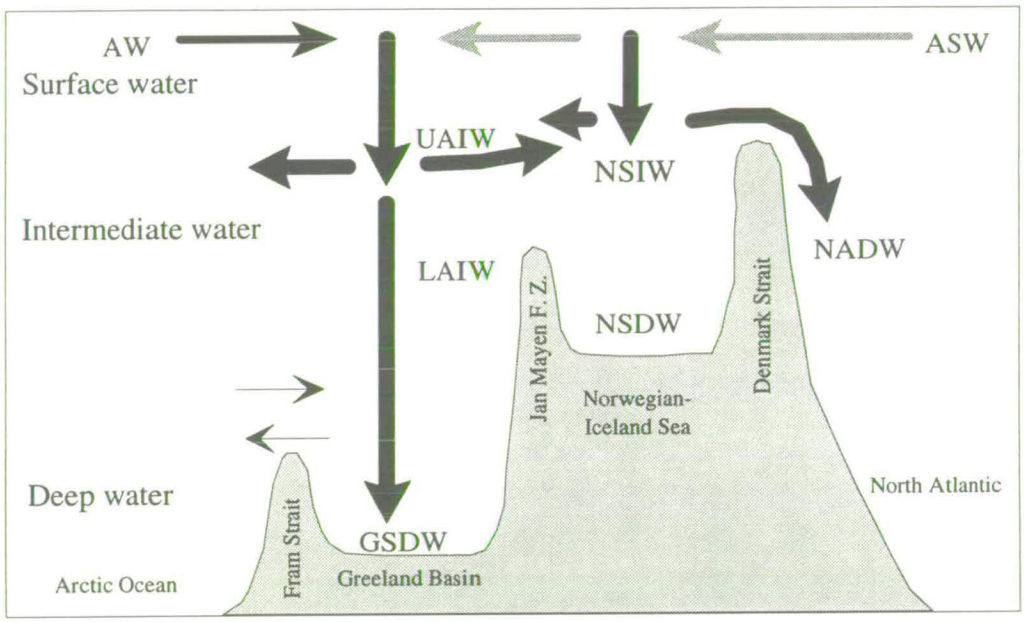

Fig. 1.3. Schematic representation of the deep water formation in the Greenland-Norwegian-Iceland Seas. AW-Arctic Water; ASW-Atlantic Surface Water; UAIW-Upper Arctic Intermediate Water; LAIW-Lower Arctic Intermediate Water; NSIW-Norwegian Sea Intermediate Water; GSDW-Greenland Sea Deep Water; NSDW-Norwegian Sea Deep Water; NADW-North Atlantic Deep Water.

The sample preparation and analytical techniques used in this study are described in detail in Appendix 1. The cores themselves consist predominantly of a blue-grey coloured mud, which is fairly homogenous, and quite often silty. In places small stones are visible within the mud, these show up very clearly in the x-ray photographs (plate 4, p. 88) and are described in detail in chapter 3. The sedimentology of the cores is dealt with in more detail in chapter 3 also. All the data tables are contained in Appendix 3. A list of the foraminifera identified from cores PCM7 and PCM5 is contained in Appendix 2.

Chapter 2. Chronostratigraphy using oxygen isotope stratigraphy and magnetic susceptibility

2.1. Introduction

To make meaningful interpretations of Fram Strait paleoceanography and the history of Spitsbergen ice rafting from the piston cores examined in this study, it is first necessary to produce a chronostratigraphic framework from these cores. One of the most commonly used methods to construct an age model in deep sea records involves the use of oxygen isotope stratigraphy. In this study oxygen isotope stratigraphy was used to produce an age model as accurately as possible, but was additionally refined using a magnetic susceptibility stratigraphy. This is particularly helpful in those sections of the record where no foraminifers are available for oxygen isotope stratigraphy, and is useful to determine interstadials especially in stage 5. A brief explanation of the theory behind these techniques will follow.

The theory of oxygen isotope stratigraphy is based on the variation in abundance of two isotopes of the oxygen atom, ^{16}O and ^{18}O, in the global hydrological system. The oxygen isotopic composition of the global oceans is dominantly controlled by low latitude evaporation and high latitude precipitation. Evaporation from low latitude oceans preferentially removes the lighter oxygen isotope, ^{16}O. Storm tracts moving to higher latitudes preferentially loose the heavy oxygen isotope, ^{18}O, during precipitation. This causes polar ice sheets to become enriched in the light oxygen isotope, ^{16}O, when compared to the average composition of ocean water. The isotopic composition is measured, and expressed as a ratio of $^{18}O/^{16}O$, then compared to a standard value known as PDB. The PDB standard was obtained from carbonate from the belemnite *Belemnitella americana* from the Upper Cretaceous Peedee formation from South Carolina (Epstein and Urey, 1951). It is then expressed as the deviation of ^{18}O in parts per thousand, ‰, from this standard value. For example a $\delta^{18}O$ value of 2.5‰ indicates the sample measured has 2.5 parts per thousand more ^{18}O atoms than the standard to which it is compared. The enrichment of polar ice sheets in ^{16}O means that during glacial periods, when these ice sheets were much larger, the oceans were more highly enriched in ^{18}O compared to interglacial times.

This concept was first realised by Emiliani (1955), who used the $^{18}O/^{16}O$ ratio in carbonate of foraminifera in marine cores to deduce glacial and interglacial periods during the Quaternary. Foraminifera are marine organisms that precipitate calcareous

shells from marine water. The oxygen isotopic composition of the marine water at the time when they lived is incorporated into their shells. Foraminifera precipitate their shells in approximate isotopic equilibrium with the surrounding water, although factors such as water temperature, and species vital effects may distort the isotopic signature. These are summarised in Patience and Kroon (1991). On death the foraminifera settle to the ocean floor and are buried, accumulating over time, and thus provide a record over time of glacial/interglacial variations.

It is the global synchroneity of oxygen isotopic variation in ocean water, and therefore foraminifera, that allows correlation between records from different geographical areas. Emiliani (1955) established the first oxygen isotope stratigraphy for the Quaternary from foraminiferal tests sampled from a low latitude marine core. He divided the isotope record up into stages. Periods with low $\delta^{18}O$ values were assigned odd stage numbers, these are the interglacial periods, and periods with high $\delta^{18}O$ values were assigned even numbers, the glacial periods. The numbering system starts with the present interglacial as stage 1, and continues back through the glacial/interglacial cycles. This has been adopted as the standard oxygen isotopic nomenclature, and is used in this study.

Foraminiferal oxygen isotopic records have been produced from many cores throughout the global oceans. Imbrie *et al.* (1984) took the oxygen isotopic records from five high resolution cores from low latitudes and combined them, stacked them, to produce a standard global isotope record known as the SPECMAP record. This record was accurately dated, and is often correlated to new isotope records to produce an age model for an otherwise undated core. In this study we have correlated the oxygen isotopic records from our piston cores to a composite isotope record produced by Duplessy *et al.* (1988). This composite record was produced by stacking the isotope records of five cores taken from the Norwegian Sea. The age model for this composite was obtained by correlation with the SPECMAP record. Our age model has been refined in the upper section by correlation with two acccurately radiocarbon dated records from the Norwegian/Greenland Sea, core M 23259 and M 23071 from Sarnthein *et al.* (1992), and by using magnetic susceptibility stratigraphy.

The magnetic susceptibility of sediments is primarily determined by their content of magnetic minerals, but also by the grain-size and composition of magnetic material present. Several studies have used the variation in magnetic susceptibility as a stratigraphic tool in marine records, for example Hounslow (1990) and Bloemendal (1989). Magnetic susceptibility has also been used for stratigraphic correlation with

deep-sea oxygen isotope records, for example the susceptibility records from Chinese loess and paleosol deposits (Maher and Thompson, 1991). Lake sediment stratigraphy is also commonly deduced from magnetic susceptibility records, Thompson *et al.* (1975) and Snowball and Thompson (1990). In the present study correlation between magnetic susceptibility and the oxygen isotope stratigraphy, and correlation between cores using magnetic susceptibility, has been used to refine the age model during periods of lower resolution in oxygen isotope stratigraphy.

For all cores the isotope stratigraphy was deduced from measurements of the oxygen isotopic ratio in the skeletons of the planktic foraminifer *Neogloboquadrina pachyderma* (sinistral) (Ehrenberg). In the following section the isotope curves themselves will be described, interpretation will be presented after.

2.2. Description of the $\delta^{18}O$ records from the Spitsbergen margin

2.2.1. PCM5

The oxygen isotopic record for PCM5 is shown in fig. 2.1. The $\delta^{18}O$ value in the highest portion of the core at 2cm depth is relatively light compared to the rest of the record, 3.2 ‰, then a flat plateau with values of 4‰ occurs down to 125cm. Below this point the record shows a period of heavy $\delta^{18}O$ values, between 4.5 and 4.8‰ down to 200cm, followed by lighter values (3.8 to 4.2‰) until a depth of 295cm. From here to 445cm the amplitude and frequency of isotopic variation increases. Two light spikes, the first with a $\delta^{18}O$ value of 3‰ between 300 and 312cm, and the second being 1.5 - 2.0‰ from 325 to 340cm, are separated by a heavier peak characterised by $\delta^{18}O$ values of 3.8 - 4‰. After the second light spike a more prolonged heavy episode between 345 and 385cm, with $\delta^{18}O$ values ranging from 3.8 to 4.5‰, is recorded. This is followed by a generally lighter section until 415cm with $\delta^{18}O$ values of 3.5 to 4‰. A $\delta^{18}O$ maximum at 445cm gives way to a plateau of relatively heavy values, heavier than 4.2‰, down to the base of the core at 685cm.

2.2.2. PCM30

The top of core PCM30, shown in fig. 2.1, is characterised by a sharp fall towards heavier $\delta^{18}O$ values, from 3‰ to values generally greater than 4.5‰ from 37 to 182cm.

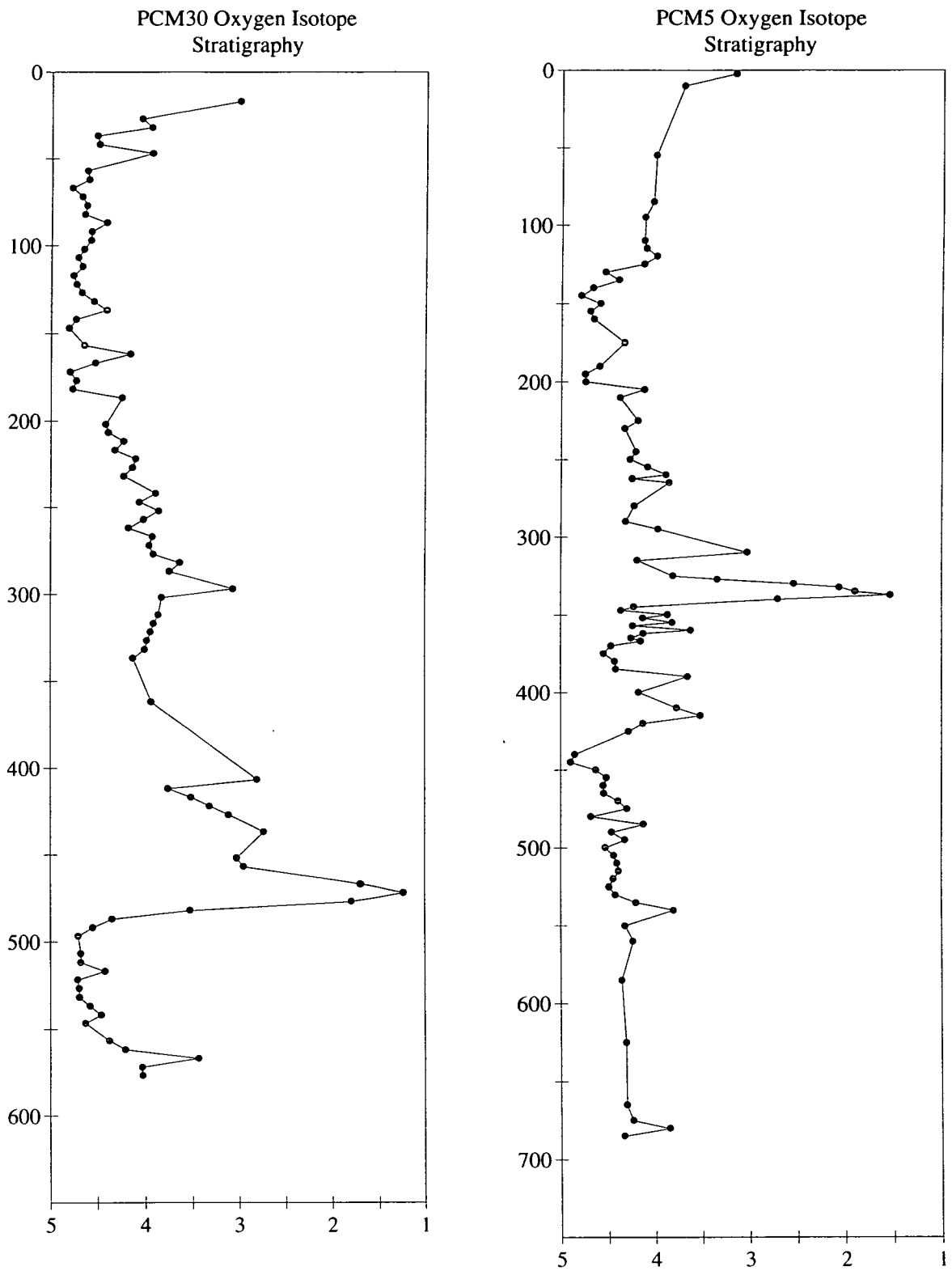

Fig. 2.1. Oxygen isotope stratigraphy for PCM30 and PCM5, plotted against depth in cm, oxygen isotope measurements are per mil w.r.t. PDB standard.

An overall trend towards lighter $\delta^{18}O$ values follows, culminating in a spike with a $\delta^{18}O$ value of 3‰ at 297cm. Oxygen isotopic values increase slightly to 3.9 - 4.1‰ between 302 and 362cm, unfortunately followed by a gap in the isotope record due to lack of foraminifera in the samples. However, at 407cm a light spike of 2.8‰ was found. The slight fall of 1‰ is followed by a sharp rise in $\delta^{18}O$ values to a relatively heavy peak with a value of 3.7‰ at 412cm. From here depletion in $\delta^{18}O$ occurs only interrupted by a short step in the record at 460cm before a continuation in the lightening trend culminates in $\delta^{18}O$ values of 1.2 - 1.7‰ at 472cm. These are the lightest values in the core. A dramatic increase in $\delta^{18}O$ values occurs, which are the heaviest found in the core, 4.7‰ at 497cm. The $\delta^{18}O$ values remain greater than 4.5‰ until 547cm, where a slight decrease to values to about 4‰ down to 577cm is found. The last 50cm of the core are barren of foraminifera and therefore no isotope stratigraphy is possible.

2.2.3. PCM7

The isotope record for PCM7 is shown in fig. 2.2. The upper part of the record is produced from the trip core, which is presented above the main core record. The trip core $\delta^{18}O$ record shows a general trend towards heavier values, starting at 2.5‰ and reaching a value of 3.4‰ at its base of 100cm. The top of the main core exhibits relatively light $\delta^{18}O$ values of 2.6 - 2.9‰ down to 25cm, followed by a section with increasing values culminating in a maximum $\delta^{18}O$ value of 4‰ at 65cm. Below the maximum, values decrease rapidly to a distinct plateau with $\delta^{18}O$ values of 2.6 - 3.2‰. A rapid $\delta^{18}O$ increase just below 125cm gives way to values between 3.8 and 4‰ from 135 to 245cm, which was interrupted by a distinct light isotope excursion at 175cm, culminating in $\delta^{18}O$ values of 3.6‰. The heaviest $\delta^{18}O$ value of 4.7‰ was measured at 265cm, values remain just above 4.2‰ until 330cm. The lower part of the core is characterised by smaller amplitude variations in $\delta^{18}O$ with values between 3.6 and 4.2 ‰. Sections with heavier $\delta^{18}O$ values occur at 410 - 460cm, 515 - 525cm, and 660 - 727cm.

2.2.4. PCM56

The oxygen isotope record of PCM56 shows smaller $\delta^{18}O$ amplitude variations compared to the other cores, see fig. 2.2. At the top of the core $\delta^{18}O$ values are relatively light at 3.7‰ until 25cm, where a rise occurs followed by a plateau characterised by $\delta^{18}O$ values of around 4.1‰ which stretches to 330cm.

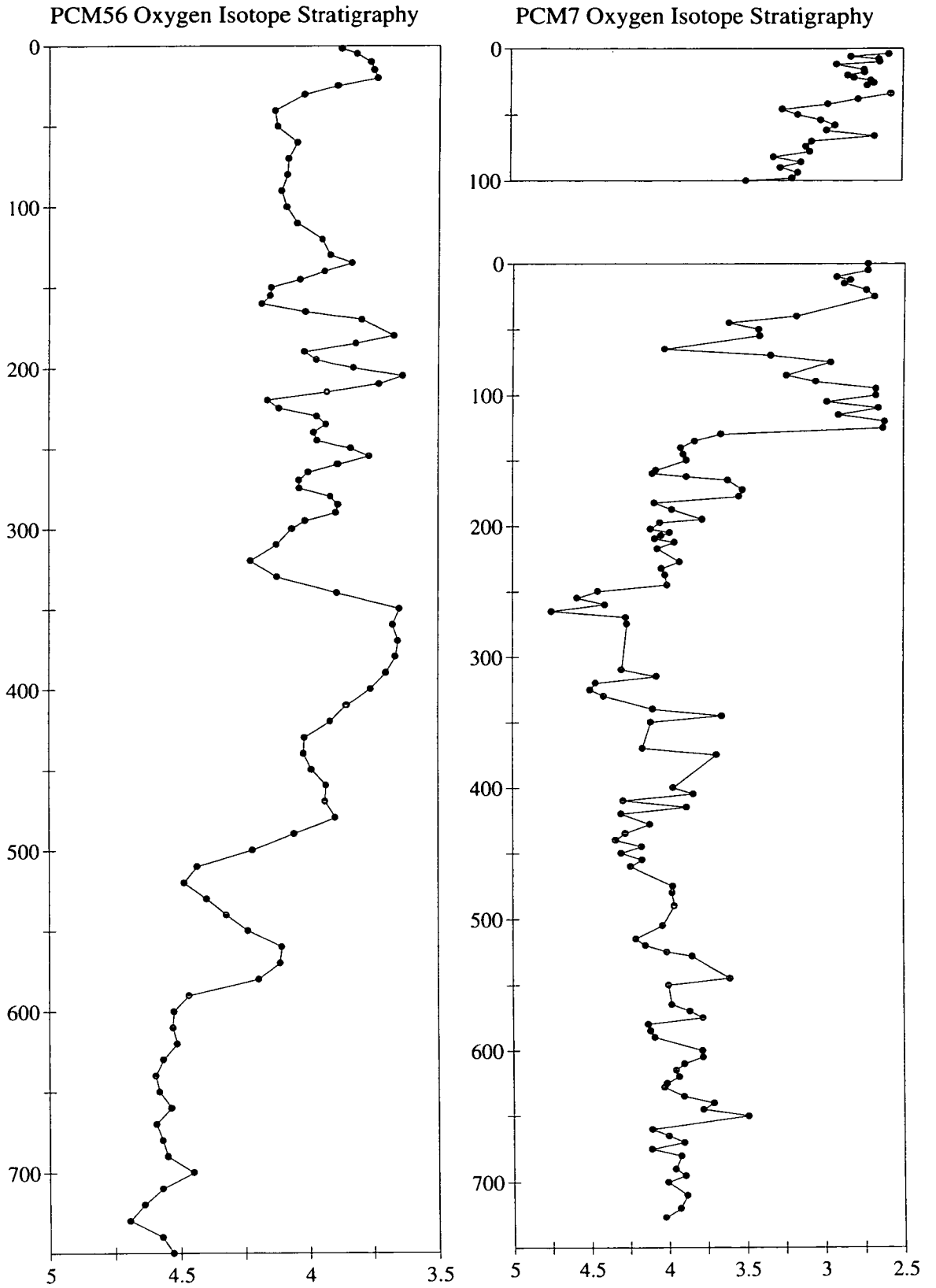

Fig. 2.2. Oxygen isotope stratigraphy for PCM56 and PCM7, plotted against depth in cm, isotope measurements are per mil relative to PDB standard.

Within this period there are several short duration light $\delta^{18}O$ spikes with values of roughly 3.6‰, notably at 140cm, 170cm, 210cm, and 255cm. There is a sharp drop in $\delta^{18}O$ values at 340cm, with values ranging from 3.5 to 3.7‰ until 410cm. Below this point, there is an increase in $\delta^{18}O$ with values around 4‰ until 490cm. From there, $\delta^{18}O$ values increase sharply to higher values of, 4.3 to 4.5‰, up to 530cm. A sharp light is recorded at 575cm with $\delta^{18}O$ values of 3.8‰ before heavy values resume at 580cm down to the base of the core.

2.3. Oxygen isotope chronostratigraphy

To obtain an initial oxygen isotope chronostratigraphy a comparison was made to the stacked record of the Norwegian Sea produced by Duplessy *et al.* (1988). This curve is a stacked benthic record of oxygen isotopic variation produced from benthic foraminifera from five cores from the Norwegian Sea. Although the actual values are not necessarily the same as the values in the Fram Strait cores, the overall shape of the curves are similar and major stage boundaries and events can be recognised. In all $\delta^{18}O$ records the glacial stages 2 and 6 were visually recognised, see figs. 2.3 and 2.5. However, it was not easy to make further reliable subdivisions, the recognition of warm periods appeared to be difficult particularly within stage 5. This is caused by a complex history of meltwater input into the Fram Strait leading to a reduction in foraminiferal abundances (see Paleoceanography chapter). These subdivisions were found, however, by using core to core correlations with magnetic susceptibility, as discussed later in this chapter.

To obtain a more detailed age model for the top section of PCM7 correlation has been made with two cores from the Norwegian/Greenland Sea, M 23259 and M 23071, from Sarnthein *et al.* (1992), the position of these cores is shown in fig. 4.5, and details of the cores are reproduced in table 4.1. These two cores have been accurately radiocarbon dated, and are shown along with PCM7 and PCM56 in fig. 2.4.

Actual ages for stage boundaries in this study were calculated by correlation with the cores mentioned above, the position of the boundary was placed at the midpoint between sections of rapid changes in $\delta^{18}O$ values from high to low, or vice versa, in the approximate areas of stage boundaries. Further tie points have been made between the cores in this study and the composite record of Duplessy *et al.* (1988) and cores M 23259 and M23071; these tie points are shown in table 2.1.

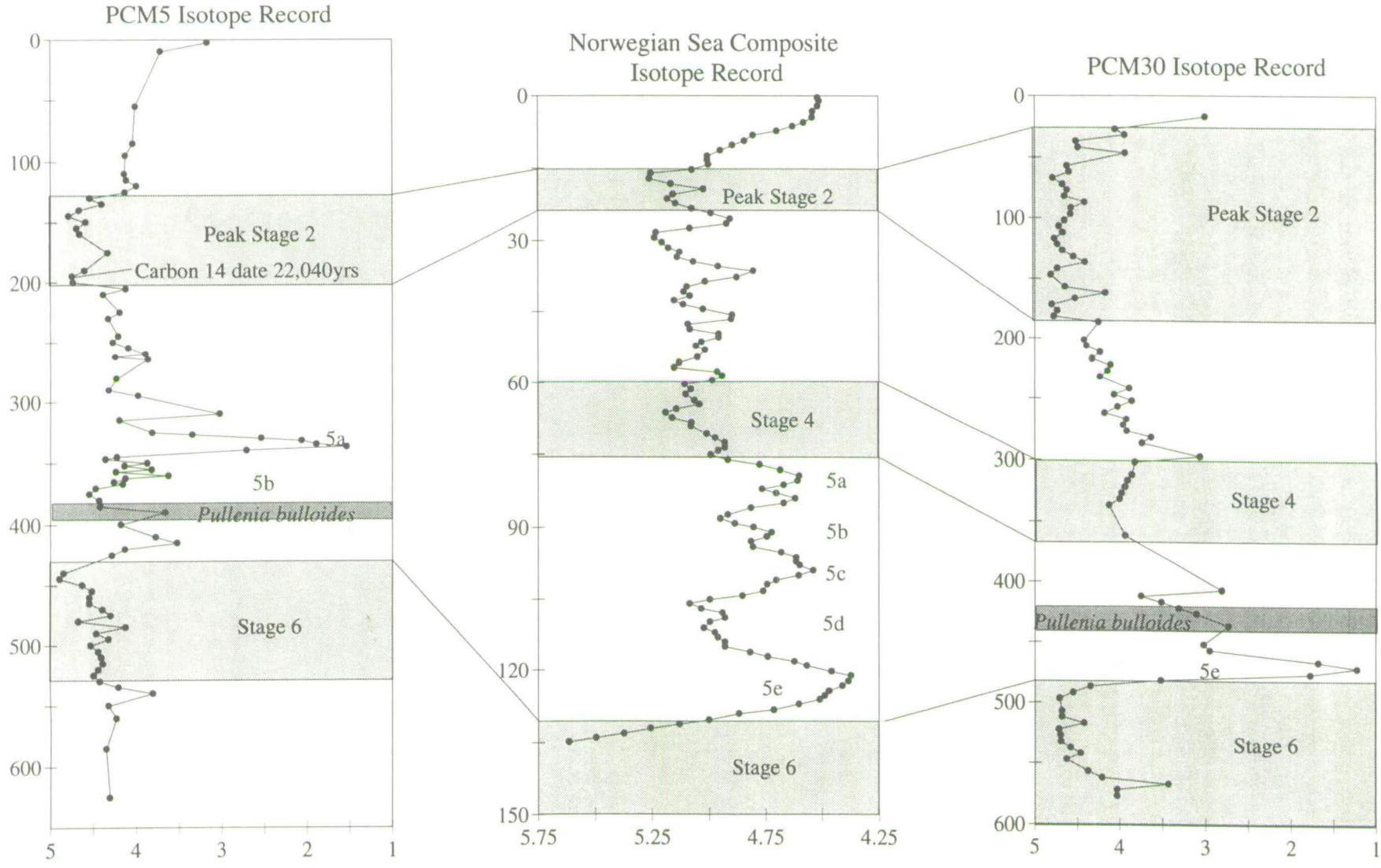

Fig. 2.3. Correlation of oxygen isotope stratigraphy from PCM5 and PCM30 with stacked benthic record of Duplessy et al (1988). PCM5 and PCM30 plotted against depth, stacked record plotted against time, isotope measurements per mil w.r.t. PDB.

Tie Points	PCM5 depth	PCM30 depth	PCM7 depth	PCM7 trip core
From M 23259 and M 23071				
9kyrs				**28cm**
10.6			**45cm**	
11.92			**65**	
12.3			**120**	
13.11			**150**	
13.6			**172.5**	
12.84	10cm		**140**	
^{14}C Date 22.04	**195**	**177cm**	**325**	
From stacked				
benthic curve				
16k yrs	**145**	**117**	**265**	
25			**345**	
36			**375**	
45			**475**	
50			**545**	
59	**265**	**297**	**605**	
64			**650**	
65		**337**		
75	325	**362**		
80	332.5	**372**		
84	**337.5**	**377**		
89	350			
93	375	412		
95	390	437		
100		442		
102	400			
107	405			
110	407.5	452		
117	410			
121		**472**		
126	437.5			
136	**445**	**497**		
140	**480**	567		
Stage boundary tie points				
Stage 1-2 (12.5 ka)	**0cm**		**130cm**	
Stage 2-3 (25ka)	**200cm**	**192cm**	**345cm**	
Stage 3-4 (59ka)	**265cm**	**297cm**	**605cm**	
Stage 4-5 (71ka)	**312.5cm**	**352cm**		
Stage 5-6 (134ka)	**440cm**	**487cm**		

Table 1. Table listing tie points used in compilation of age model for cores in this study. Based on correlation with cores M23071 and M23259 (Sarnthein et al., 1993) and stacked benthic composite curve from the Norwegian Sea, (Duplessy , 1988). Depth values in bold type are tie points made by correlation with oxygen isotope stratigraphy only, the other values in the table represent tie points achieved by core to core correlation using magnetic susceptibility, and correlation between susceptibility and oxygen isotope stratigraphy.

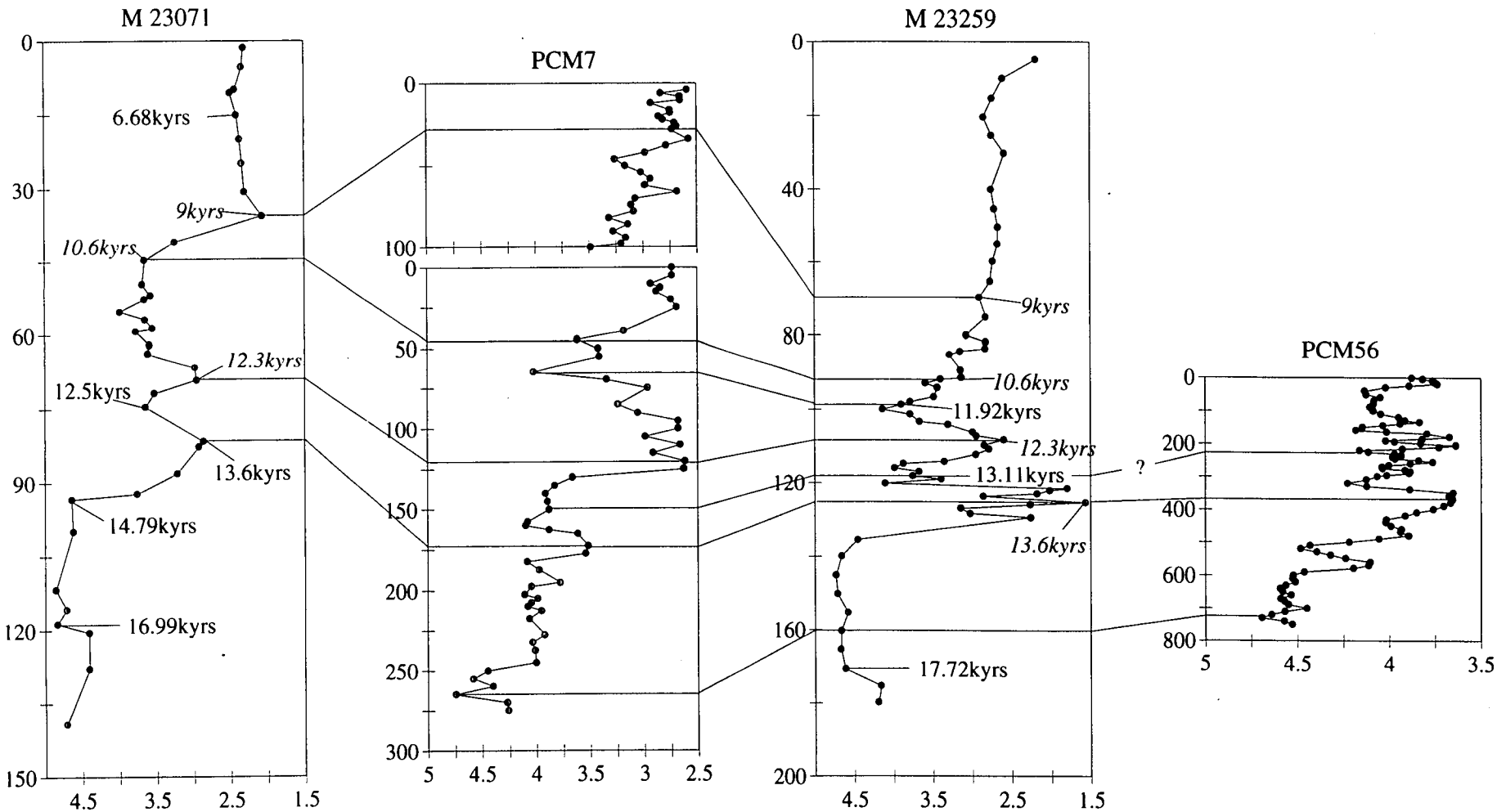

Fig. 2.4. Correlation between oxygen isotope stratigraphies of cores PCM7 and PCM56 of this study with cores M 23071 and M 23259 from Sarnthein et al. (1993). All cores plotted against depth, the ages in normal text on M 23071 and M 23259 are radiocarbon determinations, the ages in italics are time slice interpretations from Sarnthein et al. (1993). These points have been correlated to PCM7 and PCM56 to determine the age model for these cores. All isotope measurements are the per mil variation from PDB standard.

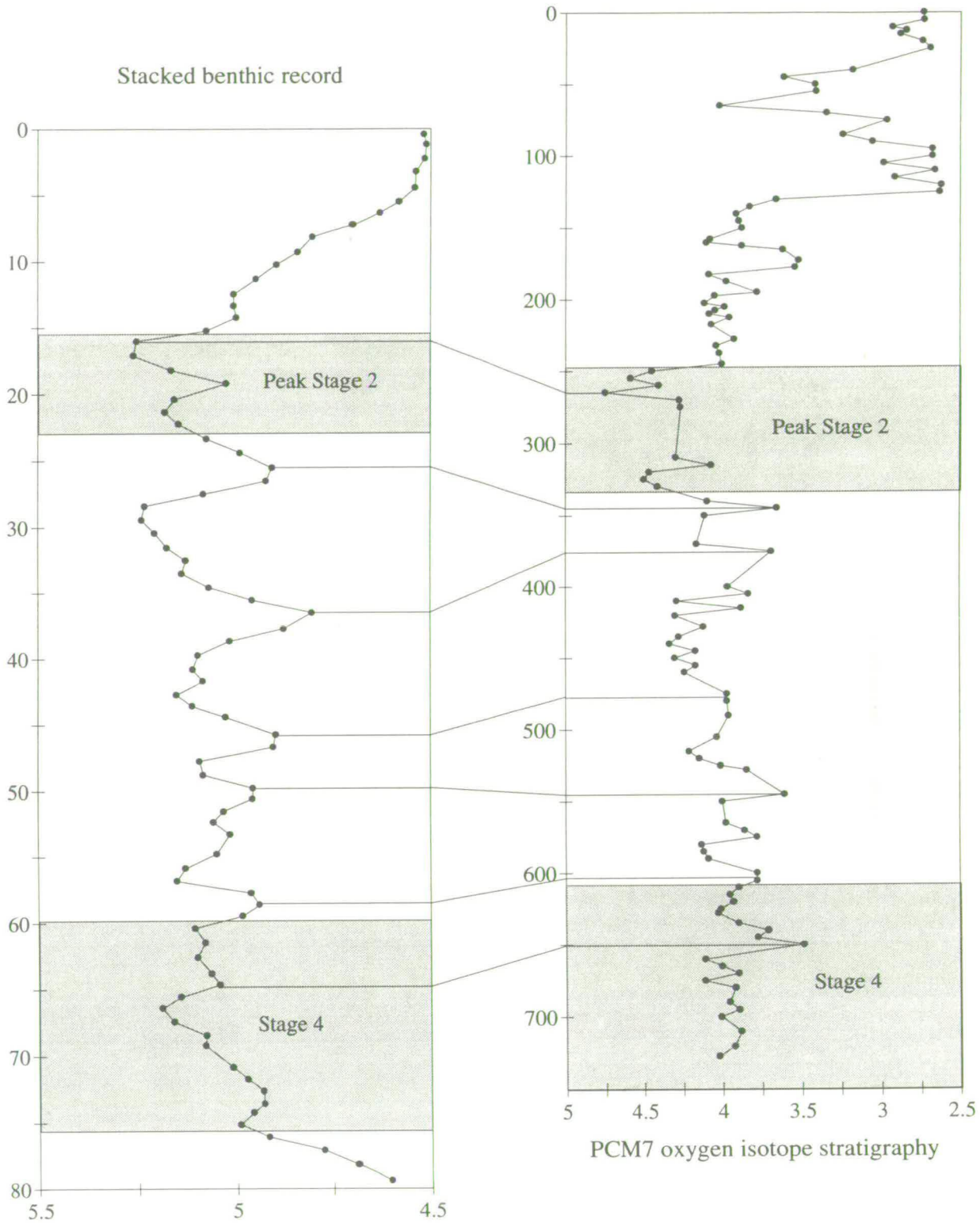

Fig. 2.5. Correlation between oxygen isotope record of PCM7 and stacked benthic oxygen isotope record from Duplessy et al (1988). PCM7 plotted against depth, the stacked record against time. Isotope scale expressed as per mil w.r.t. PDB.

In table 2.1 the tie points that are marked in bold are those that were made purely on the basis of oxygen isotope correlations. The age model was refined by adding the remaining tie points by core to core correlation on the basis of magnetic susceptibility, and correlation between susceptibility and isotope stratigraphy.

2.3.1. PCM5 and PCM30

The two planktic isotope curves of PCM5 and PCM30 show a remarkable similarity, seen in fig. 2.1 both plotted against depth. These two cores are correlated with the Norwegian Sea composite record in fig. 2.3. One radiocarbon date has been measured on PCM5 at a depth of 195cm, this gave an age of 22,040 +- 320 years (a reservoir correction of 400 years has been subtracted). This section is heavy in $\delta^{18}O$ values, thus has been interpreted as oxygen isotope stage 2 (the last glaciation). The boundaries of stage 2 and its subsequent ages were found by correlation with the stacked record, and by placing the boundaries at the midpoints of the sections of rapid change from high to low values (of vice versa) as mentioned above. The step at 130cm in PCM5 corresponds to an early phase of deglaciation, a second trend to lighter oxygen isotope values at the core top represents the transition to the Alleröd (beginning of isotope stage 1). This is supported by the correlation with PCM7 based on magnetic susceptibility. Fig. 2.6 shows the top of PCM5 correlating with 135cm in PCM7, where the major decrease in $\delta^{18}O$ values occurs. This transition is dated here using coiling directions of the foraminifer *N. pachyderma* (see below). In PCM30 the initial deglaciation step seen in PCM5 at 130cm occurs at 37cm, and stage 2 continues down to 182cm, this correlation agrees with the susceptibility correlation shown in fig. 2.6.

The major step from stage 2 to stage 3 in PCM5 and PCM30 can be found by correlation with the composite record. Both cores exhibit a clear stage 3 record showing increasingly lower oxygen isotopic values, culminating in a light spike of roughly 3.8‰ at 265cm in PCM5, and 3‰ at 297cm in PCM30. Stage 4 is clearly represented in PCM30 between 302-362cm, this can be correlated with the slightly heavier peak in composition of stage 4 in the composite curve. Stage 4 can then be identified in PCM5 by using the magnetic susceptibility correlation (outlined below). From this correlation stage 4 in PCM5 is represented by the higher $\delta^{18}O$ values between 280-325cm, but also contains a light isotope spike at 310cm.

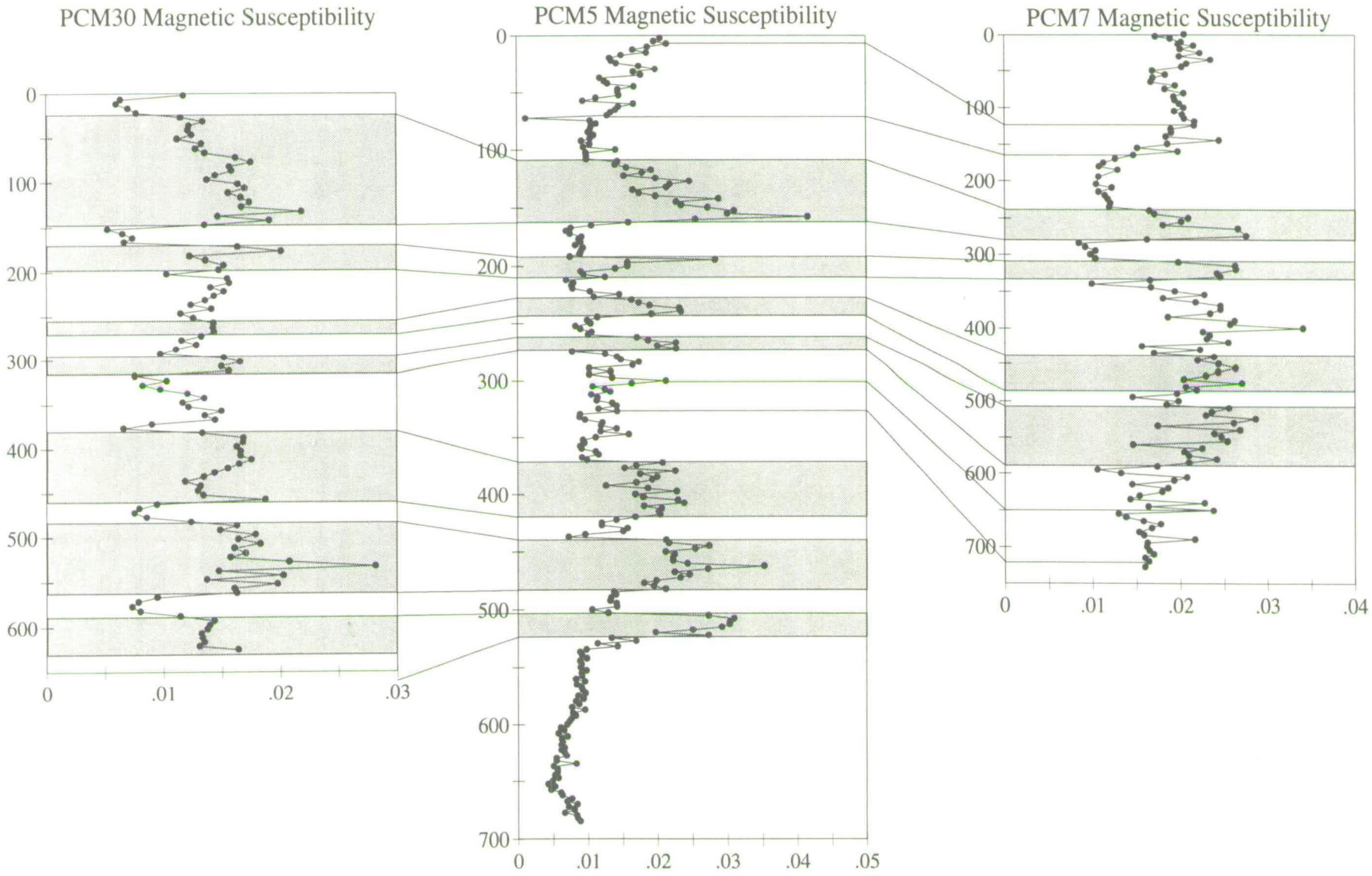

Fig.2.6. Correlation between PCM5, PCM7, and PCM30 based on magnetic susceptibility. The vertical scale is depth in cm, the horizontal scale is magnetic susceptibility expressed as mass in units of e-6m /kg.

The stage 5 $\delta^{18}O$ record is not so straight forward. Substage 5e in marine deep sea records is one of the key warm intervals in the late Pleistocene. It is easily recognisable by its $\delta^{18}O$ values being slightly lighter than Holocene values, indeed in both cores in this study a very light $\delta^{18}O$ spike does occur (see fig. 2.1). Thus at first sight it would appear that the light spike at 335cm in PCM5 must correlate with a similar spike at 472cm in PCM30, but this is not the case. There are two lines of evidence which prove these two spikes are not time equivalent. The first is the magnetic susceptibility correlation between the two cores, shown in fig. 2.6. The broad peak from 370-420cm in PCM5 clearly correlating with a similar peak between 380-460cm in PCM30, the following trough - peak - trough series seen in PCM5 can also be seen in PCM30. This indicates that the light spike in PCM30 at 472cm corresponds to a depth slightly greater than 420cm in PCM5 and cannot possibly correlate to the spike at 340cm in PCM5.

The second line of evidence, confirming that the two peaks do not correlate, involves the distribution of a certain benthic foraminiferal species in the two cores. The distribution of *Pullenia bulloides* (Orbigny) was first used in the Norwegian-Greenland Sea as a stratigraphic indicator by Haake and Pflaumann (1989). They found an abrupt appearance of *P. bulloides* during the late part of stage 5 only. They interpreted this period characterised by the presence of *P. bulloides* as being indicative of isotope substage 5a. This criteria has been used to identify isotope substage 5a in the Norwegian-Greenland Sea in several subsequent studies, for example by Köhler and Spielhagen (1990), and Hebbeln (1992). In this study a similar abrupt appearance of *P. bulloides* has been identified in both PCM5 and PCM30. This peak is found between 385-390cm in PCM5, and between 422-437cm in PCM30, these two portions of the cores must therefore be time equivalent. In PCM5 this faunal marker is found below the prominent isotope spike, in PCM30 it is found above the spike, the spikes therefore do not correlate. It is therefore a problem to identify substage 5e, but the position of the light spike in PCM30 directly above the heavy $\delta^{18}O$ values interpreted as stage 6 suggest that this is substage 5e. This is confirmed by core to core correlation using magnetic susceptibility, and the distinct pattern of magnetic susceptibility variations relative to $\delta^{18}O$ record of PCM30 (see below). Thus the light spike in PCM5 must be younger. Köhler and Speilhagen (1990) point out that substage 5a in the Fram Strait is characterised by a very light $\delta^{18}O$ spike, often lighter than the spike found in substage 5e, the spike in PCM5 is therefore almost certainly substage 5a. Again this is supported by the magnetic susceptibility correlations discussed later in this chapter.

Stage 6 can be recognised in both PCM5 and PCM30, and can be directly correlated with the composite curve. The record from PCM30 ends within stage 6, PCM5 however continues possibly into stage 7, the transition most likely occurring at 535cm. Interpretation of the rest of PCM5 is not certain, it seems likely that stage 7 continues down to the base of the core.

2.3.2. PCM7 and PCM56

The dating for PCM7 is based on correlation with PCM5 which contains a ^{14}C date, correlation with cores M 23259 and M 23071 from Sarnthein *et al.* (1992), and correlation with the stacked benthic record of Duplessy *et al.* (1988). Fig. 2.4 shows the oxygen isotope curve of PCM7 plotted in depth with the isotope curves of M 23259 and M 23071, fig. 2.5 shows the oxygen isotope curve of PCM7 in depth with the stacked benthic curve of Duplessy *et al.* (1988). The oxygen isotope record of PCM56 is shown in fig. 2.2 in depth, this core is dated by correlation with the oxygen isotope record of PCM7, fig. 2.4.

The oxygen isotope curve of core PCM7 contains an expanded section at the top characterised by relatively light $\delta^{18}O$ values, representing the transition from the last glacial period to the present interglacial (Holocene or stage 1). An age model has been produced for this top section by correlation with two radiocarbon dated cores from the Norwegian/Greenland Sea, M 23259 from 72°02'N 09°16'E and M 23071 from 67°05'N 02°55'E. This correlation is shown in fig. 2.4, the radiocarbon dates for M 23259 and M 23071 are marked in normal type, the dates marked in italics are time slice ages constructed from 55 time-calibrated planktic $\delta^{18}O$ records by Sarnthein *et al.* (1992). The tie points used in this correlation are shown in table 2.1. The major oxygen isotope shift in PCM7 at 130cm culminating in $\delta^{18}O$ values of 2.6‰ at 120cm has been correlated to the 12.3ka time slice from Sarnthein's cores. This correlation is supported by foraminiferal assemblages changes in these cores. Sarnthein *et al.* (1992) report the first major influx of subpolar fauna into the Norwegian/Greenland sea just after this time slice. The foraminiferal abundance counts for PCM7 record an influx of the subpolar planktic species *Neogloboquadrina pachyderma* (Ehrenberg) (dextral) at 125cm (just after the major isotope shift), the paleoceanographic consequences of these changes are dealt with in chapter 6. The earlier major shift in oxygen isotope values seen in M 23259 and M 23071 at 13.6ka therefore correlates to the smaller amplitude shift seen in PCM7 at 177.5cm. The heavy $\delta^{18}O$ value at 11.92ka in M 23259 correlates fairly conclusively with a similar

heavy episode in PCM7 at 65cm, as does the less extreme episode at 10.6ka with 45cm in PCM7. The time slice age of 9ka from M 23259 and M 23071 has been correlated to a point near the top of the trip core, 28cm, this marks the position where the oxygen isotope values become more stable in PCM7. The top of the trip core has been given an approximate age of 10ka, leaving a small gap between the trip core and the main core. The section from 250cm to the base of PCM7 has been correlated to the stacked benthic curve, this is outlined below.

The correlation of peak stage 2 with the stacked benthic record of Duplessy *et al.*, (1988) fig. 2.5, is supported by the correlation of PCM7 with PCM5. The double peak during stage 2, seen between 130-200cm in PCM5, correlates with the period between 250-330cm in PCM7, the ^{14}C date of 22,040 +- 320 years at 195cm in PCM5 correlates to 325cm in PCM7. The earlier peak at 265cm in PCM7 has been interpreted as the peak of the last glaciation, by correlation with the Duplessy record, and assigned an age of 16ka years. The section of the core older than stage 2 has also been correlated to the stacked benthic record of Duplessy *et al.* (1988). The light spike at 650cm in PCM7 has been correlated to the spike at 65ka years in the stacked record, within stage 4, the end of stage 4 in PCM7 occurs at 605cm, correlating to 59ka yrs in the stacked record. The base of PCM7 represents some point towards the beginning of stage 4, stage 5 is not reached in this core. Several correlation points within stage 3 can be made between the two records, and are shown in fig. 2.5. All tie points used to the age model for PCM7 are shown in table 1.

The oxygen isotopic record for PCM56 represents a highly expanded section. The whole 750cm of the core probably correlates to the section between peak stage 2 and a point just before the major drop in oxygen isotope composition at 130cm in PCM7, this is shown in fig. 2.4. This represents a time interval from approximately 17ka at the base of the core to approximately 13ka at its top. The reduction in oxygen isotopic composition at 580cm correlates to the first major decease in values after peak stage 2 in PCM7 at 245cm. The pronounced trough from 410-340cm in PCM56 is equivalent to a similar feature seen in PCM7 from 177.5-165cm. The upper 340cm of PCM56 is interpreted as being equivalent to the high oxygen isotope section in PCM7 from 160-130cm. The major drop in values seen in PCM7 at this point are not present in PCM56.

2.4. Magnetic susceptibility stratigraphy

As mentioned earlier magnetic susceptibility has been used as a correlation tool between marine records. It has also been possible to correlate marine magnetic susceptibility records to records of oxygen isotope stratigraphy to produce an age model for the core. In this study it has been possible to accurately correlate between cores using magnetic susceptibility. This has enabled refinements to be made to the oxygen isotope age model where one core may have a poor isotope record compared to another. It has also been possible to correlate magnetic susceptibility directly to the oxygen isotope record for PCM5 and PCM30, this has allowed further refinement of the age model, particularly within isotope stage 5, which has a poor oxygen isotope record due to low foraminiferal abundance. The first section below outlines the correlation between cores using magnetic susceptibility, and is followed by a description of the correlation between susceptibility and oxygen isotope records.

2.4.1. Correlation between cores:

The susceptibility records of PCM5 and PCM30 show a remarkable similarity, fig. 2.6. The sharp trough in PCM5 from 165 to 192cm correlates with a similar feature in PCM30, at 150 to 165cm. The preceding peak with values reducing upwards reaching another trough at 105cm in PCM5 can be seen in PCM30 where the trough is reached at 20cm. PCM5 has a more complete section at its top, though PCM30 has a higher sedimentation rate. The peak in PCM5 at 195cm correlates to the peak at 177cm in PCM30, the next peak in PCM5 at 240cm can be correlated to a peak in PCM30 at 262cm. The peak at 265cm in PCM5 corresponds to one at 297cm in PCM30. The next obvious correlation point is the broad peak in PCM5 with highest value at 405cm, this corresponds to a similar feature in PCM30 culminating in a peak at 455cm. The following trough and peaks in the two cores match well (peak value at 462cm in PCM5 and 530cm in PCM30). The final trough and peak in PCM30 is clearly visible in PCM5, which carries on for over a metre of sedimentation not found in PCM30. Overall PCM5 shows a longer record with extra sediment recovered at both top and bottom, but PCM30 possesses a higher sedimentation rate and, therefore, should show more detail.

Several features of the magnetic susceptibility record of PCM7 can also be correlated to PCM5 and PCM30, see fig. 2.6. The obvious trough in PCM5 at 165 to 192cm is found in PCM7 at 285 to 305cm. The preceding peak, trough, and then rising values

to the surface in PCM5 can be traced in PCM7 also, the top of PCM5 correlating to approximately 135cm in PCM7. The peak at 195cm in PCM5 correlates to a similar feature at 315cm in PCM7. The next two peaks in PCM5, 240cm and 270cm, are also seen in PCM7 at 455cm and 525cm. The sharp peak at 650cm in PCM7 correlates to a similar isolated peak at 300cm in PCM5, the base of PCM7 correlates to approximately 320-327cm in PCM5. The magnetic susceptibility record for PCM56 is much harder to correlate to any of the other cores, and so has not been attempted.

2.4.2. Correlation between magnetic susceptibility and oxygen isotopes:

Magnetic susceptibility over certain periods correlates remarkably with the oxygen isotope record. This is best seen in PCM30, fig. 2.7, high magnetic readings correlate with high $\delta^{18}O$ values, thus in general cold glacial periods have high susceptibility values. This correlation between susceptibility and isotope ratio helps to fill the sampling hiatus in the isotope record, where foraminifers do not occur, or where the stable isotope signal is difficult to interpret. This assumes that high magnetic susceptibility values consistently correlate to colder periods and the overall trends do suggest that this is the case, see figs. 2.7 and 2.8. Peak stage 6 shows high susceptibility readings, but at the base a distinct trough in susceptibility values between 567cm and 582cm correlates to lower oxygen isotope ratios during mid-stage 6 , 567-577cm. The next major trough in susceptibility occurs during another section of light oxygen isotope values (isotope substage 5e, see section on stratigraphy), 462-477cm, there is then a short peak in both parameters (substage 5d) before another minor trough then peak, interpreted as isotope substage 5b. The high magnetic values of substage 5b continue to 382cm. This suggests that substage 5b extends up to 382cm, and substage 5a is found between 372-377cm, a period of low magnetic susceptibility. Isotope substage 5a is not represented in the oxygen isotopes, so this correlation helps define more closely the subdivisions of stage 5. The heavy oxygen isotope values of stage 4 are characterised by a period of high magnetic susceptibility values but with a marked trough, 332-317cm, in its centre. The trend of increasing oxygen isotopic values during stage 3, from 292-187cm, is mirrored in the magnetic susceptibility readings, both records culminating in a peak during early stage 2, at 177cm. There is then a marked low in magnetic susceptibility values more extreme than the slight drop in $\delta^{18}O$ values would suggest. This episode is present in all the magnetic records, fig. 2.6, and its cause is uncertain. The rest of peak stage 2 with high oxygen isotope ratios is characterised by high magnetic susceptibility readings.

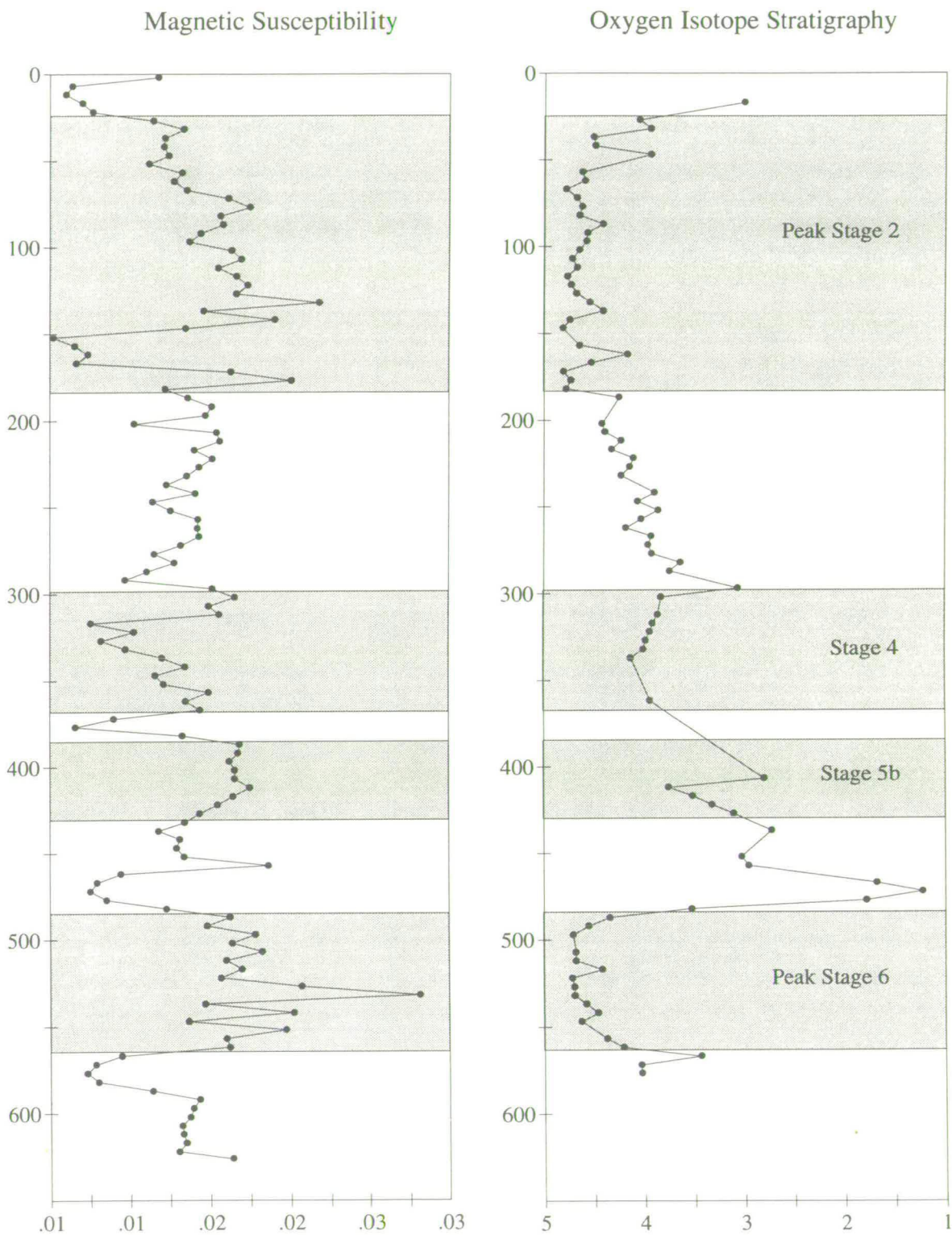

Fig. 2.7. Correlation between magnetic susceptibility and oxygen isotope stratigraphy for PCM30, against depth. Isotope scale per mil w.r.t. PDB, susceptibility scale mass in units of $10^{-6}m^3/kg$.

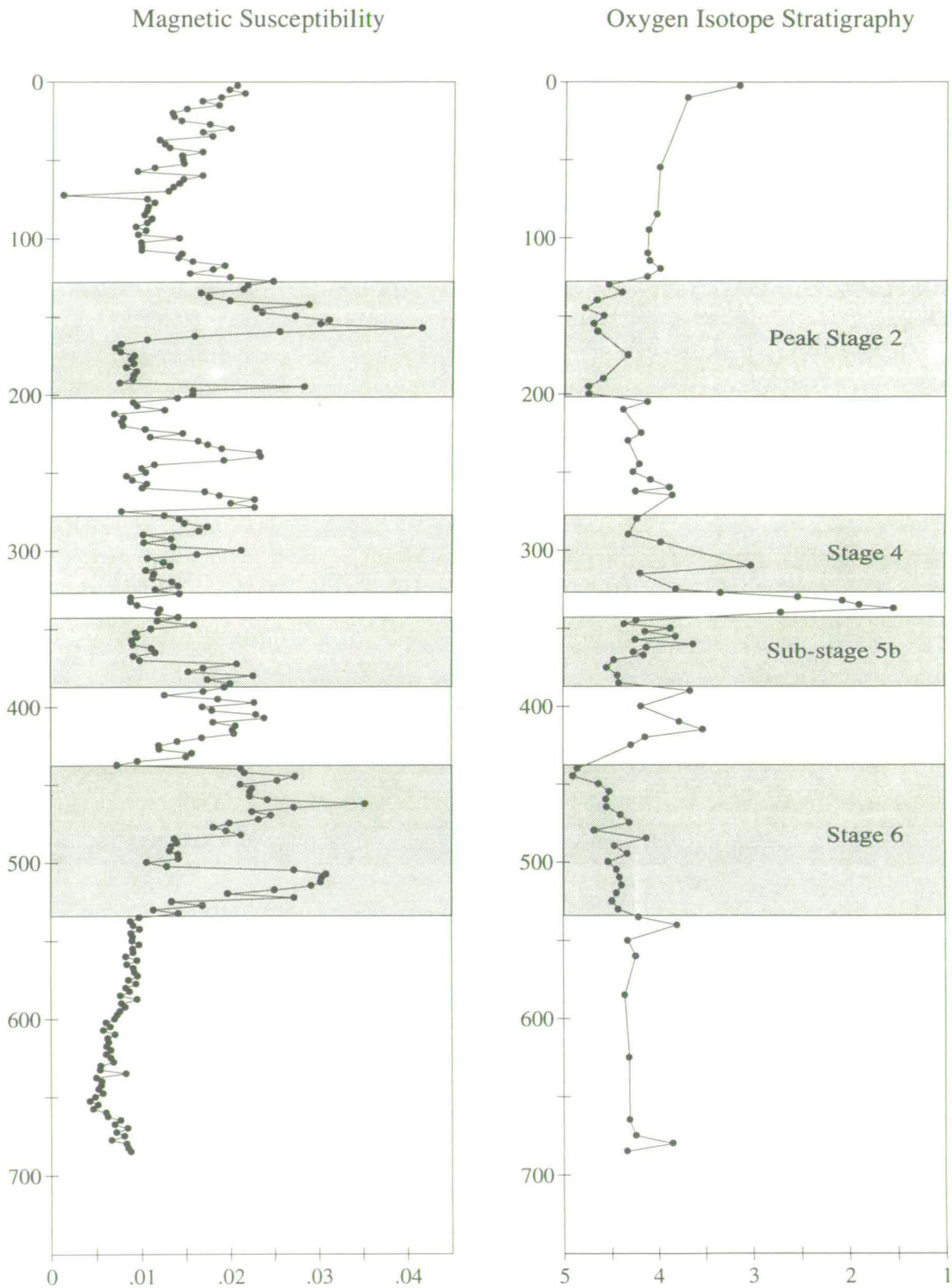

Fig 2.8. Correlation between magnetic susceptibility and oxygen isotope stratigraphy for PCM5, against depth. Isotope scale per mil w.r.t. PDB, susceptibility scale 10^{-6} m^3 /kg

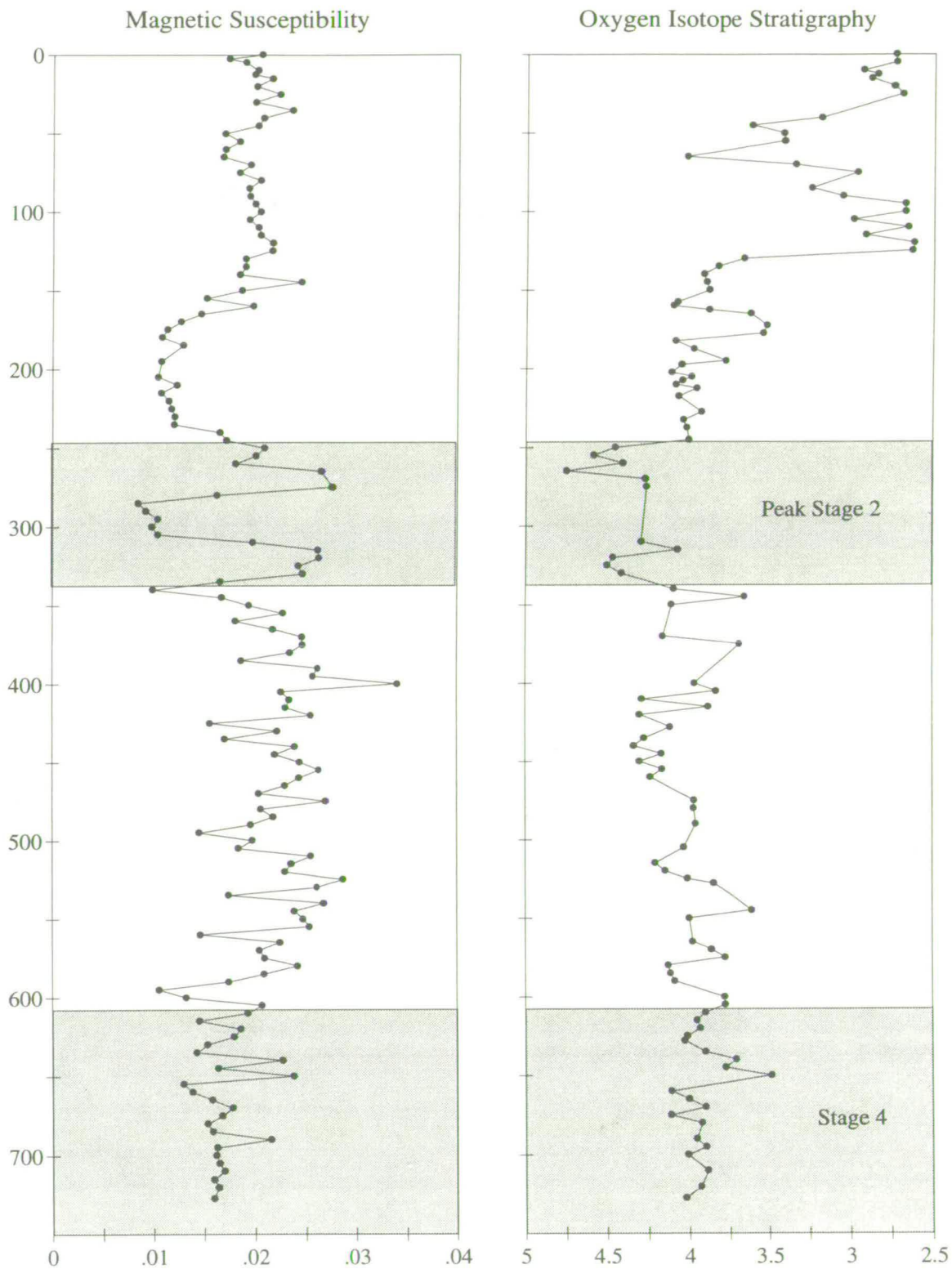

Fig. 2.9. Correlation between magnetic susceptibility and oxygen isotope stratigraphy for PCM7, against depth, (cm). Isotope scale per mil w.r.t. PDB, susceptibility scale mass in units of $10^{6}m^{3}/kg$.

The magnetic susceptibility values drop at the top of the core correlating with the initial melting event during stage 2 causing lower oxygen isotopic ratios at 17cm. The correlation for PCM5 is shown in fig. 2.8, the initial moderate to light oxygen isotopic ratios of stage 7, from 685-540cm are characterised by low susceptibility values. There are two major peaks in susceptibility during stage 6 with a trough which correlates with only slightly lighter oxygen isotopic values at 485cm. The susceptibility low after the end of stage 6 marks the position of substage 5e in PCM5, though it is not clearly visible in the isotopic record. There are three minor troughs at 335, 325, and 310cm which suggest substage 5e is fairly expanded in PCM5. The heavy oxygen isotope period of substage 5b has a poor correlation with susceptibility, but a minor trough in magnetic susceptibility is found during substage 5a at 340cm. Stage 4 is characterised by a minor peak in magnetic susceptibility readings, stage 3 shows again a poor record with distinct peaks and troughs not seen in the isotopic record. The heavy oxygen isotope values of stage 2 are accompanied by high magnetic readings, except for the sharp trough mentioned earlier, then values drop during the early deglacial phase of stage 2.

The record for PCM7 shows a very poor correlation during stages 4 and 3, the magnetic susceptibility shows no real correlation to oxygen isotopic signature, fig. 2.9. One possible explanation for this is that the isotope record during stage 3 and 4 records global isotopic variations rather than local effects recognised in the other cores. Stage 2 shows a similar picture to PCM5 and PCM30, two peaks in magnetic values correlating to the peaks during stage 2. The initial melting phase of stage 2 at 245cm, leading to lighter oxygen isotopic ratios, correlates to a low period in magnetic susceptibility. The susceptibility readings increase again at 160cm, this correlates to a rise in oxygen isotopic values at this position also. The top section of the core shows no correlation, magnetic susceptibility values remaining constant while oxygen isotope values fluctuate from interglacial to heavy stadial values.

For large sections of the cores examined in this study magnetic susceptibility appears to correlate with the oxygen isotope record. Periods of high susceptibility correspond to periods of high isotope ratio, glacial periods, and low susceptibility to interglacials. The correlation fails during stages 3 and 4, and also during the present interglacial record shown in PCM7. It appears to correlate well when there is a local influence on the oxygen isotopic ratio, stages 2, 5, 6, and 7, and not so well when the isotopes reflect a more widespread global influence (stage 3 and 4). This does not explain the lack of correlation during the present interglacial, the top section of PCM7, which is assumed to be a locally derived record.

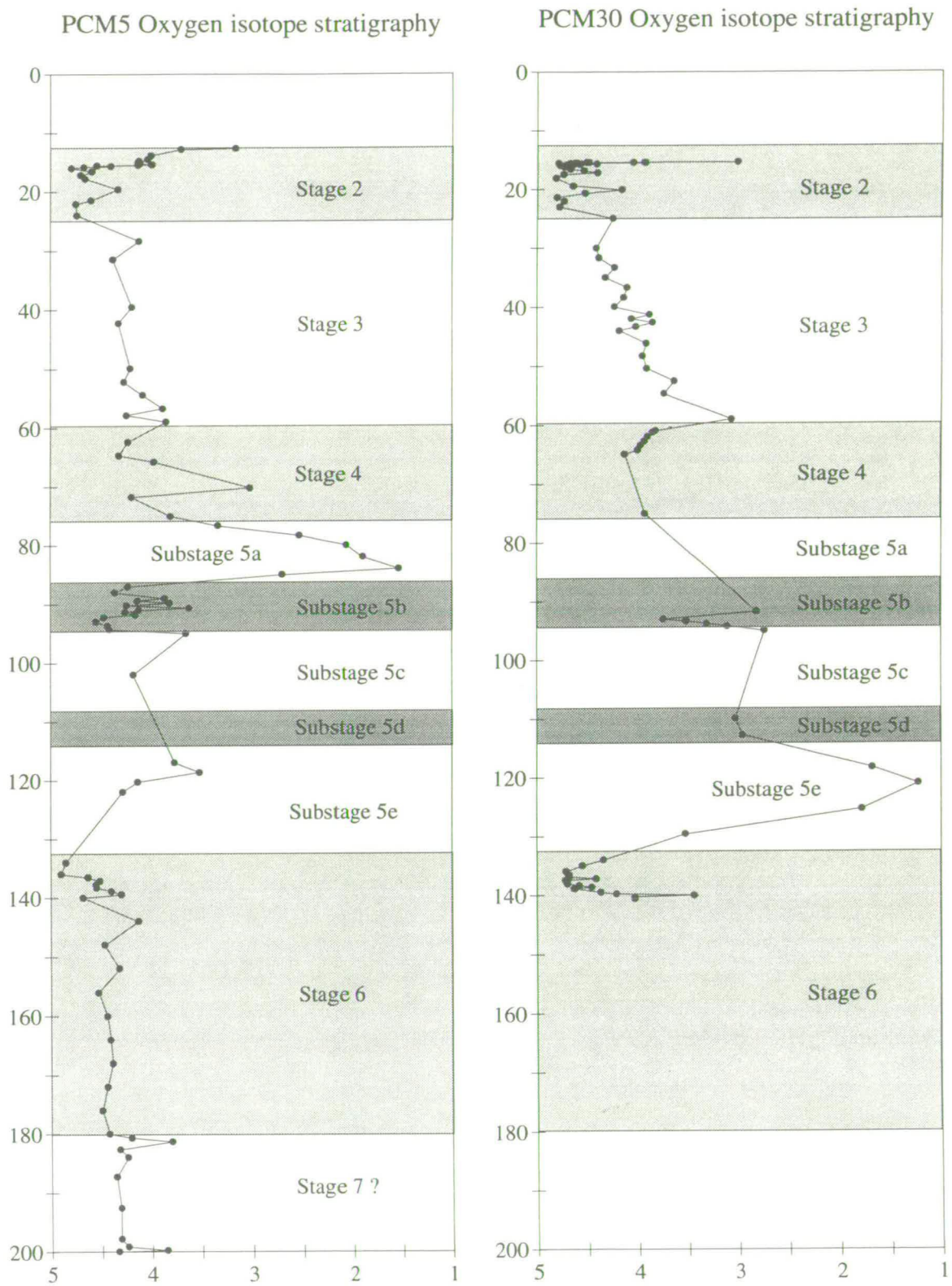

Fig. 2.10. Age model for PCM5 and PCM30 from oxygen isotope stratigraphy, after refinement using magnetic susceptibility correlation. Vertical scale age in ka, horizontal scale oxygen isotope composition in per mil w.r.t. PDB. Glacial and stadial stages have been shaded.

This correlation has been used to improve the age model for the cores, the refined age model is shown in fig. 2.10, main glacial periods shaded and substages of stage 5 are marked, the colder substages are shaded also. The tie points used between the isotope records in this study, the Duplessy composite curve, and cores M 23259 and M 23071 of Sarnthein et al. (1993) are summarised in table 1.

2.5. Sedimentation rates

From the age model produced above variations in sedimentaion rate can be observed by plotting age against depth, this is shown in fig. 2.11. In these plots the nearer horizontal, or shallower, the line the faster the sedimentation rate. All three cores show very shallow lines for the upper 200cm of sediment. After this initial section the lines rapidly steepen suggesting a drop in sedimentation rate. This apparent drop in sedimentation rate is caused by compaction of the sediment on burial.

The glacial isotopic stages 2, 4 and 6, and the stadial substage 5b are shaded and labelled in fig. 2.11. Table 2.1 below gives the average sedimentation rates, expressed as cm per thousand years, for isotopic stages for each core.

Isotope stages	PCM5 (cm/ka)	PCM30 (cm/ka)	PCM7 (cm/ka)
Stage 2	17.5	21.5	17.2
Stage 3	1.9	3.1	7.6
Stage 4	3.75	4.1	9.2
Stage 5 (whole)	1.9	2.2	
Substage 5b	4	5.5	
Stage 6	2.6	15.8	

Table 2.1. Approximate sedimentation rates for PCM5, PCM30 and PCM7 averaged over isotopic stages, based on linear interpolation between stage boundaries. The value for the whole of stage 5 includes substage 5b, but a separate value for the stadial substage 5b is also shown.

Stage 2 in all cores shows very rapid sedimentation rates, this is partially due to compaction of the deeper buried section lower in the core, but all cores show a definite step at the stage 2-stage 3 boundary. The average sedimentation rate for stage 3 in PCM7 is slightly lower than the rate for stage 4, 7.6 compared to 9.2cm/ka. The stage 3 sedimentation rates in PCM5 and PCM30 are similar to rates in stage 5 for

both cores, these values are significantly lower than the values for stage 4. The cold stadial substage 5b in PCM5 and PCM30 have significantly higher sedimentation rates than the rest of stage 5. The sedimentation rates within stage 6 are less clear, values for PCM30 are very high 15.8cm/ka, for PCM5 they are only 2.6cm/ka. This is most probably due to uncertainty about the position of the stage6-stage 7 boundary in PCM5, the age model at the base of this core may be slightly inaccurate. PCM30 only records the latest period of stage 6, which may explain the very rapid sedimentation rates, similar rates are experienced during the same period of PCM5.

In general the sedimentation rates for PCM7 are higher than the other two cores, this is partially due to a shallower coring depth for this core. The rates for PCM30 are slightly higher than for PCM5, this again may be due to a shallower depth at the cores site of PCM30 than PCM5, though sediment source is undoubtedly an important factor also. A second general trend seen in sedimentation rates are the higher values during glacial stages 2, 4 and 6, and stadial substage 5b.

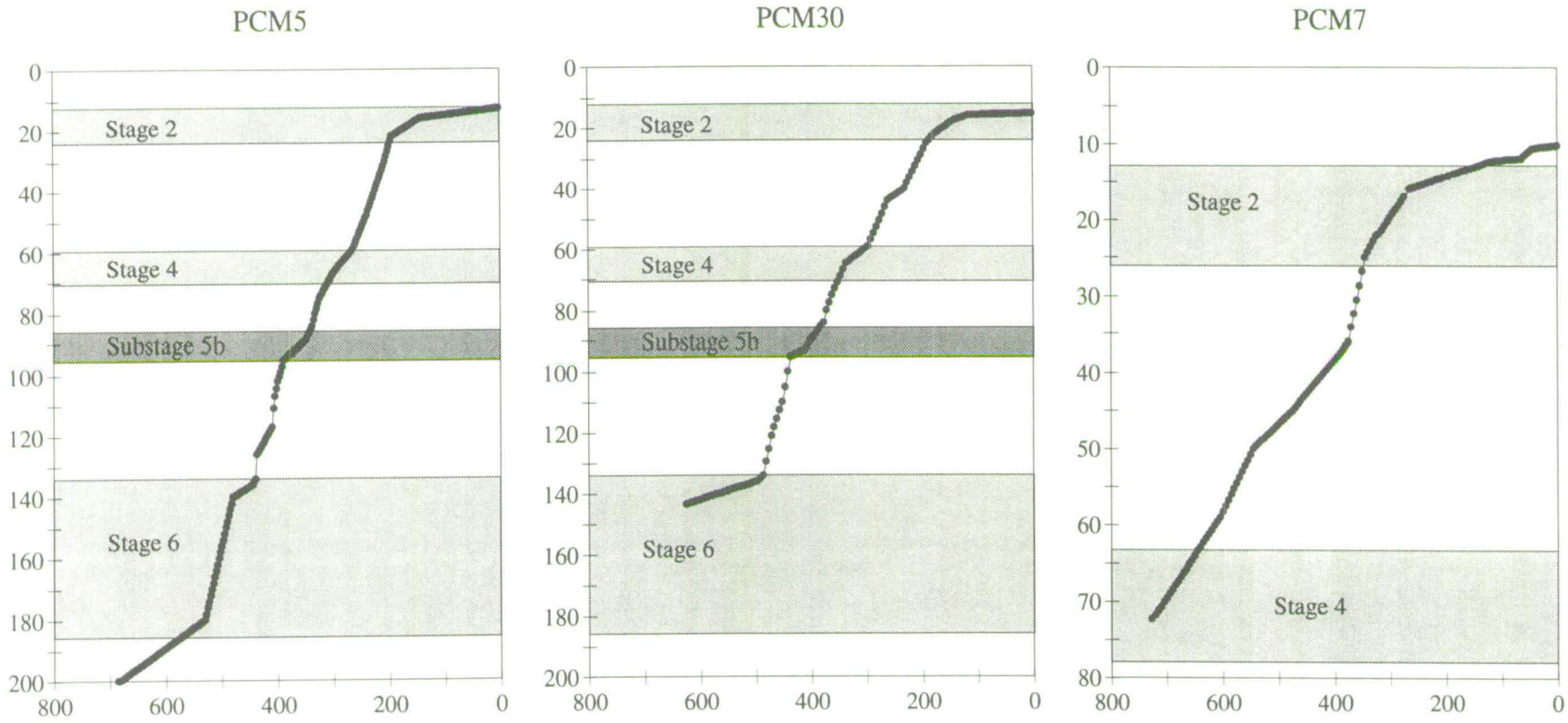

Fig. 2.11. Sedimentation rate curves for three cores, PCM5, PCM30, and PCM7. The plots are age on the vertical axis against depth on the horizontal axis. Note the differences in age scale. Glacial stages and cold stadial stages are shaded. Shallower angled lines represent periods of faster sedimentation. All cores show a rapid sedimentation for the uppermost 200cm or so, then a marked decrease, this is due to compaction. The shaded cold periods do tend to show higher sedimentation rates.

Chapter 3. The history of ice rafting from the Svalbard ice cap over the last 200 ka from the sedimentology of marine cores

3.1. Aims and rationale

The aim of this chapter is to review the sediment supply to the continental slope of western Spitsbergen, the facies associations produced on the slope, and to compare the timing of sedimentary changes in the different cores investigated. The sedimentology of the cores in this study are examined using x-ray photography and particle size analysis.

The sedimentary facies associations of glacially influenced continental slope environments are poorly understood when compared to other environments. The processes and sedimentary facies on glaciated margins are highly variable in time and space. The location of glaciers, their thermal regime (whether warm or cold based), and the position of the glacier grounding line (either at or near to the ice front or at the proximal extremity of an ice shelf) all play important roles in the formation of deposits on the slope.

In this study an accurate time frame has been achieved from oxygen isotope stratigraphy, see chapter 2. The degree of ice rafting is assessed from clast counts from x-ray photographs of the cores, and also particle size measurements. Using this data a model of the input of IRD to the continental margin of Spitsbergen has been produced. This allows an interpretation of the history of the Svalbard ice cap to be made. The accurate time constraint on this data makes it possible to test the hypothesis suggested by Boulton *et al.* (1983) for an anti-phase relationship between climate change and ice growth/decay in high latitude areas.

3.2. Sediment supply to the continental margin

3.2.1. Sediment supply from icebergs

There are several factors influencing the input of ice rafted detritus (IRD) to the marine system, these will be outlined briefly below.

Iceberg detritus content

The quantity of detritus within the icebergs is highly variable and obviously important to the sediment supply. There are several positions within an ice mass where detritus is concentrated, basal debris, englacial debris and supraglacial debris. The quantity of basal debris present in an iceberg depend on the thermal regime at the base of the ice when calving occurs, and from where the iceberg calves. If the iceberg is calved from an ice shelf, Drewry and Cooper (1981) have shown that its basal debris content will be low. Much of the basal debris will have melted out or will melt out soon after calving. Calving from an ice shelf can produce icebergs with high basal debris if there are extensive zones of bottom freezing present. Calving from an outlet glacier or an ice tongue commonly produces debris rich icebergs with thick basal diamict layers.

Englacial and supraglacial debris is also common in icebergs, and may contribute to IRD deposits. The quantity of this material within an iceberg depends on its previous history within the ice mass. The quantity of nunataks (mountain tops protruding above an ice mass) near to the flow path of glaciers is important, more nunataks will lead to higher concentrations of supraglacial debris. The harshness of the climate will also affect the supply of debris, harsher climates with more intense frost shattering will lead to high debris supplies to the ice mass.

Iceberg production rates

The rate of production of icebergs is obviously an important factor controlling the concentration of IRD in marine sediments. Iceberg production rates are controlled mainly by the ice flux. The greater the amount of ice flowing through the system the larger the number of icebergs produced. The flux rate of ice produced at the outlets to ice masses is controlled by the catchment size. If a major outlet fjord has a large number of minor glaciers draining into it, then the flux rate will be high leading to higher iceberg production. The flux rate is also controlled by accumulation rates. Glaciers act as conveyor belts, ice deposited in interior areas of the ice mass flows through the system and is eventually released at the edges of the ice mass, either by melting or calving of icebergs. Higher accumulation rates produce larger ice fluxes, larger volumes of ice flowing faster through the system produce more icebergs. Sea level also has an important influence on iceberg production. Once an ice mass advances onto the continental shelf it comes into contact with the sea, the buoyancy effect of the sea on the ice will lead to rapid calving. Any rise in sea level, caused by isostatic depression due to the weight of ice, will lead to enhanced calving.

Iceberg carry distance

The distance an iceberg travels before it has totally melted will affect the supply of IRD, and the position in the marine realm the IRD is deposited in. The physical size of the iceberg is important, this is controlled by the fracture patterns within the ice mass. Icebergs from ice shelves tend to be very large as fractures are relatively rare, large tabular bergs are produced. Calving from a fjord head would produce smaller icebergs due to a higher concentration of fractures, and the smaller dimensions of the ice front. Obviously larger icebergs will survive for longer and have a greater chance of being carried beyond the continental shelf to allow IRD deposition in slope environments. Water temperature is also crucial, icebergs calving into relatively warm waters may be large or rich in debris, but will melt rapidly and deposit all their material on the continental shelf close to the ice front. Dowdeswell and Murray (1990) predicted icebergs calving from subpolar glaciers such as Svalbard and Alaskan glaciers may carry debris in the order of 100km from the tidewater ice front. Icebergs from Antarctic and high polar ice sheets may survive 1000km or more. During glacial periods areas such as Svalbard would act as high polar areas, icebergs surviving much longer in the colder surface waters.

Trajectory of iceberg flow

Once calving has produced icebergs their flow directions are controlled by ocean currents. Current regimes may lead to a concentration of IRD in certain areas below the iceberg flow paths. For example a strong along shelf current may carry icebergs along the shelf preventing them from reaching the continental slope, so the slope could be starved of IRD even though calving rates are high. The position of pack ice may influence iceberg drift patterns also.

3.2.2. Thermal regime of ice mass

The thermal characteristics of the ice mass can influence the quantity of material available for sedimentation. A temperate ice mass will contain large quantities of meltwater, and subsequently large amounts of suspended sediment will be released as a surface plume. A polar ice mass will have very little meltwater, ablating virtually only by calving, such sediment laden plumes would be rare. Fine material from these plumes eventually settles out and is redistributed by ocean currents. As material sinks from the plume into saline water flocculation occurs increasing settling velocities. This material forms partially sorted silts and muds, and may show laminations also. Cold dense meltwater plumes may become more dense than the surrounding waters if

they carry enough suspended sediment, in this case they sink to form gravity controlled bottom flows, (Vorren et al., 1989). Such currents would flow across the shelf and down the continental slope acting as turbidity currents.

3.2.3. Ocean circulation

The ocean current regime and general climatic patterns will influence sediment supply to the continental slope. Surface currents control the tracks of melting icebergs, and water mass type, controlled by the climatic regime, will control the rapidity of melting of icebergs and also the rate of calving. Deeper marine currents, such as contour currents, keep fine material suspended leading to the deposition of relatively coarse-grained sediments, these have been recognised from the Antarctic continental margin by Anderson *et al.* (1979 and 1980). Where sedimentation of fines and ice rafted material occurs, weakly to well stratified compound glacial marine sediments accumulate. Long slope contour currents can act as a sediment supply also, carrying fine material into the area.

3.3. Previous studies using ice rafted detritus (IRD)

The distribution of coarse grain-sized material in marine cores can be used to identify periods of intense ice rafting from surrounding landmasses. Ice rafted input into the marine system can provide evidence for changes in oceanic circulation, and the size and distribution of land based ice sheets. The occurrence of ice rafted detritus in marine cores has been extensively used recently in the North Atlantic to recognise periods of intense outflow of icebergs from the Laurentide ice sheet, Heinrich (1988), Bond *et al.* (1992), Broecker *et al.* (1992), Andrews and Tedesco (1992), and Grousset *et al.* (1993).

Distinct layers of ice rafted detritus (IRD), since termed Heinrich layers, were recognised by Heinrich (1988) in 13 piston cores from the Dreizck seamount area of the North Atlantic (at 19°40'W, 47°23'N). Heinrich found 11 layers extending back to the isotope stage 5/6 boundary. Bond *et al.* (1992) recognised the first six Heinrich events in a range of cores across the width of the North Atlantic. Both studies reached the conclusion that these events recorded periods of intense ice rafting from the Laurentide ice sheet.

The forcing mechanism for these rapid expansions is uncertain, the frequency suggested by Heinrich, 11,000 years, is higher than any of the Milankovitch orbital periodicities, but lower than the Dansgaard-Oescher oscillations of ^{18}O profiles seen in cores from the Greenland ice sheet. Bond *et al.* (1992) suggested these ice rafting events occurred as a result of rapid expansions of the Laurentide ice sheet leading to large scale calving of icebergs into the North Atlantic. Reduction of foraminiferal abundances and the rise in dominance of the species *Neogloboqudrina pachyderma* (sinistral) were used to infer a drop in sea surface water temperatures. Andrews and Tedesco (1992), also recognised Heinrich events from several cores in the Hudson Strait, and suggested that large scale surging of a Hudson Strait ice stream could be the principal cause of Heinrich events. This suggestion could explain Heinrich events during relatively warm (isotopically light) periods. More recently Oerlemans (1993) examined the hypothesis that cooling events caused expansions of the Laurentide ice sheet leading to increased ice calving depositing Heinrich layers in the North Atlantic, as suggested by Bond *et al.* (1992). He uses a model of the Laurentide ice sheet to show that cooling during peak glacial periods causes a reduction in ice calving, but cooling during a deglacial period causes a still stand in glacial retreat leading to rapid increase in calving. He concludes that Heinrich events are unlikely to reflect a direct response of the Laurentide ice sheet to climate cooling.

Bond *et al.* (1992) speculated whether the Greenland, Fennoscandian, or Barents Shelf ice sheets underwent similar events, and if so whether there might be a time correlation between Laurentide ice sheet and other N. hemisphere ice sheet events. IRD has also been investigated from marine cores from the Greenland Sea, in order to elucidate the glacial history of Spitsbergen (Hebbeln, 1992). As discussed in chapter 1 the glacial history of the Svalbard archipelago is far from certain. Miller *et al.* (1989) suggested on the basis of terrestrial records that no major ice advance reached the continental shelf along the western coast of Spitsbergen during the last four marine isotopic stages, and that the last major advance occurred during stage 5 (greater than the advance during stage 2). Mangerud *et al.* (1992), however, concludes from terrestrial and marine records that there were three major ice advances on Spitsbergen during this period; one during isotope substage 5d, one during isotope stage 4 and early stage 3, and one during late stage 2. Svendsen *et al.* (1992) provide evidence from marine cores that glaciers reached the edge of the continental shelf during the Late Weichselian (isotope stage 2) and were not merely restricted to fjord mouths. Using the presence of IRD and organic carbon accumulation rates in eight cores from the Fram Strait, Hebbeln (1992) identified two phases of ice cap growth on

Spitbergen during the last 130,000 years. These phases occur during late stage 4 and early stage 3, and during stage 2 (agreeing partially with Mangerud's conclusions).

One important aspect in these studies is the criteria used to characterise ice rafted material. Several different criteria have been used, Ruddiman (1977) interpreted the presence of material coarser than 62μm as indicative of ice rafting, Hebbeln (1992) used this fraction also. Heinrich (1988) used the fraction between 180-3000μm as ice rafting indicators, Bond *et al.* (1992) used the fraction coarser than 150μm, and Andrews and Tedesco (1992) use the abundance of detrital carbonate as indicators of IRD. In this study clast counts from x-ray photographs are made and compared to particle size data to get a clearer idea of the constituents of IRD.

3.4. Results

In this present study three cores have been examined for IRD content, PCM5, PCM7, and PCM30. The weight percent material coarser than 63μm and 600μm has been measured on samples from these three cores. Samples from PCM5 were also passed through a Coulter LS-100 particle size analyser to see fine fraction variations, results from these two particle size techniques were then compared. The sedimentary characteristics of the cores from x-ray photographs of their undisturbed halves have been described and separate facies identified. Counts of the abundance of clasts larger than 2mm from these x-rays have been made. The results are described below.

3.4.1. Description of x-ray Characteristics

The x-ray photographs of three cores have been examined, PCM5, PCM7 and PCM30. Interpretative logs have been drawn for each core, see figs. 3.1, 3.2, 3.3. Four distinct sedimentation patterns have been used to subdivide the cores. These four separate patterns, or facies types are as follows;

1. Homogeneous material with rare clasts. No sedimentary structures are visible, clasts when present are randomly distributed in the sediment.
2. Sediment with common clast abundance. Cores have clasts in moderate abundance randomly distributed throughout. Clasts tend to be moderately sorted compared to type 3 sediments, the larger grains being most abundant. Sedimentary structures are usually absent, but occasionally weak laminations may be seen.

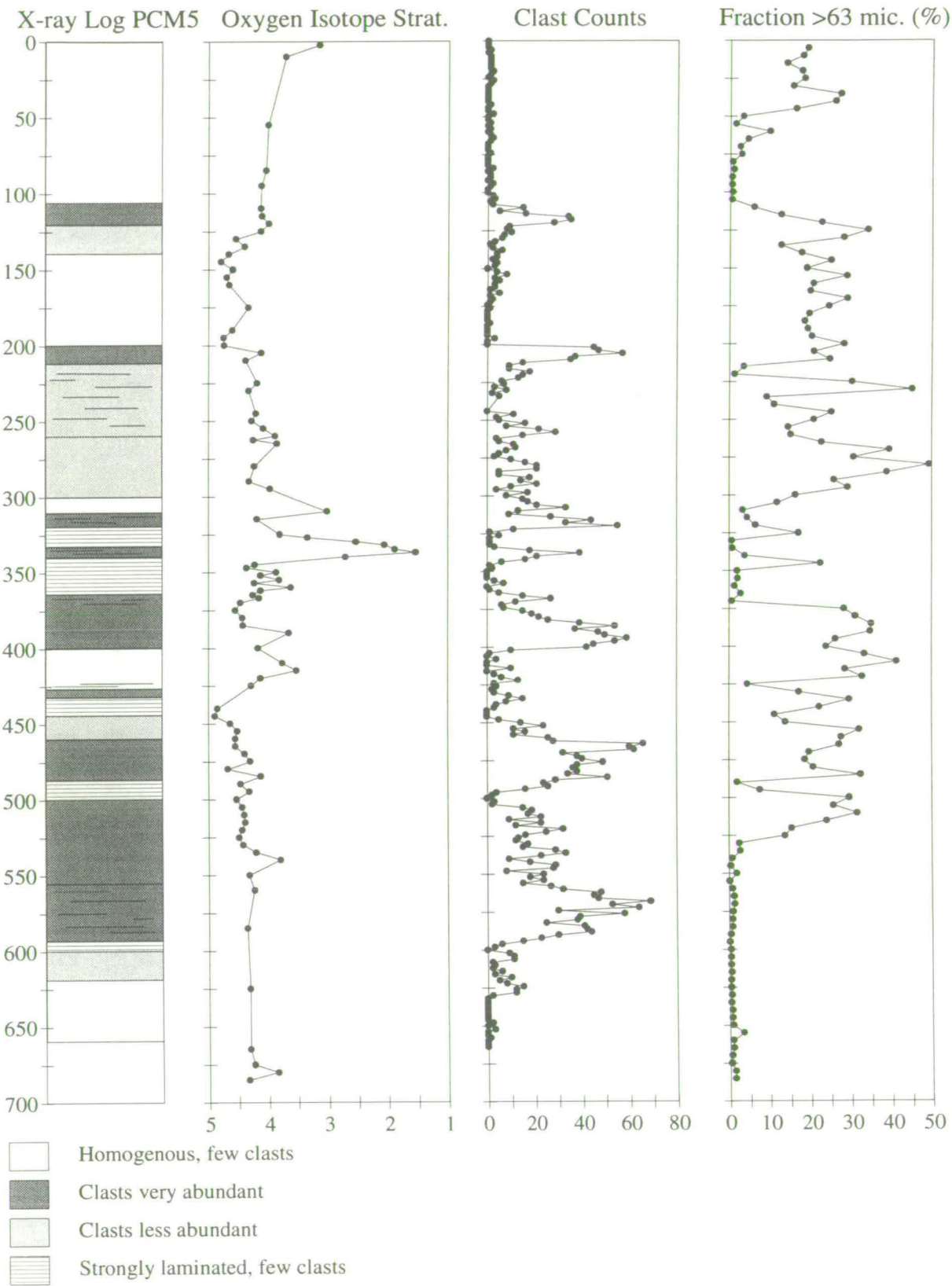

Fig. 3.1. Interpretative log of x-ray photographs of PCM5 showing distinctive sediment types. Also plotted are oxygen isotope stratigraphy, clast counts, and sand fraction all plotted against depth.

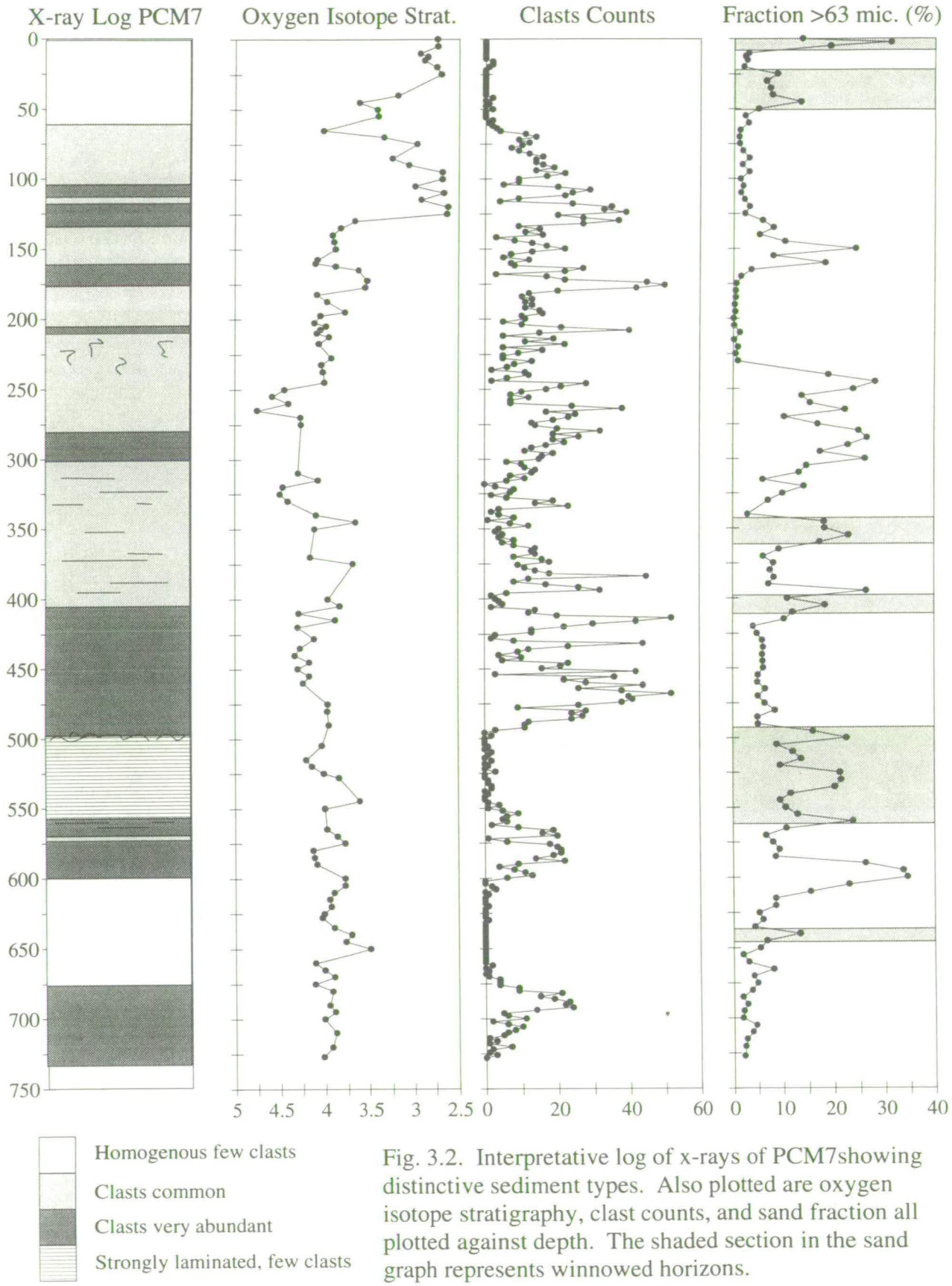

Fig. 3.2. Interpretative log of x-rays of PCM7showing distinctive sediment types. Also plotted are oxygen isotope stratigraphy, clast counts, and sand fraction all plotted against depth. The shaded section in the sand graph represents winnowed horizons.

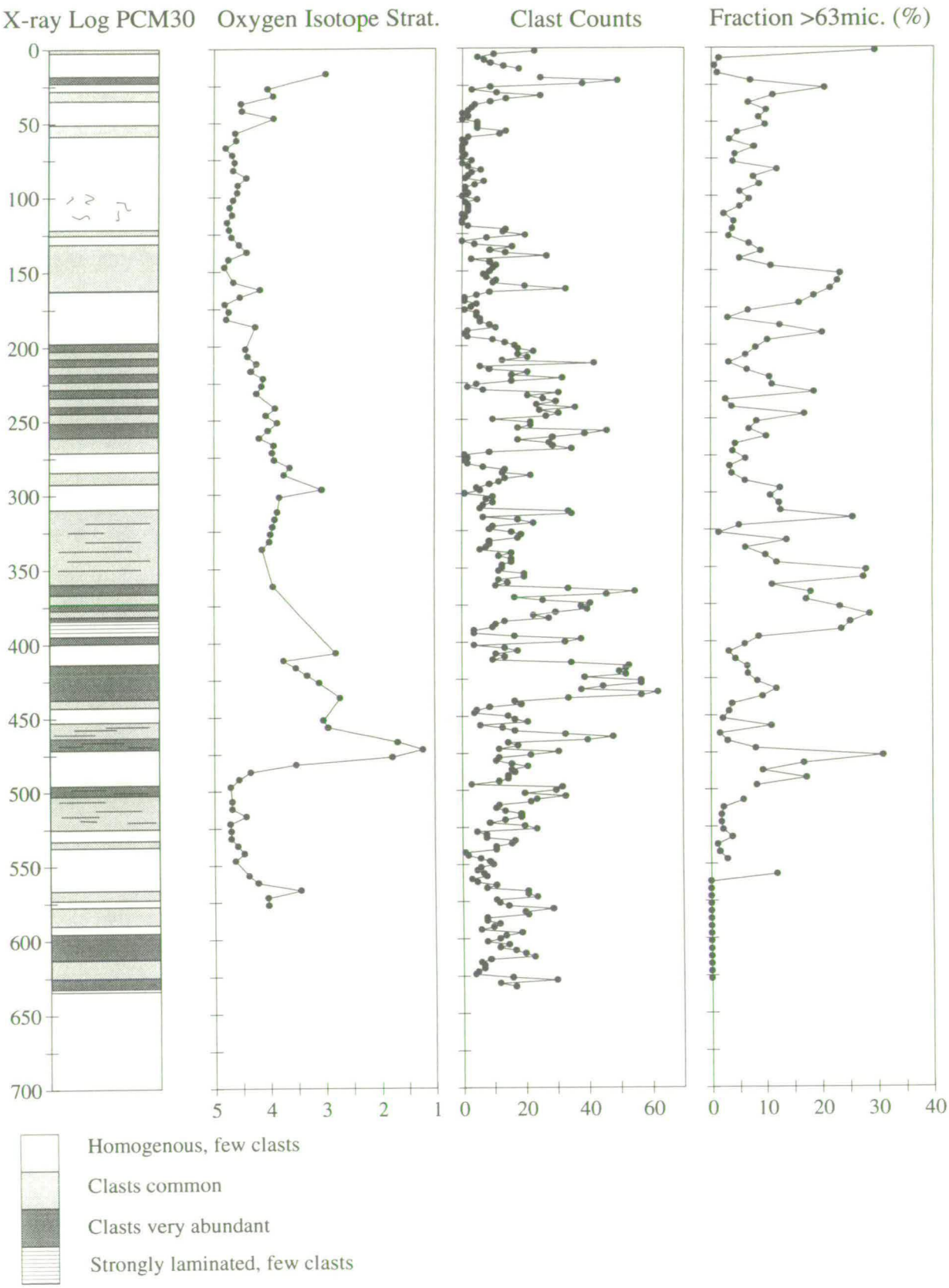

Fig. 3.3. Interpretative log of x-ray photographs of PCM30 showing distinctive patterns of sedimentation. Also plotted are oxygen isotope stratigraphy, clast counts, and sand fraction, all plotted against depth.

3. Sediment with very high clast abundance. These sections are packed with coarse grained material, which is very poorly sorted, and randomly distributed. Sedimentary structures are again usually absent, though some weak laminations are sometimes present.
4. Strongly laminated sediment. Clasts tend to be very rare in these sections if present at all. Laminations are unevenly spaced, and cross bedding is common.

A brief description of the sedimentary characteristics of the x-rays will be given in the following section, the cores will be described from the base up. Examples of the x-ray photographs are shown in plate 4.

PCM5.

The basal section up to 618cm consists of homogeneous sediment with very few clasts, this grades into a deposit with common clasts which has a sharp upper boundary at 600cm. From 600-592cm strong laminations are present, they become disturbed towards the upper boundary, within this section no clasts are present. The upper boundary is gradational, clast numbers increasing upwards, passing up into deposits with a high abundance of coarse material. The coarse material is very poorly sorted, ranging from large clasts several cm across down to very small grains barely visible. Fairly strong laminations are visible in the background sedimentation until 556cm, above this the coarse grained deposit continues with no sedimentary structures visible until 500cm. The next section has sharp lower and upper boundaries at 500 and 488cm respectively. This section has strong laminations initially, which get weaker towards the top, clasts are absent at the base but become increasingly abundant upwards.

The next section has large amounts of poorly sorted material, vague laminations are found towards the top at 460cm, the coarse material then reduces and laminations disappear until 444cm where a disturbed boundary with the following high laminated section is present. This section has very closely spaced laminations and is devoid of clasts, it also shows cross-bedding. There is a narrow section from 432-428cm where clasts appear, these soon die out to be replaced by a less strongly laminated homogeneous deposit with no clasts at all, with a sharp upper boundary at 400cm. Above this boundary there is a huge influx of poorly sorted coarse grained material, this begins to thin out at 379cm, and eventually disappears at the sharp contact with the next unit, some weak laminations are seen in the upper part of this section. The strongly laminated unit above spans from 364-320cm, the laminations are closely

spaced and highly cross-bedded, lenticular structures are also present, virtually no clasts are seen. Within this section there is a thin band where coarse material becomes abundant, laminations are still present though much weaker, and more widely spaced, its boundaries are gradational.

The next section of the core up until 200cm is dominated by the presence of clasts. Initially the abundance of coarse material is very high but gradually decreases at 310cm where there is a section with virtually no clasts, vague laminations are still present. At 300cm clast abundance increases again and no sedimentary structures can be seen, from 260cm clast abundance drops off again and disturbed laminations can be seen. The last 12cm of this section from 212-200cm records a major influx of poorly sorted coarse material, this has a very sharp top boundary.

Above this the nature of sedimentation changes markedly, the next 60cm consist of homogeneous material with no internal structure at all and very rare clasts. There is a gradual trend of increasing number of clasts towards the top of this unit, clasts becoming frequent by 140cm, and very abundant from 122-107cm. At this point they die out fairly rapidly and the upper 107cm of the core are dominated by the homogeneous deposit with very rare clasts and no sedimentary structures.

PCM7.

From the base of the core up to 676cm the sediment is dominated by high coarse material content, initially at the base of the core the number of clasts is low but increases fairly rapidly. No internal structures are visible over this section. Towards the top the coarse material content drops off until at 676cm it is virtually absent. The next 76cm until 600cm are composed of homogeneous material with few clasts and no internal structures. At 600cm there is a rapid increase in coarse material influx, poorly sorted with a wide range in grain-size, this is reduced for a short section from 573-569cm. After this the coarse material returns, but there are weak laminations visible, then at 557cm the abundance of coarse material drops off rapidly, there is not a sharply defined boundary though. Above this portion of the core strong laminations become visible these persist until 498cm. Throughout this section scattered clasts are seen, there is also a distinct decrease in lamination thickness towards the top, the laminations appear parallel. The upper boundary is marked by disturbed bedding and a gradual increase in clast abundance.

The next section is dominated by generally high quantities of coarse material, very poorly sorted and little internal structure visible. Within this unit there are distinct sections where coarse material becomes less common, from 444-438cm and 429-420cm, the lower boundaries tend to be relatively sharp and upper boundaries more gradational. At 405cm there is a prolonged section with fewer clasts until 300cm. In this unit laminations can be seen, and there are distinct bands with fewer clasts. At 300cm there is a definite change to a deposit richer in clasts and with less distinct laminations. There is a slight decrease in clast abundance at 270cm, the sediment then remains fairly unchanged until 209cm. At this point there is a thin layer 3cm thick which is packed with coarse material. This reduces gradually to similar concentrations as before until another layer with a rapid increase in coarse material is seen from 176-160cm. There are two more distinct sections with increased coarse material content, both have fairly distinct bases and gradational upper surfaces, they are found between 133-116cm and 111-106cm. This whole section shows very little internal structure, occasionally vague laminations can be seen.

From 106cm upwards there is a moderately low abundance of clasts randomly scattered through the core. There is a gradual decrease in their number upwards until at 60cm the clast abundance is virtually zero. No internal structures can be seen over this section. The upper 60cm of the core consist of homogeneous material with very low clast counts and no internal structures.

PCM30.

The base of the core is characterised by a high concentration of poorly sorted coarse debris. This material reduces rapidly leaving a deposit with common clasts from 625-612cm. At this point an influx of coarse material returns until 595cm. The next section until 502cm shows a record fluctuating between periods of moderate clast influx and periods of very little clast influx, no sedimentary structures are visible until the upper unit from 526-502cm where some weak laminations become apparent. The boundaries between these units are gradational. A brief section of high clast input is present from 502-497cm, this also shows some laminations, and grades upwards into a section with rare clasts and no sedimentary structures which has a fairly sharp upper boundary at 471cm.

The next section is dominated initially by high clast content which reduces slightly in its upper half, this unit spans 471-452cm and has weak laminations throughout. The clasts die out becoming rare for the next 10cm until 442cm, and then increases

slightly until 438cm. At this point a sharp boundary is encountered, the subsequent unit has a high clast content and is very poorly sorted with no internal structures. The clast content decreases gradually until at 413cm clasts become very rare, and an homogeneous deposit takes over until 400cm.

Above this is a 5cm section with sharp upper and lower boundaries with a very high clast content. These die out rapidly to be replaced by a strongly laminated deposit with few clasts from 395-384cm. These laminations are highly disturbed initially becoming more regular towards the top. Clast abundance then increases rapidly and fluctuates between highly abundant and common until 310cm, some laminae become visible from 360cm. At 310cm the clast content reduces, and an homogeneous deposit with rare clasts appears until 271cm. Within this section there is a layer where clasts become common from 292-285cm. The upper boundary is gradational with relatively small clasts appearing first and becoming more abundant. The next section until 197cm is characterised by rapidly fluctuating clast content between very abundant and common, each layer from 5-10cm thick, no sharp contacts occur in this section except at the top.

From 197-163cm clasts become rare, and an homogeneous deposit dominates until clasts become more common again at 163cm this lasts until 131cm. A narrow band of homogeneous sediment with rare clasts lasts until 125cm then clasts become common until 122cm then reduce again. This next homogeneous unit lasts until 59cm and has virtually no clasts present and no sedimentary structures. At 59cm there is a sharp boundary and clasts become common dying out gradually to be replaced by homogeneous sediment from 51-35cm. This grades up into a clast rich deposit which dies out rapidly at 29cm replaced by homogeneous sediment, this lasts until 23cm. There is then a very distinct band with high clast content from 23-19cm with a sharp upper boundary. The upper 19cm has few clasts and no sedimentary structures, though the top most 2cm do show some clasts.

3.4.2. Counts of clasts larger than 2mm.

The abundance of particles with a greater than 2mm diameter have been counted for PCM7, PCM5, and PCM30 from x-ray photographs (plate 4 shows examples of these x-ray photographs). Details of the sampling system are outlined in the section on analytical techniques in appendix 1. The counts were made every 2cm and the results obtained described below.

PCM7.

The number of clasts counted from 2cm intervals in X-rays of PCM7 varies from 0 to a maximum of 52. Three distinct sections occur where clast numbers are negligible, 670-600cm, 550-494cm, and 66-0cm. The rest of the record is characterised by abrupt sharp spikes, but some definite trends can be identified, see fig. 3.4. The record will be described in more detail below.

At the base of the core, there are very few clasts, below 5 per sample, but occurrence increases smoothly to reach a peak of 20-25 clasts from 692-682cm. Abundances rapidly drop off to below 5 by 676cm, and remain at this level until 600cm. Clast numbers rise smoothly again to a peak of 21 at 580cm, then decrease smoothly to below 5 by 562cm and remain low until 492cm. After this point the clast occurrence is generally higher, with rapid fluctuations. From 488cm until 446cm there is a major peak in clast counts, between 20-52, after which values tend to be below 10 with brief peaks rising to 40 clasts until 364cm. The more prominent peaks occur at 432cm, 420-412cm, 394cm, and 384cm. There is then a section of more stable numbers below 10 clasts until 312cm, at this point a general trend to higher abundances begins reaching a double peak of about 35 at 280cm and 264cm. The next section of the core upto 132cm is characterised by relatively low clast numbers, between 5-20, with occasional peaks. The numbers then increase rapidly to between 20-40 from 132-118cm. Values then drop sharply at 116cm, peak again at 112-106, drop at 104cm, then rise again to a more sustained peak of about 20 clasts at 98cm. Numbers remain relatively high, 10-20, until 68cm, after this they drop to 0-2 for the rest of the core.

PCM5.

The clast counts in PCM5 have higher peak values than PCM7, ranging from 0 to 69. The record for PCM5 shows clearer cycles than PCM7, high distinct peaks separated by low troughs. These variations, shown in fig. 3.5, are described more fully below.

The base of the core up to a depth of 630cm has no clasts present at all. There is then a small double peaked section with values reaching 10-15 before a rapid rise to a major peak from 590-560cm. Clast numbers reach their highest value throughout the core of 69 at 568cm, and range from 30-70 over this section. There is then a lower plateau of values ranging from 15-25 clasts over the section 558-506cm. A well defined trough with numbers below 5 from 504-496cm soon gives way to another section of high clast abundances of 30-60 from 494-450cm. From 448-402cm counts are generally below 5, but with three smaller peaks superimposed at 434cm, 422cm, and 410cm.

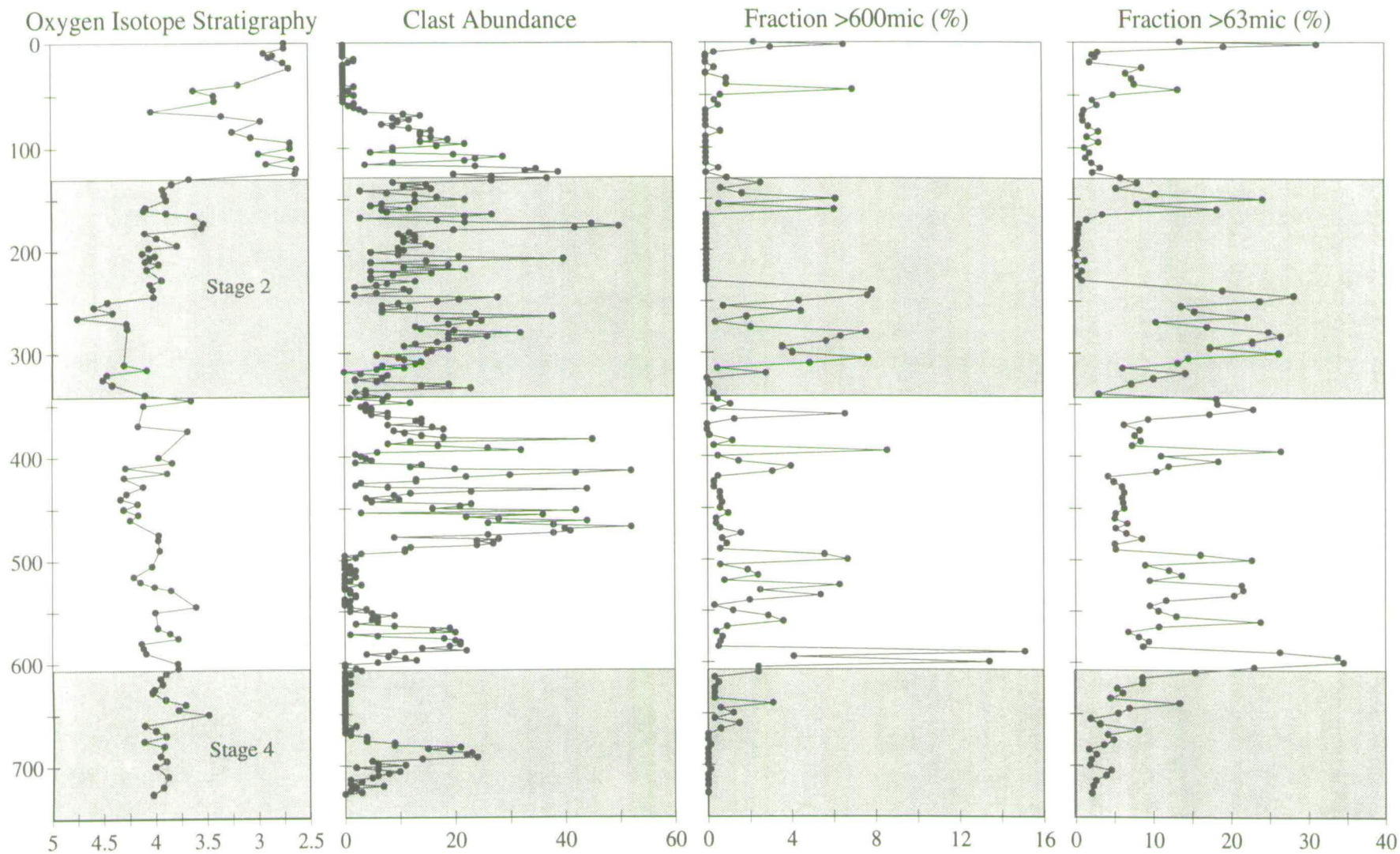

Fig. 3.4. Particle size data and clast counts for PCM7, all plotted against depth (cm). Oxygen isotope stratigraphy shown on left, glacial stages shaded. Clast abundance scale is no. clasts >2mm per 2 cm slice of core, particle size scale expressed as dry wt. %.

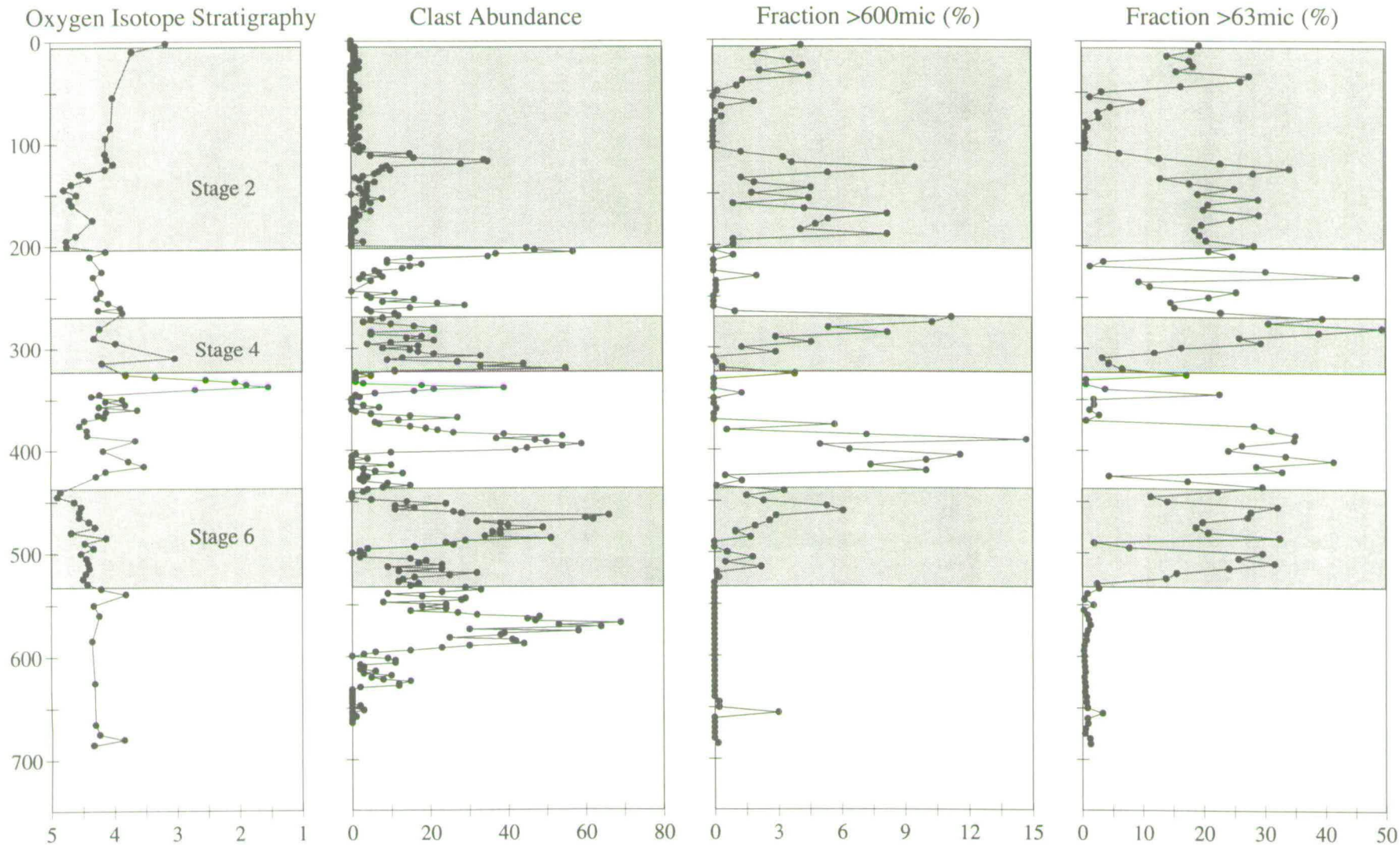

Fig. 3.5. Particle size data and clast counts for PCM5, all plotted against depth (cm). Oxygen isotope stratigraphy shown on the left, glacial stages are shaded. Clast abundance scale is no. clasts >2mm per 2cm slice of core, particle size scale expressed as dry wt. %.

The next peak has an asymmetrical appearance, rising very rapidly to 59 counts at 394cm, then decreasing gradually reaching 0 clast abundance by 360cm. Numbers remain low until 344cm, a short sharp spike reaching 39 clasts then lasts until 336cm, numbers return to near 0 briefly before the next peak at 320cm. This peak is also asymmetrical in shape, but has a rather more ragged outline. The highest value of 55 is encountered at 320cm, but clast numbers rapidly decrease, and fluctuate between 5-25 until 246cm. The opposite trend then occurs with clast numbers increasing gradually, reaching a peak of 57 at 206cm, then dropping off to 0 by 200cm. The next section from 200-168cm has values of 0 or 1, at this point the abundances increase slightly to between 1-5 until 130cm. There is then an exponential build up in clast counts reaching a peak of 35 at 118cm, then a rapid plummet to around 0 at 108cm. The rest of the core is characterised by very low clast abundances of below 2.

PCM30.

The clast counts from PCM30 do not show such clear cycles as PCM5, values range from 0-62, and tend to fluctuate rapidly, fig. 3.6. A description of the trends that are discernible are given below.

From the base of the core until 568cm there are a moderate number of clasts, 10-30, from 568-542cm there is a distinct trough, with lower numbers of below 10 clasts. Values then increase gradually to reach a peak of 33 clasts at 504cm before decreasing rapidly to a short trough. Over the next section up to 450cm clast numbers are fairly constant at about 20, but has two peaks superimposed on this, one of 31 clasts at 474cm, and the other of 48 clasts at 464cm. From 448-444cm there is a definite low in abundance with below 5 clasts, this is followed by a section of sustained high abundance from 438-414cm, between 40-62 clasts. The following section of low abundances is interrupted by one isolated peak of 38 clasts at 398cm. The next major high in clast abundance occurs between 384-364cm with values from 25-45. A drop with values ranging from 10-20 then occurs lasting until 284cm, though one peak of 35 clasts is present within this section at 314-312cm. From 280-274 clasts are virtually absent, below 5, from the record, but rapidly increase to high values from 270-196cm. This section is characterised by abundances of over 20, one short section from 230-226cm occurs where clast numbers drop to about 5.

After this section clast numbers remain below 10 until 164cm, where they increase rapidly to 30 before dropping to 10-20 until 134cm. At this point there is a minor trough with no clasts, 130cm, then a short peak of values between 15-20 clasts from 126-122cm.

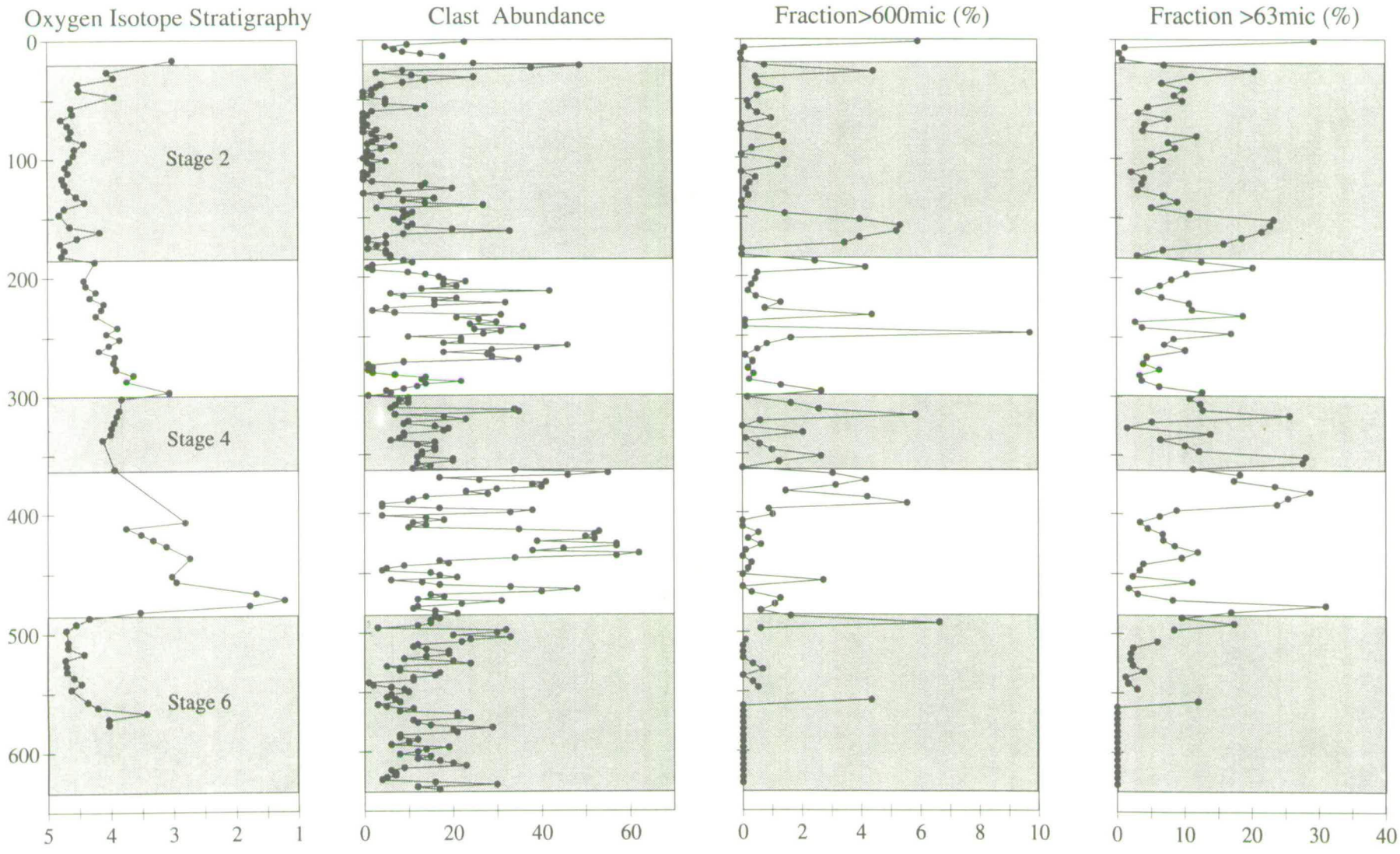

Fig. 3.6 Particle size data and clast counts for PCM30, all plotted against depth (cm). Oxygen isotope stratigraphy shown on left, glacial stages shaded. Clast abundance scale is no. clasts >2mm per 2cm slice of core, particle size scale expressed as dry wt. %.

There is then a sustained section of very low clast numbers from 0-5 until 36cm, within this section there is a minor peak where numbers reach 14 from 58-56cm. Clast numbers increase again from 34cm reaching a dominant peak of 49 at 22cm before lowering to numbers between 10-20 until the top of the core.

3.4.3. Grain-size from dry sieving measurements:

In this study the grain-size distribution of the coarser than 63μm and coarser than 600μm fractions were measured, the results are expressed as dry weight percent. A description of the processing and sampling technique used is given in Appendix 1. In all cores the percentage material coarser than 63μm correlates very well with the coarser than 600μm results. The results shall be described for each core separately.

PCM5.

The same general pattern of rapid fluctuations is present in PCM5 also, seen in fig. 3.5, changes from 1 or 2% to 30 or 40% occur within one or two samples, and a maximum value of 50% coarser than 63μm is reached. In some areas differences between the two size records are present. The greater than 600μm fraction reaches a peak of 14%, but values are generally under 10% throughout the core, the troughs commonly between 0-1%.

From the base of the core until 530cm there is a very low abundance of coarse material, below 3% coarser than 63μm, and negligible quantities of material coarser than 600μm. At this point, which coincides with the start of isotope stage 6, there is a rapid increase in coarser input to the samples. From 525-375cm the amount of material coarser than 63μm ranges between 15-40%, with two minor troughs of below 5% one at 490cm the other at 425cm. The coarser than 600μm shows three distinct peaks over this same interval increasing in magnitude upwards. The first one very small from 515-500cm about 2%, the second from 485-440cm having a peak of 6%, and the final one 420-375cm having a much larger peak of 15%. This final peak occurs within the beginning of isotope stage 5. Values for both parameters then remain low until 310cm, 1-2% greater than 63μm, 0-1% greater than 600μm (except for an isolated peak at 345cm). There is then a gradual increase in both parameters reaching a peak between 280-270cm of 50% over 63μm, and 10% over 600μm. At this point the greater than 600μm material reduces to negligible amounts until 200cm, this period represents isotope stage 3. The coarser than 63μm fraction remains moderately high throughout this period, over 10% except for one trough at 210cm,

and climbs to even higher values within peak stage 2 and just after, between 20-30%, decreasing gradually to below 1% at 105cm. The coarser than 600μm fraction increases rapidly at 195cm, reaching values between 5-10% until 165cm, values then reduce slightly to below 5% before rising to another peak of 9.5% at 125cm, then dropping gradually to 0% by 105cm. In the rest of the core the two fractions mirror each other, remaining low until 80cm, then increasing gradually to a peak at 35cm, 27% over 63μm, and 4% over 600μm. Values remain at or just below this level until the top of the core.

PCM7.

The particle size results for PCM7 are plotted in fig. 3.4 alongside the oxygen isotope stratigraphy. The greater than 63μm and greater than 600μm curves are described together, the only difference between the two is the magnitude of peaks. The record is characterised in general by very rapid fluctuations before and after large isolated peaks. The peaks in coarser than 63μm material are generally between 15-35%, and the low troughs under 5%, the highest values encountered are 34% at 600cm. For coarser than 600μm peaks attain values from 4-8%, and the troughs are commonly under 1%.

At the base of the core, within stage 4, there is a low abundance of material coarser than 63μm, below 5%, and negligible amount coarser than 600μm. During stage 4 there is a gradual increase in grain-size culminating in a peak of over 30% coarser than 63μm, and 13% greater than 600μm, at the beginning of stage 3, 600cm. During the early period of stage 3, up to 490cm, there is a background abundance of over 10% material coarser than 63μm, superimposed on this are 3 peaks with over 20%, these values are 1% and 7% respectively for coarser than 600μm fraction. This is followed by a period of lower grain-size until 420cm, about 5% greater than 63, and 1% greater than 600μm. The last section of stage 3, up to 345cm, is characterised by higher amounts of coarse material, two peaks of between 20-25% separated by a period of 7-8% material greater than 63μm, up to 8% greater than 600μm. The initial period of stage 2 has low amounts of coarse material, but this rapidly builds up to a peak of 25-30% coarser than 63μm between the two heavy isotopic peaks at 325 and 255cm. Values then drop to 10-15% during the peak glacial period from 260-255cm, then rise to a high of 28% at 240cm. Values for the coarser than 600μm reach 8% during peaks, 305-280cm and 245-240cm, and drop to 1% during the heavy isotope glacial peaks between. The values then plummet to below 1% greater then 63μm from 230-170cm, and no material coarser than 600μm. At this point values suddenly

rise again reaching a peak of 24% at 150cm, then drop off to between 1-5% from 130-50cm in the coarser than 63μm fraction, material coarser than 600μm remains below 1% for this period. From 45-25cm values between 6-14% and about 1% for greater than 63μm and 600μm respectively are present. There is then a trough before the final peak in values of the top 5cm of the core, 15-30% and 2-7% for the two size ranges.

PCM30.

The variations over much of PCM30 are rather more muted when compared to the previous two cores, shown in fig. 3.6. Peak values tend to be slightly lower, generally below 30% coarser than 63μm and roughly 6% coarser than 600μm, while the values in the troughs tends to be higher, a background of 5% coarser than 63μm. The two size ranges tend to match each other very accurately in this core.

The base of the core from 627-562cm contains no material coarser than 63μm at all, this is within early stage 6. At 557cm there is a rapid increase in both fractions, up to 12% coarser than 63μm, and 4% coarser than 600μm, this is a short lived peak and values reduce immediately to below 5% and 1% for the two fractions until 502cm. A gradual increase in the greater than 63μm material culminates in a peak of 30% after the end of stage 6. The greater than 600μm fraction peaks at the end of stage 6, 6%, before dropping to moderate values of 1% until 450cm, where it drops to negligible quantities until 407cm. Over this section the coarser than 63μm fraction drops to below 5% from 467-442cm, there is then a minor peak of 12% at 432cm then gradual decrease to 3% at 407cm, and then a rapid increase to a peak of 28% at 382cm. Values remain relatively high until 297cm, above 10% except for a minor trough of 1% at 327cm. The coarser than 600μm fraction follows the variations in 63μm material over this section, reaching a peak of 5% at 392cm, staying relatively high until a rapid drop to 0% at 362cm. Values then fluctuate rapidly until a more prolonged section of low values are reached between 287-257cm, below 0.5%. Over this section the coarser than 63μm material drops to it's background values of 5-6%.

From 262-132cm four distinct peaks are present superimposed on these background values. The peaks are between 15 and 20% material coarser than 63μm, and are mirrored by peaks between 4.5 and 9% in the coarser than 600μm fraction (the background for 600μm material is less than 0.5% over this section). These four peaks are found at 247cm, 232cm, 192cm and from 172-152cm. At this point the coarser than 63μm record is characterised by a gradual increase in values from 3% at 127cm

to 20% at 27cm, values then drop to 1% until a sharp peak of 29% at the top of the core occurs. The coarser than 600μm fraction remains at stable values of below 1.5% from 147cm until a peak of 4.4% at 27cm is reached. The quantity of material coarser than 600μm then drops to negligible amounts until a peak of 6% at the top of the core, similar to the coarser than 63μm fraction.

3.4.4. Grain-size distribution from Coulter LS-100 measurements

Samples taken every 5cm from PCM5 were passed through a Coulter LS-100 particle size analyser. The principles and details of this technique are described in appendix 1. One important limiting factor of this technique is there is an upper limit to the grain-size that can be measured on the machine. For this reason all samples have to be sieved at 500μm to remove material too coarse to be measured. This means that the volume percentage results obtained are in some places slightly higher than they should be. This technique was used on PCM5 because it is very accurate at measuring fine grained material of clay and silt grain-size. From the results obtained the volume percent material in the clay, silt and sand fractions has been plotted, these are shown in fig. 3.7 along with the oxygen isotope stratigraphy (note the change in horizontal scale, clay and sand fraction 0-60%, silt fraction 30-90%). These graphs will be described briefly below.

Clay fraction.

There is a fairly constant background value of 20% with sharp fluctuations above and below this value. Values of 20-25% are found initially from 685-615cm, they then increase slightly to 25-30% until 500cm. The next section is characterised by sharp peaks superimposed on background values of around 20%, the peaks are 47% at 490-495cm, 37% at 460cm, 40% at 450-445cm, 35% at 425-420cm and 30% at 370-365cm. From 340 to 265cm values increase slightly to around 30% with several lower spikes, 12% at 280cm and 15% at 270cm. A marked trough is found at this point, only 6-8% from 260-245cm, after a short peak of 30% values decrease again to 10-15%, and drop to as low as 5% at 200cm. A dramatic increase to values over 30% is then found lasting until 160cm, here the record first decreases then increases rapidly to 45% at 150cm. It then decreases to 25% for 10cm, then rises to 32% for 10cm and drops to 20% at 125cm. There is then a gradual increase to values of around 30% until 55cm, at this point values decrease to 20-25% until the top of the core.

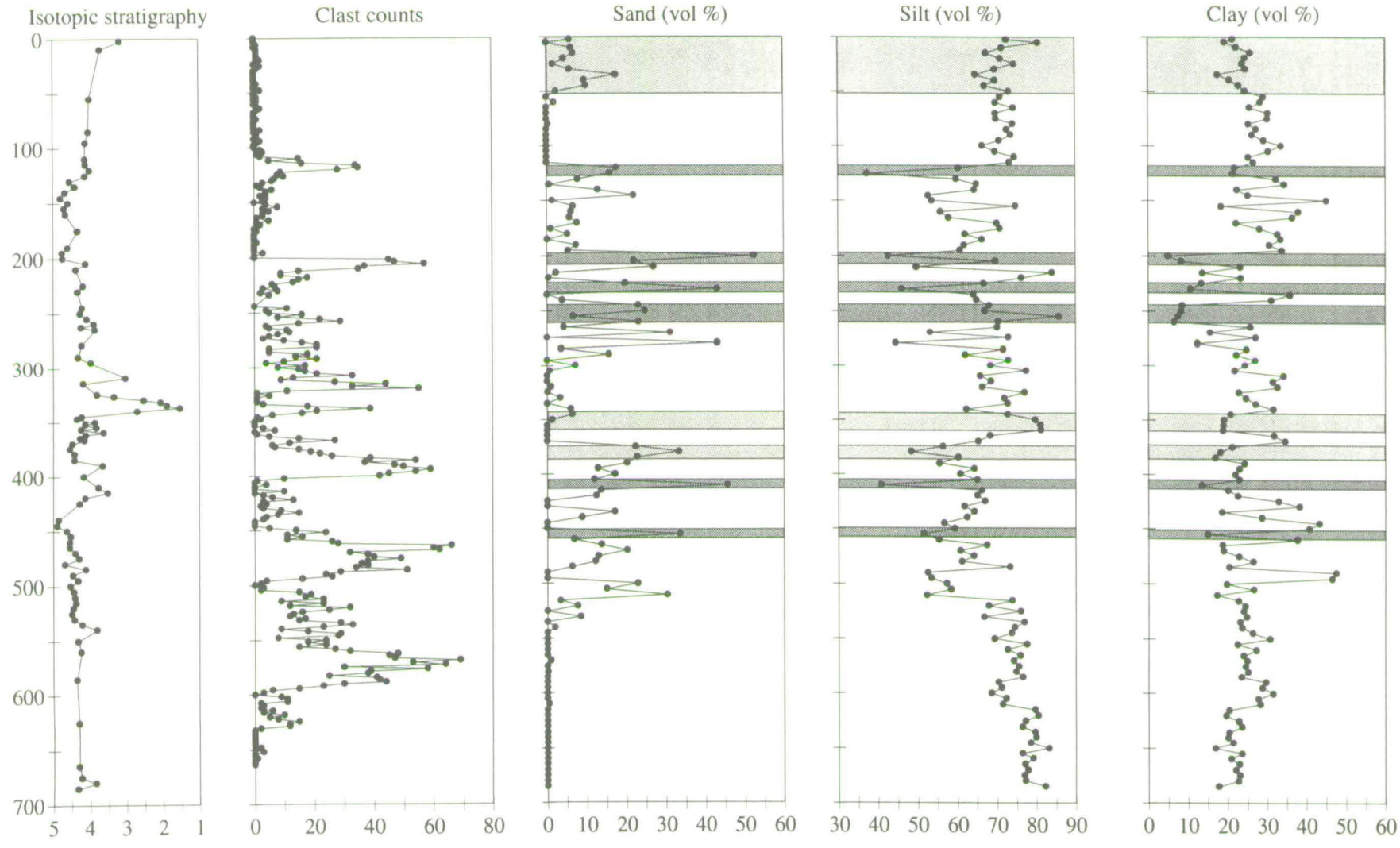

Fig. 3.7. Particle size data from PCM5, volume % measurements from Coulter Counter analysis, clast counts from x-ray photographs. Oxygen isotope stratigraphy shown on left, all plotted against depth. The light shaded sections represent periods of moderate winnowing, the darker shading represents periods with strong winnowing.

Silt fraction.

The silt fraction makes up the bulk of sediment throughout the core, rarely dropping below 50%, and commonly 70% or above. Values begin at around 80% from 685-615cm, a reduction to 70-75% is seen from 610-515cm. There is a sharp drop to 50-55% at this point until 490cm, where values rise to 60-70% until 465cm. Values then drop to 55%, there is then a gradual rise to values of 65% at 420cm followed by a gradual decrease to a trough of 50% at 380cm. This is followed by an increase to values of 80% from 360-350cm, values then drop to between 65-75% until 285cm. From this point until 120cm the record is fairly spiky, but a general decrease in silt fraction can be seen with several very low spikes (correlating to periods of high sand fraction. At 120cm the values become more stable, 65-75%.

Sand fraction.

The volume of material in the sand fraction is, understandably, less than in the other fractions. Background values are zero and peaks are superimposed on this. The sand fraction remains at zero from the base of the core until 535cm, there are then four peaks in abundance between 535 and 375cm. The first peak from 530-500cm reaches values from 20-30%, the next peak is slightly larger, from 485-455cm with highest values of 33%. The third peak is a minor one, 440-435cm up to 17%, and the fourth peak is the largest from 420-375cm with values around 15-20% and a peak of 45%. There is then another section of very low values until 305cm. The next section from 300-120cm is characterised by very rapid fluctuations in sand content, often changing from zero to 20 or 30% from one sample to the next. Peaks of 20% or over are found at 280cm, 270cm, 260cm, 250cm, 230cm, 210-200cm (up to 52% at 200cm), and 145cm. A section of no sand content is then encountered until 55cm when values increase to 5-10% (peak of 17% at 35cm) until the core top.

3.4.5. Comparison of Coulter Counter and dry sieved results

Particle size analysis of PCM5 has been carried out using two techniques. Using a Coulter LS-100 particle size analyser, and by dry sieving residue material after washing. The Coulter counter uses the principle of Frauhofer diffraction of laser light, light falling on suspended sediment particles is deflected (diffracted) by an amount dependant on, among other things, the diameter of the particle. It gives a value of maximum diameter of particle. Unfortunately material coarser than 500μm has to be removed before measurements are made. So in this case where there are sections of the core with significant amounts of material coarser than 500μm it will

over estimate the actual values. The actual value obtained is in volume percent. This technique was used because it could accurately measure the clay and silt fractions. The dry sieving technique was used to measure material between 63-600μm and material coarser than 600μm. The values are expressed as dry weight percent. This technique enabled the coarser fractions to be measured more accurately.

The sand fraction content of PCM5 using both these methods is shown in fig. 3.8. This shows that although the actual values are not the same the general trends are identical using both techniques. The coulter counter values are generally lower than the dry sieved values. There are several reasons why the values are not closer. Firstly the coulter counter values are for a grain-size between 63-500μm, whereas the dry sieved measurements are for a grain-size between 63-600μm, the larger values in dry sieved results are therefore not so surprising. Also the values are expressed in two different forms, one in volume percent and one in weight percent. The coulter counter assumes a constant density for all particle sizes, which is an unlikely scenario.

Taking the above into account the measurements from the coulter counter are still a very useful measure of clay and silt content of PCM5, for coarser grain-sizes the dry sieved results are more accurate.

3.5. Correlation between particle size distribution and clast counts

In this section the clast counts will be correlated with the coarser than 63μm fraction, or sand fraction, produced from the dry sieving measurements. The correlation between these two parameters is mixed, good in some areas but very poor in others. This correlation will be briefly outlined for PCM5 and PCM7 below.

PCM5.

The correlation between the two parameters in PCM5, fig. 3.5, is considerably better than in PCM7. Both parameters are low at the base of the core. The first major peak in clast counts from 560-600cm is not seen at all in the sand fraction. The relatively high clast numbers found from 560-510cm do correspond partially to a peak in sand material from 500-530cm. At this point a distinct trough appears in both measurements, this is followed by a major peak in both parameters too. The sand fraction remains high, with two minor troughs, until 375cm. During this period clast counts reduce to fairly low values from 445-405cm, but then increase dramatically to correlate with the end of the major peak in sand material.

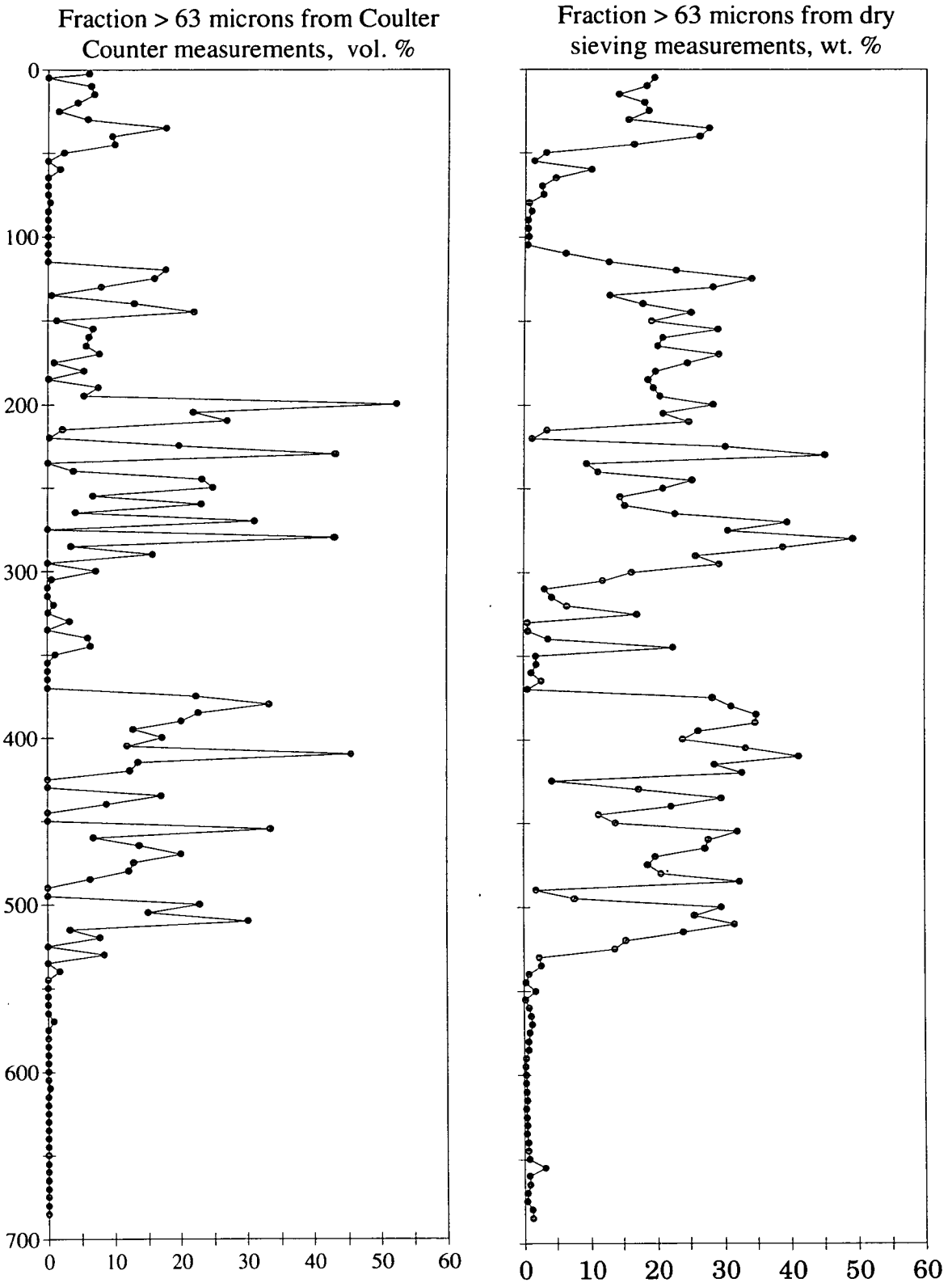

Fig. 3. 8. Comparison of particle size methods used for analysis of PCM5. Graph on the left shows volume % sand fraction from Coulter LS-100 particle size analyser, graph on the right shows weight % sand fraction from dry sieving measurement.

The next section from 364-322cm is characterised by low clast numbers except for a peak at 338cm, the sand fraction matches this, the peak at a similar position. Both parameters increase during stage 4, beginning to increase around 320cm. The sand fraction remains high until 115cm. The clast counts are high for the first part of this section, and at the end of this section, in the central part the two records are radically different. The peak in sand fraction found at the top of the core is not represented in clast counts.

PCM7.

In this section the clast counts will be correlated to the fraction >63μm only, the sand fraction, fig. 3.4 shows this correlation. At the base of the core the high abundance of clasts coincides with low amounts sand. The next peak in clast counts between 600-550cm correlates with a high in the sand fraction, the clasts then disappear until 500cm while the sand fraction remains abundant. At this point the clast abundance increases and remains relatively high until near the top of the core at 70cm. The sand fraction drops off, however, during this initial period until 420cm. There are two further major troughs in the sand fraction which coincide with relatively high clast counts, 230-265cm and 125-55cm. The top 70cm of the core have very few clasts, but have relatively high abundance of sand fraction. The correlation between these two parameters is predominantly poor throughout PCM7.

3.6. Interpretation of particle size data and x-ray photographs

3.6.1. Characterisation of IRD

In previous studies, as mentioned in the introduction, material coarser than 63μm has commonly been used to represent IRD in marine cores. This assumption may be valid for material cored far from continental landmasses in deep abyssal environments, but in this study this is not the case. The material cored is predominantly from the continental slope, ice masses may have commonly reached the shelf edge during glacial periods, so coarse material may be supplied by processes other than ice rafting. In this study three parameters were measured to quantify ice rafted detritus input in the Greenland Sea, clast counts and percentage material coarser than 63μm and 600μm. The measurements of material coarser than 63μm and 600μm correlated very well, so these two parameters record the same process. The clast counts differ quite dramatically from this record in places, so in some areas must be influenced by different processes.

3.6.2. Interpretation of clast counts from x-ray photographs

At first sight, it seems likely, that counts of clasts greater than 2mm and commonly several cm in size, reflects input of dropstones from floating icebergs. There are, however other possibilities. From clast counts and from the x-rays themselves fluctuations in the concentration of clasts are clearly visible, figs. 3.1, 3.2, 3.3 and plate4. Changing concentration of clast content and presence of sedimentary structures were used to differentiate between four types of deposits. The first type is characterised by sections where clasts are very abundant, a wide range in size of clasts (from barely visible to several cm) are found, and these are poorly sorted. These sections have the appearance of rapid dumps of material over a short time. Other sections where clasts are described as common in the interpretative logs, figs. 3.1, 3.2, 3.3, are dominated by a much smaller range in clast size, and are randomly scattered in a matrix of finer material. The final two types of deposit have few clasts and are differentiated on presence of laminations. The third type consists of homogeneous material with occasional clasts present, and no laminations. The final type of material differentiated from the x-rays was characterised by strong laminations, sometimes parallel but commonly cross-bedded or disturbed. Clasts were rare in these deposits.

The clasts in the latter three types of deposits almost certainly do originate from icebergs, so are true dropstones, or IRD. The material found in sections where clasts are termed very abundant may originate from other sources. Ice at its maximum extent at the shelf edge may push material over the edge, or basal meltout may wash detritus over the edge, this material would be very poorly sorted and consist of a wide range of particle sizes, it would also have the appearance of a rapid dump of poorly sorted material, this is one option for the origin of sediment with very abundant clasts.

Another option is origination from debris flows caused by collapse of an oversteepened slope. Boulton, (1990) suggested this process is common on glaciated continental slopes. It seems unlikely that this would account for anything more than a small proportion of the material found in these cores. If debris flows were common, correlation between cores based on magnetic susceptibility and oxygen isotope stratigraphy (see chapter 2) would not be possible. So any debris flows that are present must be of minor importance.

A third possible origin for material packed with poorly sorted clasts is from icebergs. It is common for icebergs to have large amounts of debris lying on their surface, as a result of concentration by ablation, supraglacial moraine, or material washed on to the ice surface by meltwater streams, (Gilbert, 1990). This material may be dumped *en masse* due to iceberg instability; for example icebergs tipping over, forming the type of deposit with abundant clasts found in the cores of the present study. Dropstones released as single particles from iceberg melting would also contribute to this type of deposit.

The final type of deposit found in the x-ray phototgraphs is one with strong laminations, sometimes cross-bedded of disturbed. Clasts (dropstones) are usually absent from these deposits, but are found occasionally. The presence of laminations, and especially cross-bedding, suggests this material was deposited in an environment characterised by currents. Anderson *et al.* (1979) described laminated sediments from the continental slope of Antarctica, this material was interpreted as a contourite. It seems likely that the deposits found in this study with strong laminations are also contourites. This is supported by evidence from the continental margin of the Barents Sea in Vorren *et al.* (1989). During interglacials strong along slope currents are formed by relatively warm Atlantic water flowing north in the Norwegian Current, this winnows slope sediments leaving a sandy lag. This becomes the West Spitsbergen Current further north possibly having a similar effect on slope sediments found in the study area, acting as a contour current. Another interpretation is that these sediments were deposited by turbidity currents formed by cold dense water flowing off the shelf and down the slope.

3.6.3. Interpretation of particle size data, the effects of winnowing

Data from the dry sieved measurements suggests that the sand fraction and fraction coarser than 600μm are controlled by the same process as they correlate perfectly. Some of this material is produced from iceberg melting, but there are distinct sections where the sand content does not correlate with the clast counts from the x-rays, so there must be other processes causing peaks in sand fraction. High concentrations of sand may result from a similar ice meltout or ice tongue push mechanism as suggested above for the occurrence of high clast numbers, for example during early stage 6, early substage 5b, and just after peak stage 2 in PCM5, fig. 3.4.

Sections where sand content is high but clast counts from x-rays are low must result from a different process. Sections influenced by winnowing have been identified in PCM5 from the Coulter Counter particle size measurements, fig. 3.7. The proportion of clasts is independent of the winnowing process. Sections with low clay content and high sand content have been shaded in fig. 3.7 and represent winnowed horizons. The darker shading represents strong winnowing, low clay and low silt with high sand. Less intense winnowing is identified by lighter shading, these sections have high silt content, so weaker currents not strong enough to remove the silt fraction were dominant. Winnowing must have been produced by stronger than normal bottom currents. These currents may have been contour currents, as mentioned above, from the northward flowing West Spitsbergen Current, another explanation would be the formation of turbidity currents by cold dense meltwater flowing over the shelf edge. The recognition of winnowed horizons is slightly more problematical for PCM7 as no fine grained particle size data is available. Winnowed horizons have been identified by the high percentage of material coarser than 63μm during sections with low clast content. If the coarse material does not correlate with high clast sections then it is most likely that it does not originate from icebergs, so must have been produced by either winnowing or by high foraminiferal abundances. Fig. 3.2 shows the fraction coarser than 63μm plotted with clast counts and the x-ray interpretive log. The winnowed horizons have been shaded. A good correlation can be seen between the winnowed horizon at 490-560cm and the section with strong laminations from 495-555cm seen in the x-rays. This confirms the idea that at least some of the laminated sections are produced by currents, though PCM5 shows a poor correlation between winnowed horizons and laminated sediments. The winnowed horizons appear to be more common during interglacial or interstadial periods, as noted by Vorren *et al.* (1989) from the Barents Sea margin, for example the top 50cm in PCM7, and during parts of stage 3, 555-495cm in PCM7 and 220-250cm in PCM5, see figs. 3.2 and 3.7. The absolute abundance of foraminiferal tests may also cause a peak in the sand fraction, see figs. 3.9 and 3.10. Possible sections where high foraminiferal abundance may influence the particle size distribution have been shaded.

3.6.4. Explanation of differences between sand fraction and clast counts

The sections with high clast counts but low percent material coarser than 63μm are less easy to explain. One would expect a section with abundant clasts to have a high weight percent coarser than 63μm value also. This is not always the case and may be a result of the measuring techniques used.

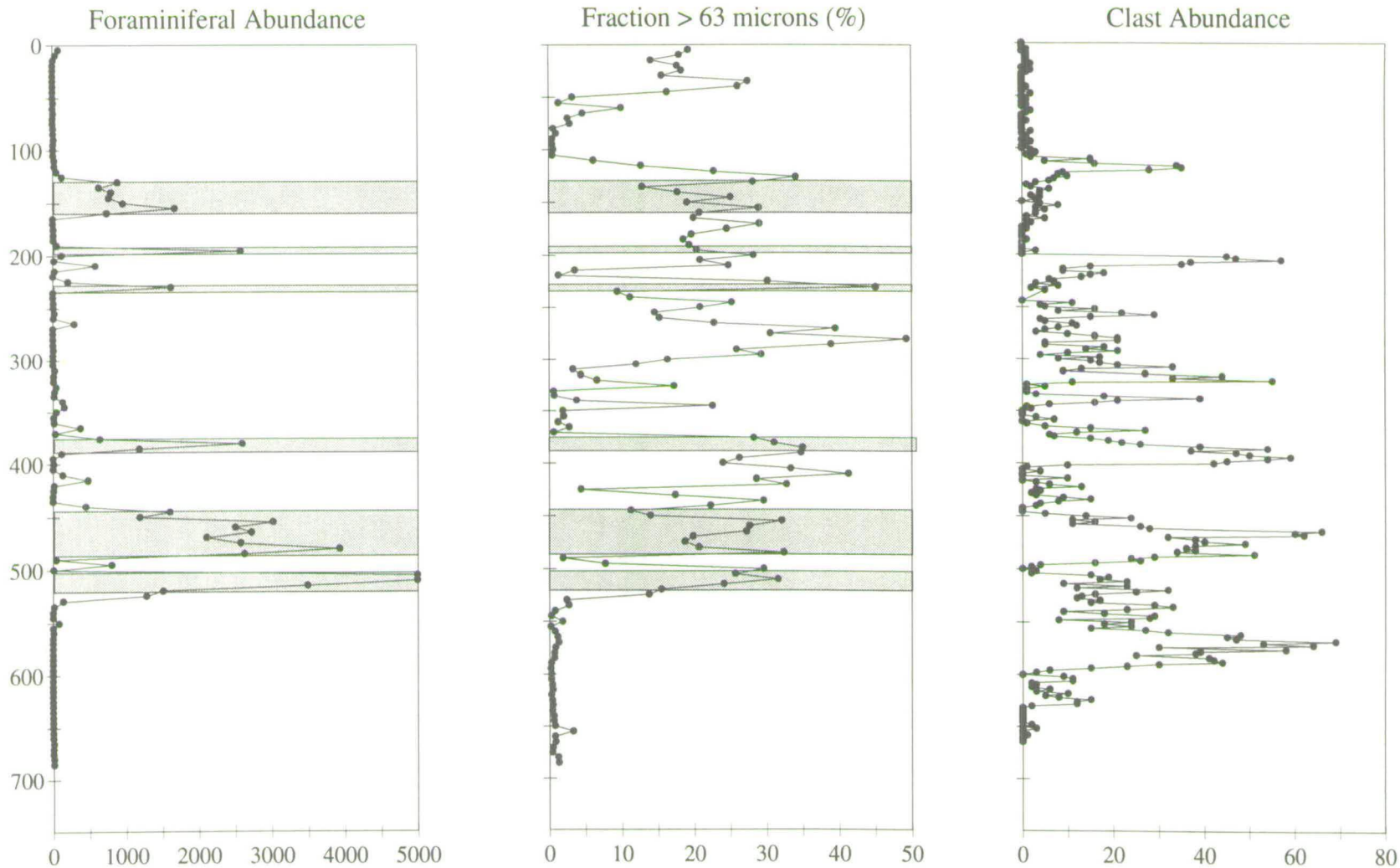

Fig. 3.9. Record of foraminiferal abundance with the particle size data for PCM5. Some of the peaks in the greater than 63mic fraction may be caused by high foraminiferal abundance, these sections are shaded above. All graphs plotted against depth, foraminiferal abundance scale is specimens/gm dry wt.

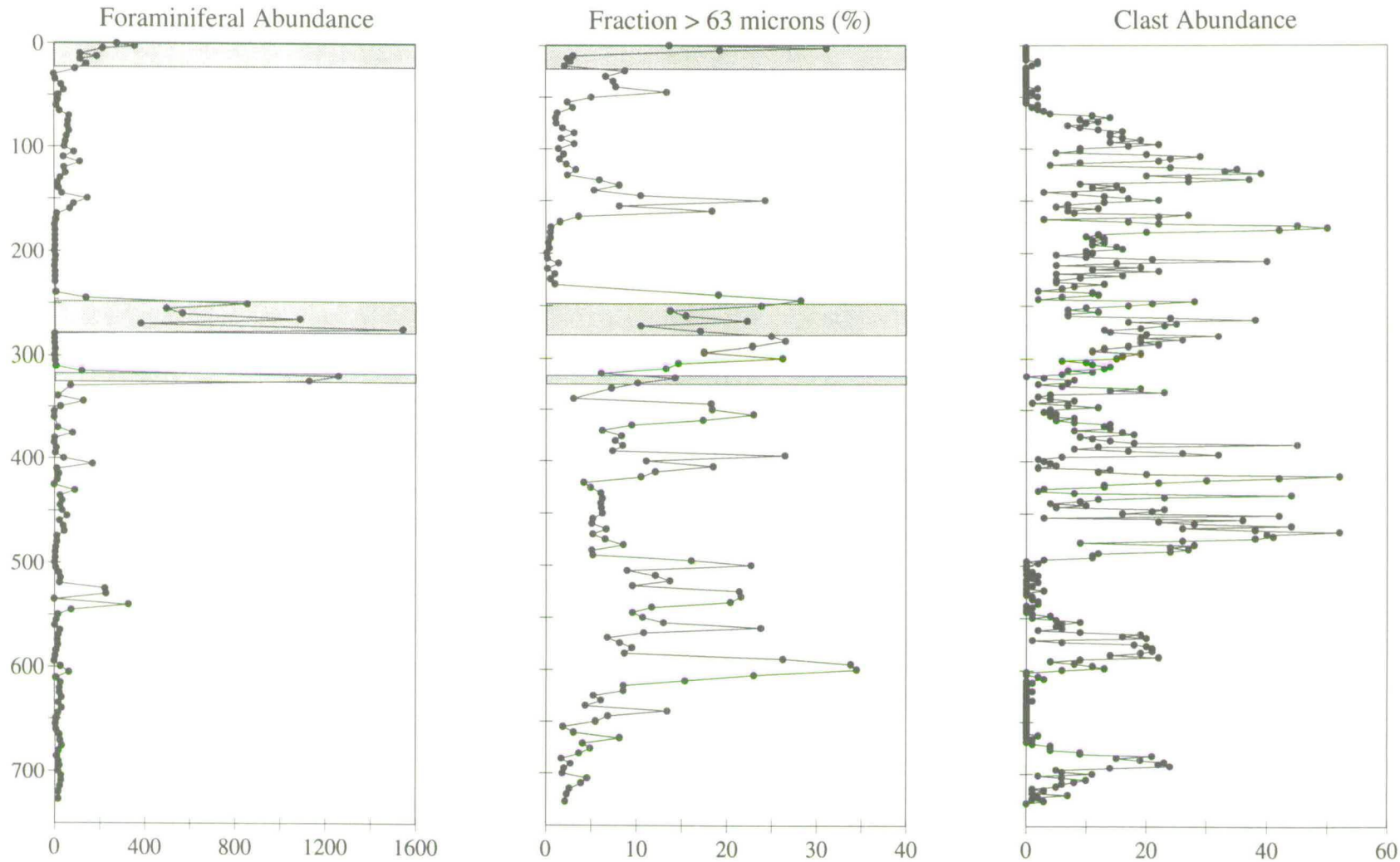

Fig. 3.10. Record of foraminiferal abundance with particle size data from PCM7. Some of the peaks in the greater than 63 micron fraction may be caused by high foraminiferal abundance, these sections are shaded. All graphs plotted against depth, foraminiferal abundance scale is specimens/gm dry wt.

The clast counts are a qualitative measure, they do not relate to sample weight, so a large increase in clast numbers may have a relatively minor impact on the weight of various fractions in the sample. The composition of the clasts may account for some discrepancy between the two parameters. Some clasts seen in the x-ray photographs may be composed of frozen clumps of fine grained material. These would be seen in the x-rays as discrete particles, but during the processing procedure for the particle size measurements they would be broken up into their constituent particles possibly finer than 63μm.

In this study measurements of particle size and clast counts have been found to be affected by different processes. The actual clast counts from x-ray photographs are in most cases an accurate measure of IRD input to the system caused by iceberg calving, and are thus a measure of calving rates. Periods of very high clast abundance are also influenced by material washing out from the base of an ice mass at the shelf edge. The abundance of the fraction coarser than 63μm record different processes though. Peaks in this grain-size may result from winnowing, or from ice washout and pushing material over the edge of the continental shelf, some peaks are also obviously influenced by increased clast abundance. This has important implications for studies such as that of Hebbeln (1992), where the fraction coarser than 63μm was assumed to represent IRD input in the cores examined. Further offshore away from the influences of slope processes and bottom currents the coarser than 63μm fraction probably is an accurate representation of IRD input. In this study, however, proximity to the continental slope and submarine fan complexes as well as strong bottom current fluctuations also influence material coarser than 63μm.

3.7. Source of IRD

There is strong evidence suggesting the source area for the material coarser than 63μm is the local Spitsbergen landmass, this is provided by geochemical measurements. Measurements of the percentage silica content in PCM5 were made by x-ray fluorescence spectrometry (for details of this technique see Appendix 1). These are shown in fig. 3.11 plotted with the dropstone counts and the fraction coarser than 63μm. A clear correlation between the silica content and coarser than 63μm fraction is present. There are two possible sources of silica in the marine system, detrital quartz or biogenic silica produced by organisms such as diatoms. Since productivity in this high arctic environment is relatively low, the biogenic silica input must also be low when compared to the terrestrial input.

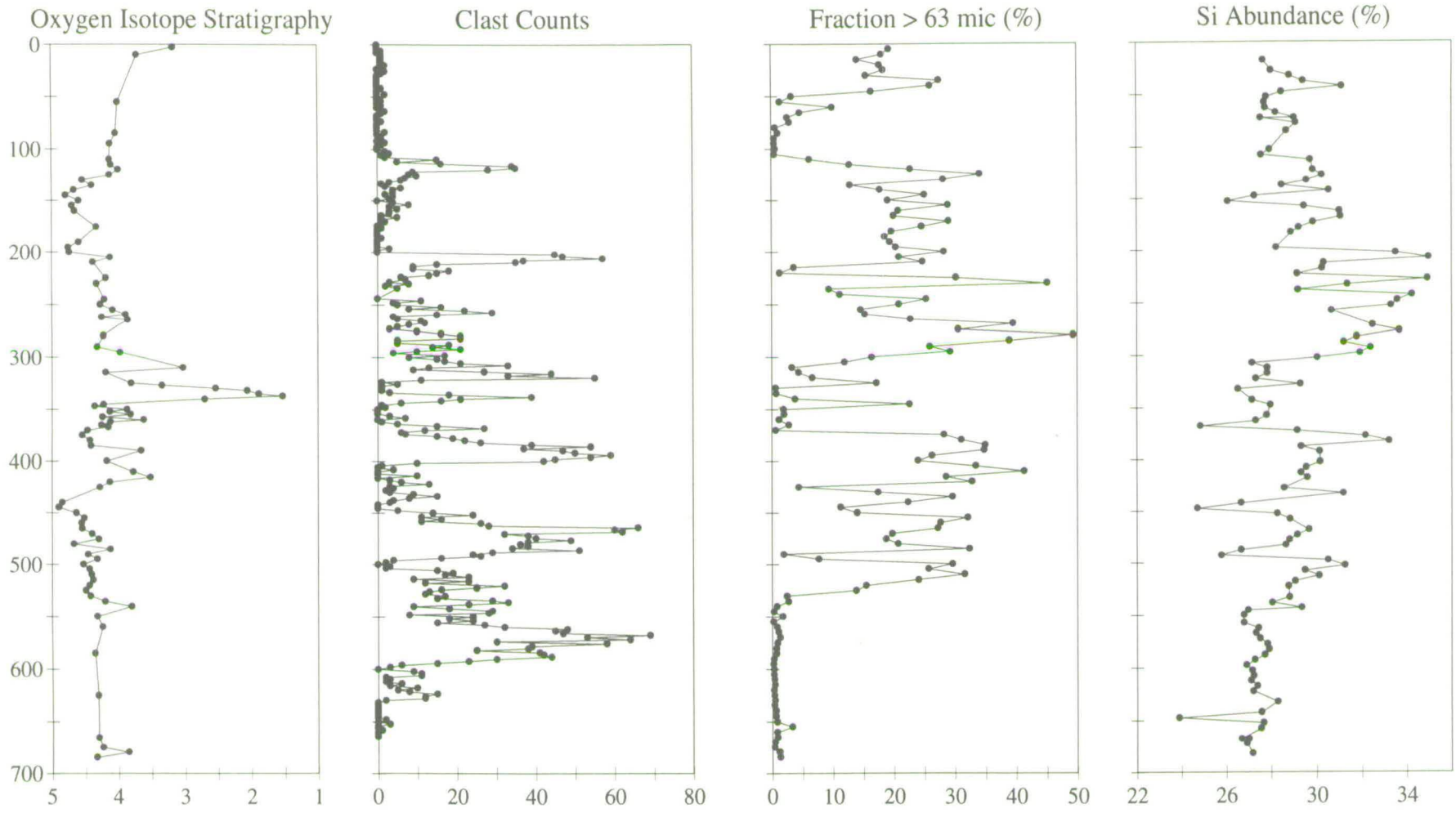

Fig. 3.11. Results from PCM5 showing the correlation between silica content and the fraction greater then 63 microns. All plotted against depth, oxygen isotope stratigraphy shown on left. The clast counts do not correlate with the silica content implying there are several sources of dropstones, not just the local fjord systems.

Quartzites and sandstones crop out over large areas of Spitsbergen (Ager, 1980 and Harland, 1961). The extensive Hecla Hoek group contains a high proportion of quartzites, and bodies of Devonian Old Red Sandstone occur in central and northern Spitsbergen, and also Triassic sandstones in central and eastern Spitsbergen. It seems most likely that these rocks provided the silica measured in PCM5. The strong correlation between silica and grain-size coarser than 63μm suggests this material was produced by eroding glaciers on the local Spitsbergen landmass.

The proximity of the sites in this study to the Spitsbergen continental margin suggests that IRD in cores, taken from dropstone counts, reflects iceberg flux from Spitsbergen. The dropstone counts do not always correlate well with the silica content in PCM5, fig. 3.11, this suggests that the icebergs may have sources other than the local west Spitsbergen fjords. Some icebergs almost certainly originate from other ice masses, possibly from the Barents Shelf carried north by the Norwegian Current, or from the Greenland ice sheet being carried in the Greenland Sea gyres. Input of IRD from these other ice masses would most probably have a minor influence on total IRD concentrations. It is also likely that icebergs produced from calving on the eastern and southern margins of the Svalbard ice mass (from other islands in the Svalbard archipelago such as Edgeoya and Barentsoya, and the eastern coast of Spitsbergen) would be carried by surface currents around the southern tip of Spitsbergen. At this point they would become entrained in the West Spitsbergen Current and be carried northwards along the western margin of Spitsbergen. The possible sources of icebergs from the Svalbard archipelago are shown in fig. 3.17.

Western Spitsbergen has a mountainous terrain, whose west coast is cut by four deep fjords (from the north, Kongsfjorden, Isfjorden, Bellsund and Hornsund) which are continued across the western continental shelf as linear troughs extending down to 300m below sea level. At the present day glaciers only calve into the sea at fjord heads. When western Spitsbergen is more heavily glaciated and ice domes extend to the western seaboard, analogues elsewhere (Antarctic Peninsula, N.W. Greenland) suggest that major fast flowing ice streams occupied the four major fjords and their related shelf troughs. These would have drawn down ice from the surrounding highlands allowing a major flux of ice across the grounding line generating icebergs from the fjords. These would combine with icebergs calving from the eastern ice mass to produce large peaks in IRD during periods of rapid calving. High calving rates may be produced by several factors, breakup of a relatively extensive ice mass, rapid advance of ice tongues caused by high moisture supply, or by a relative sea level

rise breaking up an ice mass on the continental shelf, these were discussed in the introduction.

3.8. General history of Svalbard ice cap from x-ray interpretation and particle size data

An interpretation of the general characteristics of the Svalbard ice cap can be made from the concentration of clasts, and general characteristics of x-ray photographs of cored material in this study. Particle size data have also been considered in this interpretation.

The base of PCM5 provides a record of oxygen isotope stage 7. Figures 3.12, 3.13, and 3.14 show the clast counts and sand fraction along with oxygen isotope stratigraphy plotted against time, glacial stages and cold substages are shaded. The base of PCM5 shows no IRD present and very little material coarser than 63μm, this represents an interglacial period when the ice cap was relatively small, glaciers far up the fjords. Then towards the end of stage 7, 192.5 ka, the amount of IRD begins to increase reaching a peak at 185 ka before dropping off to slightly lower values until the end of stage 7, the >63μm fraction remains very low during this period. The most likely explanation for this is the rapid build up of the Svalbard ice cap. Towards the end of the interglacial period relatively warm sea surface temperatures (SST's) and warm air currents encourage high evaporation, which ultimately leads to rapid accumulation of the ice cap. High accumulation rates would result in rapid advance of ice onto and across the continental shelf. The buoyancy effect of the sea and summer melting would in turn produce rapid calving, which leads to the peak in IRD. The high clast composition of this peak suggests material is being dumped *en masse* by heavily laden icebergs. The slight drop in IRD towards the end of stage 7 resulted from a lowering in temperatures leading to the glacial stage 6, this would reduce calving rates due to lower accumulation, also a sea level fall would increase the stability of an ice mass on the shelf causing a lower IRD supply.

At the start of stage 6 a rapid increase in grain-size occurs, clast content remains high, and is very poorly sorted. This corresponds to the ice tongues reaching the edge of the continental shelf and pushing coarse material over the edge, basal melting would also flush coarse terrestrially derived material onto the continental slope. The still advancing ice tongues combined with summer melting would retain high calving rates.

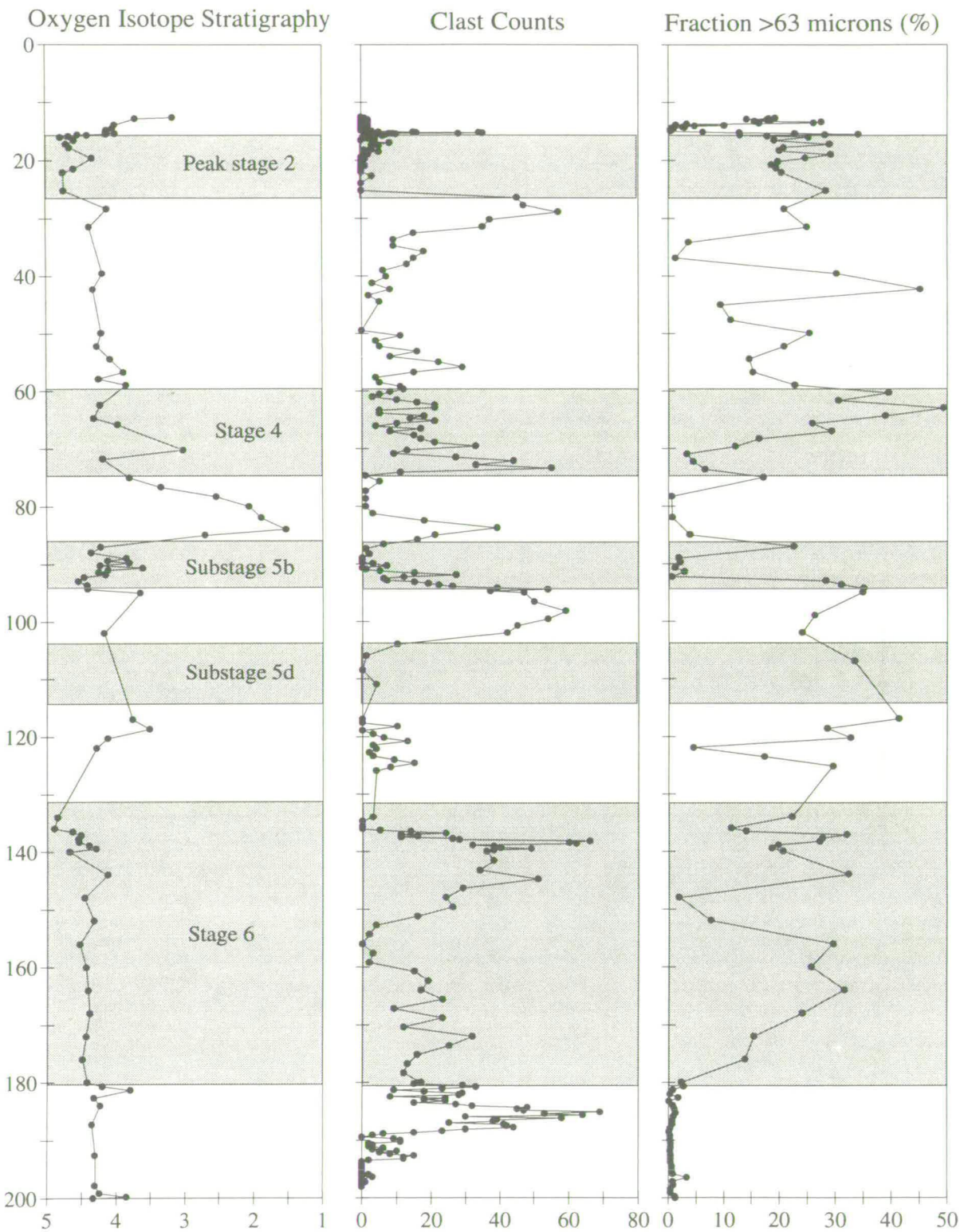

Fig. 3.12. IRD and particle size record of PCM5 plotted against age. Oxygen isotope stratigraphy on the left with glacial stages and substages shaded, horizontal scale isotope composition in per mil w.r.t. PDB. Clast counts horizontal scale clast numbers per 2cm slice of core, fraction >63 microns scale expressed as dry wt. %..

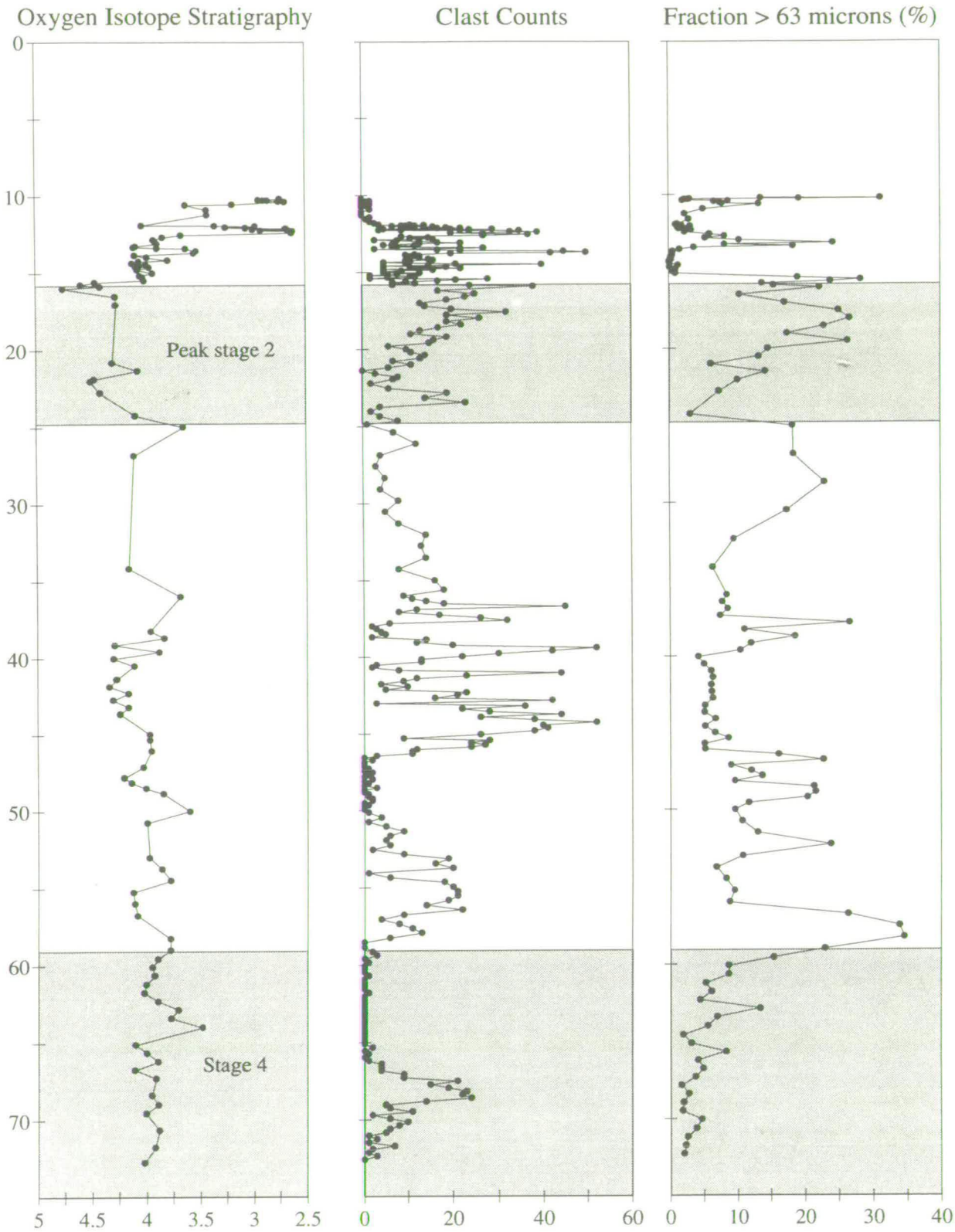

Fig. 3.13. IRD and particle size record for PCM7 plotted against age on vertical axis, kyrs. Oxygen isotope stratigraphy on the left with glacial stages shaded, horizontal scale isotopic composition per mil w.r.t. PDB. Clast counts horizontal scale clast numbers per 2cm slice of core, fraction >63 microns scale expressed as dry wt. %.

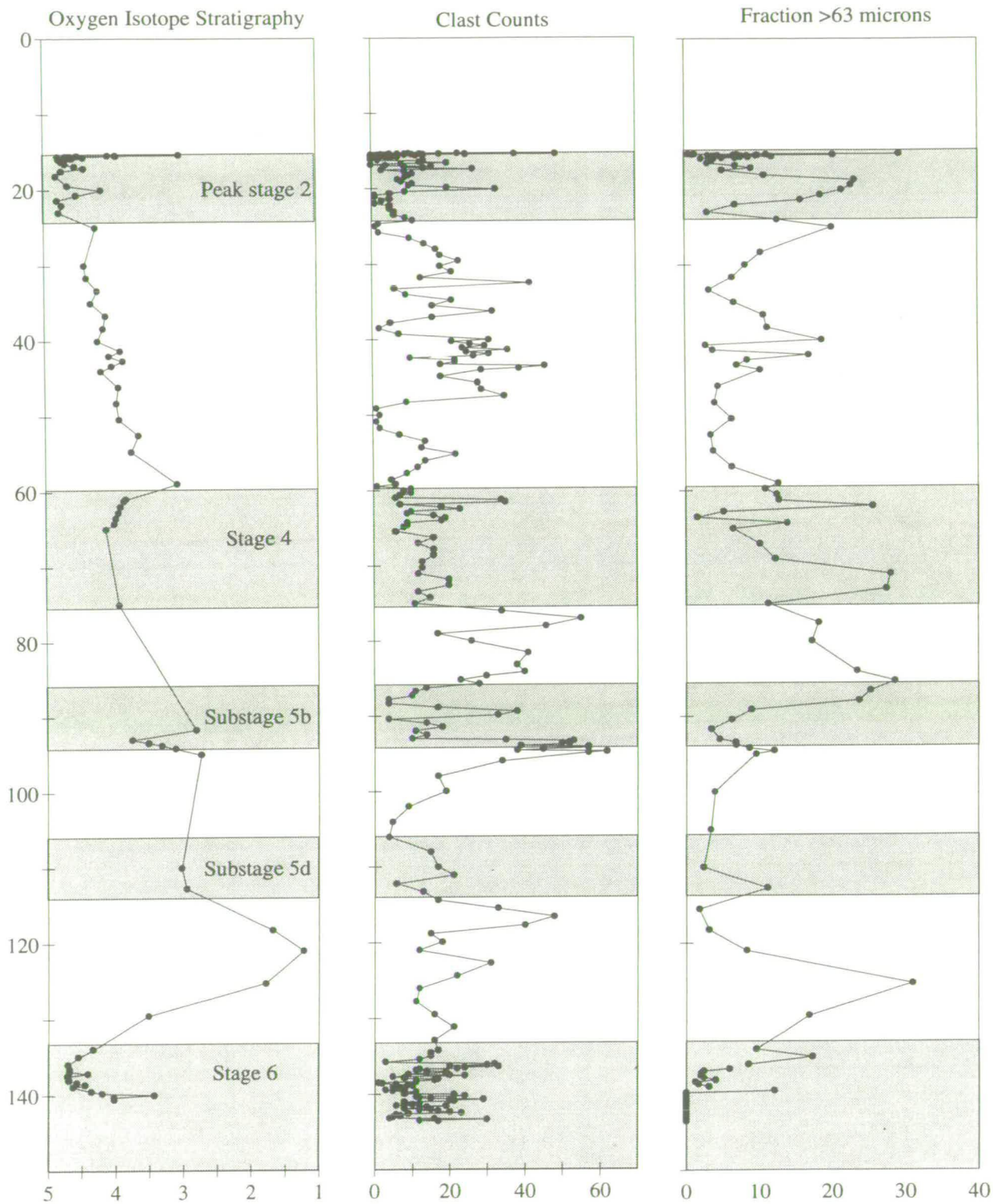

Fig. 3.14. IRD and particle size record of PCM30 plotted against age. Oxygen isotope stratigraphy on the left with glacial stages and substages shaded, vertical scale age in kyrs, horizontal scale isotopic composition in per mil w.r.t. PDB. Clast counts horizontal scale clast numbers per 2cm slice of core, >63micron fraction scale dry wt. %.

Within early stage 6, approximately 152-160 ka, the IRD disappears for a short period, this coincides with an early peak in stage 6 glaciation as evidenced by the oxygen isotope record. Reduction in calving during a peak glacial period may be caused by several factors. The whole area may be locked in sea ice preventing the free movement and melting of icebergs. Alternatively the ice cap may not have been so large due to a lack of moisture supply (due to cold temperatures over the oceans reducing evaporation), accumulation rates may have been very low, with little ice movement (glaciers frozen to their beds) causing low iceberg calving rates. For this initial period of stage 6 the first idea seems most plausible, this is supported by the foraminiferal abundance counts. The period immediately before and immediately after this period of low calving is characterised by very high foraminiferal abundances, over 3000 specimens/gm dry wt. see fig. 3.9, but during this episode abundances drop to virtually zero. This dramatic drop cannot be attributed to dilution due to increased sedimentation rate, it must be due to a drop in productivity. The most likely cause of this is a thick year round sea ice layer preventing light reaching the ocean surface, this will be dealt with in more detail in the chapter on Foraminiferal Assemblages. So the reduction in calving rate is most probably due to a thick year round sea ice cover reducing iceberg movement, accumulation rates would also reduce due to the cold ice that covered the Norwegian-Greenland Sea. This scenario also explains the lack of IRD at the end of stage 6, approximately 134-136 ka, where oxygen isotope values reach their maximum suggesting peak glacial conditions. During both these periods the abundance of the fraction coarser than 63μm is reduced slightly, but is still present. This suggests that even during these periods of freezing in there is still some ice motion pushing material over the shelf break, or the extra weight of the ice on the shelf edge may cause some sediment collapse forming turbidity currents leading to a concentration of coarser material. The period between these two peak glacial events has high IRD and high sand content, due to the resumption of summer melting causing high calving rates and more material pushed over the shelf edge. This melting would allow nutrients to be released to the surface waters and also allow light to reach this area, this would cause a bloom in productivity recorded in high foraminiferal abundances, see fig. 3.9.

The record of stage 6 in PCM30 is not so complete as in PCM5, only the latest section is represented in the isotope record. The IRD record for this section differs from PCM5, there is a fairly high peak during most of the latter part of stage 6 with only a short lived minor drop towards the end that may represent the period of very low IRD seen in PCM5 at the glacial maximum. During a strong glacial period, when it is assumed that the ice was at or near the shelf edge, the major source of iceberg would

be the main outlet fjords of the Spitsbergen ice cap. These two cores would probably receive icebergs from different fjord systems. PCM30 was cored further north on the edge of a submarine fan complex produced from the mouth of the Kongsfjorden system, see fig. 3.17. Its position on this fan complex explains the higher background dropstone numbers being below the flow lines of calving icebergs from the fjord. PCM5 and PCM7 were cored to the south between the two major fjord systems Kongsfjorden and Isfjorden on a step in the continental slope. They would receive IRD from icebergs calving from Isfjorden (or Bellsund and Hornsund further south) being carried northwards by the West Spitsbergen Current, or a similar current. The cores to the south of the area, PCM5 and PCM7, would also be more strongly influenced by icebergs carried around from the southern and eastern margins of the ice cap.

In PCM30 there is very little material coarser than 63μm during stage 6, except right at the end during the deglacial melting phase. PCM30 is situated on a submarine fan, extending from the shelf, and is not affected so greatly by the push mechanism as PCM5 or PCM7.

The record for stage 5 is similar for both PCM5 and PCM30. During substage 5e (the Eemian interglacial) the IRD content of PCM30 is high, PCM5 has a slightly lower content. This suggests some ice was present even during the Eemian. This is the result of large scale melting of the ice cap formed during stage 6 leading to high iceberg calving rates. The lower than expected IRD content of PCM5 may be due to the relative extreme warmth of the Eemian (warmer than the present according to Miller *et al.*, 1989) causing the melting of a large proportion of the icebergs soon after calving before reaching the edge of the continental shelf. In both cores there is an initial high peak in the fraction coarser than 63μm, corresponding to large scale melting. In PCM5 this remains high during the whole of substage 5e, even when the ice tongues were far from the shelf edge, this period was most probably caused by winnowing by a strong boundary current. It was suggested by Vorren *et al.* (1989) that contour currents along the edge of the Barents shelf were more vigorous during interglacial times, these would continue along the shelf edge of Spitsbergen also.

Substage 5d is very poorly recorded in this area, but coincides with a drop in IRD supply. The ice cap would have retreated substantially during substage 5e, calving would be significantly reduced due to colder conditions with lower moisture supply during substage 5d. The Spitsbergen ice cap would begin to build up again during this colder period, but at a slow rate due to low moisture supply. The IRD supply

increases dramatically within substage 5c, a warmer interstadial period. It remains high for the early section of substage 5b, but drops off to almost zero towards the end of this substage. The rapid increase during substage 5c is best explained by a continuation in ice cap growth. Substage 5c at this high latitude may have been a weak interstadial with low temperatures allowing accumulation of ice on Svalbard. Temperatures would have been higher than during substage 5d however, so the moisture supply from warmer air currents from further south would be higher than the preceding stadial period. This would cause a rapid build up of ice soon reaching the fjord mouths where calving would take place, enhanced by the warm based fast flowing nature of the ice tongues. Rapid accumulation allowed the ice tongues to remain on, or even advancing across, the continental shelf during this period of rapid calving.

This peak in IRD continued for the early part of substage 5b, but dropped off soon after the start to very low values for the late period of this substage. This may be the responce of the ice mass to the cooler climate of substage 5b. Colder sea surface temperatures would lead to reduced accumulation, and therefore a reduced ice flux. Continued calving of the marine based ice mass would lead to the retreat of ice reducing the IRD content deposited on the continental slope.

An extensive melting event then took place at the end of substage 5b and start of 5a (this has been recognised in other studies from the Fram Strait for example Kohler and Spielhagen, 1990), identified from the oxygen isotope record of PCM5. This is accompanied by a significant spike in IRD input, and reflects a rapid iceberg calving event of the ice tongues at some position on the continental shelf. This event seems more intense in PCM30 than PCM5, this may be because PCM30 is closer to a source of icebergs and melting ice. The end of substage 5a in PCM5 is characterised by very low IRD content, whereas PCM30 has high IRD throughout 5a. This suggests the northern section of the Spitsbergen ice cap continued to supply large quantities of icebergs whilst further south the supply reduced. Alternatively this could be produced by a change in iceberg trajectory due to stronger along shelf currents. There is also a high abundance of material coarser than 63μm during this period caused by melting of the large ice mass nearby.

Stage 4 has moderate to high IRD content in both cores. The Svalbard archipelago probably had an intermediate stadial type climate during this period. Such a climate would have a moisture supply large enough to cause accumulation at a fast enough rate to lead to calving, and IRD accumulation offshore. The record for mid-late stage

4 is also present in core PCM7, fig. 3.13, and in much higher resolution too. This core shows a period of virtually zero IRD input during the latter part of stage 4. This is unlikely to have been produced by large scale freezing in of the area as in stage 6 and 5b. Stage 4 has traditionally be interpreted as a stadial event rather than a major continental glaciation. It seems more likely that this period of low IRD input has another explanation. One possible explanation is a still stand in ice movement caused by low supply, no accumulation, during a relatively cold climate. The ice cap would not actually melt but just remain roughly where it stood, or waste away slowly. Calving would be very low accounting for the lack of IRD in the cores. The period of low IRD is seen to a lesser extent in the other cores also, see figs. 3.12 and 3.14.

The stage 3 record is more clearly represented in PCM7, see fig. 3.13, due to a higher sedimentation rate so it will be described from this record. The IRD record of PCM7 correlates well with PCM30, but not so well with PCM5. During stage 3 the correlation of the IRD content to the oxygen isotope stratigraphy is very poor. This suggests that the isotope record is being produced by larger scale global variations rather than local variations seen in stages 5 and 6.

The start of stage 3 has a substantial IRD peak, from 58ka to 51ka, see fig. 3.13. This is caused by a slight climatic amelioration. It seems unlikely that this represents a major melting phase, but the ice tongues may have retreated far up the major fjords possibly even onto land. This may explain the distinct period of low IRD from 50ka until 47ka, continued warming trend leading to the withdrawal of the ice tongues from the fjord heads reducing calving. The other possible explanation is that of a similar process as the period at the end of stage 4, cooler temperatures causing a still stand in ice reducing calving. At this point the IRD content increases and remains high, but with large fluctuations until 32ka. This period is one of general build up of ice with minor fluctuations superimposed. Warmer events causing the sharp peaks in IRD, and colder episodes causing reduction in calving leading to troughs in IRD. The IRD content then remains fairly low until 24ka. This period in PCM5 is characterised by much higher amounts of IRD, than in PCM30. This may be a reflection of the drift patterns of the icebergs, perhaps being carried further offshore missing the core site of PCM7 to some extent.

The record of material coarser than 63μm during stage 3 is rather confusing. It is unlikely that ice reached the edge of the continental shelf until the start of stage 2, so only the peaks within stage 2 can be explained by material being pushed over the shelf edge by advancing ice. The first peak in early stage 3 correlates with the dropstone

counts, in PCM7 and PCM5 especially see figs. 3.12 and 3.13, so this was probably produced by iceberg melting. The next peak between 46 and 53 ka, see fig. 3.13, occurs during a period of low IRD, and may represent a winnowing peak, or perhaps the collapse of an unstable shelf edge developing turbidity currents. The peaks towards the end of stage 3 correlate to periods of low IRD content, so are most likely caused by the same process.

The record of stage 2 IRD is similar from all three sites, though the actual amount of material is different. There is a distinct trend of increasing IRD content, particularly within PCM5 and PCM7. The stage 2 record of IRD fluctuations is shown in more detail for PCM5 and PCM30 in fig. 3.15, both these cores show a major peak in IRD just after the heavy oxygen isotope period between 16ka and 15.3ka ago. This represents a major melting event just after the glacial maximum, leading to large scale calving. PCM30 shows minor peaks in IRD between 25ka and 16ka, in general these correlate with periods of relatively lighter oxygen isotope values. This implies these IRD peaks are formed by warming events leading to increased calving, for example the peak at 20ka, and from 17-17.5ka.

During peak stage 2, 25-16 ka, and the initial deglaciation period the amount of coarser material in the cores is high. This can be explained by ice at the shelf edge pushing material over, and by rapid melting at the start of deglaciation. Once the ice has retreated from the shelf edge the amount of coarse material washed over the edge drops rapidly, this explains the disappearance of this coarse material soon after deglaciation begins.

The latter part of stage 2 and the deglaciation period into the Holocene are represented in higher resolution in core PCM7. This period, from 18ka to 10ka, is shown in detail in fig. 3.16. This period is characterised by rapid pulses of IRD input during periods of relatively lighter oxygen isotope values. The process causing these peaks in IRD is similar to that described above for the peaks in stage 2 of PCM30. There are several discrepancies however. The initial IRD peak at 16ka most likely correlates to the minor warming event suggested in the isotopic record slightly younger than 16ka, this is slightly out of phase most probably due to lack of resolution in the isotope record. The distinct IRD peak at 15.1ka correlates with a very minor change in $\delta^{18}O$ value, it seems likely that the full amplitude of the warming event is not represented in the isotope values due to sampling resolution. The final discrepancy lies at the top of the core, after the Younger Dryas stadial event.

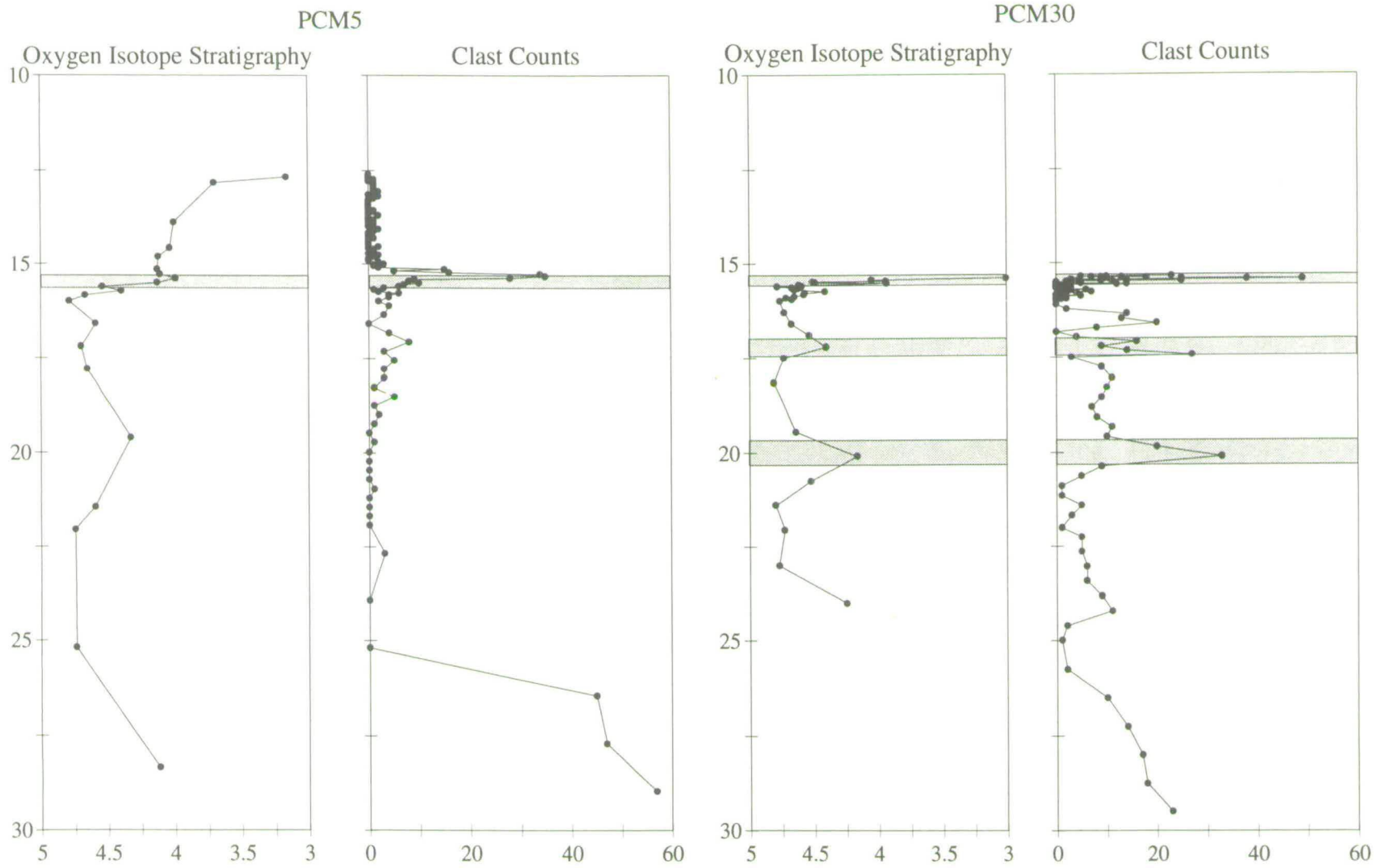

Fig. 3.15. IRD record of PCM5 and PCM30 showing more detail of the period from 30kyrs to 10kyrs, isotopic composition scale per mil w.r.t. PDB, clast scale number of clasts per 2cm slice of core. Shaded areas represent periods when high clast abundance correlates with light oxygen isotope composition.

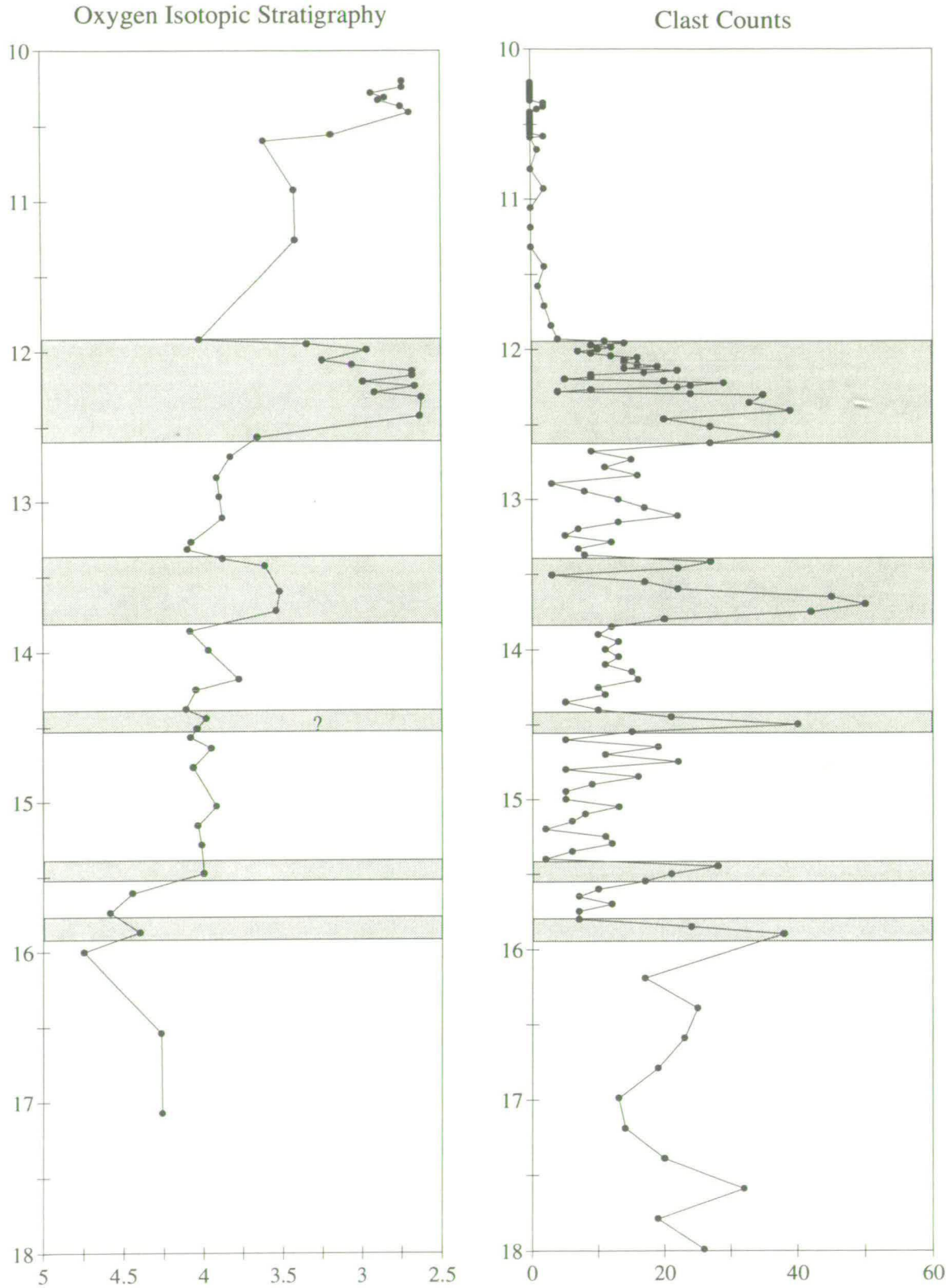

Fig. 3.16. IRD record for PCM7 from mid-way through stage 2 until 10kyrs ago, vertical scale age in kyrs. Isotopic stratigraphy shown on the left, horizontal scale isotopic composition, per mil w.r.t. PDB. Claste counts on the right, scale is number of clasts per 2cm slice of core. The shaded areas represent periods of increased iceberg calving due to warming events.

The warming event after the Younger Dryas at 10.5ka has no corresponding IRD peak as would be expected from the break-up of ice accumulating during the Younger Dryas. This suggests that there was very little build-up of ice on Spitsbergen during the Younger Dryas, and that this period was characterised by cold dry conditions with a low moisture supply. This agrees with evidence presented by Svendsen and Mangerud (1992) who failed to find evidence for glacial advance on Spitsbergen during this period.

The top of PCM7 also has two peaks in coarser than 63μm fraction, one just after the Younger Dryas and one right at the top, these peaks are most likely due to winnowing by a return of a more vigorous circulation system during a high stand in sea level. Interglacials in general are characterised by much stronger circulation systems, stronger boundary currents are therefore more likely to affect the core sites during interglacial periods. This explains the dominance of winnowing during stage 1, stage 5e, and to a certain extent during periods within stage 3.

3.9. Comparison with land based interpretations of the Svalbard ice cap

Mangerud and Svendsen (1992) have made interpretations of the extent of ice on Spitsbergen over the last glacial cycle from studies of cliff sections at the head of Isfjorden. They concluded that oxygen isotope stage 5e was warmer than the present, from the occurrence of *Mytilus edulis* in the lowest marine formation. They recognised several post-Eemian (stage 5e) tills representing major glaciations around 110 ka, 75-50 ka, and 25-10 ka. They interpret the intervening periods as having glaciers on Svalbard not significantly larger than present.

This interpretation is in partial agreement with the ideas outlined above. The glacial advance suggested as around 110 ka correlates with oxygen isotope stage 5d. From the IRD evidence presented above a major ice advance may have started within stage 5d but was more extensive during stages 5c and 5b, so ice masses would be on the continental shelf from around 110-85ka. This suggests that the interstadial recognised by Mangerud and Svendsen (1992) from 110-75ka, the Phantomodden interstadial, was infact of much shorter duration: from 85-7 ka correlating to oxygen isotope stage 5a. The major advance from 75-50 ka is recognised in the data presented here. The retreat of this advance is recognised in the IRD data before it is seen in the land based stratigraphy, as expected. Mangerud and Svendsen (1992) then interpret an interstadial, the Kapp Ekholm interstadial, from 50-25 ka. From this study this

interstadial seems too long, the data here suggest it ended around 46 ka, and ice then began building up towards the stage 2 glaciation from 25-10 ka. This seems more feasible given the major ice volumes during stage 2, ice reaching the shelf edge. Mangerud and Svendsen (1992) suggest only 15 ka for the build up and collapse of this major ice mass, this seems too short, it would be more likely that the ice began advancing during stage 3, as suggested by this study.

The general patterns of ice advance and retreat recognised in the IRD data agree with reconstructions of ice mass size from land based studies, but the detailed timing of events are not the same. Some discrepancies can be explained by time lags between ice expansion and IRD reaching the continental slope, but it seems likely that there are some problems with the dating methods used on the land based stratigraphy and/or the age model presented in this study.

3.10. Model of iceberg calving from the Svalbard ice cap

From the observations noted above a model of IRD input to the continental margin of Spitsbergen has been made, this is described in the following section. In the following model six different states of ice distribution have been proposed to explain the IRD fluctuations found in the cores in this study. In this model it is assumed that all IRD found in the cores examined is produced from icebergs calving from the margins of the Svalbard ice cap. Although this is an oversimplification the vast majority of IRD probably does originate from the Svalbard archipelago so this assumption is valid. A graphic representation of this model is presented in fig. 3.18.

1. Interglacial Peak: The Svalbard ice cap would be relatively small, similar size or smaller than the present day. During these periods iceberg calving would be low, IRD input to the core sites would therefore be low also. The abundance of material coarser than 63μm during these periods can be either high or low. Peaks that occur are due to a more vigorous circulation system producing contour currents along the slope, turbidity currents may also act as a winnowing agent. This situation is present during substage 5e and the latter period of the stage 1 record in PCM7, from 11 ka onwards.

2. Build up to glaciation: The climate begins the cooling trend towards a glacial period, but is still relatively warm. Moderate SST's and warm air currents encourage evaporation from the ocean surface. This provides a high moisture supply leading to rapid accumulation of the Svalbard ice cap.

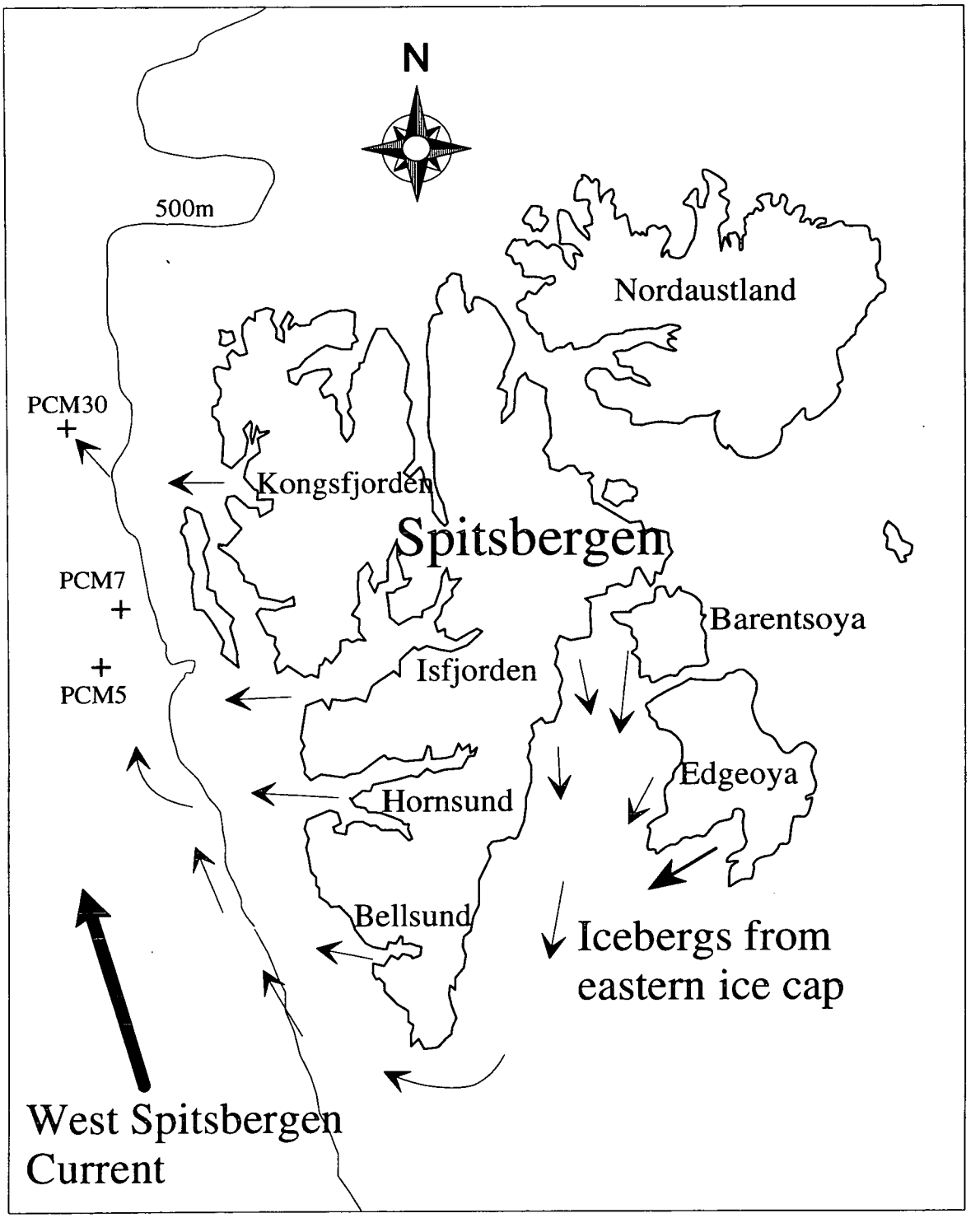

Fig. 3.17. Map of Svalbard showing iceberg drift patterns from the eastern ice cap. Icebergs would be carried around the southern tip of Spitsbergen by the East Spitsbergen Current, become entrained in the West Spitsbergen Current and carried north. The majority of icebergs would probably originate from the western fjords though. Some icebergs may also be carried into the area by the West Spitsbergen Current from the edge of the Barents Shelf. The position of the cores studied are marked, as is the edge of the continental shelf.

1. Interglacial Peak

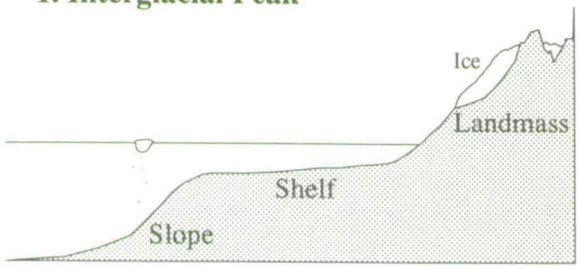

Relatively small land based ice cap, may reach fjord heads in places. Calving rate low, few icebergs, so little IRD deposited on shelf. Sediment supply to slope localised due to along shelf currents.

2. Build up to Glaciation

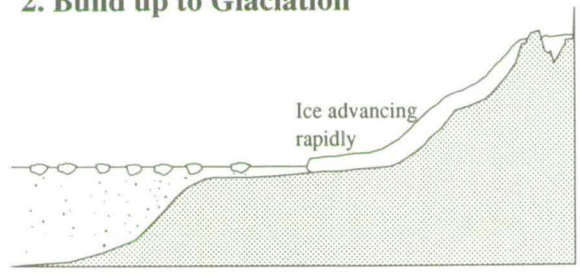

Climate has started to cool, leading to accumulation of ice. Ice tongues advancing rapidly onto shelf, the calving rate is high due to the effect of the relatively warm sea breaking up the ice tongues. Large numbers of icebergs produce high quantities of IRD on shelf and slope.

3. Full Glacial

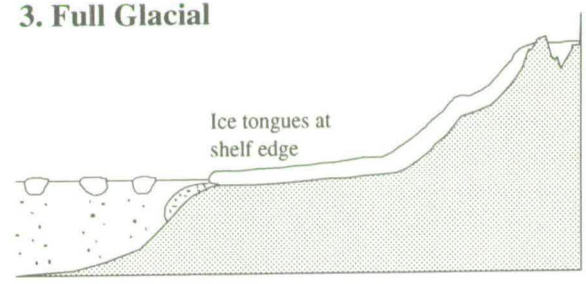

Ice cap at maximum extent, ice tongues at shelf edge. Summer melting causes high calving and iceberg production leading to large volumes of IRD. Basal melting supplies large amounts of poorly sorted material to slope also.

4. Permanent Pack-ice

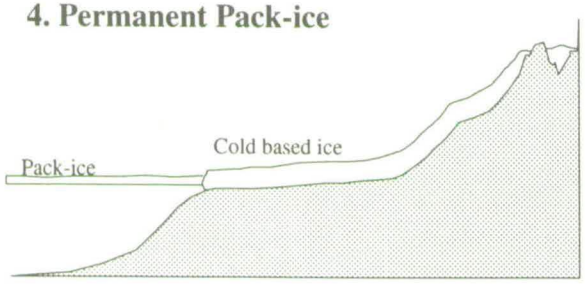

Peak glacial conditions, thick layer of permanent pack-ice, very little summer melting, so low amounts of detritus released to system. Very low accumulation rates due to cold ice covered Norwegian Sea.

5. Glacial Stillstand

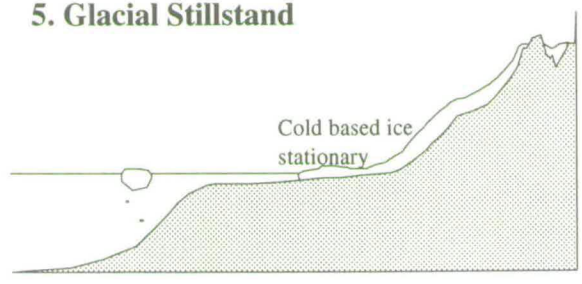

Glacial conditions still prevail, but ice tongues are not as extensive. Low moisture supply results in low ice accumulation, ice cold based so movement is low. Very few icebergs produced, and melting rates would be low so little IRD supplied to slope.

6. Deglaciation

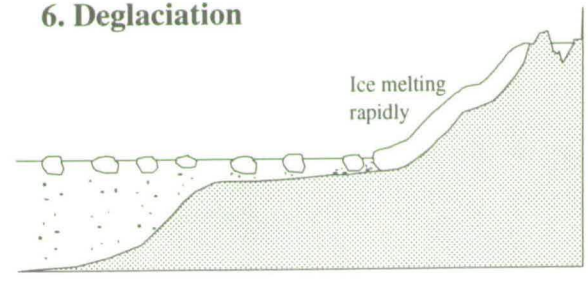

Ice rapidly melting from a glacial position, due to sea level rise, and warmer ocean currents. High calving rates, so large numbers of icebergs produced. Fast melting leads to high flux of IRD to continental margin.

Fig. 3.18. Schematic diagram of the six phases of IRD supply to the continental slope suggested by the model in the text. Diagrams not drawn to scale, and do not take into account input of icebergs from sources other than the Svalbard ice cap.

Glaciers would be warm based and thus fast flowing, once ice tongues reached the fjord heads high calving rates would be induced by the buoyancy and relative warmth of the water. Peaks in IRD would be formed by these icebergs, initially small but increasing in magnitude as the ice tongues advance and approach the shelf edge, calving increasing. The coarser than 63μm material is generally low during these periods as ice would not have reached the shelf edge, though ice rafting and winnowing may lead to some peaks. This situation is found towards the end of stage 7, from 193-180 ka, during substage 5c, and towards the end of stage 3, from 46.5 ka.

3. Full glacial conditions: The ice cap is at it's maximum extent, ice tongues reaching the edge of the continental shelf. Summer melting causes high iceberg calving rates leading to high IRD peaks. Basal meltwater and ice movement push material over the shelf edge leading to peaks in material coarser than 63μm, and very large quantities of poorly sorted clasts. These conditions occur during parts of stage 6, substage 5b, and stage 2 in this study.

4. Permanent pack-ice formation: Ice has extended to the edge of the continental shelf, and a thick cover of permanent sea ice has formed, this occurs during peak glacial conditions when the coldest temperatures occur. Very little if any summer melting occurs, icebergs are trapped in sea ice, and no further calving is possible. Accumulation rates are very low due to cold surface temperatures of the Norwegian-Greenland Sea due to ice cover, so ice flow is further reduced. IRD content found in the cores is very low, foraminiferal abundances are very low also, light intensities below the pack ice are too low to support high numbers. The coarser than 63μm fraction is reduced but still moderately high due to collapse of the shelf edge under the weight of ice forming turbidity currents. This scenario is found in PCM5 during parts of stage 6, from 141.8-142.8 ka, and 134-136 ka, and it also occurs briefly during substage 5b, from 89-90.5 ka.

5. Glacial stillstand/wastage: These conditions occur during less extreme stadial conditions than above, but still with cold glacial temperatures. Ice tongues are situated somewhere between shelf edge and fjord heads. Cold air streams, and cold SST's cause low evaporation rates, so moisture supply to the Spitsbergen landmass is low. Precipitation over Spitsbergen is low so ice accumulation rates are low, ice movement is therefore reduced. Ice flow rates are also low because basal temperatures are low, there is very little meltwater about to facilitate sliding, ice tongues may even be frozen to the bedrock. The ice cap remains stable or wastes away slightly due to lack of supply. This is reflected by a low rate of calving so low

supplies of IRD to the core sites. Melting rates of calved icebergs would also be low. An example of this regime is found during the latter part of stage 4 shown in PCM7 from 58.5-66.2 ka, and during part of stage 3 from 46.4-50.1 ka.

6. Deglaciation: This involves rapid melting of a major ice mass at the end of a glacial period. High calving rates cause large peaks in IRD. The large amount of meltwater present would wash large volumes of coarse material over the shelf edge initially, until the ice tongues have retreated a significant distance from the edge. These conditions predominate just after major glacial periods, and are facilitated by sea level rise and warmer ocean currents, for example at the stage 6-substage 5e boundary, and the boundaries between substages 5b and 5a, and stage 2 to stage 1 transition.

3.11. Summary

1. Counts of clasts larger than 2mm from x-ray photographs have proved a more accurate measure of IRD than the fraction coarser than 63μm in cores from the continental slope of Spitsbergen. The fraction coarser than 63μm was found to be heavily influenced by winnowing, and to a lesser extent by foraminiferal abundances. This is in part due to the proximity of a continental landmass to the study area, and would be less important to studies carried out far from land.

2. It has been assumed that the majority of clasts seen in the x-ray photographs were deposited from icebergs calving from the Svalbard ice mass, this is supported by the correlation between silica content and clast counts in PCM5.

3. A model has been proposed that explains the abundance of clasts in the cores of this study. This model predicts the state of the ice mass from clast counts, foraminiferal abundances and oxygen isotope analysis of planktic foraminifera.

4. The calving rate is the most important factor controlling IRD input to the slope, this is influenced by rate of ice movement, which in turn is influenced by moisture supply.

5. Periods of rapid ice advance produce IRD peaks. These occur when moisture supply is highest, when sea surface temperatures are relatively warm. They do not necessarily correlate to the coldest periods.

6. The qualitative history of the Svalbard ice mass based on IRD content from this study partially agrees with the terrestrial evidence of ice advances. Ice advances can be identified during oxygen isotope stages 2, 4 and 6 from both lines of evidence. An advance during stage 5 is recognised from both terrstrial and marine evidence, though the timing does not agree. The terrestrial evidence suggests the advance took place during substage 5d, the marine record suggests this advance reached a peak during substage 5b.

Plate 4

Examples of x-ray photographs used for clast counts showing the various types of sediment found in the cores. The vertical scale bar is 10cm. Sections with large numbers of clasts are clearly visible in the left hand x-ray. The base of this x-ray shows a section with high clast abundance and laminations. The middle x-ray shows sections with abundant clasts and also one section with clear laminations devoid of clasts. The third x-ray, on the right, shows a homogeneous section with no clasts or sedimentary structures.

Chapter 4. Oxygen isotope records of planktic and benthic foraminifera and paleoceanography of the Fram Strait

4.1. Introduction

An introduction into oxygen isotope analysis has been presented in chapter 2. In chapter 2, the oxygen isotope stratigraphy obtained from the oxygen isotopic composition in the shells of planktic foraminifera was used to produce a chronostratigraphic framework. To construct age models is obviously very useful, enabling correlation between records from different areas in time, but oxygen isotope analysis is also a very useful tool for paleoceanographic reconstruction. Information on changes in surface and bottom waters can be obtained if both planktic and benthic foraminiferal species are analysed. The oxygen isotopic composition of foraminiferal tests is controlled by the oxygen isotopic composition of the global oceans as a result of changes in global ice volume and species specific fractionation. Variations in these parameters will be outlined below.

The oxygen isotopic composition of the worlds oceans is not constant over time. Evaporation at low latitudes preferentially removes the isotopically lighter ^{16}O from the oceans. Atmospheric water vapour then travels towards the poles, on this journey the isotopically heavier ^{18}O is preferentially lost through precipitation leading to further enrichment in ^{16}O in water vapour. So precipitation at high latitudes is isotopically light, -30‰ to -40‰, polar ice sheets are therefore enriched in ^{16}O compared to mean ocean water. Expansion of these polar ice sheets in response to climatic forcing removes significant quantities of ^{16}O from the oceans, this causes a change in the mean oceanic composition. A reduction in polar ice sheet volume will return large volumes of meltwater to the oceans enriched in ^{16}O, this would alter the mean composition of the oceans, reducing the $^{18}O/^{16}O$ ratio. The difference in oxygen isotopic composition of the oceans between full glacial and full interglacial periods is approximately 1.2‰ (Berger, 1979). These changes will be preserved by the oxygen isotopic composition of both planktic and benthic foraminifera, which on dying accumulate on the sea floor and become incorporated in the sedimentary record.

Temperature of ocean water also has an effect on the oxygen isotopic composition of foraminifera. At lower temperatures, there is a greater fraction of ^{18}O relative to ^{16}O, so foraminifera living in cold water will be enriched in ^{18}O compared to specimens living in warmer water (Urey, 1947, Shackleton and Opdyke, 1973). This temperature

effect has been quantified as approximately 0.23‰/1°C (Epstein, 1953). Planktic species, living in surface waters, record not only changes in ice volume but also local oceanographic trends, such as changes in surface current distribution or, especially in this study, influx of meltwater from the nearby continental ice cap. Benthic foraminifera living at the sea floor experience little temperature variation, in general bottom waters are very cold, just above freezing point (Broecker, in prep). Extreme meltwater effects do not penetrate much below surface waters due to the low density of meltwater compared to normal marine water. Benthic oxygen isotope compositions should therefore record changes in ocean isotopic composition caused by ice volume effects rather than the local temperature and meltwater effects often recorded in planktic foraminifera.

This is however not necessarily the case, the accuracy of using benthic foraminiferal species as indicators of ice volume will be tested using an independant global ice volume curve produced by Fairbanks (1989). Fairbanks (1989) used a series of drilled coral reefs from offshore Barbados to estimate the sea level rise from the last glacial maximum until the present. This sea level curve was converted to a curve recording the change in oxygen isotope composition of ocean water by applying a calibration of 0.011‰ $\delta^{18}O$ per metre change in sea level (Fairbanks and Matthews, 1978). As mentioned above, temperature changes in bottom waters tend to be low, and meltwaters are usually restricted to surface waters due to their low densities. The benthic oxygen isotope records produced here should, if meltwaters are not mixed into deep waters, match the global ice volume curve of Fairbanks. Discrepancies between the two must be explained by changes in bottom water temperature/salinity characteristics.

Not all foraminifera precipitate calcium carbonate in equilibrium with ambient sea water, fractionation is often caused by secretion of tests in disequilibrium with ocean waters (Shackleton *et al.*, 1973). Physiological differences may result in large variations in the oxygen isotope ratio between species, and between a species and the ambient sea water. This type of fractionation is assumed constant so, once calculated, it can be taken into account by applying a correction factor. Such correction factors have been used on measurements of some of the benthic species analysed in this study, outlined below. Migration of planktic foraminifera during their life cycle may also cause changes in the oxygen isotopic composition (Berger *et al.*, 1981). Juvenile stages usually inhabit shallower waters, while adult stages may live at deeper depths, this would lead to an enrichment in the $\delta^{18}O$ of adult stages compared to juveniles. This problem can be eliminated by analysing specimens of a limited size range.

The oxygen isotopic composition recorded in the planktic foraminifera depends, among other things, on the depth habitat of particular species in the water column. We have chosen to analyse *Neogloboquadrina pachyderma* (sinistral) (Ehrenberg) from our records due to its overwhelming abundance compared to other planktic species. The depth habitat of this species, along with other planktic species, has been studied in detail by Carstens and Wefer (1992) using plankton tows from the Arctic Ocean, Fram Strait and Greenland Sea. Their results suggest *N. pachyderma* (sinistral) lives in the surface 50m in the Arctic Ocean, but in the Fram Strait and Greenland Sea they live at depths between 100-200m at present. This depth is below the pycnocline where water temperatures are close to 0°C. This change to a deeper habitat is attributed to the influx of North Atlantic water into the southern part of the study area. *N. pachyderma* (sinistral) prefers colder Polar type waters rather than relatively warm saline North Atlantic type waters. This suggests that oxygen isotope measurements made on *N. pachyderma* (sinistral) record no temperature change at all. When they originate from cold polar waters they live in the upper 50m, and when they originate from North Atlantic waters, such as the West Spitsbergen Current, they live at depths of 100-200m in waters close to 0°C.

Johannessen *et al.* (in press) have studied the $\delta^{18}O$ composition of planktic foraminifera from core top samples from the Norwegian Sea between 60 and 72°N. They compared the expected $\delta^{18}O$ composition of calcite precipitated in equilibrium with ocean water, from modern hydrological data, with $\delta^{18}O$ measurements of Recent specimens of *N. pachyderma* (sinistral). From this, they concluded that in Arctic waters this species lives in the surface 30m, where temperatures are close to 0°C. Measurements of the subpolar species *Neogloboquadrina pachyderma* (dextral) suggest that this species lives in the top 20-30m of the North Atlantic Current, or West Spitsbergen Current. *N. pachyderma* (dextral) has an isotopic composition of approximately 1.4‰ in this North Atlantic water, specimens of *N. pachyderma* (sinitral) analysed from this water mass have an isotopic composition of approximately 2.3‰. Johannessen *et al.* suggests this 0.9‰ difference is produced by calcification during different seasons, *N. pachyderma* (dextral) secreting its test during summer, and *N. pachyderma* (sinitral) secreting its test during cooler seasons, spring or autumn. A more likely explanation of this difference is that *N. pachyderma* (sinistral) lives at greater depths in the North Atlantic Current, as suggested by Carstens and Wefer (1992). This may be because competion at the surface is too high or, most probably, they prefer to live in the cooler deeper waters.

The 0.9‰ difference between the sinistral and dextral varieties measured from North Atlantic waters equates to a temperature difference of 4°C between surface waters and the waters at the depth the sinistral variety calcifies. This must be taken into account when interpreting the oxygen isotope curves for the planktic species later in this chapter. At the present day summer surface temperatures in the West Spitsbergen Current (North Atlantic water) are approximately 4°C (Quadfasel and Meincke, 1987) so *N. pachyderma* (sinistral) lives in water with a temperature of only 1-2°C.

The importance of measuring the shells of both planktic and benthic foraminifera in Fram Strait cores will be discussed in depth in this chapter, along with the paleoceanographic implications and meltwater history deduced from these results.

4.2. Aims and implications of oxygen isotope records from this study

Sarnthein *et al.* (1992) have used oxygen isotope records from cores within the Norwegian-Greenland Sea to identify episodes of increased meltwater production, this work is described later. From their results they mapped the movement of these meltwater plumes. They recognised clear meltwater events in cores from the Norwegian Sea and off the Barents Shelf, but have very poor records for further north in the Greenland Sea. One of the cores in this study, PCM7, shows an expanded section from the last glacial maximum to approximately 8 ka ago. A method has been used to accurately assess the meltwater influence on the $\delta^{18}O$ values in *N. pachyderma* (sinsitral) from this core, using a curve of global ice volume produced by Fairbanks (1989), and therefore recognise more clearly the meltwater history of the Greenland Sea.

Oxygen isotope measurements of benthic foraminifera have also been used in this study to assess changes in bottom waters. The common assumption that benthic foraminifera record global ice volume changes only, and do not experience temperature or meltwater effects is tested using the Fairbanks ice volume curve. Periods of enhanced bottom water circulation will be recognised from benthic $\delta^{18}O$ measurements also.

Over longer time scales a much clearer picture of the oceanography during stage 5 is produced from oxygen isotope measurements from PCM5 and PCM30; the oxygen isotope resolution within stage 5 is greater in PCM5 and PCM30 than in any other published records from the Greenland Sea. Combining these two cores all substages

within stage 5 can be recognised. The meltwater events during stage 5 can be clearly identified, and can be quantified using estimates of the temperature influence from the top of PCM7 and also from data from Johannessen *et al.* (in press). Measurements from benthic foraminifera are used in these cores also to identify periods where some temperature or meltwater influence reached the bottom waters.

4.3. Previous oxygen isotope research in the Norwegian-Greenland Sea and comparison with data from this study

Oxygen isotope studies are relatively rare in high Arctic areas such as the Norwegian-Greenland Sea, especially in the northern part of this area, the Fram Strait and the continental margin of Spitsbergen. Some of the oxygen isotope records that have been produced for this area are mentioned in table 4.1 below, the position, water depth, and reference of these cores are shown. Fig. 4.5 documents the position of these cores in the Norwegian-Greenland Sea.

Table 4.1. Details of cores from literature which are compared to the cores in this study, the cores in this study are included at the top.

Core	Water Depth	Position	Reference
PCM56	468m	79° 55'N 08° 49'E	This study
PCM30	1137m	79° 35'N 06° 41'E	This study
PCM7	1073m	78° 38'N 07° 54'E	This study
PCM5	2139m	78° 29'N 07° 43'E	This study
MG-123	3050m	79° 16'N 00° 48'E	Morris (1988)
21535	2557m	78° 44'N 01° 52'E	Köhler and Speilhagen (1990)
PS 21295	3112m	78° 00'N 02° 25'W	Jones and Keigwin (1988)
1294-4	2500m	78° 00'N 05° 00'E	Hebbeln (1992)
M 23259	2518m	72° 02'N 09° 16'E	Weinelt et al. (1991)
V27-60	2525m	72° 11'N 08° 35'E	Duplessy, Labeyrie, Blanc (1988)
K11	2900m	71° 47'N 01° 36'W	Duplessy, Labeyrie, Blanc (1988)
23199	2000m	66° 22'N 05° 13'E	Haake and Pflaumann (1989)
M 23071	1308m	67° 05'N 02° 55'E	Sarnthein et al. (1992)
HM 52-43	2781m	64° 31'N 00° 44'E	Sarnthein et al. (1992)
TROLL 3.1	332m	60° 47'N 03° 43'E	Lehman and Keigwin (1992)

4.3.1. Comparison and re-interpretation of Fram Strait oxygen isotope records

Four of these oxygen isotope records are from Fram Strait cores: 1294-4, 21535, MG-123, and PS 21295. PS 21295, which was studied by Jones and Keigwin (1988), shows a poor resolution record from 16.5 ka to 2 ka, and is plotted with PCM7 in fig. 4.6. This core has been radiocarbon dated and provides a record from 16.5ka to 2.25ka, it does not show the relatively high amplitude fluctuations in $\delta^{18}O$ values seen in PCM7. The glacial values of approximately 4.6‰ are similar to values measured in PCM7. The deglacial record of this core does not agree closely with the other cores from the Norwegian/Greenland Sea. The initial light oxygen isotope spike is dated at 14.48ka rather than 13.6ka as seen elsewhere (see below). This age may be inaccurate due to the low sedimentation rates of this core, and/or poor oxygen isotope resolution. The $\delta^{18}O$ value at this point is similar to the values found between 177.5-165cm in PCM7 at 13.6 ka. The increase in $\delta^{18}O$ values in PS 21295, culminating in the peak with a $\delta^{18}O$ value of 4.4‰ at 12.63 ka, agrees well with the increase seen in PCM7 from 155-130cm, from approximately 13.4 to 12.5 ka. This suggests that the Fram Strait and Spitsbergen margin experienced similar meltwater and surface current conditions during this period. The $\delta^{18}O$ record for PS 21295 then shows a gradual reduction in $\delta^{18}O$ values from this point reaching stable values of 3.5‰ at 7.2ka. The record seen in PCM7 is different, it shows a rapid reduction in $\delta^{18}O$ values dropping to 2.6‰ by 12.3ka, followed by an increase to 4.0‰ at 12ka, then a reduction at 10.5ka and an increase and subsequent gradual reduction to values of 2.6‰ by 8.5ka.

The other records from the Fram Strait span a much longer period than this, as far back as oxygen isotope stage 6. These are shown in fig. 4.4 along with PCM5 and PCM30. The stage definitions and interpretations, along with comparison with cores from this study, are dealt with in the following section. One of the records extends back to oxygen isotope stage 7, MG-123. The stage 6 record of two of the cores, MG-123 and 21535-8, correlates well with PCM5 and PCM30, although oxygen isotope values are slightly higher in the latter two records. This suggests oceanic conditions were fairly stable and similar over the whole of the Greenland Sea during stage 6.

The record for stage 5 is rather more problematical particularly the Eemian or substage 5e. This was discussed by Köhler and Speilhagen (1990) using the records of cores MG-123 and 21535-8. They concluded that substage 5e in the Fram Strait was characterised by heavier oxygen isotope ratios than those from substage 5a. Their explanation for this is that substage 5a times were characterised by lower salinity

surface waters due to more intense iceberg melting than during substage 5e, rather than having higher sea surface water temperatures.

From correlation with PCM30 and PCM5 the positioning of substage 5e in cores MG-123 and 21535-8 appears incorrect, and also seems likely to be incorrect for core 1294-4, see fig. 4.4. (the stage assignments in brackets are those suggested from correlation with cores from this study). The oxygen isotopic ratio of substage 5e in PCM30 is 1.2‰, this light $\delta^{18}O$ value is certain to have been heavily influenced by meltwater. The position of substage 5e in MG-123 at 250cm has an oxygen isotope value of 3.5 ‰, this is too heavy for this period, even accepting that being further offshore this core would be less affected by meltwater from the Spitsbergen landmass. This event is more likely to be during substage 5c, having similar $\delta^{18}O$ values to substage 5c in PCM5 and PCM30. Also its position in relation to substages 5a, 5b, and stage 6 support its interpretation as substage 5c. There appears to be no event in core 21535-8 that could realistically be correlated to substage 5e, the oxygen isotopic ratios do not drop below 3.7‰. The assignment of substage 5e in core 1294-4 at the base is dubious also, the $\delta^{18}O$ values drop to just below 3‰, while being lower than the previous two cores this still seems too heavy. Again this event is more likely to be substage 5c, the oxygen isotope value for sustage 5c in PCM30 is 2.7‰, similar to the event seen in 1294-4. Also, supporting this new assignment, if the position of substage 5a and stage 4 are correct then substages 5b, 5c, and 5d are very condensed, and substage 5d had a greater influence than 5b, whereas in fact the opposite is the case in this area, as discussed in chapter 5 on correlation with the Summit ice core, and evidenced in the oxygen isotope curves of PCM5 and PCM30.

It seems likely that substage 5e is not recorded in these cores as an event of light oxygen isotopic composition because it has not been sampled. The values seen in MG-123 and 21535-8 at the start of stage 5 are similar to values measured within stage 6, it seems likely that these high values are caused by reworking of planktic foraminifera from stage 6. This idea is supported by the absence of low oxygen isotope values for substage 5e in PCM5, which was taken from a similar water depth as these cores though not so far out in the Fram Strait. Planktic foraminiferal abundances within PCM5 are exceptionally high during stage 6, and very low during stage 5, especially substages 5e and 5a. The signature of planktic foraminifera from substage 5e would be drowned out by reworking of foraminifera from stage 6. Another alternative may be that during substage 5e times the central Fram Strait was still under the influence of Arctic surface waters, the warmer Atlantic waters being confined to areas nearer the coast of Spitsbergen and flowing westwards at a higher

latitude. This is the situation at the present day, so a similar situation is likely to have occurred during substage 5e times. Johannessen *et al* (in press) have shown that *N. pachyderma* (sinistral) has an oxygen isotopic composition of approximately 3.5‰ in areas influenced by Arctic waters, and about 2.5‰ in areas influenced by North Atlantic waters. Even assuming this, it seems unlikely that substage 5e is present in cores 21535-8 or MG-123. The assignment of substage 5e in MG-123 would mean that substages 5d, 5c and 5b are hardly represented at all, a similar situation occurs in core 1294-4.

Substage 5a is clear in MG-123, 21535-8, and 1294-4, having isotopic ratios of 2.7‰, 3.6 ‰, and 3.8 ‰ respectively. These values are significantly heavier than the value of 1.5 ‰ measured for substage 5a in PCM5. There is a sampling hiatus over this period in PCM30 which explains why such low $\delta^{18}O$ values were not recorded. This is most probably caused by a reduction in the influence of meltwater in the more distant cores of the central Fram Strait. It is also possible that these cores are not of high enough resolution to have sampled the most extreme period of substage 5a. The possible alternative explanation suggested for substage 5e mentioned above may also follow for substage 5a (under the influence of Arctic waters not North Atlantic waters). Substage 5b is recorded clearly in MG-123, approximately 220-240cm, the oxygen isotopic ratios of between 4.2 and 4.3 ‰ are very similar to those found in PCM5. The position of substage 5b in the other cores is less clear, in core 21535-8 it is most likely to be represented by the section between 245 and 290cm, and in core 1294-4 between 300 and 350cm.

The position of stage 4 can be correlated accurately between all five cores, all with oxygen isotopic ratios of between 4 and 4.5 ‰. Stage 3 is very poorly represented in core 1294-4, but considerably better in the other cores. The general trend within stage 3 in the three cores 21535-8, PCM5 and PCM30 is similar, slightly increasing values of $\delta^{18}O$ upwards. This suggests a gradual freezing in or growth of ice culminating in the last glacial phase, stage 2. The trace for core MG-123 shows if anything the reverse, with the lightest ratios towards the end of stage 3. The reason for this is unclear.

Another important characteristic of these records is their paucity of resolution over the last deglaciation and Holocene period when compared to the record of core PCM7. The actual $\delta^{18}O$ values reached in the upper sections of these cores, interpreted as the Holocene, are considerably heavier than those found in PCM7, between 3.0 and 3.5‰ compared to 2.5‰ in PCM7. This could be due to several reasons, firstly these cores

do not record full interglacial conditions due to non-deposition or erosion of the Holocene sediments by bottom currents, or secondly these values are Holocene values and are heavier because these cores lie within a different cooler water mass. Support for the first idea comes from the records for PCM5 and PCM30 which are also incomplete with the Holocene missing. PCM5 is taken from a water depth of 2139m (1000m deeper than PCM7), and PCM30 was taken from significantly further offshore than PCM7. The three other cores were taken from water depths of 2500m or deeper, and are much further out into the Fram Strait than any of the cores in this study. They would therefore be more likely to suffer from the erosional bottom currents that presumably removed the Holocene records from PCM5 and PCM30. The other possibility is that these cores from the central Fram Strait are in an area under the influence of Polar surface waters flowing southwards rather than North Atlantic surface waters flowing northwards. The oxygen isotope signature of the Holocene in the central Fram Strait supports this idea. Measurements from Johannessen *et al.* (in press) for areas under Polar waters at the present time are approximately 3.5‰, similar to the values at the top of the central Fram Strait cores. These cores may therefore be under the influence of colder Polar surface waters, but they are also of a much lower resolution than PCM7 over this deglacial and Holocene period.

All of the five cores show a higher resolution during glacial or stadial periods, stages 2, 4, and 6, and to a certain extent during substage 5b, compared to interglacial periods. In PCM5 and PCM30 this is due to higher sedimentation rates during these periods, and also much higher foraminiferal abundances at these times, this allows a much clearer, higher resolution curve to be produced with fewer sampling breaks.

4.3.2. Comparison of cores from the Norwegian Sea to Spitsbergen margin cores

The oxygen isotope record of PCM7 is unique for the Spitsbergen margin-Fram Strait area. No other published marine oxygen isotope records show such an expanded high resolution curve for this period. There are, however, oxygen isotope records from the Norwegian Sea further south that possess good records of the oxygen isotope stage 2-stage 1 transition. These are documented in table 4.1 above, and comparison with PCM7 will be outlined below.

Further south there are three cores taken from the southern margins of the Greenland Sea basin. Cores K11 and V27-60 from the central area show poor resolution over the

deglacial period (Duplessy *et al.*, 1988). After the initial deglacial reduction in $\delta^{18}O$ from values of 4.6‰, there is a brief period of heavier values before the Holocene $\delta^{18}O$ values of 2.5-3.0‰ are reached. These Holocene $\delta^{18}O$ values are similar to those found at the top of PCM7, suggesting that similar oceanographic conditions existed in this central area as along the Spitsbergen margin.

The third core from this area M 23259 (Sarnthein *et al.*, 1992) shows a similar resolution to PCM7 over this period. This core is situated near the edge of the Barents Shelf (fig. 4.5) and Sarnthein *et al.* (1992) suggest that the $\delta^{18}O$ record is heavily influenced by meltwater from the Barents Shelf. M 23259 shows a very rapid melting event, $\delta^{18}O$ values dropping from 4.7‰ to approximately 2‰ by 13.6 ka. This event is less pronounced and spread over a much larger section in PCM7, culminating in $\delta^{18}O$ values of 3.5‰ at 13.6ka. This difference can be explained by the current system. During glacials Sarnthein *et al.* (1992) suggest surface currents flow to the south, so meltwater from the initial melting phase of the Spitsbergen and Barents Shelf ice masses would be carried southwards. The meltwater signature of M 23259 would be more extreme than cores from the Spitsbergen margin due to the extra meltwater from the Barents Shelf. The next deglacial event seen in M 23259 culminates in $\delta^{18}O$ values of 2.5-3.0‰ at 12.3 ka. This point also coincides with the first influx of subpolar foraminifera into the Greenland Sea (Sarnthein *et al.*, 1992). This correlates with the major fall in $\delta^{18}O$ values in PCM7 at 130cm, which also coincides with the first major influx of subpolar foraminifera in this core (see chapter 6). This light oxygen isotope spike is therefore produced by both temperature and meltwater, this will be discussed in more detail in section 4.4. Both records then show an increase in oxygen isotope composition of planktic foraminifera with $\delta^{18}O$ values close to 4.0‰ at 12 ka ago. Values then decrease to flatten out at approximately 2.5‰ by about 9 ka ago in M 23259. PCM7 shows a decrease in $\delta^{18}O$ values to 2.6‰ but then a further increase to values of about 3.3‰, values drop off to 2.6-2.7‰ by the top of PCM7, 8.5 ka ago.

Further south again two other cores studied by Sarnthein *et al.* (1992), from off the Norwegian coast in the Norwegian Sea, show a similar resolution to PCM7 over the last deglaciation. These cores, HM 52-43 and M 23071 from 64 and 67°N have been plotted in fig. 4.6 along with PCM7. The position of M 23071 is shown in fig. 4.5. These two cores show a very similar meltwater history to that of M 23259, and PCM7. The amplitude of the meltwater changes is less than in either M 23259 of PCM7, but the Holocene $\delta^{18}O$ values at the top of each core are considerably lower

than the other cores from further north, values ranging from 2.2 to 2.4‰ compared to the range of 2.6 to 2.7‰ for M 23259 and PCM5.

Another core from a similar area in the Norwegian Sea, 23199 from 66°N (fig. 4.5) was analysed by Haake and Pflaumann (1989). This record extended back as far as oxygen isotope stage 7, with very clear substage 5e $\delta^{18}O$ values of 2.5‰, similar to Holocene values. In general, Norwegian Sea oxygen isotope records seem to record a clearer substage 5e signature than records further north from the Greenland Sea. This is supported by the composite benthic oxygen isotope curve produced by Duplessey *et al.* (1988) from 5 cores from the Norwegian Sea. This is shown in fig. 2.3. This record has a low resolution for the Holocene, but shows a good record for stage 5. Substage 5e is easily identifiable with near Holocene $\delta^{18}O$ values. This record is very similar to the SPECMAP record of Imbrie *et al.* (1984).

4.4. Description of $\delta^{18}O$ Results

Stable oxygen isotope measurements have been made on four cores from the continental margin of Spitsbergen, PCM5, PCM7, PCM30 and PCM56. Samples of the planktic foraminifera *N. pachyderma* (sinistral), a polar species, were analysed for all cores in the size range >125μm. The planktic $\delta^{18}O$ records have been described in chapter 2 so will not be described again here. Measurements were also made on benthic species of three of the cores, PCM5, PCM7 and PCM30, which will be described here. Unfortunately due to the variation in abundance of benthic species within a core and between cores several species were measured to produce oxygen isotope curves as complete as possible. For PCM5, cored from water 2139m deep (deeper than the other cores), specimens of a characteristically deep water living species were measured, *Eponides umbonatus* (Reuss). The palaeoenvironmental significance of this species and other species measured is discussed more fully in the Foraminiferal Abundance chapter. For the other two cores, PCM7 and PCM30, taken from shallow water depths 1074m and 1154m respectively, different species had to be analysed. For both cores no one species was present in high enough numbers throughout the core to be used alone to produce an oxygen isotope curve. For this reason measurements were made from two species, *Melonis barleeanum* (Williamson) and *Cassidulina teretis* (Tappan). The results were then combined to produce a more complete oxygen isotope record.

As mentioned in the introduction species fractionation can affect the oxygen isotopic signature of certain foraminifera. These fractionation factors are assumed constant so a correction can be made to express the results in equilibrium with the ocean water at time of precipitation. The planktic foraminifer *N. pachyderma* (sinistral) precipitates carbonate in equilibrium with the ocean water it is living in, so no correction has to be made to these measurements. Streeter and Shackleton (1979) calculated that *M. barleeanum* has a constant fractionation factor of -0.4‰, so the oxygen isotopic composition within the carbonate precipitated by this species is 0.4‰ lighter than the composition of the surrounding ocean water. A correction factor of +0.4‰ has been added to all measurements from this species. Calculations carried out by Rokoengen *et al.* (1991) concluded that *C. teretis* precipitates carbonate in equilibrium with ocean water, thus no correction factor is necessary for this species. The other benthic species analysed in this study, *E. umbonatus*, was found to precipitate carbonate 0.47‰ lighter than ocean water by Belanger *et al.* (1981), thus a correction factor of +0.47‰ has been added to these measurements. Once these corrections have been made measurements from different species can be combined to produce a more complete record, it also allows interpretation of environmental changes to be made from comparison of results from different cores.

The results obtained from stable oxygen isotope analysis will be described in the following section. Details of the analytical technique can be found in Appendix 1.

4.4.1. The benthic $\delta^{18}O$ record of PCM5.

For this core the benthic species *E. umbonatus* was analysed (fig. 4.1). Due to the low abundance of benthic foraminifera within this core this was the only species which was found in high enough numbers to be analysed. Unfortunately even this species gives a patchy record with major gaps in places.

No measurements were possible from the base of the core, the first analyses were made at 550cm. Initial $\delta^{18}O$ values of 4.7‰ rise to 4.9‰ from 525-495cm, then drop to 4.7‰ until 470cm. There is then an increase in $\delta^{18}O$ values reaching a peak of 5.17‰, the highest values in the core at 445cm. This is followed by a two stage drop in $\delta^{18}O$ values reaching a low of 4.17‰ at 385cm. The resolution over this section is particularly poor with just four points between 385 and 440cm. After this a rapid rise results in $\delta^{18}O$ values attaining 5‰ at 367cm; this is followed by a drop to 3.8‰ at 365cm.

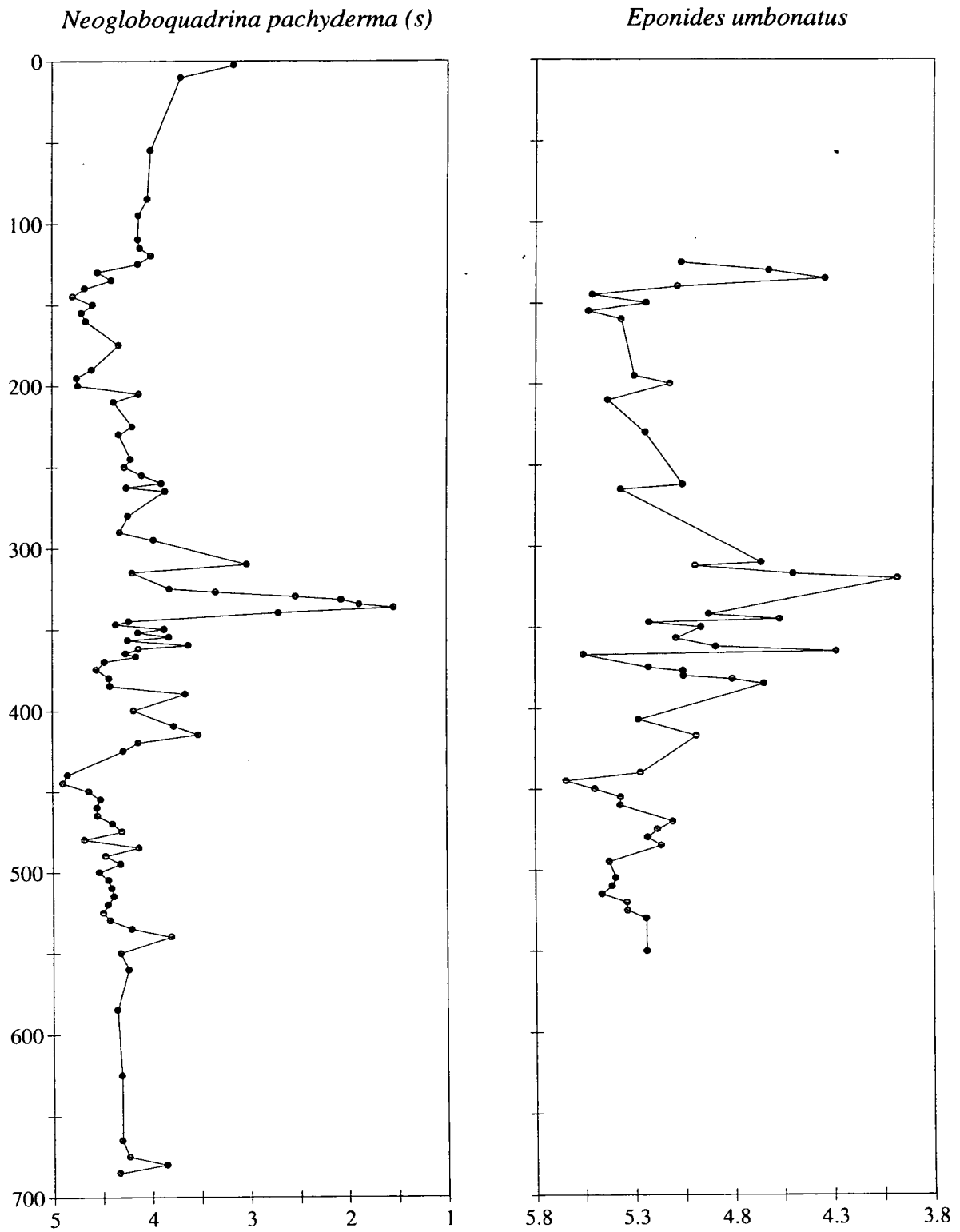

Fig. 4.1. Oxygen isotope data for PCM5. Planktic species on the left, benthic species on the right. Vertical scale depth in cm, horizontal scale per mil deviation of oxygen isotope composition w.r.t. PDB standard.

This point is most probably incorrect, possibly affected by reworking as the next section has values of around 4.5‰ until 342cm. There is then a short section with no measurements, the next $\delta^{18}O$ value being 3.5‰ at 320cm, this is the lowest value measured in the core, and is followed by a rapid increase in $\delta^{18}O$ to 4.6‰ at 357cm. This is followed by a more gradual trend of increasing $\delta^{18}O$ values culminating in a relatively stable plateau of measurements between 4.5 and 5‰ from 265-145cm. This is followed by a sharp drop to 3.8‰ at 135cm, and an equally sharp rise to 4.6‰ at 125cm. The upper 120cm of the core did not contain enough specimens for measurement.

4.4.2. The benthic $\delta^{18}O$ record of PCM30

Two benthic species were analysed from PCM30 to produce as complete a record as possible, these were *C. teretis* and *M. barleeanum*. Unfortunately there are still gaps in the record, but due to higher benthic abundances these are less common than in PCM5. Fig 4.2 shows the results from both species plotted on the same axis, small circles represent *C. teretis*, larger triangles *M. barleeanum*, no correction factors have been applied to these results. In the graph of combined benthic results, the correction factors outlined above have been applied to produce a single curve. This curve will be described in more detail below.

The base of the core is virtually barren, and no measurements were possible until 562cm, the $\delta^{18}O$ record starts off with relatively low $\delta^{18}O$ values of 4.3‰. The $\delta^{18}O$ values then increase to 5.4‰ before dropping to around 4.6‰ until 507cm. There is then a significant gap where no analyses were possible. The next sample analysed at 457cm has the lightest $\delta^{18}O$ value of the whole core, 3.57‰, values then increase sharply to 4.4‰ at 452cm and remain at or slightly above this level until 402cm. A sampling hiatus is then present until 337cm, similar to the planktic record, $\delta^{18}O$ values of around 5‰ then continue to 307cm. There is then a minor gap until 287cm where values of 4.4‰ occur rising to 4.5-4.6‰ until 242cm. Values then increase gradually reaching a peak of 5.4‰ at 222-207cm, there is then a reduction to 5.1-5.3‰ until 147cm. A fairly stable plateau of $\delta^{18}O$ values between 5.4 and 5.6‰ then persists until 42cm. At this point $\delta^{18}O$ values drop to 4.6-4.7‰ until 22cm, rise to 4.8-5‰, and finally drop to a low of 4‰ at the top of the core.

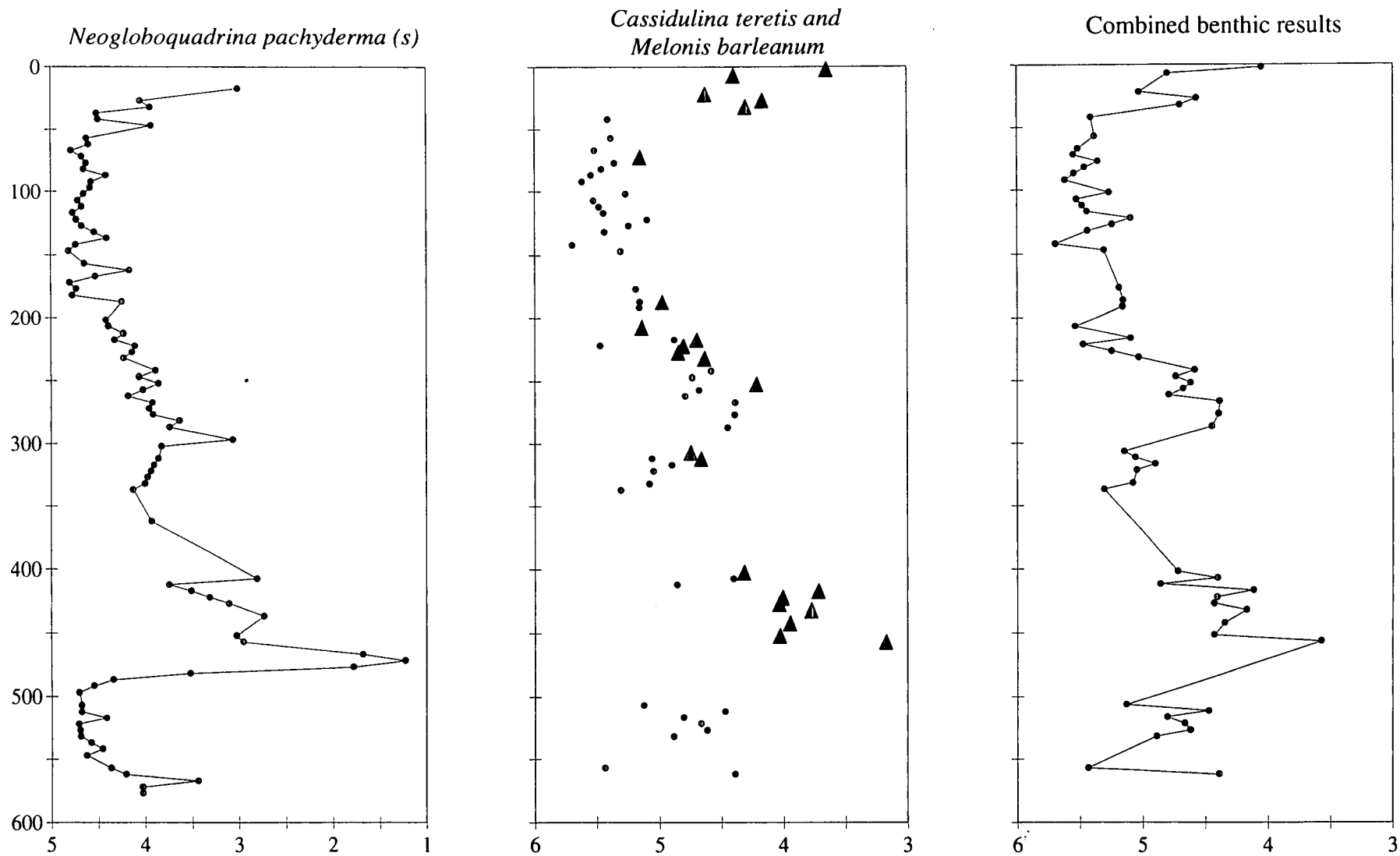

Fig. 4.2. Oxygen isotope measurements of planktic and benthic foraminifera from PCM30. Second graph, *Melonis barleanum* triangles and *Cassidulina teretis* circles. For the combined benthic curve a correction factor of 0.4 per mil was added to analyses of *M. barleanum*

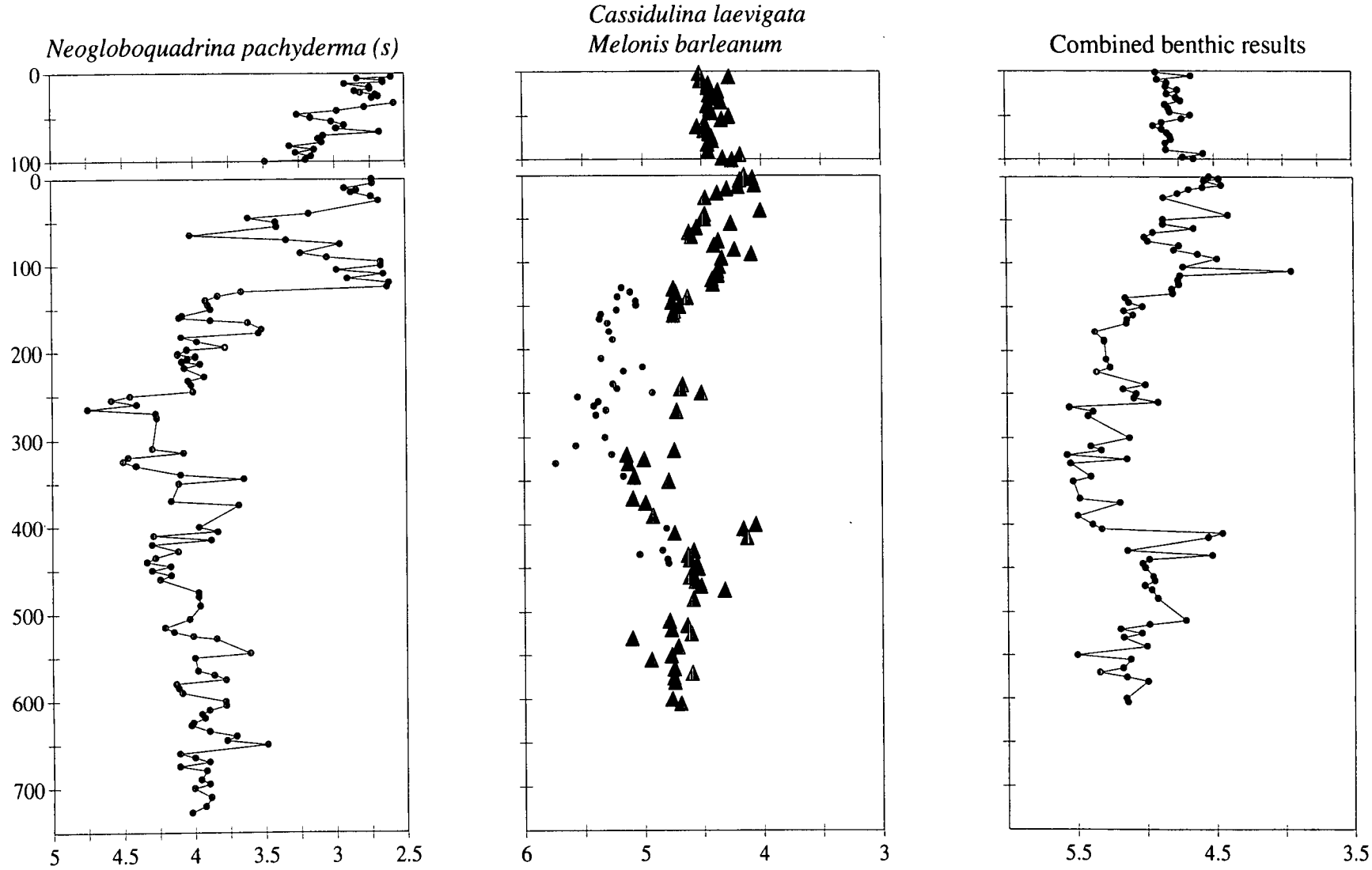

Fig. 4.3. Oxygen isotope data for PCM7. Planktonic species on the left, then two benthic species, the third graph shows a combined benthic isotope curve produced by adding 0.4 per mil to the values of *Melonis barleanum* (triangles). Vertical scale depth in cm, horizontal scale per mil deviation in oxygen isotope composition w.r.t. PDB standard.

4.4.3. The benthic $\delta^{18}O$ record of PCM7

The same species were analysed as in PCM30, namely *C. teretis* and *M. barleeanum*. The results, before a correction factor was applied to produce a combined benthic curve, are shown in fig. 4.3. The majority of measurements were carried out on *M. barleeanum*, which are represented by the large triangles. Analyses of *C. teretis* (small circles in the plot) were made to fill in some of the sampling gaps between 120cm and 450cm. A correction factor of +0.4‰ was added to the $\delta^{18}O$ measurements of *M. barleeanum* to produce the combined benthic curve. This curve will be described in more depth below.

The base of the core up to 610cm was to poor in benthics for analyses to be carried out. The initial section analysed from 605-510cm has $\delta^{18}O$ values of between 5.1-5.2‰. Values then drop to a stable plateau of around 4.9-5.0‰ until 430cm. At this point there is a sharp drop in $\delta^{18}O$ values to 4.5‰ to 400cm, although one point with a value of 5.1‰ is found at 410cm which may be reworked. A stable plateau is then reached with $\delta^{18}O$ values of between 5.3-5.5‰ from 390-255cm, this is then replaced by a short section with $\delta^{18}O$ values of around 5.0‰ from 250-220cm. Values rise to about 5.3‰ until 160cm then drop back to 5.0‰ until 130cm. A drop to 4.7-4.8‰ until 75cm is interrupted by a $\delta^{18}O$ value of 3.9‰ at 100cm, this point is probably a poor measurement. Values then increase to 4.9-5.0‰ and decrease gradually at first but more quickly later to 4.4-4.6‰ from 12.5cm until the top of the core. The trip core above the main part of the core has stable $\delta^{18}O$ values throughout of 4.8-5.0‰.

4.5. Meltwater and current circulation history of the Fram Strait over the last 200 ka from oxygen isotope evidence

As mentioned in the introduction benthic foraminifera living on the ocean floor should record global ice volume fluctuations. Deep waters are in general very cold and experience little temperature fluctuations. The amplitude of the ice volume effect from full glacial to full interglacial is approximately 1.2‰ (Berger, 1979). The benthic $\delta^{18}O$ records should have a similar amplitude if ice volume changes dominate the $\delta^{18}O$ record. Low density meltwater spikes should not penetrate deep enough to affect benthic foraminifera, but a process has been suggested by The Nansen Arctic Drilling Program Science Committee (1992) to enable isotopically light meltwater to penetrate to significant depth. Continued melting and re-freezing at the ice front will produce a volume of meltwater with the isotopic signature of ice, but with a high salinity.

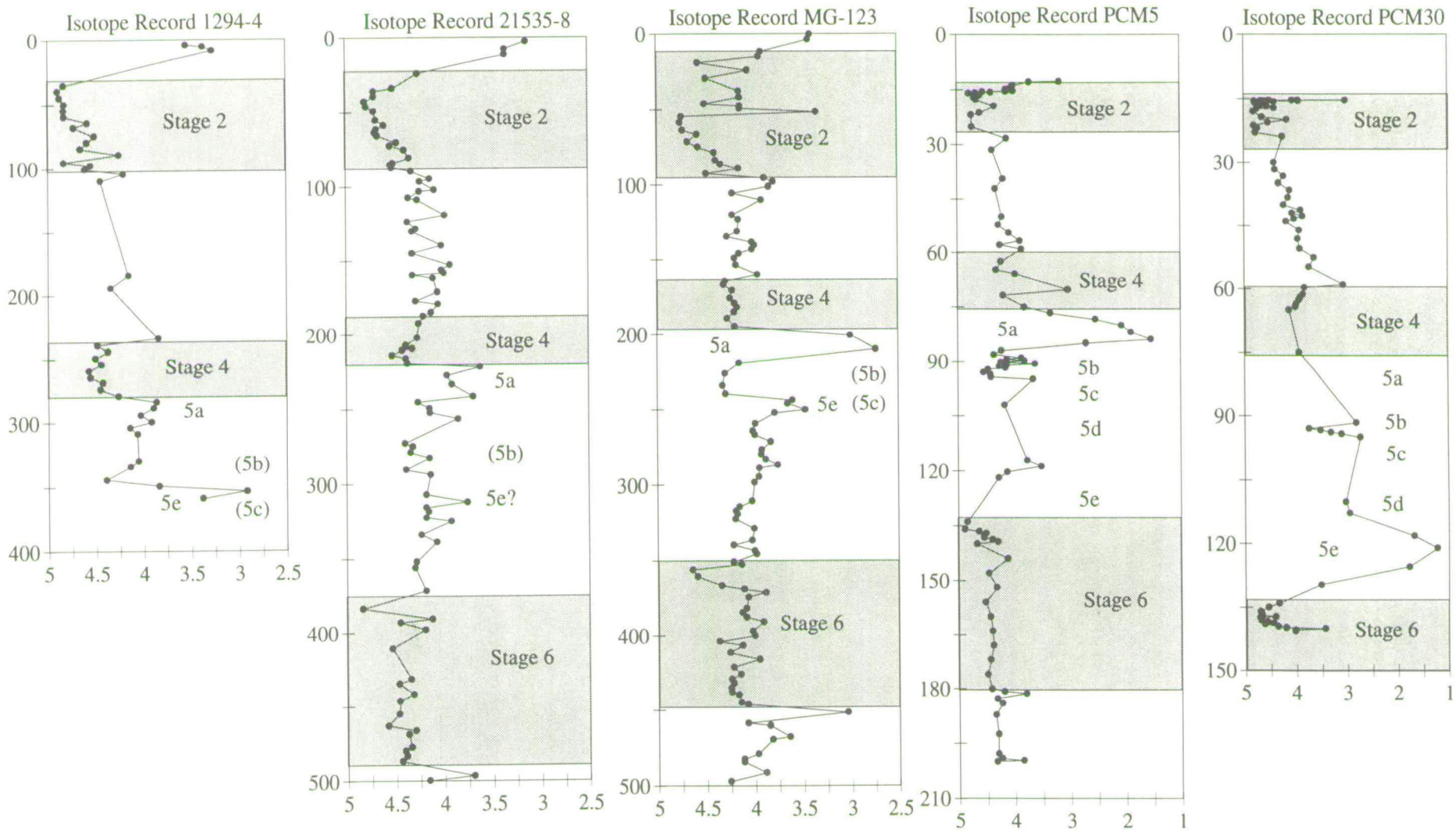

Fig. 4.4. Oxygen isotope data from Fram Strait cores plotted with data from PCM5 and PCM30 from this study, glacial stages are shaded, present authors interpretation. Original authors stage assignments for Fram Strait cores are shown, re-interpretations from this study shown in brackets. Fram Strait cores plotted against depth in metres, PCM5 and PCM30 plotted against age, note change in isotope scale.

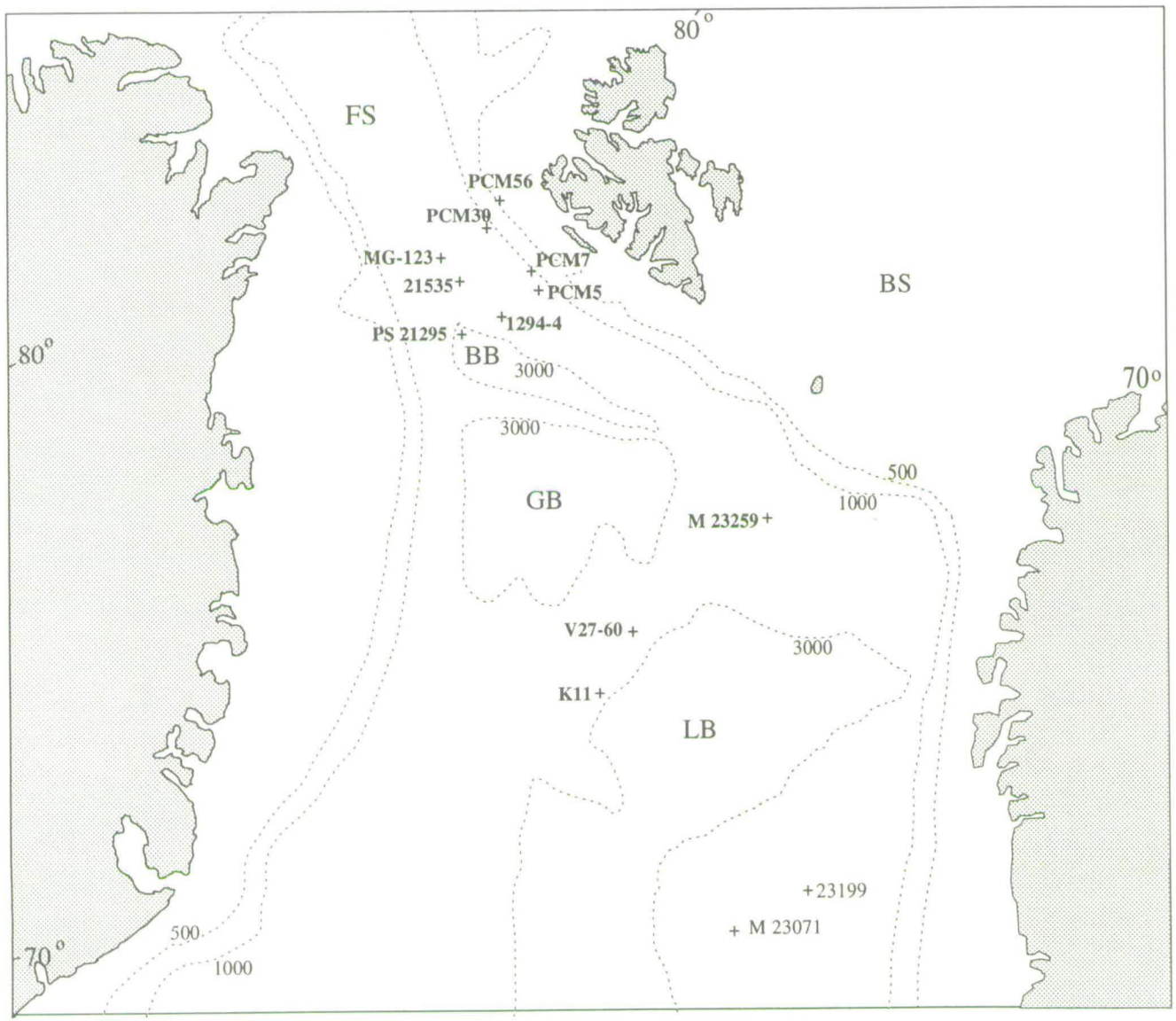

Fig. 4.5. Map of Greenland Sea and Barents Shelf showing position of cores from this study and other cores referred to in text;

PCM56, PCM30, PCM7, PCM5 from this study.
1294-4, from Hebbeln, (1992).
21535, from Kohler and Speilhagen, (1990).
MG-123, from Morris, (1988).
PS 21295, from Jones and Keigwin, (1988).
M 23259, from Weinelt et al. (1992).
V27-60, from Duplessy et al. (1988).
K11, from Duplessy et al. (1988).
23199, from Haake and Pflaumann (1989).
M 23071, from Sarnthein et al. (1992).

FR - Fram Strait
BB - Boreas Basin
GB - Greenland Basin
LB - Lofoten Basin
BS - Barents Shelf

Submarine contours in metres.

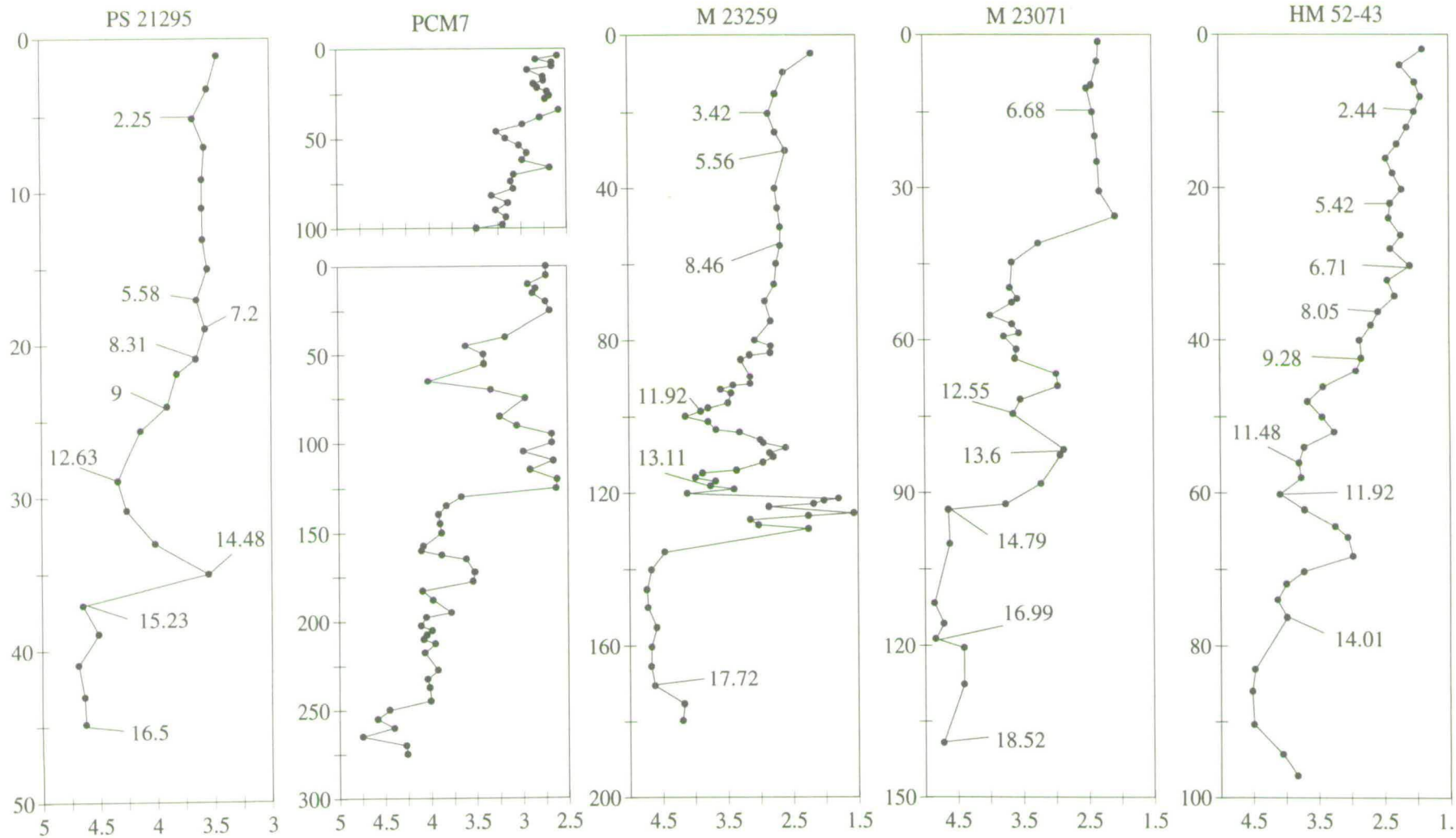

Fig. 4.6. Oxygen isotope data of the last deglaciation from Norwegian/Greenland Sea cores, see fig. 4.5 for position of cores. All vertical scales are depths in cm, radiocarbon dates have been marked also. Horizontal scale is the oxygen isotope scale expressed as per mil variation from PDB standard, all measurements were made on the planktic foraminifera, *Neogloboquadrina p. (sinistral).*

Re-freezing of meltwater causes a concentration of salt in remaining unfrozen meltwater, this becomes more and more concentrated as melting and re-freezing continues. Very cold dense brines with a light oxygen isotope signature are formed, these would flow down the continental slope influencing the oxygen isotopic composition of benthic foraminifera on the way. This process has been observed off the continental margin of Antarctica. There is evidence that meltwater does have an effect on the benthics in some brief sections of the cores in this study, these events will be mentioned in the following discussions.

4.5.1. History from 200,000 to 136,000 years

The oxygen isotope record of stage 6 is represented in PCM5 and PCM30 (figs. 4.7 and 4.8). The planktic $\delta^{18}O$ record shows typical glacial values similar to stage 2, 4.5‰ for most of stage 6 in PCM5 (fig. 4.7) then rising to 4.6-4.8‰ for the end of stage 6. These heavy oxygen isotope values were produced by cold Polar surface waters originating from the Arctic Ocean to the north, temperatures would be near 0°C, and sea ice would be common. The benthic $\delta^{18}O$ record of PCM5 shows heavy glacial values of 5-5.5‰. The benthic stage 6 record of PCM30 is inconsistent. There are several points with values of 5-5.5‰ but also one section occurs with values below 5‰, the reason for this is uncertain. The normal glacial $\delta^{18}O$ values of 5-5.5‰ represent cold bottom waters, with a temperature at or below 0°C, and high global ice volumes.

4.5.2. History from 136,000 to 85,000 years

The stage 5 oxygen isotope records of both planktics and benthics are characterised by rapid high amplitude fluctuations. Combining the records from PCM5 and PCM30 provides a fairly complete record for stage 5. PCM30 records the early period of stage 5, substages 5e, 5d and 5c, while PCM5 records the later period more clearly, substages 5c, 5b and 5a.

Substage 5e

The planktic record for substage 5e from PCM30 (fig. 4.8) shows remarkably light $\delta^{18}O$ values ranging from 1.2-1.7‰. As mentioned earlier this core records a better oxygen isotope record of substage 5e than any other published data from the Greenland Sea, the values recorded are considerably lighter than any other recorded values for this period. The amplitude of the glacial-interglacial shift at the stage 6-5 boundary is 3.4‰, which is much greater than expected.

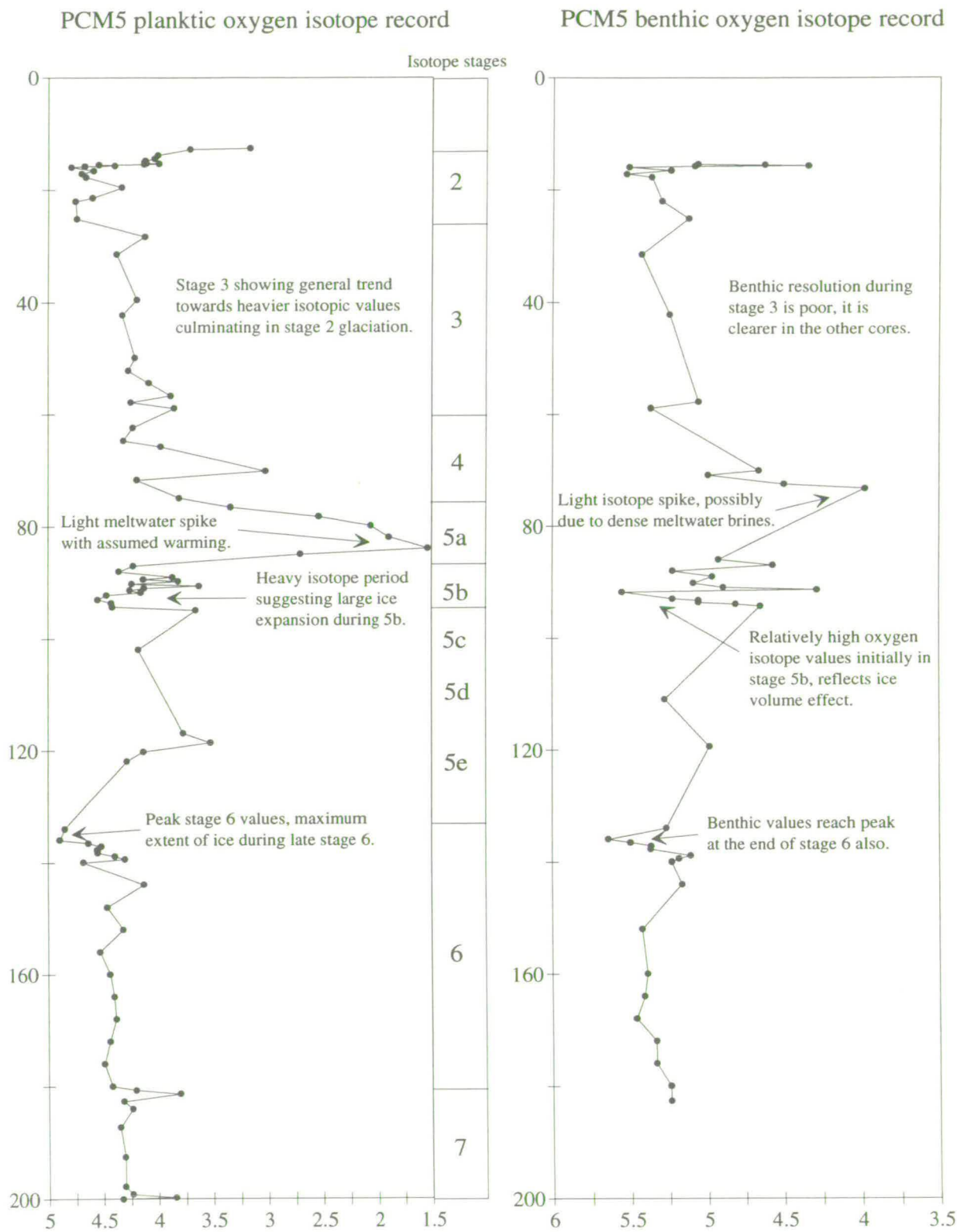

Fig. 4.7. Planktic and benthic oxygen isotope records for PCM5 plotted against age on vertical axis. Oxygen isotopic composition on horizontal axis, per mil w.r.t. PDB. The oxygen isotope stages are labelled in the box beside the planktic curve.

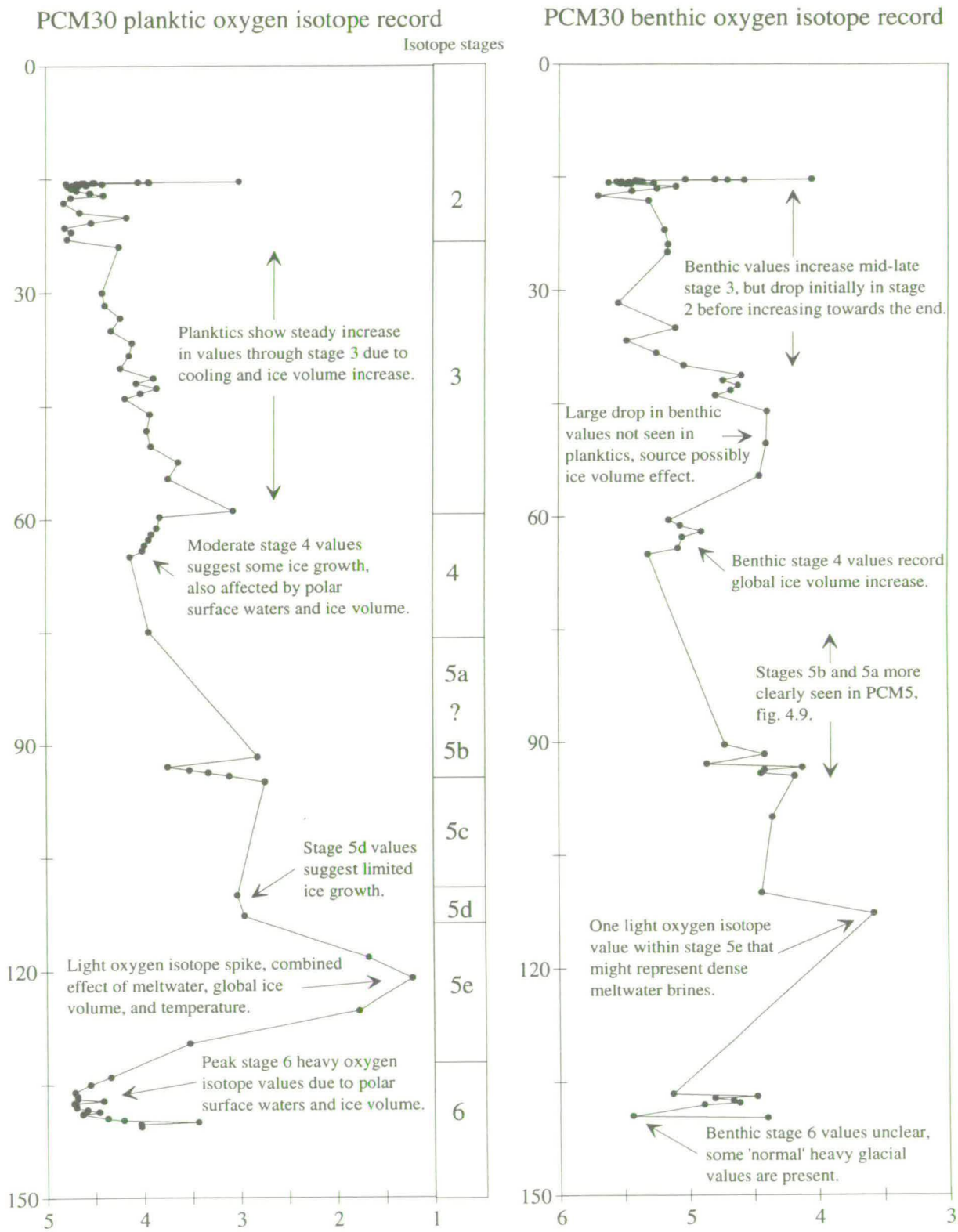

Fig. 4.8. Planktic and benthic oxygen isotope records for PCM30 plotted against age on vertical axis. Oxygen isotopic composition on horizontal axis, per mil w.r.t. PDB. The oxygen isotope stages are labelled inthe box beside the planktic curve, taken from age model of chapter 2.

Normal interglacial $\delta^{18}O$ values for this area are approximately 2.5-2.6‰, as shown by the top of PCM7 in fig. 4.10, and other cores mentioned earlier. Assuming that during substage 5e the global ice volume was similar to the present interglacial, an ice volume effect of 1.2‰ can be expected. If this is subtracted from the total oxygen isotope amplitude (3.4‰) a shift of 2.2‰ remains. This must be produced by the combined effects of temperature and meltwater. Substage 5e, also known as the Eemian interglacial, is considered from global evidence as warm or slightly warmer than the present (LIGA members, 1991).

Surface currents during stage 6 are estimated at near 0°C. North Atlantic water entering the Norwegian-Greenland Sea has an initial temperature of 6-8°C. By the time this current reaches the Spitsbergen margin, in the form of the present day West Spitsbergen Current, its temperature will have dropped to 3-4°C (Quadfasel and Meincke, 1987). So surface waters during substage 5e were most probably around 4°C warmer than glacial values perhaps slightly higher, this would produce an isotopic effect of 0.8-1‰. However, as mentioned in the introduction, *N. pachyderma* (sinistral) does not live near the surface of North Atlantic waters. They prefer to live at depths of around 50m according to Johannessen *et al.* (in press), or in a depth range of 100-200m according to Carstens and Wefer (1992), who studied the distribution of *N. pachyderma* (sinistral) in plankton tows. Temperatures at this depth would be low, 1-2°C at most and quite possibly around 0°C. Temperature effects are thus probably small and most of the shift is due to salinity. This minor temperature change would produce a $\delta^{18}O$ shift of between 0-0.4‰. Assuming a maximum temperature effect of 0.4‰, this leaves a 1.8‰ oxygen isotope shift to be accounted for by meltwater influx. Johannessen *et al.* (in press) calculated a salinity effect of 0.6‰ in $\delta^{18}O$ per 1‰ salinity change from the North Atlantic Mixing Line (Craig and Gordon, 1965). Using this calculation, the meltwater spike recorded in PCM30 would be produced by surface water with a salinity of 3‰ less than normal. This suggests that during substage 5e a large body of water with a salinity of 32‰ covered large areas of the Spitsbergen continental margin. This is an exceptionally intense meltwater influx and could explain the lack of subpolar foraminifera found in the samples of this age. Such a meltwater lid may have allowed only the deeper living polar species to survive.

The benthic $\delta^{18}O$ record for substage 5e unfortunately is not as good as the planktic record (fig. 4.8). There is one point that may represent the latter period of substage 5e. Using this point the stage 6-5e oxygen isotope amplitude is 1.7‰ (taking an average stage 6 $\delta^{18}O$ value of 5.2‰ and substage 5e value of 3.5‰). The usual

benthic glacial-interglacial amplitude produced by the ice volume effect is 1.2‰. The amplitude in PCM30 is 0.5-0.7‰ greater than this. This suggests there is some temperature or meltwater effect present in the PCM30 benthic record. There are two possible explanations for this greater than expected amplitude. The production of dense meltwater brines, mentioned earlier, could produce a lighter oxygen isotope value. Melting and re-freezing of meltwater at the ice margin concentrates salt, producing very cold, saline isotopically light meltwater that could sink and flow down the continental slope. The other alternative is a different deep water mass influencing bottom water conditions in the area during substage 5e. The mixing of Atlantic surface water entering the Greenland Sea with Polar surface water and further cooling and sinking could form a cold saline intermediate water mass. This situation happens at the present time, and is the proposed method of production of a large proportion of North Atlantic Deep Water (NADW), this will be discussed in more detail in the Paleoceanography chapter. It seems unlikely that such a deep water mass would have formed in this area during substage 5e due to the intense meltwater lid produced by melting. This would exclude North Atlantic waters from the area, this idea is supported by the lack of subpolar foraminifera in the cores at this time. So during substage 5e dense meltwater brines are the most likely cause of an increased glacial-interglacial $\delta^{18}O$ amplitude in the benthic foraminifera.

Substages 5d and 5c

The oxygen isotope record during substage 5d from PCM30, with planktic $\delta^{18}O$ values of 3‰ and with benthic $\delta^{18}O$ values of 4.5‰, suggest stadial type conditions, see fig. 4.8. The increase in benthic $\delta^{18}O$ values from substage 5e to 5d may represent a return to glacial style deep waters, and therefore a reduction in the production of NADW, if it was produced during substage 5e, or may be due to the ice volume effect. Substage 5c is poorly represented in both cores, and probably acts as a period of ice build-up, as suggested in chapter 3.

Substage 5b

The other periods of stage 5 are more clearly represented in PCM5 (fig. 4.7). Substage 5b is characterised by a group of relatively heavy oxygen isotope values. The planktic $\delta^{18}O$ values for early substage 5b are 4.5‰, these decrease to 4.0-4.2‰ towards the end. Substage 5b represents a period of significant ice build-up on the Spitsbergen margin, possibly as large as stages 6 and 2, this was shown from ice rafting evidence in chapter 3. The planktic $\delta^{18}O$ values are slightly lower during substage 5b than during stages 6 and 2. This may be due to a reduced ice volume effect, global ice volumes being slightly smaller during substage 5b than peak glacial

times. The benthic $\delta^{18}O$ values are surprisingly low initially, but rapidly increase to reach typical glacial values midway through substage 5b. The $\delta^{18}O$ values increase from 4.2‰ to 5.1‰. This amplitude is similar to the one of the ice volume effect, which most likely affects the benthics over this section. Towards the end of substage 5b both planktic and benthic $\delta^{18}O$ values fluctuate quite markedly, this may represent initial melting at the substage 5b-5a transition.

Substage 5a

Substage 5a in PCM5 shows a similar isotopic spike to substage 5e in PMC30 (fig. 4.7). Oxygen isotope values drop from 4.1‰ to 1.5‰, resulting in an amplitude of 2.6‰. The ice volume amplitude from substage 5b to substage 5a must be less than from stage 6 to substage 5e. Global ice volume was greater during full glacial stage 6 than stadial 5b, and would be less during substage 5e than substage 5a. A maximum estimate of 0.9‰ difference leaves a 1.5‰ shift due to temperature and meltwater effects. Sea surface temperatures during substage 5a were most probably less than during substage 5e, and using the assumption that *N. pachderma* (sinistral) lives below 50m the temperature effect on $\delta^{18}O$ values would be small, probably zero. From the calculations of Johannessen *et al.* (in press) this could be accounted for by a water body with salinity 2.5‰ less than normal. The salinity values of this surface meltwater cap would be approximately 32.5‰ (assuming a normal salinity of approximately 35‰). This calculation is a maximum estimate of the meltwater effect as there may be some temperature effect. From these assumptions the meltwater influx to the Spitsbergen margin during substage 5a was extensive, though not quite as great as during substage 5e, and can also be used as an explanation for the low abundances of foraminifera during this period.

The benthic $\delta^{18}O$ record of the substage 5b-5a transition, though not particularly good, does allow the minimum amplitude of change to be seen, which is shown in fig. 4.10. As in the substage 5e record of PCM30 the benthic $\delta^{18}O$ record for substage 5a is incomplete, but one value is found corresponding to late substage 5a. From the age model for PCM5 this point lies within stage 4, but has most probably been re-worked from substage 5a, and can therefore be used to calculate the substage 5b-5a $\delta^{18}O$ amplitude. The substage 5b-5a oxygen isotope amplitude has a value of 1.5‰. Using a slightly reduced ice volume effect assumed for the substage 5b-5a transition above, leaves an excess of at least 0.6‰ to be explained by temperature or meltwater effects. The same two possibilities as outlined above for substage 5e can be used here, but as with substage 5e dense meltwater brines are the more likely explanation.

4.5.3. History from 85,000 to 25,000 years

The most complete record of stage 4 is found in core PCM30 (fig. 4.8). Stage 3 can be seen clearly in PCM7 and PCM30 (figs. 4.9 and 4.8). This period of the $\delta^{18}O$ record in PCM5 is poor. The stage 4 $\delta^{18}O$ values from PCM30 are 4‰ for planktics and 5‰ for benthics. The absolute $\delta^{18}O$ values are on average 0.5‰ lower during stage 4 than during peak glacial periods. This is best explained by a reduced global ice volume during stage 4 compared to the situation during peak glacials. The oceanography of the Spitsbergen margin was probably similar to the situation in glacial periods; a well stratified water column and cold Polar surface waters flowing south.

The beginning of stage 3 is marked by a distinct drop in benthic $\delta^{18}O$ values to 4.5-4.7‰ in PCM30 (fig. 4.8). A similar drop is seen in the benthics of PCM7 (fig. 4.9) though slightly later. The planktic $\delta^{18}O$ records do not show such a prolonged drop, PCM30 shows an initial drop but values immediately rise, and continue rising steadily throughout stage 3. This suggests a gradual cooling of the area, reduced meltwater fluxes, lower surface temperatures, and increased global ice volumes. The planktic oxygen isotope stage 3 record of PCM7 shows a more fluctuating system with distinct periods of meltwater production, but with small amplitudes. The isotopically light benthic event may be an ice volume effect, recording a reduction in global ice volume at the end of stage 4, but it is not represented in the planktic record. It may therefore represent a change in deep water characteristics. It could not be produced by an intermediate water mass forming from Atlantic water as there is no planktic foraminiferal, or planktic oxygen isotope evidence for influx of Atlantic waters during this time. It is also unlikely to result from the formation of dense meltwater brines, as no meltwater is recorded in the planktic foraminifera either. The most likely reason appears to be the global ice volume effect. After this period the benthic $\delta^{18}O$ values tend to increase towards the glacial stage 2 values. The benthic $\delta^{18}O$ values reach full glacial values before the planktics in PCM7 and PCM30.

4.5.4. History from 25,000 to 8,500 years

The oxygen isotope record of stage 2 and the transition from stage 2 to stage 1 is represented in most detail in PCM7 (fig. 4.10). Stage 2 is also recorded in PCM5 and PCM30, the latter period for both cores are shown in fig. 4.11.

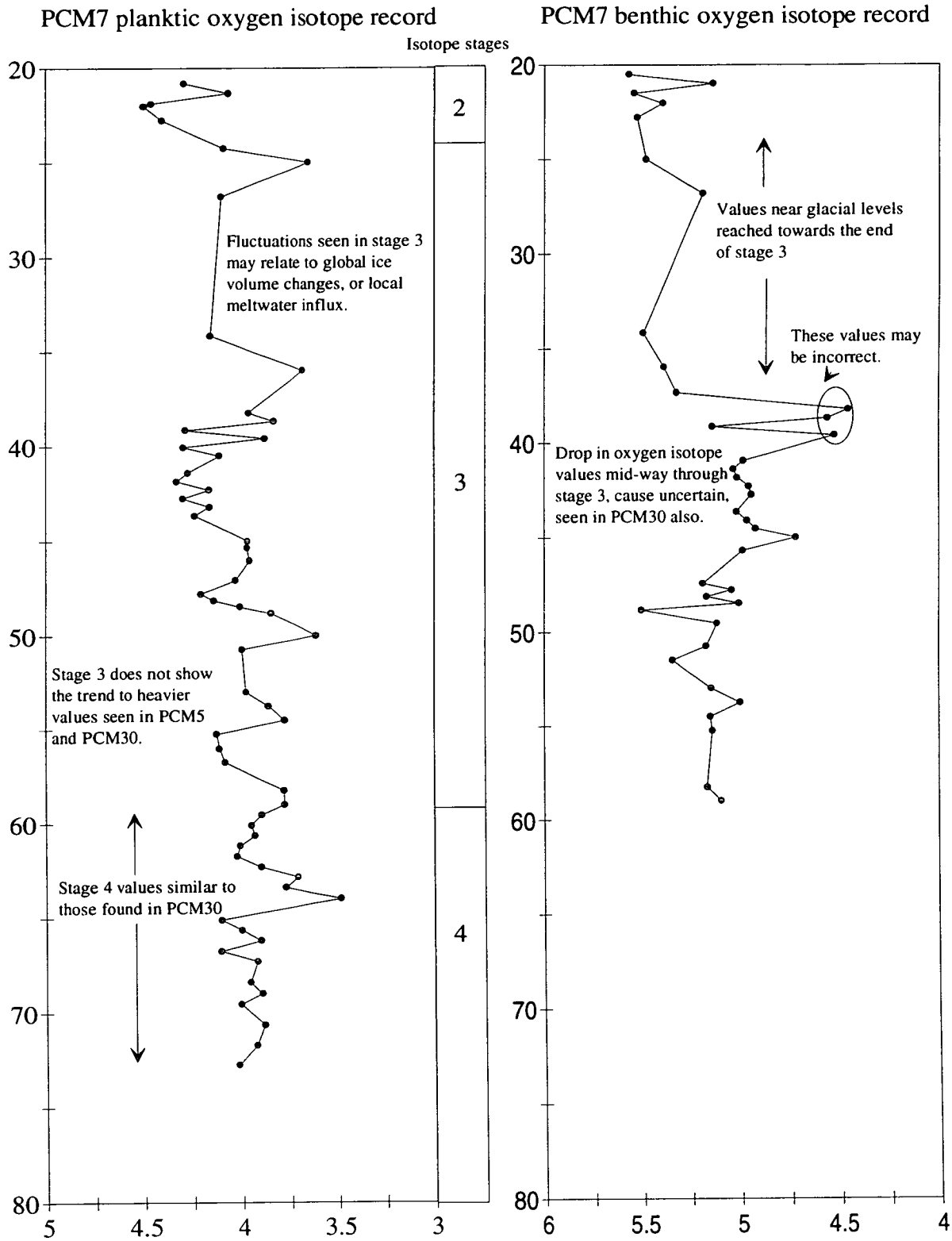

Fig. 4.9. Planktic and benthic oxygen isotope records for PCM7 plotted against age on vertical axis. Oxygen isotopic composition on horizontal axis, per mil w.r.t. PDB. Oxygen isotope stages are labelled in the box beside the planktic curve, taken from age model of chapter 2.

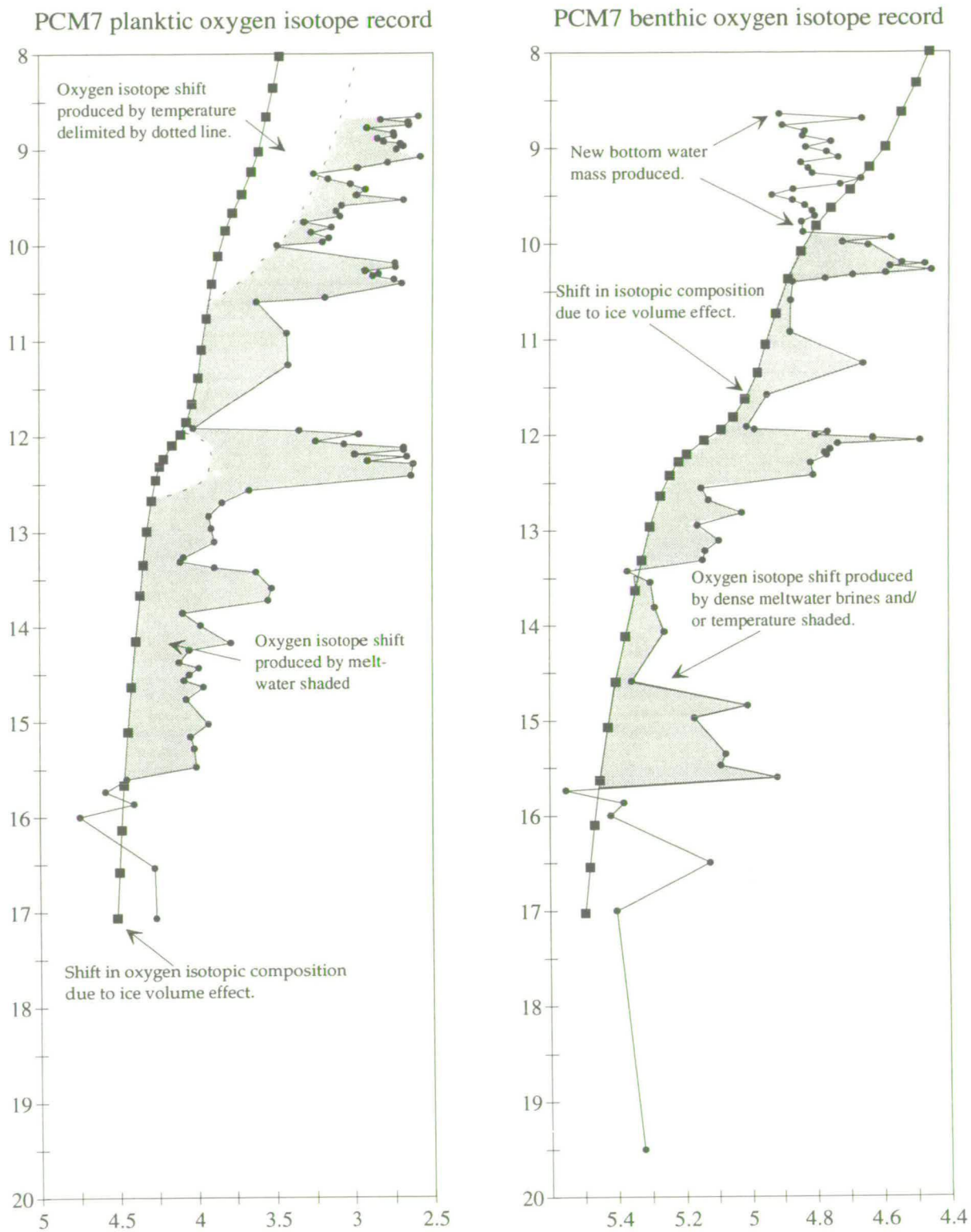

Fig. 4.10. Planktic and benthic oxygen isotope records for PCM7 plotted against age in kyrs, vertical scale. Joined circles on graph represent oxygen isotope measurements w.r.t. PDB from the core. Large squares represent an estimation of the ice volume effect from the Fairbanks (1989), explained in text. Dotted line in planktic graph represents isotopic shift caused by temperature change, shaded area represented isotopic shift due to meltwater influx. In benthic graph shaded area represents influence of dense meltwater brines, with possibly some temperature effect, see text for explanation.

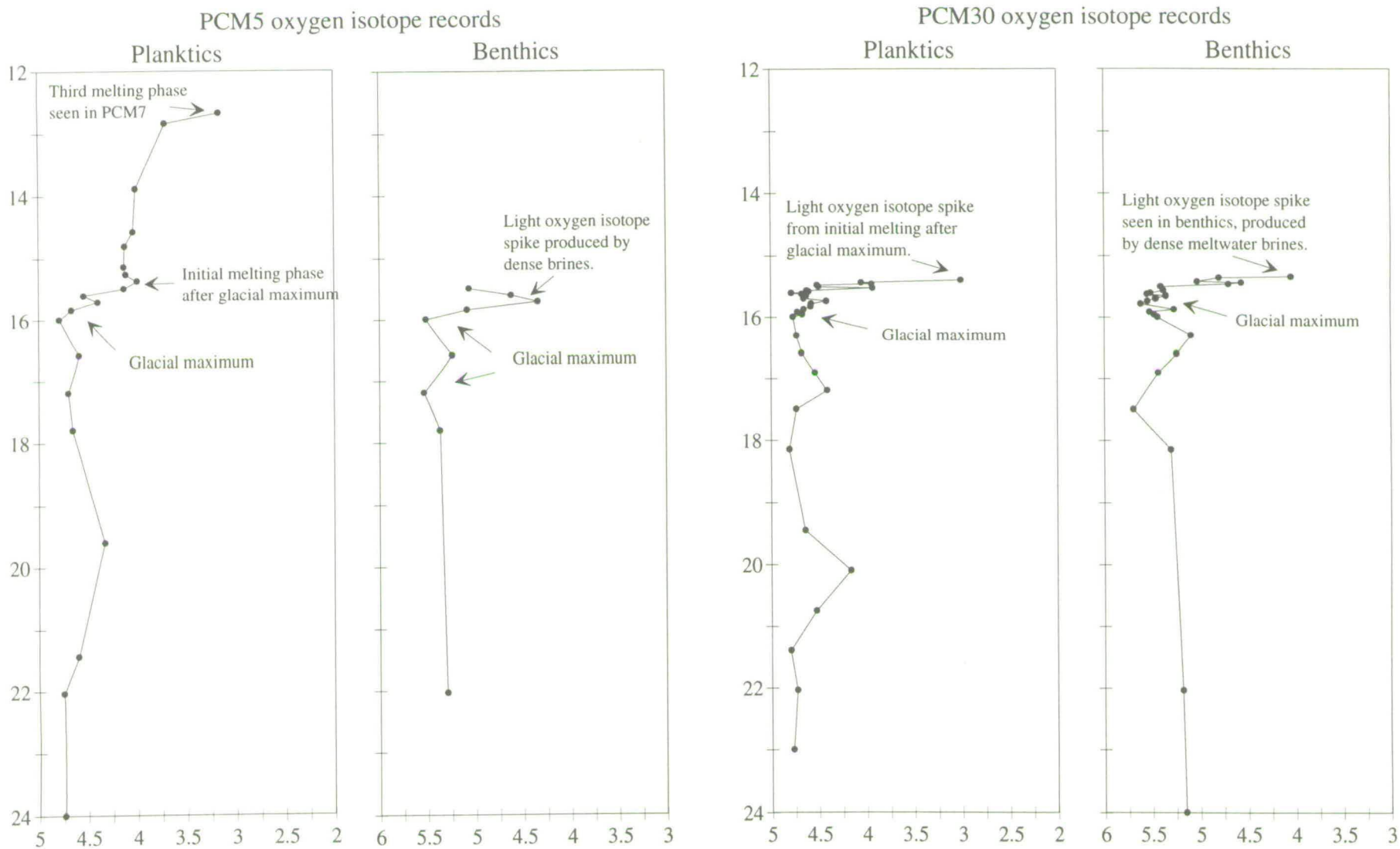

Fig. 4.11. Planktic and benthic oxygen isotope records from PCM5 and PCM30. The records are plotted against time for the period 12ka to 24ka years to show detail of the initial melting phase after the peak of the last glaciation. Oxygen isotope composition on the horizontal scale, per mil w.r.t. PDB standard.

All three cores show peak stage 2 $\delta^{18}O$ planktic values of 4.7-4.8‰, typical glacial values with surface water temperatures around 0°C and abundant sea ice formation. Benthic $\delta^{18}O$ values in all three cores average 5.5‰, leaving a benthic minus planktic value of between 0.5-1.0‰. This contrast may be produced by different water mass characteristics, possibly a salinity difference since temperature effects should be low as both water masses are close to 0°C, though the deeper water mass might be slightly below freezing. Vital effects in the planktics may cause some of the variation also. Johannessen *et al.* (in press) suggest a vital effect of 0.5‰ for living specimens of *Neogloboquadrina pachyderma*, which has not be taken into account in this study.

The record from PS 21295 from the central Fram Strait (Jones and Keigwin, 1988) also records the later part of stage 2 and stage 1. This record is shown in fig. 4.6 along with PCM7 and other cores from the Norwegian Sea. PS 21295 shows an initial melting event at 14.5ka ago, values then increase to 4‰ by 12.6ka, and then reduce gradually reaching 3.5‰ during the Holocene. These Holocene values indicate that the area was under the influence of Polar surface waters throughout the whole of the Holocene. The period of heavy $\delta^{18}O$ values at 12.6ka in PS 21295 is represented by much lighter $\delta^{18}O$ values in PCM7 with a difference of at least 1.4‰ between the two. This suggests a decoupling of the current system between the central Fram Strait and the Spitsbergen margin at approximately 12.5ka. The isotopic effects of meltwater and temperature increase experienced on the Spitbergen margin did not extend into the central Fram Strait. Atlantic waters were kept close to the eastern side of the basin, only flowing westwards at higher latitudes, 80°N or higher. The other explanation is that the isotope resolution in PS 21295 is too poor to register the changes seen in PCM7 over this period.

Just after the peak glacial period at 16ka melting began in the area, see figs. 4.10 and 4.11. This is also seen in the benthics of PCM5 and PCM30. The benthic record of PCM5 ends soon after the initial melting episode, but does record this phase in which $\delta^{18}O$ values drop from peak glacial values of 5.6‰ to values of 4.5‰. PCM30 shows a similar event in the benthic record; $\delta^{18}O$ values dropping from 5.6‰ to 4.1‰ at the very top of the core. Some of this drop may be accounted for by global ice volume changes, but only a small amount, perhaps 0.1-0.2‰. The rest of the $\delta^{18}O$ shift measured in benthics must be caused by dense meltwater brines mentioned earlier. The benthic record in PCM7 is more complete and shows this event also. The benthic oxygen isotope values drop from glacial values of 5.6‰ to about 5‰ initially, then rise to 5.3‰. This rise to 5.3‰ occurs once the effect of the dense meltwater brines has gone due to mixing, the benthic values are then 0.2-0.3‰ lighter

than full glacial values. This 0.2-0.3‰ drop represents the ice volume change over this initial deglacial event.

The planktic and benthic oxygen isotope records for PCM7 are shown in fig 4.7 along with a curve representing the change in isotopic composition expected due to the ice volume effect from Fairbanks (1989), as mentioned in the introduction. This curve, shown as joined squares in fig 4.7, has been superimposed on the planktic and benthic curves assuming full glacial $\delta^{18}O$ foraminiferal composition, with a $\delta^{18}O$ value of 4.5‰ for planktics and 5.5‰ for benthics. Benthic foraminifera are expected to record changes in ice volume, but little change in temperature or salinity. If this were so one would expect the benthic curve to match the ice volume curve accurately, but fig. 4.10 shows this is not the case. The shaded section between the two curves represents the excess $\delta^{18}O$ shift not accounted for by ice volume. This must be produced by temperature and meltwater effects on bottom waters.

For the planktic $\delta^{18}O$ record only part of the section between the two curves has been shaded. This shaded area represents the excess $\delta^{18}O$ shift produced by meltwater. In two sections a dotted line delimits a portion of the difference between ice volume effect and actual readings. These sections left unshaded represent a $\delta^{18}O$ shift of 0.2-0.4‰ produced by the possible maximum temperature increase. The amplitude of the temperature effect has been estimated based on the appearance of subpolar foraminifera in samples. The appearance of subpolar foraminifera is produced by the influx of North Atlantic surface waters into the area. At the present day, the West Spitsbergen Current originating from North Atlantic water has a temperature of 4-5°C. This would be expected to produce a temperature effect of 0.8-1.0‰ in the oxygen isotope values measured. As mentioned earlier this is not the case, because *N. pachderma* (sinistral) lives at water depths of 100m in North Atlantic waters (Carstens and Wefer, 1992), water at this depth would be only 1-2°C at most, and possibly closer to 0°C, producing a $\delta^{18}O$ temperature effect of 0.2-0.4‰.

The first influx of subpolar foraminifera between 12.5-12 ka ago is interpreted as having a temperature effect of 0.2‰ at most because the subpolar foraminifera made up only 20% of the assemblage, see chapter 6. The second influx of subpolar foraminifera from 10.5 ka onwards was more significant, so a temperature effect rising to 0.4‰ by the top of the trip core has been assumed.

Changes in planktic and benthic oxygen isotope records are synchronous to a certain extent, both record an initial melting event at 15.5 ka. The planktic values drop to an

average of 4.0‰ until 13.7 ka. This represents a meltwater effect of 0.5-0.6‰, surface waters with a salinity of 1‰ less than normal could acccount for this (using the mixing line of Craig and Gordon, 1965). There is then a second major melting event at 13.6 ka, $\delta^{18}O$ values drop to 3.5‰. This represents a further drop in salinity by 0.8‰. So surface waters with a salinity of about 33‰ must have been present during this period. Oxygen isotope values then rise to about 4.0‰ again due to mixing of the meltwater with more saline surface waters increasing their salinity until roughly 12.6 ka.

The benthic $\delta^{18}O$ curve registers the initial melting event due to the influence of dense meltwater brines. These reduce the $\delta^{18}O$ values by 0.4‰, equivalent to a salinity reduction of about 0.7‰. The effect of these brines has worn off before 14 ka as the oxygen isotope curve of the benthic foraminifera rises and intersects the ice volume curve again. This implies the benthics at this point, 14-13.4 ka, record the ice volume effect only because the two curves are very close. The benthics do not record the melting event at 13.6 ka, but show a second influx of dense brines at 13.3 ka, values drop to 5.1‰. This is approximately 0.2‰ below the ice volume curve, and can be explained by water with a salinity of 0.3‰ below present values.

A third major melting event is recognised 12.3 ka ago in both the planktic and benthic $\delta^{18}O$ curves. The planktic oxygen isotope values drop to 2.6‰, and the benthic values drop to 4.75‰. This event coincides with a major global melting event seen in a steepening of the ice volume curve at this point. There is still a 1.6‰ $\delta^{18}O$ amplitude in planktics produced by temperature and salinity changes. As mentioned above 0.2‰ of this shift can be explained by a temperature increase, this leaves a 1.4‰ shift produced by meltwater. A surface meltwater plume with a salinity value of 2.2‰ less than present values would cause this shift. The benthic foraminifera record an excess of 0.35‰ $\delta^{18}O$ shift produced by dense brines, equivalent to a salinity drop of 0.7‰.

The subpolar planktic foraminifera then disappear and oxygen isotope values increase again to 4.0‰ in planktics and 5.0‰ in benthics. The meltwater plumes have totally dissipated, and Polar surface waters have invaded the area again. At this point, 12 ka ago, both planktic and benthic $\delta^{18}O$ curves match the ice volume curve, so both were recording ice volume changes only. Therefore at this time the oceanographic regime had returned to a glacial style system.

This episode was short lived and meltwaters began to influence both surface and deep waters again. The benthic foraminifera record a minor influx of cold brines that rapidly dissipated, leaving the benthic $\delta^{18}O$ curve near the ice volume curve again from 11.0-10.5 ka. Over this period the planktic foraminifera record a meltwater influence, which produced a 0.5‰ $\delta^{18}O$ shift.

A fourth meltwater event can be recognised at 10.5 ka again in the $\delta^{18}O$ records of both planktic and benthic foraminifera. The planktic foraminifera also record a second influx of subpolar species at this point, so some temperature increase must be taken into account. As mentioned above a temperature increase of 1-2°C has been assumed for this period resulting in an oxygen isotope shift of 0.2-0.4‰ at most. The planktic $\delta^{18}O$ values drop to 2.6‰, the ice volume effect at this time accounts for a 0.5‰ $\delta^{18}O$ shift. Glacial values of 4.5‰ result in an amplitude of 1.9‰. Subtracting the ice volume and temperature effects from this leaves 1.0-1.2‰ shift in $\delta^{18}O$ values produced by meltwater. This reflects a meltwater plume with a salinity 1.8-2.0‰ less than normal sea water. Benthic $\delta^{18}O$ values drop to an average of 4.55‰. This produces an oxygen isotope shift of 0.35‰ caused by meltwater, equivalent to a salinity drop of 0.5-0.6‰ in a deep water plume.

The meltwater effects on the $\delta^{18}O$ composition of both planktic and benthic foraminifera had dissipated by 10 ka ago. The planktic $\delta^{18}O$ values increased to 3.5‰, and the temperature effect accounted for the whole oxygen isotope shift. Meltwater influences return at 9.6 ka, and from 9.1 ka to the top of the core at approximately 8.7 ka ago. At 10 ka ago, the benthic oxygen isotope values increased to 4.8‰ and values remained at approximately this level throughout the rest of the core. Fig 4.7 shows the benthic oxygen isotope curve actually crossing the ice volume curve at 10 ka ago, and remaining above the curve from then on. This means that either the temperature of bottom waters decreased or the salinity increased. As temperatures were 0°C or slightly less a temperature decrease is unlikely, so salinity must have increased. The oxygen isotope values at 9 ka ago are approximately 0.2‰ greater than expected from Fairbanks' ice volume curve. This represents an increase in salinity of bottom waters by 0.3‰. This sudden change over to bottom waters with higher salinity must represent the formation of a new deep water mass. This new water mass formation coincides with the timing of influx of North Atlantic surface waters. It seems likely that the new water mass was produced by mixing of high salinity North Atlantic water with cold Polar surface waters producing an intermediate cold water mass with relatively high salinity.

This intermediate water mass forms in the Greenland Sea at the present day and is termed Greenland Sea Intermediate Water, and is a major component of North Atlantic Deep Water that flows southwards out of the Norwegian-Greenland Sea. The evidence presented above suggests that a circulation system similar to the present day first began in the Greenland Sea at approximately 10 ka ago. Deep water formation did not occur in the Greenland Sea prior to this. This does not rule out the formation of NADW further south in the Norwegian Sea at an earlier time however.

4.6. Influence of North Atlantic surface waters flowing into the Norwegian Sea to the Fram Strait

The present day pattern of surface current circulation in the Norwegian-Greenland Sea is shown in fig. 1.2. During interglacial periods the North Atlantic current flows into the southern section of the Norwegian Sea and continues northwards along the western margin of Norway and along the western margin of Spitsbergen, keeping to the eastern section of the Norwegian-Greenland Sea. Minor 'arms' of this current separate and flow into the Barents Sea at its southern boundary, and north of Spitsbergen flow NE into the Arctic Ocean. Another arm of water flows west across the top of the Fram Strait to form the return Atlantic flow at depth along the eastern margin of Greenland. The influence of this current can be assessed from $\delta^{18}O$ measurements of a range of cores from this area.

Core M 23259 (from 72°N 9°E, Weinelt *et al.*, 1991) shows a glacial-interglacial $\delta^{18}O$ amplitude of 1.9‰, of which 1.2‰ is produced by the ice volume effect. This leaves a 0.7‰ shift due to temperature increase assuming meltwater effects are negligible during the late Holocene. This is equivalent to a temperature increase of 3-4°C in surface currents produced by influx of the North Atlantic surface waters (at 50-100m water depth as measurements were made on *N. pachyderma* sinistral). It is not so easy to deduce the Holocene temperature increase in surface waters from the Spitsbergen margin from PCM7 as this record ends at approximately 8.5ka ago. At this time meltwater may still have had an influence on the oceanic $\delta^{18}O$ composition. However assuming the meltwater influence was minor at this time, using the $\delta^{18}O$ value at the top of the core of 2.7‰ a glacial-interglacial range of 1.8‰ is seen. Subtracting the ice volume effect of 1.2‰ leaves a 0.6‰ shift produced by temperature assuming little meltwater influence. This relates to a temperature increase of 2-2.5°C in surface waters down to a depth of 100m. Measurements from the central Fram Strait from core PS 21295 show a glacial-interglacial range of 1.2‰.

This is equal to the ice volume effect, suggesting there is no increase in surface water temperatures in this area between glacial and interglacial times. So the North Atlantic waters do not influence the central Fram Strait, flowing close to the eastern margins of the basin.

Two cores are found to the south at latitude 66-67°N (fig. 4.5): core 23199 from Haake and Pflaumann (1989), and core M 23071 from Sarnthein *et al.* (1992). Core M 23071 shows a high resolution record similar to cores PCM7 and M 23259, see fig 4.6. The meltwater events recognised in core M 23071 are less extreme than those of cores M 23259 and PCM7. This is most probably due to mixing of the meltwater experienced at the edge of the Barents Shelf and Spitsbergen margin causing a reduction of its effect further south. The full interglacial $\delta^{18}O$ values experienced at this site average 2.4‰ and the glacial-interglacial range for this site is 2.2‰. The other core from this area, core 23199, has a much lower resolution, but the glacial-interglacial range can be easily seen. Glacial $\delta^{18}O$ values average 4.7‰ and interglacial (Holocene) values average 2.5‰, a similar difference of 2.2‰ as in core M 23071. Assuming an ice volume effect of 1.2‰, this leaves a 1‰ temperature effect assuming negligible meltwater effect during the late Holocene. This relates to a 4-5°C temperature increase in surface currents, not surprisingly slightly higher than the cores further north.

HM 52-43 from 64°N provides another record further south (Sarnthein *et al.*, 1992). This core shows a similar record for the deglaciation from stage 2 to stage 1 as M 23071 and M 23259. Holocene oxygen isotope values are slightly lighter though, reaching a $\delta^{18}O$ value of approximately 2.2‰. This results in a glacial-interglacial range of 2.3‰, and so a 1.1‰ temperature effect relating to a temperature increase of about 5°C in surface currents to a depth of 50-100m.

By comparing the oxygen isotopic signature of a series of cores at different latitudes in the Norwegian-Greenland Sea it is possible to see the warming effect of Atlantic water surface currents. Influx of Atlantic water into the southern Norwegian Sea may result in temperature increases of approximately 8°C. As this current, known as the Norwegian Atlantic Current, flows north its effect diminishes. By the time it reaches approximately 64°N a temperature increase of 5°C is experienced, this drops to 3-4°C by the time it reaches the edge of the Barents Shelf, and 2-2.5°C on reaching the Spitsbergen margin. This reduction is caused by continued mixing with the surrounding colder Polar surface currents, and can be seen in the reduction of the influx of subpolar foraminifera northwards. These are estimates and are based on the

assumption that meltwater has little influence on the Holocene oxygen isotope measurements.

4.7. Conclusions

1. Deglaciation from the stage 2 maximum to the Holocene took place in 4 major steps, these can be recognised in the planktic oxygen isotope record as meltwater events. The initial step was approximately 15.5 ka ago, the second step 13.6 ka ago, the third step 12.3 ka ago, and the fourth step 10.5 ka ago. Minor meltwater events can also be recognised, for example at 9.6 ka and 9 ka ago. Meltwater brines are also seen in the benthic oxygen isotope record from 15.5 ka ago until 10 ka ago but to a lesser extent.

2. From comparison of a global ice volume curve (from Fairbanks, 1989) with the benthic oxygen isotope curve of PCM7, it is clear that benthic foraminifera in this area do not record the ice volume effect accurately. The oxygen isotopic composition of the benthics is also affected by dense meltwater brines. The formation of a new deepwater mass also affects the isotopic composition of benthic foraminifera.

3. Oxygen isotope measurements of *N. pachyderma* (sinistral) will not record the true warming of surface waters. This is because this species lives at water depths of greater than 50m in North Atlantic waters. Temperatures in surface waters at this depth originating from the North Atlantic are probably only 1-2°C warmer than Polar surface waters at a similar depth.

4. North Atlantic surface waters first reached the Spitsbergen continental margin 12.5 ka ago, and lasted until approximately 12 ka ago. This surface current re-appeared from 10.5 ka ago, and had a stronger influence from 10 ka onwards. It was this stronger North Atlantic surface current which led to the formation of GSIW from 10 ka onwards.

5. It is possible to identify the diminishing effect of North Atlantic surface waters from south to north through the Norwegian-Greenland Sea by the reducing glacial-interglacial $\delta^{18}O$ amplitudes to the north. This is produced by the increased mixing of North Atlantic waters with Polar surface waters further north.

6. During the last deglacial cycle the formation of a new deep water mass was recognised. Mixing of North Atlantic surface waters with Polar surface waters leads to the formation of Greenland Sea Intermediate Water (GSIW). In this study this water mass was first recognised on the Spitsbergen continental margin from 10 ka ago. This marks the point where a bottom circulation system similar to the present day began. It is GSIW and a similar water mass in the Norwegian Sea which are the major contributors to North Atlantic Deep Water.

7. Cores from the central Fram Strait do not record influx of North Atlantic surface waters during stage 5 or the Holocene, this can be seen from the lower glacial-interglacial $\delta^{18}O$ amplitudes. These areas are under the influence of Polar surface waters all the time similar to the present day, while the areas closer to the Spitsbergen margin are influencd by North Atlantic currents at certain times mentioned above.

8. Re-interpretation of the stage 5 stratigraphy for of the central Fram Strait cores has been made using the more complete records of PCM5 and PCM30 from the continental margin of Spitsbergen. Substage 5e is not recorded in any of the central Fram Strait records considered in this study, substage 5a is seen but with a much smaller amplitude. The larger amplitudes of the Spitbergen margin are produced by firstly influx of warmer North Atlantic currents, and secondly intense meltwater plumes which are less pronounced in the central Fram Strait further from the meltwater source.

9. During substages 5e and 5a times the continental margin of Spitsbergen was characterised by intense surface meltwater plumes affecting waters as deep or deeper than 100m. Dense meltwater brines also affected the benthic $\delta^{18}O$ record during these periods. The affect of these plumes seems to have dissipated by the time waters reach the central Fram Strait. These meltwaters may have caused the reduction in foraminiferal abundances during substages 5a and 5e, and may also explain the absence of subpolar foraminifera during these periods. Meltwater was more intense during substage 5e than 5a, this disagrees with the conclusion of Köhler and Speilhagen (1992) from analysis of cores from the central Fram Strait.

Chapter 5. Carbon isotopes from planktic and benthic foraminifera as evidence for biological productivity, meltwater and circulation history in the Fram Strait

5.1. Introduction

Carbon isotopes can be used as a tool for paleoceanographic reconstruction, but many factors have to be considered when interpreting results. The carbon isotopic composition of deep sea sediments is influenced by the following factors; 1. Global changes in the rates of exchange of the ocean carbon reservoir with the biosphere, soil and sediments. 2. Changes in surface water productivity. 3. Internal changes in water mass structure and circulation. 4. Species-specific fractionation effects, termed 'vital effects'. 5. Microhabitat effects.

Shackleton and Kennett (1975) analysed the carbon isotopes of the shells of both planktic and benthic foraminifera, and recognised a difference in $\delta^{13}C$ values between the two. The carbon isotope composition of foraminifera reflects the composition of total dissolved CO_2 ($\Sigma\ CO_2$) in the water the foraminifera secrete their shells from. Surface waters are always enriched in the heavier isotope ^{13}C relative to deep waters (planktic foraminifera are enriched in ^{13}C relative to benthic foraminifera). Changes in ocean circulation and surface water productivity act to enrich surface waters in ^{13}C over short time-scales of 100's to 1000's of years. Over longer time-scales carbon exchange with external reservoirs affects the $^{12}C/^{13}C$ ratio of $\Sigma\ CO_2$ in sea water (Berger and Vincent, 1986).

Carbon exchange with external reservoirs such as the biosphere, soil and sediments, tends to produce variations over longer time scales that correlate with sea level change (Berger 1977; Broecker 1982; Woodruff and Savin 1985). Periods of high sea level (interglacial periods) coincide with periods of ^{13}C enrichment in the oceans (Berger, 1977). This variation is thought to be a product of carbon being deposited in marginal sediments during times of transgression, then eroded and returned to the ocean during times of regression (Tappan, 1968; Berger, 1977; Broecker, 1982; Woodruff and Savin, 1985). During a high stand of sea level organic carbon, enriched in ^{12}C, is removed and stored in marginal sediments. This produces an enrichment in ^{13}C in the $\Sigma\ CO_2$ of the oceans. In addition, when isotopically light organic carbon is stored in forests and soils (the biosphere), enrichment in ^{13}C occurs in the oceans (Shackleton, 1977). When these forests are reduced and soil eroded, isotopically light ^{12}C is

returned to the oceans causing a relative depletion in ^{13}C of dissolved oceanic carbon. Interglacial periods tend to support a greater biomass in the form of forests which are reduced during glacial periods. This effect also helps cause the ^{13}C enrichment in the oceans during high stands of sea level or interglacials. These external reservoir exchanges tend to have time-scales of 10,000 years to millions of years.

In general planktic foraminifera record a carbon isotopic signature enriched in ^{13}C by approximately 1‰ relative to benthics (Berger and Vincent, 1986). This difference is produced by photosynthesis in surface waters; this preferentially removes the lighter ^{12}C isotope from ΣCO_2 in sea water. Precipitated organic matter becomes enriched in ^{12}C, which then, after sinking, is re-oxidised. This process removes ^{12}C from surface waters and deposits it in deeper waters, causing surface water enrichment in ^{13}C and deep water enrichment in ^{12}C of ΣCO_2. The term 'biological pumping' has been used to refer to this removal of carbon from surface waters and concentration in deeper waters (Deuser and Hunt, 1969, Craig, 1970, Kroopnick, 1974). This biological pumping also acts to deplete micronutrients such as phosphate, nitrate and silicate in surface waters, they are released back into the water column by respiration and decay of organic matter at depth (Berger and Vincent, 1986). An increase in surface water productivity will lead to increased photosynthesis, and therefore greater enrichment of ^{13}C in the ΣCO_2 of surface waters and a corresponding greater depletion in deep waters.

There is a direct association between dissolved oxygen use and $\delta^{13}C$ (the amount of oxygen used is termed 'apparent oxygen utilisation' or AOU) since oxygen is used for the decay of organic material enriched in ^{12}C. Different ocean basins have different oxygen concentrations in deep waters depending on the renewal of these deep waters (Duplessy *et al.*, 1984). The deep basins of the North Atlantic at the present time are occupied by relatively young waters, rich in oxygen, and consequently a high $\delta^{13}C$ signature of ΣCO_2 occurs in these waters as much of the organic matter is yet to be decayed (Kroopnick, 1980; Berger and Vincent, 1986). These young deep waters originate in the Norwegian-Greenland Sea where dense surface waters sink to form North Atlantic Deep Water (NADW) (Worthington, 1976). During glacial periods, when the formation of NADW is thought to have been much reduced, older bottom waters, depleted in oxygen and therefore depleted in ^{13}C, were present. Pacific deep waters are much older than Atlantic ones, deep water circulation carries water from the deep Atlantic into the deep Pacific. These older deep waters are depleted in oxygen, and the ΣCO_2 of this water is relatively low in ^{13}C as much of the organic material has been decayed and the lighter ^{12}C isotope has been released. The ΣCO_2 in

modern NADW has an average $\delta^{13}C$ value of +1.0 to +0.5‰ PDB (PDB is the standard samples are commonly measured against, similar to $\delta^{18}O$ measurements). Σ CO_2 in Pacific deep waters have $\delta^{13}C$ values of +0.5 to -0.5‰. The global average surface water $\delta^{13}C$ is +2.0‰. These values are all from Kroopnick (1985).

The microhabitat of foraminifera will produce variations in the $\delta^{13}C$ signature (Grossman, 1987). Oxidation of organic carbon in the sediment will reduce the $\delta^{13}C$ value of Σ CO_2 in the pore fluids. Thus the $\delta^{13}C$ value of foraminiferal species depends on the depth within the sediment they live. The deeper they live the greater the depletion of ^{13}C they will record due to the oxidation of organic matter in the sediment (Woodruff *et al.*, 1980, Belanger *et al.*, 1981). For example, *Cibicidoides wuellerstorfi* (Schwager) lives at the sediment water interface and therefore is thought to record accurately the $\delta^{13}C$ composition of Σ CO_2 in deep waters (Grossman, 1987). *Oridorsalis umbonatus* (Reus) (*Eponides umbonatus* (Reuss) in this study) lives at depths of roughly 1cm in the sediment. At this depth, the $\delta^{13}C$ signature recorded by *O. umbonatus* is 1‰ depleted in ^{13}C due to oxidation of organic material (Vincent and Berger, 1981). Species of the genus *Cassidulina*, even though infaunal, have been found to secrete their test in equilibrium with the Σ CO_2 of deep waters (Grossman, 1987). Specimens of *Cassidulina teretis* (Tappan) have been measured in this study, and should therefore record accurately deep water changes in $\delta^{13}C$. The other species used in this study, *Melonis barleeanum* (Williamson), is also an infaunal species, so should be depleted in ^{13}C. These assumptions will be discussed later.

Benthic carbon isotope studies have been useful in understanding deep water oceanographic conditions both for recent times and back into the fossil record. It is important to understand disequilibria effects of benthic species when making oceanographic interpretations. Graham *et al.* (1981) examined 9 benthic species from 149 samples measuring oxygen and carbon isotopes. They concluded that none of these species secreted calcium carbonate in isotopic equilibrium with ocean water. Of the species studied *Planulina wuellerstorfi* (*Cibicidoides wuellerstorfi* in this study) had the smallest disequilibrium effect of -1.0‰ with respect to $\delta^{13}C$. They concluded this species showed the most systematic relationship between $\delta^{13}C$ of its test and $\delta^{13}C$ of bottom waters, and was therefore the most useful species for paleoceanographic reconstruction. From this study the disequilibium effects for the following species were calculated for $\delta^{13}C$, *Oridorsalis tener* (*E. umbonatus* of this study) -2.1‰, *Globocassidulina subglobosa* -1.5‰, and *Melonis pompilioides* -1.4‰.

Belanger *et al.* (1981) came to similar conclusions from $\delta^{13}C$ measurements from a range of benthic species. They found *P. wuellerstorfi* most accurately recorded the isotopic composition of deep waters. They suggest *O. tener* is of limited use due to its habitat in the upper 1cm of sediment. Other species living within bottom sediments would be affected to a greater extent than *O. tener*. They suggested that species with lower $\delta^{13}C$ values lived in an environment with less dissolved oxygen, i.e. within sediment, or originate from older water masses where more oxygen has been used up in organic activity (respiration).

Species vital effects are also important in the final $\delta^{13}C$ signature of planktic foraminifera. Berger *et al.* (1978) measured $\delta^{13}C$ of different size fractions for different species of planktic foraminifera and found that the $\delta^{13}C$ values varied depending on size and species. The size dependant fractionation can be reduced if all analyses are made on adult specimens of a similar size. Juvenile forms are heavily depleted in ^{13}C as they incorporate ^{13}C-depleted carbon from their metabolism. The larger adult specimens record more accurately the $\delta^{13}C$ composition of the surface waters. Species vital effects also have an influence on the $\delta^{13}C$ values recorded in benthic foraminfera (Vincent and Berger, 1981, Graham *et al.*, 1981, Grossman, 1987).

Johannessen *et al.* (in press) measured the $\delta^{13}C$ of $\Sigma\ CO_2$ from surface waters and Recent planktic foraminifera from the Norwegian-Greenland Sea between 60°N and 72°N. Three main surface water masses were recognised, Polar water from the Arctic Ocean, North Atlantic water, and Arctic water (a mixture of Polar and N. Atlantic waters). The carbon and oxygen stable isotopic composition of these water masses were calculated from $\delta^{13}C$ and $\delta^{18}O$ measurements of the planktic foraminifera living within them. The lowest $\delta^{13}C$ values are found in the North Atlantic waters 0.2 to 0.5‰, Polar waters have a slightly higher value of 0.5 to 0.6‰, and Arctic waters have the highest $\delta^{13}C$ values of 0.7 to 0.9‰. They suggest the enhanced $\delta^{13}C$ content of Arctic waters compared to Polar and N. Atlantic surface waters is due to partial thermal equilibration between atmosphere and ocean surface water.

This study examines the $\delta^{13}C$ record of planktic and benthic foraminifera through time in one of the areas of formation of NADW. The $\delta^{13}C$ signature may provide information about the timing and intensity of NADW formation through time, but, undoubtedly, will be complicated by other factors such as productivity, meltwater and species vital effects.

5.2. Results

Stable isotope measurements were made on planktic foraminifera from four cores, PCM5, PCM7, PCM30 and PCM56, and benthic measurements were made on three cores, PCM5, PCM7 and PCM30. On all four cores measurements were made from the same planktic species, *Neogloboquadrina pachyderma* (sinistral). All analyses were made on specimens larger than 125μm to reduce the size fractionation effect mentioned above.

Due to variations in abundance of benthic foraminifera within one core and between cores different species had to be measured. For PCM5 (from 2139m water depth) the deep water species *E. umbonatus* (often referred to in the literature as *Oridosalis umbonatus* or *O. tener*) was analysed. The two other cores, PCM7 and PCM30 are from a shallower depth, 1074m and 1154m respectively, and different species had to be analysed to produce an isotope curve as complete as possible. Measurements were made from specimens of *Melonis barleeanum* and *C. teretis*.

5.2.1. The $\delta^{13}C$ planktic foraminiferal record of core PCM5

The $\delta^{13}C$ of both planktic and benthic species are shown in fig. 5.1. The $\delta^{13}C$ values for planktic foraminifera range from -0.65‰ to a peak of 0.7‰. At the base of the core the values are approximately -0.2‰ from 685 until 665cm, they then increase to 0.15‰ then gradually decrease to a low of -0.5‰ at 540cm. At this point, $\delta^{13}C$ values increase to close to 0.0‰ from 525 to 485cm. The next section is characterised by slightly lower $\delta^{13}C$ values of -0.2 to -0.3‰ until 455cm. After this section, there is a trend to higher values that has minor negative troughs superimposed on it. This section culminates in the highest values found in the core of 0.7‰ from 385 to 380cm. This is followed by a major reduction in $\delta^{13}C$ values to the lowest values measured in the core. These are found from 340 to 335cm and are about -0.6‰. Values then increase to a plateau of about 0.1‰ from 290 to 245cm, and then a further increase to 0.4‰ from 230 to 195cm. Within this section there is one value of -0.2‰ at 205cm. There is then a brief trough with $\delta^{13}C$ values of -0.1‰ from 190 to 175cm before values return to levels from 0.3 to 0.5‰ until 145cm. At this point, there is a sharp drop in $\delta^{13}C$ values to between 0.0 and -0.3‰ from 135 to 55cm. At the very top of the core values increase to 0.6‰ at 2.5cm.

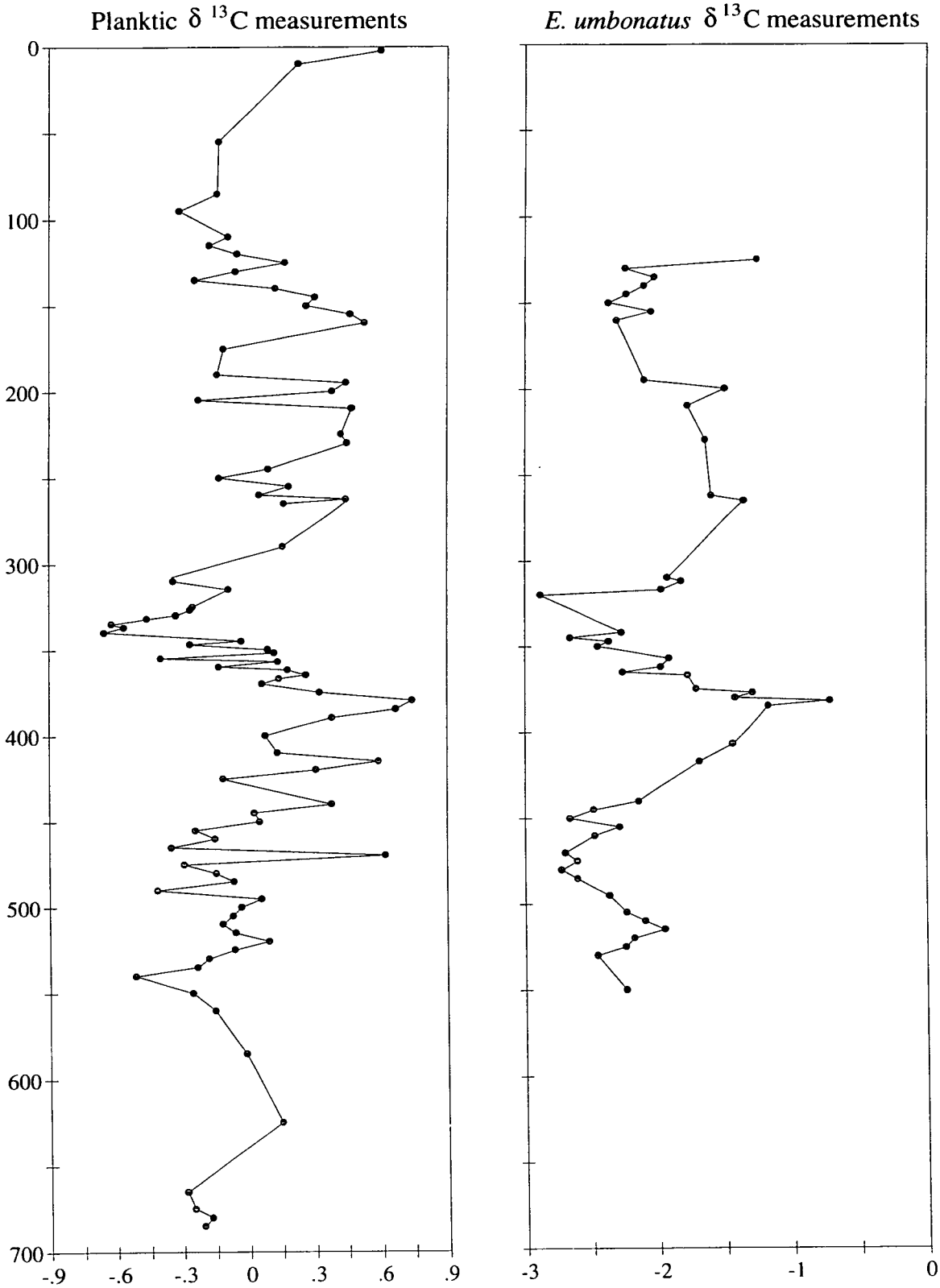

Fig. 5.1. Carbon stable isotope measurements from planktic and benthic foraminifera from PCM5. Vertical scale depth in cm, horizontal scale isotopic variation in per mil variation w.r.t. PDB.

5.2.2. The $\delta^{13}C$ benthic foraminiferal record of core PCM5

Measurements were made on the benthic species *E. umbonatus* in PCM5, the $\delta^{13}C$ curve is plotted in fig. 5.1. Due to low abundances of benthic foraminifera in certain sections of PCM5, benthic measurements were only possible between 125 and 550cm. As mentioned in the introduction, this species has a fractionation effect of -1.1‰ due to vital effects, this has not been added to the plot of fig. 5.1. The $\delta^{13}C$ values measured from PCM5 vary from -2.9‰ to a peak of -0.77‰.

The base of the measured section from 550 to 440cm is characterised by low $\delta^{13}C$ values from -2.0 to -2.7‰, being particularly low from 485 to 460cm. There is then a trend towards heavier $\delta^{13}C$ values culminating in a peak of -0.7‰ at 382cm; values between -1.5 and -0.7‰ are present between 407 and 377cm. The $\delta^{13}C$ signature then decreases again to -2.8‰ from 350 to 320cm. Values of $\delta^{13}C$ then increase to a plateau of intermediate values with an average of -1.5‰ from 317 to 200cm. At this point, values decrease to between -2.0 and -2.3‰ until 130cm. The top measurement at 125cm shows an increase to a $\delta^{13}C$ high of -1.2‰.

5.2.3. The $\delta^{13}C$ planktic foraminiferal record of core PCM7

Fig 5.2 shows the $\delta^{13}C$ plots for both planktic and benthic species for PCM7. The values of $\delta^{13}C$ measurements on *N. pachyderma* in PCM7 show a high degree of variability in the upper section of the core. Throughout the whole core $\delta^{13}C$ values range from a low of -0.5‰ to a high of 0.4‰. The fluctuations will be described in more detail below.

The base of the core is characterised by a relatively stable plateau of $\delta^{13}C$ values of -0.1 to -0.5‰ from 727 to 570cm. The next section shows an increase in $\delta^{13}C$ values to around -0.1 to 0.1‰ at 545cm, there is then a gradual trend of increasing values with minor troughs superimposed. This trend culminates in $\delta^{13}C$ values of about 0.2‰ at 340cm; two noticeable troughs occur at 445cm and 400-375cm. From there a two stepped decrease follows in values to approximately 0.0‰ at 320cm and then to -0.2‰ from 310 to 270cm. The $\delta^{13}C$ values then rapidly increase to 0.2‰ from 260 to 250cm; values remain between 0.0 and 0.2‰ until 202cm except for a trough with a $\delta^{13}C$ value of -0.18‰ at 232cm.

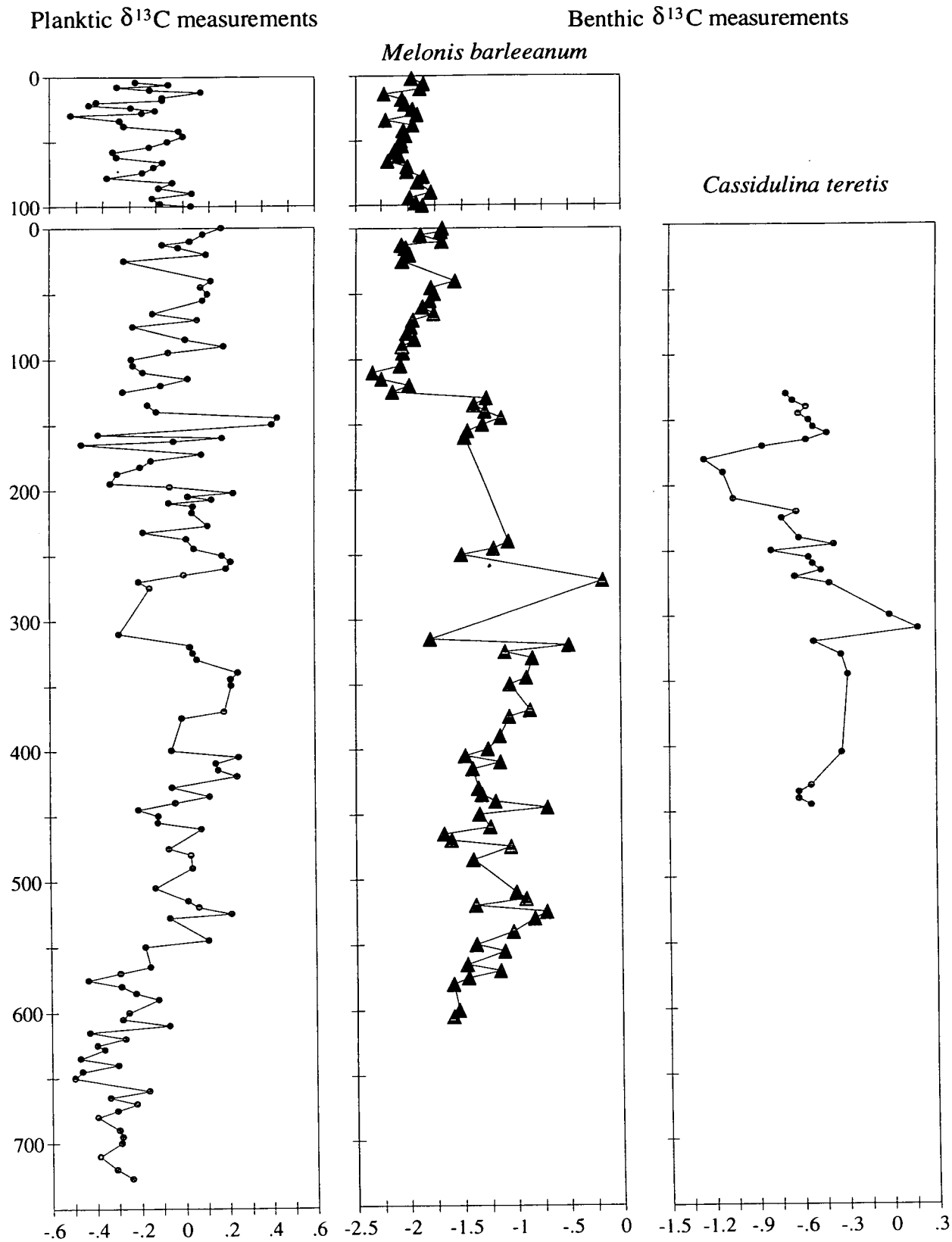

Fig. 5.2. Carbon stable isotope measurements from planktic and benthic foraminifera from PCM7. Vertical scale depth in cm, horizontal scale isotopic variation in per mil w.r.t. PDB standard.

The top of the PCM7 $\delta^{13}C$ record shows very rapid fluctuations with high amplitudes producing a very spiky looking graph. From 195 to 177cm $\delta^{13}C$ values from -0.1 to -0.3 ‰ are recorded and give way to a very spiky section which is followed by a distinct peak from 150 to 145cm with $\delta^{13}C$ values of about 0.4‰. Values then decrease to between 0.0 and -0.2‰ from 140 to 95cm, where a general trend towards higher $\delta^{13}C$ values can be identified. This trend culminates in $\delta^{13}C$ values of 0.1‰ from 55 to 40cm; there is then a trough with a value $\delta^{13}C$ of -0.2‰, after which values increase again to 0.1‰ until the top of the main core. The trip core is characterised by initial $\delta^{13}C$ values of 0.1‰, decreasing to -0.2‰ by 58cm and then increasing to 0.15‰ at 46cm. Values drop to -0.3‰ at 20cm, then rise slightly to an average of 0.0‰ by the top of the trip core.

5.2.4. The $\delta^{13}C$ benthic foraminiferal record of core PCM7

Measurements have been made on two benthic foraminiferal species for core PCM7. The $\delta^{13}C$ results for both species are shown in fig. 5.2. The two species measured from PCM7 are *M. barleeanum* and *C. teretis*. The results from these two species will be described separately.

Measurements from specimens of *C. teretis* have been made between 445 and 130cm of the main core. Values of $\delta^{13}C$ range from a peak of 0.18‰ to a low of -1.26‰. The initial $\delta^{13}C$ values of about -0.6‰ from 445 to 430cm increase slightly to -0.3‰ until 330cm, then increase rapidly to 0.18‰ at 310cm. This is followed by an equally rapid decrease to $\delta^{13}C$ values of -0.4‰ at 275cm, from where a steady decrease to values of -0.7‰ at 220cm is found. There is then a distinct step to lower $\delta^{13}C$ values of -1.0 to -1.3‰ from 210 to 180cm, followed by a rapid increase again to values of -0.4 to -0.7‰ from 165 to 130cm, the final measurements made using this species.

The majority of $\delta^{13}C$ measurements on benthic foraminifera from PCM7 are from specimens of *M. barleeanum* from 605 to 0cm in the main core and throughout the trip core. The $\delta^{13}C$ values measured range from a peak of -0.16‰ (although this is an isolated point and may be a flyer) to a low of -2.3‰. These values are considerably lower than those made from *C. teretis*. Reasons for this will be discussed in the interpretation section later. The fluctuations in $\delta^{13}C$ values from *M. barleeanum* will be described in more detail below.

The lowest section measured from 605 to 580cm is characterised by $\delta^{13}C$ values of about -1.5‰,. From here values increase gradually to a peak of -0.7‰ at 525cm. This is followed by a decrease in $\delta^{13}C$ values to between -1.2 to -1.6‰ from 485 to 400cm. At this point, values increase to between -1.0 and -0.6‰ until 325cm. There is then a dramatic decrease to a $\delta^{13}C$ value of -1.7‰ at 315cm followed by a dramatic increase to a value of -0.16‰ (the highest value in the core, although as mentioned earlier this may be a flyer), and an immediate decrease again to between -1.0 and -1.5‰ from 250 to 240cm. A sampling hiatus occurs in the core until 160cm. Between 160 and 130cm, $\delta^{13}C$ values are relatively stable and average -1.2‰. This is followed by a major decrease to $\delta^{13}C$ values of -2.0‰ at 125cm. Values remain relatively stable at between -2.0 and -2.3‰ until 90cm, at which point a gradual trend appears towards higher values culminating in a peak of -1.5‰ at 40cm. Values then drop back to -2.0‰ before rising slightly to -1.7‰ at the top of the main core. The trip core is characterised by very stable $\delta^{13}C$ values ranging from -1.8 to -2.0‰, being slightly higher for the basal 20cm.

5.2.5. The $\delta^{13}C$ planktic foraminiferal record of core PCM30

The $\delta^{13}C$ record measured from specimens of the planktic foraminifer *N. pachyderma* (sinistral) is shown in fig. 5.3 along with the carbon isotopic data for benthic species. The $\delta^{13}C$ values from the *N. pachyderma* range from a peak of 0.45‰ to a low of -0.65‰. The distinct trends visible in this record will be described below.

The base of the core from 577 to 482cm is characterised by $\delta^{13}C$ values fluctuating between values of approximately -0.2‰ to values of approximately 0.0‰. The low $\delta^{13}C$ values are found between 577-557cm, from 537-532cm and from 512-507cm; whereas the high $\delta^{13}C$ values are found in the sections from 547-542cm, 527-517cm and from 497--487cm. At this point, there is a distinct drop to very low $\delta^{13}C$ values of -0.3 to -0.5‰ from 477-467cm. From there the $\delta^{13}C$ values increase initially to values of about 0.2‰ from 452 to 437cm and again to values of 0.3 to 0.4‰ from 427 to 412cm. The next section has a low resolution but $\delta^{13}C$ values of approximately 0.2‰ are present until 337cm. The $\delta^{13}C$ values then decrease to a low of -0.2 to -0.3‰ from 327 to 312cm. The next section is characterised by initially a slow increase until 250cm followed by a more rapid rise in $\delta^{13}C$ values, culminating in a peak of 0.2 to 0.4‰ from 237 to 207cm. Values of $\delta^{13}C$ then drop slightly to a plateau ranging from -0.1 to 0.2‰ from 202 to 27cm.

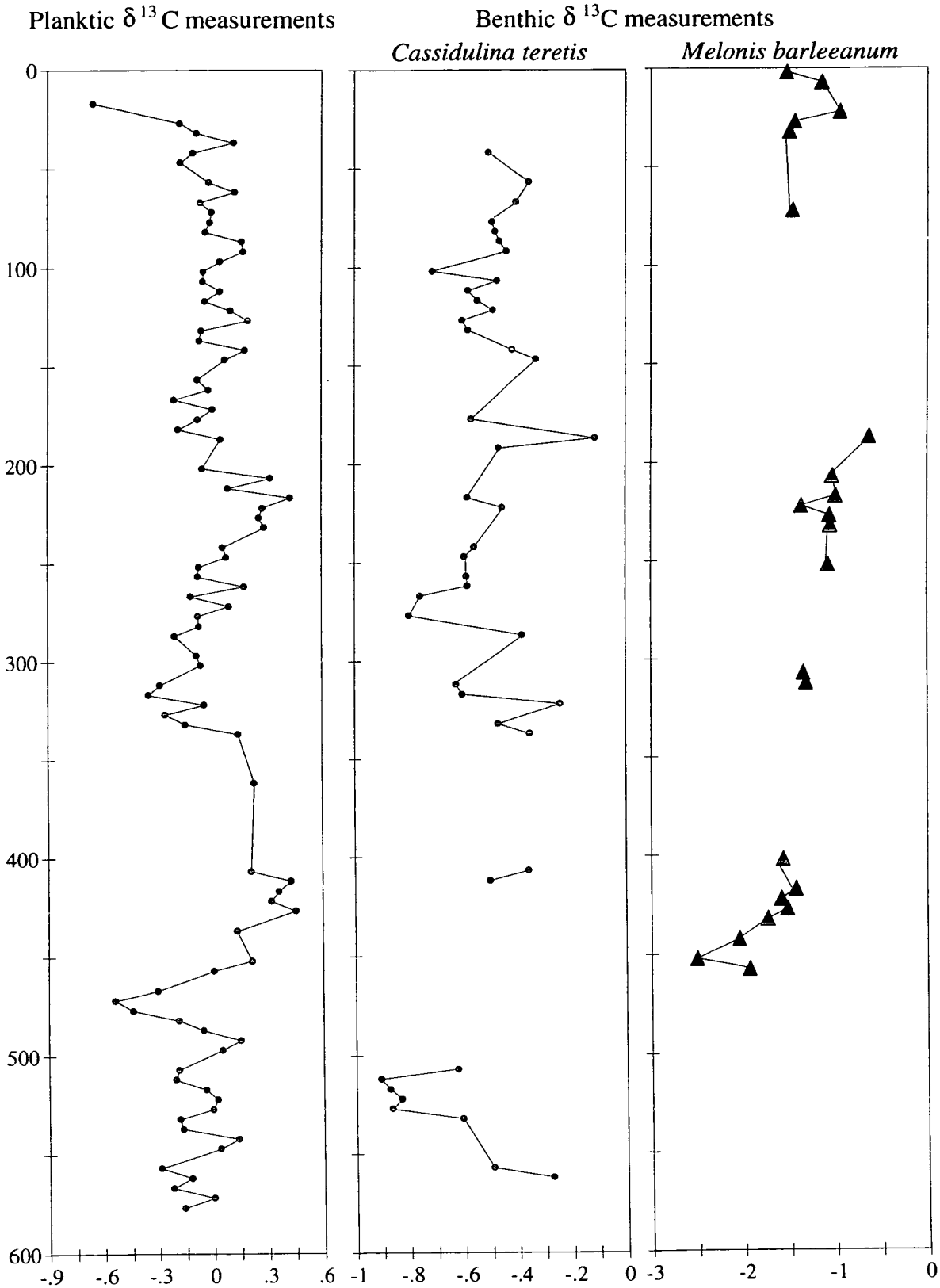

Fig. 5.3. Carbon isotopic measurements from planktic and benthic foraminifera from PCM30. Vertical scale depth in cm, horizontal scale isotopic variation in per mil w.r.t. PDB standard.

The final measurement taken at 17cm records a dramatic decrease in $\delta^{13}C$ value to -0.65‰, which is the lowest value in the core.

5.2.6. The $\delta^{13}C$ benthic foraminiferal record of core PCM30

Measurements were made on two benthic species in PCM30, these two species were *M. barleeanum* and *C. teretis*. The $\delta^{13}C$ and $\delta^{18}O$ results from both species are shown in fig. 5.3. The results from the two species will be described separately below.

Relatively few measurements were made on *M. barleeanum*, and occur in clusters. The first cluster, between 457 and 402cm, is characterised by an initial drop in $\delta^{13}C$ value from -1.9‰ to -2.5‰ at 452cm, then a rapid increase to values averaging -1.5‰ for the rest of this section. The next group of values are found between 252 and 187cm. The initial $\delta^{13}C$ values are -1.0‰ decreasing gradually to -0.6‰ by 187cm. The final group of measurements made on this species are from the top of the core from 72 to 2cm. The $\delta^{13}C$ values are initially -1.5‰ until 27cm, then increase to -1.0‰ and finally drop to -1.5‰ again at the core top.

Considerably more measurements have been made on specimens of *C. teretis*, as this species is more abundant than *M. barleeanum* in PCM30. There are however sampling hiatus' in the core which is the main reason why measurements were also made on *M. barleeanum*. Values from the base of the core begin at 562cm with a $\delta^{13}C$ composition of -0.2‰. There is a rapid decrease to a plateau of values of -0.9‰ from 527 to 512cm, then a rise back to values of -0.6‰. There is then a major sampling hiatus with two isolated $\delta^{13}C$ values of -0.4‰ from 407 to 412cm. Then from 337 to 42cm there is a relatively complete section with only minor gaps. The start of this section records $\delta^{13}C$ values of -0.2 to -0.4‰, there is then a two stepped decrease in values to -0.6‰ from 317 to 312cm then -0.8‰ from 277 to 267cm. After this $\delta^{13}C$ values rise to between -0.5 and -0.6‰ until 192cm, there is an isolated high value of -0.1‰ at 187cm then values drop again to -0.5‰ at 177cm. There is a small gap at this point until 147cm where values have dropped slightly to -0.3‰. A steady decrease to values averaging -0.6‰ from 132 to 112cm then gives way to an increase to a plateau of values between -0.45 and -0.5‰ from 107 to 77cm. There is a minor increase in $\delta^{13}C$ values to -0.3‰ then a decrease to -0.5‰ at 42cm the last measurement from this species in this core.

5.3. Discussion

5.3.1. $\delta^{13}C$ variations on a glacial to interglacial time scale

The $\delta^{13}C$ signature of the dissolved CO_2 in the global oceans varies between glacial and interglacial periods (Broecker, 1982; Boyle, 1988; Broecker and Peng, 1989). As mentioned in the introduction, this is thought to be due to greater biomass storage on land during interglacial periods (Shackleton, 1977). This organic material is depleted in ^{13}C, therefore causing an enrichment in $\delta^{13}C$ in the oceans during interglacials. Both planktic and benthic foraminiferal species should record higher $\delta^{13}C$ values during interglacials than glacials. Curry and Crowley (1987) measured the $\delta^{13}C$ composition of the planktic foraminifera *Globigerinoides sacculifer* from a series of cores from the equatorial Atlantic Ocean. These records were stacked to produce a composite curve, which records the average global variation in $\delta^{13}C$ of the oceans for the past 200,000 years. Variations, seen in this record, should be due almost exclusively to glacial-interglacial variations in the carbon budget.

This composite record has been overlain on the $\delta^{13}C$ records from planktic foraminifera of PCM5 and PCM30 (fig. 5.4). In order to facilitate a comparison an average Holocene $\delta^{13}C$ value of +0.3‰ has been assumed for the Spitsbergen margin, so the Holocene section of the composite curve has been set at 0.3‰ in fig. 5.4. The curve of Curry and Crowley (1987) is shown as a thin line, while the data from this study is shown by joined circles in fig. 5.4. This comparison shows that the $\delta^{13}C$ amplitude from our results is considerably greater than the global average $\delta^{13}C$ range produced by glacial-interglacial variations. In general, $\delta^{13}C$ values for stage 6, substage 5b and stage 2 from our data are slightly higher than suggested by the composite curve. Another clear difference between the two records is found during stage 5. The very light $\delta^{13}C$ values recorded in PCM5 during substage 5a, and in PCM30 during substage 5e correlate to periods in the Atlantic composite curve with relatively high values.

Thus in general the Fram Strait $\delta^{13}C$ records of planktic and benthic foraminifera do not show the predicted glacial-interglacial variations although there are some similarities. For instance the $\delta^{13}C$ record of *N. pachyderma* of PCM5 (fig. 5.5) shows generally low $\delta^{13}C$ values during glacial stage 6. There is a definite increase in $\delta^{13}C$ at the stage 5-6 boundary, which is similar to the composite. The remarkable difference with the composite curve, however, lies in the fact that within late substage 5b and substage 5a there is a significant period with the lowest $\delta^{13}C$ values.

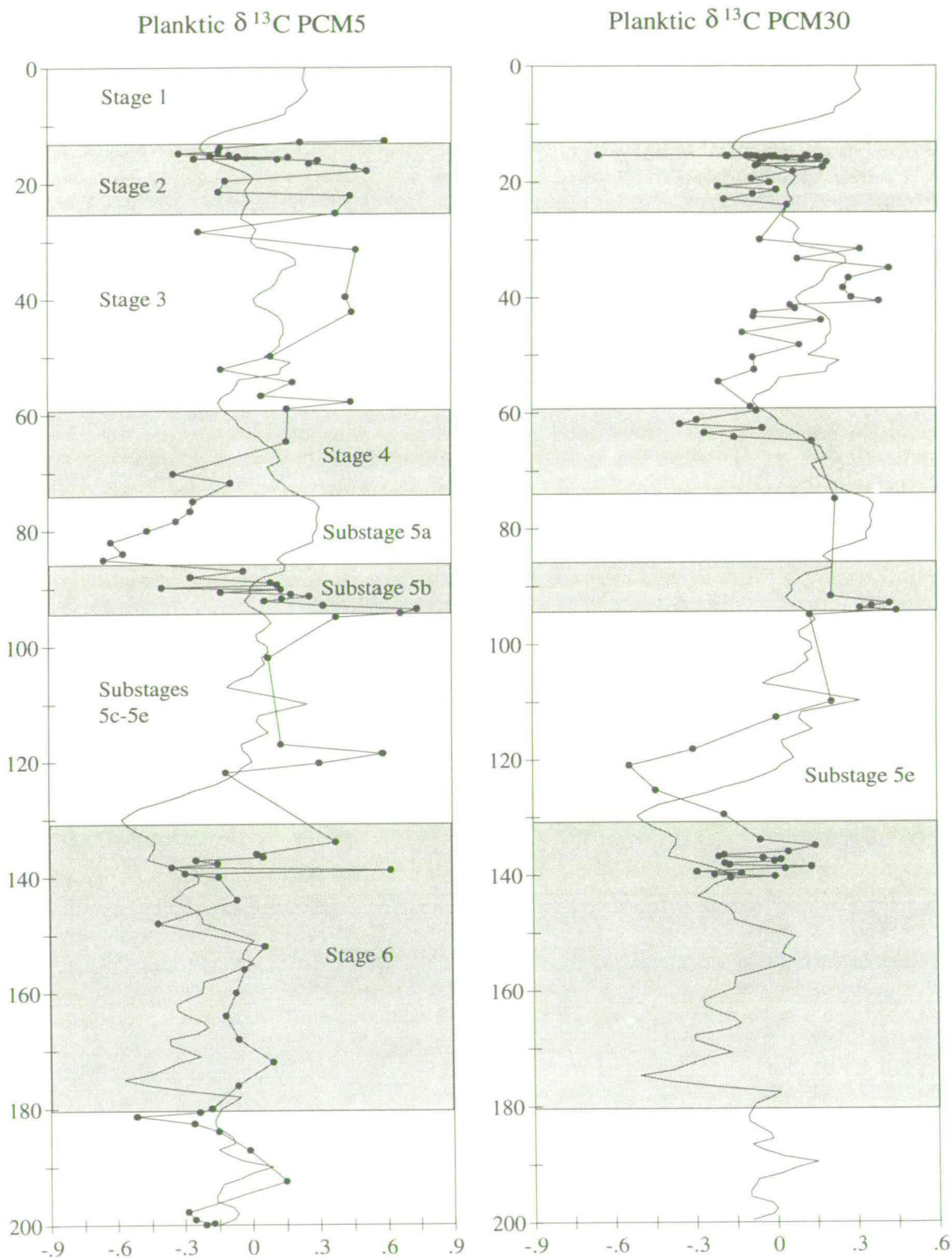

Fig. 5.4. Stable carbon isotopic data for planktic foraminifera of PCM5 and PCM30, shown as joined circles, plotted against age. Horizontal scale is isotopic variation in per mil w.r.t. PDB standard. The other line in both graphs is a composite carbon isotope curve produced from the equatorial Atlantic (Curry and Crowley, 1987). This curve acts as an indicator of global carbon 13 shift due to glacial interglacial fluctuations. Differences between this data and our data must be due to local effects, see text for discussion.

Values tend to increase during stage 3 and then decrease during peak stage 2 times. The benthic $\delta^{13}C$ record for PCM5 shows more convincingly distinct low $\delta^{13}C$ values, as predicted by the stacked curve, within stage 6 and stage 2 (fig. 5.5), but, as with the planktic foraminifera, also shows a strong decrease in $\delta^{13}C$ within late stage 5 (substage 5a particularly). PCM30 shows a similar trend (fig.5.6 shows the $\delta^{18}O$ and $\delta^{13}C$ of planktic and benthic foraminifera plotted against age) with moderately low planktic $\delta^{13}C$ values during glacial stages 6, 4 and 2, and high values during much of stage 5 and stage 3. During substage 5e, however, there is a distinct period with low $\delta^{13}C$ values. There is a sampling hiatus covering substage 5a so the light spike seen in PCM5 is not seen here. The benthic $\delta^{13}C$ record for PCM30 and the trends are not clear because two different species were measured.

The *N. pachyderma* $\delta^{13}C$ record of PCM7 (figs. 5.7 and 5.8, also showing the $\delta^{18}O$ record of *N. pachyderma,* and the $\delta^{18}O$ and $\delta^{13}C$ benthic foraminifera) shows low $\delta^{13}C$ values within stadial stage 4 and early stage 3, from 50 ka to the base, and then considerably higher values during the rest of stage 3. This is similar to the trend in the composite record of Curry and Crowley. Stage 2 shows a mixed record with one section of low $\delta^{13}C$ values that are expected, but much of stage 2 is characterised by relatively high $\delta^{13}C$ values, from 14.3 to 16ka and from 22 to 32ka, or rapidly fluctuating values (figs. 5.7 and 5.8). The stage 1 record from *N. pachyderma* in PCM7 is also characterised by highly fluctuating $\delta^{13}C$ values rather than the exclusively high values expected due to global glacial-interglacial variations in carbon fluxes. In general, the meltwater events recognised from light $\delta^{18}O$ measurements (see chapter 4) correlate to light $\delta^{13}C$ values (or to periods with highly fluctuating $\delta^{13}C$ values). For example, the meltwater event from 13.5 to 13.8ka correlates to a period with two light spikes in the $\delta^{13}C$ record. The major melting event at 12.3ka also correlates to a period of light $\delta^{13}C$ values. Further melting events at 10.5ka, 9.5ka and 9ka are also characterised by episodes with light $\delta^{13}C$ values (fig. 5.7). The benthic record from PCM7 has relatively high $\delta^{13}C$ values for stage 3 as expected, but the stage 2 section does not show the predicted fall in $\delta^{13}C$ values. There is a major shift to lower $\delta^{13}C$ values at the start of stage 1, at 12.3 ka, which then persists for the rest of the record. This is virtually the opposite to the trend expected as seen in the composite curve.

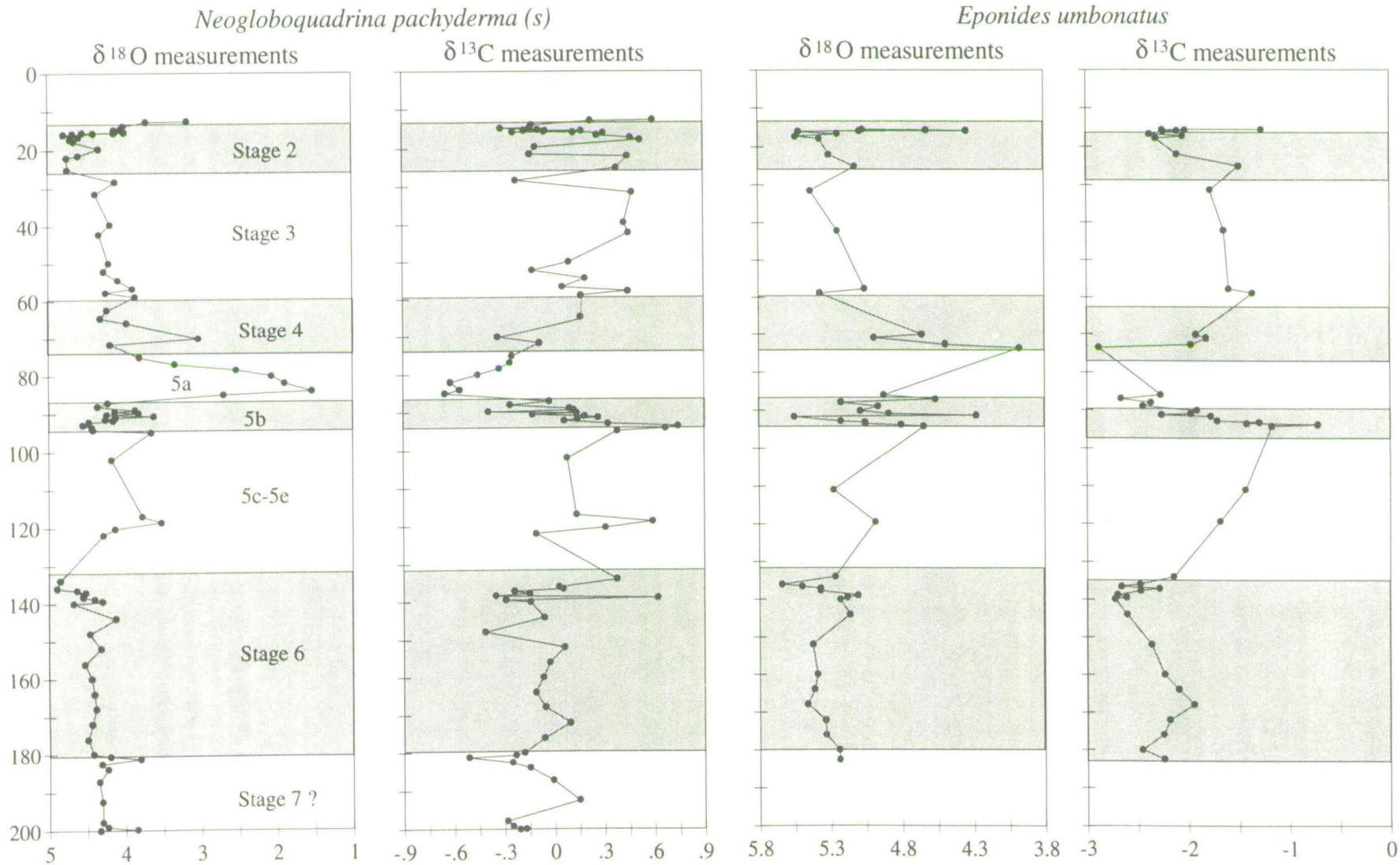

Fig. 5.5. Stable oxygen and carbon isotope measurements from planktic and benthic foraminifera from PCM5. Vertical scale age in ka, horizontal scale per mil variation w.r.t. PDB standard.

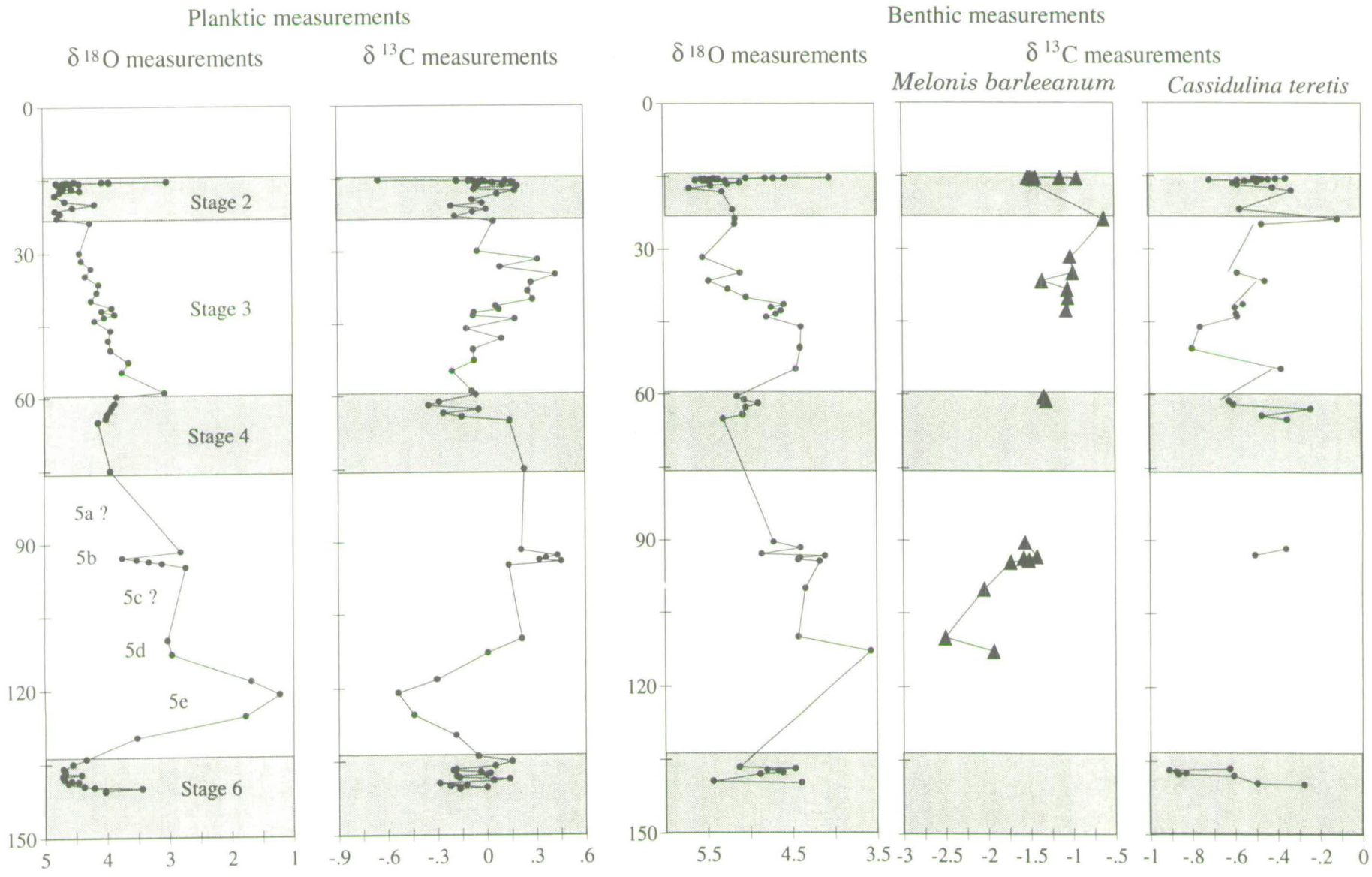

Fig. 5.6. Stable oxygen and carbon isotopic data from planktic and benthic foraminifera from PCM30. Vertical scale in ka, horizontal scale per mil variation w.r.t. PDB standard. Shaded sections represent glacial periods, isotope stages are labelled.

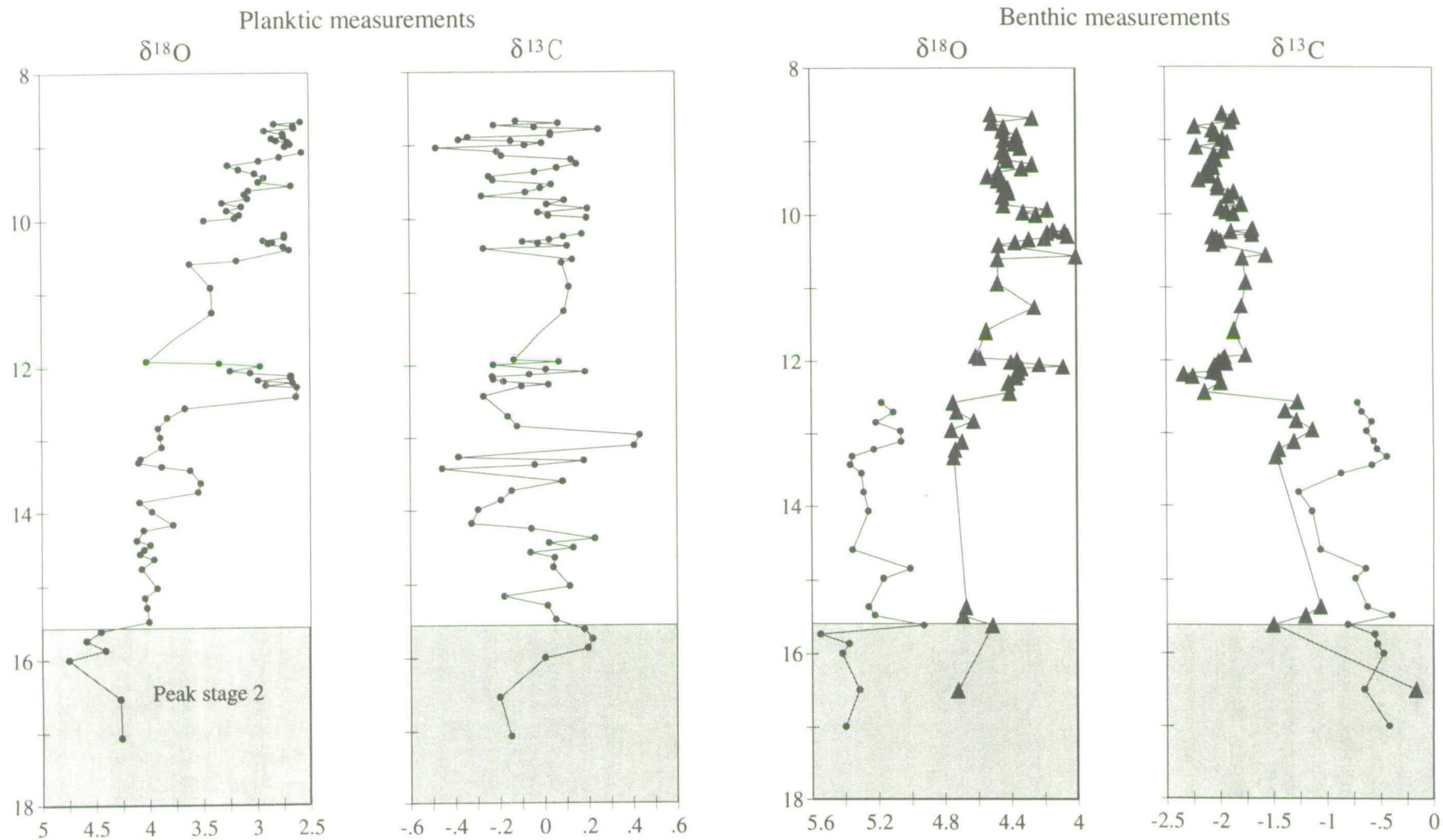

Fig. 5.7. Stable oxygen and carbon isotope measurements from planktic and benthic foraminifera from PCM7. Vertical scale in ka, horizontal scale per mil variation w.r.t. PDB standard. In the benthic plots the triangles are from the foraminifera *Melonis barleeanum* and the circles are from *Cassidulina teretis*.

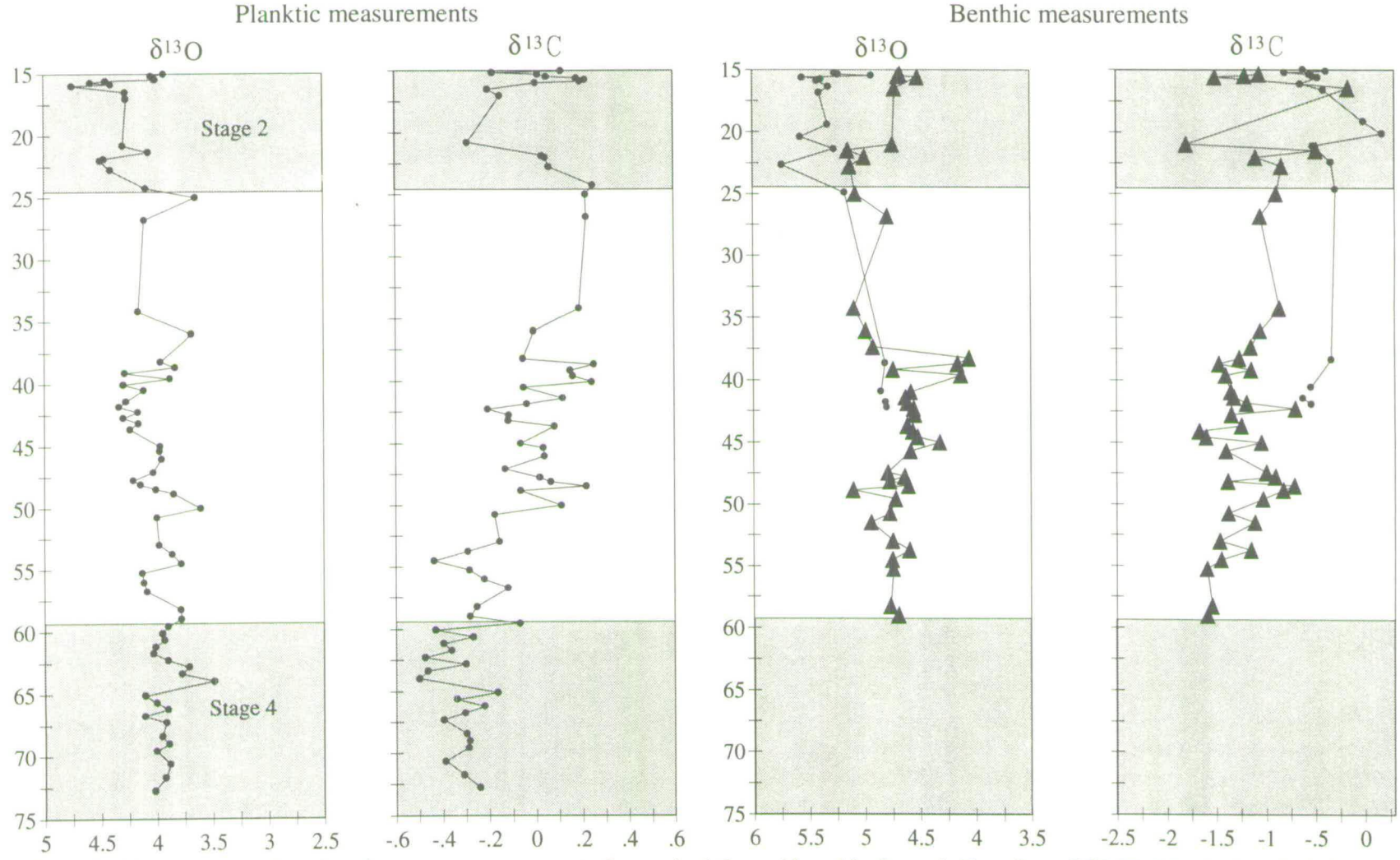

Fig. 5.8. Stable oxygen and carbon isotope measurements from planktic and benthic foraminifera from PCM7. Vertical scale in kyrs, horizontal scale per mil variation w.r.t. PDB standard. In the benthic plots the triangles are from the foraminifera *Melonis barleeanum* and the circles are from *Cassidulina teretis.*

5.3.2. Meltwater and the $\delta^{13}C$ record

The periods with a low $\delta^{13}C$ signature during substages 5e and 5a occur during periods of strong meltwater flux, as evidenced in the $\delta^{18}O$ records of cores PCM5 and PCM30 (see chapter 4). The record for the latter part of stage 2 and stage 1 of PCM7 also show low $\delta^{13}C$ values during meltwater events. It therefore seems likely that meltwater must somehow have an influence on the $\delta^{13}C$ composition of foraminiferal shells. There are several possible explanations for the low $\delta^{13}C$ values produced by meltwater influx. The first idea involves the release of terrestrial organic material when ice melts. The large volumes of ice that advance onto the continental shelf during glacial periods originate from the Spitsbergen landmass. While on land, the glaciers would pick up terrestrial material from erosion at the base of the glacier, and from material falling onto the ice from nunataks (mountains exposed above the ice mass). Advancing across the continental shelf the ice masses will continue to pick up material from the sediment surface, having a predominantly terrestrial source. This terrestrially derived material contains organic matter highly depleted in ^{13}C. Large scale melting of such an ice mass would lead to an increased influx of terrestrially derived organic material into the marine system, and consequently produce a surface water layer highly depleted in ^{13}C. During a melting period large quantities of meltwater would be emptied northwards by the major Russian rivers flowing to the north, this might also supply large amounts of organic material to the northern ocean.

The second idea involves the presence of algal blooms in ice. Large marine based ice masses are not totally devoid of life, they can support great quantities of algae. The algae are often concentrated on the underside of ice at the interface with ocean water. Such algal blooms would be depleted in $\delta^{13}C$, consequently when the ice melts this organic material would be released into the surface waters causing an depletion in $\delta^{13}C$ in surface waters. The third idea involves the isotopic equilibration between ocean water and the atmosphere, isotopically light ^{12}C is removed from the ocean due to temperature fractionation and partial pressure. Given time for full equilibration the ocean surface waters would be enriched in $\delta^{13}C$ by 3‰, this is rarely achieved due to the time taken for equilibration to occur (Charles *et al.*, 1993). It has been suggested by Johannessen *et al.* (in press) that partial thermal equilibration with the atmosphere explains the light $\delta^{13}C$ values in Arctic surface waters. So a meltwater lid would help prevent the ventilation of surface waters, reducing the removal of ^{12}C (ie. prevent thermal equilibration with the atmosphere), as suggested by Karpuz and Jansen (in press). Another explanation may simply be that such large influxes of meltwater cause great stress to the foraminifera leading to an increase in metabolic carbon used

in secretion of their tests. The low benthic $\delta^{13}C$ values measured in PCM5 during substage 5a suggest meltwater influenced the benthic foraminifera also. This supports the idea of deep meltwater brines during strong melting phases mentioned in chapter 4.

5.3.3. Productivity and the $\delta^{13}C$ record

Variations in surface water productivity may also disrupt the normal glacial-interglacial variation in $\delta^{13}C$. Periods of high productivity will lead to an enrichment in surface water $\delta^{13}C$ as photosynthesis removes ^{12}C from the water and stores it in organic matter. So periods of high foraminiferal abundance, relating to high surface water productivity, should cause a peak in $\delta^{13}C$ measurements of planktic foraminifera and a low $\delta^{13}C$ value in benthic foraminifera, as re-oxidation of this sinking organic material releases ^{12}C.

Figs. 5.9 and 5.10 show the foraminiferal abundance counts plotted against planktic and benthic foraminiferal $\delta^{13}C$ measurements for PCM5 and PCM7. Also shown in these diagrams are the planktic minus benthic foraminiferal $\delta^{13}C$ values, these plots should record the strength of the biological pump, the efficiency of the removal of organic material from surface waters and its re-oxidation at depth. The shaded sections in both plots represent periods of enhanced foraminiferal, and hence surface water, productivity. PCM5 shows two periods of high foraminiferal abundance within stage 6 (fig. 5.9). These may explain the relatively high $\delta^{13}C$ values experienced within the glacial stage 6, when lower values are expected. There is another period of high foraminiferal abundance within stage 5, from 375 to 385cm within substage 5b, this produces exceptionally high $\delta^{13}C$ values, the productivity influence backing up the global interglacial influence. Two minor foraminiferal highs at 230 and 195cm early in stage 2 also produce heavy $\delta^{13}C$ excursions. A more sustained peak in foraminiferal abundance from 130 to 160cm produces a further high in $\delta^{13}C$ values. This period is within peak stage 2 the last glaciation. The P-B $\delta^{13}C$ values are high during stage 6 and mid-stage 2. This reflects a strong pumping action, organic matter enriched in ^{12}C due to photosynthesis sinks to the sea floor, is re-oxidised, and causes an enrichment in ^{12}C of bottom water ΣCO_2. PCM7 also shows, to a certain extent, an enrichment in planktic $\delta^{13}C$ during isotope stage 2 when foraminiferal abundances are enhanced (see chapter 6 for an explanation of this glacial enhancement in productivity) see fig. 5.10.

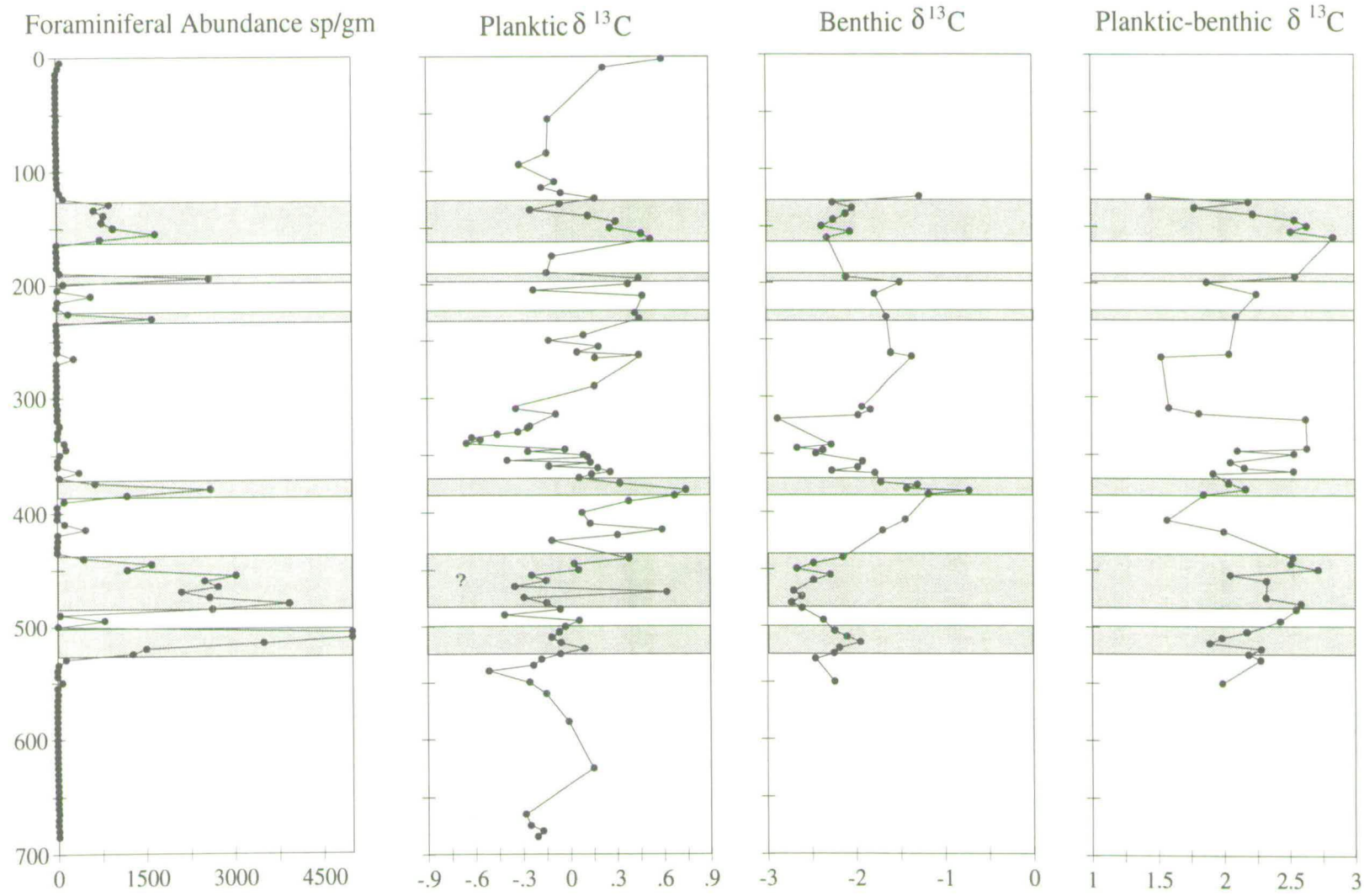

Fig. 5.9. Carbon isotopic signature of planktic and benthic foraminifera from PCM5 plotted with foraminiferal abundance counts. The shaded sections represent periods of high foraminiferal abundance correlating to high planktic carbon 13 values. The horizontal scale for carbon isotope plots is per mil variation w.r.t. PDB standard. Curve on the right shows the planktic-benthic carbon 13 values.

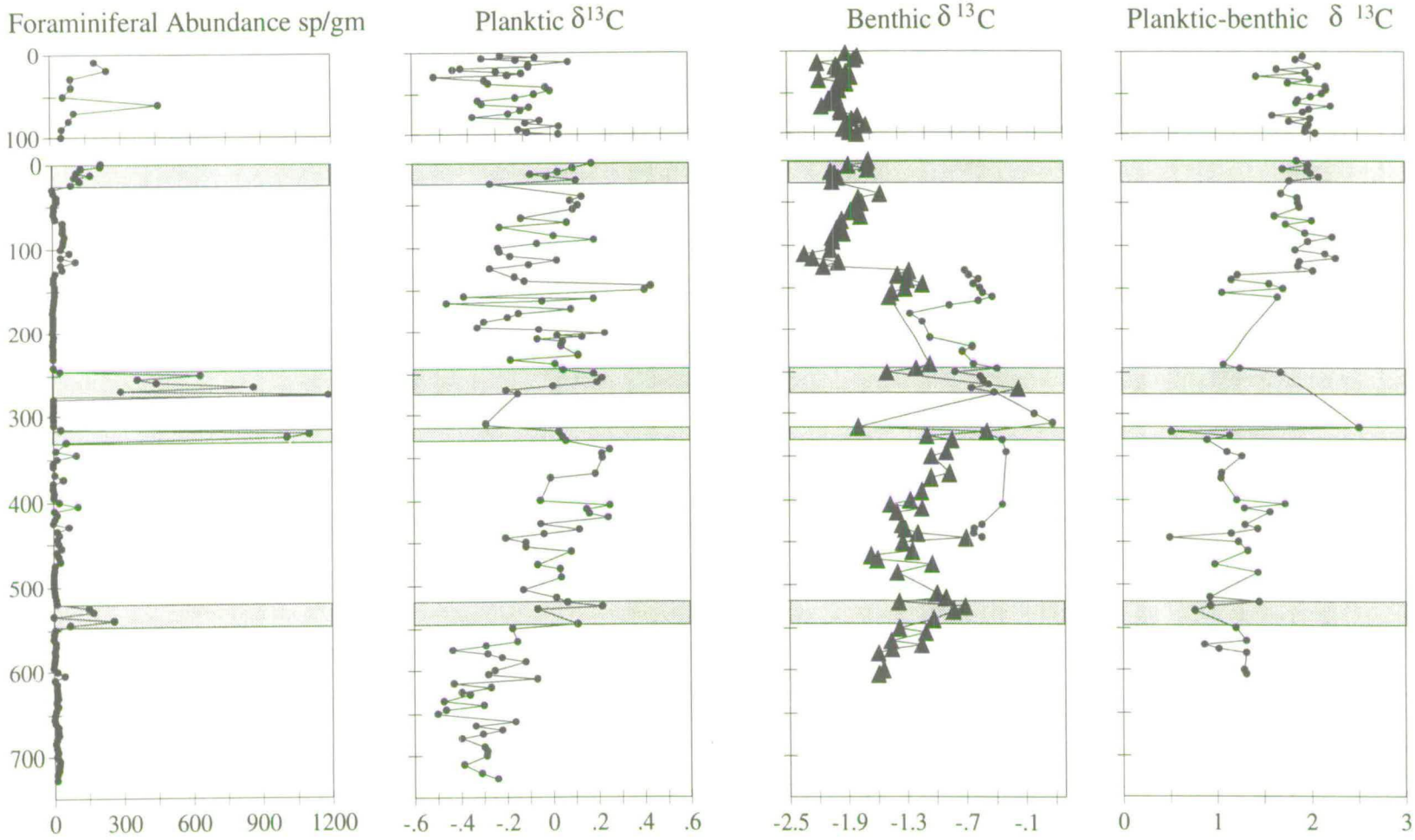

Fig. 5.10. Carbon isotopic signature of planktic and benthic foraminifera from PCM7 plotted with foraminiferal abundance counts (all against depth). The shaded sections represent periods of high foraminiferal abundances correlating to high planktic carbon 13 values. The horizontal scale for carbon isotope plots is per mil variation w.r.t. PDB standard. In the benthic plot triangles represent measurements from *Melonis barleeanum*, circles are from *Cassidulina teretis*.
The curve on the right shows the planktic-benthic carbon 13 values for PCM7.

From 245 to 275cm and from 315 to 330cm foraminiferal abundances are very high compared to the background values, these periods coincide with peak stage 2 glaciation. The corresponding $\delta^{13}C$ measurements from these periods are relatively high, especially considering they are during glacial periods when low values are expected. There is also a minor increase in foraminiferal abundance during stage 3, 525 to 545cm, which correlates to an increase in $\delta^{13}C$. The top of the main PCM7 core shows a minor increase in foraminiferal numbers, from 0 to 25cm, and an associated increase in $\delta^{13}C$ values. The P-B $\delta^{13}C$ values are not so clear for PCM7 (fig. 5.10). There are two points with high P-B $\delta^{13}C$ values within the shaded sections of stage 2 when high productivity would be expected to cause a stronger carbon pumping process, but values are predominantly low. The highest P-B $\delta^{13}C$ values are found in the upper section of the main core, from 130cm, and the whole of the trip core. These values are caused by the pronounced reduction in benthic $\delta^{13}C$ values at 130cm. This reduction correlates to a minor increase in foraminiferal abundance (fig. 5.10), this is produced by an influx of North Atlantic surface waters into the area (chapter 4). This North Atlantic water mass originates from far to the south of the Greenland Sea, and may carry organic material within it. This would encourage an increase in productivity, and lead to increased organic material sinking to the deeper waters causing a depletion of deep waters in $\delta^{13}C$. The expected increase in planktic $\delta^{13}C$ is not seen, however, but may be obscured by the effects of meltwater (causing a decrease in $\delta^{13}C$).

Periods of high surface water productivity produce distinct increases in $\delta^{13}C$ of planktic foraminifera. This ought to produce a corresponding decrease in benthic $\delta^{13}C$ as organic matter sinks and is re-oxidised at depth. This holds true for some sections of the record, stage 6 and stage 2 in PCM5, but is complicated in PCM7 by the effects of meltwater.

5.3.4. Bottom water variations as evidenced by benthic foraminiferal $\delta^{13}C$ measurements

From the results shown in figs. 5.5 to 5.8, it is obvious that the three different benthic foraminiferal species measured in this study have different $\delta^{13}C$ disequilibrium effects. These differences are produced by species specific fractionation and variations in microhabitat, as mentioned in the introduction. The stage 2 values for the different species in all three cores will be compared. Stage 2 has been chosen as it is clearly represented in all cores.

For PCM5 the species *E. umbonatus* was analysed. This is considered an epifaunal species though it actually lives in the upper 1cm of sediment (Vincent *et al.*, 1981). From fig. 5.5 it appears that the average $\delta^{13}C$ value of this species during peak stage 2 is -2.2‰. For PCM7, two species were measured, *M. barleeanum* and *C. teretis* (fig 5.7 and 5.8). *M. barleeanum* has an average peak stage 2 $\delta^{13}C$ value of -1.3‰, *C. teretis* has an average value of -0.6‰. In PCM30 only measurements from *C. teretis* were made during peak stage 2 times, and have a $\delta^{13}C$ average value of -0.5 to -0.6‰.

Graham *et al.* (1981) calculated the $\delta^{13}C$ disequilibrium effect of *O. tener* (*E. umbonatus* in this study) to be -2.1‰. If a correction factor of +2.1‰ is applied to the measurements from *E. umbonatus* from stage 2, average values of -0.1‰ are produced. The disequilibium effect of *M. barleeanum* is uncertain, but measurements from another species of this genus, *M. pompilioides*, produced a disequilibium effect of -1.4‰. If it is assumed that this disequilibium effect is the same for *M. barleeanum* the corresponding correction to stage 2 $\delta^{13}C$ values produces values of +0.1‰. This is reasonably close to the value of -0.1‰ produced by correction of the $\delta^{13}C$ values of *E. umbonatus,* suggesting that the disequilibium effect for *M. barleeanum* is about the same as for *M. pompilioides*. The stage 2 $\delta^{13}C$ values for *C. teretis* of -0.6‰ suggest a disequilibium effect of only -0.5‰ for this species. This assumes that the deep water mass at 2000m at the site of PCM5 is the same water mass found at 1100m at the core site of PCM30.

The proportion of the disequilibium effect produced by species specific fractionation and the proportion produced by microhabitat variation is interesting. Vincent *et al* (1981) suggest *E. umbonatus* living at approximately 1cm depth within the sediment has a disequilibium effect produced by microhabitat of -1.0‰. This leaves a species specific fractionation effect of 1.2‰ as the overall disequilibium effect quoted by Graham *et al.* (1981) is -2.2‰. Grossman (1984) reports species of *Cassidulina* record almost exactly the $\delta^{13}C$ of deep waters, these measurements were made from off southern California. In this study it has been found that *C. teretis* has a disequilibium effect of -0.5‰, this may be produced by living deeper within the sediment than off southern California.

Using the correction factors outlined above the glacial stage 2 $\delta^{13}C$ values of bottom waters are approximately 0.0‰. The stage 6 values are slightly less, from peak stage 6 in PCM5 measurements from *E. umbonatus* produce $\delta^{13}C$ values of -2.7‰ (fig. 5.5), this equates to a $\delta^{13}C$ value of bottom water of -0.5‰. Measurements from *C. teretis* from PCM30 during peak stage 6 produce values of -0.9‰, see fig. 5.7, a

correction factor of +0.5‰ leaves a $\delta^{13}C$ value of bottom water of -0.4‰, similar to the value produced from PCM5. Stage 6 deep waters are therefore more depleted in ^{13}C than during stage 2. This can be explained by a more intense glaciation during stage 6 times, with older more stagnant deep waters. The oxygen content would be very low due to the break down of organic material releasing ^{12}C, thus producing a relative depletion in ^{13}C. These glacial $\delta^{13}C$ values of 0‰ or less are lower than the $\delta^{13}C$ values of modern North Atlantic Deep Water, 0.5 to 1.0‰, and are in fact closer to values from older oxygen poor Pacific deep waters of today, 0.5 to -0.5‰ (from Kroopnick, 1985). This supports the idea of stagnant circulation during glacial periods, bottom waters becoming depleted in oxygen and therefore depleted in $\delta^{13}C$ also.

The end of a glacial period is thought to be characterised by an increase in oceanic circulation, interglacial periods should therefore record periods of more vigorous circulation with younger bottom waters. Younger bottom waters should have a higher oxygen content and be richer in ^{13}C, as organic carbon is still to be broken down. This change should be recorded by the $\delta^{13}C$ signature of benthic foraminifera. This increase in $\delta^{13}C$ is clearly visible at the end of stage 6 in PCM5 (fig. 5.5). The $\delta^{13}C$ values increase from -2.5‰ during stage 6 to approximately -1.2‰ during mid stage 5, and increase further to -1.0‰ during early stage 5b, the corrected value is therefore between 1.0 and 1.2‰. The decrease seen during late stage 5 is due to meltwater effects and has been discussed already. This increase in $\delta^{13}C$ due to a more vigorous circulatory system is also seen during stage 3 in PCM5 (fig. 5.5).

The transition from stage 2 to stage 1 ought to show a similar trend of increasing $\delta^{13}C$ values marking the resumption of NADW production. This period of the record is present in PCM7, and has been measured using *M. barleeanum* (fig. 5.7) but presents a rather strange picture. The $\delta^{13}C$ values towards the end of stage 2, from 13-14 ka, are approximately -1.3‰, this equates to a corrected value of 0‰. A major change to lower $\delta^{13}C$ values is then recorded at 12.3 ka, values decreasing to approximately -2.0‰, a corrected value of -0.6‰. This correlates exactly to a major decrease in $\delta^{18}O$ benthic and planktic values recording a major deglacial event. This also marks the point where subpolar foraminifera are found in the core for the first time due to an influx of North Atlantic surface waters, see chapter 4.

The oxygen isotope evidence of chapter 4 suggests that the initial influx of North Atlantic surface waters at 12.3 ka did not lead to a resumption of NADW production. The decrease in *M. barleeanum* $\delta^{13}C$ values at this point was produced by meltwater

influx. The $\delta^{18}O$ results suggest that the influx of North Atlantic surface waters from 10 ka onwards initiated renewed NADW production. This increase in deep water circulation would be expected to produce younger bottom waters enriched in $\delta^{13}C$. The record of *M. barleeanum* in PCM7 shows little change in $\delta^{13}C$ at 10 ka, still a corrected $\delta^{13}C$ value of -0.6‰. This is much lower than typical $\delta^{13}C$ values of NADW between +0.5 and +1.0‰, the reason for this is uncertain. It may be due to an increase in surface water productivity as warmer nutrient rich Atlantic waters enter the area. An increase in productivity should increase the $\delta^{13}C$ value of planktic foraminifera, but decrease the value in benthic foraminifera due to increased sinking of organic material. The foraminiferal counts from PCM7 (fig. 5.10) do show an increase in numbers before this point, 125cm or 10.4 ka, so it is a possible explanation.

5.3.5. Comparison of planktic and benthic foraminiferal $\delta^{13}C$ signatures

The difference in $\delta^{13}C$ between surface waters and deep waters can be evaluated by comparing the planktic and benthic foraminiferal $\delta^{13}C$ corrected values. The fractionation effect of the planktic foraminiferal species *N. pachyderma* (sinistral) has been calculated by Johannessen *et al.* (in press) for the Norwegian Sea as +1.4‰, so a correction factor of +1.4‰ has to be added to the planktic measurements to see the $\delta^{13}C$ value of surface waters. Surface waters are highly susceptible to changes in $\delta^{13}C$ composition due to the effects of meltwater and productivity fluctuations. Average stage 2 planktic foraminiferal $\delta^{13}C$ values from PCM30 are from -0.1 to +0.1‰ (fig. 5.6). This range is much greater in PCM5 from -0.3 to +0.3‰ (fig. 5.5), but this may be due to changes induced by productivity fluctuations. An average of close to 0.0‰ does seem accurate. Adding the correction factor of +1.4‰ produces a glacial $\delta^{13}C$ value of surface waters of approximately 1.4‰. Stage 6 planktic $\delta^{13}C$ values are slightly lower, averaging -0.2‰ for PCM5 and PCM30, this equates to a corrected value of 1.2‰. This difference matches the benthic foraminiferal $\delta^{13}C$ values which are slightly less during stage 6 compared to stage 2. For glacial periods in general the planktic foraminiferal $\delta^{13}C$ values are approximately 1.4‰ higher than the corresponding benthic values, this is slightly greater than the P-B amplitude of 1‰ suggested by Berger and Vincent (1986).

During interglacial periods planktic $\delta^{13}C$ values tend to increase as expected, except where meltwater influences are strong, as in substages 5e and 5a. The $\delta^{13}C$ values for mid stage 5 in both PCM5 and PCM30 reach values of 0.3 to 0.6‰, corrected to 1.7

to 2.0‰. The Holocene record of PCM7 is hard to interpret due to the effects of meltwater and no clear values can be seen. The benthic stage 5 $\delta^{13}C$ values seen in PCM5 are between 1.0 and 1.2‰ (fig. 5.5), a difference of approximately 0.7‰ between planktic and benthic foraminiferal species. The P-B amplitude is considerably less during interglacials than glacials this may be due to the increased effect of meltwater on surface waters decreasing the $\delta^{13}C$ composition by addition of light ^{12}C terrestrial organic material.

The glacial $\delta^{13}C$ planktic values of 1.4‰ are similar to the $\delta^{13}C$ values of present day Polar waters measured by Johannessen *et al.* (in press). This suggests that during glacials Polar surface waters reached the Spitsbergen continental margin. The stage 5 planktic foraminiferal $\delta^{13}C$ values of between 1.7 and 2.0‰ are close to the Arctic surface water values also measured by Johannessen. This water mass is a mixture of North Atlantic surface water and Polar surface water. As a result the $\delta^{13}C$ data suggests that during stage 5 North Atlantic waters did reach the Spitsbergen margin, and a mixture of North Atlantic water and Polar waters was present. The Holocene picture from $\delta^{13}C$ measurements is unclear due to the effects of meltwater, other parameters such as the $\delta^{18}O$ signature and foraminiferal abundances are more useful for this period.

5.4. Conclusions

1. Major glacial-interglacial fluctuations can be seen in the $\delta^{13}C$ signature of both planktic and benthic foraminifera, having an amplitude of between 0.6 and 0.9‰. These first order ranges are complicated by the effects of meltwater and surface water productivity.

2. Meltwater influxes have a major influence on the $\delta^{13}C$ values of planktic, and to a lesser extent, benthic foraminifera. Influx of meltwater causes a depletion in $\delta^{13}C$ values due either to the release of terrestrial material carried in the ice on melting, release of algal blooms from within the ice, or change in metabolic uptake of carbon of foraminifera due to stress.

3. Surface water productivity can be estimated by the foraminiferal abundance counts made on PCM5 and PCM7 (figs. 5.9 and 5.10). Periods of high foraminiferal abundance correlate to periods with increased $\delta^{13}C$ values in *N. pachyderma*

(sinistral). This is due to increased photosynthesis in surface waters storing light ^{12}C in organic matter that subsequently sinks to bottom waters.

4. During oxygen isotope stages 6 and 2 greater planktic-benthic $\delta^{13}C$ values indicate a stronger biological pump.

5. The deep water glacial $\delta^{13}C$ values measured from benthic foraminifera (after correction) range between 0.0 and -0.5‰. These values are similar to old, oxygen poor Pacific deep waters, and were probably produced by stagnant circulation during glacial periods.

6. The corrected stage 5 deep water $\delta^{13}C$ values from benthic foraminifera were between 1.0 and 1.2‰. These higher values were produced by a more vigorous circulatory system of an interglacial. They are similar to the present day $\delta^{13}C$ values of NADW, suggesting some deep water production may have taken place during stage 5 in this area.

7. Measurements from the benthic foraminifera *M. barleeanum* from the top of PCM7 show the opposite trend to the expected one. A major deglaciation event at 12.3 ka can be recognised from $\delta^{18}O$ measurements. This ought to produce a more vigorous circulation system leading to renewed bottom water production, and therefore an enrichment in $\delta^{13}C$ of bottom waters. Measurements over this period in PCM7 show a depletion in $\delta^{13}C$ over this transition. The reason for this is uncertain but may reflect the effects of meltwater, or possibly an increased surface water productivity associated with the influx of North Atlantic surface waters. The microhabitat of this species within the sediment may also affect the $\delta^{13}C$ values.

8. The difference between planktic $\delta^{13}C$ values and benthic $\delta^{13}C$ values is greater during glacials than interglacials. During glacial periods the difference is on average 1.4‰, but decreases to 0.7‰ during interglacials. The normal planktic-benthic foraminiferal $\delta^{13}C$ range is 1.0‰ (from Berger and Vincent, 1986). The reduced interglacial difference may be due to the effects of meltwater adding terrestrial organic material to surface waters, this would reduce the $\delta^{13}C$ value to nearer the benthic values. The increased range during glacial may be due to reduction in $\delta^{13}C$ benthic values due to intense stagnation of circulation in this high latitude area.

Chapter 6. Abundance records of planktic and benthic foraminifera as indicators of intensity of surface water circulation and productivity

6.1. Introduction

Fluctuations in relative and absolute abundances of both planktic and benthic foraminifera have been recognised throughout the modern worlds oceans for a long time. Accurate counts of different species present have been made in order to identify different assemblage groups related to particular environments. Different assemblages can then be used to characterise different water masses and, in the case of benthic foraminifera, different water depths and environments. The faunal composition of past samples can then be analysed and used to recognise environmental and paleoceanographic fluctuations. This is particularly useful for glacial-interglacial fluctuations, but also for environmental changes on shorter time scales. Some of the recent studies of planktic and benthic foraminifera from the Norwegian-Greenland Sea area will be outlined in the section below.

6.2. Previous Research

Studies of planktic foraminifera

Variations in planktic foraminifera have been used extensively to recognise different surface water masses (Bé, 1977; Hemleben and Spindler, 1983; Brummer and Kroon, 1988). CLIMAP (1976) used Recent surface samples to characterise the species content of certain biogeographic provinces. Past samples were then analysed and temperature and salinity estimates of surface currents were made using the information obtained from the Recent samples. Using planktic foraminifera to make estimates of temperature and salinity is somewhat dangerous because their distribution is most probably effected by other factors as well, but most workers agree that certain water masses are characterised by certain assemblages of species. Planktic foraminiferal abundances have been used extensively for paleoceanographic reconstruction's in the Norwegian Sea (Kellogg, 1973; and 1980; Lehman and Keigwin, 1992; and Haake and Pflaumann, 1989).

Interpretations of variations in planktic foraminiferal species are less complex than benthic variations. Definite links between water mass and planktic foraminiferal assemblages can be made, for example the CLIMAP study mentioned above. Surface

currents in the Norwegian-Greenland Sea at present control the planktic assemblages found across the basins; these currents are shown in fig. 6.1. The warm Norwegian Atlantic Current on the eastern side of the basins supports a different, more diverse assemblage than the colder East Greenland Current to the west. The colder surface currents originating from the Arctic Ocean are dominated by one species, *Neogloboquadrina pachyderma* (Ehrenberg) (sinistral), whereas the surface waters sourced from the North Atlantic are dominated by *N. pachyderma* (dextral), *Globigerina quinqueloba* (Natland) with minor abundances of *Globigerina bulloides* (d'Orbigny). These differences were recognised by Kellogg (1973, 1980).

Lehman and Keigwin (1992) recognised influxes of Atlantic water into the Norwegian Sea by faunal analysis of the TROLL 3.1 core off the coast of southern Norway. During the last glacial period the planktic foraminiferal assemblage consisted of near 100% *N. pachyderma* (sinistral), a polar species. At this time, surface waters originated from further north, possibly the Arctic Ocean. At approximately 13.5ka the faunal assemblage changed, the sinistral variety of *N. pachyderma* being replaced by the dextral variety common in temperate to subpolar environments of the North Atlantic. This marks the first influx of North Atlantic surface waters into the Norwegian Sea. At two times since 13.5 ka cold Polar surface currents have replaced North Atlantic surface waters, once for a brief period at 11.73 ka and again from 11.16 to 10.5 ka ago. Evidence for this comes from the replacement of *N. pachyderma* (dextral) by the cold water variety *N. pachyderma* (sinistral).

Sejrup *et al.* (1984) examined the foraminiferal and stable isotopic record of two cores from slightly further north in the Norwegian Sea, approximately 65°N on the southeastern slope of the Norway Basin. They recognised a major change in the planktic fauna from one dominated by *N. pachyderma* (sinistral) to one dominated by *N. pachyderma* (dextral) at an age close to 10ka.. Using this as an indicator of the palaeoposition of the oceanic polar front, they claim that the polar front did not reach 65°N in the Norwegian Sea until 10ka. This disagrees with the evidence from the TROLL 3.1 core, and also with data from litteral molluscs suggesting that the polar front attained a more northerly position in the Norwegian Sea between 12.6 and 11ka (Mangerud, 1977).

Kellogg (1973) carried out planktic foraminiferal absolute abundance counts on 7 cores from the Norwegian-Greenland Sea. Four climatic modes were recognised from this data, in which the absolute foraminiferal abundances vary along with warm water and cold water faunas.

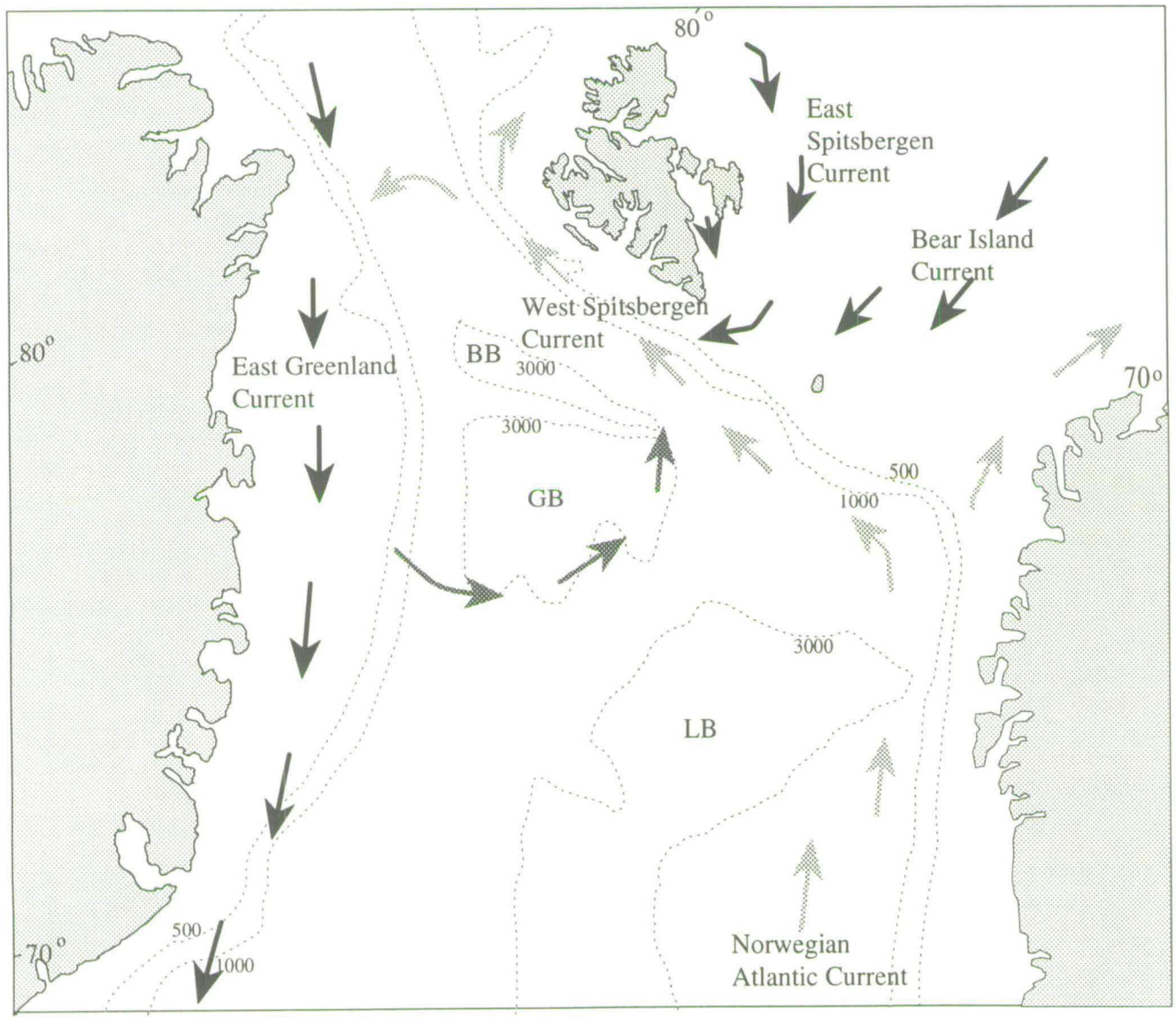

Fig. 6.1. Map of Greenland Sea showing surface current circulation of the present day.

Warm currents, light shading;
Norwegian Atlantic Current
West Spitsbergen Current

Cold currents, dark shading;
East Greenland Current
East Spitsbergen Current
Bear Island Current

Interglacial conditions were characterised by high foraminiferal abundances and high percentages of warm water forms. Interstadial conditions were recognised with high foraminiferal absolute abundances but lower percentages of warm water fauna. Moderate glacial conditions with low foraminiferal content and characterised by high percentages of cold water fauna were identified, and peak glacial periods are either barren or have very low foraminiferal absolute abundances.

More recently, Kellogg (1980) reconstructed surface water temperatures in the Norwegian Sea from faunal composition data of 24 Norwegian Sea cores for the last glacial maximum (18ka), the last interglacial (120ka), and oxygen isotope substage 5a (82ka). From this study it was concluded that the Eemian (the last interglacial) was probably characterised by slightly warmer temperatures than the Holocene. During weak interglacial periods, such as substage 5a, the Norwegian Sea was covered by permanent pack ice, with a tongue of seasonally ice free water stretching up the centre of the sea as far as 76°N. He also concluded that during the last glacial, oxygen isotope stage 2, the Norwegian-Greenland Sea was covered by permanent pack ice to approximately latitude 60°N. Haake and Pflaumann (1989) analysed the faunal composition of two cores from the Vöring Plateau (68°N). Except for Holocene surface samples, they record a planktic foraminiferal fauna dominated by the polar species *N. pachyderma* (sinistral) as far back as oxygen isotope stage 6. The Recent surface samples had a higher proportion of *N. pachyderma* (dextral) and *G. bulloides*, indicators of North Atlantic water influence. So they found no evidence of Atlantic water influx during the Eemian (oxygen isotope 5e).

Belyaeva and Khusid (1990) examined the foraminiferal assemblages of sediments from the Mendeleev Ridge in the Arctic Ocean. They observed higher abundances of both planktic and benthic foraminifera during interglacial periods. Influx of relatively warm intermediate waters to the Arctic Ocean from an Atlantic source, and partial thawing of the ice cover to allow light penetration led to higher productivity. During glacial periods permanent pack ice reduced the penetration of sunlight to the surface waters causing a drop in surface water productivity. Typical interglacial planktic foraminiferal abundances reached 5000-10,000 sp/gm, glacial periods were characterised by values of about 100 sp/gm.

Sejrup *et al.* (1984) used faunal and oxygen isotopic evidence to interpret changes in the oceanography between the Late Weichselian (oxygen isotope stage 2) and the Holocene (stage 1). Two cores off southern Norway revealed low production rates of foraminifera during peak glacial periods. Planktic foraminiferal abundances during

glacial periods were below 100 sp/gm dry weight, interglacial values reach a peak of 1700 sp/gm.

Elverhoi et al. (1993) examined the foraminiferal oxygen isotope record and ice rafted detritus (IRD) record of a series of cores from the continental margin of Spitsbergen. They recognised two periods of increased foraminiferal abundance from 25 to 23ka and from 19 to 15ka (ages are radiocarbon years). These two periods also contained coccoliths, and a high proportion of ice rafted material (coarser than 500μm). They concluded these periods must have been characterised by ice free conditions as evidenced by the high foraminiferal abundances and the presence of coccoliths. Also chalk fragments were found which are thought to be sourced from the North Sea as this is the closest source of chalk to the area. These must have been carried by icebergs. They concluded that two periods within oxygen isotope stage 2 were characterised by ice free conditions caused by influx of North Atlantic waters, and envisage a narrow ice free corridor stretching from the North Sea along the coast of Norway up as far as the coast of Spitsbergen 80°N.

Studies of benthic foraminifera

Several studies have been carried out examining changes in benthic foraminiferal fauna with depth in the Norwegian-Greenland Sea (Belanger and Streeter, 1980; Sejrup *et al.*, 1981 and Corliss and Chen, 1988). Some studies have extended this work to look at variations of benthic fauna over time, using such changes for paleoceanographic interpretations (Streeter *et al.*, 1982 and Haake and Pflaumann, 1989). In order to make interpretations based on past faunal changes it is essential to understand the present distribution patterns. This enables the recognition of relationships of physical and chemical parameters with faunal distributions. In this section I will outline the conclusions from past work from palaeoecological studies of benthic foraminifera in the Norwegian-Greenland Sea.

Belanger and Streeter (1980) examined assemblages of benthic foraminifera in 36 core top samples from the continental slope and deep basin of the Norwegian-Greenland Sea. Four overlapping depth dependant biofacies were recognised. The shallowest and most diverse biofacies was found between 600-1200m, and was characterised by *Melonis barleeanum* (Williamson), *Pullenia bulloides* (d'Orbigny), and *Islandiella norcrossi* (Cushman). From 950-1500m, samples were dominated by *Cassidulina teretis* (Tappan); the next biofacies was found between depths of 1250-3200m dominated by *Cibicides wuellerstorfi* (Schwager). The final assemblage characterised by *Oridorsalis tener* (Brady) (*Eponides umbonatus* (Reuss) in this

study) and *Epistominella exigua* (Brady) dominated below 2900m, but was present at shallower depths up to 1000m.

In a similar study, Sejrup *et al.* (1981) identified, using 42 surface samples from the Norwegian continental margin between 62°N and 65°N, 5 biofacies groups. These biofacies extend from the shelf down the slope to deep bathyal regions. Biofacies 1 was found on the continental shelf and was dominated by *Bulimina marginata* (d'Orbigny) and *Textularia bocki* (Hogland) with other associated species, and extended down to 400m water depth. Biofacies 2 was dominated by *Trifarina angulosa* (Williamson) and *Cibicides lobatulus* (Walker and Jacob) and was found from 400-700m on the upper part of the continental slope. The base of this biofacies was determined by the base of the Norwegian Current (a northward flowing relatively warm saline current). The 3rd biofacies spanned water depths sampled by the cores of this study, present from 700-1200m on the continental slope. *Nonion barleeanum (M. barleeanum* in this study), *Cassidulina reniforme* (Norvang), *Cassidulina laevigata* (d'Orbigny), and *P. bulloides* are the dominant species in this assemblage. Water temperatures at this depth are generally below 0°C, and salinities about 34.92‰; the base of this biofacies coincides with the pycnocline (below this level the water density becomes fairly stable). The 4th biofacies, between 1200-1600m, was marked by the dominance of *C. laevigata*, and co-occurrences of *C. wuellerstorfi*, *E. exigua* and *E. umbonatus*. Temperature and salinity values were very stable below 1200m, -1°C and 34.92‰ respectively. The final assemblage recognised by Sejrup *et al.*, found below 1600m, was dominated by *C. wuellerstorfi*, *E. exigua* and *E. umbonatus*.

There are definite similarities between the different assemblages recognised in the two studies mentioned above (Belanger and Streeter, 1980 and Sejrup *et al.*, 1981) as expected. The important question though is what causes these changes in assemblage composition. The shelf biofacies and biofacies 2 from Sejrup *et al.* (1981) are controlled by water mass characteristics. The shelf biofacies 1 is found where warm saline Atlantic water impinges on the sea floor, and biofacies 2 is found in the transition zone between Atlantic water and colder homohaline deep water. Why the faunal changes occur below this depth, and similarly the changes in faunal assemblages in deeper water identified by Belanger and Streeter (1980) are not so easy to understand. Changes in temperature and salinity at these depths are small and do not account for such assemblage changes. Belanger and Streeter (1980) present variations in water properties with depth for stations in the Greenland Basin and Norwegian Basin. In the Greenland Basin temperature is high in the surface waters, but rapidly drops to stabilise at -1°C by 300-400m water depth. Salinity stabilises at a

value of 34.9‰ even shallower at about 100-200m. In the Norwegian Basin temperature decreases gradually from 5°C at the surface to -1°C by 1400m and remains constant below this, whereas salinity is stable at 34.9‰ over the whole water column. So in neither basin are temperature or salinity the driving mechanisms behind benthic foraminiferal variations. Belanger and Streeter (1980) summarise the main parameters influencing foraminiferal distribution. These can be split up into two groups: (1) physical-environmental parameters and (2) biological-environmental parameters. Physical parameters include temperature, salinity, hydrostatic pressure, nature of substrate, light intensity, pH, concentration of O_2, nutrients and trace elements. Biological parameters include substrate concentration of labile organic carbon, competition, predation and disease.

The physical-environmental parameters measured by Belanger and Streeter (1980), temperature, salinity, oxygen, phosphate, silica and nitrate concentrations, show no bathymetric discontinuities that could explain the bathymetric zonation of benthic foraminifera seen. In particular, the dominance of *C. wuellerstorfi* from 1250-3200m, and its replacement by *O. tener* from 2900m coincides with no major change in oceanographic parameters. They conclude that hydrostatic pressure-temperature interdependance may regulate the barotolerance of species, and may be an important factor in assemblage composition, but a wide range of physical and biological-environmental parameters, mentioned earlier, may affect in a more subtle way the dominance of benthic foraminifera.

Corliss and Chen (1988) classified benthic foraminifera of the Norwegian Sea into 9 separate morphotypes. These were used to recognise microhabitat patterns which they suggest are related to the organic carbon content of deep sea sediments. The main distinction between morphotypes relates to the mode of life of the foraminifera: epifaunal, living in the top 1cm of sediment or on the sediment surface or infaunal, living below 1cm in the sediment. Examples of epifaunal species from their study include *Planulina wuellerstorfi* (*C. wuellerstorfi* of this study), *Pyrgo murrhina* (Schwager) and *Oridosalis umbonatus* (*E. umbonatus* of this study). Examples of infaunal species include *C. laevigata, Melonis zaandami* (Van Voorthuysen) (*M. barleeanum* in this study) and *P. bulloides*. The upper water column from 200-500m contains both infaunal and epifaunal groups, from 500-1500m the infaunal species dominate, then below 1500m the epifaunal species dominate.

The morphotypes recognised have a regular pattern varying with depth. The infaunal-epifaunal variations were compared to water mass distribution, calcium carbonate

content, grain size, and organic carbon content. From this comparison morphotype patterns were not related to water mass distribution, calcium carbonate content, grain size or dissolved O_2 concentration. The epifaunal-infaunal data appeared to be related to organic carbon content. Shallow waters with a wide range in organic carbon values contain both epifaunal and infaunal morphotypes. From about 500-1500m organic carbon has a high concentration and is related to infaunal dominance, whereas deeper waters with low organic carbon are dominated by epifaunal morphotypes. It is suggested that epifaunal forms dominate in areas with low organic carbon (food supply) because they can forage at the surface where labile organic matter is most abundant.

From these studies of benthic foraminifera in the Norwegian-Greenland Sea distinctive biofacies have been recognised which inhabit certain water depths. Factors controlling the distribution of benthic foraminifera are less well understood. Hydrostatic pressure combined with temperature may be important, and a link between variations in infaunal and epifaunal species with organic carbon content has been established (Corliss and Chen, 1988).

Some studies have looked at benthic faunal changes over time, Streeter *et al.* (1982) from the Norwegian-Greenland Sea, and Haake and Pflaumann (1989) from the Vöring Plateau. Both these studies examined benthic faunal variations from oxygen isotope stage 6 to the present. Both found in general benthic foraminiferal abundances to be much higher during interglacial periods. They concluded that productivity was higher during these periods due to ice free surface waters causing planktic blooms which supplied organic matter to benthics for food supply. They found specimens of *C. wuellerstorfi* to be more abundant during interglacial periods, and *O. umbonatus* (*O. tener* or *E. umbonatus*) to be more abundant during glacial periods. From this they concluded that *C. wuellerstorfi* represented higher productivity ice free conditions, and *O. umbonatus* dominated during periods of sea ice cover, where productivity, and therefore food supply were very low.

6.3. Objectives of foraminiferal abundance counts

The main aim of this chapter is to document the faunal changes in both benthic and planktic foraminifera, and the total abundance changes in foraminifera present on the continental slope of Spitsbergen. Faunal changes are related to changes in circulation patterns over time, and are also used as a proxy for productivity changes. The

changes in absolute foraminiferal abundance highlight periods of enhanced productivity assuming sedimentation rate and winnowing do not play a major part, these effects will be assessed. The major surface circulation changes that take place during a deglacial phase are assessed from planktic foraminiferal faunal changes, while changes in deep water circulation are evaluated from benthic foraminiferal faunal changes. In particular this chapter aims to identify influxes of North Atlantic surface waters to the area and deduce the resulting changes in deep water circulation. The detailed timing of such changes have important implications for the global ciculation system as a whole, and are investigated in detail for the stage 2-stage 1 transition. Similar techniques are then used to interpret the palaeoceanography during oxygen isotope stage 5.

6.4. Description of foraminiferal absolute abundance counts

Planktic and benthic foraminifera were counted from two cores, PCM5 and PCM7. The results of these counts are described briefly below, sample preparation and counting procedures are outlined in Appendix 1. Counts of individual species, which are thought to have paleoecological significance, will be described below. The species described below are shown in plates 1, 2 and 3. A taxonomic list of the species identified in these counts is given in Appendix 2.

6.4.1. PCM5

All absolute abundance counts are expressed as number of specimens per gram of dry weight sediment. The results of absolute planktic and benthic foraminiferal abundance counts along with the benthic:planktic ratio are shown in fig. 6.2. Normally the planktic:benthic ratio is plotted, but in this study I have chosen to plot this in reverse as this highlights the periods with increased benthic foraminiferal absolute abundance more clearly. These results have several interesting features. Firstly, the planktic and benthic foraminiferal absolute abundances match each other, secondly in general the planktic foraminiferal abundance is over ten times greater than the benthic foraminiferal abundance, and thirdly the rapidity with which abundances change.

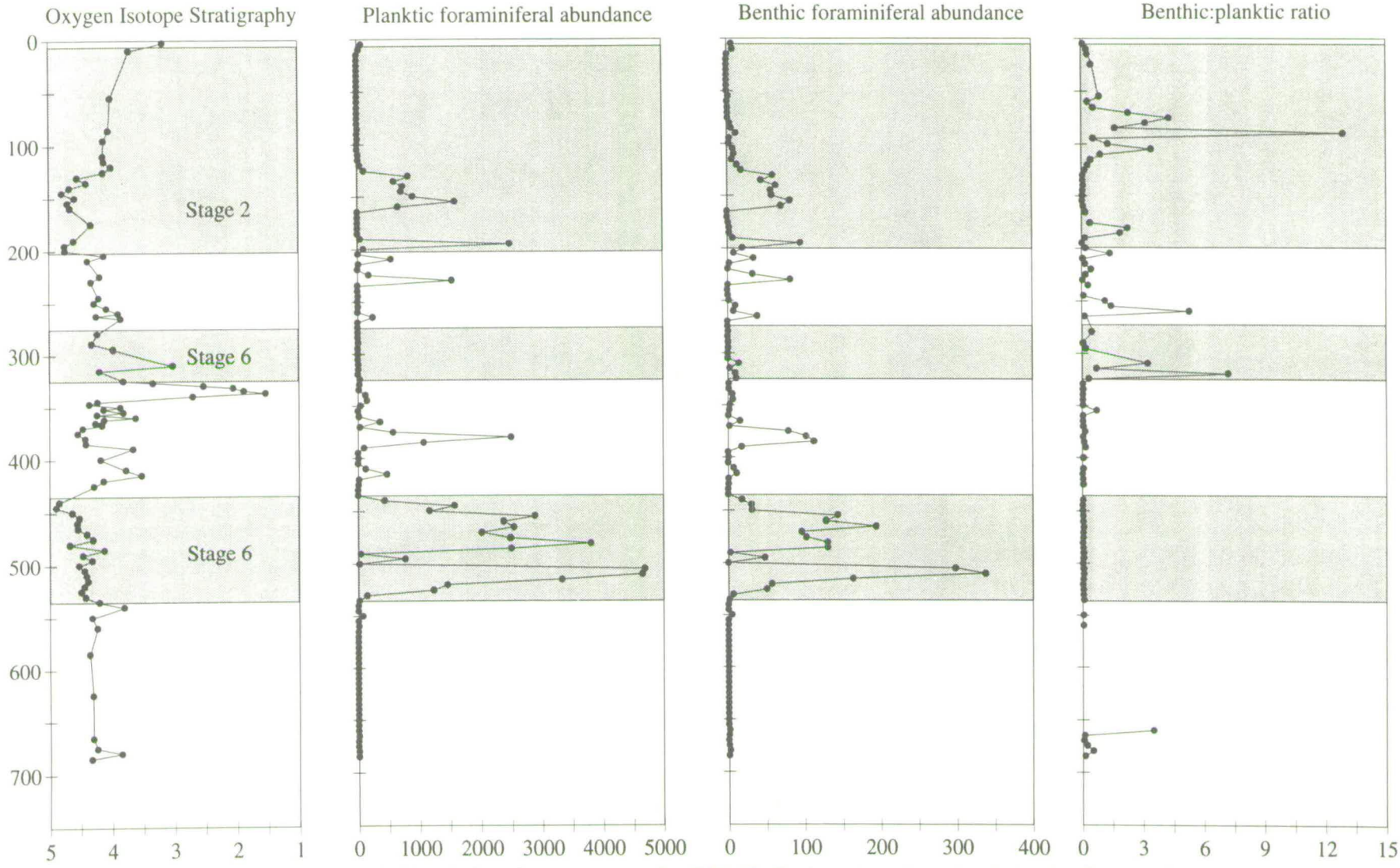

Fig. 6.2. Planktic and benthic foraminiferal abundance counts for PCM5 all plotted against depth (cm). Oxygen isotope stratigraphy on the left, scale per mil variation w.r.t. PDB standard. Planktic and benthic abundances expressed as no. specimens per gram dry wt sediment. The B:P ratio is shown on the right.

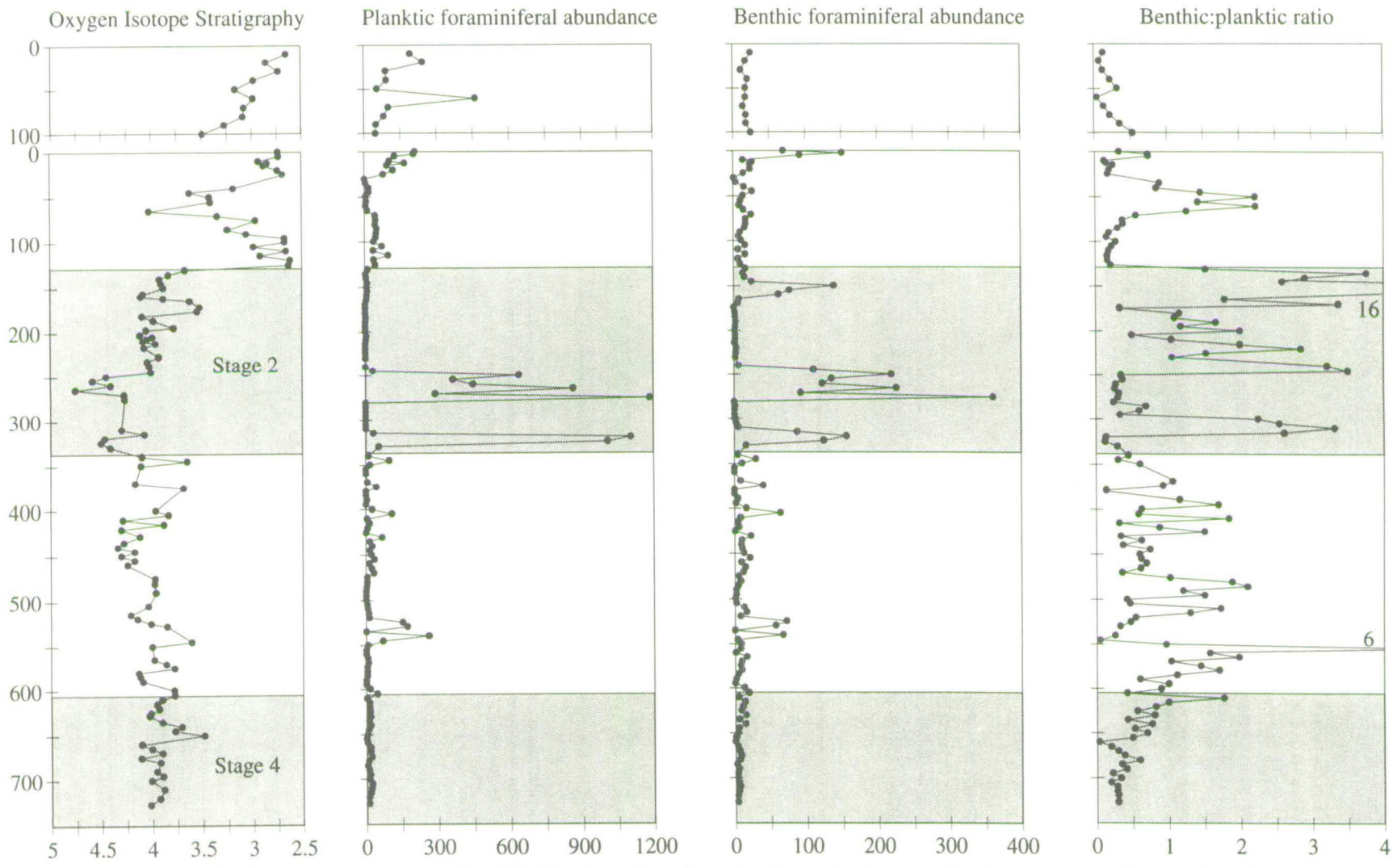

Fig. 6.3. Foraminiferal abundance counts for PCM7, plotted against depth (cm). Oxygen isotope stratigraphy on the left, scale per mil variation w.r.t. PDB standard. Planktic and benthic abundances expressed as no. specimens per gram dry wt. sediment. B:P ratio is shown on the right.

The planktic foraminiferal abundance record

The planktic foraminiferal abundance record varies from 0 to 4700 specimens per gram (sp/gm). Absolute abundance values change from close to zero to several thousand sp/gm over one or two samples. The base of the core is characterised by very low abundances, close to 0sp/gm until 540cm, where one isolated sample occurs at 550cm with a minor peak of 73sp/gm. A dramatic increase occurs at 535cm with values reaching a peak of 4700sp/gm at 505cm, then dropping off to just 10sp/gm at 500cm. Abundances upwards rise to a more sustained peak of over 1000sp/gm from 485-445cm, but rapidly drop to below 10sp/gm from 435-395cm, although a minor peak of 400sp/gm occurs from 415-410cm. Slightly higher in the core values again jump to over 1000sp/gm, with a peak of 2500sp/gm at 380cm, but are reduced to 300-500sp/gm from 375-365cm. The next section has moderately low abundances of around 100sp/gm until 325cm. There is a further drop in abundances to below 10sp/gm from 325 to 235cm, with one minor peak of 250sp/gm at 265cm. There are several isolated peaks in this interval of around 1000sp/gm, superimposed on background values below 10sp/gm; these peaks are at 230cm, 210cm, and the largest at 195cm. Low values then continue to 165cm. From there an interval with relatively high abundances of 500-1500sp/gm occurs from 160-125cm. Values then drop back to around 10sp/gm until 10cm, where a minor increase occurs again to 70sp/gm.

The benthic foraminiferal abundance record

As previously mentioned the benthic foraminiferal abundances match those of the planktics, but are considerably lower. Fluctuations occur just as rapidly (fig. 6.2). As with the planktic record, the base of the core until 530cm is virtually barren with low abundances of 0-1sp/gm. The next section exhibits the same three peaks as seen in the planktic record. The first one is the largest with 337sp/gm at 510cm, the second peak has values from 100-150sp/gm, and the third peak values of approximately 100sp/gm. The next section has relatively low values below 10sp/gm from 360-235cm, except for a spike of 38sp/gm at 265cm (the same position as the planktic abundance spike). Over the next section, the same three isolated peaks as found in the planktic foraminiferal abundance record can be recognised in the benthic record with abundances from 50-100sp/gm at 230cm, 210cm, and 195cm. A section with very low abundances then gives way to a more prolonged but subdued peak of 50-90sp/gm from 160-130cm. Values then drop, but maintain relatively moderate abundances of 5-15sp/gm until 80cm. They then drop to nearly 0sp/gm, until the top 10cm where a slight increase to 8sp/gm is found.

Benthic:Planktic ratio

The ratio of benthic to planktic abundance can be used to identify sections where either planktic or benthic foraminifera become more abundant relative to each other. It is commonly used as a sea level indicator; benthic foraminiferal specimens are more abundant than planktic ones in shallower shelf waters; further offshore planktics become more and more abundant relative to benthics (van der Zwaan *et al.*, 1990).

In PCM5, the B:P ratio is predominantly very low (fig. 6.2). Thus in general planktic foraminifera are far more abundant than benthic foraminifera. There are several sections, however, where the ratio increases above 1 (shaded in fig. 6.2), implying benthics are more abundant than planktics. These sections always occur when total foraminiferal abundance is low. This must be interpreted with care, as they may be caused by reworking of low numbers of foraminifera from more abundant sections. The initial peak in the B:P ratio curve at the base of the core can be ignored because it occurs in a section with planktic and benthic abundances of near 0sp/gm. The next section where the B:P ratio increases above 1 is found from 320-310cm. A similar peak can be seen from 250-260cm. A more prolonged and significant peak is found between 120-70cm. Possible explanations for these peaks will be discussed later.

Absolute Abundance variations of individual foraminiferal species

The variation in abundance of specimens of individual benthic and planktic foraminiferal species have been counted. Results of the most common, or significant, species have been plotted in figs. 6.4 and 6.5 as number of specimens per gram of dry sediment versus depth. The distribution of the concentrations of these important species will be briefly described below. In general the total number of specimens of separate species follows closely the absolute abundance of total foraminifera.

N. pachyderma (sinistral) (Ehrenberg); Plate 1, figs. 1, 2, 3 and 4.

This species is by far the dominant planktic species found in PCM5 comprising over 95% of the planktic foraminiferal assemblage for the whole core. For this reason a separate plot of *N. pachyderma* (sinistral) has not been made. Its abundance is very similar to the total planktic foraminiferal abundance of fig. 6.2. This distribution has been described above, so will not be repeated here.

E. umbonatus (Reuss); Plate 1, figs. 10 and 11.

E. umbonatus is one of the most abundant benthic foraminiferal species in PCM5. The abundance variation of specimens of this species is shown in fig. 6.4. The abundance of this species is zero from the base of the core to 540cm.

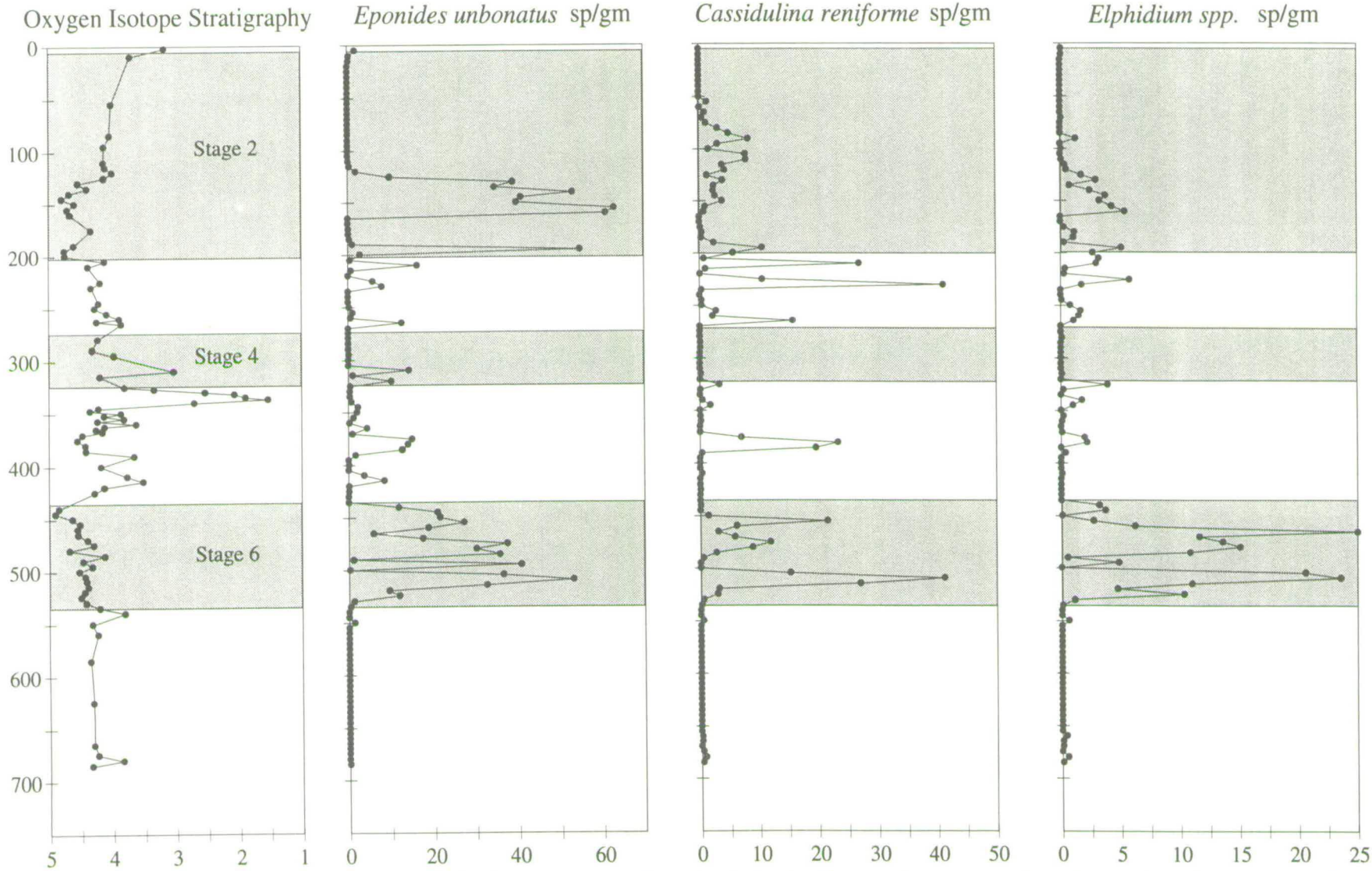

Fig. 6.4. Foraminiferal abundances for PCM5 all plotted against depth (cm). Oxygen isotope stratigraphy on the left, scale per mil variation w.r.t. PDB standard. Abundances of species expressed as no. specimens per gram dry wt. sediment.

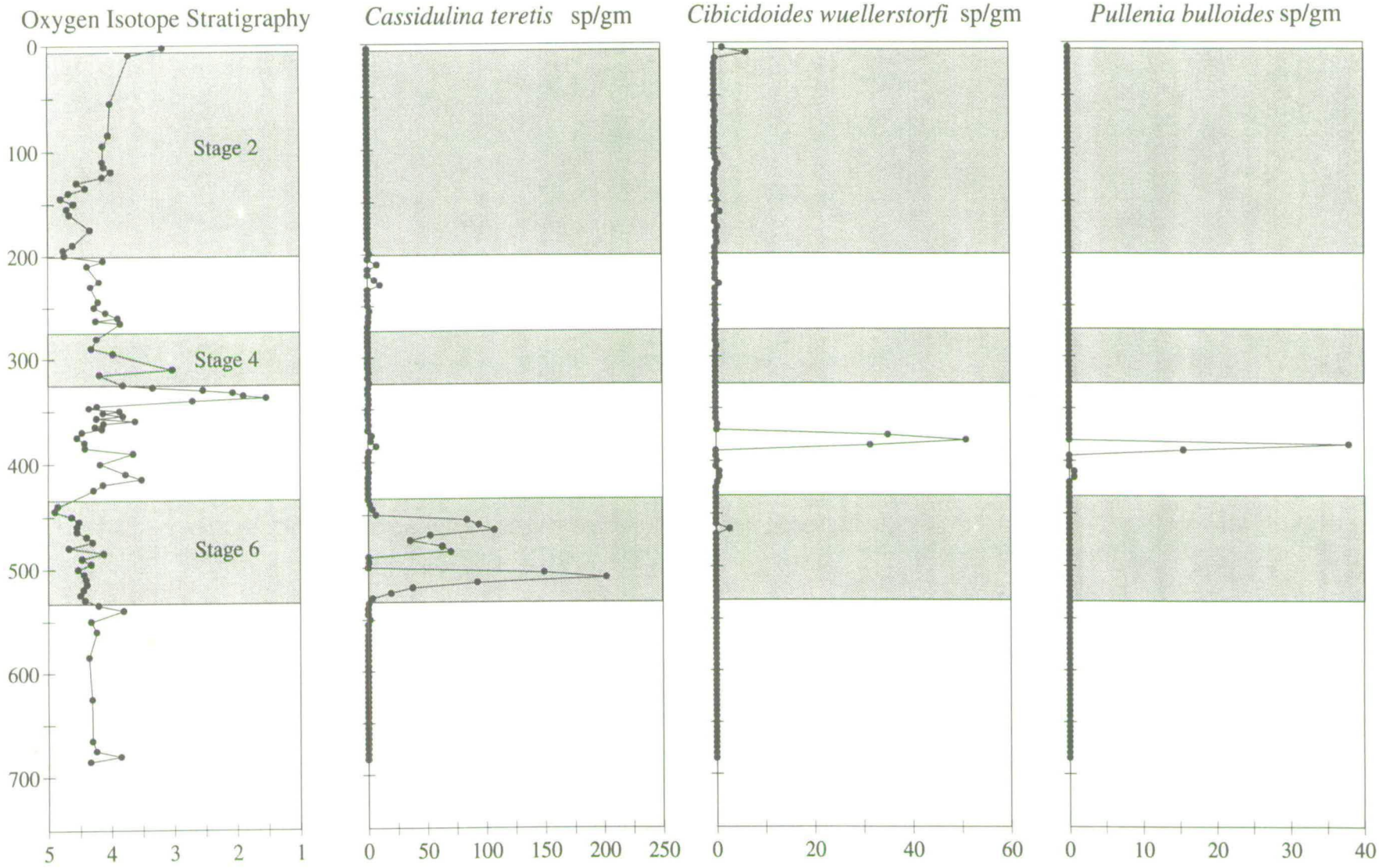

Fig. 6.5. Foraminiferal abundance counts for PCM5, all plotted against depth (cm). Oxygen isotope stratigraphy on the left, scale per mil variation w.r.t. PDB standard. Species abundances expressed as no. specimens per gram dry wt. sediment.

From 525 to 440cm the abundance is generally much higher, ranging from 10 to a peak of 53 sp/gm at 510cm. Two samples within this section, however, display abundance values of 0 sp/gm; these are at 500 and 490cm. The next section from 435 to 200cm is in general characterised by very low abundance values, close to zero, but with short spikes in abundance of approximately 10-20 sp/gm superimposed. These spikes are found at 415, 385-375, 320, 310, 265, 230 and 210cm. At 195cm, there is a much larger spike in abundance of *E. umbonatus* with a maximum of 55 sp/gm; values drop immediately to zero from 190 to 165cm. At this point, abundances rapidly increase again and remain at high levels of 40 to 60 sp/gm from 160 to 130cm. Then the abundance of this species drops to zero at the top of the core, though a very minor increase to 1 sp/gm is found in the top sample.

C. reniforme (Norvang); Plate 2, figs. 6 and 7.

C. reniforme also has relatively high abundances in PCM5 (fig. 6.4). The abundance of this species at the base of the core, similar to *E. umbonatus*, is zero from 685 to 530cm. Then values increase to 15-40 sp/gm from 515 to 505cm, but values rapidly drop to zero from 500 to 490cm and rise to between 5 and 20 sp/gm from 485 to 455cm. The abundance of this species drops to zero between 445 and 390cm, but rises to a short peak of 20 sp/gm from 385 to 380cm. The next section shows very low abundances at or close to zero from 370 to 270cm. After this, a series of isolated peaks in absolute numbers of *C. reniforme* can be seen, ranging from 10 to 40 sp/gm with backround values of zero. These peaks are at 265, 230, 210, and 195cm. Continuing upwards a section occurs with sustained but relatively low abundances of between 2 and 10 sp/gm from 150 to 80cm After this abundances drop to zero for the rest of the core.

Elphidium spp.; Plate 3, figs. 1, 2, 3 and 4.

Individual species of the genus *Elphidium* were not distinguished, but have been grouped together as *Elphidium spp.* (fig. 6.4). The pattern of absolute abundances of specimens of this group is very similar to the other species mentioned above, though absolute numbers are in general lower. The first major peak in abundance is found from 525 to 505cm with values of 10 to 20 sp/gm. A peak with similar values is found from 485 to 460. Values then remain below 5 sp/gm for the rest of the core. Minor peaks in abundance of between 2 and 5 sp/gm are found at the following depths; 380-375, 325, 225, 210-195, and 160-130cm. The abundance of *Elphidium spp.* is at or close to zero sp/gm for the rest of the core.

C. teretis (Tappan); Plates 2, figs. 2 and 3.
The absolute abundance of *C. teretis* specimens is very high in certain sections, but over much of core PCM5 this species is absent (fig. 6.5). The abundance of this species is zero from 685 to 535cm. Values rapidly from there rise to a peak of 150 to 200 sp/gm at 510-505cm. The concentration of this species drops to zero again but jumps to another peak of between 50 and 100 sp/gm from 485 to 455cm. Over the rest of the core, this species is virtually absent, with values below 2 sp/gm except for a minor increase to 10 sp/gm at 230 and 210cm.

Cibicidoides wuellerstorfi (Schwager); Plate 2, figs. 10 and 11.
C. wuellerstorfi specimens are very rare in sediments of PCM5 (fig. 6.5). A major peak is found at 385-375cm where the absolute abundance rises to between 30 and 50 sp/gm. Values then drop to below 1 sp/gm for the rest of the core except for one sample at 10cm where the numbers of this species increase to 6.5 sp/gm.

Pullenia. bulloides (d'Orbigny); Plate 2, figs. 8 and 9.
The absolute abundance of *P. bulloides* follows the same pattern as *C. wuellerstorfi,* and is shown in fig. 6.5 also. The abundance of this species is zero for the whole core except for a short lived spike at 390 to 385cm, where abundances of between 15 and 38 sp/gm are found.

6.4.2. PCM7

The records of foraminiferal variations from core PCM7 have similar characteristics to those of core PCM5. In general, the benthic and planktic records again match each other, though there are some definite exceptions. The absolute abundance of planktic foraminifera are again higher than those of benthic foraminifera, but not to the same extent as in PCM5: only 2 or 3 times higher. The records are also characterised by rapid fluctuations in abundance values for both groups. The planktic and benthic foraminiferal abundances and B:P ratio are shown in fig. 6.3.

The planktic foraminiferal abundance record
The planktic foraminiferal abundance values for PCM7 reach a peak of 1190sp/gm, but are generally much lower, below 100sp/gm. The base of the core is characterised by abundances of 0-20sp/gm from 727-550cm. There is a sharp rise in abundance to 260sp/gm at 540cm, and 150sp/gm from 530-525cm. Values then decrease rapidly to below 10sp/gm until 475cm, at which point they rise again to 15-30sp/gm until

400cm, there is a larger peak of 100sp/gm at 405cm. The next section is characterised by predominantly low values under 10sp/gm until 335 cm. There are two distinct peaks where abundances suddenly jump to 50-100sp/gm during this section at 375 and 345cm. At 330cm, abundances rapidly increase to just over 1000sp/gm from 325-320cm, but then decrease to 1sp/gm or below from 310-280cm. At this point, values suddenly increase to 1180sp/gm, the highest throughout the core, and remain at 400-800 sp/gm until 250cm. Abundances there drop rapidly to 1 or 2 sp/gm again until 165cm, where there is a gradual increase to approximately 10sp/gm. A further increase to 30-50 sp/gm occurs from 130-70cm. Values then drop to approximately 10sp/gm again until 30cm, from where they rise to average about 100sp/gm through the remainder of PCM7, and the trip core also. There is a slightly higher peak of 450sp/gm at 60cm within the trip core.

The benthic foraminiferal abundance record

In general the benthic foraminiferal abundances match the major peaks in planktic foraminiferal abundance, but there are sections where the two significantly differ. The benthic foraminiferal values are commonly 1/3 of the planktic foraminiferal values. The benthic foraminiferal values at the base of the core are initially relatively low, about 5sp/gm from 727-645cm. From there, they increase slightly to 10-20 sp/gm until 600cm, where they drop to almost 0 sp/gm. Values remain below 10 sp/gm, until a peak of 50-70 sp/gm is found from 540-525cm. This coincides with a peak in planktic foraminiferal abundance also. This peak is split by a trough, where no benthic foraminifera occur at all at 535cm. Values then gradually increase to 10-20 sp/gm from 470-430cm. The next section matches the planktic curve; generally low abundances with minor peaks superimposed at 405cm, 375cm, and 345cm of 30-60sp/gm. The major peak seen in the planktic foraminiferal abundance at 325cm can also be seen in the benthic foraminiferal abundances from 325-315cm with abundances reaching 150 sp/gm at 320cm. Benthic abundances fall rapidly below 1 sp/gm until 280cm, where the prolonged peak, seen in the planktic foraminiferal abundance, also occurs in the benthic one. A maximum peak of 360 sp/gm at 275cm gives way to values between 100-200 sp/gm until 245cm. There values drop to below 5 sp/gm until 165cm, where a major peak is found from 160-145cm with values reaching 139 sp/gm at 150cm. Values drop to a relatively stable backround level of 10-20 sp/gm until 10cm, where a sudden increase to values between 50-150 sp/gm is found. Abundances then drop back to the previous levels, or slightly higher, of 20-30 sp/gm throughout the trip core.

Benthic:Planktic Ratio

The generally higher benthic foraminiferal abundances relative to planktic foraminiferal abundances in PCM7 result in higher B:P ratios showing more fluctuations than in PCM5 (fig. 6.3). One important observation is that the B:P ratio in sections with high planktic foraminiferal abundance, 150sp/gm or more, is very low, 0.3-0.5. It is in sections where overall abundances are lower that benthic specimens become relatively more important, and thus B:P ratios increase to values greater than 1 (these sections are shaded in fig. 6.3). Initially the ratio is below 0.5, from the base of the core until 660cm, where the values increase as benthic specimens become more abundant relative to planktic specimens. Values reach 1 or greater from 620-550cm, but then drop below 0.5 until 520cm. The next section is characterised by rapid fluctuations with values between 0.5-2. A major peak in the B:P ratio is found from 300-315cm, with values ranging from 2-4. This is just after the major peak in planktic foraminiferal abundance. Values then drop to below 0.5 while total foraminiferal abundances remain high. In contrast values increase to between 1 and 3 over the next section where total abundances drop to very low values. This peak is less important as it reflects a drop in abundance to nearly 0 sp/gm in both planktic and benthic foraminiferal specimens rather than a relative increase in benthic foraminiferal abundance.

There is a much more significant increase in the B:P ratio to greater than 3, reaching a peak of 16 at 150cm. This represents a major peak in benthic foraminiferal abundance which is not represented in the planktic foraminiferal abundance record. Values drop to 0.3 or lower from 125-75cm, which is the result of an increase in planktic foraminiferal abundance and a slight decrease in benthic foraminiferal abundance. The B:P ratio increases significantly to 1-2 from 70-35cm due to a distinct drop in planktic foraminiferal abundance. The remainder of core PCM7 and the trip core are characterised by B:P ratio values of below 1, as planktic foraminiferal abundances increase to moderate values of 100sp/gm or more.

Absolute abundance variation of individual foraminiferal species

Absolute abundance counts of both planktic and benthic specimens of individual species have been made. The results are shown in figs. 6.6 to 6.9, expressed as number of specimens per gram of dry sediment versus depth. In general, all species follow the variations of planktic or benthic total abundances closely, but major departures from this trend will be outlined below.

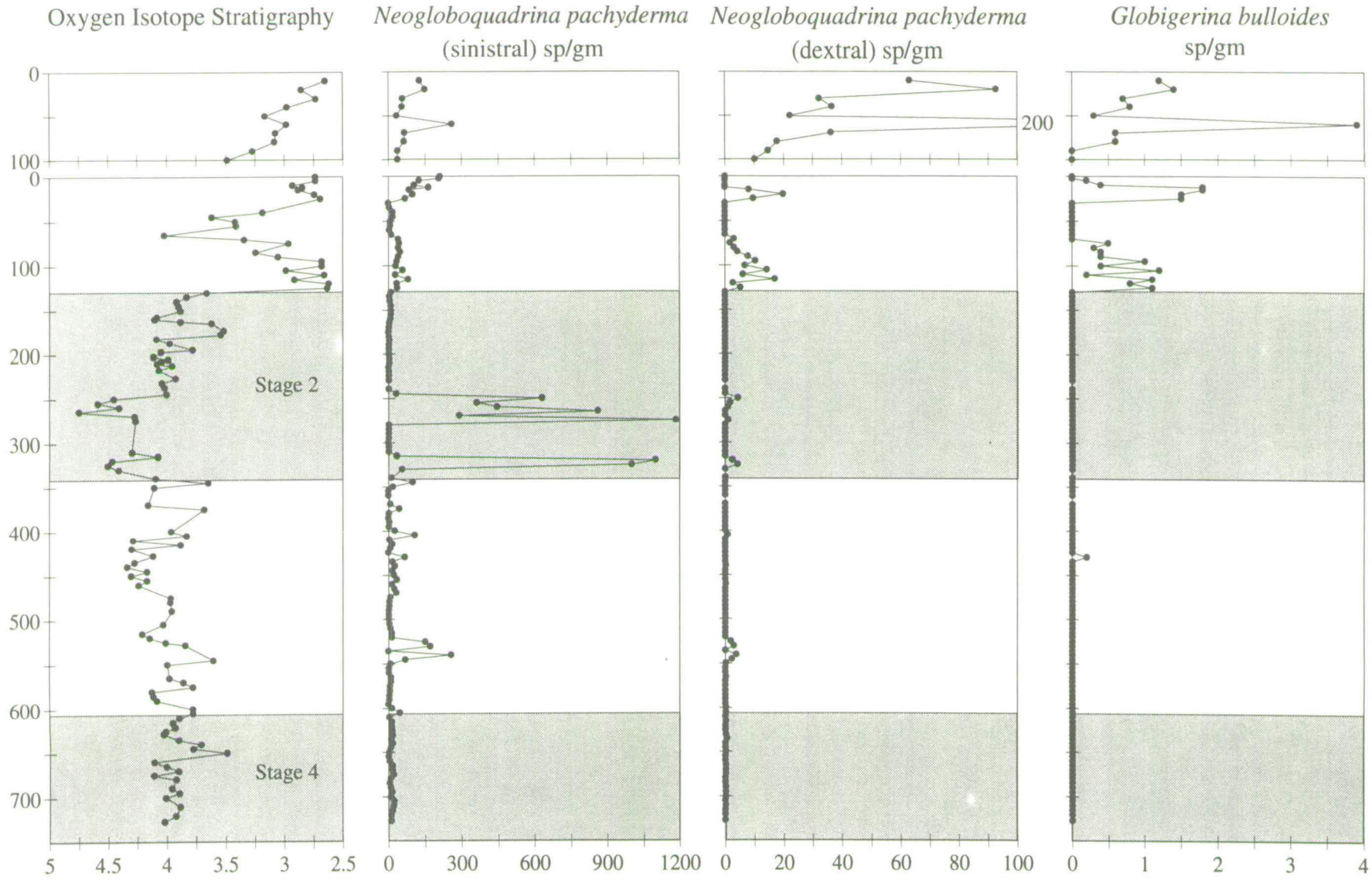

Fig. 6.6. Foraminiferal abundance counts for PCM7, all plotted against depth (cm). Oxygen isotope stratigraphy on the left, scale per mil w.r.t. PDB. Abundances of species expressed as no. specimens per gram dry wt. sediment.

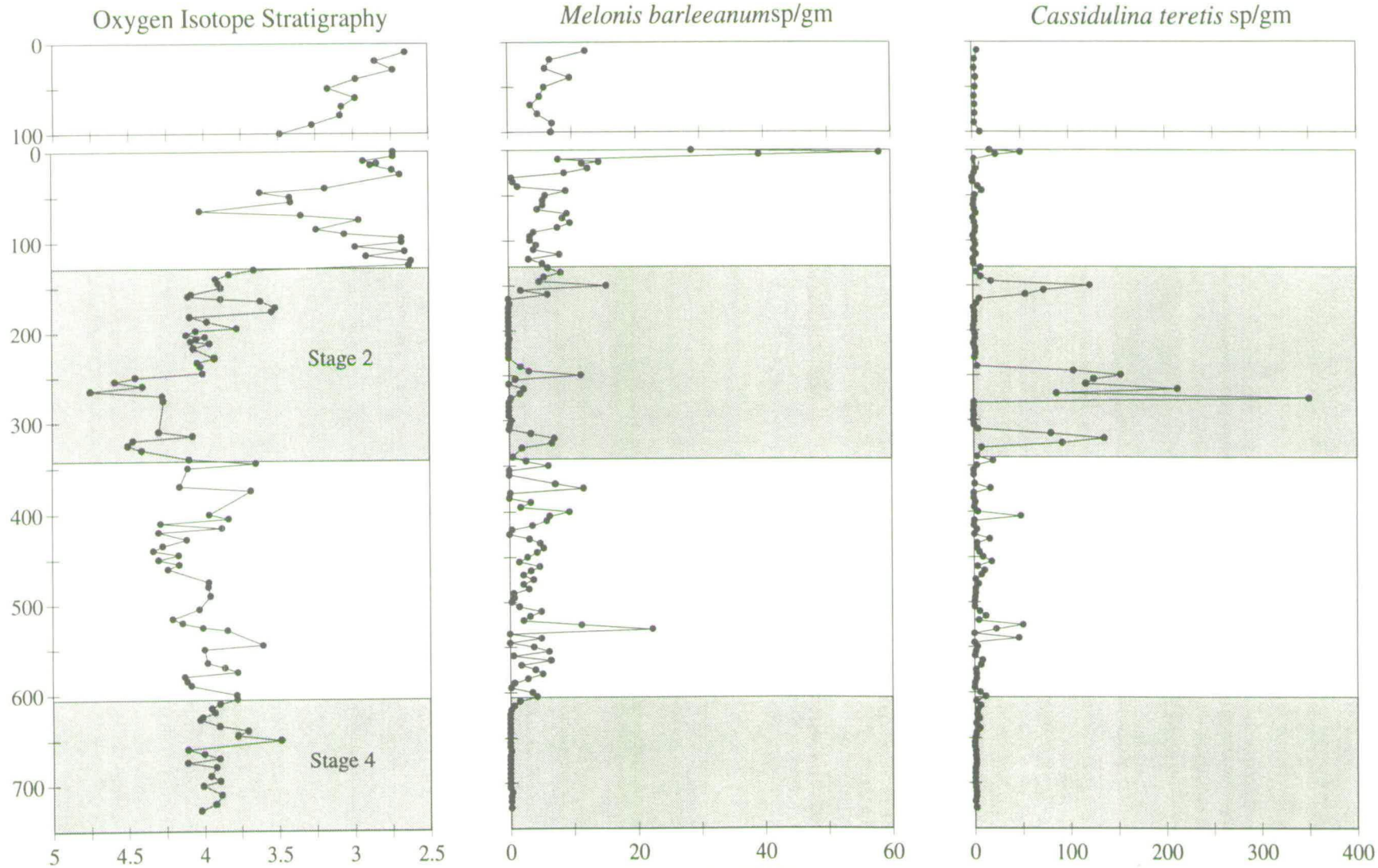

Fig. 6.7. Foraminiferal abundance counts for PCM7, all plotted against depth (cm). Oxygen isotope stratigraphy on the left, scale per mil variation w.r.t. PDB standard. Species counts expressed as no. specimens per gram dry wt. sediment.

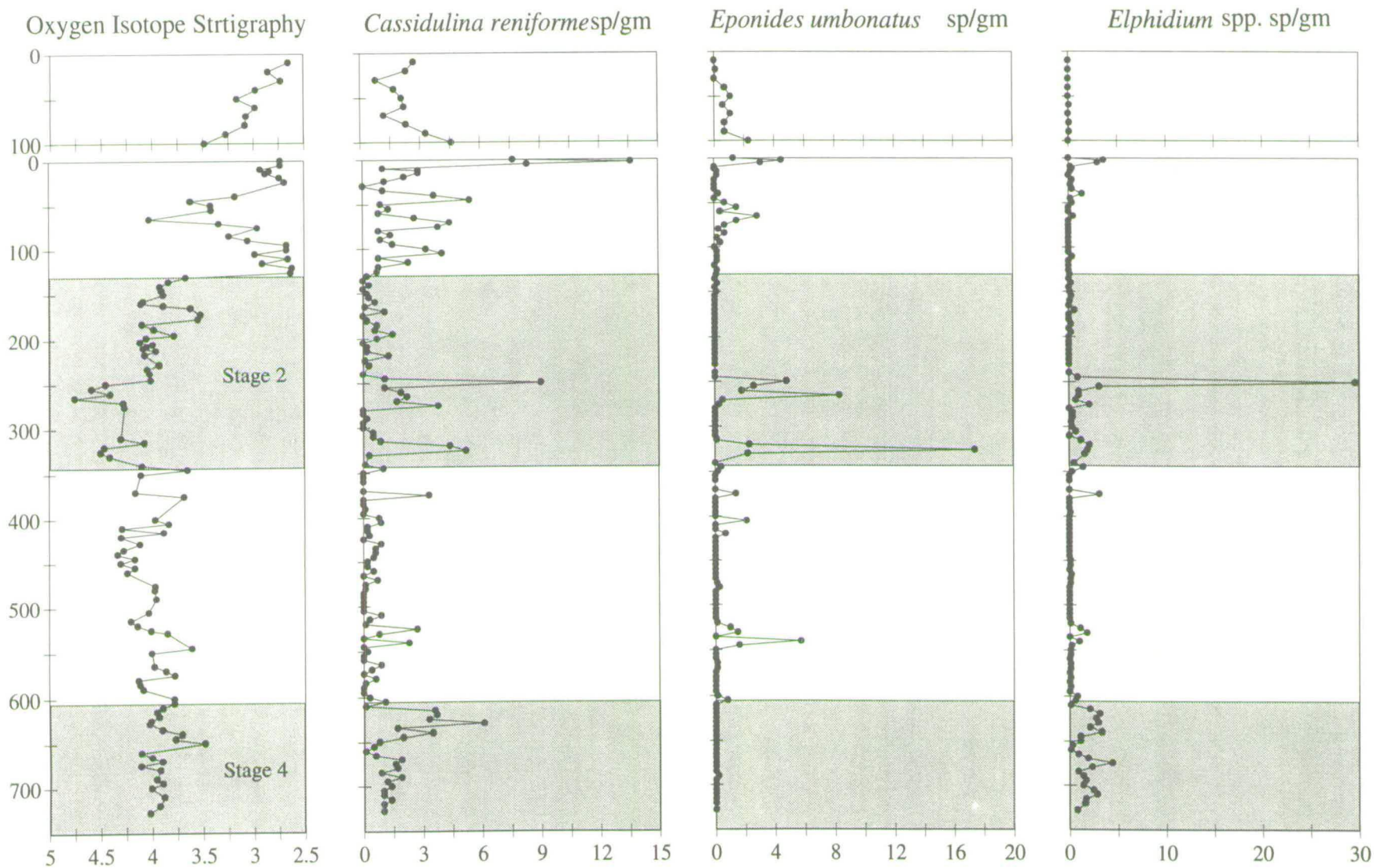

Fig. 6.8. Foraminiferal abundance counts from PCM7, all plotted against depth (cm). Oxygen isotope stratigraphy on the left, scale per mil variation w.r.t. PDB standard. Abundance of species expressed as no. specimens per gram dry wt. sediment.

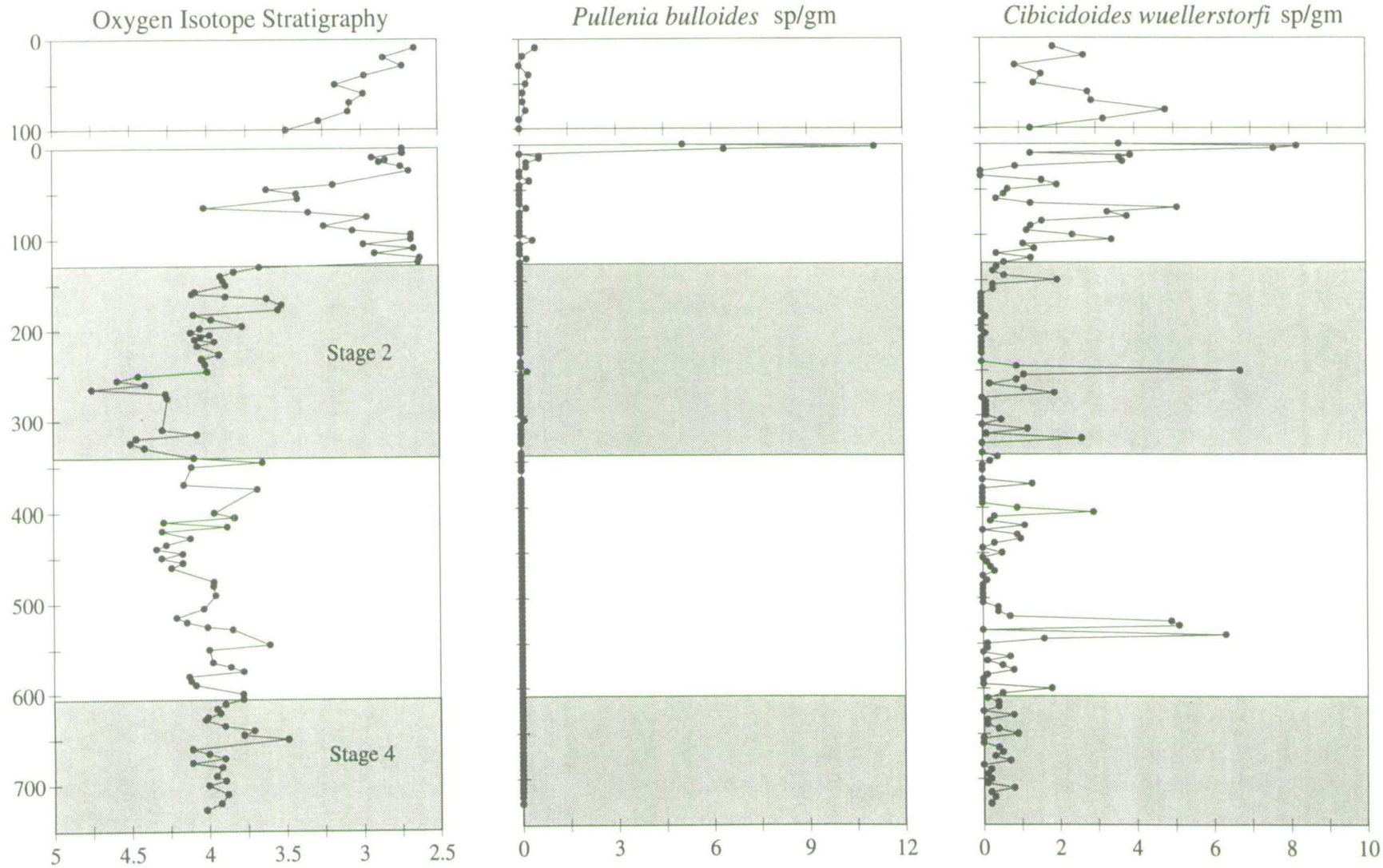

Fig. 6.9. Foraminiferal abundance counts for PCM7, plotted against depth (cm). Oxygen isotope stratigraphy on the left, scale per mil variation w.r.t. PDB standard. Benthic abundances expressed as no. specimens per gram dry wt. sediment.

N. pachyderma (sinistral); Plate 1, figs. 1, 2, 3 and 4.

This is by far the dominant planktic foraminiferal species, and commonly comprises 95 to 100% of the planktic foraminiferal assemblage. The total abundance of this species is shown in fig. 6.6. The *N. pachyderma* (sinistral) abundance follows closely the total abundance of all planktic foraminifera, but the only difference is that slightly lower values occur in the upper 130cm of the main core and the trip core. The variations of total planktic foraminiferal abundance have been described above thus will not be repeated.

N. pachyderma (dextral); Plate 1, figs. 5, 6 and 9.

The variation in *N. pachyderma* (dextral) abundance is shown in fig. 6.6, values are in general low, ranging from 0 to 200 sp/gm. Values are below 3 sp/gm from the base of the core until 130cm. From 125 to 70cm, the abundance of *N. pachyderma* (dextral) rises to between 5 and 20 sp/gm. Values drop to 0 sp/gm until 30cm, where they increase from 25 to 15cm to 10 to 20 sp/gm, but drop to 0 sp/gm again until the top of the main core. The trip core has a much higher abundance of this species, starting with values of 10 sp/gm, then rapidly increasing to 200 sp/gm at 60cm; after this values decrease to between 30 and 90 sp/gm until the top of the core.

Globigerina bulloides; Plate 1, figs. 7 and 8.

The abundance of this species is very low compared to the species of *Neogloboquadrina,* with values below 4 sp/gm throughout the core (fig. 6.6). There are no specimens of *G. bulloides* from the base of the core until 130cm, where values rise to between 0.5 and 1 sp/gm from 125 to 75cm, after this they drop to zero until 30cm. At this point, the abundance increases to 2 sp/gm from 25 to 12.5cm, then decrease slightly to 0.5 sp/gm for the rest of the main core. The trip core begins with low values, but values increase to between 0.5 and 4 sp/gm from 70cm until the top.

M. barleeanum (Williamson); Plate 2, fig. 1.

M. barleeanum is common throughout core PCM7 and the trip core with values ranging from 0 to 20 sp/gm, with a maximum peak of 60 sp/gm (fig. 6.7). Initially the abundance of *M. barleeanum* is zero from the base of the core until 615cm. The next section from 610 to 315cm has values of between 0 and 10 sp/gm and an average of 4-5 sp/gm. Within this section there is one spike in abundance of 20 sp/gm at 530cm. From 310 to 275cm abundance drops to zero, but from 270 to 240cm values rise to between 2 and 15 sp/gm before dropping to zero again until 165cm. From 160 to 45cm values range from 5 to 10 sp/gm, forming a stable plateau of values. There is a brief drop with values below 1 sp/gm until 30cm, where the abundance values

increases to 15 sp/gm from 25 to 10cm. From there it rises again to between 30 and 60 sp/gm until the top of the main core. The trip core is characterised by stable abundances of 5 to 10 sp/gm throughout.

C. teretis; Plate 2, figs. 2 and 3.

The abundance of *C. teretis* is greater than any other benthic foraminiferal species in PCM7 with a maximum peak of 350 sp/gm (fig. 6.7). The abundance of this species is very low initially, below 2 sp/gm from 727 until 545cm. Values increase to between 20 and 50 sp/gm from 540 to 525cm. From there values remain low with sporadic peaks in abundance until 330cm. In this section values are commonly below 5 sp/gm, but peaks of 15 to 40 sp/gm are found at 455, 430, and 405cm. From 325 to 315cm the abundance of this species increases dramatically to between 80 and 136 sp/gm, but at this level values drop to zero until 280cm. At this point, there is another major increase in abundance to 350 sp/gm at 275cm, values then drop slightly to an average of 120 sp/gm until 245cm. Abundances drop to below 2 sp/gm from 240 to 165cm. This is followed by a rise in abundance to between 50 to 120 sp/gm from 160 to 150cm, where values drop to below 5 sp/gm until 10cm. The top of the main core shows a minor increase in abundance to 20-50 sp/gm. The trip core shows low stable values below 10 sp/gm throughout.

E. umbonatus; Plate 1, figs. 10 and 11.

E. umbonatus has a generally low abundance in PCM7 with several short sections where abundance suddenly increases (fig. 6.8). This species has an abundance of close to zero from 727 to 550cm, where a minor peak occurs with values between 1 and 5 sp/gm from 545 to 525cm. Values remain below 1 sp/gm until 340cm, at which point there is a sudden increase to 18 sp/gm at 330cm. The abundance of *E. umbonatus* drops back to zero again from 320 to 270cm. Values rise to 3-10 sp/gm from 265 to 250cm, then drop to zero until 100cm. At this point, the abundance counts rise slightly to between 0 and 2 sp/gm until 50cm, drop to zero until 10cm, where they rise to 4 sp/gm for the upper 10cm of the main core. The trip core is characterised by abundances initially of 2 sp/gm at 100cm, but decrease gradually to 0 sp/gm by 30cm.

C. reniforme; Plate 2, figs. 6 and 7.

Absolute abundance variations of *C. reniforme* are similar to those of *E. umbonatus* (fig. 6.8). The base of the core is characterised by relatively high abundances of 1 to 5 sp/gm from 727 to 615cm. Values drop to below 1 sp/gm until 545cm, where there is a brief section with abundances of 1 to 2 sp/gm from 540 to 525cm. The abundance

of *C. reniforme* remains below 1 sp/gm until 335cm, except for one sample at 375cm with an abundance of 4 sp/gm. Values rise to 6 sp/gm from 320 to 325cm, then drop to below 1 sp/gm until 280cm. From there they increase to between 2 and 9 sp/gm from 275 to 245cm. A long section from 240 to 130cm is characterised by abundances of *C. reniforme* of below 1 sp/gm . At 130cm, there is a distinct rise in abundance, fluctuating between 1 and 6 sp/gm until the top of the main core. The final 10cm of the core is characterised by abundances of approximately 10 sp/gm. The trip core has a generally higher abundance of between 2 and 5 sp/gm throughout.

Elphidium spp; Plate 3, figs. 1, 2, 3 and 4.

Specimens of different species of *Elphidium* were not subdivided, but have been counted together. Specimens of *Elphidium spp.* are relatively rare total specimen abundance is shown in fig. 6.8. The base of the core is characterised by values between 1 and 4.5 sp/gm from 727 to 600cm. There is then a section with no specimens of *Elphidium spp.* until 545cm; values increase to 1-2 sp/gm from 540 to 525cm, then drop to zero again until 380cm. At 375cm, there is a minor increase to 3 sp/gm before returning to zero. From 345 to 315cm values increase to between 1 and 2 sp/gm, then drop back to zero but rise to between 1 and 2 sp/gm from275 to 255cm. A major peak in abundances of 26 sp/gm occurs at 250cm. After this, the abundance of *Elphidium spp.* decreases to zero until 10cm, from where values rise to 3 sp/gm from 5 to 2.5cm. The trip core has no specimens of *Elphidium spp.* throughout its length.

C. wuellerstorfi; Plate 2, figs. 10 and 11.

The absolute abundance of *C. wuellerstorfi* in PCM7 (fig. 6.9) is variable ranging from 0 to 9 sp/gm. The abundance of this species at the base of the core low; below 1 sp/gm until 550cm, values then rise to between 4 and 6 sp/gm from 540-525cm. Absolute abundance values drop to below 1 sp/gm again until 245cm, although two samples with 2 sp/gm are found at 405 and 325cm. At 250cm, there is an isolated peak in abundance of 6.7 sp/gm before dropping to 0 sp/gm until 160cm. At this point, the abundances increase but remain below 1 sp/gm. They rise to between 1 and 5 sp/gm from 125 to 65cm. Then from 60-25cm, abundances drop to approximately 1 sp/gm before rising to between 2 and 8 sp/gm from 20cm until the top of the main core, and for the whole of the trip core.

P. bulloides; Plate 2, figs. 8 and 9.

This species is rare in PCM7, only being present in several samples at the top of the main core (fig. 6.9). It is present in samples at 5, 2.5 and 0cm in the main core with

abundances of 6-11 sp/gm, and in no other samples throughout the main core and the trip core.

6.5. The significance of absolute abundance variations of planktic and benthic foraminifera for the productivity of high latitude seas over the last 200 ka

There are several factors which could lead to variations in concentration of foraminiferal tests encountered in samples. These include changes in surface water productivity, sedimentation rates, current winnowing and carbonate dissolution.

At first sight, it may appear that the rapid foraminiferal abundance changes, seen in cores PCM5 and PCM7, are due to dilution effects. This is not the case however, the foraminiferal fluctuations almost certainly reflect productivity changes along the Spitsbergen margin. As mentioned in chapter 2, sedimentation rates are generally higher during glacial periods, stages 2, 6 and substage 5b. These are the periods that coincide with the intervals of increased foraminiferal abundances (figs. 6.2 and 6.3). Also, the rapidity of change is exceptional. For example in core PCM5 (fig. 6.2) foraminiferal abundances drop from 4500 sp/gm at 505cm to below 10 sp/gm at 500cm. PCM7 shows similar fluctuations for example from 0 sp/gm at 280cm to 1100 sp/gm at 275cm, see fig. 6.3. It seems unlikely that such dramatic shifts in abundance could be accommodated by sedimentation rate fluctuations alone. Comparison of the foraminiferal abundances with dropstone counts from chapter 3 support this also. Periods with high dropstone counts reflect periods of intense ice calving and melting; summer melting of an ice mass at the edge of the continental shelf during glacial periods (see chapter 3 for more detail). These periods are therefore characterised by enhanced sedimentation rates. Fig. 3.5 shows the sections with high foraminiferal abundances from 450-550cm correlating with sections of high dropstone numbers for PCM5, the peak in foraminiferal abundance at 380cm also correlates with high dropstone counts.

Winnowing would be expected to increase the abundance of foraminifera by removing fine grained clay particles. Sections within PCM7 that have been interpreted as being influenced by winnowing (due to the increased concentration of the coarser than 63μm fraction in some sections with no corresponding increase in dropstone numbers, see chapter 3) do not correlate with high foraminiferal abundances. Certain sections between 450-650cm (fig. 3.4) have high concentrations of the fraction coarser than 63μm, but these sections do not correlate with significant peaks in foraminiferal

abundance. So foraminiferal abundances are not influenced to a great extent by winnowing processes. Sedimentation rates and winnowing may have some influence on abundance values but productivity seems to be the driving force in foraminiferal abundance variations.

Productivity of the oceans in general is linked to solar radiation and nutrient supply in surface waters. In low latitudes, where sunlight is not a limiting factor, nutrient supply becomes limiting. Carbon, hydrogen, oxygen, nitrogen and phosphorous are needed for organic production. Carbon, hydrogen and oxygen are in abundant supply in the oceans, so it is nitrates and phosphates that are the limiting factors. Nutrients are removed from surface waters by sinking of organic material to greater depths. Nutrients are generally higher in deep waters which collect the 'rain' of organic material from the photic zone. Upwelling of these nutrient-rich deep waters may return nutrients to surface waters resulting in productivity blooms. Upwelling commonly occurs at continental margins where winds drive surface currents offshore, to be replaced by upwelling nutrient rich deep waters, for example the Peru coast. Upwelling is also found where surface currents diverge, for example at the equator.

Productivity in high latitudes is limited by solar radiation during winter months. When sunlight is absent primary productivity in high latitude areas is nil. During summer months, when sunlight is available, other factors become limiting. During exceptionally cold periods permanent pack ice may form, i.e. during glacial periods. If thick enough, this will prevent solar radiation reaching surface waters and reduce productivity to virtually nil. Smith *et al.* (1987) studied the phytoplankton biomass and productivity at the margins of sea ice in the Fram Strait. Productivity was at a peak at and just beyond the edge of the sea ice, decreased rapidly under the ice with distance from the edge of the ice, and decreased away from the ice margin in open water areas. Mixing of surface waters with nutrient rich deep waters is prevented by a stable depth stratification produced by low salinity surface waters due to melting ice. Another supply of nutrients is therefore necessary.

Input of terrestrial detritus to surface waters acts as an alternative source of nutrients. This may occur through river transport, aolian transport, or in high latitude areas through the process of ice rafting. Continental ice masses erode large volumes of sediment or rock which is then transported within the ice. During major ice expansion ice tongues often advance beyond the landmass onto the continental shelf. In some instances ice may advance to the shelf edge. Eventually calving will take place and icebergs rich in terrestrial material will be produced. Icebergs and sea ice commonly

have concentrations of nutrients such as nitrate, ammonia and silicates an order of magnitude higher than ambient sea water (Jacobs *et al.*, 1979). On melting, this material is released causing an increase in nutrient levels in surface waters resulting in increased productivity. This mechanism was suggested by Sancetta (1992) to explain high primary productivity in glacial North Atlantic sediments rich in ice rafted detritus. Icebergs may also increase productivity by causing turbulence and increased mixing, large ones may cause upwelling due to melting (Sancetta, 1992). Sea ice can also have a marked effect on productivity levels. The high productivity at the sea ice margin recorded by Smith *et al.* (1987), is produced partially by release of nutrients concentrated in the sea ice by aolian transport and partially by ice edge upwelling.

As mentioned earlier, it is assumed that changes in foraminiferal abundances in PCM5 and PCM7 are produced by fluctuations in surface water productivity. If planktic productivity is high, then benthic productivity tends to be high also, because of the rain of organic material from the plankton blooms reaching the sea floor. These planktic blooms may not necessarily be planktic foraminifera, other planktic organisms such as diatoms, coccoliths or dinoflagellates may cause blooms. So benthic foraminiferal abundances need not always coincide with planktic foraminiferal abundances.

As mentioned earlier the absolute abundances of foraminifera in both PCM5 and PCM7 are highest within the glacial periods, especially stages 2, 6 and substage 5b (figs. 6.2 and 6.3). Abundances during stages 3, 4 and most of stage 5 were very low, intermediate abundances were encountered within stage 1 from PCM7. These high glacial abundances are the exact opposite of foraminiferal abundances observed elsewhere in the Norwegian-Greenland Sea and Arctic Ocean as recorded by Sejrup *et al.* (1984), Kellogg (1973) and Belyaeva and Khusid (1990), but agree with the results of Elverhoi *et al.* (1993). High foraminiferal abundances are assumed to be due to higher surface water productivity during glacial periods.

Past studies have assumed that during peak glacial periods the Greenland Sea, and the majority of the Norwegian Sea were covered by year round permanent pack ice. These assumptions were based on low foraminiferal abundances during glacial periods, and resulting temperature estimates from transfer functions (Kellogg, 1980, McIntyre *et al.*, 1976). Data from this study suggests that the Spitbergen margin was in fact seasonally ice free during peak glacial periods, agreeing with Elverhoi *et al.* (1993).

The high abundances during stages 2, 6 and 5b also coincide with periods of intense dropstone content, see chapter 3. These dropstone concentrations have been interpreted as being produced by calving and summer melting of extensive ice tongues at the shelf edge during glacial periods. The high foraminiferal abundances are produced by productivity blooms. Such blooms in surface water productivity are produced by an increase in nutrients supply. The source of these nutrients must be melting icebergs and sea ice, and ice edge upwelling as mentioned earlier. So during the glacial periods of stages 2, 6 and also substage 5b there must have been extensive areas free from pack ice along the Spitsbergen margin, but also close to an ice margin supplying nutrients.

There is evidence to suggest that during certain periods within glacials permanent pack ice was present. During stage 6 there are two periods when foraminiferal abundances drop from 1000sp/gm or more to below 10sp/gm; once from 505cm to 500cm, then again at 445cm. These periods coincide with peak $\delta^{18}O$ values, and also periods when IRD disappears, see figs. 3.9 and 3.10. A permanent pack ice cover during these peak glacial periods explains the lack of foraminifera, thick ice cover preventing sunlight reaching surface waters, thus reducing productivity levels. Pack ice would also reduce the input of IRD by locking up icebergs, and due to lower melting rates because of intense cold surface water temperatures. This idea has already been mentioned in the model of ice rafting in chapter 3.

6.6. The timing and intensity of North Atlantic Surface Water influx into the Fram Strait from planktic foraminiferal evidence

From accurate species counts it is possible to identify periods of Atlantic surface water flowing into the area. Carstens and Wefer (1992) studied the recent planktic foraminiferal assemblages in the Arctic Ocean. They recognised two main zones, a northern zone (polar waters) characterised by *N. pachyderma* (sinistral), and a southern zone (subpolar waters) characterised by *N. pachyderma* (dextral), and *G. quinqueloba*. The northern zone was under the influence of cold Polar surface waters while the southern zone recorded the influx of warmer, more saline, North Atlantic waters into the Arctic Ocean. The subpolar species are common in North Atlantic surface waters entering the Norwegian-Greenland Sea. The proportion of right coiling forms compared to left coiling forms is a useful indicator of the presence of Atlantic water in such high latitude areas. Keigwin and Jones (1992) used the percentage abundance of left and right coiling varieties of *N. pachyderma* in the TROLL 3.1 core

from the southern coast of Norway. The last glacial period (oxygen isotope stage 2) was characterised by near 100% left coiling *N. pachyderma*, but periods were recognised when the dextral coiling variety almost totally replaced the sinistral variety. These periods were interpreted as marking the influx of Atlantic surface waters into the Norwegian Sea after the last glaciation.

From the results of PCM7 and PCM5 certain periods can be identified when North Atlantic waters entered the area. These periods are recognised by the presence of *N. pachyderma* (dextral) and by the presence of minor abundances of *G. bulloides*. PCM5 has such low numbers of *N. pachyderma* (dextral) that they have not been plotted. The planktic foraminiferal assemblage of PCM5 is always dominated by the sinistral variety, very close to 100%. There are rare occurrences of the dextral variety, but in any population of *N. pachyderma* from Polar waters there are always some specimens of *N. pachyderma* (dextral), and similarly in any population of *N. pachyderma* (dextral) from Subpolar waters there are always some specimens of the sinistral variety. This concept has been studied in more detail by Brummer and Kroon (1988). Although *N. pachyderma* was not investigated in their study, the basic principles are the same for all species. The abundance of *N. pachyderma* (dextral) never rises above 2-3% in PCM5. This suggests that PCM5 records no major influx of Atlantic water. The percentage of *N. pachyderma* (dextral) and of *G. bulloides* are shown in fig. 6.10 for the period 8 to 26 ka from PCM7. Also plotted in this figure is the $\delta^{18}O$ record from planktic foraminifera for this period from PCM7. This clearly shows the periods when North Atlantic waters first entered the area after the last glacial period (oxygen isotope stage 2). These periods are shaded in the diagram. The first time North Atlantic waters reached 78°N along the western margin of Spitsbergen after the last glaciation was at approximately 12.5ka. This correlates with the major oxygen isotope shift produced by meltwater and temperature changes (see chapter 4). These northward flowing Atlantic waters were then replaced by Polar surface waters again at 12ka; the foraminiferal assemblage dominated by *N. pachyderma* (dextral) and *G. bulloides* was replaced by the *N. pachyderma* (sinistral) assemblage. Atlantic waters re-appeared in the area from 10.5-10.3ka, but were replaced by Polar waters between approximately 10.3 and 10ka. From then on Atlantic waters were present until recent times according to the planktic foraminiferal record of PCM7.

These ages for the influx of Atlantic waters into the Norwegian-Greenland Sea do not agree with those produced from the TROLL 3.1 core (Lehman and Keigwin, 1992), who proposed Atlantic water entered the area at 13.6ka.

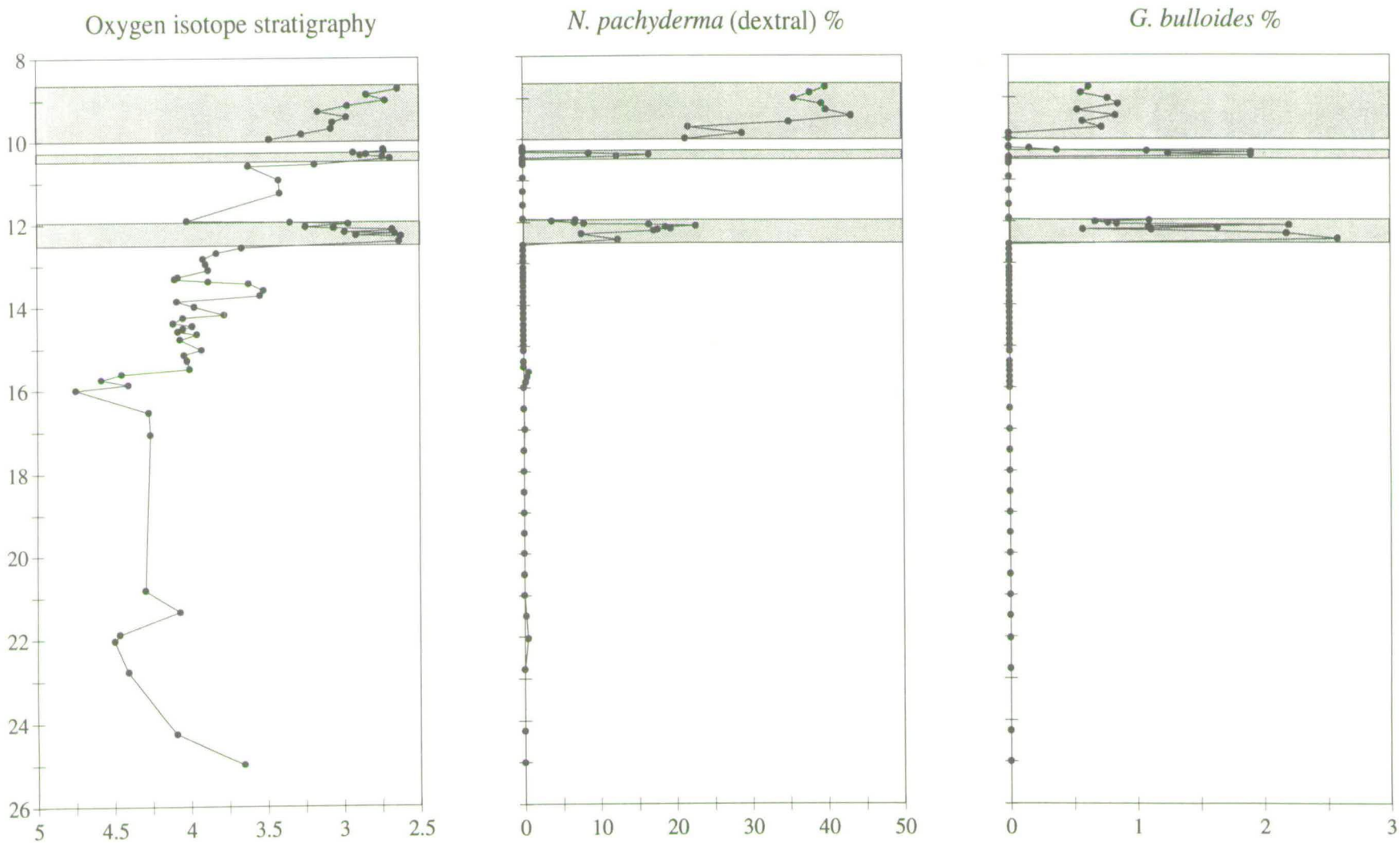

Fig. 6.10. Oxygen isotope stratigraphy for PCM7 shown on the left, plotted against age for the period 8 to 26 ka. Horizontal scale per mil variation w.r.t. PDB standard. The curves on the right show the percentage abundance of two species of planktic foraminifera dominant in North Atlantic water. The shaded sections represent periods when North Atlantic surface waters were present on the west Spitsbergen margin.

They do, however, corroborate the mollusc evidence of Mangerud (1977) from a terrestrial section on the western coast of Spitsbergen. They suggest that North Atlantic waters entered the Norwegian-Greenland Sea approximately 12.6ka, long before 10ka as suggested by Sejrup *et al.* (1984).

It is also possible to make a qualitative statement about the relative strength of the North Atlantic current reaching the study area at this time. Further south, the TROLL 3.1 core records a variation from near 100% sinistral variety to near 100% dextral variety, when Atlantic waters first entered the Norwegian Sea. At this southerly position the current is strong, and little mixing with Polar waters has occurred. As the current flows further north it weakens and becomes increasingly mixed with colder Polar waters. This is seen in the reduction of the dextral variety of *N. pachyderma* in PCM7, initially only 10 to 20%. The top of PCM7 records a higher percentage of *N. pachyderma* (dextral), 35 to 40%, suggesting the current is more influential during this later period from 10ka onwards. This would suggest that the $\delta^{18}O$ record for this section is influenced more by temperature change than during the earlier invasion of Atlantic waters at 12.3ka. Atlantic waters actually entered the Norwegian-Greenland Sea earlier than recorded in PCM7 (Lehman and Keigwin, 1992). This initial invasion must have been too weak to bring a great proportion of Atlantic surface waters near the Spitsbergen margin.

The record of PCM5 covers the time period from approximately 200 to 13ka. This core therefore records faunal changes within oxygen isotope stage 5, and more importantly substage 5e, the last interglacial or the Eemian. The planktic foraminiferal fauna for the whole of PCM5 is characterised by very high percentages of *N. pachyderma* (sinistral), 95 to 100%. This suggests that at no time during the period 200 to 13ka Atlantic surface waters reached the northerly latitudes of the Spitbergen margin at 78°N. This result is surprising as substage 5e is thought to have been slightly warmer than the present, and coccolith and diatom evidence suggest that Atlantic waters did reach the Spitsbergen margin (Miller *et al.*, 1989; LIGA Members, 1991; Mangerud and Svendsen, 1992). The absolute abundances of planktic foraminifera during stage 5 were very low, except for the stadial substage 5b (fig. 6.2). One possible explanation is that carbonate dissolution was higher during substage 5e, and the majority of foraminifera were dissolved. Though it is more likely that the planktic foraminiferal productivity was very low during this period, thus there is no foraminiferal record of substage 5e in the cores studied (see also stable oxygen isotope record of PCM5).

6.7. The significance of relative variations in benthic and planktic foraminiferal abundances

The two cores, from which faunal analysis has been made, are relatively close together geographically on the Spitsbergen margin, at 78°N on the continental slope (fig. 3.17) but they are from different depths. Core PCM5 comes from a deeper site, 2139m, while PCM7 was cored from 1073m of water. This difference in water depth has a major influence on the composition of benthic foraminiferal assemblage present (see below), and on the absolute abundance of benthic foraminifera. This is expressed in the B:P ratios from the two cores (figs. 6.2 and 6.3) because the dilution by the absolute abundance of planktic foraminifera is the same in the two cores. In general when the total foraminiferal abundances are relatively high, above 50 sp/gm, the B:P ratio is very low. Locally the B:P ratio rises to greater than 1, even as high as 12 at 90cm. These high values always coincide with periods of very low foraminiferal abundance, usually below 10 sp/gm. With such low abundances the B:P ratio becomes very unreliable.

The B:P ratio for PCM7 is lower than for PCM5, this is due to the greater benthic foraminiferal absolute abundances in PCM7. This is expected as benthic foraminifera become more abundant in shallower water compared to planktic ones. The reason for this is that organic material on the ocean floor tends to be higher near a terrstrial source, and is, therefore higher in shallower waters. The B:P ratio is commonly used as a relative water depth indicator, higher in shallower water.

The upper section of PCM7 shows interesting trends in B:P ratio, from 160cm to 0cm in the main core. These trends are caused by changes in the planktic foraminiferal absolute abundances rather than changes in benthic foraminiferal absolute abundances, which are relatively stable. The periods when planktic foraminifera become rare are most likely produced by influxes of meltwater, in which the planktic foraminifera cannot live. The meltwater influxes do not affect the benthics as much, their food supply continues, either from phytoplankton rain, terrestrial material carried in the meltwater, or nutrients from the melting ice.

6.8. Benthic foraminifera as indicators of organic carbon supply and palaeocirculation changes

The benthic foraminiferal species shown in figs. 6.4 to 6.9 are the most dominant species from PCM5 and PCM7, and the ones that have the most palaeoecological or paleoceanographic significance. Other species were recognised but they occur only in very small numbers and are not mentioned in the following discussion, but are listed in Appendix 2. A distinct difference in the composition of the fauna can be recognised between the two cores The cause of these changes is uncertain as mentioned in the introduction. Changes in organic carbon supply seem to play a role in the control of faunal distribution (Corliss and Chen, 1988) possibly in combination with hydrostatic pressure differences. Physical parameters are of minor importance, since water mass characteristics are very stable in the Greenland Sea below 300 or 400m (Belanger and Streeter, 1980); where temperature is about -1°C, and salinity is about 34.9‰.

Certain benthic foraminifera have particular microhabitats, some live on, or above the sediment water interface, and are termed epifaunal, while some live within the sediment, termed infaunal. Corliss and Chen (1988) suggested that the relative proportion of specimens living either infaunally or epifaunally may be useful in palaeoceanographic interpretation (see section on previous research). For this reason the proportion of epifaunal versus infaunal specimens has been calculated for cores PCM5 and PCM7 (figs. 6.11 to 6.13). Shifts in the epifaunal to infaunal proportion may reflect changes in deep water circulation. This study can also be used to test the hypothesis that differences can be observed between the microhabitat of the benthic foraminiferal faunal at different water depths (as suggested by Corliss and Chen, 1988). The epifaunal species recognised in this study are *E. umbonatus*, *C. wuellerstorfi* and *Elphidium spp.* The other main species recpgnised in this study are considered infaunal, these are *C. teretis*, *C. reniforme*, *M. barleeanum* and *P. bulloides*.

The number of epifaunal and infaunal specimens and their ratio for PCM7 and PCM5, (figs. 6.11 to 6.13) show some of the major changes in foraminiferal faunal composition over time, and at different depths. The results from this study show that in general the ratio of epifaunal:infaunal specimens is greater for PCM5, the deeper core, than in core PCM7.

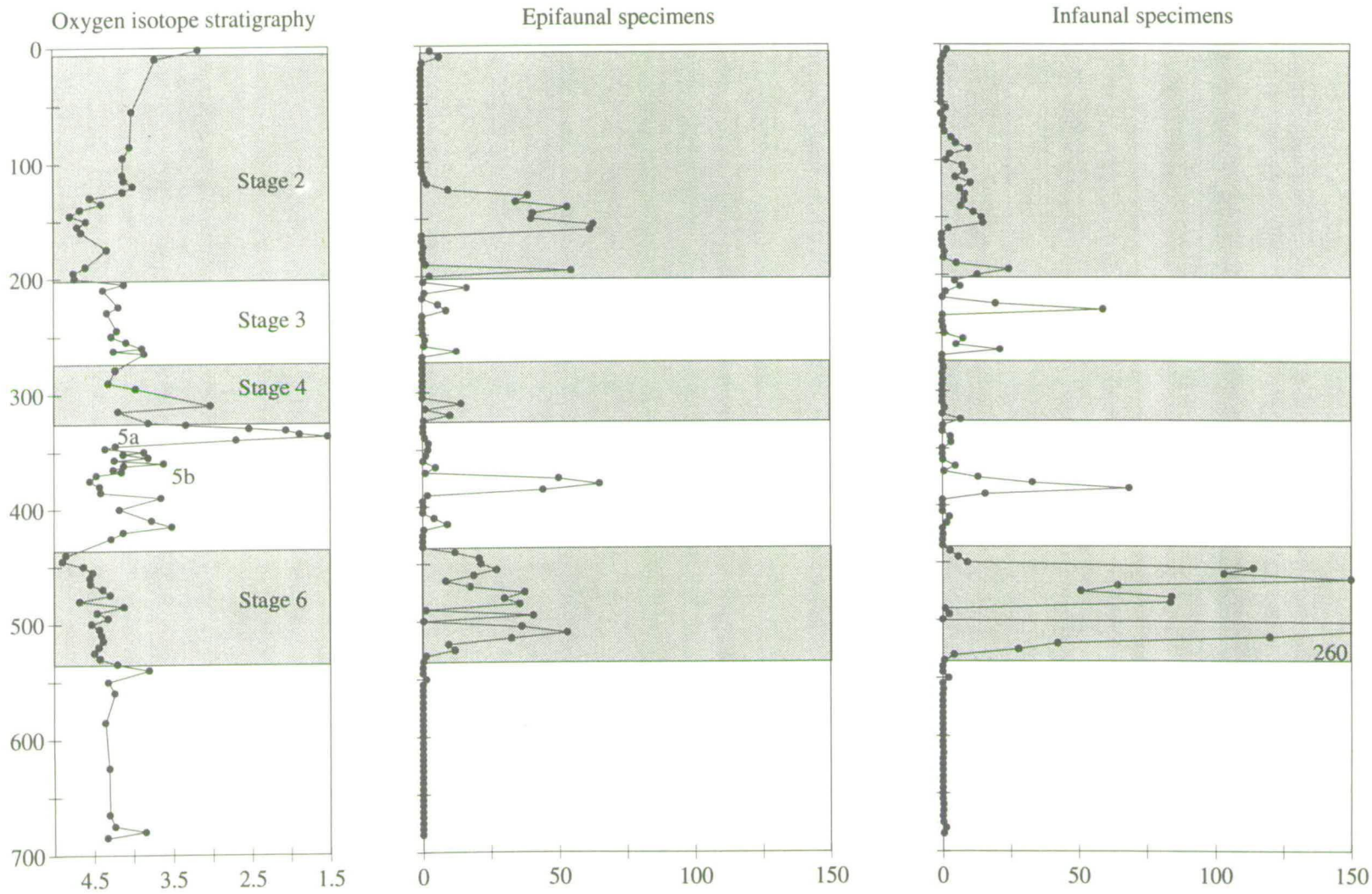

Fig. 6.11. Graph showing number of epifaunal and infaunal specimens found in PCM5, plotted against depth. The horizontal scale is in specimens per gram. The oxygen isotope stratigraphy is shown on the left for reference, isotope stages are shown on this plot.

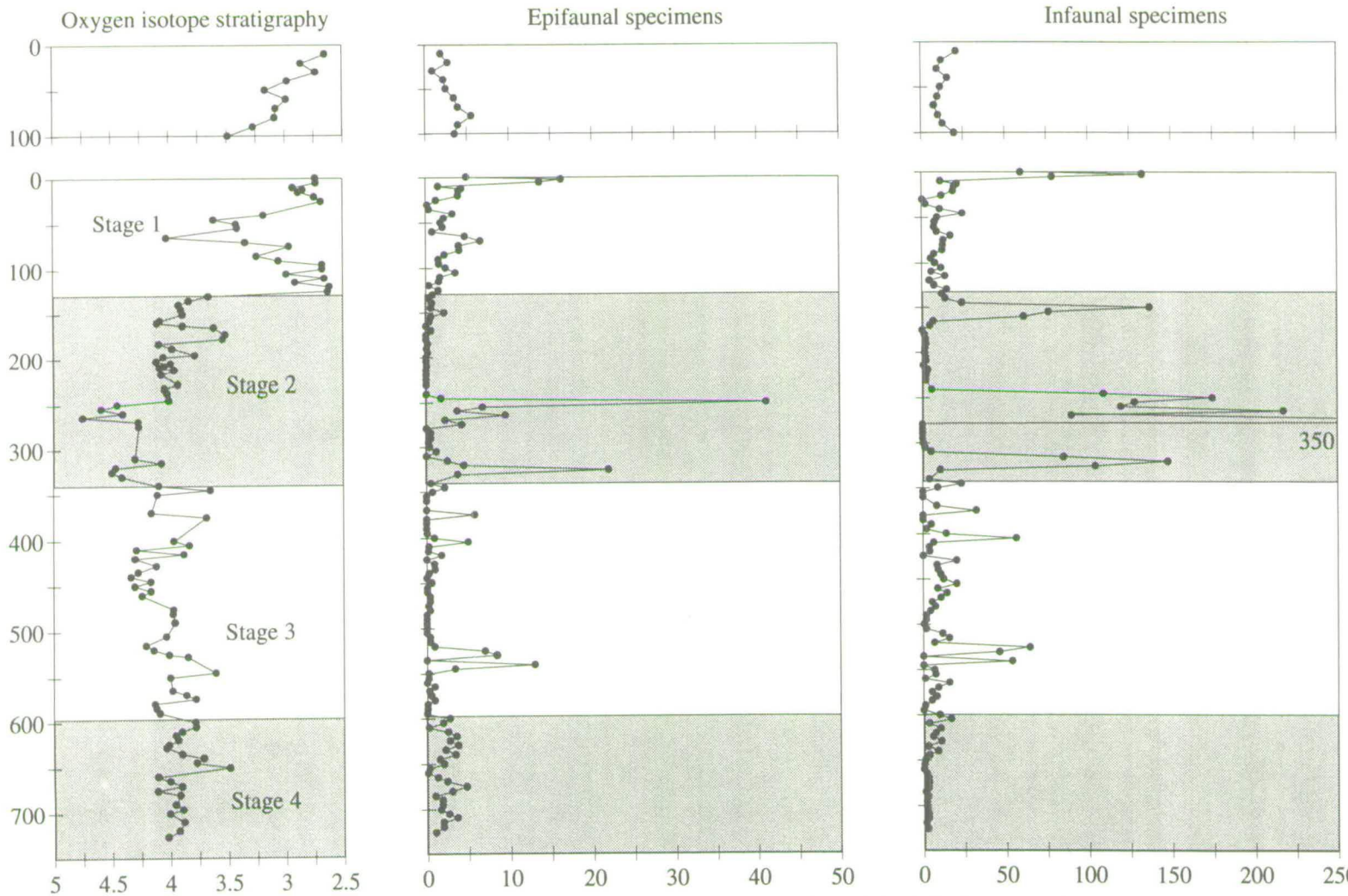

Fig. 6.12. Graph showing number of epifaunal and infaunal specimens found in PCM7, plotted against depth. The horizontal scale is in specimens per gram of dry sediment. The oxygen isotope stratigraphy is shown on the left for reference, isotope stages are labelled.

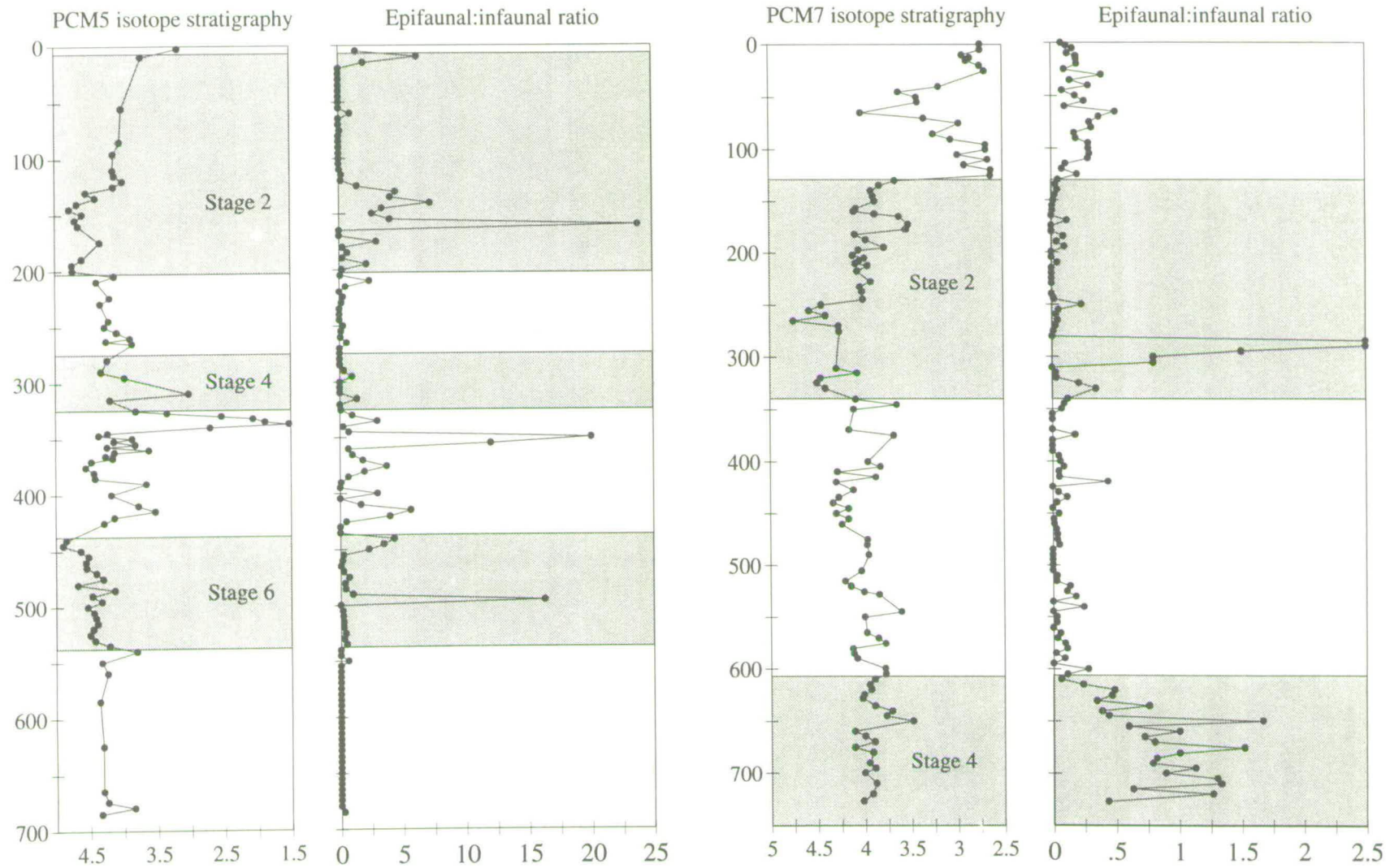

Fig. 6.13. Graph showing epifaunal :infaunal ratio for PCM5 and PCM7, plotted against depth. Note the change in horizontal scale, 0-25 for PCM5 on the left, but only 0-2.5 for PCM7 on the right. The oxygen isotope curves for both cores are shown with glacial periods shaded.

Comparing the oxygen isotope stage 2 records for both cores (130-340cm in PCM7 and 10-205cm in PCM5) epifaunal specimens are approximately 5 times more abundant than infaunal ones during peak stage 2 in PCM5, but under 0.5 times as abundant in PCM7. The peak of 2.5 during stage 2 in PCM7 is misleading. This peak occurs during a period of very low benthic foraminiferal absolute abundance, only 0-5 sp/gm, so should not be relied upon. This observation agrees with that of Corliss and Chen (1988) mentioned in the introduction. They recognised that infaunal specimens were much more abundant in water depths from 500-1500m, and that epifaunal specimens dominate below 1500m. PCM7 is from a water depth of close to 1000m, while PCM5 is from a water depth of over 2000m. This suggests that the organic carbon content is higher at the shallower core site.

Using the conclusion from Corliss and Chen (1988), that an increase in epifaunal specimens at the expense of infaunal specimens is caused by a reduction in organic carbon flux, it is possible to qualitatively estimate the organic carbon flux over the past 200 ka from the epifaunal-infaunal variations. The variation of infaunal and epifaunal specimens seen in PCM5 (fig. 6.11) shows a large increase in infaunal specimens within oxygen isotope stage 6. This therefore relates to an increase in organic carbon flux during stage 6 as compared to stage 2, where epifaunal specimens are relatively more important. Supporting evidence is drawn from the planktic foraminiferal absolute abundances. It is assumed that the planktic foraminifera preyed upon the phytoplankton blooms, which provide a high proportion of the food supply used by the benthic foraminifera. If this is the case, then the planktic foraminiferal absolute abundances should be higher during stage 6 compared to stage 2, owing to the higher proportion of infaunal specimens found during stage 6. Fig. 6.2 shows that the absolute abundance of planktic foraminiferal specimens is considerably higher during stage 6 than stage 2. This strengthens the idea that it is possible to use epifaunal-infaunal variations to identify changes in the abundance of food supply, or organic carbon flux, over time. It also supports the premise that epifaunal specimens become more abundant when food supply is lower (Corliss and Chen, 1988), living at the sediment surface they will scavenge what little food rains down from above, so there is no food left for the infaunal species.

One of the most palaeoecologically important species identified in this study is *C. teretis*. Although *C. teretis* has low background abundances, it also produces peaks of very high abundances contributing 80-90% of the total benthic foraminiferal abundance in PCM7, and up to 60% in PCM5 (figs. 6.7 and 6.5). *C. teretis* is a common species found in the Arctic ocean at the present time, found in water with a

temperature of -0.5 to 0.5°C, and down to a water depth of 1700m (Murray, 1991). In PCM7 this species is most abundant during glacial periods, 275-245cm, and 315-325cm. It is also the species that forms the sudden spike in benthic foraminiferal abundance at 160-145cm, 13.3-12.9ka. This suggests that this species is an early colonizer, and it is the first infaunal species to bloom once a large food supply becomes available. It is also likely that *C. teretis* can survive during periods of low dissolved oxygen supply during stagnant circulation periods, such as peak glacial times. During peak glacial times a stable water stratification is formed, this prevents the production of new deep waters. Deep waters are, therefore generally older, and much of the oxygen in them has been used up by the organisms living at that depth. In core PCM5 *C. teretis* is virtually absent from the top down to 450cm, but then suddenly becomes very abundant from 455-485cm and from 505-525cm (fig. 6. 5). These two peaks are within isotope stage 6. *C. teretis* is an infaunal species so its abundance should be higher when food supply is greatest, ie. when surface water productivity if greatest. So, if it is assumed that *C. teretis* becomes more abundant when surface productivity is high, we can conclude that during stage 6 the surface productivity as recorded in core PCM5 was greater than during stage 2 (which is supported by the planktic foraminiferal abundances). The epifaunal species *E. umbonatus* was dominant during stage 2, when food availability would have been lower, and oxygen content would be low due to stagnant glacial circulation. The dominance of *C. teretis* during stage 2 in PCM7, and its absence during stage 2 in PCM5 suggests that during stage 2 the food supply to the benthics was greater in shallower waters at the core site of PCM7.

It has been concluded earlier (section 6.4) that surface productivity in this area may have been caused by release of nutrients from a melting ice front, either from ice masses originating from the Spitsbergen land mass, or from sea ice. The higher productivity during stage 6 suggests that the ice edge was nearer to core site PCM5, actually extending right to the shelf break. During stage 2 the continental ice edge would have been further from this core site, in a more landward position causing a reduction in supply of organic material from the melting ice front. The ice front would have been nearer the core site of PCM7 (which is slightly nearer shore); thus producing the high abundances of *C. teretis* in PCM7. There is a much longer period for ice to build-up during stage 6 than the time for ice build-up during stage 2. This is also supported by the idea of the formation of a permanent pack ice cover during certain periods of stage 6, as evidenced by the sudden drop in foraminiferal abundances and dropstone concentrations (described in chapter 3). This is not seen so

clearly in stage 2, foraminiferal abundances do drop, but dropstone concentrations remain high during these periods.

Another important species found predominantly in PCM7 is *M. barleeanum* (fig. 6.7). *M. barleeanum* has a background abundance of approximately 10 sp/gm throughout PCM7, except for two sections where no specimens are found, from 625-727cm and from 165-235cm. This species is very rare in PCM5 due to the greater water depth at the core site of PCM5. This is supported by previous studies, mentioned in the introduction, in which it was found that *M. barleeanum* was most abundant in samples from water depths down to 1200m (Belanger and Streeter, 1980, and Sejrup *et al.*, 1981). According to Murray (1991), this species is not closely related to a certain water mass, but it is influenced more by food supply, and thus it can be found in sediments with higher organic carbon content. In this study, *M. barleeanum* appears not to be associated with high supply of organic carbon at all times. For instance this species is relatively rare during peak stage 2 when surface water productivity is at a peak, and hence food supply to the benthos. It is more abundant towards the top of the core, where North Atlantic water is influencing the area. Perhaps its low numbers during stage 2 are due to competition with *C. teretis,* which appears to be an initial colonizer, and therefore reacts more quickly to the appearance of a food supply. The sudden appearance of *C. teretis* and *M. barleeanum* at 150cm in PCM7 (13.2 ka) suggests organic carbon contents increased in the sediments at this time. This is approximately 1000 years before North Atlantic surface waters are thought to have reached this area (from planktic foraminiferal and oxygen isotope evidence, chapter 4). The increase in benthic foraminiferal abundance at 150cm may be due to an increase in nutrient supply from summer melting during a relatively small advance of ice.

One of the most important species found in PCM5 was *E. umbonatus* (fig. 6.4). This species has been recorded in previous studies as being dominant in deeper waters, below 1600m according to Sejrup *et al.* (1981). In PCM7, the abundance of *E. umbonatus* is very low, but minor are peaks found during peak stage 2 (fig. 6.8), its abundance in PCM5, however, is much higher (fig. 6.4) supporting a preferred deeper depth habitat. This species is one of the most important epifaunal species recognised in this study, together with the other numerically important species *C. wuellerstorfi*. *E. umbonatus* is more abundant during times of poor circulation, and thus low dissolved oxygen contents in bottom waters. It is also related to periods of high food supply, for example during stage 2 and stage 6 in PCM5 (fig. 6.4). It is also common when food supply is low, partially due to its epifaunal microhabitat. During less

stagnant periods, when the oxygen content of bottom waters is higher, and more food is available, this species appears to be replaced by another epifaunal species *C. wuellerstorfi*.

The abundance of *C. wuellerstorfi* in core PCM5 is sporadic, it is present in only two sections. It is found in the top 10cm, and from 375-385cm in core PCM5 (fig. 6.5); the actual abundances at these times are moderately high though, 10 sp/gm in the top 10cm and 50 sp/gm at 380cm. This species is more common in core PCM7 (fig. 6.9), although it is still found in relatively low numbers, below 10 sp/gm. In PCM5 the spike in abundance of *C. wuellerstorfi* at 375-385 coincides with a similar spike in abundance of the benthic species *P. bulloides*, 385-390cm (fig. 6.5). This species is not found at any other time within PCM5, the stratigraphic importance of this spike has been discussed in chapter 2, its paleoecological importance will now be discussed. *P. bulloides* is also present in PCM7, but is very rare. There is one major peak in abundance at the top of the main core, isolated occurrences near this point are most likely produced by reworking from the major spike. This species has been identified in previous studies of the Norwegian Sea, it was found associated with *M. barleeanum* between 600 and 1200m by Belanger and Streeter (1980). The reason for its absence over much of the record in both cores is uncertain, but may be due to the generally low food supply in this area caused by low productivity. It is not as well adapted as other species like to *M. barleeanum*, and *C. teretis* to this environment.

The presence of *C. wuellerstorfi* has been used in the past as an indicator of North Atlantic Deep Water (NADW) (Weston and Murray, 1984, Lutz and Coulbourn, 1984), but is also abundant in Norwegian Sea Bottom Water (Mackensen *et al.*, 1985). Mackensen *et al.* (1985) concluded that *C. wuellerstorfi* was associated with deep sea environments with a relatively high food supply, while *E. umbonatus* was associated with deep sea environments with a relatively low food supply. The peak in abundance of *C. wuellerstorfi* in PCM5 was found during oxygen isotope substages 5c to 5b. There is little evidence suggesting an influx of North Atlantic water at this time from the planktic foraminiferal fauna, but there was almost certainly a stronger circulation system at this time than during the major global glaciations of stages 6 and 2. This is supported by the $\delta^{13}C$ values from benthic foraminifera of core PCM5 (chapter5). The $\delta^{13}C$ values of *E. umbonatus* at this time rises to typical NADW type values, suggesting deep water production was taking place. This stronger circulation system may have supplied more oxygen to the deep water environment, and food (as evidenced by higher surface water productivity) causing a bloom in *C. wuellerstorfi* and *P. bulloides*. These two species prevented an increase in numbers of *E.*

umbonatus due to competion and also *C. teretis* (these two species dominate during periods of high food supply with lower oxygen content). The second peak in *C. wuellerstorfi* found in the upper 10cm of core PCM5 is related to a period of increased circulation. This coincides with the initial influx of North Atlantic waters into the area stimulating deeper water circulation again, leading to re-oxygenation of deep waters and increased nutrient supply. In PCM7 the abundance of *C. wuellerstorfi* is partially associated with influx of North Atlantic surface waters. The lower section of PCM7 has very low abundances of *C. wuellerstorfi*, generally below 1 sp/gm. Abundances are higher when total benthic foraminiferal abundances are higher, for example within peak stage 2 (245-275cm). The absolute abundance increases slightly at 130cm, or 12.3 ka, when North Atlantic waters were first recognised in this area. The numbers then decreased from 65cm, 11 ka, and increase from 25cm, 10.4 ka, until the top of the core and remain relatively high for the whole of the trip core. This pattern is similar to the distribution pattern for *N. pachyderma* (dextral) (fig. 6.6), the species marking the influx of North Atlantic surface water into the area. So for the top of PCM7 the relative abundance of *C. wuellerstorfi* may record the initiation of NADW formation, or at the very least an increase in food supply to the bottom waters. This inceased food supply was caused by the influx of more productive North Atlantic surface waters. In PCM5 the occurrence of the two species *P. bulloides* and *C. wuellerstorfi* reflects initiation of deep water circulation, and possible NADW production.

C. reniforme is a species present in moderate numbers in both cores (figs. 6.4 and 6.8). *C. reniforme* can live on the continental shelf, but is also found in low numbers on the slope down to 1300m, Sejrup and Guibault (1980) consider this an Arctic species. In PCM5 it is common when ever total benthic abundances are high, but also after the initial melting event at 125cm, 15.5ka, when all other benthic species are very rare. In PCM7 the abundance is patchy being moderately high at the top of the core, but also at the base from 615-727cm, 60-72ka. This represents oxygen isotope stage 4, and is a period of low benthic abundance in general. This suggests that *C. reniforme* can survive in conditions of low food supply, and low oxygen supply when other species die out. The other alternative is that this species could be reworked from the continental shelf, pushed over the shelf edge by grounded ice at its maximum extent, or carried within icebergs.

One group of species was recognised in moderately high numbers that was almost certainly reworked from the shelf, this was the group *Elphidium* spp. This group consisted of various different species of *Elphidium* which were not subdivided. Most

species of *Elphidium* live on the continental shelf, so this group represents reworked specimens in PCM5 and possibly in PCM7. From this evidence reworking was most intense within PCM7 during glacial periods, peak stage 2 and stage 4. PCM5 records high *Elphidium* spp. abundances during late stage 3, stage 2 and stage 6. This reworking was probably produced by icebergs grounding on the shelf, and subsequent freezing of material onto their bases. This material would contain benthic foraminifera which would be released on melting to the continental slope and other areas. Some foraminifera would also be pushed over the shelf edge at times of maximum ice extent, this was suggested in chapter 3.

6.9 Conclusions

1. Foraminiferal productivity peaks are found during glacial periods not during interglacial periods as found in previous studies. This proves the Spitsbergen margin was seasonally ice free during glacial periods and not covered in permanent pack ice as previously thought. The peaks in productivity were probably produced by an increase in nutrient supply from melting sea ice and from input of terrestrial material from ice from Spitsbergen.

2. Permanent pack ice was present at certain periods during isotope stage 6, 505-500cm and 445cm. Evidence for this comes from the disappearance of foraminifera and IRD from samples during these periods. Permanent pack ice would reduce the flux of IRD from icebergs, and prevent solar radiation reaching surface waters thus reducing surface water productivity.

3. The influx of North Atlantic surface waters were recognised by the appearance of subpolar planktic foraminiferal species *N. pachyderma* (dextral) and minor occurrences of *G. bulloides*. North Atlantic water first reached this area at 12.5 ka, disappeared at 12 ka, then was present again from 10.5 to 10.3 ka, and from 10 ka to the top of the core at 8.5 ka. This is supported by the oxygen isotope evidence outlined in chapter 4.

4. The relative strength of the influx of N. Atlantic waters into the area can be assessed from the percentage of *N. pachyderma* (dextral) present. Initially from 12.5 to 12 ka *N. pachyderma* (dextral) comprised only 10-20% of the planktic assemblage suggesting a relatively weak N. Atlantic current. From 10 to 8.5 ka this percentage rose to 35-40% due to a stronger current. So for this later period of influx the $\delta^{18}O$

record from the planktic foraminifera probably has a higher temperature effect included than for the previous periods of Atlantic influx.

5. There is no evidence from planktic foraminifera of an influx of N. Atlantic water to the Spitsbergen margin from 200 ka to 12.5 ka, not even during isotope substage 5e. This may be due to an increase in carbonate dissolution during isotope stage 5 as suggested by the very low absolute foraminiferal abundances during this period. Or it may be due to the large volumes of meltwater produced which the foraminifera cannot survive in.

6. In general the abundance of benthic formainifera match the abundance of planktic foraminifera. Blooms in planktic foraminiferal abundance are produced by phytoplankton blooms, which in turn supply organic material to the ocean floor leading to a bloom in benthic foraminiferal productivity. The B:P ratio for PCM7 is greater than for PCM5, this is due to the shallower water depth at the core site of PCM7. Planktic foraminifera are 5-10 times more abundant than benthics in PCM5, and 2-3 times more abundant than benthics in PCM7.

7. The epifaunal:infaunal ratio is greater for the deeper core, PCM5. This supports the conclusion of Corliss and Chen (1988) that epifaunal species are more dominant at water depths greater than 1500m (PCM5 is from a water depth of over 2000m), while infaunal species are more common from 500-1500m (PCM7 is from a water depth of 1134m).

8. Infaunal species are more abundant during periods of increased food supply to bottom waters, as evidenced by the higher infaunal specimen abundance during stage 6 compared to stage 2 in PCM5.

9. The infaunal species *C. teretis* was dominant during periods of stagnant ocean circulation (low oxygen supply), in combination with high food supply from surface productivity. It is considered a colonizer, an opportunist which appears once food supply increases. During a stagnant period with a lower food supply the epifaunal species *E. umbonatus* takes over. When food supply is high and circulation is relatively stronger, leading to greater oxygen supply to bottom waters, the epifaunal species *C. wuellerstorfi* and the infaunal species *P. bulloides* become dominant. These last two species mark the initiation of deep water production.

10. The changes in relative abundance of *C. teretis* and *E. umbonatus* can be used as a measure of nutrient supply to bottom waters and indicators of circulation intensity. The relative increase in abundance of C. teretis during stage 6 compared to stage 2 suggests stage 6 was a more intense glacial period than stage 2, with a greater stagnation of circulation, and the ice margin further out at or just beyond the shelf edge. During stage 6 the ice edge was nearer PCM5, while during stage 2 the ice edge was nearer PCM7 (closer to the shelf break).

11. The abundance of *M. barleeanum* and *C. wuellerstorfi* in core PCM7 appears to be weakly associated with the influx of North Atlantic surface waters. The absolute abundance of both species increased slightly when N. Atlantic water entered the area at 12.5 ka.

Plate 1

Figs. 1, 2, 3 and 4. *Neogloboquadrina pachyderma* (sinistral) (Ehrenberg). View of aperture showing some of the variation present within the species. *N. pachyderma* (sinistral) is the dominant species found living in polar waters. Scale, x150, x312.5, x140 and x160 respectively.

Figs. 5, 6 and 9. *Neogloboquadrina pachyderma* (dextral) (Ehrenberg). View of aperture side showing intraspecific variability found in this study. The appearance of *N. pachyderma* (dextral) in samples from this study records the influx of North Atlantic waters into the study area. Scale, x125, x200 and x162.5 respectively.

Figs. 7 and 8. *Globigerina bulloides* (d'Orbigny). View showing large open and central aperture. This is an indicator species of subpolar waters in the Norwegian-Greenland Sea. Scale, x110 and x90 respectively.

Figs. 10 and 11. Eponides umbonatus (Reuss). Fig. 10 shows the coiling side and fig. 11 shows the aperture of this species. E. umbonatus is characteristic of deep water environments with relatively low food supply. It is also the species used in stable isotope analysis for PCM5. Scale, x162.5 and x150 respectively.

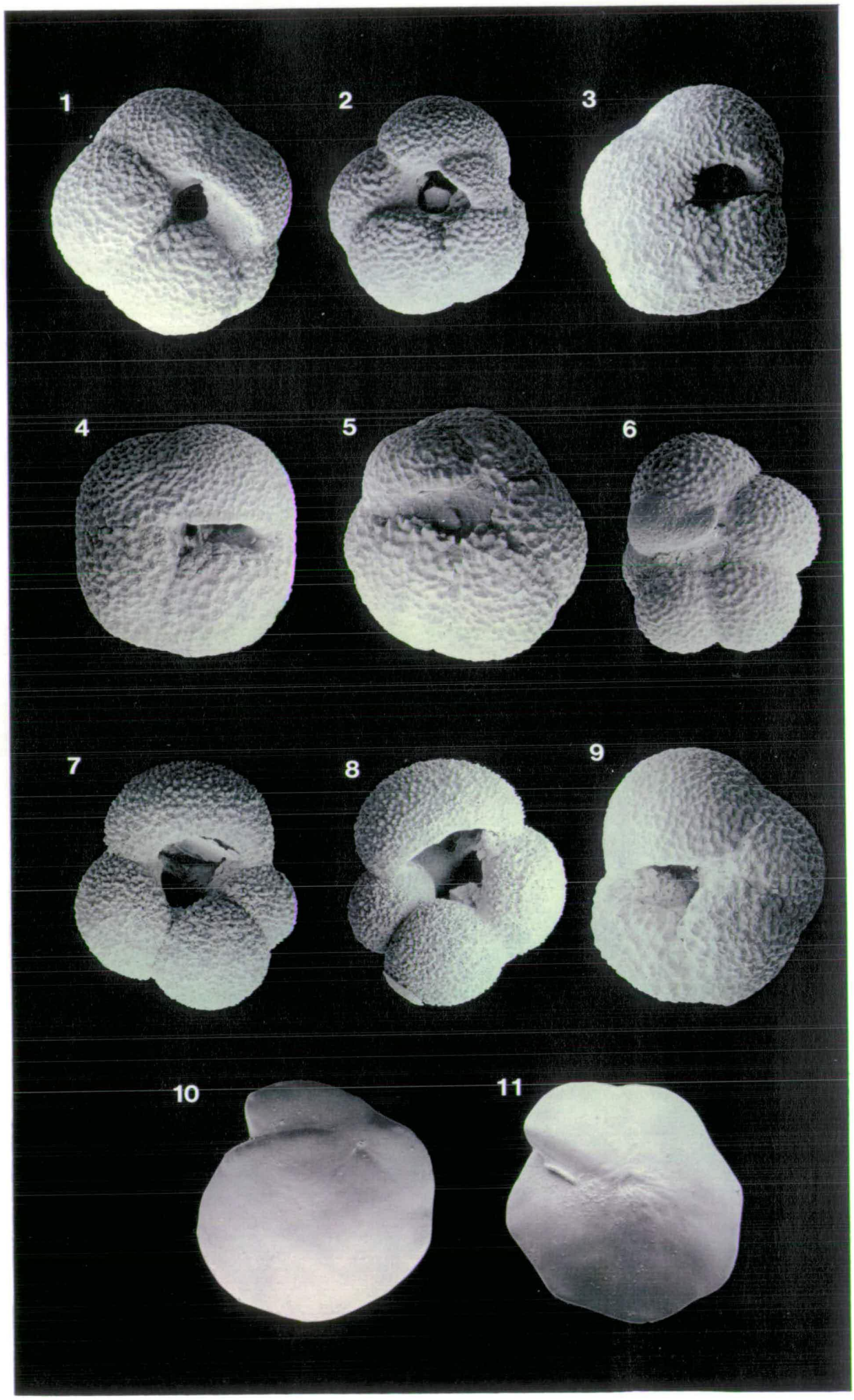
1
2
3
4
5
6
7
8
9
10
11

Plate 2

Fig. 1. *Melonis barleeanum* (Williamson). Side view clearly showing the pores in the wall. *M. barleeanum* is moderately abundant throughout the shallower core PCM7, but blooms when deep water circulation is renewed at approximately 10ka. It is associated with high food supply from renewed deep water circulation. This species was used for stable isotope analysis for cores PCM7 and PCM30. Scale x110.

Figs. 2 and 3. *Cassidulina teretis* (Tappan). Two views of the aperture of *C. teretis* showing the distinctive long flap, there are also groups of pores on the surface which are diagnostic. This species was found to be dominant during periods of relativley high food supply with poor circulation. *C. teretis* was used for stable isotope measurements from cores PCM7 and PCM30. Scale, x120 and x150 respectivley.

Figs. 4 and 5. *Islandiella helenae* (Feyling-Hansen and Buzas). Two views of the aperture of *I. helenae* which is used to differenciate this species from *C. teretis*. *I. helenae* has a complex aperture with flaps and teeth and the test surface is missing the diagnostic pores of *C. teretis*. Scale, x115 and x100 respectively.

Figs. 6 and 7. *Cassidulina reniforme* (Nørvang). Fig 6 shows the aperture, fig. 7 the reverse view. *C. reniforme* lives on the shelf down the slope, some specimens are undoubtedly reworked. Scale, x250 and x300 repectivley.

Figs. 8 and 9. *Pullenia bulloides* (d'Orbigny). Fig. 8 shows an oblique view of the slit like aperture, fig. 9 shows a side view of the smooth spherical test. This species blooms when deep water production is renewed, but dies off soon after. Scale, x160 and x140 respectively.

Figs. 10 and 11. *Cibicidoides wuellerstorfi* (Schwager). Side views shown in both figs., *C. wuellerstorfi* is more abundant during periods of high food supply and vigorous deep water circulation. It is associated with NADW production in the Greenland Sea. Scale, x80 and x65 respectively.

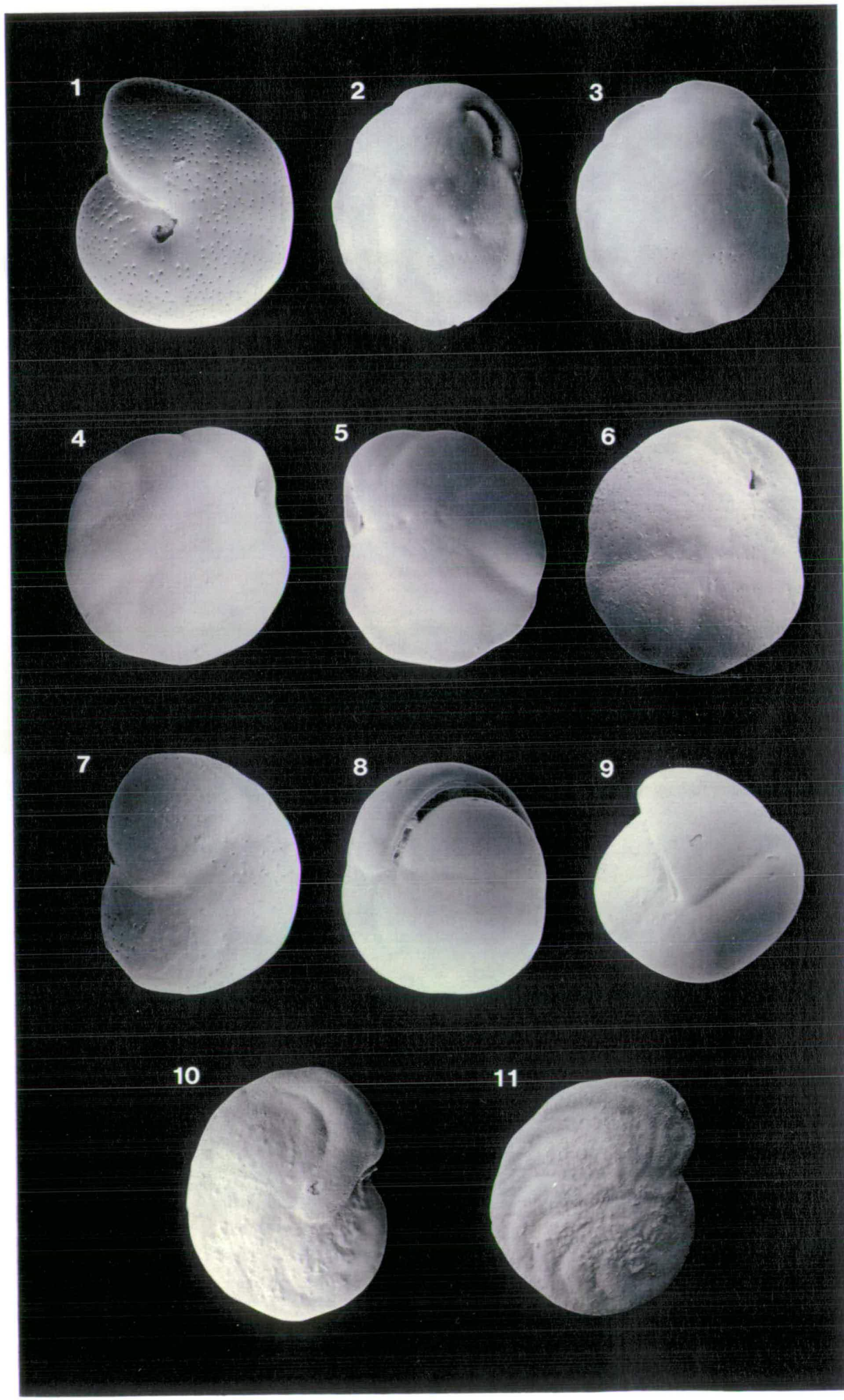
1
2
3
4
5
6
7
8
9
10
11

Plate 3

Figs. 1 and 2. *Elphidium excavatum* (Terquem) forma *clavata* Cushman. Fig. 1 side view of typical *E. excavatum* forma *clavata*, fig. 2 possible variation of the species. These are relatively shallow water foraminifera and are, therefore, probably reworked from the shelf during glacial periods. Scale, x100 and x120 respectively.

Fig. 3. *Elphidium groenlandicum* Cushman. Side view of this typical shelf species probably reworked during glacial periods. Scale x70.

Fig. 4. *Elphidium albiumbilicatum* (Weiss). Side view, this species is also probably reworked from the continental shelf. Scale x175.

Figs. 5 and 6. *Cibicides lobatulus* (Walker and Jacob). Fig. 5 view of flat side showing previous whorls, fig. 6 view of convex side showing chambers of final whorl. This species is also diagnostic of shelf environments and is probably reworked in the cores of this study. Scale, x80 and x120 respectively.

Fig. 7. *Oolina hexagona* (Williamson). Oblique side view of specimen. Scale x325.

Fig. 8. *Quinqueloculina seminula* (Linné). Oblique end on view showing aperture, details of teeth not visible. Scale x120.

Fig. 9. *Pyrgo* sp. Side view of specimen, two chambers visible. Scale x30.

Fig. 10. *Stanforthia loeblichi* (Feyling-Hansen). Side view of specimen showing long aperture with flap. Scale x105.

Fig. 11. *Bulimina marginata* (d'Orbigny). Side view of specimen showing characteristic frills. This species is usually associated with relatively warm subpolar deep waters, but is very rare in this study. Scale x65.

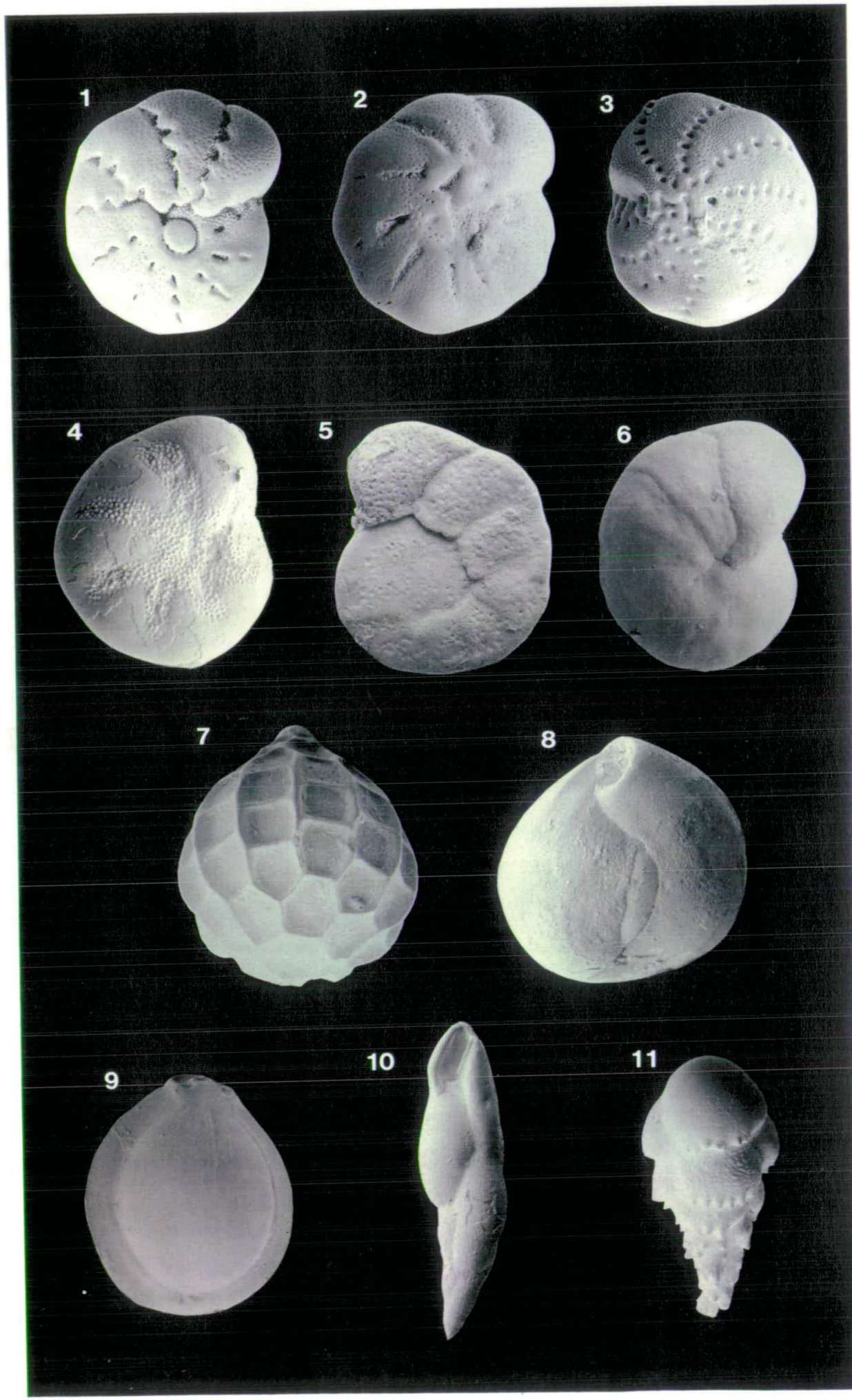
1
2
3
4
5
6
7
8
9
10
11

Chapter 7. Reading the Fram Strait records and their implications for the timing of Spitsbergen ice advances and palaeoceanographic changes over the last 200 ka

7.1. Introduction

The aim of this concluding chapter is to bring together the results from the different parameters measured and provide a clearer picture of the paleoceanography and glacial history of the Spitsbergen margin. The results will also be compared to other globally significant records in an attempt to put the Fram Strait records in a global context. To achieve this, the $\delta^{18}O$ records produced from this study will be compared to the Summit ice core (GRIP members, 1993) and the solar insolation record produced by Berger (1978).

Three marine cores from the continental margin of Spitsbergen, between lat. 78°N and 80°N, were analysed in this study, cores PCM5, PCM7 and PCM30. The cores were obtained from the continental slope at water depths of between 1000m and 2300m. Oxygen isotope stratigraphy combined with radiocarbon dating were used to produce an age model for the cores. Using these methods core PCM5 was found to extend from late oxygen isotope stage 7 to the oxygen isotope stage 2 - stage 1 boundary (approximately 200 ka to 12.5 ka), PCM30 covered oxygen isotope stage 6 to mid-stage 2 (approximately 150 ka to 15 ka), and PCM7 covered late stage 4 to early stage 1 (the time range from 75 ka to 8.5 ka).

From the data provided by these cores interpretations of the glacial history of the Spitsbergen ice cap and the palaeoceanographic history of the Fram Strait and Greenland Sea area were made. The following parameters were examined to produce the conclusions presented in this thesis: 1) Stable isotope measurements of $\delta^{18}O$ and $\delta^{13}C$ on planktic and benthic foraminifera: 2) absolute abundance counts and species counts of planktic and benthic foraminifera: 3) particle size measurements: 4) clast counts from x-ray photographs and 5) magnetic susceptibility measurements.

7.2. Correlation of marine oxygen isotope records with Summit ice core record

Ice cores are a source of very high resolution data which, under optimum conditions, have few sampling gaps. Measurements have been made on several ice cores from both the Greenland ice sheet and the Antarctic ice sheet, for example the Vostok ice

core from the Antarctic ice sheet (Lorius *et al.*, 1985). This record reaches marine isotope stage 7. Three ice cores, Camp Century, Dye3 and Renland ice cores, were drilled to the base of the Greenland ice sheet, and studied by Johnsen *et al.* (1972), Dansgaard *et al.* (1982), and Johnsen (1992) respectively. These all reach ice deposited in the last glaciation.

A new ice core from the central area of the Greenland ice cap has recently been analysed by Johnsen *et al.* (1993), and Dansgaard *et al.* (1993). It became known as the Greenland Ice-core Project (GRIP) Summit ice core, shortened to Summit ice core for the following discussion. This core comes from the centre of the ice mass where lateral flow of ice is at a minimum, so disruption of the record should be at a minimum. The ice core was drilled to a depth of 3000m into silty ice very close to bedrock. A time scale for the core has been achieved back to 14.5 ka by counting annual layers from the surface. The chronology has been extended to the base of the core by ice-flow modelling, confirmation of this chronology has been attained by the close correlation of the Summit isotope profile with that of the Vostok ice core (from the Antarctic ice sheet), the SPECMAP marine isotope record, and the Devil's Hole terrestrial isotope records. The record extends back as far as 250 ka, isotope stage 7 the Holstein Interglacial.

7.2.1. The $\delta^{18}O$ record produced from the ice core

One of the useful measurements made on the ice core is the $\delta^{18}O$ signature of melted samples of the ice. The water molecules from this melted ice preserve the isotopic signature of the precipitation at the time of its deposition. The isotopic composition of ice forming at polar regions is governed predominantly by the air temperature at the time of formation (Johnsen *et al.*, 1993). The isotopic composition of the ocean water in the source areas for the precipitation also has an effect on the ice composition, but only minor when compared to the temperature effect.

During a glacial period evaporation of moisture from the oceans leads to an enrichment in the heavy oxygen isotope, ^{18}O, in the marine environment. This enrichment is also enhanced by a decrease in temperature. This signature is taken up by marine organisms such as foraminifera, and can be measured to produce records such as those of marine cores PCM7, PCM5 and PCM30 of this study. Water molecules preserved as ice in polar continental ice sheets during glacial periods will record the exact opposite to marine cores: they will be depleted in the heavy ^{18}O, and enriched in the lighter ^{16}O. The lighter ^{16}O is preferentially removed during

evaporation from the oceans causing this enrichment in heavy ^{18}O in the marine environment and its depletion in polar ice sheets. During an interglacial the polar ice sheets partially melt returning proportionally more of the light ^{16}O isotope to the oceans, thus causing a dilution in ^{18}O in the marine record during these warm periods. Warmer air temperatures produce precipitation with an oxygen isotopic signature enriched in ^{18}O (Johnsen *et al.*, 1993).

The $\delta^{18}O$ record produced from the Summit ice core is therefore directly linked to air temperature changes over Greenland and the surrounding source areas for precipitation. Near surface air temperatures are controlled to a large degree by the temperature of surface ocean currents which the air comes into contact with and the height of the ice sheet. So changes in the $\delta^{18}O$ signature of the Summit ice core can also be used to imply changes in ocean circulation. The marine $\delta^{18}O$ record is controlled by water temperature and by global ice volumes.

A complete record of the $\delta^{18}O$ variations for the Summit ice core shows several curious trends (Dansgaard *et al.*, 1993). The lower section of the record is reproduced in fig. 7.1. The plot on the left in fig. 7.1 shows the detailed data plotted against depth, the curve on the right shows a smoothed version of this data plotted against the age model produced for the ice core, the data has been smoothed by a 5kyr gaussian low-pass filter. The measurements for the Holocene are remarkably stable, the rest of the record is characterised by very rapid high amplitude fluctuations in $\delta^{18}O$. The last glacial period from 80 ka to 20 ka was punctuated by a series of warm periods with an increase in surface air temperatures of 5-8°C. These episodes were short lived lasting only a few centuries (Johnsen *et al.*, 1993).

The record of isotope stage 5e, the Eemian interglacial, also shows similar rapid $\delta^{18}O$ fluctuations. The age model produced for the core suggests the duration of the Eemian was longer than previously assumed, nearly 20ka from 133 to 114ka (Dansgaard *et al.*, 1993). The Eemian has been split into 3 main warm phases separated by 2 cooler periods (Greenland Ice-core Project (GRIP) members, 1993). The $\delta^{18}O$ measurements suggest air temperatures were 2°C warmer during Eemian times than the present, and the cooler periods within the Eemian were characterised by temperatures similar to those experienced during substages 5c and 5a. These shifts in temperature were very rapid occurring in a matter of decades. This contrasts starkly with the stable climate of the Holocene, and suggests the possibility of climatic instability during the Holocene if global warming continues producing a climate similar to the Eemian (Dansgaard *et al.*, 1993).

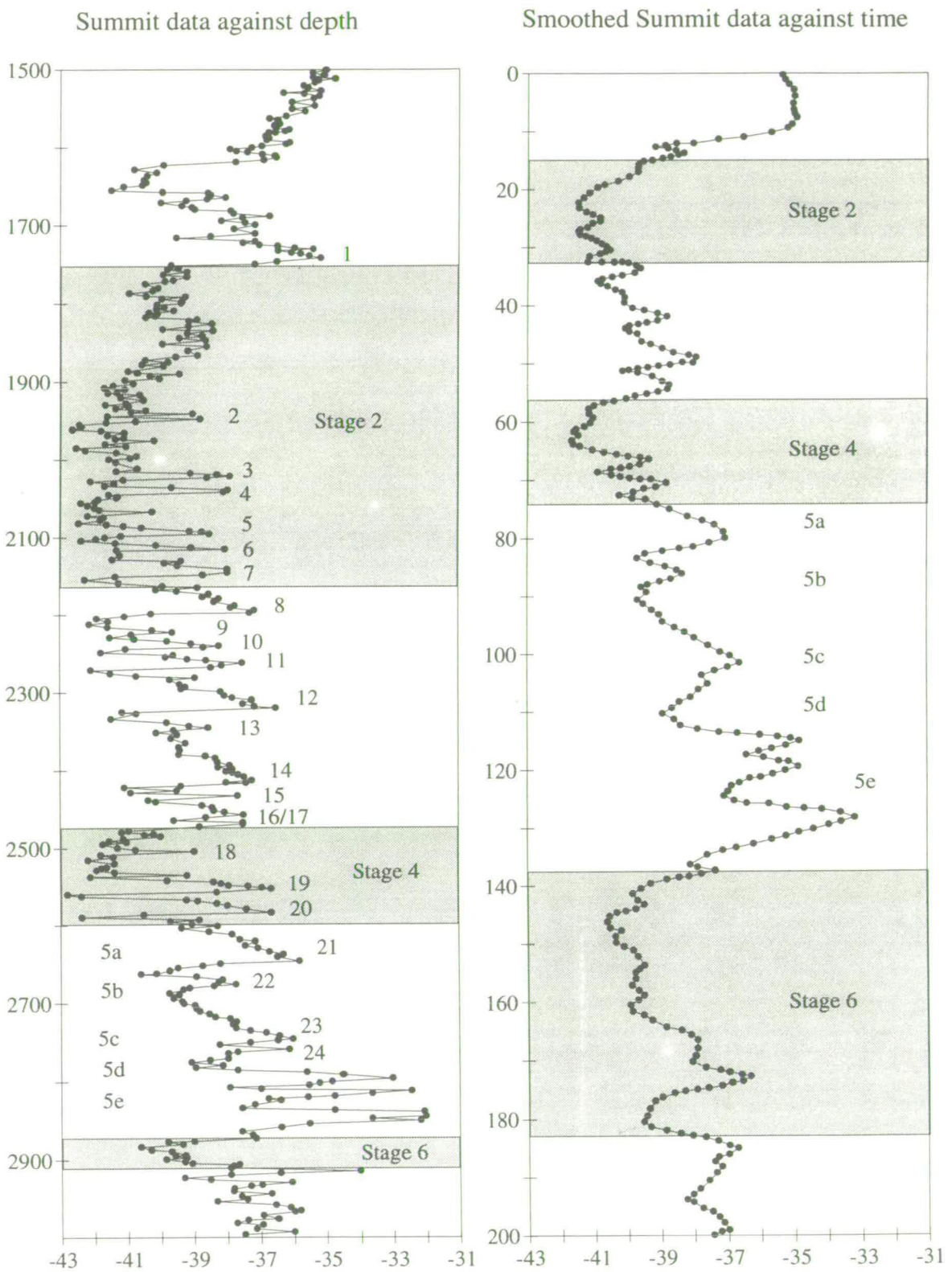

Fig. 7.1. Summit ice core oxygen isotope record. On the left plotted against depth, numbers to right of curve represent glacial interstadials, main glacial isotope stages shaded, and substages of isotope stage 5 labelled. The plot on the right is the same data plotted against time, the curve has been smoothed with a 5-kyr gaussian low-pass filter. All data from Dansgaard et al. (1993). Isotope scale per mil variation w.r.t. SMOW standard.

7.2.2. Correlation between $\delta^{18}O$ records of the Summit ice core and marine cores PCM5, PCM7 and PCM30

The question now arises as to whether it is possible to correlate between the high resolution Summit ice core isotopic data and $\delta^{18}O$ data from marine cores, and if the rapid fluctuations seen in the ice core can be identified in the marine realm. The correlation between the Summit ice core and the marine isotope records of this study, PCM7, PCM5 and PCM30 is made below.

The isotope record from melted water within the ice core shows a remarkable correlation with the planktic isotope record of PCM7, shown in fig. 7.2 (the ice core data was adapted from Dansgaard *et al.*, 1993). The top of the Summit profile in this diagram is approximately 10ka calendar years B.P., the top of the trip core of PCM7 is approximately 8.5ka radiocarbon years. This remarkable correlation illustrates the possibility of recognising events represented in terrestrial ice cores in deep marine records, though it is necessary to have a core of high resolution. PCM7 shows a high resolution over the period from the last glacial peak to the top of the core at 8.5 ka. The sedimentation rate up to the peak of stage 2 is approximately 15 cm/ka. As a result isotope samples were measured approximately every 300 years (samples taken every 5cm). This is high enough resolution to recognise many of the events found within the Summit ice core.

The record for the upper section of the cores, from stages 2 and 1, correlate well. The major temperature fluctuations recorded by the ice core for stages 2 and 1 are also preserved in the $\delta^{18}O$ record of the marine core PCM7. This suggests these temperature changes over Greenland reflect changes in ocean temperature and/or global ice volume as recorded by planktic foraminifera. The rapid fluctuations evident in stages 3 and 4 of the ice core can not be correlated with any confidence with the marine record, probably because sedimentation rates are too low for the sampling resolution during this period.

Longer term correlation between the ice core and marine records is possible using PCM5 and PCM30 which extend to oxygen isotope stages 7 and 6 respectively (fig. 7.3). The rapid temperature fluctuations recorded in the ice core during stages 3 and 4 are not visible in the marine cores, this is again most likely to be due to poor resolution in the marine cores over this period. PCM5, however, does record one major spike in $\delta^{18}O$ values within stage 4, at 310cm, which might correlate with one of the warming events recognised during early stage 4 in the ice core.

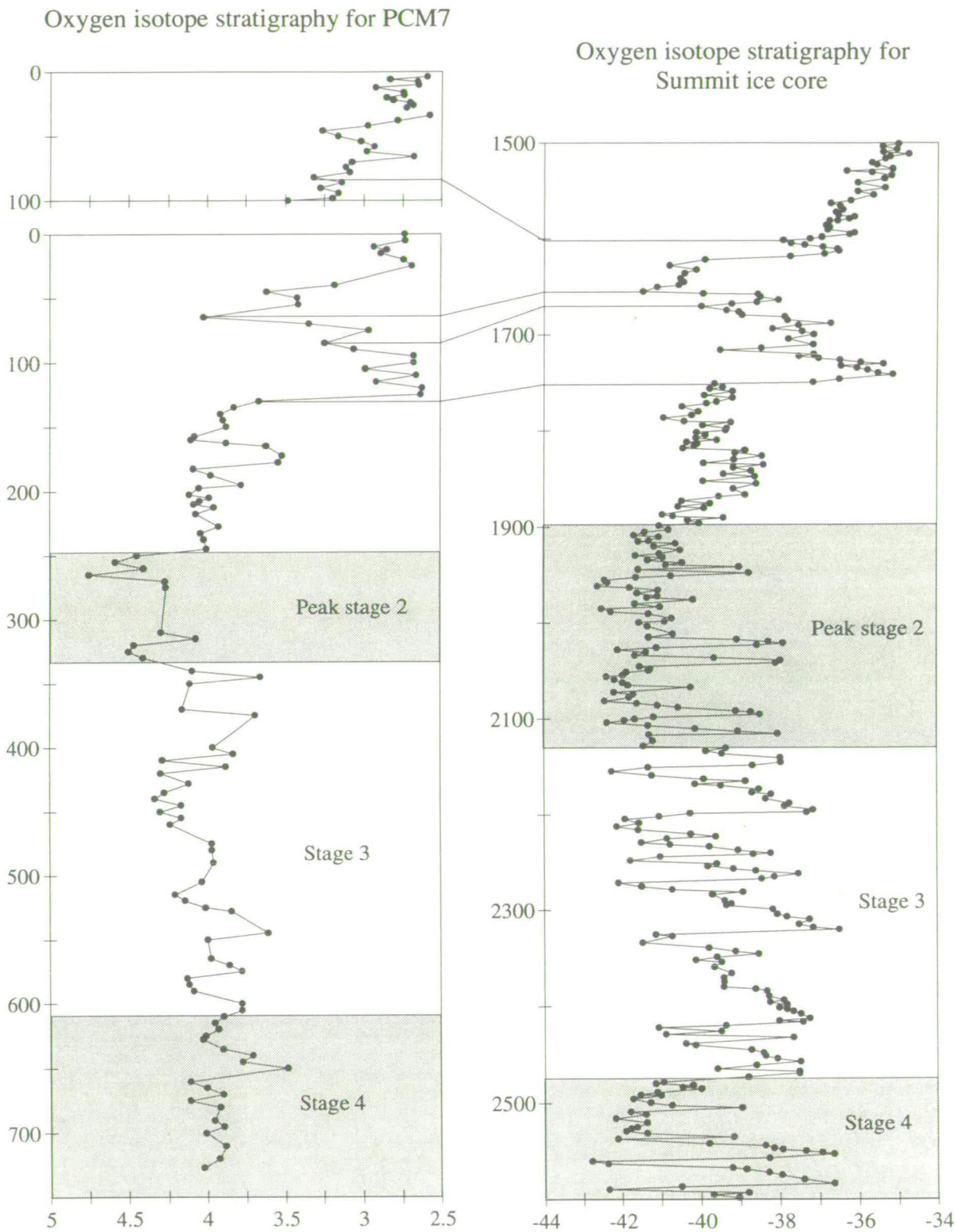

Fig. 7.2. Summit ice core oxygen isotope record on the left, oxygen isotope record of PCM7 on the right, both records plotted against depth (cm). Summit isotope data is expressed as per mil variation w.r.t. SMOW standard, isotope data for PCM7 expressed as per mil variation w.r.t. PDB standard. Summit data from Dansgaard et al. (1993). Oxygen isotope stages labelled, glacial stages shaded.

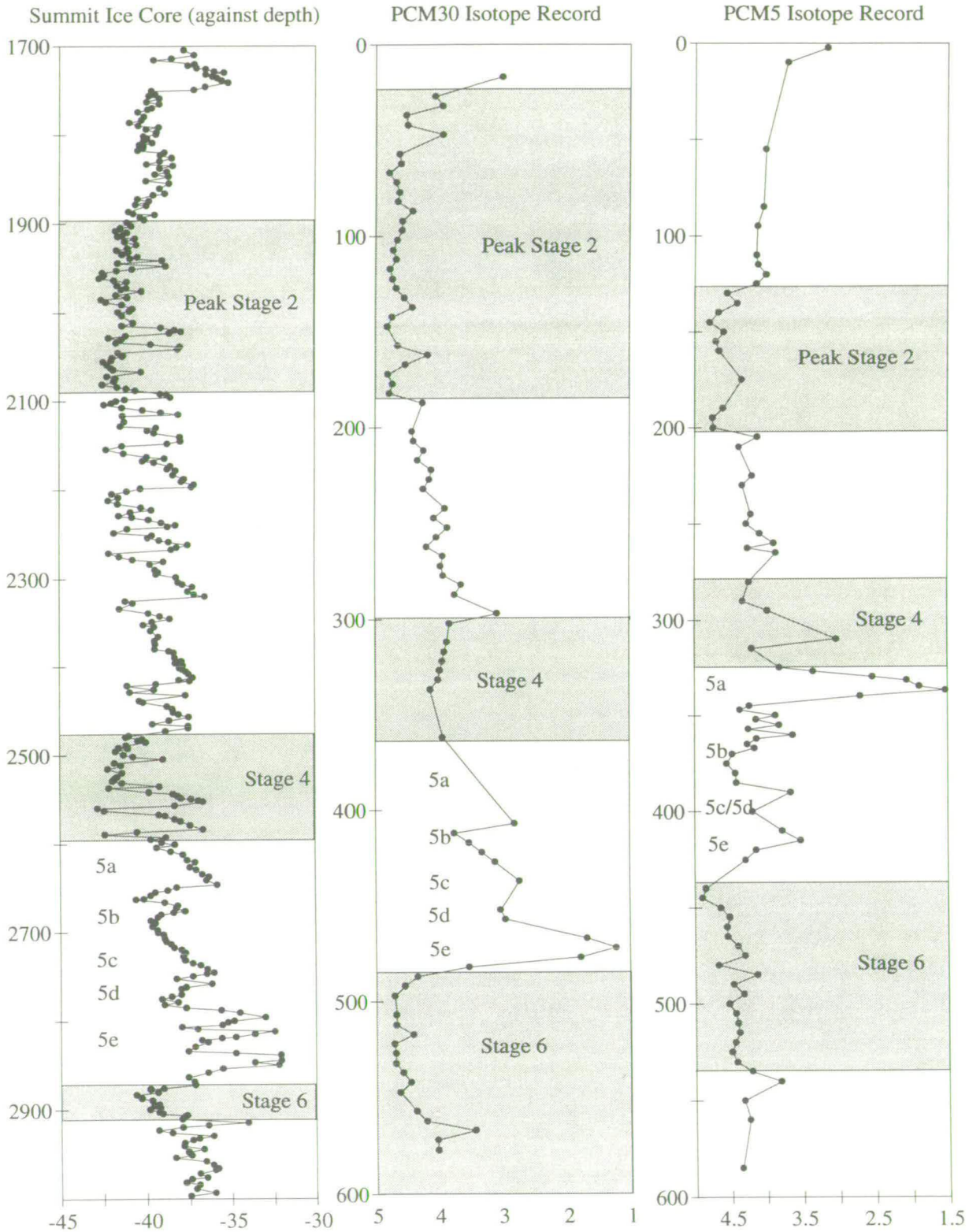

Fig. 7.3. Summit ice core oxygen isotope record on the left with oxygen isotope stratigraphy of marine cores PCM30 and PCM5 from this study. All data plotted against depth (cm). Summit isotope data expressed as per mil variation from SMOW standard, the isotope scale for PCM30 and PCM5 is expressed as per mil variation w.r.t. PDB standard. The isotope stages and substages are labelled, glacial stages are shaded.

The picture of late stage 5 produced from the ice core matches the marine record well. The warm event of substage 5a in the ice core is seen as a major isotopic spike in PCM5. This is influenced by meltwater influx as well as temperature and global ice volume exchanges (see chapter 4). Substage 5b is the dominant cold event within stage 5 from the ice core records. This agrees with the $\delta^{18}O$ record of PCM5, as the twin peaked shape can be recognised in both PCM5 and the Summit ice core. Substages 5c and 5d are poorly defined in the ice core, because they are not as intense as the other events within stage 5. A similar pattern can be recognised in the marine cores, where substages 5c and 5d are also difficult to define. Finally in stage 5 there is the substage 5e record mentioned earlier. The major fluctuations within substage 5e recognised in the ice core are not seen in the marine $\delta^{18}O$ records. A single strong isotope spike represents the substage 5e record in PCM30. The isotope record of the marine cores is not of high enough resolution for the fluctuations seen in the ice core to be visible. The sedimentation rate over stages 3 to 5 in PCM5 and PCM30 is considerably slower than the upper section of PCM7. Fig. 2.11 shows depth plotted against age for the three main cores of this study. This illustrates the rapid sedimentation rate during the upper core sections and during glacial stage 6. The sedimentation rate from stages 4 and 5 in PCM30 is approximately 3cm/ka. Samples taken every 5cm therefore represent a time interval of around 1.6 ka. The sedimentation rate during stage 6 in PCM30 increases to 18 cm/ka (and 10 cm/ka in PCM5). This represents a sample approximately every 300 years. The stage 6 record from all the three cores is relatively straight forward to correlate.

The Summit ice record suggests that the climate during stage 5 in the Greenland Sea area differs from the globally accepted situation. Substage 5e was not the stable warm interglacial as previously envisaged, substage 5d appears only to have a minor influence on the area; substage 5b was a much longer lasting and higher amplitude cooling event. Most global records suggest substage 5d was a more intense cold event than substage 5b; see for example the SPECMAP isotope record of Imbrie *et al.* (1984). The Summit record also shows a relatively long duration of warmer conditions during substage 5a, not as warm as substage 5e but more intense than substage 5c. There does seem to be some uncertainty in the interpretation of ice core records. The interpretation of duration of events, and the rapid switching from a warm state on the one hand to a cold state on the other is valid, but the amplitude of changes is not so certain. For example, stage 4 appears to be a colder event than either stages 2 or 6, both of which are known to have been more extreme in terms of temperature and ice advance. The greater importance of substage 5b over 5d suggested in the ice core is, however supported by the marine cores. The position of

substages 5d and 5c in cores PCM5 and PCM30 are not certain, but substage 5b is very clear in PCM5 (385-345cm) and also in PCM30 (412-427cm) and dominates the stage 5 record.

The difficulty with correlating a marine oxygen isotope curve with the Summit ice core lies in the lack of resolution of the oxygen isotope curve due to fluctuations in foraminiferal abundances. Sampling hiatuses are common when foraminiferal abundances are low, for example during stage 5 in PCM5 and PCM30. The correlation of another parameter with no sampling gaps, such as magnetic susceptibility, with the Summit ice core may be useful. The magnetic susceptibility record of PCM5 is of a higher resolution than the oxygen isotope curve, sampled every 2.5cm compared to every 5cm, and contains no sampling gaps (see chapter 2). The magnetic susceptibility record is plotted with the Summit ice core record in fig. 7.4. Rapid fluctuations can be seen in the susceptibility record, the cause of these is uncertain but a tentative correlation can be made with the Summit ice core. This shows that substage 5e was not adaquately sampled for oxygen isotope analysis. This was because the foraminiferal abundances were too low for analysis during this period. A similar attempt at correlation has been made for the magnetic susceptibility record of PCM7 and the Summit ice core during stages 2 and 3 (fig. 7.5). These correlations have been made purely to show the possible potential of using a parameter such as magnetic susceptibility as a proxy for palaeoclimatic change. The advantages over oxygen isotope measurements are a greater speed and ease of measurement and the lack of sampling gaps in the record. Magnetic susceptibility measurements could be used in conjunction with the oxygen isotope record to produce stronger correlations, but should not replace oxygen isotope measurements. More research is needed to understand the cause of the high frequency fluctuations in magnetic susceptibility readings.

7.3. Relationship between solar insolation fluctuations, the Summit ice core and the Fram Strait records

The variation in solar radiation received at the earth's surface varies over time. These variations are considered to be caused by fluctuations in orbital parameters (Imbrie *et al.* 1984). Berger (1978) calculated the difference in solar radiation received at various positions on the Earth's surface. The yearly average solar insolation receipt at latitude 80°N has been plotted for the past 200 ka in fig. 7.6 along with the smoothed Summit ice core $\delta^{18}O$ data.

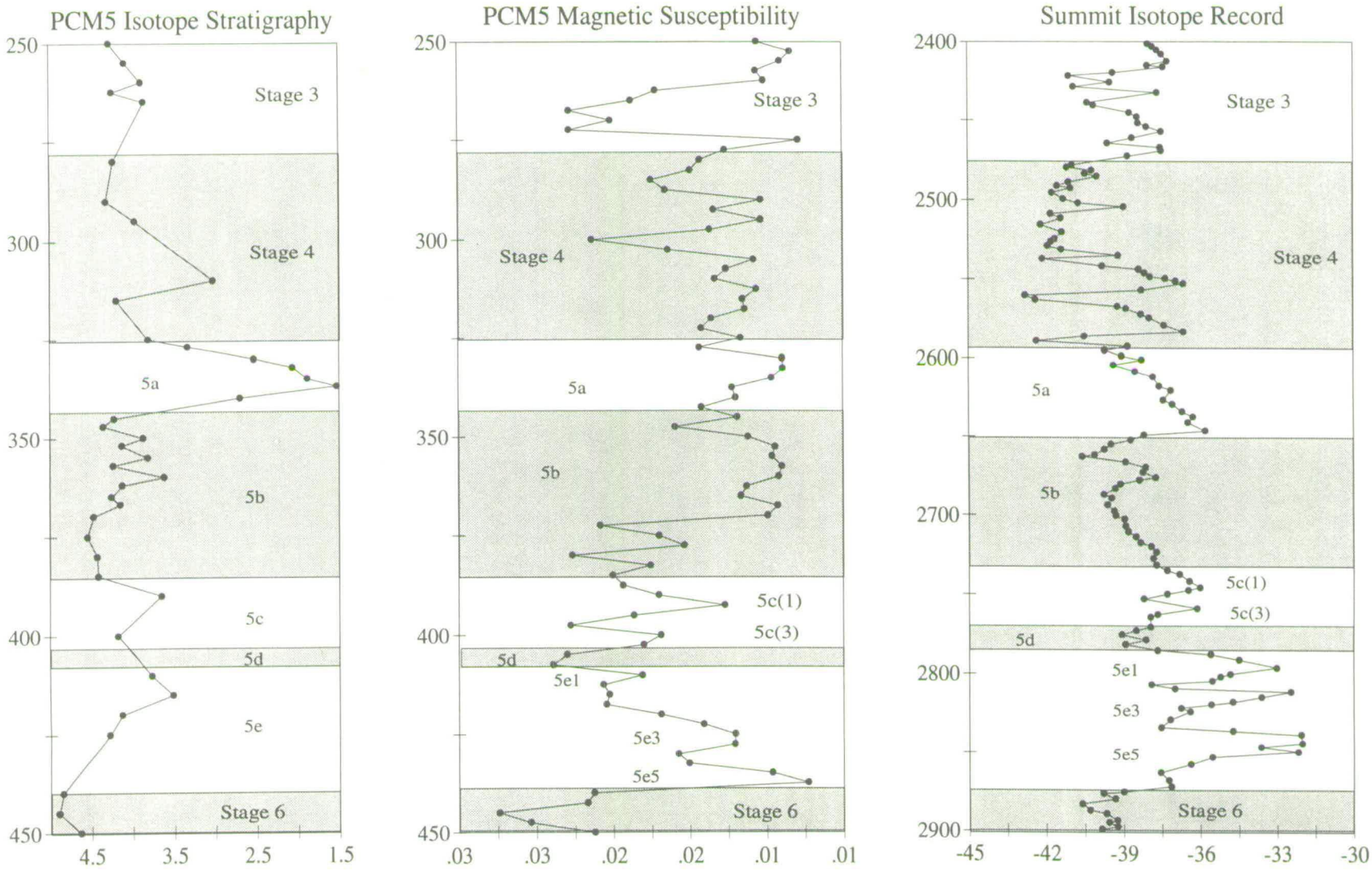

Fig. 7.4. Comparison between magnetic susceptibility measurements of PCM5 with Summit oxygen isotope data. Oxygen isotope record of PCM5 shown on the left for reference. This plot shows the greater resoltion of the magnetic susceptibility readings compared to the oxygen isotope readings, and the high frequency fluctuations present in the susceptibility readings.

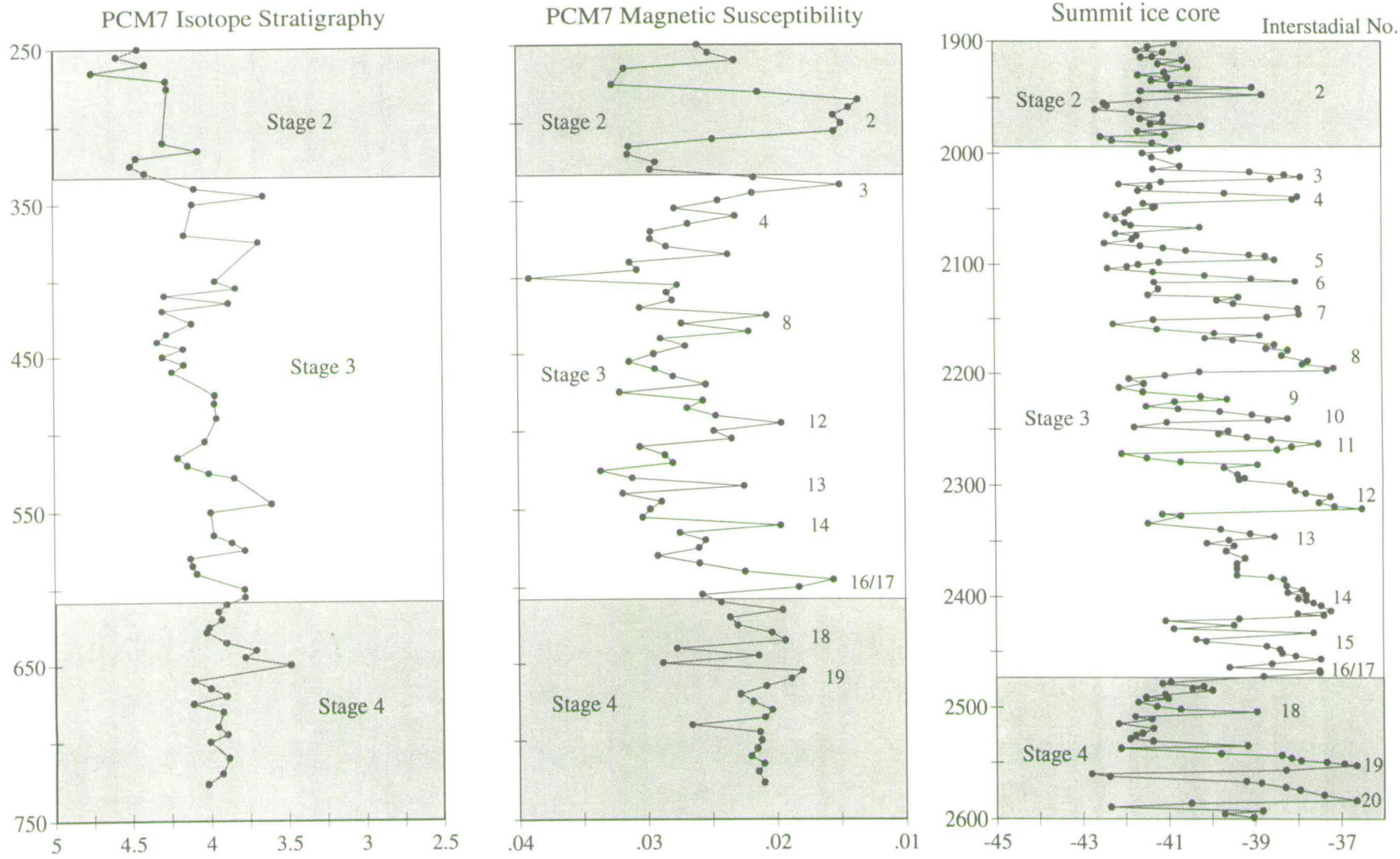

Fig. 7.5. Comparison of magnetic susceptibility for core PCM7 with Summit ice core data, the oxygen isootope stratigraphy of PCM7 is shown on the left. An attempted correlation between the high frequency events in the magnetic susceptibility record and the interstadial events recognised in the Summit ice core has been made. This is designed to show the potential for correlation of parameters such as magnetic susceptibility with ice core records.

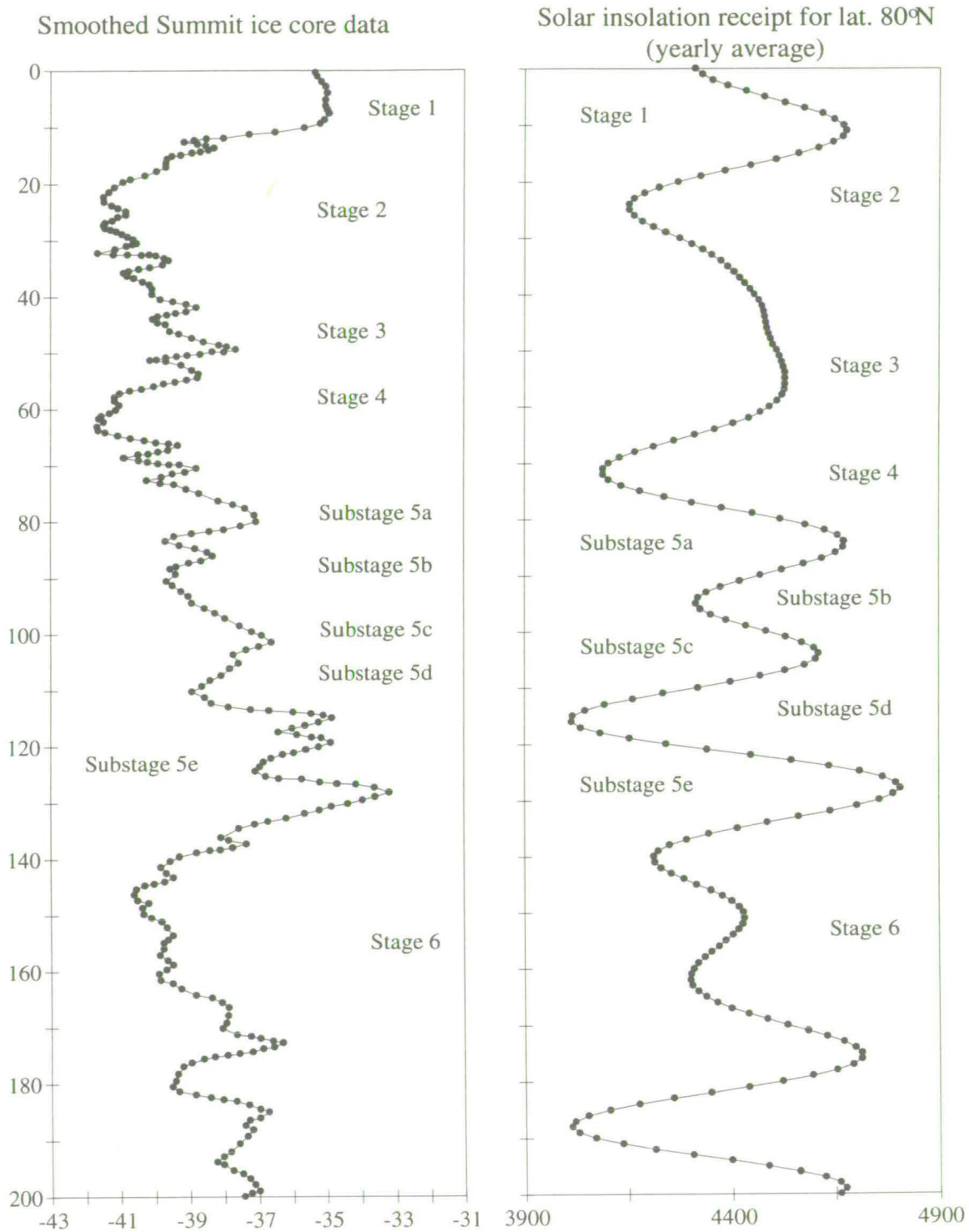

Fig. 7.6. Comparison between smoothed Summit ice core data on the left (Dansgaard et al., 1993), and record of solar insolation variation over the past 200 ka (from Berger, 1978). The scale for the Summit ice core is per mil variation w.r.t. PDB standard. The solar insolation scale is watts per square meter. Notice the general similarity between the two records, except for during stage 5 where the ice core has a greater amplitude during substage 5b, while the solar insolation has a greater amplitude during substage 5d. Also notice the time lag between the major troughs in insolation receipt, glacials, and the major troughs in Summit isotope values relating to temperature minima.

One would expect these two records to be very similar, indeed they are similar, but certain differences can be recognised. The most significant difference is found within stage 5. The Summit ice core documents a major fall in temperature during substage 5b, and only a minor change within substage 5d. The insolation data suggest the major cold event during stage 5 took place within substage 5d, and substage 5b was relatively unimportant. The insolation data further suggest substage 5d was the most extreme cold event during the last 200 ka at 80°N, with stage 4 being more extreme than much of stage 6 and stage 2. Another major difference is present in the phase relationships between these two curves, an offset being visible. The Summit ice core data tends to lag behind the solar insolation receipt, since the temperature changes over the Greenland ice sheet respond after the solar radiation drops. This is particularly noticeable in the substage 5d, substage 5b, stage 4 and stage 2 records (fig. 7.6), where the Summit record shows a lag of approximately 5-10 ka. This may reflect the time lag between a reduction in energy input (solar radiation), and the resulting temperature drop induced by ice advance, increase in height of the Greenland ice sheet and changes in ocean circulation. Support for this idea is gained from comparison of the solar insolation data with the oxygen isotope records of PCM5 and PCM30 (fig. 7.7), which show these lags, albeit less clearly.

The $\delta^{18}O$ evidence from cores PCM5 and PCM30 suggests that stages 2 and 6 were both more extreme than any period during stage 5 and stage 4. Fig. 7.7 shows the isotopic data of PCM5 and PCM30 plotted with the solar insolation curve for lat. 80°N. The terrestrial evidence is also at odds with the solar insolation data. The last major ice advance occurred during stage 2, when ice reached the continental shelf edge along the Spitsbergen margin (Svendsen *et al.*, 1992). The logical explanation for these discrepancies is that the size of an ice advance does not simply increase with temperature decrease. One of the most important parameters to ensure major ice advance is the moisture supply (Boulton *et al.*, 1982). A larger moisture supply will increase the rate and amplitude of ice advance. This is evidenced by the lack of major glaciers in very cold areas of the Arctic which are isolated from relatively warm ocean currents or storm tracks which could provide moisture. The major moisture supply for ice masses around the Norwegian-Greenland Sea is from evaporation from the ocean. Evaporation will be greater from a relatively warm sea, although relatively cold temperatures are needed to allow ice to accumulate on land. The high frequency of storms generated by the Iceland-Greenland cyclone track (Kellogg, 1980) from the eastern coast of North America also provides a significant moisture source. A balance between the two is needed to allow rapid evaporation and accumulation of snow and ice on land. This does not necessarily occur during the coldest periods.

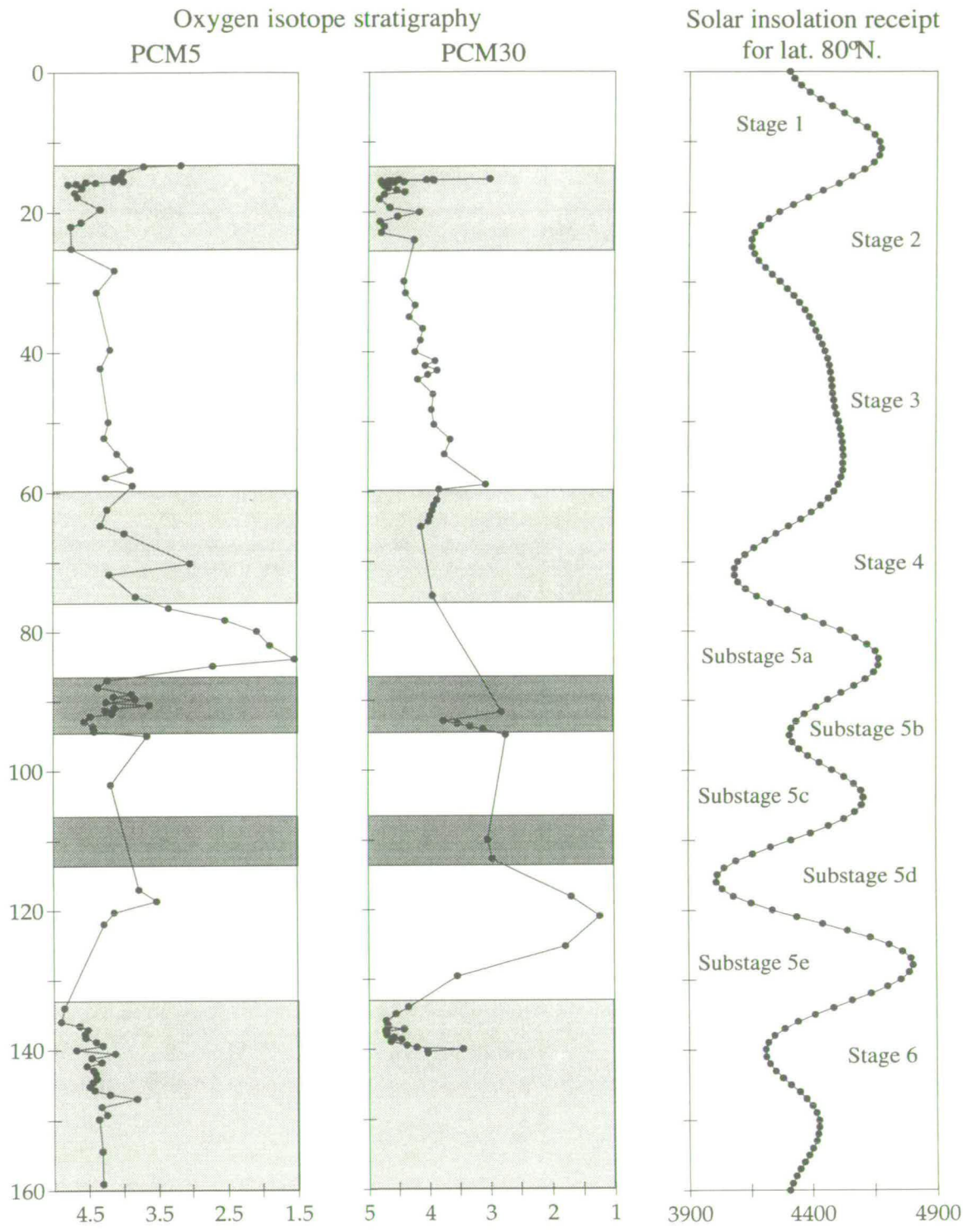

Fig. 7.7. Comparison between oxygen isotope results from marine cores PCM5 and PCM30 and record of solar insolation variation over the last 160 ka. The oxygen isotope data has a scale of per mil variation w.r.t. PDB standard. The scale of solar insolation is watts per square meter. Notice the difference between the sets of data within stage 5, the solar insolation data shows the lowest values within substage 5d, while the marine cores shows substage 5b as the most extreme event within stage 5.

Boulton *et al.*, (1982) postulated an antiphase relationship between ice advance in high latitude areas and mid latitude areas. Large ice advances would be found on Spitsbergen and Greenland during mid latitude interstadials, when relatively warm North Atlantic waters and storm tracks penetrated into the Iceland-Norwegian Sea providing a moisture supply. In such a model major mid latitude European ice masses would advance when the Polar Front was at its southerly extreme, i.e. during the coldest periods. Storm tracks would be diverted to mid latitudes thus starving the high latitude ice masses.

It is possible that during stage 3 the moisture supply to the Spitsbergen and Greenland ice masses was enhanced by some Atlantic water influence. Such an influence was not, however, seen in the planktic foraminiferal record (only specimens of *N. pachyderma* (sinistral) were found in PCM7 during stage 3), but this does not preclude minor Atlantic water influx into some portions of the Norwegian-Greenland Sea, and an associated increase in storms. The warmer sea surface temperatures would provide moisture leading to advances of high latitude ice sheets culminating in the large ice sheet of stage 2, reaching the Spitsbergen shelf edge. By comparison, the ice sheets of stage 4 were relatively starved due to cold surface waters, and thus little evaporation could occur to supply the continental ice masses with moisture. The major ice advance found during substage 5b from cores PCM5 and PCM30 agrees with the Summit ice core, but not the insolation record. This may be due to a sustained build-up beginning perhaps as early as substage 5d, but only reaching its full extent during substage 5b. The relatively cold conditions during substage 5d would not promote as rapid an advance as warmer conditions during substage 5c. It may be that a relatively warm prolonged period is required to produce an ice advance reaching the continental shelf, while very cold conditions lead to a starvation of ice masses, producing only minor ice advances.

It has recently been suggested by Imbrie *et al.*, (1994) that the 100ka cyclicity seen in many environmental records may be produced by internal driving mechanisms. The northern hemisphere ice sheets are envisaged as the driving force. Once these ice sheets reach a critical size, they stop responding linearly to Milankovitch forcing, and drive climatic and oceanic responces themselves which mimic the Milankovitch cycles. Ice sheets grounding on the continental shelves become unstable, leading to mass wasting, and resulting deglaciation setting in motion the 100ka oscillations. There seems to be a growing body of evidence pointing to an internal driving mechanism for ice sheet growth and decay, not relying solely on insolation changes from orbital parameters. Ice sheets reaching a critical mass, then collapsing causing

deglaciation. Andrews and Tedesco (1992) suggested that the Heinrich events of the North Atlantic are caused by large scale surging of the Laurentide ice mass. This would explain why their cyclicity does not fit with solar insolation changes. Oerlemans (1993) reached a similar conclusion, that Heinrich layers are caused by rapid ice advance once the Laurentide ice mass reaches a critical size, and is not dependant on climate cooling.

The results from this study suggest that solar insolation is not the sole driving force in the global climate causing ice sheet growth and decay. The IRD records of PCM5 and PCM30 do not correlate with the solar insolation records particulary well (fig. 7.8). This supports the above mentioned idea that the Milankovitch cyclicity may not be the all encompassing driving mechanism it was previously thought to be. Potentially ice sheet dynamics such as surging may play a role in the appearance of dropstones in these records. Indeed it has been suggested that the catastrophic collapse of the Laurentide ice sheet may be the cause of Heinrich events (Andrews and Tedesco, 1992). Once the Laurentide ice sheet reaches a certain critical size pressure melting takes place at its base. Geothermal heat also adds to the basal melting leading to increased lubrication and surging of the ice sheet. A model of the Laurentide ice sheet has been produced that explains the 7ka periodicity of Heinrich events by the mechanism outlined above (MacAyeal, 1993a; MacAyeal, 1993b). However, the dynamics of the Spitsbergen ice sheet would not produce such a periodicity, major surging events have not been modelled for this ice cap. Our data suggests that the moisture supply plays an important role in the ice sheet build up. Major dropstone events do correlate to meltwater spikes, but only if there was enough time and moisture supply for the ice sheet to grow during interdtadial periods like stage 3 and substage 5c. Spectral analysis was attempted on the dropstone record of PCM5, unfortunately no clear cyclicity was seen.

7.4. Glacial history of the Spitsbergen margin as evidenced from marine cores - Comparison with terrestrial data

A reconstruction of the glacial history of the Spitsbergen ice mass over the past 200 ka has been made in chapter 3 from the evidence of marine cores. The main source of data for this reconstruction was the presence of ice rafted detritus (IRD) in the marine cores seen in x-rays of the undisturbed half of the cores. It was assumed that due to the proximity of the core sites to the Spitsbergen margin the majority of IRD seen in the cores originated from the Spitsbergen ice cap.

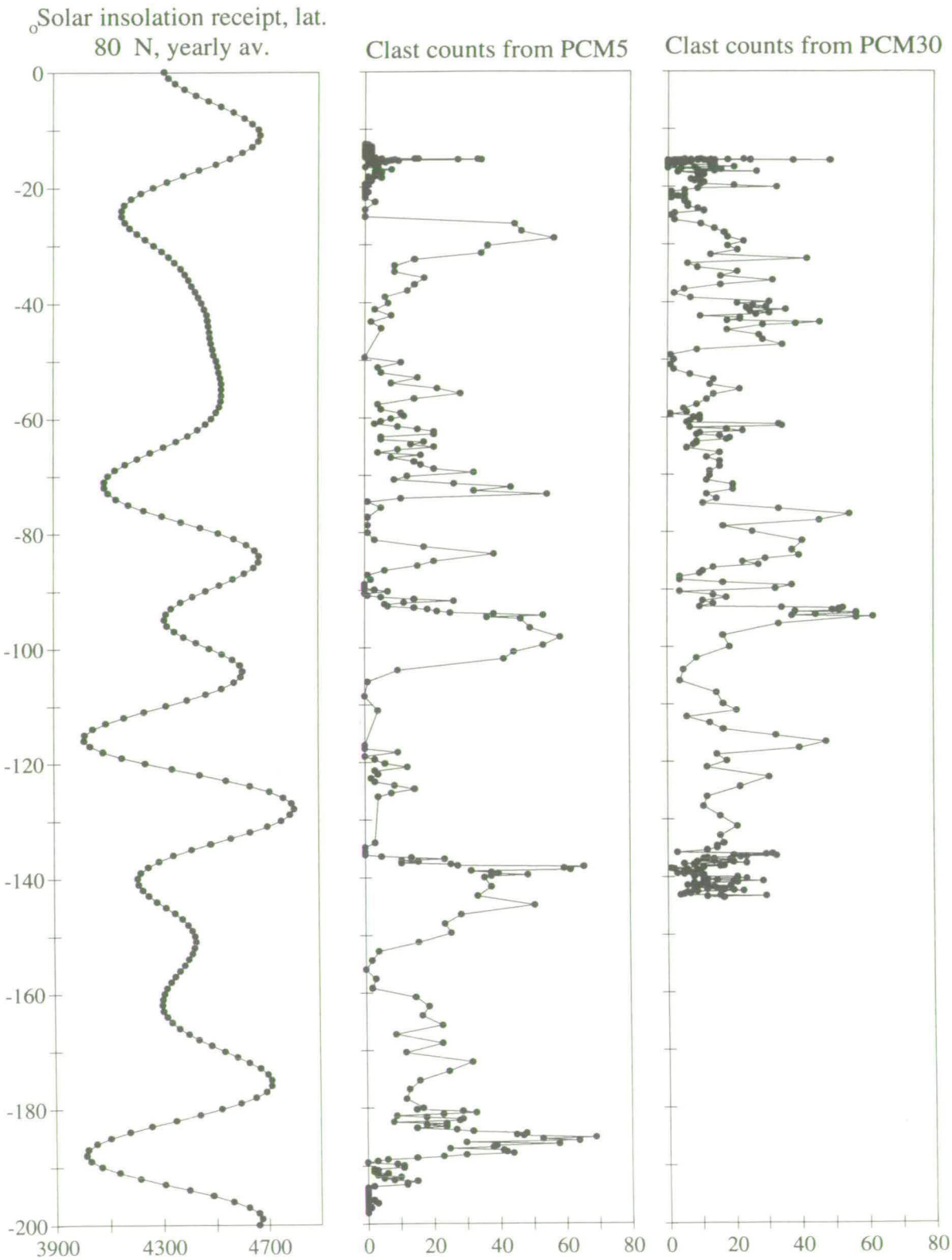

Fig. 7.8. Comparison between solar insolation receipt and dropstone records of PCM5 and PCM30. Note the poor correlation between the two sets of data, this is more fully explained in the text.

This was supported by the close correlation between silica content and IRD content within core PCM5 (large areas of Spitsbergen consist of sandstones, a source of quartz forming the silica peaks).

From the sedimentology of cores PCM5, PCM7 and PCM30, periods were recognised when dropstones were abundant due to rapid iceberg calving and melting. Periods were also recognised when large quantities of poorly sorted coarse detritus were seen in the cores. This material was interpreted as having been pushed over the shelf edge when the ice masses were at their maximum extent. These periods where also identified by the oxygen isotope signature, occurring during periods of high $\delta^{18}O$ composition of foraminifera corresponding to glacial periods (for example during stages 2 and 6). Interglacial periods were recognised by the almost total lack of IRD in the cores and by the light $\delta^{18}O$ foraminiferal composition. Fig. 3.18 summarises the IRD record and calving scenarios identified from the cores in this study. The IRD peaks seen in the cores may have been produced by several scenarios. Some IRD peaks were produced by rapid expansion of ice across the continental shelf during the build up to a glacial peak, or alternatively surging plays a role. When ice was at its maximum extent at or near the shelf edge, IRD was being produced in large amounts due to summer melting. There were also strong IRD peaks during the early melting phases after a glacial maximum. So peaks in IRD can occur not only during glacial maximum periods, but also during the build up, and rapid retreat of the ice front. Certain periods were also recognised during peak glacial periods when permanent pack ice covered the whole area and drastically reduced the influx of IRD to the core sites (also reducing the planktic foraminiferal productivity). Stadial periods were seen to have low IRD quantities possibly because the moisture supply was very low, ice would stagnate therefore reducing calving rate, starving the area of IRD during these periods.

From this evidence a model was proposed to explain the IRD fluctuations found in the cores. The model consists of six different states of ice distribution over the continental margin of Spitsbergen, and is summarised in fig. 3.18. Using this model an interpretation of the history of the Spitbergen ice cap was made. The ice advances recognised from the data from cores PCM5, PCM7 and PCM30 are summarised in fig. 7.9 along with the conclusions from two other studies from this area. The conclusions from the study of Hebbeln (1992) are based on IRD recognised in a series of cores from the Fram Strait and Spitsbergen margin, and those from Mangerud and Svendsen (1992) are based on the examination of sediments exposed in cliff sections at the head of Isjforden on Spitsbergen.

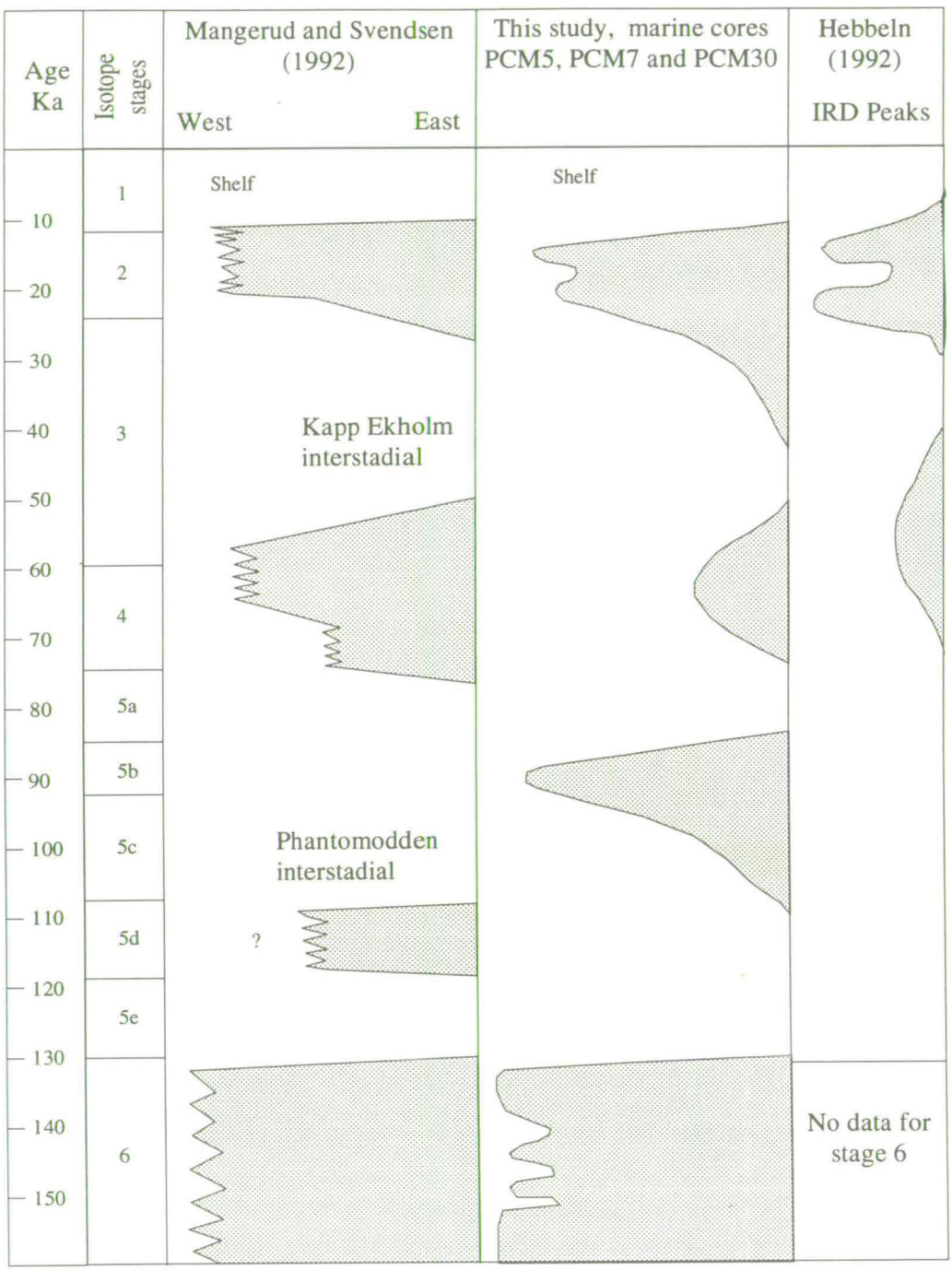

Fig. 7.9. Summary diagram showing on the left advance and retreat of Svalbard glacial terminus' from Mangerud and Svendsen (1992). The curve on the right shows the input of terrestrial material to Fram Strait sediments, from IRD content of marine cores, from Hebbeln (1992). The curve in the centre represents an interpretation of the relative iceberg calving rates, and extent of advance of Svalbard glaciers from results from marine cores PCM5, PCM7 and PCM30 from this study. The age and oxygen isotope stages are shown on the left.

The results of this study suggest four ice advances over the past 200 ka. The largest advance occurred during stage 6. Periods within stage 6 were identified when permanent pack ice covered the Spitsbergen margin year round, as evidenced by the sudden reduction in IRD and foraminiferal abundances in core PCM5. The planktic and benthic foraminiferal evidence presented in chapter 6 also supports the conclusion that stage 6 was a more intense glacial period than any other period since. The abundance of *C. teretis* during stage 6 and very high planktic foraminiferal abundances suggests a high food supply from the ice edge close by. During stage 2 this species is absent from PCM5 and was replaced by the epifaunal species *E. umbonatus* (which can survive with a lower food supply) and planktic foraminiferal abundances are lower. This suggests that the ice margin was further away during stage 2, i.e. further inland nearer core site PCM7. This agrees with other evidence from terrestrial records in this area (Mangerud and Svendsen, 1992; Miller et al., 1989).

Evidence for an advance of ice during stage 5 is conflicting. The results of Mangerud and Svendsen (1992) suggest the advance took place during substage 5d, the size of this advance is uncertain. The oxygen isotope evidence and foraminiferal evidence from the cores in this study suggest the advance during stage 5 reached a peak during substage 5b (agreeing with the Summit ice core evidence). There is evidence that the advance may well have begun during substage 5c, and disappeared during substage 5a (from the presence of IRD). Though the absence of IRD in the cores does not exclude the possibility of the advance beginning earlier during substage 5d. Hebbeln (1992) finds no evidence of an advance during stage 5 at all. Boulton *et al.* (1982) recognised a major advance starting during substage 5d and only disappearing during substage 5a. This idea agrees more closely with the results of this study, though our evidence suggests the advance was slightly later. That is to be expected as our data is from the continental slope, and will only record an advance once the ice reaches the shelf and begins calving. All studies indicate an advance of varying sizes during stage 4 and early stage 3.

It is now generally accepted that a major advance also occurred during stage 2, when ice reached the shelf edge (Svendsen *et al.*, 1992). The beginning of this advance is still uncertain. Mangerud and Svendsen (1992) suggested a very rapid build up starting late on in stage 3, whilst our evidence points to a slower build up beginning earlier during mid to late stage 3. This greater time period seems more likely considering the magnitude of the advance. There is no evidence from terrestrial sites for significant ice advance during Younger Dryas times. The particle size and IRD

data from core PCM7 also supports this (fig. 3.16). No increase in IRD is found during or immediately after the Younger Dryas suggesting an ice advance onto the shelf. The oxygen isotope and foraminiferal abundance data, however, do indicate changes in oceanography at this time. Colder surface waters returned during the Younger Dryas and disappeared immediately afterwards; this is discussed in more detail below.

7.5. Palaeoceanography and meltwater history of the Fram Strait and Spitsbergen margin

The palaeoceanography of the Fram Strait and Spitsbergen margin over the last 200 ka is poorly understood. The initial problem to overcome, when studying the palaeoceanography of an area, is the problem of age control. This is especially difficult in the Fram Strait-Spitsbergen margin area during stage 5 due to low foraminiferal numbers and the local effects of meltwater. The age control for this study, and most other studies, has been achieved using oxygen isotope stratigraphy (as mentioned earlier). Palaeoceanographic interpretations have been made using oxygen and carbon stable isotope analysis of planktic and benthic foraminifera, absolute abundance counts of planktic and benthic foraminifera, counts of individual foraminiferal species and the IRD record.

The present oceanography of the area has been outlined in chapter 1, and is summarised in fig. 1.2. There are three main surface water masses affecting the Greenland Sea (Swift and Aagaard, 1981). Atlantic waters flowing up the eastern side of the Norwegian-Greenland Sea forming the relatively warm and saline Norwegian Atlantic Current and West Spitsbergen Current. Polar surface water flows to the south from the Arctic Ocean. This forms the East Greenland Current flowing along the eastern Greenland margin, and is cold with a low salinity. The third surface water mass in this area lies between the former two , and is termed Arctic water (Helland-Hansen and Nansen, 1909). This is a mixture of warm saline North Atlantic water and cold fresher Polar water. It forms an anticlockwise circulating gyre in the central Greenland Sea. It is bounded to the west by the Polar front and to the east by the Arctic front.

Arctic Intermediate Water (AIW) lies below the surface currents, formed from mixing and cooling of dense warm Atlantic waters with cold Polar waters. This forms an upper and lower layer. There is partial cooling and mixing of these intermediate

layers to form the cold dense deep waters of the Greenland Sea Deep Water (GSDW), also added to by very cold waters from the continental shelves (Carmack and Aagaard, 1973; Swift and Aagaard, 1981 and Quadfasel and Meincke, 1987). The upper AIW flows to the south into the Iceland Sea, across the Jan Mayen Fracture Zone. This upper AIW constitutes a major proportion of the overflow of dense water into the North Atlantic through the Denmark Strait forming NADW (Swift and Aagaard, 1981). At the present time the Greenland Sea is one of the main areas of formation of North Atlantic Deep Water (NADW), due to the northward flow of North Atlantic surface water into the area.

The production of NADW is reduced during glacial periods, and is formed further south in the North Atlantic itself (Duplessy *et al.*, 1980). During deglaciation the influx of North Atlantic surface waters to the Norwegian-Greenland Sea leads to the renewal of production of NADW, causing redistribution of heat from low to high latitudes, encouraging high latitude melting. This process can be interrupted by the effects of meltwater, for example during the Younger Dryas (Broecker *et al.*, 1988). The effects of meltwater in the Greenland Sea can be partially assessed from the cores in this study. This will be discussed later.

It was previously thought that the Norwegian-Greenland Sea was covered by year round pack ice during glacial periods (McIntyre *et al.*, 1976 and Kellogg, 1980). The results of foraminiferal counts from this study shows conclusively that the Spitsbergen margin was seasonally ice free during peak glacial periods, for example during stages 2 and 6. The absolute abundances of foraminifera are much higher during glacial periods. There must have been seasonally ice free conditions to support these numbers. The nutrient supply supporting such high foraminiferal abundances originated from melting pack ice, and, possibly more importantly, terrestrially derived organic material carried to the shelf edge by ice tongues extending from the outlet glaciers of the Spitsbergen ice mass. This is supported by the correlation between IRD and foraminiferal abundances of cores PCM7 and PCM5 (see figs. 3.9 and 3.10). Ice edge upwelling of nutrient rich deep waters may have contributed as well. Productivity, as estimated from foraminiferal abundances (chapter 6), is considerably lower during interglacial periods in the cores in this study. This may simply reflect a much higher productivity during glacials in cores near the ice edge. Foraminiferal abundances would be considerably lower under the ice or away from the melting ice edge, the source of nutrients. This result is the opposite to observations made from past studies from the Norwegian-Greenland Sea and Arctic Ocean (Kellogg, 1973; Sejrup *et al.*, 1984 and Belyaeva and Khusid, 1990). Here peak glacial periods are

characterised by seasonally ice free conditions, due to summer melting, with productivity being locally very high, due to the nutrient supply from melting sea ice and melting ice tongues.

The influx of North Atlantic surface waters to the Spitsbergen margin can be recognised by the appearance of a subpolar foraminiferal fauna, characterised by *N. pachyderma* (dextral) and *G. bulloides,* replacing the Polar fauna which is dominated by *N. pachyderma* (sinistral). Over the past 200 ka, covered by the cores in this study, the subpolar fauna was only recognised during the last glacial-interglacial transition. This has very important palaeoceanographic implications, as periods of North Atlantic influx to the Greenland Sea ought to promote the production of NADW. Thus producing a more vigorous global circulation system leading to an interglacial climate.

There is no foraminiferal evidence for renewed influx of N. Atlantic waters into the area during any part of the last interglacial (stage 5). This is particularly strange as substage 5e has been identified as being as warm or slightly warmer than present in the Greenland Sea (Miller *et al.*, 1989 and LIGA Members, 1991). A major melting event can be identified from the $\delta^{18}O$ record of planktic foraminifera in core PCM30 during substage 5e. A similar event can be recognised during substage 5a in core PCM5 (chapter 4, figs. 4.9 and 4.10). It seems unlikely that during these major melting episodes, North Atlantic waters did not reach the area, but subpolar foraminifera are not recorded in core PCM5 at this time. The absolute foraminiferal abundances during much of stage 5 are very low, possibly due to increased carbonate dissolution. The other possibility is that the large volumes of meltwater produced by these melting events may produce an environment in which the foraminifera cannot live. Estimates of the intensity of this meltwater spike (chapter 4) suggest a body of water with salinity 3‰ less than normal marine salinity would have been present in the Fram Strait. One of these ideas may explain the absence of *N. pachyderma* (dextral). Also the oxygen isotope record of PCM5 does not show substage 5e due to low foraminiferal abundance.

Measurements of $\delta^{13}C$ from benthic foraminifera (chapter 5) provides evidence of more vigorous circulation during stage 5, similar to the standard interglacial circulation. Heavier $\delta^{13}C$ values are normally indicative of relatively new oxygenated deep waters (for example North Atlantic interglacial periods), while lighter $\delta^{13}C$ values are commonly found in old stagnant deep waters (North Atlantic glacial periods). Corrected $\delta^{13}C$ values of between 1.0 and 1.2‰ were observed from

specimens of the benthic foraminiferal species *E. umbonatus* from core PCM5. These $\delta^{13}C$ values are heavier than those measured during stages 6, 4 and 3, and similar to the $\delta^{13}C$ values of NADW today, 0.5 to 1.0‰ (Kroopnick, 1985). These results suggests deep water production took place during stage 5. This implies that N. Atlantic waters did reach the Greenland Sea during stage 5. There is some support for this idea in the absolute abundances of certain benthic foraminiferal species. Around late substage 5c-early substage 5b two species, *P. bulloides* and *C. wuellerstorfi*, suddenly became dominant (see fig. 6.5). These two species possibly mark the onset of new deep water circulation, and most likely the formation of NADW in this area. North Atlantic waters certainly invaded the Norwegian Sea during stage 5 (Miller et al., 1989; Mangerud and Svendsen, 1990 and LIGA members, 1991), so NADW production would have taken place there if not further north in the Greenland Sea .

Faunal evidence, from core PCM7, suggests that the initial influx of N. Atlantic waters reached the Spitsbergen margin after the last glacial maximum of stage 2 at 12.3 ka. There is, however, oxygen isotopic evidence of two melting episodes before this time; the first one at 15.5 ka, then another event at 13.6 ka. This demonstrates that it is possible to have significant melting events with no faunal evidence of the influx of N. Atlantic waters, and this may well have been the case during substage 5e. A meltwater lid above the Atlantic Water may have killed the foraminiferal. To facilitate full deglaciation, however, North Atlantic waters are almost certain to appear in the area. The initial melting event identified at 15.5 ka coincides with melting episodes recognised in other cores from the Fram Strait and the Norwegian Sea (Jones and Keigwin, 1988 and Sarnthein *et al.*, 1992). The second meltwater event recognised in core PCM7, at 13.6 ka, was identified in several cores from the Norwegian Sea (Sarnthein *et al.*, 1992). One core, M 23259 from off the Barents Shelf, also identified a major melting event at 12.3 ka with an associated influx of subpolar foraminifera (Sarnthein *et al.*, 1992), the same situation as observed in PCM7. This could be an artifact, however, of the age model used in this study, as correlation was made to core M 23259 in the production of the age model. Independant radiometric dates for core PCM7 are forthcoming and will either confirm or refute a contemporaneous timing of meltwater events compared to the Barents Sea. The influx of North Atlantic waters for the first time at 12.3 ka is supported by evidence from molluscs from a marine section along the Spitsbergen margin examined by Mangerud (1977). North Atlantic waters entered the Norwegian further south earlier than this however. Lehman and Keigwin (1992) recognised an influx of subpolar foraminifera associated with the influx of North Atlantic water 13.6 ka, from

the TROLL 3.1 core from off the southern coast of Norway. This influx of Atlantic water was not strong enough to reach as far north as the Greenland Sea.

Polar waters re-invaded the Spitsbergen margin at 12 ka (subpolar foraminifera being replaced by polar ones) until 10.5 ka, when it was replaced by Atlantic waters again from 10.5 to 10.3 ka. The subpolar fauna disappeared from 10.3 until 10 ka, then Atlantic waters returned up to the present day. The final influx of Atlantic water at 10 ka was considerably stronger than the previous occurrences (evidenced by an increase in the percentage of subpolar fauna compared to the earlier influxes). The cold spell from 12 to 10.5 ka can be seen in M 23259 and other cores from the Norwegian sea (Sarnthein *et al.*, 1992), but further details are difficult to resolve, due to the lower resolution of these cores.

Diatom data from the Norwegian-Greenland Sea (Koç *et al.*, 1993) shows an ice free corridor extending north-south along the coast of Norway to approximately 70°N by 13.4 ka. The rest of the area is interpreted as being covered by sea ice. This agrees partially with the data from this study, showing a significant melting phase, but no evidence of North Atlantic waters reaching the Spitsbergen margin at 13.6 ka. The diatom flora does not show the significant warming event at 12.3 ka, which resulted from the influx of North Atlantic waters as far north as the Spitsbergen margin. This would have created at least a narrow ice free corridor, and quite possibly more extensive ice free areas in the Norwegian-Greenland Sea. The decrease in diatom flora identified from 11.2 to 10.2 ka agrees fairly well with the timing of the retreat of Atlantic waters as evidenced from the planktic foraminifera of core PCM7. The major incursion of North Atlantic waters producing considerable ice free areas in the Norwegian-Greenland Sea identified from the diatom flora had occurred by 9 ka: this is in agreement with our data. The timing of the events from the diatom evidence agree with that of the foraminiferal studies from core PCM7 (and other cores mentioned earlier), but the magnitude of the changes are significantly different. The major warming from diatom evidence occurred between 10.2 and 9 ka, while the foraminiferal evidence suggests an earlier major warming event took place at 12.3 ka, followed by a further warming event at 10 ka.

7.6. The recognition and influence of meltwaters locally and their effect on deep water circulation

The production of meltwater from the Greenland, Svalbard and Arctic ice masses has had a major influence on the palaeoceanography of the Greenland Sea, and palaeocirculation of global oceans. It has been suggested that the production of large volumes of low salinity meltwater may form a 'lid' of low density surface water in the North Atlantic Ocean (Broecker *et al.*, 1988). The low salinity of this 'lid' will prevent sinking of surface waters (usually produced by winter cooling) therefore shutting down the production of NADW. This would reduce the global circulation system, preventing the re-distribution of heat from tropics to poles, leading to general cooling at mid to high latitudes, causing ice advance. He suggested this mechanism as the causal factor of the Younger Dryas readvance recognised over much of the Northern Hemisphere.

This process may well take place in the Norwegian-Greenland Sea as well. Meltwater influxes can be recognised from the oxygen isotope record of both planktic and benthic foraminifera. Two major meltwater events have been recognised in stage 5, during substages 5e and 5a, from cores PCM30 and PCM5 respectively (fig. 4.4). The resolution of PCM30 and PCM5 over this time period is not great enough to observe possible ice readvances which may have occurred due to these meltwater 'lids'. These light $\delta^{18}O$ meltwater spikes were also identified in the benthic foraminiferal $\delta^{18}O$ record (figs. 4.9 and 4.10). The benthic foraminiferal meltwater spikes probably originated from the formation of dense meltwater brines. Meltwater brines could be produced by repeated melting and re-freezing leading to a concentration of salt, producing cold saline meltwater that sinks to the sea floor adding to the Greenland Sea Deep Water (see chapter 4). Over much of the stage 2 to stage 1 transition meltwater had a major influence on both planktic and benthic foraminiferal $\delta^{18}O$ records (shown in fig. 4.7).

One possibility that has not been considered is that North Atlantic waters flowing northwards during substages 5e and 5a might sink below the meltwater 'lid' recognised in the planktic foraminiferal $\delta^{18}O$ records. A strong meltwater cap would have very low salinity (see chapter 4 for estimates) and would, therefore, have a low density compared to North Atlantic waters. The large contrast might prevent mixing causing the North Atlantic water to sink below the meltwater as is flows northwards. A similar situation is seen in the Arctic Ocean today. Such a mechanism would help explain the lack of subpolar foraminifera during substages 5e and 5a in the cores of

this study. The Atlantic waters would be too deep for the foraminifera to live in and the surface waters would too low a salinity for them. This idea also explains the evidence for renewed deep water formation during stage 5 seen in the benthic $\delta^{13}C$ record of PCM5. The Atlantic water below the meltwater would sink to produce deep water circulation as it does at the present time. The benthic foraminiferal $\delta^{13}C$ signature records such a process, and the presence of *P. bulloides* and *C. wuellerstorfi* also support renewed deep water circulation. Such a mechanism has serious implications for the salt conveyor system suggested by Broecker (1982). Broecker suggests a meltwater 'lid' would prevent deep water renewal, thus reducing circulation, but in the idea outlined above sinking could still occur below a meltwater 'lid' leading to deep water formation and increased global circulation.

The period of renewed NADW production should be visible in the $\delta^{18}O$ and $\delta^{13}C$ records of the benthic foraminifera of core PCM7. The results from these two lines of data provide conflicting evidence for the production of NADW. The benthic $\delta^{13}C$ values from *M. barleeanum* from core PCM7 show no evidence of renewed deep water production over the last deglaciation (fig. 5.7). The $\delta^{13}C$ values should get heavier when new deep water circulation is initiated. The opposite trend is seen at the point when North Atlantic waters first enter the area. This may reflect the microhabitat of *M. barleeanum*, which is an infaunal species living deeper than *C. teretis* or *E. umbonatus* (which is an epifaunal species), so would not record so accurately changes in bottom water $\delta^{13}C$ composition.

The benthic foraminiferal $\delta^{18}O$ curve does, however, show the meltwater effect on the benthics, as well as the changes in bottom water circulation (fig. 4.7). The meltwater effect is represented by the shaded section between the drop in $\delta^{18}O$ due to the ice volume effect (Fairbanks, 1989) and the foraminiferal $\delta^{18}O$ curve (fig. 4.7). From 15.5 ka until 10 ka the foraminiferal $\delta^{18}O$ values are decreasing at a faster rate than the predicted change due to global ice volume changes (the difference between the two being produced by meltwater brines on the sea floor). There is no evidence for renewed deep water circulation, or production of new deep water over this period. At 10 ka, however, the benthic foraminiferal $\delta^{18}O$ curve suddenly changes, increasing and cutting across the predicted $\delta^{18}O$ change from ice volume decreasing. This must be produced by a significant change in deep water characteristics, marking the time when a new circulation regime began. Immediately prior to this change a very strong melting event can be recognised in both planktic and benthic $\delta^{18}O$ records (10.5 to 10.2 ka). This coincides with an increase in the percentage of subpolar planktic foraminifera found in core PCM7, from 10.5 to 10.3 ka (see fig. 6.10). The subpolar

foraminifera disappear from 10.3 to 10 ka. It seems likely that this disappearance was due to the meltwater influx affecting the surface waters rather than the Atlantic water influx stopping. After this there is a significant increase in the percentage of subpolar foraminifera, between 35 and 40% compared to the previous values of approximately 20%. This suggests a considerably stronger Atlantic water influx at 10 ka and coincides with the sudden increase in benthic $\delta^{18}O$ values. Therefore the renewed production of a deep water circulation at 10 ka was produced by a stronger influx of Atlantic water than the earlier influxes at 12.3 and 10.5 ka.

The time when this deep water production began at about 10 ka, is also marked by a distinctive change in the benthic foraminiferal assemblage. There is a sudden appearance of *P. bulloides*, and also a marked increase in abundance of *C. wuellerstorfi* and *M. barleeanum* (fig. 7.10). These increases actually occur slightly earlier than 10 ka. The exact timing of these events awaits independant dates which are in progress. *C. wuellerstorfi* has been suggested as being an indicator species of NADW by Weston and Murray (1984), and Lutze and Coulbourn (1984). The sudden appearance of *P. bulloides* associated with a significant increase in the abundance of *C. wuellerstorfi* can be used in this area as a marker for the onset of renewed deep water production. The abundances of both drop off rapidly, especially *P. bulloides*, suggesting that these species are the colonizers marking the initial change, but that other species invade soon after new deep water production has started. The sudden rise in *M. barleeanum* may be due to an increase in nutrient supply, which has a major influence on this species (Murray, 1991).

The earlier influxes of North Atlantic waters, from planktic foraminiferal faunal evidence, did not lead to renewed deep water production according to the benthic foraminiferal $\delta^{18}O$ record, or the individual benthic foraminiferal species abundances. This was due to the weaker strength of the North Atlantic influx during these periods. Evidence from this study has shown that NADW production is not initiated every time North Atlantic surface waters enter the Greenland Sea, a certain strength of influx is needed before deep circulation can begin again. It has also shown that renewed deep water circulation did not begin until approximately 10 ka in the Fram Strait-Spitsbergen margin area. It is likely that the initiation of a more vigorous circulation system after the last glaciation began earlier further south in the Norwegian Sea.

The results of this study have shown that the benthic foraminiferal fauna is not simply related to change in water depth, or water mass type. There seems to be a much stronger link between species present, nutrient supply and palaeocirculation.

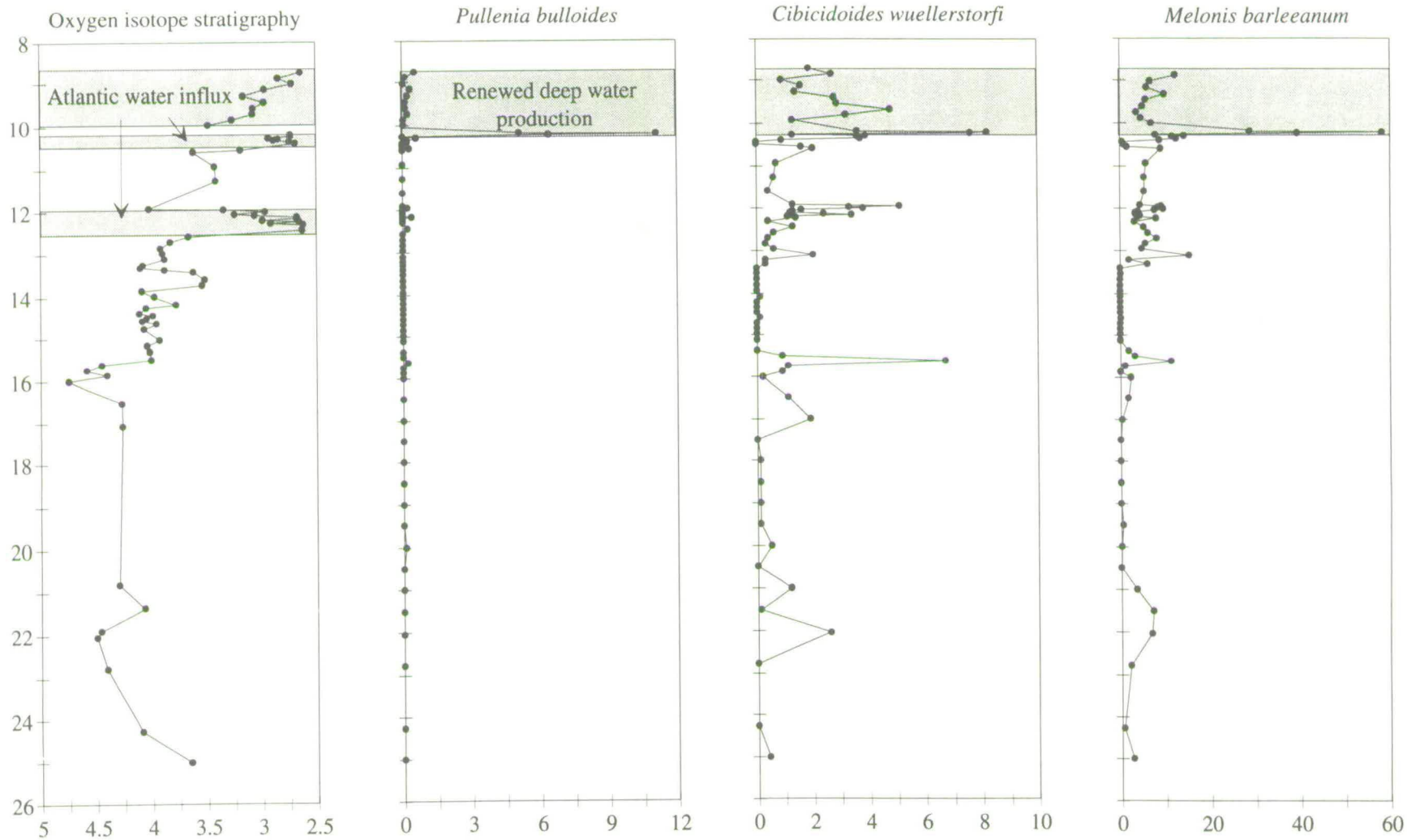

Fig. 7.10. . Planktic foraminiferal oxygen isotope, and benthic foraminiferal species absolute abundances for PCM7 for the time period 26 to 8 ka. Periods of North Atlantic water influx are shaded on the oxygen isotope curve. Periods of renewed deep water production are shaded on the benthic abundance plots. The sudden increase in the absolute abundance of the three benthic foraminiferal species at 10.2 ka marks the onset of deep water circulation in this area. The species abundance counts are in specimens per gram of sediment.

The variation in abundance of benthic foraminiferal species over time can be used in conjunction with stable oxygen and carbon isotope analysis (from both planktic and benthic foraminifera) to recognise subtle changes in ocean circulation and nutrient supply. Using these techniques in isolation severely limits the palaeoceanographic conclusions that can be made. This is highlighted by the recognition of influx of North Atlantic surface waters into the Fram Strait during the deglaciation from stage 2, and the recognition of the initiation of deep water circulation at a later date.

7.7. Concluding remarks

This study examined samples every 5cm, so the resolution is not as high as it could be. The top of PCM7, from 16 ka to 8.5 ka, has a sedimentation rate of approximately 50 cm/ka, producing a sample every 100 years. It is now thought that major changes in ice sheet stability and, therefore, ocean circulation can occur over a decadal time scale (from the Summit ice core record, Johnsen *et al.*, 1993). This makes it even more important to study marine cores at a much higher resolution than in the past. This could be carried out in the future by sampling cores with a similar resolution as PCM7 every cm. This would produce marine climatic data with a decadal resolution. Such a study would be very informative in the Fram Strait area and would improve our knowledge of the timing and extent of deep water circulation over the last deglaciation. It would also aid our understanding of the responses of benthic foraminiferal fauna to changes in palaeoceanographic circulation, making the causal factors of species variation clearer. A similar study in other more southerly areas, such as the Norwegian Sea, would expand our knowledge of changes in surface water, and corresponding changes in deep water circulation during a deglaciation cycle. This would help to increase our understanding of the processes in action during deglaciation, and the possible driving mechanisms of the rapid climatic shifts that have been identified recently from ice core evidence. Such studies would also help elucidate the present debate on the actual influence of Milankovitch periodicity on global climatic change.

References

Aagaard, K., Swift, J. and Carmack, E. (1985): Thermohaline circulation in the Arctic Mediterranean Seas. Journal of Geophysical Research 90 (4833-4846).

Ager, D. V. (1980): The Geology of Europe. London: McGraw-Hill.

Anderson, J. B., Kurtz, D. and Weaver, F. (1979): Sedimentation on the Antarctic continental slope. SEPM Special Publication No. 27 (265-283).

Anderson, J. B., Kurtz, D., Domack, E. and Balshaw, K. (1980): Glacial and glacial marine sediments of the Antarctic continental shelf. Journal of Geology 88 (399-414).

Alexander, I. ,Kroon, D. and Thompson, R. (1993): Late Quaternary paleoenvironmental change on the Northeast Australian margin as evidenced in oxygen isotope stratigraphy, mineral magnetism and sedimentology. In; Davies, P.J., McKenzie, J.A., *et al.*. Proc. ODP, Sci. Results, 133: College Station, TX (Ocean Drilling Program).

Andrews, J., Tedesco, K. (1992): Detrital carbonate-rich sediments, northwestern Labrador Sea: Implications for ice sheet dynamics and iceberg rafting (Heinrich) events in the North Atlantic. Geology 20 (1087-1090).

Bé, A. W. H. (1977): An ecological zoogeographic and taxonomic review of Recent planktonic foraminifera. In: Ramsay, A. T. S. (Ed.): Oceanic Micropalaeontology, 1 (1-100).

Belanger, P. (1982): Paleoceanography of the Norwegian Sea during the past 130,000 years: coccolithophorid and foraminiferal data. Boreas 11 (29-36).

Belanger, P., Streeter, S. (1980): Distribution and ecology of benthic foraminifera in the Norwegian-Greenland Sea. Marine Micropaleontology 5 (401-428).

Belanger, P., Curry, W. B. and Matthews, R. K. (1981): Core-top evaluation of benthic foraminiferal isotopic ratios for palaeo-oceanographic interpretations. Palaeogeography, Palaeoclimatology, Palaeoecology 33 (205-220).

Belyaeva, N. and Khusid, T. (1990): Foraminiferal assemblages in sediments from the Mendeleev Ridge, Arctic Ocean. In Bleil, U, Thiede, J. (eds.), Geological History of the Polar Oceans: Arctic versus Antarctic. (447-454). Kluwer Academic Publishers. Netherlands.

Berger, W. H. (1971): Sedimentation of planktonic foraminifera. Marine Geology, 11 (325-358).

Berger, W. H. (1977): Carbon dioxide excursions and the deep sea record: aspects of the problem. In: Andersen, N. and Malahoff, A. (eds.), The Fate of Fossil Fuel CO2 in the Oceans. Plenum Press, New York (505-542),

Berger, W. H. (1978): Long-term variations of calorific solar radiation resulting from the earths orbital elements. Quaternary Research 9 (139-167).

Berger, W. H. (1979): Stable isotopes in foraminifera. In: Foraminiferal Ecology and Paleoecology, SEPM Short Course No. 6, Houston (156-198).

Berger, W. H., Killingley, J. and Vincent, J. (1978): Stable isotopes in deep sea carbonates:Box Core ERDC-92, west Equatorial Pacific. Oceanologica Acta 1 (203-216).

Berger, W., H., Be, A. W. H. and Vincent, E. (eds.) (1981): Oxygen and carbon isotopes in foraminifera. Palaeogeography, Palaeoclimatology, Palaeoecology 33 (1-277), Special Issue.

Berger, W. H. and Vincent, E. (1986): Deep-sea carbonates: Reading the carbon-isotope signal. Geologische Runschau 75/1 (249-269).

Bloemendal, J. (1989): Paleoenvironmental implications of the magnetic characteristics of sediments from Deep Sea Drilling Project Site 514, southeast Argentine Basin. In Ludwig, W. and Krasheninnikov, V. *et al.* (eds.) Initial Reports DSDP, Vol. 71.

Bond, G., Heinrich, H., Broecker, W., Labeyrie, L., McManus, J., Andrews, J., Huon, S., Jantschik, R., Clasen, S., Simet, C., Tedesco, K., Klas, M., Bonani, G., Ivy, S. (1992): Evidence for massive discharges of icebergs into the North Atlantic ocean during the last glacial period. Nature 360 (245-251).

Boulton, G. S. (1990): Sedimentary and sea level changes during glacial cycles and their control on glaciomarine facies architecture. In Dowdeswell, J., Scourse, J. (eds.), Glacimarine Environments: Processes and Sediments. Geological Society Special Publication 53 (15-52).

Boulton, G. S., Baldwin, C. T., Peacock, J. D., McCabe, A. M., Miller, G., Jarvis, J., Horsefield, B., Worsley, P., Eyes, N., Chroston, P., Day, T., Gibbard, P., Hare, P. and von Brunn, V. (1982): A glacio-isostatic facies model for the Quaternary events in Spitsbergen and the Arctic. Nature 298 (437-441).

Boyle, E. A. (1988): Vertical oceanic nutrient fractionation and glacial/interglacial CO_2 cycles. Nature 331 (55-56).

Broecker, W. S. (1982): Ocean chemistry during glacial time. Geochem. Cosmochim. Acta. 46 (1689-1705).

Broecker, W. S. (1982): Glacial to interglacial changes in ocean chemistry. Progr. Oceanog., 11 (151-197).

Broecker, W. S. (in prep.): The glacial world according to Wally. Draft of book in preparation.

Broecker, W. S., Andree, M., Wolfi, W., Oeschger, H., Bonani, G., Kennett, J. and Petreet, D. (1988): The chronology of the last deglaciation: Implications to the cause of the Younger Dryas. Paleoceanography 3 (1-19).

Broecker, W. S., Bond, G., Klas, M., Clark, E., McManus, J. (1992): Origin of the North Atlantic's Heinrich events. Climate Dynamics 6 (265-273).

Broecker, W. S. and Peng, T. H. (1989): The cause of the glacial to interglacial atmospheric CO_2 change: A polar alkalinity hypothesis. Global Biochem. Cycles 3 (215-239).

Brummer, G. A. and Kroon, D. (1988): Planktonic foraminifers as tracers of ocean climate history. Free University Press, Amsterdam (1-346).

Carmack, E. and Aagaard, K. (1973): On the deep water of the Greenland Sea. Deep-Sea Research 20 (687-715).

Carstens, J. and Wefer, G. (1992): Recent distribution of planktonic foraminifera in the Nansen Basin, Arctic Ocean. Deep Sea Research 39 (507-524).

Charles, C., Wright, J. and Fairbanks, R. (1993): Thermodynamic influences on the marine carbon isotope record. Paleoceanography 8 (691-697).

CLIMAP Project Members (1976): The surface of the Ice Age Earth. Science 191 (1131-1144).

Corliss, B. and Chen, C. (1988): Morphotype patterns of Norwegian Sea deep-sea benthic foraminifera and ecological implications. Geology 16 (716-719).

Craig, H. (1970): Abyssal carbon-13 in the South Pacific. J. Geophys. Res. 74 (691-695).

Craig, H. and Gordon, I. (1965): Deuterium and oxygen-18 in the ocean and the marine atmosphere. In: Tongiorgi, E. (ed.) : Stable isotopes in oceanographic studies and palaeotemperatures. Consiglio Nazionale Delli Ricerche, Laboratorio Di Geologica Nucleare, Pisa.

Curry, W. and Crowley, T. (1987): The $\delta^{13}C$ of Equatorial Atlantic surface waters: Implications for ice age pCO_2 levels. Paleoceanography 2, No. 5 (489-517).

Dansgaard, W., Clausen, H., Gundestrup, N., Hammer, C., Johnsen, S., Kristinsdottir, P. and Reeh, N. (1982): A new Greenland deep ice core. Science 208 (1273-1279).

Dansgaard, W., Johnsen, S., Clausen, H., Dahn-Jansen, D., Gundestrup, N., Hammer, C., Hvidberg, C., Steffensen, J., Sveinbjornsdottir, A., Jouzel, J. and Bond, G. (1993): Evidence for general instability of the past climate from a 250 kyr ice core record. Nature 364 (218-220).

Deuser, W. G. and Hunt, J. M. (1969): Stable isotope ratios of dissolved inorganic carbon in the Atlantic. Deep Sea Research 16 (221).

Dowdeswell, J. and Murray, T. (1990): Modelling rates of sedimentation from icebergs. In: Dowdeswell, J. and Scourse, J. (eds.), Glaciomarine Environments: Processes and Sediments. Geological Society Special Publication No. 53 (121-138).

Drewry, D. and Cooper, A. (1981): Processes and models of Antarctic glaciomarine sedimentation. Annals of Glaciology 2 (117-122).

Duplessy, J. C., Moyes, J. and Pujol, C. (1980): Deep water formation in the North Atlantic Ocean during the last Ice Age. Nature 286 (479-481).

Duplessy, J. C., Shackleton, N., Matthews, R., Prell, W., Ruddiman, W., Caralp, M. and Hendy, C. (1984): ^{13}C record of benthic foraminifera in the last interglacial ocean: implications for the carbon cycle and the global deep water circulation. Quat. Res., 21 (225-243).

Duplessy, J. C., Labeyrie, L. and Blanc, P. L. (1988) Norwegian Sea deep water variations over the last climatic cycle : Paleoceanographic implications. In 'Long and short term variability of climate'.

Elverhoi, A., Dokken, T. and Hebbeln, D. (1993): Abstracts from the PONAM Fourth Annual Workshop, Cambridge.

Emiliani, C. (1955): Pleistocene temperatures. Journal of Geology 63 (538-578).

Emiliani, C. (1966). Palaeotemperature analysis. Journal of Geology 74 (109-126).

Epstein, S. (1953): Temperature shell growth relationships of shallow water biota. Journal of Geology 61 (424-438).

Epstein, S. and Urey, H. C. (1951): Carbonate water isotopic temperature scale. Geological society of America Bulletin 62 (417-425).

Fairbanks, R. (1989): A 17,000 year glacio-eustatic sea level record: influence of glacial melting rates on the Younger Dryas event and deep ocean circulation. Nature 342 (637-642).

Fairbanks, R. and Matthews, R. (1978): The marine oxygen isotope record in Pleistocene coral, Barbados, West Indies. Quaternary Research 10 (181-196).

Gilbert, R. (1990): Rafting in glacimarine environments. In: Dowdeswell, J. and Scourse, J. (eds.), Glaciomarine Environments: Processes and Sediments. Geological Society Special Publication No. 53 (105-120).

Graham, D., Corliss, B., Bender, M and Keigwin, L. (1981): Carbon and oxygen isotopic disequilibria of recent deep-sea benthic foraminifera. Marine Micropalaeontology 6 (483-497).

GRIP (Greenland Ice Project Members) (1993): Climate instability during the last interglacial period recorded in the GRIP ice core. Nature 364 (203-207).

Grossman, E. L. (1984): Carbon isotope fractionation in live benthic foraminifera-comparison with inorganic precipitate studies. Geochem. Cosmochim. Acta 48 (1505-1512).

Grossman, E. L. (1987): Stable isotopes in modern benthic foraminifera: a study of vital effects. Journal of Foraminiferal Research 17 (48-61).

Grousset, F. E., Labeyrie, J., Sinko, J., Cremer, M., Bond, G., Duprat, J., Cortijo, E. and Huon, S. (1993): Patterns of ice rafted detritus in the glacial North Atlantic (40-55°N). Paleoceanography Vol. 8, No. 2 (175-192).

Haake, F. and Pflaumann, U. (1989): Late Pleistocene foraminiferal stratigraphy of the Voring Plateau, Norwegian Sea. Boreas 18 (343-356).

Harland, W., B. (1961): An outline structural history of Spitsbergen. In: Raasch, G., O. (ed.): Geology of the Arctic. University of Toronto Press, Toronto.

Hebbeln, D. (1992): Weichselian glacial history of the Svalbard area: correlating the marine and terrestrial records. Boreas 21 (295-304).

Hebbeln, D. and Wefer, G (1991): Effects of ice coverage and ice-rafted material on sedimentation in the Fram Strait. Nature 350 (409-411).

Heinrich, H. (1988): Origin and consequences of cyclic ice rafting in the northeast Atlantic Ocean during the past 130,000 years. Quaternary Research 29 (142-152).

Helland-Hansen, B. and Nansen, F. (1909): The Norwegian Sea. Its physical oceanography based upon the Norwegian researches 1900-1904. Report on Norwegian Fishery and Marine Investigations Vol.2, Part 1 (390pp).

Hemleben, C. and Spindler, U. (1983): Recent advance on living planktic foraminifera. Utrecht Micropalaeontological Bulletin 30 (141-170).

Hounslow, M. W. (1990): A magnetic susceptibility stratigraphy for Pleistocene and Pliocene sediments in the vicinity of the Barbados Ridge. In Moore, J. and Mascle, A. (eds.) Proceedings of the Ocean Drilling Program, Scientific Results, Vol. 110.

Imbrie, J., Hays, J., Martinson, D., McIntyre, A., Mix, A., Morley, J., Pisias, N., Prell, W. and Shackleton, N. (1984): The orbital theory of pleistocene climate: support from a revised chronology of the marine d18O record. In A. L. Berger *et al.* (eds.) Milankovitch and Climate Part 1. D. Reidel Publishing Company.

Imbrie, J., Berger, A., Boyle, E., Clemens, S., Duffy, A., Howard, W., Kukla, G., Kutzbach, J., Martinson, D., McIntyre, A., Mix, A., Molfino, B., Morley, J., Peterson, L., Pisias, N., Prell, W., Raymo, M., Shackleton, N. and Toggweiler, J. (1994): On

the structure and origin of major glacial cycles 2. The 100,000 year cycle. Palaeoceanography 8 No. 6 (699-735).

Jacobs, S., Gordon, A. and Amos, A. (1979): Effects of glacial ice melting on the Antarctic surface water. Nature 277 (469-471).

Johannessen, T., Jansen, E. and Ravelo, A. Distribution of oxygen and carbon isotopes in recent planktonic foraminifera from the Greenland, Iceland and Norwegian Seas and their relationship to different water masses, nutrients and circulation. In press.

Johnsen, S. (1992): Meddr. Gronland Geoscience 30 (pp22).

Johnsen, S., Dansgaard, W., Clausen, H. and Langway, C. (1972): Oxygen isotope profiles through the Antarctic and Greenland Ice Sheets. Nature 235 (429-434).

Johnsen, S., Clausen, H., Dansgaard, W., Fuhrer, K., Gundestrup, N., Hammer, C., Iversen, P., Jouzel, J., Stauffer, B. and Steffensen, J. (1993): Irregular glacial interstadials recorded in the new Greenland ice core. Nature 359 (311-313).

Jones, G. and Keigwin, L. (1988): Evidence from Fram Strait (78°N) for early deglaciation. Nature 336 (56-59).

Karpuz, N. and Jansen, E. (1992): A high resolution diatom record of the last deglaciationfrom the SE Norwegian Sea: Documentation of rapid climate changes. Paleoceanography 7 (499-520).

Karpuz, N. and Jansen, E.: A high resolution diatom record of the last deglaciation from the SE Norwegian Sea: Documentation of rapid climatic changes. In press.

Karpuz, N. and Schrader, H. (1990): Surface sediment diatom distribution and Holocene paleotemperature variations in the Greenland, Iceland, and Norwegian Seas. Paleoceanography 5 (557-580).

Kellogg, T. (1973): Late Pleastocene climatic record in the Norwegian and Greenland Sea deep-sea cores. Columbia University, Ph.D., 1973. University Microfilms, Ann Arbor, Michigan.

Kellogg, T. (1980): Paleoclimatology and paleo-oceanography of the Norwegian and Greenland Seas: glacial-interglacial contrasts. Boreas 9 (115-137).

Koç, N., Jansen, E. and Haflidason, H. (1993): Paleoceanographic reconstructions of surface ocean conditions in the Greenland, Iceland and Norwegian Seas through the last 14 ka based on diatoms. Quat. Sci. Reviews 12 (115-140).

Köhler, S. and Spielhagen, R. (1990): The enigma of oxygen isotope stage 5 in the central Fram Strait. In Bleil, U., Thiede, J. (eds.), Geological History of the Polar Oceans: Arctic versus Antarctic (489-497). Kluwer Academic Publishers. Netherlands.

Kroopnick, P. (1974): Modelling the dissolved O_2-CO_2-^{13}C system in the eastern equatorial Pacific. Deep Sea Research, 21 (211-229).

Kroopnick, P. (1980): The distribution of 13C in the Atlantic Ocean. Earth and Planetary Science Letters 49 (469-484).

Kroopnick, P. (1985): The distribution of $\delta^{13}C$ in Σ CO_2 in the world oceans. Deep Sea Research 32 (57-84).

Lehman, S. and Keigwin, L. (1992): Sudden changes in North Atlantic circulation during the last deglaciation. Nature 356 (757-762).

LIGA members (1991): Report of the 1st discussion group: The last interglacial in high latitudes of the northern hemisphere: Terrestrial and marine evidence. Quaternary International 10-12 (8-28).

Lorius, C., Jouzel, J., Ritz, C., Merlivat, L., Barkov, N., Korotkevich, Y. and Kotlyakov, V. (1985): A 150,000 year climate record from Antarctic ice. Nature 316 (591-596).

Lutze, G., F. and Coulbourn, W., T. (1984): Recent benthic foraminifera from the continental margin of northwest Africa: Community, structure and distribution. Marine Micropalaeontology 8 (361-401).

MacAyeal, D. R. (1993a): A low order model of the Heinrich event cycle. Paleoceanography 8 (767-773).

MacAyeal, D. R. (1993b): Binge/purge oscillations of the Laurentide ice sheet as a cause of the North Atlantic's Heinrich events. Paleoceanography 8 (775-784).

Mackensen, A., Sejrup, H. and Jansen, E. (1985): The distribution of living benthic foraminifera on the continental slope and rise off southwest Norway. Marine Micropalaeontology 9 (275-306).

Maher, B. A. and Thompson, R. (1991): Mineral magnetic record of the Chinese loess and paleosols. Geology 19 (3-6).

Mangerud, J. (1977): Late Weichselain marine sediments containing shells, foraminifera and pollen at Agotnes, western Norway. Norsk Geologisk Tidsskrift 57 (13-19).

Mangerud, J. and Svendsen, J. (1990): Deglaciation chronology inferred from marine sediments in a proglacial lake basin, western Spitsbergen, Svalbard. Boreas 19 (249-272).

Mangerud, J., Bolstad, M., Elgersma, A., Helliksen, D., Landvik, J., Lonne, I., Lycke, K., Salvigsen, O., Sandahl, T. and Svendsen, J (1992): The glacial maximum on Spitsbergen, Svalbard. Quaternary Research 38 (1-31).

Mangerud, J. and Svendsen, J. (1992): The last interglacial-glacial period on Spitsbergen , Svalbard. Quaternary Science Reviews 11 (633-664).

Mantyla, A. W. and Reid, J., L. (1983): On the abyssal circulation of the World Ocean. Deep-Sea Research 30 (805-833).

Martinson, D., Pisias, N., Hays, J., Imbrie, J., Moore, T. and Shackleton, N. (1987): Age dating and the orbital theory of the Ice Ages : Development of a high resolving 0 to 300,000 year chronostratigraphy. Quaternary Research 27 (1-29).

McIntyre, A., Kipp, N., Crowley, T., Kellogg, T., Gardiner, J., Prell, W. and Ruddiman, W. (1976): Glacial North Atlantic 18,000 years ago: A CLIMAP reconstruction. Geological Society of America Memoir 145 (43-76).

Miller, G. H., Sejrup, H. P., Lehman, S. J., Forman, S. L. (1989). Glacial history and marine environmental change during the last interglacial - glacial cycle, Western Spitsbergen, Svalbard. Boreas 18 (273-296).

Morris, T. H. (1988): Stable isotope stratigraphy of the Arctic Ocean: Fram Strait to central Arctic. Paleo. Paleo. Paleo. 64 (201-219).

Murray, J. W. (1991): Ecology and Palaeoecology of Benthic Foraminifera. Longman Scientific and Technical (pp397).

Nansen Arctic Drilling Program Science Committee (1992): The Arctic Ocean Record: Key to global change (initial science plan) (pp102).

Nørvang, A. (1945): The zoology of Iceland. Foraminifera 2(2) (1-79).

Oerlemans, J. (1993): Evaluating the role of climate cooling in iceberg production and the Heinrich events. Nature 364 (783-785).

Patience, A. and Kroon, D. (1991): Application of oxygen isotope chronostratigraphy to the dating of Late Cenozoic marine sediments. In Smart, P. and Francis, P. (eds.): Quaternary dating methods - a users guide. Technical Guide 4. Quaternary Research Association, Cambridge (199-221).

Quadfasel, D. and Meincke, J. (1987): Note on the thermal structure of the Greenland Sea gyres. Deep-Sea Research 34, No. 11 (1883-1888).

Rokoengen, K., Erlenkeuser, H., Lofaldli, M., Skarbo, O. (1991): A climatic record for the last 12,000 years from a sediment core on the Mid-Norwegian continental shelf. Norsk Geologisk Tidsskrift 71 (75-90).

Ruddiman, W. (1977): Late Quaternary deposition of ice-rafted sand in the subpolar North Atlantic (lat 40 to 65°N). Geological Society of America Bulletin 88 (1813-1827).

Sancetta, C. (1992): Primary production in the glacial North Atlantic and North Pacific oceans. Nature 360 (249-251).

Sancetta, C., Imbrie, J. and Kipp, N. (1973): Climatic record of the past 130,00 years in the North Atlantic deep-sea core V23-82: Correlation with the terrestrial record. Quaternary Research 3 (110-116).

Sarnthein, M. and Tiedemann, R. (1990): Younger Dryas style cooling events at glacial terminations I-IV at ODP site 658: Associated benthic $d^{13}C$ anomalies constrain meltwater hypothesis. Paleoceanography 5 (1041-1055).

Sarnthein, M., Jansen, E., Arnold, M., Duplessy, J., Erlenkeuser, H., Flatoy, A., Veum, T., Vogelsang, E. and Weinelt, M. (1992): $\delta^{18}O$ time slice reconstruction of meltwater anomalies at termination I in the North Atlantic between 50 and 80 °N. In Bard, E. and Broecker, W. S. (eds.): The Last Deglaciation: Absolute and Radiocarbon Chronologies (183-200). Springer-Verlag Berlin Heidelberg.

Sejrup, H., P. and Guibault, J., P. (1980): *Cassidulina reniforme* and *C. obtusa* (Foraminifera), taxonomy, distribution and ecology. Sarsia 65 (79-85).

Sejrup, H. P., Fjaeran, T., Hald, M., Beck, L., Hagen, J., Miljeteig, I., Morvik, I. and Norvik, O. (1981): Benthonic foraminifera in surface samples from the Norwegian continental margin between 62 N and 65 N. Journal of Foraminiferal Research 11 (277-295).

Sejrup, H. P., Jansen, E., Erlenkeuser, H. and Holtedahl, H. (1984): New faunal and isotopic evidence on the Late Weichselian - Holocene oceanographic changes in the Norwegian Sea. Quaternary Research 21 (74-84).

Shackleton, N. (1977): Carbon-13 in *Uvigerina*: tropical rainforest history and the equatorial Pacific carbonate dissolution cycle. In: N. R. Andersen and A. Malahoff (eds.) The fate of fossil fuel CO2 in the oceans; -Plenum Press, New York (401-427).

Shackleton, N. and Opdyke, N. (1973): Oxygen isotope and palaeomagnetic stratigraphy of Pacific core V28-238: Quaternary Research 3 (39-55).

Shackleton, N., Wiseman, J. and Buckley, H. (1973): Non-equilibrium isotopic fractionation between seawater and planktonic foraminiferal tests. Nature 242 (177-179).

Shackleton, N. and Kennett, J. P. (1975): Paleotemperature history of the Cenozoic and initiation of Antarctic glaciation: oxygen and carbon isotope analysis in DSDP Sites 277, 279 and 281. Init. Repts. DSDP 29 (743-755).

Smith, W., Baumann, M., Wilson, D. and Aletsee, L. (1987): Phytoplankton biomass and productivity in the marginal ice zone of the Fram Strait during summer 1984. Journal of Geophysical Research 92 (6777-6786).

Snowball, I. and Thompson, R. (1990): A mineral magnetic study of Holocene sedimentation in Lough Catherine, Northern Ireland. Boreas 19 (127-146).

Streeter, S. and Shackleton, N. (1979): Paleocirculation of the deep North Atlantic: 150,000 year record of benthic foraminifera and oxygen-18. Science 203 (168-171).

Streeter, S. Belanger, P., Kellogg, T. and Duplessy, J. (1982): Late Pleistocene paleoceanography of the Norwegian-Greenland Sea: Benthic foraminifera evidence. Quaternary Research 18 (72-90).

Svendsen, J. I. and Mangerud, J. (1992): Paleoclimatic inferences from glacial fluctuations on Svalbard during the last 20,000 years. Climate Dynamics 6 (213-220).

Svendsen, J. I. Mangerud, J., Elverhoi, A., Solheim, A. and Schuttenhelm, R. (1992): The Late Weichselain glacial maximum on western Spitsbergen inferred from offshore sediment cores. Marine Geology 104 (1-17).

Swift, J. H. and Aagaard, K. (1981): Seasonal transitions and water mass formation in the Iceland and Greenland seas. Deep-Sea Research 28A No. 10 (1107-1129).

Tappan, H. (1968): Primary production, isotopes, extinction and the atmosphere. Palaeogeog., Palaeoclim., Palaeoec. 4 (187-210).

Thompson, R., Battarbee, R., O'Sullivan, P. and Oldfield, F. (1975): Magnetic susceptibility of lake sediments. Limnology and Oceanography 20 no. 5.

Urey, H. C. (1947): The thermodynamic properties of isotopic substances. Journal of the Chemical Society 1947 (562-581).

Vincent, E. and Berger, W., H. (1981): Stable isotope composition of benthic foraminifera from the Equatorial Pacific. Nature 289 (639-643).

Vorren, T. O., Lebesbye, E., Andreassen, K. and Larsen, K. B. (1989): Glacigenic sediments on a passive continental margin as exemplified by the Barents Sea. Marine Geology 85 (251-272).

Watson, D. (1990): Mineral magnetic investigation of some cores off the coast of Spitsbergen. Ph.D. Thesis, Edinburgh University.

Weinelt, M., Sarnthein, M., Vogelsang, E and Erlenkeuser, H. (1991): Early decay of the barents Shelf ice sheet - spread of stable isotopesignals across the eastern Norwegian Sea. Norsk Geologisk Tidsskrift 71 (137-140).

Weston, J. F. and Murray, J. W. (1984): Benthic foraminifera as deep sea water mass indicators. In Oertli, H. J. (ed.) Benthos '83 (605-610).

Woodruff, F., Savin, S. and Douglas, R. (1980): Biological fractionation od carbon and oxygen isotopes by recent benthic foraminifera. Marine Micropalaeontology 5 (3-11).

Woodruff, F. and Savin, S. M. (1985): $\delta^{13}C$ values of Miocene Pacific benthic foraminfera: correlations with sea level and productivity. Geology 13 (119-122).

Worthington, L. V. (1976): "On the North Atlantic circulation." John Hopkins Press, Baltimore/London.

van der Zwaan, G. J., Jorissen, F. J. and de Stigter, H., C. (1990): The depth dependancy of planktic/benthic ratios: Constraints and applications. Marine Geology 95 (1-16).

Appendix 1. Analytical techniques

A 1.1. Sediment collection and sampling

The piston cores analysed in this study were collected during an expedition of the Geological Survey of the Netherlands, with the survey vessel Hr. Ms. Tydeman of the Hydrographic Survey of the Netherlands in 1988. The cores were sliced in half and stored at the Dutch Geological Survey in Haarlem, The Netherlands.

Samples were taken from one of the halves of the cores in October 1990, the other half was left undisturbed. The samples were taken using plastic plugs with a diameter of approximately 2cm. The sampling interval varied between 2.5cm and 5cm, sampling frequency is reported in table 1.1 along with the core length, water depth and core location. These samples were then brought to Edinburgh University where various analyses were carried out on them.

A 1.2. Magnetic susceptibility

Magnetic susceptibility measurements were made on the samples before any other treatment using a Bartington Instruments susceptibility meter. The meter was calibrated using a paramagnetic salt ($FeSO_4.7H_2O$) standard. The value obtained was then divided by the sample weight to produce a measure of mass specific susceptibility expressed in units of $10^{-6}m^3kg^{-1}$.

A 1.3. Stable isotope analysis

Samples were first dried in an oven at 60°C for 24 hours, this was to allow total sediment dry weight to be measured. The samples were then wet sieved through a 63μm stainless steel sieve, and the residue dried in an oven at 60°C. The dried samples were then sieved at 125μm, and specimens of the planktic foraminifera *Neogloboquadrina pachyderma* (sinistral) were picked under a binocular microscope for all cores. Different benthic foraminiferal species were picked for the cores, for PCM5 *Eponides umbonatus* was picked, for PCM7, and PCM30 *Cassidulina teretis* and *Melonis barleanum* were picked. Once picked, the specimens were washed in methyl alcohol (AR) and cleaned in an ultrasonic bath for several seconds to remove

any attached contaminants. Excess methyl alcohol was removed with tissue paper and remaining alcohol allowed to evaporate. Foraminiferal sample weights used in analysis were between 0.05 and 0.1mg and comprised between 10-15 specimens for planktic measurements, 5-10 for measurements on *M. barleanum*, and 10-20 for specimens of *C. teretis*.

Once cleaned the foraminifera were added to orthophosphoric acid (sg.1.9) at 90°C and the CO^2 gas evolved was analysed using a VG Isogas Prism mass spectrometer. Samples were analysed using a standard marble reference (SM1), and values obtained converted to a PDB standard (Craig, 1957). Precision for oxygen analysis was 0.085% (standard deviation for 100 analyses of a standard carbonate, SM1, conducted over several months).

A 1.4. Foraminiferal abundance counts

Foraminiferal abundance counts were made on the samples after they were processed for stable isotope analysis. The foraminifera picked for stable isotope analysis were taken into account. Counts of individual species content were made for each sample, where possible at least 300 planktic and 100 benthic foraminiferal specimens were counted from each sample to produce a representative value of total abundance. The sample was accurately split when abundances were too high to count all the specimens present. Using the dry weight measurements made during initial processing the absolute abundance of planktic and benthic individual species in number of specimens per gram dry weight were calculated. Percentages were also calculated for certain species.

A 1.5. Grain size measurements from sieved residue

These measurements were made on cores PCM5, PCM7 and PCM30 using the same samples as used for stable isotope analysis. Once the dried residue was obtained it was weighed, and the weight percent material coarser than 63μm was calculated (the samples were sieved at 63μm during the initial sampling preparation, after their dry weight was measured). These samples were also dry sieved through a stainless steel 600μm mesh sieve and weighed, the dry weight percent material coarser than 600μm was then calculated.

A 1.6. Coulter LS 100 measurements

Subsamples were taken before processing for the stable isotope measurements was carried out. A Coulter LS-100 particle size analyser was used to measure the particle size variations of subsamples from PCM5. This instrument uses the principle of Frauhofer diffraction of laser light in which light falling on suspended sediment particles is deflected (diffracted) by an amount dependent on the diameter of the particle. The samples were soaked overnight in water to facilitate deflocculation. After a visual inspection for good dispersion, the samples were wet sieved at 500μm and the suspension retained. Material coarser than 500mm had to be removed due to the limited size range the machine can accurately measure. The sample volume was then made up to approximately 150mL. Samples were further disaggregated with ultrasound for 3 minutes before being run through the instrument.

A 1.7. X-ray photography

X-ray photographs of the undisturbed half of cores PCM5, PCM7, and PCM30 were taken using a Hewllet Packard 43805-N x-ray system with Agfa-Gevaert NDT systems D7Pb film. Contact prints were made of these x-rays, and the number of clasts greater than 2mm in diameter were counted. The counts were made of sections 2cm in width, and over the whole width for each core.

A 1.8. X-ray fluorescence spectrometry

X-ray fluorescence spectrometry was performed on a Philips PW 1480 sequential automatic x-ray spectrometer and PW1510 sample changer. This allowed major element compositions to be measured, though only silica content has been presented in this thesis.

Fused 45mm discs were prepared from finely ground bulk sediment. The finely ground sediment was mixed with an ultrapure flux, Spectroflux 105, with a ratio of 5.333:1 (by weight, flux:sediment). This mixture was melted in a crucible in a muffle furnace at 1100°C for 20 minutes. The crucibles were allowed to cool and any weight loss made up with additional flux and refused over a Meker burner. The mixture was then pressed into a disc on a 220°C hotplate. The discs were then stored in a desicator until such time as they could be analysed.

Depth	Age	Magnetic Susceptibility	Depth	Age	Magnetic Susceptibility
2.5	12.67	0.0206	145	16.00	0.0228
5	12.73	0.0197	147.5	16.30	0.0236
7.5	12.78	0.0215	150	16.60	0.0273
10	12.84	0.0188	152.5	16.90	0.0311
12.5	12.90	0.0167	155	17.20	0.0301
15	12.95	0.0186	157.5	17.50	0.0416
17.5	13.01	0.0150	160	17.80	0.0255
20	13.07	0.0134	162.5	18.10	0.0160
22.5	13.13	0.0135	165	18.40	0.0107
25	13.18	0.0143	167.5	18.70	0.0077
27.5	13.24	0.0175	170	19.00	0.0070
30	13.30	0.0199	172.5	19.30	0.0076
32.5	13.35	0.0167	175	19.60	0.0092
35	13.41	0.0178	177.5	19.90	0.0088
37.5	13.47	0.0119	180	20.20	0.0091
40	13.52	0.0125	182.5	20.50	0.0083
42.5	13.58	0.0130	185	20.80	0.0094
45	13.64	0.0168	187.5	21.10	0.0092
47.5	13.70	0.0145	190	21.40	0.0090
50	13.75	0.0145	192.5	21.70	0.0076
52.5	13.81	0.0146	195	22.04	0.0283
55	13.87	0.0114	197.5	23.62	0.0158
57.5	13.92	0.0094	200	25.19	0.0158
60	13.98	0.0167	202.5	26.76	0.0141
62.5	14.04	0.0146	205	28.34	0.0091
65	14.09	0.0141	207.5	29.91	0.0095
67.5	14.15	0.0135	210	31.48	0.0126
70	14.21	0.0129	212.5	32.83	0.0070
72.5	14.27	0.0012	215	34.18	0.0080
75	14.32	0.0105	217.5	35.53	0.0077
77.5	14.38	0.0113	220	36.88	0.0079
80	14.44	0.0106	222.5	38.23	0.0104
82.5	14.49	0.0105	225	39.58	0.0147
85	14.55	0.0102	227.5	40.93	0.0110
87.5	14.61	0.0110	230	42.28	0.0164
90	14.66	0.0105	232.5	43.63	0.0174
92.5	14.72	0.0093	235	44.98	0.0190
95	14.78	0.0104	237.5	46.33	0.0232
97.5	14.84	0.0095	240	47.68	0.0234
100	14.89	0.0142	242.5	48.80	0.0193
102.5	14.95	0.0099	245	49.94	0.0115
105	15.01	0.0099	247.5	51.07	0.0100
107.5	15.06	0.0099	250	52.20	0.0105
110	15.12	0.0144	252.5	53.34	0.0084
112.5	15.18	0.0140	255	54.47	0.0090
115	15.23	0.0157	257.5	55.60	0.0106
117.5	15.29	0.0193	260	56.73	0.0101
120	15.35	0.0179	262.5	57.87	0.0172
122.5	15.41	0.0153	265	59.00	0.0188
125	15.46	0.0198	267.5	59.57	0.0228
127.5	15.52	0.0248	270	60.14	0.0201
130	15.58	0.0219	272.5	60.71	0.0228
132.5	15.63	0.0214	275	61.28	0.0078
135	15.69	0.0166	277.5	61.85	0.0126
137.5	15.75	0.0175	280	62.42	0.0143
140	15.80	0.0199	282.5	62.99	0.0149
142.5	15.86	0.0288	285	63.56	0.0175

A.1. PCM5 Magnetic susceptibility measurements

Depth	Age	Magnetic Susceptibility	Depth	Age	Magnetic Susceptibility
287.5	64.13	0.0165	430	123.56	0.0158
290	64.70	0.0103	432.5	124.38	0.0151
292.5	65.27	0.0134	435	125.20	0.0096
295	65.84	0.0103	437.5	126.00	0.0073
297.5	66.41	0.0136	440	134.00	0.0213
300	67.00	0.0213	442.5	135.00	0.0217
302.5	67.80	0.0164	445	136.00	0.0274
305	68.60	0.0108	447.5	136.29	0.0254
307.5	69.40	0.0126	450	136.58	0.0212
310	70.20	0.0133	452.5	136.87	0.0225
312.5	71.00	0.0106	455	137.16	0.0222
315	71.80	0.0115	457.5	137.45	0.0222
317.5	72.60	0.0114	460	137.74	0.0243
320	73.40	0.0135	462.5	138.03	0.0353
322.5	74.20	0.0142	465	138.31	0.0273
325	75.00	0.0116	467.5	138.59	0.0225
327.5	76.67	0.0143	470	138.87	0.0247
330	78.34	0.0089	472.5	139.15	0.0233
332.5	80.00	0.0089	475	139.44	0.0199
335	82.00	0.0096	477.5	139.72	0.0181
337.5	84.00	0.0122	480	140.00	0.0195
340	85.00	0.0120	482.5	142.00	0.0212
342.5	86.00	0.0142	485	144.00	0.0138
345	87.00	0.0119	487.5	146.00	0.0140
347.5	88.00	0.0159	490	148.00	0.0134
350	89.00	0.0112	492.5	150.00	0.0132
352.5	89.40	0.0094	495	152.00	0.0142
355	89.80	0.0096	497.5	154.00	0.0142
357.5	90.20	0.0090	500	156.00	0.0107
360	90.60	0.0092	502.5	158.00	0.0129
362.5	91.00	0.0112	505	160.00	0.0273
365	91.40	0.0116	507.5	162.00	0.0309
367.5	91.80	0.0092	510	164.00	0.0304
370	92.20	0.0099	512.5	166.00	0.0303
372.5	92.60	0.0208	515	168.00	0.0292
375	93.00	0.0170	517.5	170.00	0.0251
377.5	93.33	0.0153	520	172.00	0.0197
380	93.66	0.0226	522.5	174.00	0.0273
382.5	94.00	0.0175	525	176.00	0.0135
385	94.33	0.0200	527.5	178.00	0.0169
387.5	94.66	0.0193	530	180.00	0.0114
390	95.00	0.0170	532.5	180.33	0.0143
392.5	97.00	0.0127	535	180.66	0.0098
395	99.00	0.0187	537.5	180.99	0.0089
397.5	100.50	0.0228	540	181.32	0.0092
400	102.00	0.0169	542.5	181.65	0.0098
402.5	104.50	0.0180	545	181.98	0.0089
405	107.00	0.0230	547.5	182.31	0.0091
407.5	111.00	0.0239	550	182.64	0.0090
410	117.00	0.0181	552.5	182.97	0.0098
412.5	117.82	0.0207	555	183.30	0.0091
415	118.64	0.0203	557.5	183.63	0.0092
417.5	119.46	0.0205	560	183.96	0.0083
420	120.28	0.0169	562.5	184.29	0.0096
422.5	121.10	0.0141	565	184.62	0.0084
425	121.92	0.0120	567.5	184.95	0.0091
427.5	122.74	0.0121	570	185.28	0.0093

A.1. PCM5 Magnetic susceptibility measurements

Depth	Age	Magnetic Susceptibility
572.5	185.61	0.0096
575	185.94	0.0086
577.5	186.27	0.0094
580	186.60	0.0083
582.5	186.93	0.0087
585	187.26	0.0077
587.5	187.59	0.0096
590	187.92	0.0078
592.5	188.25	0.0082
595	188.58	0.0076
597.5	188.91	0.0074
600	189.24	0.0070
602.5	189.57	0.0061
605	189.90	0.0066
607.5	190.23	0.0058
610	190.56	0.0071
612.5	190.89	0.0062
615	191.22	0.0064
617.5	191.55	0.0061
620	191.88	0.0067
622.5	192.21	0.0061
625	192.54	0.0066
627.5	192.87	0.0069
630	193.20	0.0055
632.5	193.53	0.0054
635	193.86	0.0083
637.5	194.19	0.0050
640	194.52	0.0056
642.5	194.85	0.0056
645	195.18	0.0053
647.5	195.51	0.0057
650	195.84	0.0049
652.5	196.17	0.0043
655	196.50	0.0052
657.5	196.83	0.0046
660	197.16	0.0061
662.5	197.49	0.0063
665	197.82	0.0077
667.5	198.15	0.0070
670	198.48	0.0085
672.5	198.81	0.0073
675	199.14	0.0081
677.5	199.47	0.0067
680	199.80	0.0084
682.5	199.90	0.0085
685	200.00	0.0089

A.1. PCM5 Magnetic susceptibility measurem

Depth	Age	Magnetic Susceptibility	Depth	Age	Magnetic Susceptibility
0	10.2	0.0205	365	32.32	0.0218
2.5	10.22	0.0172	370	34.15	0.0246
5	10.24	0.0189	375	36	0.0246
10	10.28	0.0201	380	36.45	0.0234
12.5	10.31	0.0198	385	36.9	0.0186
15	10.33	0.0215	390	37.35	0.0263
20	10.37	0.0200	395	37.8	0.0257
25	10.41	0.0223	400	38.25	0.0341
30	10.45	0.0199	405	38.7	0.0226
35	10.5	0.0235	410	39.15	0.0234
40	10.56	0.0207	415	39.6	0.0230
45	10.6	0.0202	420	40.05	0.0255
50	10.93	0.0169	425	40.5	0.0156
55	11.26	0.0183	430	40.95	0.0222
60	11.59	0.0169	435	41.4	0.0171
65	11.92	0.0167	440	41.85	0.0239
70	11.95	0.0194	445	42.3	0.0220
75	11.98	0.0183	450	42.75	0.0244
80	12.01	0.0204	455	43.2	0.0264
85	12.04	0.0193	460	43.65	0.0243
90	12.07	0.0194	465	44.1	0.0229
95	12.1	0.0199	470	44.55	0.0204
100	12.13	0.0204	475	45	0.0271
105	12.16	0.0193	480	45.35	0.0206
110	12.19	0.0202	485	45.7	0.0218
115	12.22	0.0205	490	46.05	0.0196
120	12.3	0.0216	495	46.4	0.0146
125	12.43	0.0216	500	46.75	0.0198
130	12.57	0.0190	505	47.1	0.0184
135	12.7	0.0190	510	47.45	0.0255
140	12.84	0.0184	515	47.8	0.0236
145	12.97	0.0244	520	48.15	0.0230
150	13.11	0.0186	525	48.5	0.0286
155	13.22	0.0152	530	48.85	0.0261
160	13.32	0.0198	535	49.2	0.0174
165	13.43	0.0147	540	49.55	0.0269
170	13.55	0.0126	545	50	0.0239
175	13.68	0.0113	550	50.75	0.0247
180	13.81	0.0108	555	51.5	0.0254
185	13.94	0.0129	560	52.25	0.0146
195	14.18	0.0107	565	53	0.0225
205	14.44	0.0104	570	53.75	0.0205
210	14.57	0.0122	575	54.5	0.0210
215	14.7	0.0107	580	55.25	0.0242
220	14.83	0.0114	585	56	0.0209
225	14.96	0.0117	590	56.75	0.0174
230	15.09	0.0121	595	57.5	0.0106
235	15.22	0.0120	600	58.25	0.0132
240	15.35	0.0165	605	59	0.0207
245	15.48	0.0171	610	59.55	0.0193
250	15.61	0.0209	615	60.1	0.0145
255	15.74	0.0201	620	60.65	0.0186
260	15.87	0.0181	625	61.2	0.0180
265	16	0.0266	630	61.75	0.0154
275	17.07	0.0276	635	62.3	0.0143
280	17.6	0.0162	640	62.85	0.0227
285	18.13	0.0085	645	63.4	0.0164
290	18.66	0.0092	650	64	0.0238
295	19.19	0.0104	655	64.55	0.0129
300	19.72	0.0098	660	65.1	0.0138
305	20.25	0.0104	665	65.65	0.0158
310	20.78	0.0198	670	66.2	0.0178
315	21.31	0.0263	675	66.75	0.0168
320	21.84	0.0264	680	67.3	0.0153
325	22.04	0.0242	685	67.85	0.0159
330	22.78	0.0246	690	68.4	0.0216
335	23.52	0.0166	695	68.95	0.0163
340	24.26	0.0099	700	69.5	0.0162
345	25	0.0167	705	70.05	0.0165
350	26.83	0.0194	710	70.6	0.0170
355	28.66	0.0228	715	71.15	0.0160
360	30.49	0.0180	720	71.7	0.0164
			727	72.25	0.0160

Table A.2. Magnetic Susceptibility data for PCM7.

Depth	Age	Magnetic Susceptibility	Depth	Age	Magnetic Susceptibility
2	15.34	0.0118	322	62.75	0.0103
7	15.36	0.0064	327	63.50	0.0082
12	15.38	0.0060	332	64.25	0.0098
17	15.40	0.0070	337	65.00	0.0121
22	15.42	0.0077	342	67.00	0.0135
27	15.44	0.0115	347	69.00	0.0116
32	15.46	0.0134	352	71.00	0.0122
37	15.49	0.0122	357	73.00	0.0149
42	15.51	0.0121	362	75.00	0.0135
47	15.53	0.0125	367	77.50	0.0144
52	15.55	0.0112	372	80.00	0.0090
57	15.57	0.0133	377	84.00	0.0066
62	15.59	0.0128	382	85.29	0.0133
67	15.61	0.0136	387	86.57	0.0169
72	15.63	0.0162	392	87.86	0.0168
77	15.66	0.0175	397	89.14	0.0163
82	15.69	0.0157	402	90.43	0.0166
87	15.72	0.0159	407	91.71	0.0166
92	15.76	0.0144	412	93.00	0.0175
97	15.79	0.0137	417	93.40	0.0165
102	15.83	0.0164	422	93.80	0.0155
107	15.86	0.0170	427	94.20	0.0144
112	15.89	0.0155	432	94.60	0.0134
117	16.00	0.0167	437	95.00	0.0118
122	16.30	0.0174	442	100.00	0.0131
127	16.60	0.0167	447	105.00	0.0129
132	16.90	0.0218	452	110.00	0.0134
137	17.20	0.0147	457	112.75	0.0187
142	17.50	0.0191	462	115.50	0.0095
147	18.15	0.0135	467	118.25	0.0080
152	18.80	0.0052	472	121.00	0.0075
157	19.45	0.0066	477	125.30	0.0086
162	20.10	0.0074	482	129.60	0.0123
167	20.75	0.0067	487	134.00	0.0163
172	21.40	0.0163	492	135.00	0.0148
177	22.04	0.0201	497	136.00	0.0178
182	23.00	0.0123	502	136.29	0.0164
187	24.00	0.0136	507	136.58	0.0183
192	25.00	0.0152	512	136.87	0.0160
197	26.88	0.0148	517	137.16	0.0170
202	28.75	0.0103	522	137.45	0.0157
207	30.63	0.0154	527	137.74	0.0207
212	32.50	0.0156	532	138.03	0.0282
217	34.38	0.0141	537	138.32	0.0147
222	36.25	0.0152	542	138.61	0.0203
227	38.13	0.0143	547	138.90	0.0137
232	40.00	0.0136	552	139.19	0.0197
237	40.67	0.0123	557	139.48	0.0161
242	41.34	0.0141	562	139.77	0.0163
247	42.01	0.0115	567	140.00	0.0095
252	42.68	0.0126	572	140.29	0.0079
257	43.35	0.0143	577	140.58	0.0073
262	44.00	0.0143	582	140.87	0.0080
267	46.14	0.0143	587	141.16	0.0114
272	48.28	0.0132	592	141.45	0.0143
277	50.42	0.0116	597	141.74	0.0139
282	52.56	0.0128	602	142.03	0.0137
287	54.70	0.0111	607	142.32	0.0132
292	56.84	0.0097	612	142.61	0.0133
297	59.00	0.0152	617	142.90	0.0135
302	59.75	0.0166	622	143.19	0.0131
307	60.50	0.0150	626	143.48	0.0164
312	61.25	0.0156			
317	62.00	0.0076			

Table A.3. Magnetic susceptibility data for PCM30.

Depth Planktic	Age Planktic	Oxygen 18 Planktic	Carbon 13 Planktic	Depth Benthic	Age Benthic	Oxygen 18 Benthic	Carbon 13 Benthic	Oxygen 18 Benthic corrected	Depth B-P	Oxygen 18 B-P
2.5	12.68	3.162	0.598	125	15.5	4.597	-1.268	5.067	125	0.941
10	12.84	3.704	0.225	130	15.61	4.153	-2.25	4.623	130	0.084
55	13.89	4.004	-0.13	135	15.72	3.874	-2.026	4.344	135	-0.052
85	14.58	4.034	-0.136	140	15.84	4.617	-2.104	5.087	140	0.421
95	14.81	4.119	-0.311	145	16	5.044	-2.24	5.514	145	0.726
110	15.15	4.129	-0.087	150	16.6	4.772	-2.372	5.242	150	0.654
115	15.27	4.108	-0.172	155	17.2	5.064	-2.05	5.534	155	0.836
120	15.38	3.993	-0.046	160	17.8	4.898	-2.314	5.368	160	0.713
125	15.5	4.126	0.171	195	22.04	4.831	-2.103	5.301	195	0.553
130	15.61	4.539	-0.054	200	25.19	4.653	-1.497	5.123	200	0.385
135	15.72	4.396	-0.241	210	31.48	4.963	-1.782	5.433	210	1.057
140	15.84	4.666	0.124	230	42.28	4.776	-1.647	5.246	230	0.922
145	16	4.788	0.304	262	57.87	4.586	-1.599	5.056	262.5	0.814
150	16.6	4.588	0.265	265	59	4.899	-1.365	5.369	265	1.515
155	17.2	4.698	0.465	310	70.2	4.188	-1.924	4.658	310	1.638
160	17.8	4.655	0.523	312	71	4.523	-1.825	4.993	320	0.17
175	19.6	4.328	-0.107	317	72.6	4.026	-1.971	4.496	345	0.342
190	21.44	4.597	-0.138	320	73.4	3.506	-2.88	3.976	350	1.099
195	22.04	4.748	0.446	342	86	4.453	-2.273	4.923	365	0.028
200	25.19	4.738	0.379	345	87	4.094	-2.663	4.564	375	0.68
205	28.335	4.116	-0.225	347	88	4.753	-2.367	5.223	380	0.627
210	31.48	4.376	0.471	350	89	4.493	-2.447	4.963	385	0.232
225	39.58	4.185	0.424	357	90.2	4.618	-1.916	5.088	440	0.419
230	42.28	4.324	0.453	362	91	4.42	-1.975	4.89	445	0.747
245	49.94	4.204	0.093	365	91.4	3.812	-2.265	4.282	450	0.868
250	52.205	4.268	-0.128	367	91.8	5.083	-1.78	5.553	455	0.854
255	54.47	4.082	0.19	375	93	4.756	-1.715	5.226	460	0.821
260	56.735	3.886	0.052	377	93.33	4.585	-1.301	5.055	470	0.714
262.5	57.87	4.242	0.447	380	93.66	4.582	-1.424	5.052	475	0.887
265	59	3.854	0.165	382	94	4.337	-0.717	4.807	480	0.557

A.4. Oxygen and carbon stable isotope data for PCM5 from planktic and benthic foraminifera

280	62.42	4.225	
290	64.7	4.315	0.162
295	65.84	3.97	
310	70.2	3.02	-0.338
315	71.8	4.188	-0.085
325	75	3.806	-0.251
327	76.67	3.337	-0.263
330	78.34	2.532	-0.326
332	80	2.063	-0.458
335	82	1.89	-0.618
337	84	1.534	-0.563
340	85	2.702	-0.652
345	87	4.222	-0.027
347	88	4.355	-0.263
350	89	3.864	0.091
352	89.4	4.129	0.12
355	89.8	3.812	-0.394
357	90.2	4.234	0.136
360	90.6	3.617	-0.13
362	91	4.121	0.182
365	91.4	4.254	0.264
367	91.8	4.15	0.141
370	92.2	4.466	0.064
375	93	4.546	0.324
380	93.66	4.425	0.744
385	94.33	4.413	0.67
390	95	3.651	0.379
400	102	4.174	0.079
410	117	3.768	0.133
415	118.64	3.515	0.59
420	120.28	4.127	0.306
425	121.92	4.28	-0.111
440	134	4.848	0.377
445	136	4.895	0.029

385	94.33	4.175	-1.176	4.645	485	1.043
407	111	4.806	-1.438	5.276	495	1.11
417	119.46	4.516	-1.692	4.986	505	0.957
440	134	4.797	-2.147	5.267	510	1.01
445	136	5.172	-2.479	5.642	515	1.081
450	136.58	5.029	-2.664	5.499	520	0.899
455	137.16	4.897	-2.289	5.367	525	0.844
460	137.74	4.9	-2.475	5.37	530	0.82
470	138.87	4.636	-2.7	5.106	550	0.823
475	139.435	4.713	-2.611	5.183		
480	140	4.762	-2.728	5.232		
485	144	4.695	-2.609	5.165		
495	152	4.957	-2.368	5.427		
505	160	4.923	-2.242	5.393		
510	164	4.943	-2.099	5.413		
515	168	4.995	-1.949	5.465		
520	172	4.868	-2.187	5.338		
525	176	4.865	-2.249	5.335		
530	180	4.771	-2.457	5.241		
550	182.64	4.77	-2.245	5.24		

A.4. Oxygen and carbon stable isotope data for PCM5 from planktic and benthic foraminifera

450	136.58	4.631	0.054
455	137.16	4.513	-0.241
460	137.74	4.549	-0.149
465	138.305	4.544	-0.35
470	138.87	4.392	0.62
475	139.435	4.296	-0.291
480	140	4.675	-0.145
485	144	4.122	-0.062
490	148	4.462	-0.415
495	152	4.317	0.059
500	156	4.527	-0.029
505	160	4.436	-0.068
510	164	4.403	-0.115
515	168	4.384	-0.056
520	172	4.439	0.093
525	176	4.491	-0.061
530	180	4.421	-0.182
535	180.66	4.201	-0.233
540	181.32	3.801	-0.515
550	182.64	4.317	-0.256
560	183.96	4.234	-0.151
585	187.26	4.351	-0.01
625	192.54	4.307	0.148
665	197.82	4.305	-0.286
675	199.14	4.238	-0.253
680	199.8	3.849	-0.173
685	200	4.333	-0.208

A.4. Oxygen and carbon stable isotope data for PCM5 from planktic and benthic foraminifera

Depth Planktic	Age Planktic	Oxygen 18 Planktic	Carbon 13 Planktic	Depth *Melonis barleeanum*	Age *Melonis barleeanum*	Carbon 13 *Melonis barleeanum*	Oxygen 18 *Melonis barleeanum*
0	10.2	2.736	0.175	0	10.2	-1.682	4.141
5	10.24	2.733	0.092	2.5	10.22	-1.695	4.072
10	10.28	2.931	0.03	5	10.24	-1.888	4.177
12.5	10.31	2.845	-0.092	10	10.28	-1.685	4.054
15	10.33	2.883	-0.021	12.5	10.31	-2.063	4.19
20	10.37	2.743	0.107	15	10.33	-2.025	4.287
25	10.41	2.691	-0.267	20	10.37	-1.988	4.369
40	10.56	3.183	0.131	25	10.41	-2.049	4.469
45	10.6	3.615	0.082	40	10.56	-1.561	4.006
50	10.93	3.419	0.115	45	10.6	-1.783	4.474
55	11.26	3.412	0.092	50	10.93	-1.752	4.475
65	11.92	4.02	-0.134	55	11.26	-1.794	4.255
70	11.95	3.343	0.067	60	11.59	-1.865	4.545
75	11.99	2.964	-0.225	65	11.92	-1.756	4.609
85	12.06	3.243	0.01	70	11.95	-1.952	4.585
90	12.09	3.056	0.186	75	11.98	-1.969	4.361
95	12.13	2.678	-0.063	80	12.01	-2.007	4.399
100	12.16	2.678	-0.232	85	12.04	-1.937	4.226
105	12.2	2.987	-0.225	90	12.07	-2.05	4.086
110	12.23	2.66	-0.18	95	12.1	-2.04	4.332
115	12.27	2.914	0.023	100	12.13	-2.198	3.551
120	12.3	2.62	-0.099	105	12.16	-2.065	4.353
125	12.43	2.632	-0.27	110	12.19	-2.337	4.37
130	12.57	3.661	0.759	115	12.22	-2.249	4.363
135	12.7	3.828	-0.16	120	12.3	-1.987	4.413
140	12.84	3.915	-0.118	125	12.43	-2.14	4.405
145	12.97	3.897	0.432	130	12.56	-1.271	4.746
150	13.11	3.88	0.405	135	12.69	-1.389	4.724
157.5	13.27	4.078	-0.382	140	12.82	-1.283	4.623
160	13.32	4.099	0.181	145	12.95	-1.131	4.757
162.5	13.38	3.88	-0.041	150	13.11	-1.307	4.692
165	13.43	3.616	-0.457	155	13.22	-1.447	4.734
172.5	13.6	3.518	0.084	160	13.32	-1.473	4.742
177.5	13.73	3.542	-0.144	240	15.36	-1.06	4.671
182.5	13.86	4.086	-0.194	245	15.48	-1.201	4.688
187.5	13.99	3.973	-0.296	250	15.61	-1.5	4.513
195	14.18	3.777	-0.326	270	16.5	-0.167	4.721
197.5	14.25	4.047	-0.056	315	21	-1.793	4.742
202.5	14.38	4.11	0.229	320	21.5	-0.488	5.144
205	14.44	3.986	0.023	325	22.04	-1.094	4.997
207.5	14.51	4.044	0.132	330	22.78	-0.838	5.126
210	14.57	4.081	-0.062	345	25	-0.894	5.08
212.5	14.64	3.954	0.047	350	26.83	-1.051	4.79
217.5	14.77	4.066	0.04	370	34.2	-0.862	5.093
227.5	15.03	3.923	0.115	375	36.00	-1.055	4.988
232.5	15.16	4.038	-0.18	390	37.35	-1.149	4.922
237.5	15.29	4.016	0.015	400	38.25	-1.264	4.058
245	15.48	4.002	0.051	405	38.70	-1.472	4.161
250	15.61	4.448	0.181	410	39.15	-1.146	4.742
255	15.74	4.583	0.217	415	39.60	-1.404	4.129
260	15.87	4.402	0.197	430	40.95	-1.351	4.581
265	16	4.748	0.004	435	41.40	-1.319	4.632
270	16.54	4.269	-0.2	440	41.85	-1.192	4.612
275	17.07	4.262	-0.15	445	42.30	-0.702	4.554
310	20.82	4.294	-0.289	450	42.75	-1.344	4.542
315	21.35	4.069	0.716	460	43.65	-1.244	4.615
320	21.89	4.462	0.031	465	44.10	-1.668	4.564
325	22.04	4.498	0.044	470	44.55	-1.6	4.519
330	22.78	4.408	0.061	475	45.00	-1.044	4.32
340	24.26	4.092	0.249	485	45.70	-1.401	4.584
345	25	3.649	0.216	510	47.45	-0.997	4.789
350	26.83	4.106	0.219	515	47.80	-0.906	4.638
370	34.17	4.159	0.188	520	48.15	-1.381	4.77
375	36	3.683	-0.007	525	48.50	-0.713	4.602
400	38.25	3.962	-0.052	530	48.85	-0.827	5.102
405	38.7	3.831	0.251	540	49.55	-1.029	4.716
410	39.15	4.285	0.149	550	50.75	-1.379	4.771
415	39.6	3.878	0.16	555	51.50	-1.111	4.941
420	40.05	4.297	0.243	565	53.00	-1.464	4.747
428	40.5	4.113	-0.051	570	53.75	-1.153	4.596
435	41.4	4.272	0.118	575	54.50	-1.452	4.751
440	41.85	4.333	-0.037	580	55.25	-1.593	4.742
445	42.3	4.165	-0.206	600	58.25	-1.542	4.769

A.5. Oxygen and carbon stable isotope data from PCM7 for planktic and benthic foraminifera

Depth Planktic	Age Planktic	Oxygen 18 Planktic	Carbon 13 Planktic	Depth *Melonis barleeanum*	Age *Melonis barleeanum*	Carbon 13 *Melonis barleeanum*	Oxygen 18 *Melonis barleeanum*
450	42.75	4.3	-0.115	605	59.00	-1.591	4.695
455	43.2	4.163	-0.117				
460	43.65	4.238	0.081				
475	45	3.966	-0.066				
480	45.35	3.969	0.032				
490	46.05	3.956	0.038				
505	47.1	4.031	-0.129				
515	47.8	4.206	0.018				
520	48.15	4.141	0.065				
525	48.5	4.007	0.216				
528	48.85	3.844	-0.064				
545	50	3.605	0.109				
550	50.75	3.996	-0.177				
565	53	3.976	-0.155				
570	53.75	3.859	-0.291				
575	54.5	3.777	-0.436				
580	55.25	4.128	-0.284				
585	56	4.113	-0.222				
590	56.75	4.085	-0.118				
600	58.25	3.78	-0.253				
605	59	3.778	-0.281				
610	59.55	3.895	-0.069				
615	60.1	3.949	-0.43				
620	60.65	3.929	-0.269				
625	61.2	4.009	-0.397				
628	61.75	4.026	-0.361				
635	62.3	3.897	-0.475				
640	62.85	3.707	-0.3				
645	63.4	3.774	-0.464				
650	64	3.485	-0.5				
660	65.1	4.107	-0.163				
665	65.65	4	-0.338				
670	66.2	3.898	-0.22				
675	66.75	4.109	-0.306				
680	67.3	3.918	-0.396				
690	68.4	3.955	-0.299				
695	69	3.894	-0.285				
700	69.55	4.006	-0.289				
710	70.65	3.883	-0.388				
720	71.75	3.924	-0.309				
727	72.75	4.02	-0.242				

Depth *Cassidulina teretis*	Age *Cassidulina teretis*	Carbon 13 *Cassidulina teretis*	Oxygen 18 *Cassidulina teretis*	Depth Combined benthics	Age Combined bethics	Oxygen 18 Combined benthics	Depth B-P	Oxygen 18 B-P
130	12.57	-0.703	5.177	0	10.2	4.541	0	1.805
135	12.7	-0.661	5.106	2.5	10.22	4.472	5	1.844
140	12.84	-0.571	5.213	5	10.24	4.577	10	1.523
145	12.97	-0.622	5.062	10	10.28	4.454	12.5	1.745
150	13.11	-0.552	5.058	12.5	10.31	4.59	15	1.804
155	13.22	-0.524	5.224	15	10.33	4.687	20	2.026
160	13.32	-0.429	5.354	20	10.37	4.769	25	2.178
165	13.43	-0.57	5.367	25	10.41	4.869	40	1.223
170	13.55	-0.864	5.298	40	10.56	4.406	45	1.259
180	13.81	-1.261	5.286	45	10.6	4.874	50	1.456
190	14.07	-1.134	5.257	50	10.93	4.875	55	1.243
210	14.59	-1.059	5.354	55	11.26	4.655	65	0.989
220	14.85	-0.63	5.006	60	11.59	4.945	70	1.642
225	14.98	-0.73	5.167	65	11.92	5.009	75	1.797
240	15.36	-0.616	5.258	70	11.95	4.985	85	1.383
245	15.48	-0.381	5.223	75	11.98	4.761	90	1.43
250	15.61	-0.803	4.926	80	12.01	4.799	95	2.054
255	15.74	-0.549	5.552	85	12.04	4.626	105	1.766
260	15.87	-0.523	5.378	90	12.07	4.486	110	2.11
265	16	-0.466	5.417	95	12.1	4.732	115	1.849
270	16.5	-0.642	5.315	100	12.13	3.951	120	2.193
275	17	-0.41	5.4	105	12.16	4.753	125	2.173
300	19.5	-0.008	5.323	110	12.19	4.77	130	1.485
310	20.5	0.181	5.569	115	12.22	4.763	135	1.296
320	21.5	-0.517	5.267	120	12.3	4.813	140	1.108
330	22.78	-0.334	5.74	125	12.43	4.805	145	1.26
345	25	-0.293	5.172	130	12.56	5.146	150	1.212
405	38.7	-0.334	4.809	135	12.69	5.124	155	1.146
430	40.95	-0.542	4.844	140	12.82	5.023	160	1.043
435	411.4	-0.621	5.038	145	12.95	5.157	165	1.717
440	41.85	-0.623	4.805	150	13.11	5.092	170	1.78
445	42.3	-0.539	4.794	155	13.22	5.134	180	1.472
				160	13.32	5.142	190	1.284
				165	13.43	5.367	210	1.241
				170	13.55	5.298	225	1.244
				180	13.81	5.286	240	1.242
				190	14.07	5.257	245	1.086
				210	14.59	5.354	250	0.465
				220	14.85	5.006	255	0.935
				225	14.98	5.167	260	0.942
				240	15.36	5.071	265	0.635
				245	15.48	5.088	270	0.852
				250	15.61	4.913	275	1.104
				255	15.74	5.552	310	0.995
				260	15.87	5.378	315	1.073
				265	16.00	5.417	320	1.082
				270	16.50	5.121	325	0.899
				275	17.00	5.4	330	1.118
				300	19.50	5.323	345	1.831
				310	20.50	5.569	350	1.084
				315	21.00	5.142	370	1.334
				320	21.50	5.544	375	1.705
				325	22.04	5.397	405	0.73
				330	22.78	5.526	410	0.857
				345	25.00	5.48	415	0.651
				350	26.83	5.19	428	0.868
				370	34.20	5.493	435	0.76
				375	36.00	5.388	440	0.679
				390	37.35	5.322	445	0.789
				400	38.25	4.458	450	0.642
				405	38.70	4.561	460	0.777
				410	39.15	5.142	475	0.754
				415	39.60	4.529	515	0.832
				430	40.95	4.981	520	1.029
				435	41.40	5.032	525	0.995
				440	41.85	5.012	528	1.658
				445	42.30	4.954	550	1.175
				450	42.75	4.942	565	1.171
				460	43.65	5.015	570	1.137
				465	44.10	4.964	575	1.374
				470	44.55	4.919	580	1.014
				475	45.00	4.72	600	1.389
				485	45.70	4.984	605	1.117

Depth Combined benthics	Age Combined bethics	Oxygen 18 Combined benthics
510	47.45	5.189
515	47.80	5.038
520	48.15	5.17
525	48.50	5.002
530	48.85	5.502
540	49.55	5.116
550	50.75	5.171
555	51.50	5.341
565	53.00	5.147
570	53.75	4.996
575	54.50	5.151
580	55.25	5.142
600	58.25	5.169
605	59.00	5.095

Depth Planktic	Age Planktic	Carbon 13 Planktic	Oxygen 18 Planktic	Depth *Melonis barleeanum*	Age *Melonis barleeanum*	Carbon 13 *Melonis barleeanum*	Oxygen 18 *Melonis barleeanum*	Oxygen 18 *M. barleeanum* Corrected	Depth B-P	Oxygen 18 B-P
4	8.66	-0.12	2.591	2	8.63	-1.964	4.511	4.911	6	1.83
6	8.69	0.069	2.832	6	8.68	-1.855	4.262	4.662	10	2.251
8	8.72	-0.222	2.655	10	8.75	-1.886	4.502	4.902	18	2.096
10	8.75	-0.038	2.651	14	8.81	-2.219	4.434	4.834	22	1.943
12	8.78	0.251	2.923	18	8.86	-2.052	4.441	4.841	26	2.145
16	8.83	0.034	2.748	22	8.92	-2.025	4.355	4.755	30	2.621
18	8.86	0.035	2.745	26	8.98	-1.96	4.431	4.831	34	2.155
20	8.89	-0.336	2.853	30	9.03	-1.915	4.367	4.767	38	2.06
22	8.92	-0.378	2.812	34	9.086	-2.204	4.332	4.732	42	1.847
24	8.94	-0.144	2.706	38	9.142	-1.953	4.446	4.846	46	1.549
26	8.97	-0.005	2.686	42	9.198	-2.041	4.423	4.823	50	1.499
28	9	-0.082	2.73	46	9.254	-2.021	4.41	4.81	54	1.709
30	9.03	-0.481	2.146	50	9.31	-2.063	4.264	4.664	58	1.938
34	9.086	-0.207	2.577	54	9.366	-2.049	4.326	4.726	62	1.95
38	9.142	-0.186	2.786	58	9.422	-2.119	4.468	4.868	66	2.19
42	9.198	0.127	2.976	62	9.478	-2.08	4.532	4.932	70	1.759
46	9.254	0.15	3.261	66	9.534	-2.182	4.47	4.87	74	1.699
50	9.31	0.062	3.164	70	9.59	-2.003	4.432	4.832	78	1.72
54	9.366	-0.039	3.017	74	9.646	-2.005	4.411	4.811	82	1.527
58	9.422	-0.245	2.93	78	9.702	-1.856	4.403	4.803	86	1.16
62	9.478	-0.224	2.982	82	9.758	-1.909	4.442	4.842	90	1.566
66	9.534	0.037	2.68	86	9.814	-1.761	3.9	4.3	94	1.413
70	9.59	-0.012	3.073	90	9.87	-1.785	4.437	4.837	98	1.52
74	9.646	-0.079	3.112	94	9.926	-1.981	4.173	4.573	100	1.156
78	9.702	-0.275	3.083	98	9.97	-1.927	4.318	4.718		
82	9.758	0.093	3.315	100	10	-1.861	4.241	4.641		
86	9.814	0.016	3.14							
90	9.87	0.2	3.271							
94	9.926	-0.024	3.16							
98	9.97	0.023	3.198							
100	10	0.195	3.485							

A.6. Oxygen and carbon stable isotope data from PCM7 Trip core for planktic and benthic foraminifera

Depth Planktic	Age Planktic	Carbon 13 Planktic	Oxygen 18 Planktic	Depth Benthic	Carbon 13 *Cassidulina teretis*	Oxygen 18 *Cassidulina teretis*	Carbon 13 *Melonis barleeanum*	Oxygen 18 *Melonis barleeanum*	Depth Combined benthic	Age Combined benthic	Oxygen 18 Combined benthic	Depth B-P	Oxygen 18 B-P
17	15.401	-0.652	3.005	2	-	-	-1.519	3.647	2	15.338	4.047	27	0.517
27	15.443	-0.177	4.05	7	-	-	-1.138	4.398	7	15.359	4.798	32	0.761
32	15.464	-0.084	3.94	22	-	-	-0.941	4.625	22	15.422	5.025	42	0.918
37	15.485	0.12	4.511	27	-	-	-1.43	4.167	27	15.443	4.567	57	0.763
42	15.506	-0.103	4.492	32	-	-	-1.489	4.301	32	15.464	4.701	67	0.73
47	15.527	-0.174	3.932	42	-0.507	5.41	-	-	42	15.506	5.41	72	0.878
57	15.569	-0.014	4.62	57	-0.358	5.383	-	-	57	15.569	5.383	77	0.733
62	15.59	0.125	4.597	67	-0.404	5.514	-	-	67	15.611	5.514	82	0.811
67	15.611	-0.065	4.784	72	-	-	-1.457	5.151	72	15.632	5.551	87	1.134
72	15.632	0	4.673	77	-0.494	5.355	-	-	77	15.656	5.355	92	1.047
77	15.656	-0.009	4.622	82	-0.483	5.46	-	-	82	15.699	5.46	102	0.617
82	15.699	-0.035	4.649	87	-0.466	5.546	-	-	87	15.742	5.546	107	0.81
87	15.742	0.16	4.412	92	-0.439	5.618	-	-	92	15.785	5.618	112	0.81
92	15.785	0.171	4.571	102	-0.714	5.268	-	-	102	15.871	5.268	117	0.676
97	15.828	0.044	4.58	107	-0.475	5.526	-	-	107	15.914	5.526	122	0.365
102	15.871	-0.046	4.651	112	-0.583	5.479	-	-	112	15.957	5.479	127	0.569
107	15.914	-0.048	4.716	117	-0.548	5.442	-	-	117	16	5.442	132	0.898
112	15.957	0.047	4.669	122	-0.49	5.094	-	-	122	16.3	5.094	142	0.961
117	16	-0.037	4.766	127	-0.603	5.243	-	-	127	16.6	5.243	147	0.498
122	16.3	0.104	4.729	132	-0.583	5.437	-	-	132	16.9	5.437	177	0.455
127	16.6	0.196	4.674	142	-0.418	5.696	-	-	142	17.5	5.696	187	0.906
132	16.9	-0.058	4.539	147	-0.331	5.308	-	-	147	18.15	5.308	202	0.737
137	17.2	-0.069	4.408	177	-0.571	5.185	-	-	177	22.04	5.185	207	1.149
142	17.5	0.181	4.735	187	-0.113	5.154	-0.625	4.976	187	24	5.154	217	0.771
147	18.15	0.071	4.81	192	-0.47	5.161	-	-	192	25	5.161	222	1.367
157	19.45	-0.081	4.644	207	-	-	-1.023	5.138	207	31.671	5.538	227	1.104
162	20.1	-0.018	4.164	217	-0.585	4.877	-0.988	4.695	217	35.005	5.095	232	0.803
167	20.75	-0.209	4.525	222	-0.455	5.473	-1.359	4.805	222	36.672	5.473	242	0.694
172	21.4	0.006	4.799	227	-	-	-1.053	4.845	227	38.339	5.245	247	0.67
177	22.04	-0.078	4.73	232	-	-	-1.046	4.633	232	40	5.033	252	0.761
182	23	-0.186	4.773	242	-0.559	4.584	-	-	242	41.337	4.584	257	0.654
187	24	0.048	4.248	247	-0.596	4.734	-	-	247	42.004	4.734	262	0.611
202	30.004	-0.051	4.417	252	-	-	-1.069	4.216	252	42.671	4.616	267	0.465
207	31.671	0.319	4.389	257	-0.588	4.676	-	-	257	43.338	4.676	277	0.479
212	33.338	0.088	4.229	262	-0.585	4.79	-	-	262	44	4.79	287	0.709
217	35.005	0.426	4.324	267	-0.76	4.388	-	-	267	46.14	4.388	307	1.325
222	36.672	0.277	4.106	277	-0.799	4.394	-	-	277	50.42	4.394	312	1.203
227	38.339	0.256	4.141	287	-0.381	4.448	-	-	287	54.7	4.448	317	0.992
232	40	0.286	4.23	307	-	-	-1.34	4.747	307	60.5	5.147	322	1.107
237	40.67	0.391	2.913	312	-0.626	5.061	-1.31	4.66	312	61.25	5.061	332	1.077
242	41.337	0.06	3.89	317	-0.605	4.898	-	-	317	62	4.898	337	1.182
247	42.004	0.08	4.064	322	-0.243	5.044	-	-	322	62.75	5.044	407	1.598
252	42.671	-0.071	3.855	332	-0.472	5.078	-	-	332	64.25	5.078	412	1.109
257	43.338	-0.076	4.022	337	-0.354	5.308	-	-	337	65	5.308	417	0.601
262	44	0.175	4.179	402	-	-	-1.564	4.319	402	90.43	4.719	422	1.091

A.7. Oxygen and carbon stable isotope data from PCM30 for both planktic and benthic foraminifera. For the combined benthic data the two benthic species measured have been corrected and results combined .

Depth Planktic	Age Planktic	Carbon 13 Planktic	Oxygen 18 Planktic	Depth Benthic	Carbon 13 *Cassidulina teretis*	Oxygen 18 *Cassidulina teretis*	Carbon 13 *Melonis barleeanum*	Oxygen 18 *Melonis barleeanum*	Depth Combined benthic	Age Combined benthic	Oxygen 18 Combined benthic	Depth B-P	Oxygen 18 B-P
267	46.14	-0.118	3.923	407	-0.361	4.405	-	-	407	91.71	4.405	427	1.325
272	48.28	0.095	3.955	412	-0.505	4.857	-	-	412	93	4.857	437	1.43
277	50.42	-0.077	3.915	417	-	-	-1.427	3.715	417	93.4	4.115	452	1.404
282	52.56	-0.071	3.634	422	-	-	-1.583	4.007	422	93.8	4.407	457	0.62
287	54.7	-0.206	3.739	427	-	-	-1.518	4.033	427	94.2	4.433	507	0.449
297	59	-0.086	3.063	432	-	-	-1.729	3.773	432	94.6	4.173	512	-0.207
302	59.75	-0.064	3.822	442	-	-	-2.047	3.948	442	100	4.348	517	0.387
312	61.25	-0.285	3.858	452	-	-	-2.503	4.029	452	110	4.429	522	-0.05
317	62	-0.348	3.906	457	-	-	-1.931	3.173	457	112.75	3.573	527	-0.08
322	62.75	-0.043	3.937	507	-0.625	5.129	-	-	507	136.58	5.129	532	0.193
327	63.5	-0.258	3.977	512	-0.91	4.473	-	-	512	136.87	4.473	557	1.066
332	64.25	-0.149	4.001	517	-0.876	4.805	-	-	517	137.16	4.805	562	0.185
337	65	0.141	4.126	522	-0.832	4.666	-	-	522	137.45	4.666		
362	75	0.228	3.932	527	-0.868	4.618	-	-	527	137.74	4.618		
407	91.71	0.211	2.807	532	-0.607	4.887	-	-	532	138.03	4.887		
412	93	0.429	3.748	557	-0.496	5.435	-	-	557	139.48	5.435		
417	93.4	0.362	3.514	562	-0.277	4.392	-	-	562	139.77	4.392		
422	93.8	0.32	3.316										
427	94.2	0.453	3.108										
437	95	0.133	2.733										
452	110	0.213	3.025										
457	112.75	0.006	2.953										
467	118.25	-0.303	1.68										
472	121	-0.54	1.225										
477	125.3	-0.442	1.779										
482	129.6	-0.188	3.524										
487	134	-0.053	4.34										
492	135	0.151	4.551										
497	136	0.05	4.708										
507	136.58	-0.189	4.68										
512	136.87	-0.207	4.68										
517	137.16	-0.041	4.418										
522	137.45	0.021	4.716										
527	137.74	-0.003	4.698										
532	138.03	-0.186	4.694										
537	138.32	-0.169	4.579										
542	138.61	0.137	4.459										
547	138.9	0.038	4.627										
557	139.48	-0.289	4.369										
562	139.77	-0.124	4.207										
567	140	-0.224	3.435										
572	140.29	0	4.03										
577	140.58	-0.164	4.027										

A.7. Oxygen and carbon stable isotope data from PCM30 for both planktic and benthic foraminifera. For the combined benthic data the two benthic species measured have been corrected and results combined .

Depth planktic	Oxygen 18 Planktic 3 point av.	Depth Mag. Sus.	Magnetic Susceptibility	Depth Planktic	Oxygen 18 Planktic 3 point av.	Depth Mag. Sus.	Magnetic Susceptibility
2	3.88	3	0.0135	310	4.12	500	0.0161
5	3.82	10	0.0141	320	4.23	510	0.0151
10	3.76	20	0.0141	330	4.12	520	0.0154
15	3.75	30	0.0138	340	3.89	530	0.0150
20	3.74	40	0.0149	350	3.65	540	0.0152
25	3.89	50	0.0130	360	3.68	550	0.0151
30	4.02	60	0.0130	370	3.65	560	0.0149
40	4.13	70	0.0141	380	3.66	570	0.0136
50	4.12	80	0.0133	390	3.70	580	0.0137
60	4.05	90	0.0157	400	3.76	590	0.0127
70	4.08	100	0.0118	410	3.85	600	0.0157
80	4.08	110	0.0129	420	3.91	610	0.0153
90	4.10	120	0.0112	430	4.02	620	0.0129
100	4.09	130	0.0128	440	4.02	630	0.0147
110	4.05	140	0.0111	450	3.99	640	0.0144
120	3.95	150	0.0132	460	3.93	650	0.0136
130	3.91	160	0.0138	470	3.94	660	0.0127
135	3.83	170	0.0139	480	3.89	670	0.0130
140	3.94	180	0.0146	490	4.06	680	0.0138
145	4.03	190	0.0143	500	4.22	690	0.0132
150	4.15	200	0.0176	510	4.43	700	0.0140
155	4.15	210	0.0148	520	4.48	710	0.0138
160	4.18	220	0.0141	530	4.40	720	0.0141
165	4.01	230	0.0152	540	4.32	730	0.0141
170	3.79	240	0.0154	550	4.24	740	0.0146
180	3.67	250	0.0157	560	4.11	750	0.0145
185	3.82	260	0.0135	570	4.11		
190	4.02	270	0.0139	580	4.20		
195	3.97	280	0.0170	590	4.47		
200	3.83	290	0.0174	600	4.52		
205	3.64	300	0.0155	610	4.53		
210	3.73	310	0.0145	620	4.51		
215	3.93	320	0.0140	630	4.56		
220	4.16	330	0.0132	640	4.60		
225	4.11	340	0.0126	650	4.58		
230	3.97	350	0.0167	660	4.53		
235	3.93	360	0.0165	670	4.59		
240	3.98	370	0.0144	680	4.57		
245	3.97	380	0.0121	690	4.55		
250	3.84	390	0.0130	700	4.45		
255	3.76	400	0.0124	710	4.57		
260	3.88	410	0.0133	720	4.64		
265	4.00	420	0.0128	730	4.69		
270	4.04	430	0.0136	740	4.57		
275	4.04	440	0.0145	750	4.53		
280	3.91	450	0.0135				
285	3.88	460	0.0140				
290	3.89	470	0.0143				
295	4.01	480	0.0157				
300	4.06	490	0.0152				

Depth	Age	Clasts >2mm	Depth	Age	Clasts >2mm	Depth	Age	Clasts >2mm
0	12.61	0	104	15.00	3	208	30.22	37
2	12.66	0	106	15.05	1	210	31.48	35
4	12.70	0	108	15.09	2	212	32.56	15
6	12.75	1	110	15.14	15	214	33.64	9
8	12.79	0	112	15.19	5	216	34.72	9
10	12.84	1	114	15.23	16	218	35.80	18
12	12.89	1	116	15.28	34	220	36.88	15
14	12.93	1	118	15.32	35	222	37.96	13
16	12.98	1	120	15.37	28	224	39.04	6
18	13.02	1	122	15.42	9	226	40.12	7
20	13.07	2	124	15.46	8	228	41.20	3
22	13.12	1	126	15.51	10	230	42.28	8
24	13.16	0	128	15.55	7	232	43.36	2
26	13.21	2	130	15.60	6	234	44.44	5
28	13.25	1	132	15.65	3	244	49.49	0
30	13.30	0	134	15.69	1	246	50.40	11
32	13.35	0	136	15.74	2	248	51.30	4
34	13.39	0	138	15.78	6	250	52.21	5
36	13.44	0	140	15.83	4	252	53.11	16
38	13.48	0	142	15.88	4	254	54.02	8
40	13.53	0	144	16.00	2	256	54.93	22
42	13.58	1	146	16.12	4	258	55.83	29
44	13.62	0	148	16.36	3	260	56.74	15
46	13.67	0	150	16.60	0	262	57.64	4
48	13.71	2	152	16.84	4	264	58.55	5
50	13.76	0	154	17.08	8	266	59.23	11
52	13.81	0	156	17.32	3	268	59.70	12
54	13.85	1	158	17.56	5	270	60.16	8
56	13.90	0	160	17.80	3	272	60.62	5
58	13.94	1	162	18.04	3	274	61.07	3
60	13.99	0	164	18.28	1	276	61.53	10
62	14.04	1	166	18.52	5	278	61.98	16
64	14.08	2	168	18.76	1	280	62.44	21
66	14.13	1	170	19.00	2	282	62.90	21
68	14.17	0	172	19.24	1	284	63.35	5
70	14.22	0	174	19.48	0	286	63.81	5
72	14.27	0	176	19.72	1	288	64.26	18
74	14.31	1	178	19.98	0	290	64.72	14
76	14.36	0	180	20.23	0	292	65.18	21
78	14.40	0	182	20.47	0	294	65.63	10
80	14.45	0	184	20.71	0	296	66.09	4
82	14.50	0	186	20.95	1	298	66.54	17
84	14.54	2	188	21.19	0	300	67.00	8
86	14.59	0	190	21.44	0	302	67.64	15
88	14.63	1	192	21.68	0	304	68.28	17
90	14.68	1	194	21.92	0	306	68.92	21
92	14.73	0	196	22.67	3	308	69.56	33
94	14.77	2	198	23.93	0	310	70.20	13
96	14.82	1	200	25.19	0	312	70.84	9
98	14.86	0	202	26.45	45	314	71.48	27
100	14.91	0	204	27.71	47	316	72.12	44
102	14.96	2	206	28.96	57	318	72.76	33

A. 9. Abundance of clasts >2mm in PCM5.

Depth	Age	Clasts >2mm	Depth	Age	Clasts >2mm	Depth	Age	Clasts >2mm
320	73.40	55	434	124.68	15	548	182.43	8
322	74.04	11	436	125.32	8	550	182.70	24
324	74.68	1	438	126.00	4	552	182.97	18
326	75.66	5	440	134.00	3	554	183.24	24
328	77.33	1	442	134.80	0	556	183.51	15
330	78.67	1	444	135.60	0	558	183.78	27
332	80.00	1	446	136.12	0	560	184.05	32
334	81.25	3	448	136.35	5	562	184.32	48
336	82.50	18	450	136.58	14	564	184.59	45
338	83.75	39	452	136.81	24	566	184.86	47
340	85.00	21	454	137.04	11	568	185.13	69
342	85.80	16	456	137.28	16	570	185.40	53
344	86.60	6	458	137.51	11	572	185.67	64
346	87.40	1	460	137.74	26	574	185.94	30
348	88.20	2	462	137.97	28	576	186.21	58
350	89.00	0	464	138.19	66	578	186.48	39
352	89.32	0	466	138.42	60	580	186.75	38
354	89.64	0	468	138.64	62	582	187.02	25
356	89.96	3	470	138.87	32	584	187.29	41
358	90.28	7	472	139.10	38	586	187.56	42
360	90.60	0	474	139.32	40	588	187.83	44
362	90.92	1	476	139.55	49	590	188.10	30
364	91.24	5	478	139.77	38	592	188.37	23
366	91.56	15	480	140.00	36	594	188.64	15
368	91.88	27	482	141.60	38	596	188.91	6
370	92.20	12	484	143.20	34	598	189.18	3
372	92.52	6	486	144.80	51	600	189.45	0
374	92.84	7	488	146.40	29	602	189.72	9
376	93.11	15	490	148.00	24	604	189.99	11
378	93.38	19	492	149.60	26	606	190.26	11
380	93.65	22	494	151.20	16	608	190.53	2
382	93.92	26	496	152.80	4	610	190.80	3
384	94.19	39	498	154.40	2	612	191.07	2
386	94.46	54	500	156.00	0	614	191.34	6
388	94.73	37	502	157.60	3	616	191.61	3
390	95.00	47	504	159.20	2	618	191.88	10
392	96.60	50	506	160.80	15	620	192.15	5
394	98.20	59	508	162.40	19	622	192.42	8
396	99.60	54	510	164.00	17	624	192.69	15
398	100.80	45	512	165.60	23	626	192.96	12
400	102.00	42	514	167.20	9	628	193.23	12
402	104.00	10	516	168.80	23	630	193.50	2
404	106.00	1	518	170.40	12	632	193.77	0
406	108.50	0	520	172.00	32	634	194.04	0
408	111.00	4	522	173.60	25	636	194.31	0
410	117.00	0	524	175.20	16	638	194.58	0
412	117.64	0	526	176.80	13	640	194.85	0
414	118.28	10	528	178.40	12	642	195.12	0
416	118.92	0	530	180.00	17	644	195.39	0
418	119.56	3	532	180.27	15	646	195.66	0
420	120.20	6	534	180.54	29	648	195.93	2
422	120.84	13	536	180.81	33	650	196.20	0
424	121.48	3	538	181.08	23	652	196.47	3
426	122.12	4	540	181.35	9	654	196.74	0
428	122.76	2	542	181.62	18	656	197.01	0
430	123.40	3	544	181.89	29	658	197.28	1
432	124.04	9	546	182.16	28	660	197.55	0
						662	197.82	0
						664	198.09	0

A. 9. Abundance of clasts >2mm in PCM5.

Depth	Age	Clasts > 2mm.	Depth	Age	Clasts > 2mm	Depth	Age	Clasts > 2mm
2	10.22	0	92	12.11	19	182	13.85	12
4	10.24	0	94	12.13	14	184	13.90	10
6	10.26	0	96	12.14	22	186	13.95	13
8	10.28	0	98	12.15	17	188	14.00	11
10	10.30	0	100	12.17	9	190	14.05	13
12	10.32	0	102	12.18	9	192	14.10	11
14	10.34	0	104	12.20	5	194	14.15	15
16	10.36	2	106	12.21	20	196	14.20	16
18	10.38	2	108	12.22	29	198	14.25	10
20	10.40	1	110	12.24	24	200	14.30	11
22	10.42	0	112	12.25	22	202	14.35	5
24	10.44	0	114	12.27	9	204	14.40	10
26	10.46	0	116	12.28	4	206	14.45	21
28	10.48	0	118	12.29	24	208	14.50	40
30	10.49	0	120	12.30	35	210	14.55	15
32	10.50	0	122	12.35	33	212	14.60	5
34	10.52	0	124	12.41	39	214	14.65	19
36	10.53	0	126	12.46	20	216	14.70	11
38	10.54	0	128	12.52	27	218	14.75	22
40	10.56	0	130	12.57	37	220	14.80	5
42	10.58	2	132	12.62	27	222	14.85	16
44	10.59	0	134	12.68	9	224	14.90	9
46	10.67	1	136	12.73	15	226	14.95	5
48	10.80	0	138	12.79	11	228	15.00	5
50	10.93	2	140	12.84	16	230	15.05	13
52	11.06	0	142	12.89	3	232	15.10	8
54	11.19	0	144	12.95	8	234	15.15	6
56	11.32	0	146	13.00	13	236	15.20	2
58	11.45	2	148	13.06	17	238	15.25	11
60	11.58	1	150	13.11	22	240	15.30	12
62	11.71	2	152	13.15	13	242	15.35	6
64	11.84	3	154	13.20	7	244	15.40	2
66	11.93	4	156	13.24	5	246	15.45	28
68	11.94	11	158	13.29	12	248	15.50	21
70	11.96	14	160	13.33	7	250	15.55	17
72	11.97	9	162	13.37	8	252	15.60	10
74	11.99	12	164	13.42	27	254	15.65	7
76	12.00	10	166	13.46	22	256	15.70	12
78	12.01	7	168	13.51	3	258	15.75	7
80	12.03	9	170	13.55	17	260	15.80	7
82	12.04	12	172	13.60	22	262	15.85	24
84	12.06	16	174	13.65	45	264	15.90	38
86	12.07	14	176	13.70	50	266	16.19	17
88	12.08	14	178	13.75	42	268	16.39	25
90	12.10	16	180	13.80	20	270	16.59	23

A.10. Abundance of clasts >2mm in PCM7

Depth	Age	Clasts >2mm	Depth	Age	Clasts >2mm	Depth	Age	Clasts >2mm
272	16.79	19	362	31.29	8	452	42.84	42
274	16.99	13	364	32.03	14	454	43.02	3
276	17.19	14	366	32.77	13	456	43.20	36
278	17.39	20	368	33.51	14	458	43.38	22
280	17.59	32	370	34.25	8	460	43.56	28
282	17.79	19	372	34.99	16	462	43.74	44
284	17.99	26	374	35.63	18	464	43.92	26
286	18.19	19	376	36.00	9	466	44.10	38
288	18.39	22	378	36.18	11	468	44.28	52
290	18.59	17	380	36.36	14	470	44.46	40
292	18.79	13	382	36.54	18	472	44.64	41
294	18.99	11	384	36.72	45	474	44.82	38
296	19.19	19	386	36.90	12	476	45.07	26
298	19.39	16	388	37.08	8	478	45.31	9
300	19.59	15	390	37.26	17	480	45.45	28
302	19.79	6	392	37.44	26	482	45.59	24
304	19.99	10	394	37.62	32	484	45.73	27
306	20.19	11	396	37.80	6	486	45.87	24
308	20.39	14	398	37.98	2	488	46.01	12
310	20.59	13	400	38.16	3	490	46.15	11
312	20.79	7	402	38.34	4	492	46.29	11
314	20.99	11	404	38.52	5	494	46.43	3
316	21.19	6	406	38.70	2	496	46.57	0
318	21.39	0	408	38.88	14	498	46.71	2
320	21.59	3	410	39.06	12	500	46.85	0
322	21.79	8	412	39.24	20	502	46.99	0
324	21.94	7	414	39.42	52	504	47.13	0
326	22.24	2	416	39.60	42	506	47.27	1
328	22.54	6	418	39.78	30	508	47.41	0
330	22.84	19	420	39.96	22	510	47.55	2
332	23.14	14	422	40.14	13	512	47.69	1
334	23.44	23	424	40.32	13	514	47.83	0
336	23.74	4	426	40.50	3	516	47.97	2
338	24.04	2	428	40.68	2	518	48.11	0
340	24.34	4	430	40.86	8	520	48.25	1
342	24.64	8	432	41.04	44	522	48.39	0
344	24.85	1	434	41.22	23	524	48.53	3
346	25.37	7	436	41.40	12	526	48.67	0
348	26.11	12	438	41.58	9	528	48.81	0
350	26.85	4	440	41.76	4	530	48.95	1
352	27.59	3	442	41.94	10	532	49.09	1
354	28.33	5	444	42.12	5	534	49.23	2
356	29.07	4	446	42.30	23	536	49.37	2
358	29.81	8	448	42.48	21	538	49.51	0
360	30.55	5	450	42.66	16	540	49.65	1

Depth	Age	Clasts >2mm	Depth	Age	Clasts >2mm	Depth	Age	Clasts >2mm
542	49.79	0	632	62.02	0	722	71.92	2
544	49.93	0	634	62.24	0	724	72.14	1
546	50.15	1	636	62.46	0	726	72.36	3
548	50.45	4	638	62.68	0	728	72.58	0
550	50.75	1	640	62.90	0			
552	51.05	5	642	63.12	0			
554	51.35	9	644	63.34	0			
556	51.65	6	646	63.56	0			
558	51.95	5	648	63.78	0			
560	52.25	6	650	64.00	0			
562	52.55	2	652	64.22	0			
564	52.85	9	654	64.44	0			
566	53.15	19	656	64.66	0			
568	53.45	16	658	64.88	0			
570	53.75	20	660	65.10	0			
572	54.05	1	662	65.32	2			
574	54.35	6	664	65.54	0			
576	54.65	18	666	65.76	1			
578	54.95	20	668	65.98	0			
580	55.25	21	670	66.20	1			
582	55.55	21	672	66.42	4			
584	55.85	19	674	66.64	4			
586	56.15	14	676	66.86	4			
588	56.45	22	678	67.08	9			
590	56.75	9	680	67.30	9			
592	57.05	4	682	67.52	21			
594	57.35	8	684	67.74	15			
596	57.65	11	686	67.96	19			
598	57.95	13	688	68.18	23			
600	58.25	6	690	68.40	22			
602	58.55	0	692	68.62	24			
604	58.85	0	694	68.84	14			
606	59.16	2	696	69.06	5			
608	59.38	3	698	69.28	6			
610	59.60	0	700	69.50	11			
612	59.82	1	702	69.72	2			
614	60.04	0	704	69.94	6			
616	60.26	0	706	70.16	10			
618	60.48	0	708	70.38	8			
620	60.70	1	710	70.60	6			
622	60.92	0	712	70.82	5			
624	61.14	0	714	71.04	1			
626	61.36	0	716	71.26	3			
628	61.58	0	718	71.48	1			
630	61.80	1	720	71.70	7			

Depth	Age	Clasts >2mm	Depth	Age	Clasts >2mm	Depth	Age	Clasts >2mm
2	15.34	23	108	15.92	2	214	33.25	6
4	15.35	10	110	15.94	2	216	34.00	9
6	15.36	5	112	15.96	0	218	34.75	21
8	15.37	7	114	15.98	1	220	35.50	16
10	15.38	9	116	15.99	0	222	36.25	32
12	15.38	13	118	16.11	0	224	37.00	16
14	15.39	18	120	16.23	2	226	37.75	5
16	15.40		122	16.35	14	228	38.50	2
18	15.41		124	16.47	13	230	39.25	7
20	15.42	25	126	16.59	20	232	40.00	31
22	15.42	49	128	16.71	8	234	40.27	21
24	15.43	38	130	16.83	0	236	40.54	26
26	15.44	9	132	16.95	4	238	40.81	30
28	15.45	3	134	17.07	16	240	41.08	24
30	15.46	11	136	17.19	9	242	41.35	36
32	15.46	25	138	17.31	14	244	41.62	25
34	15.47	14	140	17.43	27	246	41.89	31
36	15.48	9	142	17.50	3	248	42.16	27
38	15.49	4	144	17.76	9	250	42.43	10
40	15.50	3	146	18.02	11	252	42.70	22
42	15.50	2	148	18.28	10	254	42.97	22
44	15.51	0	150	18.54	9	256	43.24	18
46	15.52	2	152	18.80	7	258	43.51	46
48	15.53	0	154	19.06	8	260	43.78	39
50	15.54	5	156	19.32	11	262	44.00	29
52	15.54	5	158	19.58	10	264	44.86	18
54	15.55	5	160	19.84	20	266	45.72	28
56	15.56	14	162	20.10	33	268	46.58	29
58	15.57	12	164	20.36	9	270	47.44	35
60	15.58	2	166	20.62	5	272	48.30	9
62	15.58	0	168	20.88	1	274	49.16	1
64	15.59	1	170	21.14	1	276	50.02	2
66	15.60	0	172	21.40	5	278	50.88	1
68	15.61	0	174	21.66	3	280	51.74	2
70	15.62	0	176	22.00	1	282	52.60	7
72	15.62	1	178	22.24	5	284	53.46	14
74	15.63	0	180	22.63	5	286	54.32	13
76	15.65	3	182	23.03	6	288	55.18	22
78	15.67	0	184	23.42	6	290	56.04	14
80	15.69	2	186	23.82	9	292	56.90	12
82	15.70	6	188	24.21	11	294	57.76	9
84	15.72	3	190	24.61	2	296	58.57	5
86	15.74	2	192	25.00	1	298	59.15	6
88	15.75	1	194	25.75	2	300	59.45	1
90	15.77	7	196	26.50	10	302	59.75	10
92	15.79	4	198	27.25	14	304	60.05	8
94	15.81	1	200	28.00	17	306	60.35	10
96	15.82	1	202	28.75	18	308	60.65	7
98	15.84	2	204	29.50	23	310	60.95	6
100	15.86	0	206	30.25	18	312	61.25	34
102	15.87	5	208	31.00	21	314	61.55	35
104	15.89	1	210	31.75	13	316	61.85	7
106	15.91	2	212	32.50	42	318	62.15	18

A.11. Abundance of clasts >2mm in PCM30.

Depth	Age	Clasts >2mm	Depth	Age	Clasts >2mm	Depth	Age	Clasts >2mm
320	62.45	23	426	94.12	57	532	137.93	8
322	62.75	10	428	94.28	57	534	138.04	17
324	63.05	9	430	94.44	45	536	138.15	16
326	63.35	16	432	94.60	38	538	138.26	11
328	63.65	19	434	94.76	62	540	138.37	11
330	63.95	18	436	94.92	57	542	138.48	1
332	64.25	9	438	96.00	34	544	138.59	2
334	64.55	9	440	98.00	17	546	138.70	6
336	64.85	8	442	100.00	19	548	138.81	9
338	65.40	6	444	102.00	9	550	138.92	10
340	66.20	16	446	104.00	5	552	139.03	6
342	67.00	12	448	106.00	4	554	139.14	5
344	67.80	16	450	108.00	15	556	139.25	7
346	68.60	16	452	110.00	17	558	139.36	8
348	69.40	13	454	111.10	21	560	139.47	3
350	70.20	13	456	112.20	6	562	139.58	5
352	71.00	12	458	113.30	13	564	139.69	11
354	71.80	20	460	114.40	17	566	139.94	8
356	72.60	20	462	115.50	33	568	140.05	21
358	73.40	12	464	116.60	48	570	140.16	21
360	74.20	15	466	117.70	40	572	140.27	24
362	75.00	11	468	118.80	15	574	140.38	11
364	76.00	34	470	119.90	18	576	140.49	12
366	77.00	55	472	121.00	12	578	140.60	15
368	78.00	46	474	122.70	31	580	140.71	29
370	79.00	17	476	124.40	22	582	140.82	20
372	80.00	26	478	126.10	12	584	140.93	21
374	81.60	41	480	127.80	11	586	141.04	8
376	83.20	38	482	129.50	16	588	141.15	8
378	84.16	40	484	131.20	21	590	141.26	12
380	84.68	30	486	132.90	16	592	141.37	10
382	85.20	23	488	134.20	17	594	141.48	6
384	85.72	28	490	134.60	15	596	141.59	19
386	86.24	14	492	135.00	15	598	141.70	14
388	86.76	11	494	135.40	12	600	141.81	12
390	87.28	10	496	135.80	3	602	141.92	8
392	87.80	4	498	136.06	32	604	142.03	15
394	88.32	4	500	136.17	30	606	142.14	12
396	88.84	17	502	136.28	20	608	142.25	17
398	89.36	38	504	136.39	33	610	142.36	20
400	89.88	33	506	136.50	24	612	142.47	23
402	90.40	4	508	136.61	22	614	142.58	9
404	90.92	14	510	136.72	12	616	142.69	6
406	91.44	18	512	136.83	11	618	142.80	7
408	91.96	11	514	136.94	14	620	142.91	7
410	92.48	14	516	137.05	19	622	143.02	5
412	93.00	10	518	137.16	19	624	143.13	4
414	93.16	35	520	137.27	14	626	143.24	16
416	93.32	53	522	137.38	9	628	143.35	30
418	93.48	52	524	137.49	20	630	143.46	12
420	93.64	50	526	137.60	24	632	143.57	17
422	93.80	52	528	137.71	5			
424	93.96	39	530	137.82	8			

A.11. Abundance of clasts >2mm in PCM30.

Depth	Age	Percent >63 microns	Percent >600 mic.	Depth	Age	Percent >63 mic.	Percent >600 mic.	Depth	Age	Percent >63 mic.	Percent >600 mic.
5	12.73	19.30	4.13	140	15.83	17.80	1.90	275	61.66	30.60	10.30
10	12.84	18.10	2.10	145	16.00	25.10	4.60	280	62.99	49.30	5.40
15	12.96	14.10	1.90	150	16.60	19.10	1.80	285	64.32	38.90	8.20
20	13.07	17.80	3.60	155	17.20	29.00	4.50	290	65.65	25.90	2.90
25	13.19	18.40	4.20	160	17.80	20.80	0.90	295	66.98	29.30	4.60
30	13.30	15.60	2.20	165	18.40	20.00	4.30	300	68.31	16.40	1.30
35	13.42	27.50	4.50	170	19.00	29.10	8.20	305	69.64	12.00	2.90
40	13.53	26.10	1.40	175	19.60	24.60	5.40	310	70.97	3.30	0.00
45	13.65	16.40	1.10	180	20.20	19.70	4.80	315	72.30	4.40	0.10
50	13.76	3.30	0.20	185	20.80	18.60	4.10	320	73.63	6.60	0.40
55	13.88	1.40	0.00	190	21.40	19.40	8.20	325	75.00	17.20	3.80
60	13.99	10.00	1.90	195	22.04	20.40	0.90	330	78.34	0.60	0.00
65	14.11	4.70	0.40	200	25.19	28.30	0.90	335	82.00	0.70	0.00
70	14.22	2.60	0.10	205	28.34	20.90	0.00	340	85.00	3.80	0.00
75	14.34	2.90	0.40	210	31.48	24.80	0.90	345	87.00	22.60	1.30
80	14.45	0.60	0.00	215	34.18	3.60	0.00	350	89.00	1.90	0.00
85	14.57	1.00	0.00	220	36.88	1.30	0.00	355	89.80	2.00	0.00
90	14.68	0.50	0.00	225	39.58	30.20	0.00	360	90.60	1.20	0.10
95	14.80	0.50	0.00	230	42.28	45.10	2.00	365	91.40	2.80	0.00
100	14.91	0.60	0.00	235	44.98	9.40	0.10	370	92.20	0.60	0.00
105	15.03	0.50	0.00	240	47.68	11.20	0.10	375	93.00	28.30	5.70
110	15.14	6.20	1.30	245	49.94	25.30	0.10	380	93.66	31.10	0.60
115	15.26	12.80	3.30	250	52.21	20.90	0.00	385	94.33	35.00	7.20
120	15.37	22.80	3.70	255	54.47	14.60	0.00	390	95.00	34.80	14.70
125	15.49	34.10	9.50	260	56.74	15.30	0.00	395	99.00	26.30	5.00
130	15.60	28.20	5.40	265	59.00	22.80	1.00	400	102.00	24.00	6.40
135	15.72	12.90	1.30	270	60.33	39.50	11.20	405	107.00	33.40	11.60

A.12. Particle size data from PCM5 from dry sieving measurements

Depth	Age	Percent >63 mic.	Percent >600 mic.	Depth	Age	Percent >63 mic.	Percent >600 mic.
410	117.00	41.30	10.00	550	182.64	1.80	0.00
415	118.64	28.60	7.40	555	183.30	0.20	0.00
420	120.28	32.80	10.00	560	183.96	0.80	0.00
425	121.92	4.40	0.50	565	184.62	1.10	0.00
430	123.56	17.40	1.30	570	185.28	1.30	0.00
435	125.20	29.60	0.10	575	185.94	0.90	0.00
440	134.00	22.30	3.30	580	186.60	0.70	0.00
445	136.00	11.30	1.50	585	187.26	0.70	0.00
450	136.58	14.00	2.30	590	187.92	0.30	0.00
455	137.16	32.10	5.30	595	188.58	0.20	0.00
460	137.74	27.70	6.10	600	189.24	0.30	0.00
465	138.31	27.20	2.90	605	189.90	0.30	0.00
470	138.87	19.80	2.60	610	190.56	0.40	0.00
475	139.44	18.70	1.90	615	191.22	0.50	0.00
480	140.00	20.70	1.00	620	191.88	0.30	0.00
485	144.00	32.40	1.70	625	192.54	0.40	0.00
490	148.00	1.90	0.00	630	193.20	0.50	0.00
495	152.00	7.70	0.00	635	193.86	0.40	0.00
500	156.00	29.60	0.60	640	194.52	0.60	0.00
505	160.00	25.70	1.80	645	195.18	0.60	0.20
510	164.00	31.60	0.50	650	195.84	0.80	0.20
515	168.00	24.10	2.20	655	196.50	3.30	3.00
520	172.00	15.50	0.10	660	197.16	0.80	0.00
525	176.00	13.80	0.20	665	197.82	0.90	0.00
530	180.00	2.40	0.00	670	198.48	0.50	0.00
535	180.66	2.70	0.00	675	199.14	0.40	0.00
540	181.32	0.80	0.00	680	199.80	1.20	0.00
545	181.98	0.30	0.00	685	200.00	1.30	0.16

A.12. Particle size data from PCM5 from dry sieving measurements

Depth	Age	Clay Fraction	Silt Fraction	Sand Fraction	Depth	Age	Clay Fraction	Silt Fraction	Sand Fraction	Depth	Age	Clay Fraction	Silt Fraction	Sand Fraction
2.5	12.65	21.32	72.69	5.99	140	15.83	22.48	64.51	13.01	280	62.99	12.37	44.58	43.05
5	12.725	19.34	80.66	0	145	16.00	25.17	52.78	22.05	285	64.32	24.78	71.67	3.55
10	12.84	22.19	71.51	6.3	150	16.60	44.99	53.67	1.34	290	65.65	22.17	62.08	15.75
15	12.955	25.74	67.47	6.79	155	17.20	18.49	74.79	6.72	295	66.98	27.00	73.00	0.00
20	13.07	24.46	71.18	4.36	160	17.80	37.95	55.95	6.10	300	68.31	24.35	68.41	7.24
25	13.185	23.75	74.6	1.65	165	18.40	36.37	57.93	5.70	305	69.64	21.88	77.47	0.65
30	13.3	24.53	69.61	5.86	170	19.00	22.21	70.10	7.69	310	70.97	34.17	65.83	0.00
35	13.415	17.54	64.8	17.66	175	19.60	28.18	70.86	0.96	315	72.30	31.52	68.48	0.00
40	13.53	20.62	69.77	9.61	180	20.20	32.61	62.04	5.35	320	73.63	32.68	66.36	0.96
45	13.645	22.84	67.18	9.98	185	20.80	33.47	66.37	0.16	325	75.00	22.88	77.01	0.11
50	13.76	24.44	73.18	2.38	190	21.40	30.60	61.89	7.51	330	78.34	24.75	71.88	3.37
55	13.875	28.96	71.04	0	195	22.04	33.79	60.82	5.39	335	82.00	27.17	72.83	0.00
60	13.99	28.25	69.87	1.88	200	25.19	4.89	42.79	52.32	340	85.00	31.61	62.32	6.07
65	14.105	25.55	74.45	0	205	28.34	8.25	69.74	22.01	345	87.00	20.75	72.81	6.44
70	14.22	30.18	69.82	0	210	31.48	23.27	49.75	26.98	350	89.00	19.04	79.78	1.18
75	14.335	30.06	69.94	0	215	34.18	13.74	84.02	2.24	355	89.80	18.94	81.06	0.00
80	14.45	25.36	74.27	0.37	220	36.88	23.44	76.24	0.32	360	90.60	18.81	81.19	0.00
85	14.565	27.25	72.75	0	225	39.58	13.37	66.76	19.87	365	91.40	31.76	68.24	0.00
90	14.68	26.23	73.77	0	230	42.28	10.73	46.12	43.15	370	92.20	34.60	65.40	0.00
95	14.795	29.22	70.78	0	235	44.98	35.85	64.15	0.00	375	93.00	21.18	56.37	22.45
100	14.91	33.53	66.47	0	240	47.68	31.19	64.97	3.84	380	93.66	18.19	48.39	33.42
105	15.025	30.31	69.69	0	245	49.94	8.56	68.18	23.26	385	94.33	16.86	60.32	22.82
110	15.14	25.35	74.65	0	250	52.21	8.20	66.96	24.84	390	95.00	24.27	55.50	20.23
115	15.255	26.68	73.32	0	255	54.47	7.55	85.76	6.69	395	99.00	22.94	64.21	12.85
120	15.37	21.92	60.45	17.63	260	56.74	6.51	70.34	23.15	400	102.00	21.96	60.84	17.20
125	15.485	21.38	37.34	15.96	265	59.00	25.75	70.06	4.19	405	107.00	22.97	65.01	12.02
130	15.6	32.2	59.92	7.88	270	60.33	15.60	53.17	31.23	410	117.00	13.54	40.91	45.55
135	15.715	34.44	64.98	0.58	275	61.66	27.08	72.92	0.00	415	118.64	20.19	66.22	13.59

A.13. Particle size data for PCM5 from Coulter-LS measurements.

Depth	Age	Clay Fraction	Silt Fraction	Sand Fraction	Depth	Age	Clay Fraction	Silt Fraction	Sand Fraction
420	120.28	22.60	65.01	12.39	560	183.96	27.26	72.74	0.00
425	121.92	32.98	66.98	0.04	565	184.62	24.10	75.90	0.00
430	123.56	38.19	61.81	0.00	570	185.28	24.97	74.15	0.88
435	125.20	18.69	64.25	17.06	575	185.94	24.54	75.46	0.00
440	134.00	28.65	62.51	8.84	580	186.60	25.16	74.79	0.05
445	136.00	43.30	56.70	0.00	585	187.26	23.49	76.51	0.00
450	136.58	40.59	59.41	0.00	590	187.92	29.65	70.35	0.00
455	137.16	15.00	51.46	33.54	595	188.58	28.84	71.16	0.00
460	137.74	37.73	55.41	6.86	600	189.24	31.52	68.48	0.00
465	138.31	18.73	67.54	13.73	605	189.90	27.71	72.29	0.00
470	138.87	18.98	60.88	20.14	610	190.56	28.27	71.41	0.32
475	139.44	22.85	64.17	12.98	615	191.22	20.42	79.58	0.00
480	140.00	26.50	61.27	12.23	620	191.88	19.61	80.39	0.00
485	144.00	20.44	73.27	6.29	625	192.54	22.87	77.13	0.00
490	148.00	47.51	52.49	0.00	630	193.20	23.65	76.35	0.00
495	152.00	46.53	53.47	0.00	635	193.86	20.35	79.65	0.00
500	156.00	19.72	57.34	22.94	640	194.52	20.08	79.92	0.00
505	160.00	26.56	58.40	15.04	645	195.18	21.49	78.51	0.00
510	164.00	17.39	52.32	30.29	650	195.84	16.87	83.13	0.00
515	168.00	22.78	73.83	3.39	655	196.50	23.68	76.32	0.00
520	172.00	24.37	67.88	7.75	660	197.16	20.90	79.10	0.00
525	176.00	24.00	76.00	0.00	665	197.82	22.90	77.10	0.00
530	180.00	24.79	66.77	8.44	670	198.48	22.16	77.84	0.00
535	180.66	23.08	76.92	0.00	675	199.14	23.09	76.91	0.00
540	181.32	23.64	74.51	1.85	680	199.80	22.77	77.23	0.00
545	181.98	26.31	73.69	0.00	685	200.00	17.74	82.26	0.00
550	182.64	30.71	69.29	0.00					
555	183.30	22.44	77.56	0.00					

A.13. Particle size data for PCM5 from Coulter-LS measurements.

Depth	Age	Percent >63 microns	Percent >600 mic.	Depth	Age	Percent >63 mic.	Percent >600 mic.	Depth	Age	Percent >63 mic.	Percent >600 mic.
0	10.20	13.7	2.3	135	12.69	8.2	2.6	285	18.00	26.6	6.4
2.5	10.22	31.2	6.6	140	12.82	5.4	0.7	290	18.50	22.9	5.7
5	10.24	19.3	3.1	145	12.95	10.5	1.7	295	19.00	17.5	3.6
10	10.28	3.1	0.4	150	13.11	24.3	6.2	300	19.50	26.3	4.1
12.5	10.31	2.4	0.0	155	13.22	8.2	0.6	305	20.00	14.7	7.7
15	10.33	2.8	0.0	160	13.32	18.4	6.1	310	20.50	13.3	4.9
20	10.37	2.1	0.0	165	13.43	3.7	0.0	315	21.00	6.2	0.5
25	10.41	8.8	0.4	170	13.55	1.6	0.0	320	21.50	14.3	2.8
30	10.45	6.7	0.0	175	13.68	0.6	0.0	325	22.04	10.2	0.0
35	10.50	7.5	1.0	180	13.81	0.5	0.0	330	22.78	7.3	0.1
40	10.56	7.8	1.0	185	13.94	0.5	0.0	340	24.26	3.1	0.3
45	10.60	13.4	7.0	190	14.07	0.3	0.0	345	25.00	18.3	0.5
50	10.93	5.1	0.7	195	14.20	0.4	0.0	350	26.83	18.4	1.1
55	11.26	2.4	0.4	200	14.33	0.1	0.0	355	28.66	23.0	0.3
60	11.59	3.0	0.6	205	14.46	0.2	0.0	360	30.49	17.4	6.6
65	11.92	1.3	0.0	210	14.59	1.4	0.0	365	32.36	9.5	1.3
70	11.95	1.1	0.0	215	14.72	0.2	0.0	370	34.20	6.3	0.0
75	11.98	1.2	0.0	220	14.85	1.0	0.0	375	36.00	8.4	0.0
80	12.01	1.9	0.0	225	14.98	0.5	0.0	380	36.45	7.7	0.1
85	12.04	3.2	0.7	230	15.11	1.0	0.0	385	36.90	8.5	1.2
90	12.07	1.7	0.0	240	15.36	19.1	7.9	390	37.35	7.4	0.3
95	12.10	3.2	0.0	245	15.48	28.3	7.7	395	37.80	26.5	8.6
100	12.13	1.4	0.0	250	15.61	23.9	4.4	400	38.25	11.1	0.5
105	12.16	2.0	0.0	255	15.74	13.8	0.8	405	38.70	18.5	1.5
110	12.19	1.5	0.0	260	15.87	15.5	4.5	410	39.15	12.1	4.0
115	12.22	2.3	0.0	265	16.00	22.3	1.9	415	39.60	10.5	3.1
120	12.30	3.4	0.6	270	16.50	10.5	0.4	420	40.05	4.2	0.5
125	12.43	2.4	0.0	275	17.00	17.1	2.1	425	40.50	5.0	0.3
130	12.56	6.0	1.0	280	17.50	25.0	7.6	430	40.95	6.1	0.3

A. 14 Particle size data from dry sieving measurements for PCM7

Depth	Age	Percent >63 mic.	Percent >600 mic.
435	41.40	6.3	0.6
440	41.85	6.1	0.6
445	42.30	6.2	0.7
450	42.75	6.3	0.6
455	43.20	5.2	1.0
460	43.65	5.1	0.4
465	44.10	6.7	0.4
470	44.55	5.2	0.6
475	45.00	6.6	1.6
480	45.35	8.6	0.7
485	45.70	5.1	0.9
490	46.05	5.2	0.6
495	46.40	16.1	5.6
500	46.75	22.7	6.7
505	47.10	9.0	0.6
510	47.45	12.1	1.9
515	47.80	13.7	2.4
520	48.15	9.6	0.8
525	48.50	21.4	6.3
530	48.85	21.6	2.5
535	49.20	20.4	5.4
540	49.55	11.7	2.0
545	50.00	9.6	0.3
550	50.75	10.7	1.2
555	51.50	13.0	2.9
560	52.25	23.8	3.6
565	53.00	10.8	0.9
570	53.75	6.8	0.4
575	54.50	8.2	0.7
580	55.25	9.5	0.6
585	56.00	8.7	0.5
590	56.75	26.3	15.1
595	57.50	33.8	4.1
600	58.25	34.5	13.4
605	59.00	23.0	2.4
610	59.55	15.4	2.4
615	60.10	8.6	0.3
620	60.65	8.6	0.5
625	61.20	5.3	0.3
630	61.75	6.1	0.3
635	62.30	4.4	0.3
640	62.85	13.4	3.1
645	63.40	6.9	0.6
650	64.00	5.5	1.2
655	64.55	1.9	0.3
660	65.10	3.1	1.5
665	65.65	8.2	0.6
670	66.20	4.1	0.0
675	66.75	4.9	0.0
680	67.30	3.7	0.1
685	67.85	1.7	0.0
690	68.40	2.7	0.0
695	68.95	2.0	0.0
700	69.50	1.8	0.0
705	70.05	4.6	0.1
710	70.60	3.9	0.0
715	71.15	2.6	0.0
720	71.70	2.3	0.0
727	72.25	2.1	0.0

A. 14 Particle size data from dry sieving measurements for PCM7

Depth	Age	Percent >63 microns	Percent >600 mic.	Depth	Age	Percent >63 mic.	Percent >600 mic.	Depth	Age	Percent >63 mic.	Percent >600 mic.	Depth	Age	Percent >63 mic.	Percent >600 mic.
2	15.34	29.42	5.97	157	19.45	22.94	5.34	312	61.25	12.77	2.60	472	121.00	8.26	1.28
7	15.36	1.40	0.13	162	20.10	21.65	5.24	317	62.00	25.72	5.85	477	125.30	31.08	1.10
12	15.38	0.53	0.00	167	20.75	18.71	3.99	322	62.75	5.26	0.61	482	129.60	16.94	0.62
17	15.40	1.03	0.00	172	21.40	16.02	3.47	327	63.50	1.57	0.00	487	134.00	9.57	1.63
22	15.42	7.18	0.79	177	22.04	6.93	0.00	332	64.25	13.93	2.05	492	135.00	17.38	6.64
27	15.44	20.51	4.46	182	23.00	3.11	0.00	337	65.00	6.48	0.11	497	136.00	8.47	0.61
32	15.46	11.27	0.49	187	24.00	12.67	2.47	342	67.00	10.14	0.60	502	136.29		
37	15.49	6.80	0.55	192	25.00	20.29	4.16	347	69.00	12.22	1.02	507	136.58	5.93	0.10
42	15.51	10.09	1.34	197	28.34	10.40	0.53	352	71.00	28.13	2.66	512	136.87	2.35	0.00
47	15.53	8.65	0.55	202	30.00	8.26	0.47	357	73.00	27.61	1.25	517	137.16	2.04	0.00
52	15.55	9.85	0.21	207	31.67	6.49	0.32	362	75.00	11.31	0.00	522	137.45	1.99	0.00
57	15.57	4.76	0.26	212	33.34	3.30	0.21	367	77.50	18.28	3.05	527	137.74	2.33	0.35
62	15.59	3.28	0.55	217	35.01	6.70	0.48	372	80.00	17.39	4.17	532	138.03	3.95	0.67
67	15.61	7.86	1.03	222	36.67	10.77	1.32	377	84.00	23.50	3.16	537	138.32	1.25	0.00
72	15.63	4.30	0.00	227	38.34	11.23	0.78	382	85.29	28.75	1.47	542	138.61	1.66	0.33
77	15.66	3.93	0.00	232	40.00	18.84	4.39	387	86.57	25.39	4.23	547	138.90	3.01	0.52
82	15.70	11.95	1.25	237	40.67	2.78	0.12	392	87.86	23.81	5.58	552	139.19		
87	15.74	7.71	1.44	242	41.34	3.83	0.12	397	89.14	8.89	0.89	557	139.48	12.04	4.36
92	15.79	8.81	0.37	247	42.00	17.06	9.70	402	90.43	6.32	1.03	562	139.77	0.00	0.00
97	15.83	5.24	0.00	252	42.67	8.51	1.66	407	91.71	3.42	0.00	567	140.00	0.00	0.00
102	15.87	7.01	1.44	257	43.34	7.12	0.85	412	93.00	4.58	0.00	572	140.29	0.00	0.00
107	15.91	5.19	1.23	262	44.00	10.25	0.52	417	93.40	6.80	0.55	577	140.58	0.00	0.00
112	15.96	2.30	0.00	267	46.14	4.48	0.12	422	93.80	6.86	0.20	582	140.87	0.00	0.00
117	16.00	4.13	0.47	272	48.28	4.01	0.35	427	94.20	8.62	0.63	587	141.16	0.00	0.00
122	16.30	3.84	0.28	277	50.42	6.39	0.21	432	94.60	12.02	0.11	592	141.45	0.00	0.00
127	16.60	3.21	0.16	282	52.56	3.46	0.40	437	95.00	9.56	0.00	597	141.74	0.00	0.00
132	16.90	7.01	0.24	287	54.70	3.79	0.24	442	100.00	3.92	0.31	602	142.03	0.00	0.00
137	17.20	9.12	0.00	292	56.84	6.37	1.32	447	105.00	3.33	0.19	607	142.32	0.00	0.00
142	17.50	5.19	0.00	297	59.00	12.71	2.68	452	110.00	2.34	0.00	612	142.61	0.00	0.00
147	18.15	10.91	1.47	302	59.75	10.90	0.18	457	112.75	11.16	2.74	617	142.90	0.00	0.00
152	18.80	23.38	3.98	307	60.50	12.47	1.65	462	115.50	1.73	0.00	622	143.19	0.00	0.00
								467	118.25	3.05	0.30	627	143.48	0.00	0.00

A.15. Particle size data from dry sieving measurements for PCM30.

Depth	Age	Planktics & benthics	Planktic Abundance	Benthic Abundance	B/P ratio	*Eponides umbonatus*	*Cassidulina reniforme*	*Cassidulina teretis*	*Elphidium spp.*	*Cibicidoides wuellerstorfi*	*Pullenia bulloides*	*Neogloboquadrina pachyderma (d)*
5	12.73	76.72	70.64	6.08	0.086	1.8	0.0	0.0	0.1	1.7	0.0	1.0
10	12.84	36.90	28.80	8.10	0.281	0.4	0.0	0.0	0.1	6.5	0.0	1.1
15	12.96	2.50	1.90	0.60	0.316	0.2	0.0	0.0	0.0	0.2	0.0	0.0
20	13.07	1.60	1.60	0.00		0.0	0.0	0.0	0.0	0.0	0.0	0.0
25	13.19	0.60	0.40	0.20	0.500	0.0	0.0	0.0	0.0	0.0	0.0	0.0
30	13.30	0.20	0.20	0.00		0.0	0.0	0.0	0.0	0.0	0.0	0.0
35	13.42	0.00	0.00	0.00		0.0	0.0	0.0	0.0	0.0	0.0	0.0
40	13.53	0.00	0.00	0.00		0.0	0.0	0.0	0.0	0.0	0.0	0.0
45	13.65	0.14	0.14	0.00		0.0	0.0	0.0	0.0	0.0	0.0	0.0
50	13.76	0.00	0.00	0.00		0.0	0.0	0.0	0.0	0.0	0.0	0.0
55	13.88	3.80	2.00	1.80	0.900	0.0	1.4	0.0	0.0	0.0	0.0	0.0
60	13.99	0.85	0.64	0.21	0.328	0.0	0.1	0.0	0.0	0.1	0.0	0.0
65	14.11	2.70	1.70	1.00	0.588	0.0	0.9	0.0	0.0	0.0	0.0	0.0
70	14.22	1.00	0.30	0.70	2.333	0.0	0.5	0.0	0.1	0.0	0.0	0.0
75	14.34	1.60	0.30	1.30	4.333	0.0	1.2	0.0	0.0	0.1	0.0	0.0
80	14.45	5.00	1.20	3.80	3.167	0.0	3.1	0.0	0.0	0.0	0.0	0.0
85	14.57	8.80	3.30	5.50	1.667	0.0	5.0	0.0	0.0	0.0	0.0	0.0
90	14.68	12.50	0.90	11.60	12.889	0.0	8.4	0.0	1.3	0.0	0.0	0.0
95	14.80	8.80	5.50	3.30	0.600	0.0	3.1	0.0	0.0	0.0	0.0	0.0
100	14.91	3.50	1.50	2.00	1.333	0.0	1.6	0.0	0.1	0.0	0.0	0.0
105	15.03	10.20	2.30	7.90	3.435	0.0	7.9	0.0	0.0	0.0	0.0	0.0
110	15.14	18.60	9.60	9.00	0.938	0.1	8.0	0.0	0.1	0.2	0.0	0.2
115	15.26	20.50	13.90	6.60	0.475	0.3	3.9	0.0	0.4	0.7	0.0	0.3
120	15.37	52.90	39.70	13.20	0.332	1.9	4.3	0.0	0.5	0.1	0.0	0.1
125	15.49	122.90	104.40	18.50	0.177	9.8	1.3	0.0	1.8	0.0	0.0	1.0
130	15.60	889.80	830.10	59.70	0.072	38.9	4.0	0.0	3.0	0.0	0.0	15.7
135	15.72	640.60	596.40	44.20	0.074	34.5	2.5	0.0	0.8	0.0	0.0	5.1
140	15.83	798.10	734.60	63.50	0.086	52.9	2.4	0.0	2.5	0.3	0.0	16.7

A.16. Foraminiferal absolute abundance and individual species counts for PCM5

Depth	Age	Planktics & benthics	Planktic Abundance	Benthic Abundance	B/P ratio	*Eponides umbonatus*	*Cassidulina reniforme*	*Cassidulina teretis*	*Elphidium spp.*	*Cibicidoides wuellerstorfi*	*Pullenia bulloides*	*Neogloboquadrina pachyderma (d)*
145	16.00	769.20	712.20	57.00	0.080	40.8	2.7	0.0	3.8	0.0	0.0	7.1
150	16.60	963.00	904.70	58.30	0.064	39.7	3.9	0.0	3.3	0.4	0.0	13.4
155	17.20	1670.00	1587.30	82.70	0.052	62.8	1.0	0.0	4.3	0.2	0.0	22.7
160	17.80	736.80	667.00	69.80	0.105	60.8	0.8	0.0	5.4	1.0	0.0	7.9
165	18.40	0.60	0.50	0.10	0.200	0.0	0.0	0.0	0.0	0.0	0.0	0.0
170	19.00	0.50	0.50	0.00		0.0	0.0	0.0	0.0	0.0	0.0	0.0
175	19.60	3.70	2.60	1.10	0.423	0.1	0.2	0.0	0.3	0.5	0.0	0.0
180	20.20	3.60	1.10	2.50	2.273	0.1	0.4	0.0	1.2	0.2	0.0	0.0
185	20.80	3.20	1.10	2.10	1.909	0.3	0.3	0.0	1.1	0.1	0.0	0.0
190	21.40	51.00	43.80	7.20	0.164	1.0	2.5	0.2	0.3	0.4	0.0	6.0
195	22.04	2571.60	2476.10	95.50	0.039	54.7	10.7	0.0	5.1	0.0	0.0	19.5
200	25.19	120.60	101.10	19.50	0.193	2.8	5.7	1.7	2.7	0.0	0.0	0.0
205	28.33	14.60	6.10	8.50	1.393	0.5	0.8	0.0	3.2	0.0	0.0	0.0
210	31.48	581.30	546.80	34.50	0.063	16.2	26.9	7.9	3.0	0.2	0.0	1.6
215	34.18	17.40	14.90	2.50	0.168	0.7	1.0	0.0	0.4	0.0	0.0	0.3
220	36.88	1.90	1.30	0.60	0.462	0.0	0.1	0.0	0.3	0.0	0.0	0.0
225	39.58	207.50	174.50	33.00	0.189	5.8	10.6	5.8	5.8	0.0	0.0	1.6
230	42.28	1618.90	1537.00	81.90	0.053	7.9	41.1	10.4	1.8	0.8	0.0	8.0
235	44.98	1.20	0.90	0.30	0.333	0.0	0.3	0.0	0.0	0.0	0.0	0.0
240	47.68	0.00	0.00	0.00		0.0	0.0	0.0	0.0	0.0	0.0	0.0
245	49.94	6.70	6.10	0.60	0.098	0.0	0.3	0.0	0.1	0.0	0.0	0.0
250	52.20	3.20	1.50	1.70	1.133	0.2	0.3	0.2	0.8	0.0	0.0	0.0
255	54.47	18.00	7.40	10.60	1.432	1.0	2.8	1.4	1.7	0.0	0.0	0.0
260	56.73	8.80	1.40	7.40	5.286	0.6	2.2	0.9	1.5	0.0	0.0	0.0
265	59.00	290.50	251.80	38.70	0.154	12.5	15.8	0.4	1.1	0.1	0.0	3.2
270	60.14	0.00	0.00	0.00		0.0	0.0	0.0	0.0	0.0	0.0	0.0
275	61.28	0.14	0.14	0.00		0.0	0.0	0.0	0.0	0.0	0.0	0.1
280	62.42	1.50	1.00	0.50	0.500	0.0	0.0	0.0	0.1	0.0	0.0	0.0

A.16. Foraminiferal absolute abundance and individual species counts for PCM5

Depth	Age	Planktics & benthics	Planktic Abundance	Benthic Abundance	B/P ratio	*Eponides umbonatus*	*Cassidulina reniforme*	*Cassidulina teretis*	*Elphidium spp.*	*Cibicidoides wuellerstorfi*	*Pullenia bulloides*	*Neogloboquadrina pachyderma (d)*
285	63.56	0.14	0.00	0.14		0.0	0.1	0.0	0.0	0.0	0.0	0.0
290	64.70	7.10	6.70	0.40	0.060	0.0	0.1	0.0	0.0	0.1	0.0	0.0
295	65.84	1.80	1.50	0.30	0.200	0.1	0.0	0.2	0.0	0.0	0.0	0.0
300	67.00	0.10	0.10	0.00		0.0	0.0	0.0	0.0	0.0	0.0	0.0
305	68.60	0.20	0.20	0.00		0.0	0.0	0.0	0.0	0.0	0.0	0.0
310	70.20	18.60	4.40	14.20	3.227	14.2	0.0	0.0	0.0	0.0	0.0	0.0
315	71.80	4.80	2.80	2.00	0.714	1.1	0.2	0.4	0.1	0.0	0.0	0.0
320	73.40	11.50	1.40	10.10	7.214	10.1	0.0	0.0	0.0	0.0	0.0	0.0
325	75.00	43.60	32.40	11.20	0.346	0.5	3.3	1.1	3.9	0.0	0.0	0.1
330	78.84	19.30	18.50	0.80	0.043	0.3	0.1	0.0	0.2	0.0	0.0	0.3
335	82.00	12.90	12.10	0.80	0.066	0.3	0.0	0.0	0.0	0.0	0.0	0.0
340	85.00	128.30	122.70	5.60	0.046	0.7	0.4	0.5	1.8	0.0	0.0	2.2
345	87.00	158.40	151.80	6.60	0.043	2.3	1.8	0.6	1.0	0.0	0.0	1.6
350	89.00	45.30	43.20	2.10	0.049	2.0	0.0	0.0	0.0	0.0	0.0	0.2
355	89.80	3.60	2.10	1.50	0.714	1.2	0.1	0.0	0.2	0.0	0.0	0.2
360	90.60	13.50	12.90	0.60	0.047	0.2	0.2	0.2	0.1	0.0	0.0	0.0
365	91.40	376.00	360.70	15.30	0.042	4.4	0.0	0.4	0.0	0.3	0.0	2.9
370	92.20	33.50	31.70	1.80	0.057	0.9	0.0	0.1	0.1	0.2	0.0	0.1
375	93.00	645.70	566.50	79.20	0.140	14.9	7.0	3.2	2.0	35.0	0.0	14.5
380	93.66	2597.60	2495.00	102.60	0.041	14.0	23.3	2.5	2.2	51.0	0.0	51.2
385	94.33	1185.70	1073.00	112.70	0.105	12.6	19.6	7.3	0.0	31.5	37.9	14.7
390	95.00	119.10	101.20	17.90	0.177	1.7	0.3	0.5	0.4	0.0	15.5	0.8
395	99.00	0.30	0.30	0.00		0.0	0.0	0.0	0.0	0.0	0.0	0.0
400	102.00	6.70	6.30	0.40	0.063	0.1	0.0	0.1	0.0	0.2	0.0	0.0
405	107.00	0.00	0.00	0.00		0.0	0.0	0.0	0.0	0.0	0.0	0.0
410	117.00	132.00	125.00	7.00	0.056	3.6	0.3	0.7	0.1	0.7	0.7	0.3
415	118.64	482.80	472.10	10.70	0.023	8.4	0.0	0.0	0.0	0.7	0.7	2.6
420	120.28	12.20	11.70	0.50	0.043	0.1	0.0	0.0	0.0	0.3	0.0	0.1

A.16. Foraminiferal absolute abundance and individual species counts for PCM5

Depth	Age	Planktics & benthics	Planktic Abundance	Benthic Abundance	B/P ratio	*Eponides umbonatus*	*Cassidulina reniforme*	*Cassidulina teretis*	*Elphidium spp.*	*Cibicidoides wuellerstorfi*	*Pullenia bulloides*	*Neogloboquadrina pachyderma (d)*
425	121.92	5.50	5.20	0.30	0.058	0.1	0.1	0.0	0.0	0.0	0.0	0.0
430	123.56	0.00	0.00	0.00		0.0	0.0	0.0	0.0	0.0	0.0	0.0
435	125.20	0.10	0.10	0.00		0.0	0.0	0.0	0.0	0.0	0.0	0.0
440	134.00	450.60	433.00	17.60	0.041	11.7	0.1	1.6	3.2	0.0	0.0	4.0
445	136.00	1603.40	1573.00	30.40	0.019	20.8	0.0	3.7	3.7	0.0	0.0	3.5
450	136.58	1189.80	1159.00	30.80	0.027	21.4	1.3	6.7	0.1	0.0	0.0	0.5
455	137.16	3018.80	2875.00	143.80	0.050	27.1	21.5	83.7	2.7	0.0	0.0	17.6
460	137.74	2493.20	2365.00	128.20	0.054	18.7	6.2	93.8	6.2	0.0	0.0	23.2
465	138.32	2723.30	2529.00	194.30	0.077	5.8	3.0	107.1	25.0	2.7	0.0	55.6
470	138.90	2104.40	2008.00	96.40	0.048	17.4	5.8	52.4	11.6	0.0	0.0	29.3
475	139.48	2574.00	2472.00	102.00	0.041	37.4	11.9	35.7	13.6	0.0	0.0	28.5
480	140.00	3926.80	3797.00	129.80	0.034	30.0	8.9	62.9	15.1	0.0	0.0	25.4
485	144.00	2623.00	2493.00	130.00	0.052	35.6	2.7	69.9	10.8	0.0	0.0	45.7
490	148.00	43.70	41.20	2.50	0.061	1.0	0.5	0.3	0.5	0.0	0.0	0.2
495	152.00	806.90	759.00	47.90	0.063	40.6	0.0	0.8	4.8	0.0	0.0	11.4
500	156.00	11.50	11.30	0.20	0.018	0.2	0.0	0.1	0.0	0.0	0.0	0.2
505	160.00	4989.40	4691.00	298.40	0.064	36.4	15.3	148.9	20.6	0.0	0.0	62.1
510	164.00	4990.40	4653.00	337.40	0.073	53.0	41.2	201.7	23.6	0.0	0.0	52.5
515	168.00	3487.50	3324.00	163.50	0.049	32.5	27.0	92.6	11.0	0.0	0.0	32.9
520	172.00	1507.50	1451.00	56.50	0.039	9.4	3.1	37.7	4.7	0.0	0.0	13.1
525	176.00	1280.00	1230.00	50.00	0.041	11.8	2.9	19.1	10.3	0.0	0.0	6.6
530	180.00	142.90	136.50	6.40	0.047	1.2	0.5	3.4	1.1	0.0	0.0	1.8
535	180.66	15.00	14.00	1.00	0.071	0.3	0.2	0.4	0.1	0.0	0.0	0.0
540	181.32	0.80	0.80	0.00		0.0	0.0	0.0	0.0	0.0	0.0	0.0
545	181.98	0.00	0.00	0.00		0.0	0.0	0.0	0.0	0.0	0.0	0.0
550	182.64	77.60	73.60	4.00	0.054	1.3	0.4	1.5	0.6	0.0	0.0	1.2
555	183.30	0.00	0.00	0.00		0.0	0.0	0.0	0.0	0.0	0.0	0.0
560	183.96	4.00	3.80	0.20	0.053	0.0	0.0	0.2	0.0	0.0	0.0	0.0

A.16. Foraminiferal absolute abundance and individual species counts for PCM5

Depth	Age	Planktics & benthics	Planktic Abundance	Benthic Abundance	B/P ratio	*Eponides umbonatus*	*Cassidulina reniforme*	*Cassidulina teretis*	*Elphidium spp.*	*Cibicidoides wuellerstorfi*	*Pullenia bulloides*	*Neogloboquadrina pachyderma (d)*
565	184.62	0.30	0.30	0.00		0.0	0.0	0.0	0.0	0.0	0.0	0.0
570	185.28	0.10	0.10	0.00		0.0	0.0	0.0	0.0	0.0	0.0	0.0
575	185.94	0.10	0.10	0.00		0.0	0.0	0.0	0.0	0.0	0.0	0.1
580	186.60	0.10	0.10	0.00		0.0	0.0	0.0	0.0	0.0	0.0	0.0
585	187.26	1.10	1.10	0.00		0.0	0.0	0.0	0.0	0.0	0.0	0.0
590	187.92	0.00	0.00	0.00		0.0	0.0	0.0	0.0	0.0	0.0	0.0
595	188.58	0.00	0.00	0.00		0.0	0.0	0.0	0.0	0.0	0.0	0.0
600	189.24	0.00	0.00	0.00		0.0	0.0	0.0	0.0	0.0	0.0	0.0
605	189.90	0.00	0.00	0.00		0.0	0.0	0.0	0.0	0.0	0.0	0.0
610	190.56	0.00	0.00	0.00		0.0	0.0	0.0	0.0	0.0	0.0	0.0
615	191.22	0.20	0.00	0.20		0.0	0.0	0.0	0.0	0.0	0.0	0.0
620	191.88	0.40	0.40	0.00		0.0	0.0	0.0	0.0	0.0	0.0	0.2
625	192.54	0.90	0.90	0.00		0.0	0.0	0.0	0.0	0.0	0.0	0.0
630	193.20	0.10	0.10	0.00		0.0	0.0	0.0	0.0	0.0	0.0	0.0
635	193.86	0.00	0.00	0.00		0.0	0.0	0.0	0.0	0.0	0.0	0.0
640	194.52	0.00	0.00	0.00		0.0	0.0	0.0	0.0	0.0	0.0	0.0
645	195.18	0.00	0.00	0.00		0.0	0.0	0.0	0.0	0.0	0.0	0.0
650	195.84	0.00	0.00	0.00		0.0	0.0	0.0	0.0	0.0	0.0	0.0
655	196.50	0.00	0.00	0.00		0.0	0.0	0.0	0.0	0.0	0.0	0.0
660	197.16	0.90	0.20	0.70	3.500	0.0	0.2	0.0	0.4	0.0	0.0	0.0
665	197.82	3.00	2.70	0.30	0.111	0.0	0.2	0.0	0.1	0.0	0.0	0.1
670	198.48	1.60	1.50	0.10	0.067	0.0	0.0	0.0	0.1	0.0	0.0	0.0
675	199.14	1.60	1.30	0.30	0.231	0.0	0.3	0.0	0.0	0.0	0.0	0.1
680	199.80	5.20	3.40	1.80	0.529	0.0	0.8	0.1	0.5	0.0	0.0	0.0
685	200.00	5.60	5.00	0.60	0.120	0.1	0.3	0.0	0.1	0.0	0.0	0.0

A.16. Foraminiferal absolute abundance and individual species counts for PCM5

Depth	Age	Planktic abundance	Benthic abundance	B/P ratio	*N.pachyderma* (sinistral)	*N.pachyderma* (dextral)	*Pullenia bulloides*	*Globigerina bulloides*	*Melonis barleeanum*	*Cassidulina teretis*	*Cassidulina reniforme*	*Elphidium spp.*	*Eponides umbonatus*	*Cibicidoides wuellerstorfi*
0	10.20	210.1	69.7	0.332	210.0	0.0	5.1	0.0	28.8	18.2	7.6	0.0	1.3	3.6
2.5	10.22	206.6	151.9	0.735	206.6	0.0	11.1	0.0	58.2	50.0	13.6	3.6	4.5	8.2
5	10.24	125.3	92.5	0.738	125.3	0.0	6.4	0.2	39.3	24.8	8.3	3.0	3.1	7.6
10	10.28	105.8	13.3	0.126	105.4	0.0	0.0	0.4	7.9	2.3	1.0	0.2	0.0	1.3
12.5	10.31	165.6	26.1	0.158	163.7	0.0	0.6	1.8	14.3	3.7	2.8	0.4	0.0	3.9
15	10.33	94.6	23.8	0.252	84.6	8.2	0.6	1.8	11.6	4.8	2.8	0.2	0.2	3.6
20	10.37	119.6	23.5	0.196	98.3	19.8	0.2	1.5	12.5	4.1	2.1	0.0	0.2	3.7
25	10.41	78.9	13.9	0.176	67.7	9.7	0.2	1.5	8.8	2.0	1.1	0.4	0.0	0.9
30	10.45	0.0	0.7		0.0	0.0	0.0	0.0	0.5	0.0	0.0	0.2	0.0	0.0
35	10.50	3.5	3.1	0.886	3.3	0.0	0.0	0.0	0.8	0.8	1.0	0.4	0.0	0.0
40	10.56	17.7	15.0	0.847	17.7	0.0	0.3	0.0	1.5	5.6	3.6	1.4	0.3	1.6
45	10.60	18.2	26.6	1.462	18.2	0.0	0.0	0.0	9.1	10.0	5.4	0.2	0.0	2.0
50	10.93	6.0	13.3	2.217	6.0	0.0	0.0	0.0	5.8	2.7	0.9	0.4	0.7	0.7
55	11.26	7.1	10.1	1.423	7.1	0.0	0.0	0.0	5.4	1.3	1.3	0.0	1.5	0.6
60	11.59	3.6	8.0	2.222	3.6	0.0	0.0	0.0	5.4	1.0	0.8	0.0	0.4	0.4
65	11.92	11.0	13.9	1.264	11.0	0.0	0.0	0.0	4.5	2.1	2.6	0.5	2.9	1.3
70	11.95	43.7	24.6	0.563	40.6	3.0	0.2	0.0	9.2	3.6	4.4	0.0	1.5	5.1
75	11.98	45.3	17.1	0.377	43.1	1.7	0.0	0.5	8.5	0.7	3.8	0.0	0.7	3.3
80	12.01	44.2	17.0	0.385	41.0	3.0	0.0	0.3	9.7	2.2	0.8	0.0	0.3	3.8
85	12.04	51.4	15.9	0.309	46.9	4.1	0.0	0.4	7.7	3.4	1.4	0.0	0.7	1.6
90	12.07	47.2	9.1	0.193	39.0	7.8	0.0	0.4	4.0	2.7	0.9	0.0	0.2	1.3
95	12.10	45.4	7.1	0.156	34.1	10.3	0.0	1.0	3.4	0.5	1.5	0.0	0.4	1.2
100	12.13	36.4	10.4	0.286	29.2	6.8	0.0	0.4	3.4	1.4	3.2	0.0	0.0	2.4
105	12.16	73.2	16.4	0.224	57.8	14.2	0.4	1.2	4.4	3.0	4.0	0.0	0.2	3.4
110	12.19	34.5	6.3	0.183	28.2	6.1	0.0	0.2	4.0	1.0	0.8	0.4	0.2	1.1
115	12.22	98.4	16.5	0.168	80.3	16.9	0.0	1.1	8.0	3.7	2.3	0.0	0.2	1.4
120	12.30	36.7	6.2	0.169	33.1	2.8	0.0	0.8	3.2	0.6	0.8	0.0	0.0	0.4
125	12.43	42.6	9.0	0.211	36.2	5.3	0.2	1.1	5.3	1.1	0.7	0.0	0.2	1.3
130	12.56	10.5	16.0	1.524	10.5	0.0	0.0	0.0	6.2	8.5	0.2	0.1	0.1	0.6

A.17. Foraminiferal absolute abundance and individual species counts for PCM7.

Depth	Age	Planktic abundance	Benthic abundance	B/P ratio	*N.pachyderma* (sinistral)	*N.pachyderma* (dextral)	*Pullenia bulloides*	*Globigerina bulloides*	*Melonis barleeanum*	*Cassidulina teretis*	*Cassidulina reniforme*	*Elphidium spp.*	*Eponides umbonatus*	*Cibicidoides wuellerstorfi*
135	12.69	3.3	12.4	3.758	3.3	0.0	0.0	0.0	8.2	3.8	0.0	0.0	0.0	0.4
140	12.82	5.1	14.8	2.902	5.1	0.0	0.0	0.0	5.6	8.2	0.3	0.2	0.2	0.3
145	12.95	9.6	24.8	2.583	9.6	0.0	0.0	0.0	4.8	19.4	0.0	0.0	0.0	0.6
150	13.11	8.3	139.5	16.807	8.3	0.0	0.0	0.0	15.3	121.7	0.2	0.1	0.1	2.0
155	13.22	9.0	77.4	8.600	9.0	0.0	0.0	0.0	1.9	74.0	0.3	0.3	0.0	0.3
160	13.32	7.1	62.5	8.803	7.1	0.0	0.0	0.0	6.1	54.8	0.6	0.1	0.0	0.3
165	13.43	3.8	6.8	1.789	3.8	0.0	0.0	0.0	0.0	6.7	0.1	0.0	0.0	0.0
170	13.55	1.6	5.4	3.375	1.6	0.0	0.0	0.0	0.1	3.6	1.1	0.6	0.0	0.0
175	13.68	0.6	0.2	0.333	0.6	0.0	0.0	0.0	0.0	0.2	0.0	0.0	0.0	0.0
180	13.81	1.3	1.5	1.154	1.3	0.0	0.0	0.0	0.0	1.3	0.2	0.0	0.0	0.0
185	13.94	2.1	2.3	1.095	2.1	0.0	0.0	0.0	0.0	1.4	0.7	0.2	0.0	0.0
190	14.07	1.5	2.5	1.667	1.5	0.0	0.0	0.0	0.0	1.8	0.6	0.0	0.0	0.1
195	14.20	1.7	2.0	1.176	1.7	0.0	0.0	0.0	0.0	0.4	1.5	0.2	0.0	0.0
200	14.33	0.7	1.4	2.000	0.7	0.0	0.0	0.0	0.0	0.7	0.7	0.0	0.0	0.0
205	14.46	4.2	2.1	0.500	4.2	0.0	0.0	0.0	0.0	2.1	0.0	0.0	0.0	0.0
210	14.59	2.2	2.3	1.045	2.2	0.0	0.0	0.0	0.1	2.0	0.2	0.0	0.0	0.1
215	14.72	0.4	0.8	2.000	0.4	0.0	0.0	0.0	0.0	0.6	0.2	0.0	0.0	0.0
220	14.85	1.3	3.7	2.846	1.3	0.0	0.0	0.0	0.0	2.3	1.3	0.0	0.0	0.0
225	14.98	1.7	2.6	1.529	1.7	0.0	0.0	0.0	0.0	2.5	0.1	0.0	0.0	0.0
230	15.11	1.9	2.0	1.053	1.9	0.0	0.0	0.0	0.0	1.7	0.3	0.0	0.0	0.0
240	15.36	1.9	6.1	3.211	1.9	0.0	0.0	0.0	1.8	4.0	0.0	0.0	0.0	0.0
245	15.48	31.7	110.9	3.498	31.7	0.0	0.0	0.0	3.2	104.8	1.1	0.9	0.0	0.9
250	15.61	636.0	219.2	0.345	632.0	4.4	0.2	0.0	11.3	154.0	9.0	29.6	4.8	6.7
255	15.74	363.1	135.7	0.374	361.4	1.7	0.0	0.0	1.0	125.8	1.1	3.1	2.6	1.1
260	15.87	446.8	122.8	0.275	445.7	1.1	0.0	0.0	0.0	117.4	1.9	1.0	1.8	0.9
265	16.00	862.2	226.2	0.262	862.2	0.0	0.0	0.0	2.3	212.8	2.2	1.0	8.3	0.2
270	16.50	290.8	92.4	0.318	290.8	0.0	0.0	0.0	1.7	86.7	1.7	0.7	0.5	1.1
275	17.00	1184.4	361.1	0.305	1183.4	1.0	0.0	0.0	0.3	350.3	3.8	2.1	0.3	1.9
280	17.50	0.8	0.2	0.250	0.8	0.0	0.0	0.0	0.0	0.2	0.0	0.0	0.0	0.0

A.17. Foraminiferal absolute abundance and individual species counts for PCM7.

Depth	Age	Planktic abundance	Benthic abundance	B/P ratio	*N.pachyderma* (sinistral)	*N.pachyderma* (dextral)	*Pullenia bulloides*	*Globigerina bulloides*	*Melonis barleeanum*	*Cassidulina teretis*	*Cassidulina reniforme*	*Elphidium spp.*	*Eponides umbonatus*	*Cibicidoides wuellerstorfi*
285	18.00	1.0	0.7	0.700	1.0	0.0	0.0	0.0	0.0	0.2	0.0	0.4	0.0	0.1
290	18.50	1.0	0.6	0.600	1.0	0.0	0.0	0.0	0.0	0.0	0.2	0.4	0.0	0.1
295	19.00	1.8	0.6	0.333	1.8	0.0	0.0	0.0	0.0	0.2	0.0	0.2	0.0	0.1
300	19.50	0.4	0.9	2.250	0.4	0.0	0.0	0.0	0.4	0.1	0.0	0.3	0.0	0.1
305	20.00	1.1	2.8	2.545	1.1	0.0	0.1	0.0	0.1	0.8	0.5	0.7	0.0	0.5
310	20.50	1.6	5.3	3.313	1.6	0.0	0.0	0.0	0.0	4.8	0.5	0.0	0.0	0.0
315	21.00	33.7	88.0	2.611	33.7	0.0	0.0	0.0	3.4	80.7	0.9	1.2	0.1	1.2
320	21.50	1102.1	156.6	0.142	1100.0	2.4	0.0	0.0	7.1	136.3	4.4	2.1	2.3	0.1
325	22.04	1005.7	125.3	0.125	1002.0	4.1	0.0	0.0	6.7	92.5	5.2	1.9	17.4	2.6
330	22.78	55.7	16.7	0.300	55.7	0.0	0.0	0.0	2.0	8.6	0.3	1.6	2.2	0.0
340	24.26	10.9	4.9	0.450	10.9	0.0	0.0	0.0	0.5	3.5	0.1	0.5	0.0	0.0
345	25.00	99.3	30.4	0.306	99.3	0.0	0.0	0.0	2.6	20.0	1.0	1.4	0.4	0.4
350	26.83	16.9	10.3	0.609	16.9	0.0	0.0	0.0	6.1	3.1	0.0	0.3	0.2	0.2
355	28.66	0.3	0.0		0.3	0.0	0.0	0.0	0.0	0.0	0.0	0.0	0.0	0.0
360	30.49	0.0	0.0		0.0	0.0	0.0	0.0	0.0	0.0	0.0	0.0	0.0	0.0
370	34.20	8.0	8.5	1.063	8.0	0.0	0.0	0.0	7.2	1.1	0.0	0.0	0.0	0.0
375	36.00	43.2	40.1	0.928	43.2	0.0	0.0	0.0	11.6	17.4	3.3	3.1	1.4	1.3
380	36.45	0.7	0.1	0.143	0.7	0.0	0.0	0.0	0.1	0.0	0.0	0.0	0.0	0.0
385	36.90	0.0	0.0		0.0	0.0	0.0	0.0	0.0	0.0	0.0	0.0	0.0	0.0
390	37.35	4.4	5.1	1.159	4.4	0.0	0.0	0.0	3.3	1.7	0.1	0.0	0.0	0.0
395	37.80	1.3	2.2	1.692	1.3	0.0	0.0	0.0	1.7	0.4	0.0	0.1	0.0	0.0
400	38.25	25.5	16.1	0.631	25.5	0.0	0.0	0.0	9.4	4.0	0.8	0.0	0.0	0.9
405	38.70	107.5	63.6	0.592	106.8	0.7	0.0	0.0	6.3	49.1	0.9	0.0	2.1	2.9
410	39.15	4.3	7.9	1.837	4.3	0.0	0.0	0.0	5.8	0.5	0.2	0.0	0.0	0.3
415	39.60	14.8	4.7	0.318	14.8	0.0	0.0	0.0	3.6	0.0	0.2	0.0	0.0	0.2
420	40.05	7.4	6.5	0.878	7.4	0.0	0.0	0.0	0.4	3.4	0.3	0.0	0.7	1.1
425	40.50	0.2	0.3	1.500	0.2	0.0	0.0	0.0	0.0	0.3	0.0	0.0	0.0	0.0
430	40.95	66.9	22.8	0.341	66.9	0.0	0.0	0.2	3.1	16.5	0.9	0.0	0.0	0.9
435	41.40	15.9	10.0	0.629	15.9	0.0	0.0	0.0	4.8	3.1	0.6	0.0	0.0	1.0

A.17. Foraminiferal absolute abundance and individual species counts for PCM7.

Depth	Age	Planktic abundance	Benthic abundance	B/P ratio	*N.pachyderma* (sinistral)	*N.pachyderma* (dextral)	*Pullenia bulloides*	*Globigerina bulloides*	*Melonis barleeanum*	*Cassidulina teretis*	*Cassidulina reniforme*	*Elphidium spp.*	*Eponides umbonatus*	*Cibicidoides wuellerstorfi*
440	41.85	25.4	9.5	0.374	25.3	0.1	0.0	0.0	5.3	3.2	0.6	0.0	0.0	0.3
445	42.30	14.8	11.0	0.743	14.8	0.0	0.0	0.0	4.3	6.1	0.5	0.0	0.0	0.0
450	42.75	21.9	13.1	0.598	21.9	0.0	0.0	0.0	2.8	9.4	0.2	0.1	0.0	0.5
455	43.20	34.9	21.8	0.625	34.9	0.0	0.0	0.0	1.5	18.8	0.2	0.1	0.0	0.0
460	43.65	13.0	9.0	0.692	12.8	0.2	0.0	0.0	4.7	3.6	0.5	0.0	0.0	0.1
465	44.10	24.0	14.8	0.617	24.0	0.0	0.0	0.0	3.3	11.0	0.0	0.2	0.0	0.2
470	44.55	31.8	11.5	0.362	31.8	0.0	0.0	0.0	2.1	8.1	0.7	0.1	0.0	0.3
475	45.00	5.8	5.9	1.017	5.8	0.0	0.0	0.0	3.7	1.6	0.1	0.1	0.1	0.0
480	45.35	4.3	8.1	1.884	4.3	0.0	0.0	0.0	2.1	5.0	0.1	0.0	0.3	0.1
485	45.70	2.1	4.4	2.095	2.1	0.0	0.0	0.0	3.0	1.3	0.0	0.0	0.0	0.0
490	46.05	1.5	1.8	1.200	1.5	0.0	0.0	0.0	0.6	1.2	0.0	0.0	0.0	0.0
495	46.40	1.2	1.8	1.500	1.2	0.0	0.0	0.0	0.7	1.1	0.0	0.0	0.0	0.0
500	46.75	1.2	0.5	0.417	1.2	0.0	0.0	0.0	0.3	0.2	0.0	0.0	0.0	0.0
505	47.10	4.1	1.9	0.463	4.1	0.0	0.0	0.0	1.5	0.4	0.0	0.0	0.0	0.0
510	47.45	7.2	12.4	1.722	7.2	0.0	0.0	0.0	4.9	5.8	0.9	0.0	0.0	0.4
515	47.80	12.5	16.3	1.304	12.5	0.0	0.0	0.0	3.2	12.3	0.3	0.0	0.0	0.4
520	48.15	13.9	7.6	0.547	13.9	0.0	0.0	0.0	2.1	4.5	0.1	0.1	0.1	0.7
525	48.50	151.5	71.9	0.475	149.6	1.9	0.0	0.0	11.2	50.2	2.7	1.1	1.0	4.9
530	48.85	172.2	56.4	0.328	169.3	2.9	0.0	0.0	22.3	22.9	0.8	1.8	1.5	5.1
535	49.20	0.4	0.0		0.4	0.0	0.0	0.0	0.0	0.0	0.0	0.0	0.0	0.0
540	49.55	260.8	66.5	0.255	257.2	3.7	0.0	0.0	4.9	46.3	2.3	1.0	5.7	6.3
545	50.00	70.7	3.3	0.047	68.6	2.1	0.0	0.0	0.0	0.0	0.0	0.2	1.6	1.6
550	50.75	8.2	7.9	0.963	8.0	0.2	0.0	0.0	3.7	3.0	0.2	0.1	0.0	0.1
555	51.50	1.3	7.8	6.000	1.3	0.0	0.0	0.0	6.1	1.5	0.0	0.1	0.0	0.1
560	52.25	0.7	1.1	1.571	0.7	0.0	0.0	0.0	0.5	0.6	0.0	0.0	0.0	0.0
565	53.00	8.5	16.8	1.976	8.3	0.2	0.0	0.0	6.4	8.3	0.9	0.1	0.1	0.7
570	53.75	9.1	9.4	1.033	9.1	0.0	0.0	0.0	1.7	6.8	0.4	0.1	0.1	0.1
575	54.50	5.2	7.5	1.442	5.2	0.0	0.0	0.0	4.0	1.2	0.0	0.0	0.0	0.5
580	55.25	5.4	9.2	1.704	5.4	0.0	0.0	0.0	5.1	2.3	0.6	0.1	0.0	0.8

A.17. Foraminiferal absolute abundance and individual species counts for PCM7.

Depth	Age	Planktic abundance	Benthic abundance	B/P ratio	*N.pachyderma* (sinistral)	*N.pachyderma* (dextral)	*Pullenia bulloides*	*Globigerina bulloides*	*Melonis barleeanum*	*Cassidulina teretis*	*Cassidulina reniforme*	*Elphidium spp.*	*Eponides umbonatus*	*Cibicidoides wuellerstorfi*
585	56.00	3.6	4.0	1.111	3.6	0.0	0.0	0.0	2.8	2.3	0.1	0.0	0.0	0.1
590	56.75	2.0	1.2	0.600	2.0	0.0	0.0	0.0	0.7	0.4	0.0	0.1	0.0	0.0
595	57.50	0.2	0.2	1.000	0.2	0.0	0.0	0.0	0.1	0.1	0.0	0.0	0.0	0.0
600	58.25	14.8	13.2	0.892	14.6	0.2	0.0	0.0	3.5	6.0	0.3	0.8	0.1	1.8
605	59.00	46.2	19.3	0.418	46.0	0.2	0.0	0.0	4.2	11.6	1.1	0.6	0.8	0.5
610	59.55	2.6	4.6	1.769	2.6	0.0	0.0	0.0	1.5	1.8	0.1	0.1	0.0	0.1
615	60.10	13.6	13.6	1.000	13.5	0.1	0.0	0.0	0.6	6.3	3.6	2.1	0.0	0.4
620	60.65	13.4	10.9	0.813	13.4	0.0	0.0	0.0	0.1	3.4	3.7	3.1	0.0	0.4
625	61.20	15.0	8.5	0.567	15.0	0.0	0.0	0.0	0.0	2.5	3.3	2.7	0.0	0.0
630	61.75	18.4	14.8	0.804	18.2	0.2	0.0	0.0	0.0	4.7	6.1	2.9	0.0	0.8
635	62.30	12.5	5.4	0.432	12.0	0.5	0.0	0.0	0.0	1.2	1.7	2.1	0.0	0.1
640	62.85	18.4	14.1	0.766	18.4	0.0	0.0	0.0	0.0	5.3	3.5	3.3	0.0	0.1
645	63.40	9.3	4.9	0.527	9.3	0.0	0.0	0.0	0.0	1.4	2.0	1.1	0.0	0.4
650	64.00	4.4	3.1	0.705	4.3	0.1	0.0	0.0	0.0	0.4	0.8	1.1	0.0	0.9
655	64.55	1.6	0.8	0.500	1.6	0.0	0.0	0.0	0.0	0.0	0.5	0.3	0.0	0.0
660	65.10	5.3	0.2	0.038	5.3	0.0	0.0	0.0	0.0	0.0	0.1	0.1	0.0	0.0
665	65.65	17.3	3.5	0.202	17.2	0.1	0.0	0.0	0.1	1.1	0.6	0.9	0.0	0.4
670	66.20	18.7	5.6	0.299	18.5	0.2	0.0	0.0	0.0	1.1	1.9	1.9	0.0	0.5
675	66.75	21.2	8.2	0.387	21.1	0.1	0.0	0.0	0.0	1.5	1.6	4.4	0.0	0.3
680	67.30	10.1	6.1	0.604	10.1	0.0	0.0	0.0	0.0	1.3	1.7	2.3	0.0	0.7
685	67.85	5.4	1.9	0.352	5.4	0.0	0.0	0.0	0.0	0.2	0.9	0.9	0.0	0.0
690	68.40	10.4	4.3	0.413	10.3	0.1	0.0	0.0	0.0	0.4	1.9	1.4	0.2	0.2
695	68.95	15.3	3.4	0.222	15.1	0.2	0.0	0.0	0.0	0.4	1.2	1.7	0.0	0.1
700	69.50	10.3	3.5	0.340	10.1	0.2	0.0	0.0	0.0	0.4	1.4	1.4	0.0	0.2
705	70.05	23.8	4.7	0.197	23.8	0.0	0.0	0.0	0.0	1.0	1.0	2.5	0.0	0.1
710	70.60	21.7	6.3	0.290	21.6	0.1	0.0	0.0	0.3	1.4	1.0	2.8	0.0	0.8
715	71.15	17.7	5.1	0.288	17.7	0.0	0.0	0.0	0.1	1.5	1.4	1.7	0.0	0.2
720	71.70	11.4	3.4	0.298	11.4	0.0	0.0	0.0	0.1	0.4	1.0	1.6	0.0	0.3
727	72.25	10.9	3.3	0.303	10.9	0.0	0.0	0.0	0.1	1.2	1.0	0.8	0.0	0.2

A.17. Foraminiferal absolute abundance and individual species counts for PCM7.

Depth	Age	Planktics	Benthics	P/B ratio	*N.pachyderma* (sinistral)	*N.pachyderma* (dextral)	*Globigerina bulloides*	*Melonis barleeanum*	*Cassidulina teretis*	*Cassidulina reniforme*	*Eponides umbonatus*	*Elphidium spp.*	*Cibicidoides wuellerstorfi*	*Pullenia bulloides*
10	8.75	191.8	25.4	7.5	127.4	63.1	1.2	12.3	5.8	2.7	0.0	0.0	1.9	0.5
20	8.89	244.3	17.6	13.9	150.3	92.6	1.4	6.7	3.4	2.3	0.1	0.0	2.7	0.1
30	9.03	90.1	11.2	8.0	57.1	32.3	0.7	5.9	2.8	0.8	0.0	0.0	0.9	0.0
40	9.17	93.2	20.6	4.5	55.7	36.7	0.8	9.8	4.2	1.7	0.7	0.0	1.6	0.3
50	9.31	55.5	17.8	3.1	33.0	22.2	0.3	5.7	3.7	2.1	1.1	0.0	1.4	0.2
60	9.45	462.8	17.4	26.6	258.6	200.3	3.9	5.0	2.7	2.2	0.6	0.1	2.8	0.1
70	9.59	103.3	14.0	7.4	66.4	36.3	0.6	3.6	3.0	1.2	1.1	0.0	2.9	0.1
80	9.73	82.2	18.3	4.5	63.7	17.9	0.6	4.7	3.3	2.3	0.7	0.1	4.8	0.2
90	9.87	51.2	18.5	2.8	36.4	14.8	0.0	7.0	2.7	3.3	0.7	0.1	3.2	0.0
100	10	47.1	25.3	1.9	37.0	10.1	0.0	6.8	8.5	4.6	2.3	0.0	1.3	0.0

A.18. Foraminiferal absolute abdundace and individual species counts for PCM7 Trip core.

Depth	Si content	Depth	Si content	Depth	Content
17.5	27.7	317.5	27.8	602.5	27.2
27.5	28	322.5	27.3	607.5	27.1
32.5	28.8	327.5	29.3	612.5	27.4
37.5	29.4	332.5	26.5	617.5	27.2
42.5	31.1	337.5	27.1	622.5	283
47.5	28.5	342.5	28	632.5	27.6
52.5	27.8	347.5	27.8	642.5	23.9
57.5	27.7	357.5	27.3	647.5	27.7
62.5	27.7	362.5	24.8	652.5	27.6
67.5	28.2	367.5	29.2	657.5	26.7
72.5	29	372.5	32.2	667.5	27
77.5	29.1	377.5	33.2	672.5	26.9
85	28.7	382.5	29.3	682.5	27.2
102.5	27.8	387.5	30.1		
107.5	27.6	392.5	30.2		
112.5	29.7	402.5	29.6		
122.5	29.9	407.5	29.3		
127.5	30.3	412.5	29.6		
132.5	29.6	417.5	28.6		
137.5	28.5	427.5	31.2		
142.5	30.5	432.5	26.7		
147.5	27.3	442.5	24.7		
152.5	26.1	447.5	28.3		
157.5	29.5	452.5	28.8		
162.5	31	457.5	29.7		
167.5	31	467.5	29.2		
172.5	29.9	472.5	28.8		
177.5	29.2	477.5	28.6		
182.5	28.9	482.5	26.7		
197.5	28.2	487.5	25.8		
202.5	33.5	492.5	30.5		
207.5	35	497.5	31.3		
212.5	30.3	502.5	29.5		
217.5	30.2	507.5	30		
222.5	29.1	512.5	29.1		
227.5	35	517.5	28.8		
232.5	31.4	522.5	28.8		
237.5	29.2	532.5	28		
242.5	34.2	537.5	29.3		
247.5	33.6	542.5	27		
252.5	33.3	545	26.8		
257.5	30.7	550	26.8		
272.5	32.5	557.5	27.4		
277.5	33.7	562.5	27.3		
282.5	31.8	567.5	27.5		
287.5	31.2	572.5	27.8		
292.5	32.4	577.5	27.9		
297.5	31.9	582.5	27.7		
302.5	30	587.5	27.3		
307.5	27	592.5	26.9		
312.5	27.8	597.5	27.1		